BEHAVIOUR AND TRANSPORTATION OF SILVER NANOPARTICLES IN AN AEROBIC WASTEWATER TREATMENT PILOT PLANT

By

MARIE-FRANCE ALINE BELINGA-DESAUNAY-NAULT

A thesis submitted to the University of Birmingham

For the degree of

DOCTOR OF PHILOSOPHY

School of Geography, Earth and Environmental Sciences

College of Environmental Health and Risk Management

University of Birmingham, UK

November 2017

Dedication

I am forever grateful to God for His grace and blessings toward me and my family in Jesus name. I dedicate this thesis to my parents, Françoise and Patrick, to my sisters, Caroline and Clémence and to my grandparents Marie, François, Cécile, Suzanne and René. I am deeply thankful for their endless love, support and encouragement for all this years and at different stages of my life.

Abstract

Investigating the behaviour, fate and transport of Silver nanoparticles (Ag-NPs) in wastewater treatment plants (WWTPs) is of great importance due to their presence in many consumer products and its potential to be toxic to environmental organisms. In this study, the transformation and fate of Ag-NPs was assessed using a multi-method characterisation approach, prior-to, during and post-aeration in the pilot sequencing batch reactor (SBR) and over a 21 day period in SBR. Synthesized 10 nm citrate and polyvinylpyrrolidone (PVP) coated Ag-NPs were spiked into OECD synthetic sewage (OECDss) media and it constituents and in the (OECDss + activated sludge (AS) media. Ag-NPs show agglomeration, dissolution and changes in surface chemistry at all measured time points i.e., at 0 hrs, at 24 hrs, at 45 hrs (during aeration) and at 48 hrs (during settling) and indicated that 80% of the citrate and PVP Ag-NPs could be removed in the form of Ag_2S, AgCl and Silver Phosphate-NPs. More than 50% of Ag-NPs accumulated within the sludge over a 21 day period (with no addition of fresh AS), and this occurred via physical adsorption on the surface of the AS flocs. This work demonstrates that Ag-NPs in wastewater can undergo a range of transformation processes, which include oxidation, dissolution, agglomeration, precipitation in an SBR pilot plant.

Acknowledgment

I am grateful to my supervisor, Professor Jamie Lead, for the opportunity he gave me to pursue this PhD topic and for his support, guidance and his immense trust in my abilities. I express my deepest gratitude to Professors Iseult Lynch and Éva Valsami-Jones for the invaluable time they spent to give their inputs on the thesis and timely support. Their kind gestures will never be forgotten. I would like to thank my co-supervisor Dr Ruth Merrifield for training, guidance and support.

Many thanks are due to Professor Cynthia Carliell-Marquet and to the rest of the team at the School of Civil Engineering for allowing me to use the Facility and for supplying the SBR plant pilot, Mark Carter for the technical, moral support and collection of the activated sludge from the WWTP and Dr. Gofetamang Ditalelo for the collaborative work. I thank Theresa Morris and Paul Stanley for the TEM and SEM training and EDS analysis, Dr. Bjorn Stolpe for the FFF training, Dr. Isabella Römer and Dr. Mila Tejamaya for the help and discussions on Ag-NPs synthesis and characterisation and Dr. Gillian Kingston and Eimear Orgill for the technical and lab support.

I am particularly grateful to Dr. Indrani Mahapatra for the guidance and endless support during of thesis. Special thanks to my friends and colleagues who helped me in many ways during the past few years – Dr. Yusuf Nur, Dr. Christine Elgy, Dr. Feng Dong, Dr. Isaac Aidoo, Gavkhar Mamadjanova, Valerie Carrasco, Dr. Pallavi Pant and Dr. Maria Pomoni. This research was funded by NERC and I am very grateful for the financial support without which this journey would not have been possible for me.

List of contents

List of Figures

Chapter 1

Chapter 2

Chapter 3

Chapter 4

Chapter 5

Chapter 6

List of tables

Chapter 1

Chapter 2

Chapter 3

Chapter 4

Chapter 5

Chapter 6

List of Abbreviations

AFM – Atomic force microscopy

Ag -Silver

Ag^+ - Silver ions, dissolved silver

AgNO3 – Silver nitrate

ANOVA – Analysis of variance

AS – Activated Sludge

BOD_5 – 5-day biological oxygen demand

$CaCl_2$ – Calcium chloride

CBA – Control bottom aeration

CMA – Control middle aeration

CBNs – Carbon based nanoparticles

CBS - Control bottom settling

CE - Capillary electrophoresis

CBS - Control bottom settling

CES - Control effluent settling

CMS - Control middle settling

CTS - Control top settling

CFF – Cross flow filtration

CNT – Carbon nanotube

COD –Chemical oxygen demand

D_H– Hydrodynamic diameter

DIW – Deionised water

DNA – Deoxyribonucleic acid

DO – Dissolved oxygen

DOC – Dissolved oxygen carbon

DLS – Dynamic light scattering

EDL – Electrical double layer

EDS (or EDX) – Energy dispersive x-rays spectroscopy

E_F – Fermi energy

EG – Energy gap (or band gap)

EM – Electron microscopy

ENPs – Engineered nanoparticles

ESEM/SEM – Environmental scanning electron microscope / scanning electron microscope

FA – Fulvic acid

FEG – Field emission gun

FIFFF – Flow-Field flow fractionation also called Field flow fractionation (FFF)

FWHM – Full width at half Maximum

GFAAS – Graphite furnace atomic adsorption spectroscopy

HA – humic acids

HDC – Hydrodynamic chromatography

HNO_3 – Nitric acid

ICPMS – Inductively coupled plasma-mass spectrometry

ICP-OES – Inductively coupled plasma-optical emission spectrometry

K_2HPO_4 – Anhydrous dipotassium hydrogen phosphate

MA – Maximum absorbance

MAD – Maximum absorbance decreased

MeO – Metal oxides

Mg_2SO_4 – Magnesium sulphate

$NaBH_4$ – Sodium borohydride

NaCl – NaCl

NOM – Natural organic matter

NP/NPs – Nanoparticle(s)

nZVI – nano zerovalent iron

OECD – the Organisation for economic co-operation and development

OECDss – OECD synthetic sewage

PCS – Photon correlation spectroscopy

PDI – Polydispersity index

PEG – Polyethylene glycol

PEG-SH – thiol-polyethylene glycol

pH – Potential hydrogen

PSD – Particle size distribution

PVP – Polyvinylpyrrolidone

QDs – Quantum dots

SPR – Surface plasmon resonance

NZVI – Nanosized zero valent iron

SEC – Size exclusion chromatography

SEM – Scanning electron microscopy

SBR – Sequencing batch reactor

SP-NPs – Silver Phosphate nanoparticles

SS - suspended solids

STM – Scanning tunnelling microscopy

STP – Specific time point

TEM – Transmission electron microscopy

TOC – Total organic carbon

TS – Total solids

TTA – Test top aeration

TMA – Test middle aeration

TBA – Test bottom aeration

TTS – Test top settling

TTS – Test middle settling

TTS – Test bottom settling

TTS – Test effluent settling

UF – Ultrafiltration

UC – Ultracentrifugation

UV-Vis – Ultraviolet-visible Spectroscopy

VS – Volatile solids

WWTP(s) – Wastewater treatment plant(s)

XAS – X-ray absorption spectroscopy

XPS– X-ray photoelectron spectroscopy

XRD – X-Ray diffraction

XRF – X-ray fluorescence

ZP – Zeta potential

Chapter 1 Introduction

Chapter Summary

In recent years, there has been significant interest in the behaviour, fate and toxicity of manufactured as well as incidental NPs, e.g., combustion derived NPs, in the environment. The research on this subject has gained interest due to the increased usage of NPs in consumer products, with the global nanotechnology market estimated to reach 3 trillion US dollars in 2015 (Kaur et al., 2014, TWC). Due to the diversity in their physical and chemical properties and toxicity, and their widespread use in consumer products and thus direct route into wastewater, understanding how NPs might behave in WWTPs has become of prime importance. Indeed, there is an increasing evidence that NPs from consumer goods enter WWTPs through the sewer system and find their way into the water stream or landfill.

This chapter first provides a definition for NPs and their origin, and describes their physical and chemical properties and commercial applications. A brief look at the link between NPs composition / properties and toxicity properties will be given. This chapter then describes fate and behaviour of NPs in the environment. Finally, this chapter gives an overview of NP behaviour in an aerobic WWTP, with a focus on NP oxidation, sulphidation and dissolution.

1.1 Definition, origin and properties of NPs

Unlike nanomaterials (NMs) which have one or more dimensions in the nanoscale, meaning between 1 and 100 nm, NPs are defined as chemical and physical materials with all three dimensions in the nanoscale (Peijnenburg et al., 2015, Handford et al., 2014). To put this into perspective, a tennis ball has a diameter of 10^8 nm and viruses and bacteria range in size between 100 and 1000 nm (Figure 1-1). Although nanotechnology has helped developed man-made or specially engineered NPs, nanosized objects have existed in the environment for millions of years, e.g., viruses, bacteria, ocean spray, volcanic ash (Stanley, 2014) and incidental NPs, (i.e., NPs which are unintentionally produced due to human activities) have also existed as early as use of fires by early humans and since the time industrial processes began.

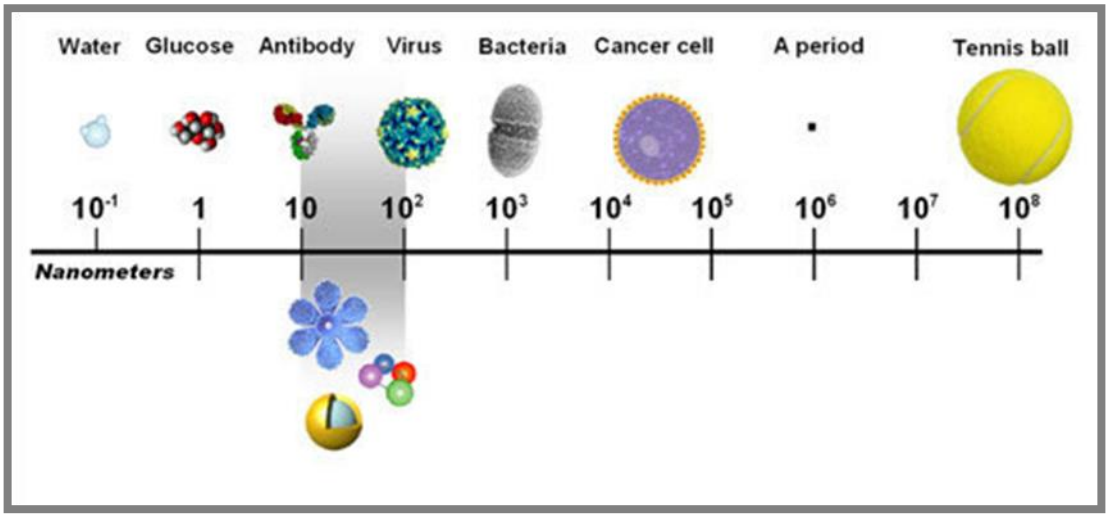

Figure 1-1: Illustration of the nanoscale relative to molecules and larger entities. Taken from (NCI, 2005)

In this chapter, we, therefore, refer to three different types of NPs, natural NPs, Engineered NPs (also known as manufactured NPs) and anthropogenic NPs, derived from emissions from

industries and combustion byproducts (Ju-Nam and Lead, 2008, Biswas and Wu, 2005, Nowack and Bucheli, 2007). Naturally occurring NPs can be generated through a variety of natural processes such as volcanic eruptions, erosion, photochemical reactions, weathering, forest fire, or plants and animals (via skin and hair shedding (Waychunas, 2009, Buzea et al., 2007). The second group of NPs commonly found in the environment are anthropogenic NPs inadvertently produced from human activities, and which are defined as incidental NPs. Engineered NPs, which are added to products for a specific function, can also be released accidentally, from wear and tear of consumer products, such as Ag-NPs from silver jewellery and cooking utensils (Nowack et al., 2012, Glover et al., 2011, Brar et al., 2010) or consumer activities, e.g. Ag-NPs released from paint outdoors (Kaegi et al., 2010). Engineered NPs (ENPs) can also be released to the environment through processing of NP-containing consumer products e.g. washing of textiles resulting in the release of embedded ENPs (Gottschalk and Nowack, 2011, Benn and Westerhoff, 2008a), and from cosmetics (Keller et al., 2013).

NPs can have optical, electrical and/or magnetic properties superior to the equivalent bulk materials, which in association with their small size and large surface area, lead to numerous applications and has resulted in a dramatic increase in the production of ENPs in recent years (Handford et al., 2014). A great variety of NPs exist currently, which can be classified (Table 1-1) based on their type (natural, anthropogenic or engineered), composition (C-containing or inorganic), formation process, size, shape, uniformity and agglomeration (Nowack and Bucheli, 2007, Buzea et al., 2007).

Table 1-1: Various approaches for classification of NPs (Nowack and Bucheli, 2007, Wagner et al., 2014)

Type	Chemical composition	Formation	Type of Nanoparticle	Examples
Natural	C-based	Biogenic	Organic colloids	Humic, fulvic acids
			Organics	viruses
		Geogenic	Soot	fullerenes
		Atmospheric	Aerosols	Organic acids
		Pyrogenic	Soot	Carbon NanoTubes (CNTs)
				Fullerenes
				Nanoglobules, onion-shaped nanospheres
	Inorganic	Biogenic	Oxides	Magnetite
			Metals	Ag, Au
		Geogenic	Oxides	Fe-oxides
			Clays	Allophane
		Atmospheric	Aerosols	Sea salt
Anthropogenic	C-based	By-products	Combustion by-products	CNTs
				Nanoglobules, onion-shaped nanospheres
		Engineered	Soot	Carbon black
				Fullerenes
				Functionalised CNTs, fullerenes
			Polymeric NP	Polyethylene-glycol (PEG) NP
	Inorganic	By-products	Combustion by-products	Platinum group metals

		Engineered	Oxides	TiO_2, SiO_2
			Metals	Ag, iron
			Salts	Metal-phosphates
			Aluminosilicates	Zeolites, clays, ceramics
Engineered	C-based	Engineered	Soot	CNTs
				Fullerenes
				Functionalised CNTs and fullerenes
				Carbon black
	Inorganic	Engineered	Oxides	TiO_2, ZnO, FeO_x, CeO_x, SiO_2
			Metals	Ag, Au, Fe,
			Semiconductors	Quantum dots

1.1.1 Naturally occurring NPs

Natural NPs are found in a variety of environments on earth, such as the atmosphere, soils, oceans and other natural water bodies and living organisms. Natural NPs can differ from ENPs in certain ways, such as non-uniform shapes due to their aggregation behaviour in the environment, ineffective passivation because they generally have no artificially added surface molecules (capping agents) to provide dispersion stabilisation, large amount and expected low toxicity (Waychunas, 2009). In the aquatic environment, these particles are formed by geochemical (abiotic) and biogeochemical (biotic) mechanisms (Wigginton et al., 2007). Natural NPs present in the environment include minerals, clays, and biological products, such as those generated by bacteria (Maurer-Jones et al., 2013, Klaine et al., 2008).

1.1.2 Accidentally produced NPs

Accidentally occurring or anthropogenic NPs are generally consequences of incidental emissions form road traffic (Shi et al., 2001), industrial activities and accidental release from discharged nanoproducts (Farre et al., 2011). There are multiple human activities causing the release of NPs into the environment in the form of airborne emissions. The increase in the commercial production of NPs over years with an estimated global production reaching over half a million tonnes by 2020 is likely to also increase the probability of their release into the environment (Maurer-Jones et al., 2013). Piccinno et al. (2012a) reported a worldwide median production volumes of industrial nanosilver to be 55 tonnes per annum.

1.1.3 Manufactured or engineered NPs

Unlike naturally occurring NPs, ENPs are generally monodispersed particles with a unique size and shape and are likely to be covered by one of a suite of synthetic surface molecules (Maurer-Jones et al., 2013). With an estimated worldwide market grown to $3 trillion in 2015 (Kaur et al., 2014), the production of ENPs by the nanotechnology industry is currently limited to a small range of NPs which are produced in high volumes and found in consumer products (Maurer-Jones et al., 2013). These ENPs include carbon based NPs (carbon nanotubes (CNTs) and fullerenes), SiO_2, Ag-NPs, titanium dioxide (TiO_2), zinc oxide (ZnO) and quantum dots (Farre et al., 2011).

1.1.3.1 Production and synthesis of manufactured NPs

There are two different approaches (Figure 1-2) that can be applied for the synthesis of NPs: the top-down and the bottom-up approaches (Domenech et al., 2012). For the top-down method, NPs are produced from a bulk material which is transformed into NPs by milling, lithography, laser ablation (Pyatenko et al., 2004) or other physical degradation process; in the bottom-up processes, the NPs are formed via association of atoms present in chemical solutions (or gases) (Domenech et al., 2012). NPs size and shape can be better controlled by using the bottom-up approach (Wang and Xia, 2004). Chemical reduction method, evaporation/condensation, thermal decomposition, electrochemical method (Yang et al., 2013c, Kim et al., 2005, Abou El-Nour et al., 2010) are some of the bottom up approaches. Another method of NPs synthesis is the green method due to its eco-friendly and cleanliness properties (Rai and Posten, 2013), where non-hazardous materials such as xanthan gum (Xu

et al., 2014) and plant extracts (Iravani, 2011, Makarov et al., 2014) are used as reducing and stabilising agents.

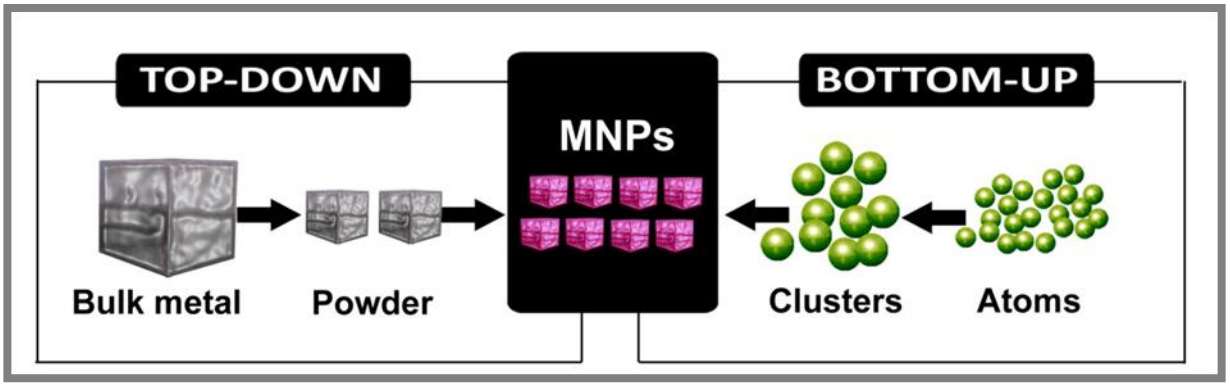

Figure 1-2: Schematic illustration of Top-down and Bottom-up approaches for the synthesis of manufactured NPs. Taken from (Domenech et al., 2012)

1.1.3.2 Carbon based NMs: fullerenes, carbon nanotubes and graphene

Carbon based NMs (CBNs) are nano-objects composed of hexagonal arrays of sp^2 carbon atoms similar to that of graphite (Cha et al., 2013). CBNs include (Figure 1-3) single or multi-walled carbon nanotubes (CNTs), fullerenes, nanodiamonds and graphene (Farre et al., 2011, Cha et al., 2013). These CBNs are produced in relatively high quantities with more than a thousand tonnes produced each year and are used in commercial applications due to their electrical properties, mechanical strength, thermal conductivity, and optical properties (Cha et al., 2013, Farre et al., 2011). The multiple applications cover the field of electronics where their conductivity and optical properties are applied in the creation of nanosensors containing CNTs (Takei et al., 2014) and carbon NPs encapsulated into carbon nanofibers (Yu et al., 2009). Another application is the usage of CBNs in the biological and life sciences sector where they might be used for their antimicrobial activity, due to the lack of efficiency of today's

antibiotics (Maleki Dizaj et al., 2015). In the aquatic environment, CBNs have their physicochemical properties and biological activity modified by the presence of natural organic matter (NOM), bacterial secretions (e.g. polysaccharides) and biomacromolecules (Kang et al., 2009).

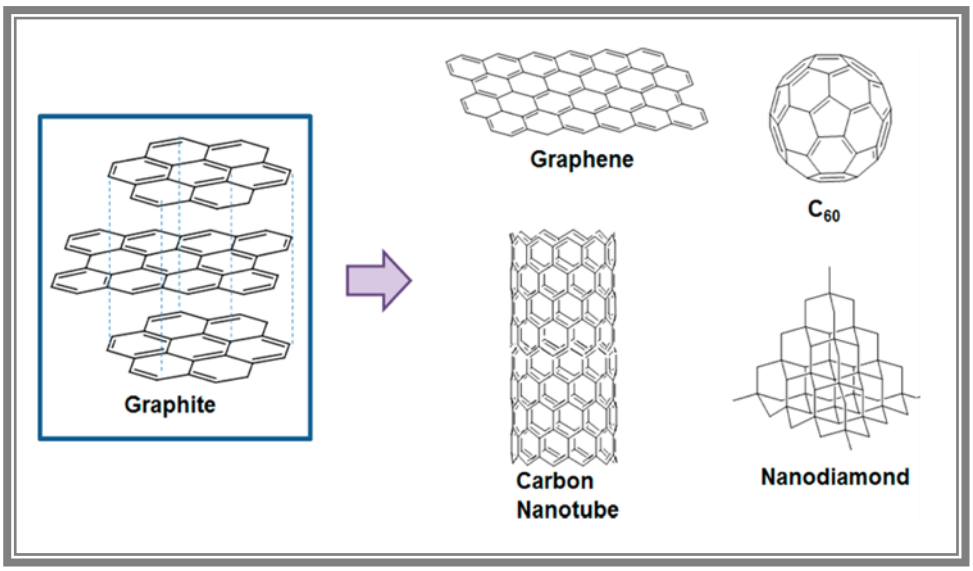

Figure 1-3: Various types of carbon-based NMs; taken from (Cha et al., 2013)

1.1.3.3 Metals oxide NPs

Metal oxide NPs (MeO NPs) exist in a range of chemical compositions such as: titanium dioxide (TiO_2), cerium dioxide (CeO_2), Ferric oxide (Fe_2O_3), silica dioxide (SiO_2), zinc oxide (ZnO), chromium oxide (Cr_2O_3), molybdenum trioxide (MoO_3), bismuth trioxide (Bi_2O_3) and binary oxides such as indium tin oxide and lithium cobalt dioxide (Salieri et al., 2015). In today's industrial applications, MeO NPs such as TiO_2, CeO_2, SiO_2 and ZnO are some of the most widely used NPs with applications in a range of products that include sunscreens, cosmetics, textiles, aerospace, sensors, paints, coatings and catalysts (Keller et al., 2010, Khin

et al., 2012, Zhou et al., 2011, Chai et al., 2015). Consumption and use of these NPs will result in release and emissions to the environment. For example, estimated worldwide production of TiO_2 -NP 3000 tonnes per year (2010), and application in consumer products may enter the environment, through the weathering of paints from exterior facades or accidental release during transport, sunscreens and cosmetics (Salieri et al., 2015).

Because of the increase in production and use of nanomaterials, the presence of engineered MeO NPs in the atmosphere (Nanayakkara et al., 2014), soil (Chai et al., 2015) and aquatic (Sharma, 2009) environments is inevitable with a range of potential effects including the risk of causing potential toxicity in the environment. In the presence of NOM or other organic molecules, MeO NPs are prevented from aggregation which could be due to binding of NOM to the NPs and stabilization due to steric effects; however, the chemical properties of the surrounding media (pH, ionic strength and ionic composition) can influence the interaction between NOM and MeO NPs and result in their agglomeration or stabilisation (Keller et al., 2010). MeO NPs have been shown to be toxic to various micro-organisms, other environmental species and human cell lines. The main reasons for toxicity are suggested to be smaller sizes of MeO NPs and hence high specific surface area and surface to volume ratio, and formation of ions. Synthesis method can also be a reason of toxicity if the nanomaterials have not been purified properly, for instance, the cationic surfactant, etyltrimethylammonium bromide (CTAB) used in the production of gold nanorods can. Toxic effects depend on the type of MeO particles (Baek and An, 2011), NP sizes (Bar-Ilan et al., 2009, Gliga et al., 2014, Ivask et al., 2014a), surface charge, surface functionality in addition to, sensitivity of test organisms, type of exposure media, exposure concentrations, duration of exposure. For example,CeO_2, ZnO, CuO, Ag-NPs are generally found to be more toxic when

compared to Au-NPs and Fe_2O_3 (Azam et al., 2012, Comfort et al., 2011) However, there are conflicting evidence of toxic effects of NPs for example, (Matzke et al., 2014, Cong et al., 2011) and it has not been possible to clearly establish the causal relationships (this could be due to many reasons, few important ones are, inadequacy of existing standard text protocols, non-standardised experimental designs, immense variety of NPs, characterisation issues, and limited round robin experiments). Toxic effects exerted by MeO NPs are due to different mechanisms of action, such as metal ion release from NPs, formation of reactive oxygen species which in turn can inhibit cell proliferation by either interfering with cell signalling pathways or damaging the cellular DNA (AshaRani et al., 2009) and, inducing cell membrane leakage (Zhang et al., 2008).

1.1.3.4 Quantum dots (QDs)

Quantum dots (QDs) are semiconductor crystals of group II – VI or III – V elements with dimensions typically less than 10 nm, smaller than the size of their exciton Bohr radii (Jamieson et al., 2007). When an array of visible light hits a QD, excited electrons are emitted from a lower energy state leaving a hole in the higher energy state and causing an increase in the effective band gap (E_G) of the QDs (Jamieson et al., 2007, Dabbousi et al., 1997). Figure 1-4shows the band gap (or energy gap), which is the energy difference between the energy levels needed by an electron emitted from the upper level of the valence band (or Fermi level = E_F) of the material to the lowest level of the conduction band (or conduction energy E_C) (Fanchi, 2004).

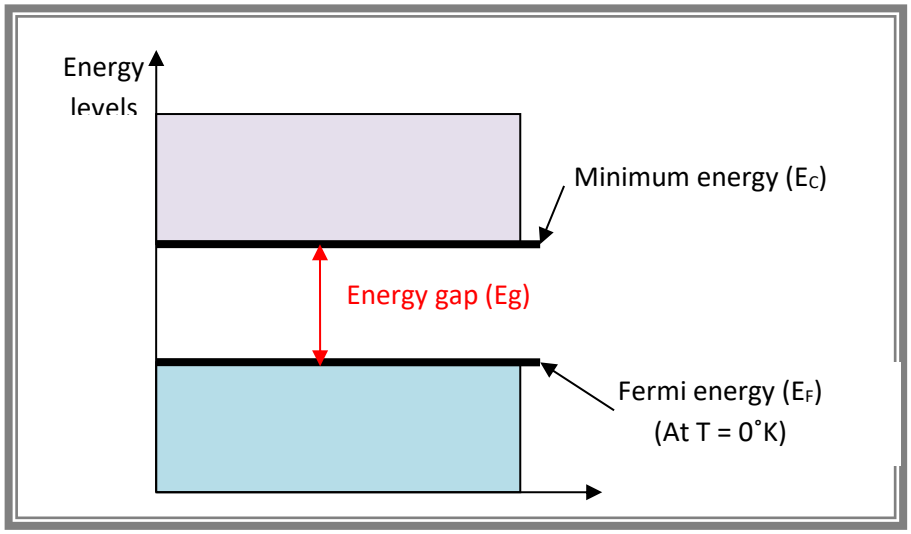

Figure 1-4: Energy levels in semiconductors (Fanchi, 2004)

This results in the QDs adsorption and emission spectrums shifting to higher energies (blue shift) as their size decreases (Dabbousi et al., 1997). This optical property of QDs, in addition to their electronic properties, gives rise to their exploitation by the nanoelectronics industry for the development of medical-imaging materials, solar cells, photovoltaics, security inks, and photonics and telecommunications products (Farre et al., 2011, Dabbousi et al., 1997). Their fluorescence may also be exploited when the fate and behaviour of NPs in living organisms are studied, allowing the sub-cellular location of the QDs to be determined using, for example, confocal microscopy (Krysanov et al., 2010).

1.1.3.5 Metal NPs: Gold and Silver NPs

As a result of their exceptional antibacterial, electromagnetic, optical and catalytic properties (Hvolbaek et al., 2007, Xu et al., 2014, Pal et al., 2007), metal NPs such as Ag-NPs and gold (Au-NPs) are widely used in industry today. These properties are dependent on the size, size distribution and morphology of the NPs (Abou El-Nour et al., 2010). For Ag-NPs, it is generally

understood the smaller their size, the higher their antibacterial and catalytic activity, which are also dependent on the chemical and physical properties of the surrounding environment (Abou El-Nour et al., 2010).

Metal NPs are used in multiple applications such as cosmetics (Cayuela et al., 2015), textiles (Airoudj et al., 2015) and food packaging (Bumbudsanpharoke et al., 2015). In the medical sector, metal NPs are used not only for their antibacterial and catalytic properties, but also for their optical properties for example when they are used in biosensors (Zhao et al., 2014, Guo et al., 2014) or intelligent drug delivery systems (Lajunen et al., 2015, Zhang et al., 2015b). This growing usage of metal/Ag-NPs increases their presence in aquatic and soil environments where they may be released via WWTPs (Gottschalk and Nowack, 2011); in these environments it is also anticipated they may have an enhanced toxicity to the biomass due to their dissolution over time (Blinova et al., 2013).

1.1.3.6 Application of manufactured NPs

There are more than a thousand nanotechnology-enabled products in the market (Weinberg et al., 2011, Maurer-Jones et al., 2013) and many new nanotechnology-enabled products are expected to enter the market in recent future. These products include cosmetics, textiles, washing machines, pharmaceuticals, medical devices, products for environmental monitoring and remediation, electronics, catalytic components, fuel cell, chemical coatings, personal care products, and food and food packaging products (Kaegi et al., 2012, Ju-Nam and Lead, 2008, Farre et al., 2011). The high demand for NP-containing consumer products is due to their superior properties compared to the equivalent bulk materials. For example, Au-NPs have a

distinct plasmon resonance peak in the optical absorption and scattering spectrum which is not present in bulk gold, making Au-NPs useful for medical diagnostics, fluorescent labels, etc. of Table 1-2 shows select NPs, their estimated production volumes, and example applications and uses.

Table 1-2: Estimated production volumes of different types of NPs and respective applications (to be completed) (Brar et al., 2010, Piccinno et al., 2012b).

Type	NP composition	Worldwide quantity estimated (in tons/year)	Application/uses
Metals	Ag	55	Antimicrobials, paints, coatings, textiles medical use, food packaging
	Pt group metals	High	Catalysts
	Sn	unknown	Paints
	Al	High	Metallic coating/plating
	Cu	unknown	microelectronics
	Zr	High	
	Se	Low	Nutraceuticals, health supplements
Alkaline earth metals	Ca	Low	Nutraceuticals, health supplements
	Mg	Low	Nutraceuticals, health supplements
Metal oxides	TiO_2	3,000	Cosmetics, paints, coatings
	ZnO	500	Cosmetics, paints, coatings
	CeO_x	55	Fuel catalyst
	SiO_2	5,500	Paints, coatings
	FeO_x	55	Water treatment
	AlO_x	55	Usually substrate bound, paintings
Carbon materials	Carbon black	High	Substrate bound, but released with tyre wear
	Carbon nanotubes	300	Used in a variety of composition materials
	Fullerenes (C60-C80)	0.6	Medical and cosmetics use
miscellaneous	Nanoclay	High	Plastic packaging
	Ceramic	High	Coating
	Quantum dots	0.6	Different compositions
	Organic NPs	Low	Vitamins, medicines, carriers for medicines and cosmetics, food additives and ingredients

1.1.4 Specific properties of NPs

NPs are defined by their size, morphology, composition, surface area, charge, functionality and speciation (Figure 1-5). To better elucidate the reasons for toxicity and for toxicity tests to be useful to bring about changes in environmental, health and safety regulations, detailed and comprehensive nanomaterial physico-chemical properties should be studied and which includes investigation of parameters, such as size and size distribution, shape, crystal structure, purity, surface area, surface properties, stability (e.g. the degree of aggregation in various experimental conditions, solubility) and surface charge. Pristine NPs synthesised (with simple core and coating) in the laboratory can be characterised by relatively simple techniques because of the controlled conditions. Whereas, characterisation of NPs in exposure medium (for toxicity studies) and complex environmental matrices pose a challenge and it needs interdisciplinary approaches. For better characterisation of the NPs, a multiple method approaches combining various characterisation techniques are needed (Abbt-Braun et al., 2004). The various properties of NPs can be measured using the characterisations techniques listed in Table 1-3.

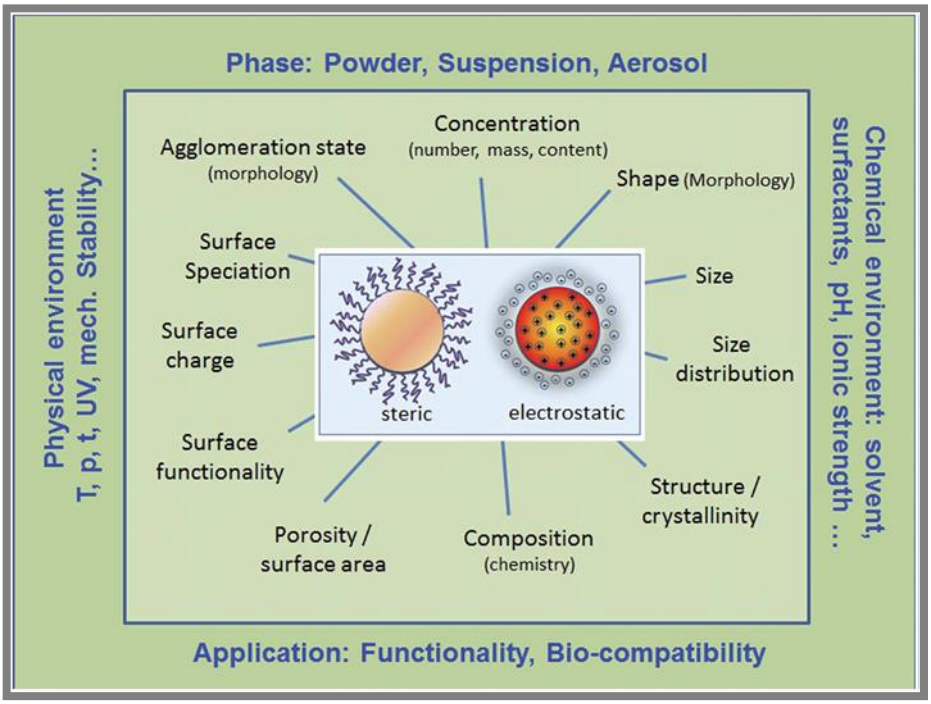

Figure 1-5: Predominant modes of stabilization of NPs, most important physico-chemical properties, and relevant forms, influencing factors and applications. Taken from (Ulrich et al., 2012).

When transferred into a different environment from their original, NPs may undergo several physicochemical changes that cause them to agglomerate, dissolve, change their surface chemistry and/or surface area, or react with their surrounding biomass (Maurer-Jones et al., 2013). There are three types of stabilisation for NPs (Figure 1-6): electrostatic stabilisation, steric stabilisation and a combination of both (Jia and Schuth, 2011). NP stability can be provided by steric stabilisation when using nonionic macromolecules as a capping agent (Tadros, 2013) such as polyvinylpyrrolidone (PVP) (Tejamaya et al., 2012) or polyethylene glycol (PEG) (Tejamaya et al., 2014). NPs can also be stabilised by a charge based approach or electrostatic stabilisation in the presence of an ionic suspension (Fabrega et al., 2011). This form of stabilisation results from the repulsive forces between similarly charged NPs in suspension which neutralise the shorter range attraction of van der Waals forces between NPs, thus protecting NPs from aggregation (Fabrega et al., 2011). However, compared to

steric stabilisation, electrostatic stabilisation is dependent on the surrounding ionic strength, as high ionic strength results in neutralisation of the NP surface charges, reducing the NPs repulsion. Ag-NPs capped with citrate is a perfect example of a charged based stabilisation (Römer et al., 2011), while PVP-capped Ag-NPs are an example of a steric stabilised NPs.

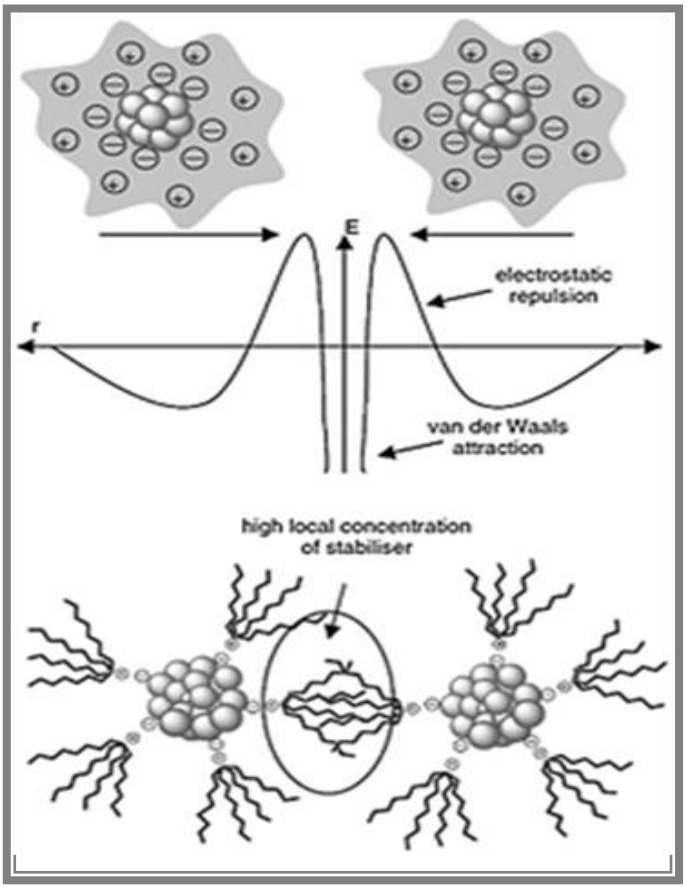

Figure 1-6: Schematic illustration of electrostatic stabilisation (top) and steric stabilisation (bottom) of metal NPs. NPs stabilised by combination of electrostatic and steric is the third type of stabilisation which is not shown in the figure. Taken from (Jia and Schuth, 2011)

Table 1-3: NPs characterisation, separation, and quantification techniques. Taken from (Lopez-Serrano et al., 2014)

Characterisation techniques	Instrumentation	Information provided
Microscopic techniques	Atomic Force Microscopy (AFM)	Size, morphology, surface texture, electrical and mechanical properties
	Scanning Tunnel Microscopy (STM)	Elemental and molecular composition
	Scanning Electron Microscopy (SEM)	Surface, size, shape morphology, crystallographic composition
	Transmission Electron Microscope (TEM)	Surface, size, shape morphology, Elemental composition, electrical conductivity
X-ray based techniques	X-ray absorption spectroscopy (XAS), X-ray fluorescence (XRF), X-ray photoelectron spectroscopy (XPS), X-Ray diffraction (XRD)	Surface, crystallographic, and elemental composition
Light scattering	Dynamic Light Scattering (DLS)	Particle size, polydispersity
Spectroscopy techniques	Ultraviolet- Visible Spectroscopy (UV-Vis)	Size, aggregation, structure, surface chemistry
Filtration techniques	**Fractionation techniques**	**Principle of separation**
	Cross flow filtration (CFF)	Diffusion coefficients through an open channel
	Field-Flow Fractionation (FFF)	Interaction with an external and perpendicular field
	Ultrafiltration (UF)	Diffusion through a membrane
	Ultracentrifugation (UC)	Deposition of particles at controlled speed and under vacuum
	Capillary electrophoresis (CE)	Electrophoretic mobility under an external electrical field
Chromatographic techniques	Size exclusion chromatography (SEC)	Interaction with the stationary phase
	Hydrodynamic chromatography (HDC)	Routes formed by open capillaries packed with non-porous materials
Plasma techniques	**Quantification technique**	**Analytical performances**
	Inductively coupled plasma-mass spectrometry (ICP-MS)	Low detection limits; isotopic analysis; multi-element analysis
	Inductively coupled plasma-optical emission spectrometry (ICP-OES)	Simultaneous NP analysis; relative low detection limits
	Laser-induced breakdown spectrometry (LIBS)	Multi-element microanalysis; little or no sample preparation
	Graphite Furnace Atomic Adsorption Spectroscopy (GFAAS)	Direct NP injection; little or no sample preparation

1.2 Fate and behaviour of NPs in the environment

In the environment, NPs can be found in the form of single, agglomerated, dissolved or sedimented particles, and can undergo modification of their surface area and chemistry; this may affect their environmental fate pathway (Farre et al., 2011, Maurer-Jones et al., 2013). The fate and behaviour of NPs in the environment can be affected by their size, morphology and composition (Weinberg et al., 2011, Farre et al., 2011) as well as their interaction with macromolecules such as natural organic matter (NOM)(Lowry et al., 2012c) or bacterial secretions (Maurer-Jones et al., 2013). In the presence of NOM, NPs are stabilised by the weakly bound capping layer of NOM at the NP surface, which limits their agglomeration as the NOM layer provides steric stabilisation preventing the NPs from coming close enough to one another to "stick" (Maurer-Jones et al., 2013, Lowry et al., 2012c). Binding of other molecules, such as bacterial secretions (polysaccharides and proteins), may increase the NPs agglomeration by, for example, bridging between particles (Maurer-Jones et al., 2013).

In the aquatic environment, the coating or stabilizers around NPs can be degraded due to the photocatalytic reaction between sunlight and NPs (Curri et al., 2003, Lowry et al., 2012c). Absorption of the photon energy from sunlight causes excitation of the electrons at the surface of the NPs leading to the NPs agglomeration (Curri et al., 2003, Lowry et al., 2012c). For example (Figure 1-7) Ag-NPs with a degraded coating can be oxidised and dissolved, releasing silver ions (Ag^+) which can be transformed into Ag – S – thiol complexes or Ag_2S (Lowry et al., 2012c). Finally the agglomeration of similar NPs (homoagglomeration) or between NPs and other complex materials present in water (heteroaggregation) can occur (Lowry et al., 2012c).

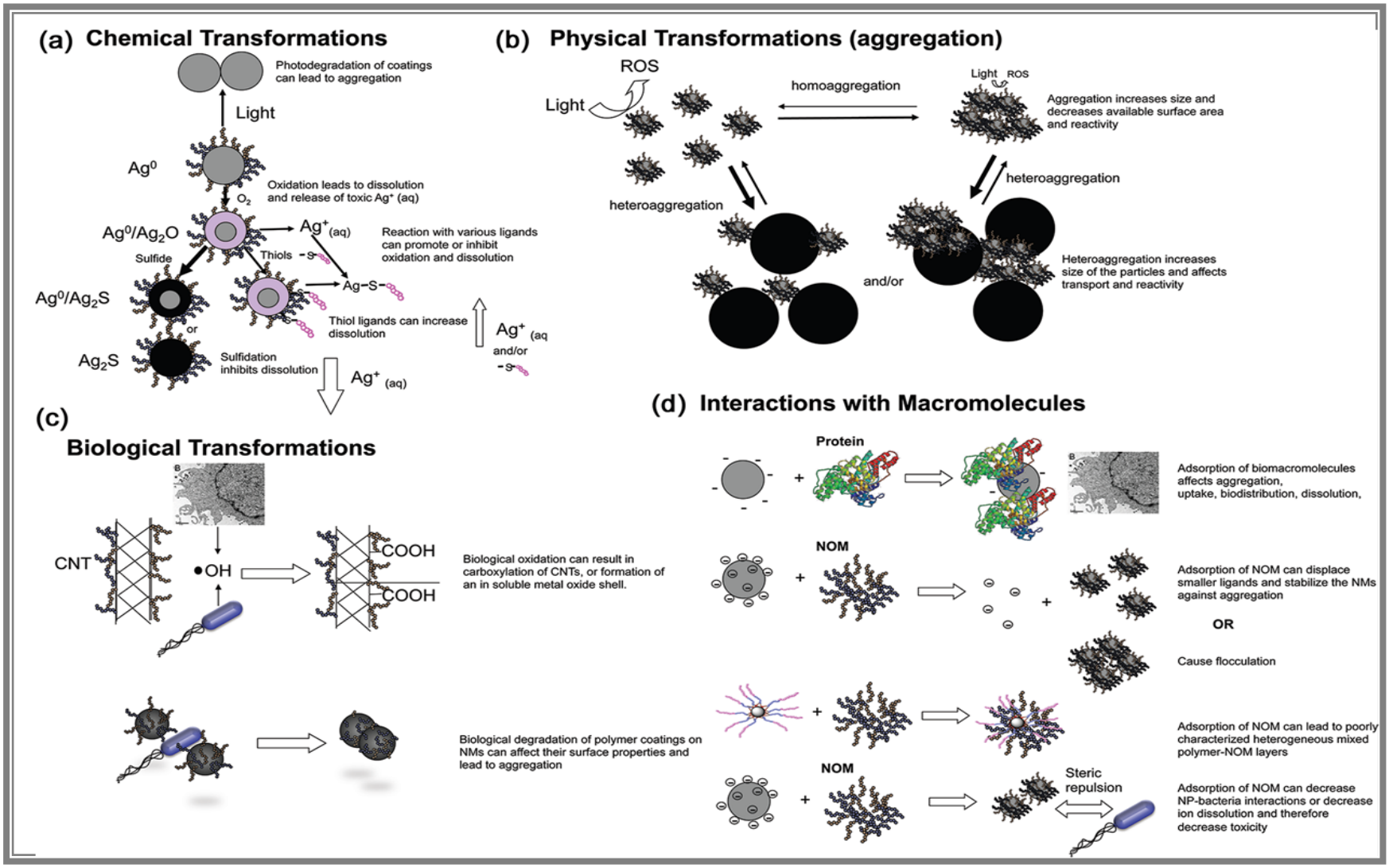

Figure 1-7: (a) Representative chemical transformation of metal NPs and the potential impacts on their behaviour and effects in the environment. Ag-NPs are used to exemplify the type of transformation that may occur. (b) Effects of physical transformations including agglomeration and heteroaggregation on the reactivity and transport of NPs. (c) biologically mediated transformation of NPs and their coatings, and subsequent impact on fate, transport and effects. (d) Effects of NPs interactions with organisms: biouptake, and subsequent fate, transport, and effects in the environment. Taken from (Lowry et al., 2012c)

1.2.1 Predicted environmental concentrations (PEC) of NPs

Different pathways of entry of NPs into the environment can be conceptually described from research studies available on conventional pollutants. NPs used in cosmetics and sunscreens can directly enter surface water during swimming (Zhang et al., 2015a). Other NPs in consumer products can enter surface and ground water via WWTP's (both municipal and industrial) effluent and sludge disposal to water streams and agricultural and forest lands respectively (Mueller and Nowack, 2008). See Figure 1-8 for broad pathways of NP flow in the technical (WWTP, landfill) and environment compartments. Exfiltration from sewer systems and overflows from WWTPs can be other routes of entry of NPs into the natural environment (Mahapatra et al., 2015). Wear and tear of nanotechnology-enabled products, and of wastes disposed in landfill can release NPs into the surrounding environment and leachate from landfill can potentially carry NPs to groundwater (Nowack et al., 2012) and incineration of products embedded with NPs can result in emissions of NPs to the air (Roes et al., 2012, Holder et al., 2013). Accidental releases of NPs from production processes and transportation are other potential sources of entry of NPs in the environment.

Predicted environmental concentrations of NPs were reported in a recent study (Sun et al., 2014a) in which probabilistic mass flow modelling approach was adopted with updated production quantities of five NPs – nano-Ag, nano-TiO_2, nano-Zn, Fullerenes, CNT (irrespective of their use in individual product categories) – along with various environmental transfer coefficients. Ag-NP production volume for the EU was reported to be 30 tonnes per year in this study(Sun et al., 2014b). PEC was estimated to be 0.17 $ng*L^{-1}$ in WWTP effluent and 0.02 $mg*kg^{-1}$ in the sludge. For the UK, Whiteley et al. (2013b) estimated 0.4 tonnes of nano-Ag released in fresh water from WWTP effluent by scaling down global and EU demand of Nano-

Ag to the UK region. According to the literature, it is difficult to predict the concentrations of NPs released into the environment (Maurer-Jones et al., 2013) and such data generated always have high uncertainties associated with them due to the difficulty of estimating production volumes of selected nanomaterial because of intellectual property issues which hampers identification of products containing nanomaterials and non-formalisation of definitions in the nanotechnology field. However, several studies (Table 1-4) have been undertaken on the prediction of NP concentrations in the environment and yearly maximum concentrations of Ag, TiO_2 and ZnO NPs combined was estimated to be 10 000 $ng*L^{-1}$ (Mueller and Nowack, 2008, Gottschalk et al., 2010, Blaser et al., 2008, Klaine et al., 2008).

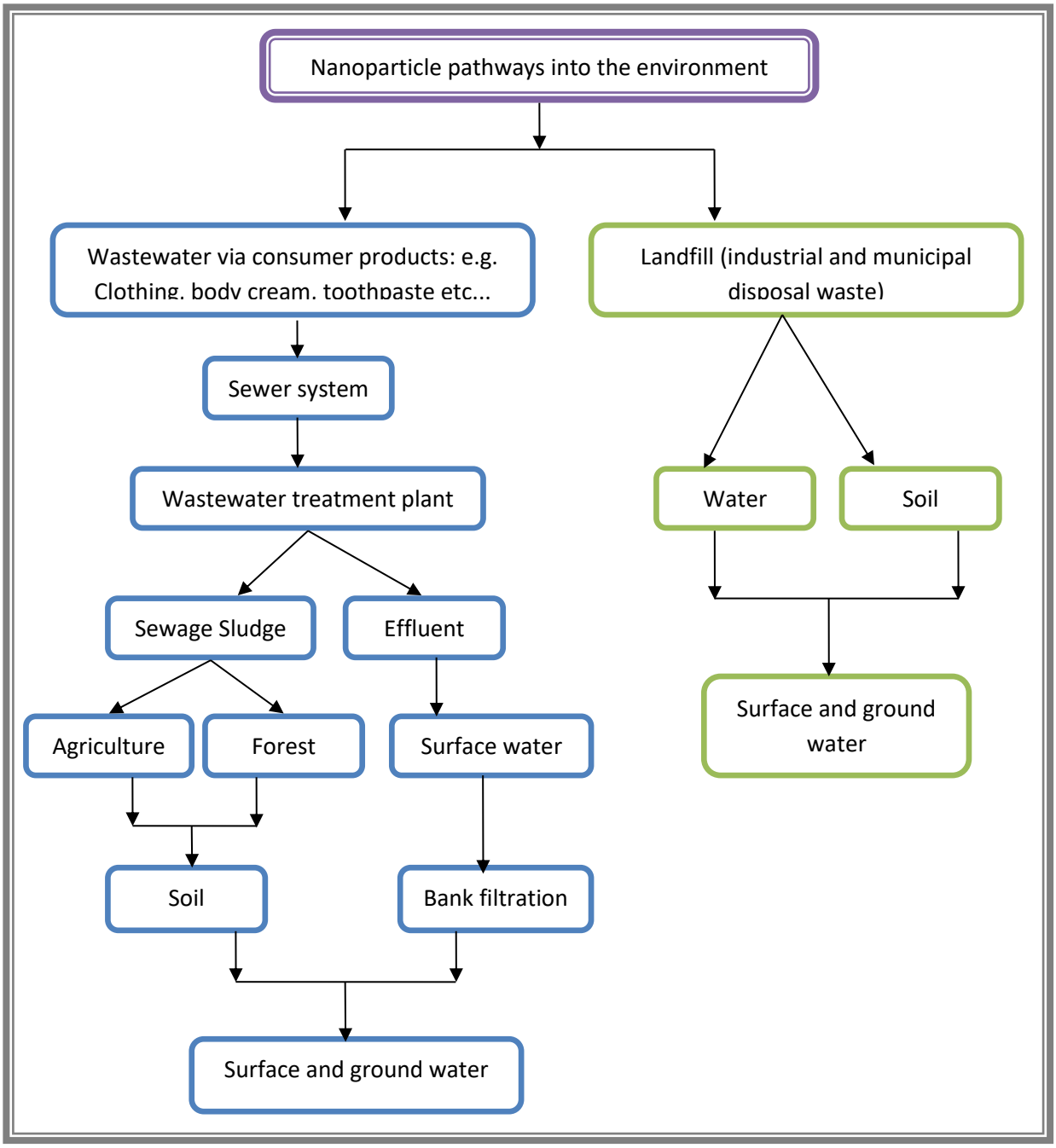

Figure 1-8: NP pathways into the environment: release into wastewater from consumer products or into water and soil from landfill (Muller et al., 2011).

Table 1-4: Predicted Environmental Concentrations (PECs) of highly produced and used NPs from the three major pathways into the environment. Taken from (Maurer-Jones et al., 2013)

NPs	Estimated PEC, pathway into environment	References
Ag	0.088 – 10 000 ng*L^{-1}, surface water	(Mueller and Nowack, 2008, Klaine and Pedro J. J. Alvarez[2], 2008, Gottschalk et al., 2010, Blaser et al., 2008)
	0.0164 – 17 µg*L^{-1}, WWTP effluent	(Gottschalk et al., 2010, Blaser et al., 2008)
	1.29 – 39 mg*kg, WWTP sludge	(Gottschalk et al., 2010, Blaser et al., 2008)
TiO_2	21 – 10 000 ng*L^{-1}, surface water	(Mueller and Nowack, 2008, Klaine and Pedro J. J. Alvarez[2], 2008, Gottschalk et al., 2010, Gottschalk and Nowack, 2011, Arvidsson et al., 2011, Praetorius et al., 2012)
	1 – 100 µg*L^{-1}, WWTP effluent	(Gottschalk et al., 2010, Kiser et al., 2009, Westerhoff et al., 2011)
	100 – 2000 mg*kg^{-1}, WWTP sludge	(Gottschalk et al., 2010, Praetorius et al., 2012, Kiser et al., 2009)
ZnO	1 – 10 000 ng*L^{-1}, surface water	(Gottschalk et al., 2010)
	0.22 – 1.42 µg*L^{-1}, WWTP effluent	(Gottschalk et al., 2010)
	13.6 – 64.7 mg*kg^{-1}, WWTP sludge	(Gottschalk et al., 2010)
Carbon-based	0.001 – 0.8 ng*L^{-1} surface water	(Gottschalk et al., 2010)
	3.69 – 32.66 µg*L^{-1}, WWTP effluent	(Gottschalk et al., 2010, Mueller and Nowack, 2008)
	0.0093 – 0.147 mg*kg^{-1}, WWTP sludge	(Gottschalk et al., 2010)

1.2.2 Toxicity and risks of NPs in the environment

The toxicity of NPs can be influenced by environmental conditions such as pH, ionic strength, sunlight, temperature, water hardness, NOM and biomass; the NP properties that may be affected are: NP type, size, morphology, surface area or chemistry (Grillo et al., 2015, Farre et al., 2011). The toxicity of NPs in the environment can be affected by their transformation through aggregation/agglomeration, dissolution, or redox-reactions and reactions with biomass (Maurer-Jones et al., 2013). For example, the dissolution of Ag-NPs increases the Ag^+ concentration in aquatic environments, hence the increase of their toxicity since Ag^+ are long-known to be toxic to many organisms (Fabrega et al., 2011). Similarly, agglomeration increases size of Ag-NPs and increase in uptake by organisms in the environment resulting in increased toxicity (Ellegaard-Jensen et al., 2012). The sulphidation of Ag-NPs in WWTP reduces the concentration of Ag^+ and limits the toxicity (Liu et al., 2011) to nitrifiers and methanogenic bacteria (Doolette et al., 2013). Table 1-5, Table 1-6 and Table 1-7 show a selection of different toxicity studies of NPs, with focussing on Ag-NPs in a range or organisms, Table 1-6 and Table 1-7 focussing on a range of different NP compositions and their effects on bacteria.

Table 1-5: Toxic effect of Ag-NPs to bacteria / bacterial communities (landfill biomass), environmental indicator species, human cells and virus

Ag-NPs							
Exposed organism	**Size (nm)**	**Coating agent and Shape**	**concentration**	**Exposure time**	**Exposure media**	**Major NP effects**	**references**
Human hepatoma (HepG2) cell	15	Protein (casein) matrix spherical	0.32 – 34 $mg*L^{-1}$	24 hrs	culture media	Oxidation of Ag-NPs Release of Ag(I) associated with presence of protein in culture media Detection of Ag-NPs associated with the cells	(Bolea et al., 2014)
Bacterial isolated freshwater	<100	PVP spherical	0.25 – 1 $\mu g*mL^{-1}$	2, 4 and 6 hrs	Milli-Q water	No release of Ag^+ and low concentration (≤ 1 ppm) observed Toxicity toward the bacteria essentially due to Ag-NPs	(Kumar et al., 2014)
Peste des petits ruminants virus	5 – 30	No coating spherical	300 $\mu g*mL^{-1}$	48 hrs	Dulbecco's modified eagle's medium (DMEM)	Ag-NPs inhibit Morbillivirus replication in vitro	(Khandelwal et al., 2014)
Landfill biomass	29	0.06% polyvinyl alcohol spherical	10 $mg*kg^{-1}$	200 days	Bioreactor landfill	Ag^+ have minimal impact on landfill methane production at 10 mg/kg concentration Ag-NPs inhibit methanogenesis and are more toxic than Ag^+	(Yang et al., 2013b)
E. coli, yeast, algae, crustaceans, and mammalian cells in vitro	10, 20, 40, 60 and 80	2 $mg*L^{-1}$ citrate spherical	e.g.: EC_{50} of 0.27 mg/L for 10 nm Ag-NPs in E coli case	24 hrs; 72 hrs; and 48 hrs	culture media; OECD 201 algae media	Toxicity of Ag-NPs strictly dependent on their dissolution	(Ivask et al., 2014b)

Table 1-6: Toxicity of different NPs (Ag, Cu, fullerene, TiO_2, SiO_2, CeO_2, ZnO, zerovalent iron, and CNTs) and NOM towards different organisms (bacteria, algae, microcrustaceans amd fish). Taken from (Grillo et al., 2015)

Type of NPs	organisms	findings	references
Ag	Ceriodaphnia dubia	Higher NOM concentrations reduced the toxicity to the micro-crustaceans	(Gao et al., 2009, Gao et al., 2012)
	MetPLATE bioassay	Higher NOM concentrations reduced the toxicity to the organisms tested	(Gao et al., 2009)
	Daphnia	NPs (50 $mg*L^{-1}$ and pH 7) caused increased toxicity to daphnia in the presence of greater quantities of NOM	(Gao et al., 2012)
	Japanese medaka embryos	A higher concentrations of NOM reduced the toxicity to the embryos	(Kim et al., 2013)
	Natural aquatic bacteria	The presence of HS reduces the cellular viability of the bacteria, and the effect was more pronounced with terrestrial humic substances (HS) than with aquatic HS	(Dasari and Hwang, 2010)
	Escherichia coli and bacillus subtilis	The addition of NOM had no significant effect on bacterial activity. Bacterial activity was reduced after addition of Calcium (Ca^{2+})	(Liu et al., 2014)
	Pseudomonas putida	The NPs interfered with the production of biofilms by the bacteria. When fulvic acid (FA) was added together with the NPs, there was increased adsorption and bioaccumulation of the NPs in the biofilms, causing a long-term effect	(Fabrega et al., 2009a)
	Pseudomonas fluorescents	NOM increased the bactericidal activity of Ag-NPs	(Fabrega et al., 2009b)
Cu	Ceriodaphnia dubia	Higher concentrations of NOM reduced the toxicity to the microcrustaceans	(Gao et al., 2009)
	MetPLATE bioassay	Higher concentrations of NOM increased the toxicity to the organisms tested	(Gao et al., 2009)
	Escherichia coli	Toxicity was reduced in the presence of 5-40 $mg*L^{-1}$ of FA	(Zhao et al., 2013)
Fullerene			
	Ceriodaphnia dubia and MetPLATE bioassay	for both organisms, fullerene showed no toxicity when the concentration of NM exceeded 3 $mg*L^{-1}$	(Gao et al., 2009)
	Escherichia coli	The antibacterial activity of fullerene was reduced at higher NOM concentrations	(Li et al., 2008)

Table 1-7: (continued) Taken from (Grillo et al., 2015)

Type of NPs	organisms	Findings	references
TiO_2	Chlorella sp.	The presence of NOM attenuated the toxicity to the algae	(Lin et al., 2012)
	Zebrafish (Danio rerio)	The toxicity of TiO_2 NPs increased in the presence of humic acid	(Yang et al., 2013a)
SiO_2	Pseudokirchneriella subcapitata	The addition of NOM in assays employing SiO_2 NPs strongly reduced toxicity	(Van Hoecke et al., 2011a)
CeO_2	Algae medium	The presence of NOM in the medium increased the stability of the NPs, resulting in reduced sedimentation	(Quik et al., 2010)
	Pseudokirchneriella subcapitata	A reduction in the toxicity of the NPs was observed. This was due to stabilisation of CeO_2 NPs by NOM and hence inhibition of direct interaction with the algal cell wall	(Van Hoecke et al., 2011b)
ZnO	Bacillus subtilis, Escherichia coli and Pseudomonas putida	HS reduced the antibacterial activity of ZnO NPs	(Li et al., 2011)
Zerovalent iron	Escherichia coli	The presence of NOM hindered the adhesion of nano zerovalent iron (nZVI) and reduced its toxicity to the bacteria	(Li et al., 2010b, Chen et al., 2011)
	Bacillus subtilis	20 $mg*L^{-1}$ of humic acids (HA) increased the toxicity to the bacteria	(Chen et al., 2011)
CNTs	Escherichia coli, Bacillus subtilis, Pseudomonas aeruginosa and Staphylococcus epidermis	HA/FA (fulvic acid) in water decreased the attachment of CNTs to the bacteria , but did not reduce the toxicity	(Kang et al., 2009)

1.2.3. Nanoregulation and proactive risk management

Regulatory changes with regard to product containing nanomaterials have been effected gradually, even though many products are still not regulated. The cosmetic product regulation was the first regulation to include definition of nanomaterials (REGULATION (EC) No 1223/2009) (Europa, 2009) and mandated notification of cosmetic products (except UV filters, colourants, preservatives) containing nanomaterials in the cosmetic products notification portal six months prior to introduction in the market. Other regulations such as the Novel Food Regulations (2015/2283) (Europa, 2015), Regulation (EU) No. 10/2011 ((EC), 2011) on plastic materials and articles intended to come into contact with food and Biocidal Products Regulation No 528/2012 (Europa, 2012) followed the Cosmetic Regulations.

However, there is no regulation with regard to disposal of Ag-NP containing products at its end of use stage and there has been no discharge limits promulgated for wastewater. In such situations, the responsibility to protect environmental health falls on individuals and on proactive measures adopted by companies and industries. For example, companies manufacturing filters for drinking water purification in developing countries can adopt extended producer responsibility where they take back water filters and manage and dispose these filters in an environmentally friendly manner. Such voluntary corporate responsibility strategies will be a concrete step towards addressing the trade-offs and conflicts regarding protecting human health and the ecosystem.

1.3 Ag-NPs in wastewater treatment plants (WWTPs)

1.3.1 Release of Ag-NPs to WWTPs

The production of consumer products containing Ag-NPs Table 1-2 has grown significantly in recent years. Some of the uses of Ag-NPs in everyday life are washing machines, textiles, deodorants, toys, water purification filters. The consumption of these products on a regular basis will increases the concentration of Ag-NPs released to the environment and particularly to the sewage system. In fact, Ag-NPs in textile products such as socks (Benn and Westerhoff, 2008a, Lombi et al., 2014) or from washing machines (Farkas et al., 2011) can be released into the sewer system via washing and enter the WWTPs (Lombi et al., 2014, Kaegi et al., 2013, Kaegi et al., 2011b). Ag-NPs can also be released from discharged consumer products or paints via weathering (Kaegi et al., 2010) and enter the WWTPs.

1.3.2 Removal of Ag-NPs from WWTPs

Municipal WWTPs are designed to remove large solid particles and dissolved organic matter present in wastewater for its safe disposal into the environment. Municipal WWTPs have three broad treatment steps – pre-treatment, primary and secondary (Figure 1-10). A tertiary treatment step (also known as advanced treatment) is present in WWTPs which receive highly recalcitrant pollutants or where disinfection and/or removal of phosphorus and nitrogen are mandatory before discharge into the environment.

In the pre-treatment step, the wastewater entering the sewage system is passed through a bar screen for the removal of floating solids in wastewater (plastics, bottles, etc.). Then in the primary treatment step, the wastewater is introduced into a tank where the grit (e.g., sand, gravel, bone chips, coffee shells and other high specific gravity materials) is removed and finally disposed to the landfill. Grit removal is based on the principle of gravitational force governed by Stoke's law and differential settling velocity of particles. Grit removal systems designed for WWTP are based on many factors, such as specific characteristics of the grit, area constraints, and downstream design of the WWTP plant. Some grit removal systems are aerated tanks, detritus or short time sedimentation, vortex chambers, and horizontal-flow velocity-controlled channels. NPs could attach themselves to the grit and be removed at this stage. The waste water is then designed to flow to a sedimentation tank (also known as primary settler) where suspended solids (SS) – organic and inorganic in nature – settle to the bottom of the tank (and is known as sludge) and lighter components of waste water like oil, grease, plastics and soaps float on the top and removed through mechanical skimming process. Coagulants like Alum and Fe_3O_4 may be added to increase sedimentation rate/settling velocity especially in the case where a high volume of industrial effluents enters with sewage and/or colloidal concentration is high. The removed pollutants are disposed of through incineration (floating solids), on landfills (grit), and sludge digestion and disposal (for sedimentation tank sludge). During the process of primary treatment solids removal efficiency as high as 70% is achieved, this includes about 30% removal of organic matter.

Removal of dissolved organic matter from wastewater is the main objective of subsequent secondary treatment processes as the organic matter (measured as Biochemical Oxygen Demand, BOD) negatively impact oxygen balance of receiving water body and hence its

aquatic life. Organic matter is primarily removed through use of micro-organisms which helps in conversion of organic matter to carbonaceous gases (CO_2 and/or CH_4), and settleable cell mass. It is at this stage of treatment some poorly degradable substances and metals are removed due to adsorption of these substances over gelatinous cell mass and removed in second stage sedimentation tanks. BOD degradation pathway can be aerobic or anaerobic, and the micro-organisms in the reactor can be in floating/suspended state (e.g., activated sludge process and its variants for aerobic and up-flow anaerobic sludge blanket reactor for anaerobic) or in attached growth (e.g. trickling filter, fluidised bed reactor, rotating biological contractor, anaerobic fixed film fixed bed reactor). Maintenance of favourable conditions for micro-organism growth, such as pH, temperature, mixing, and absence of inhibitory substances is very important in WWTP. Approximately, 85% of the BOD_5 and SS of influent water in removed at this stage.

Sequencing batch process is one of the technology variant used in the secondary stage of WWTPs for removal of BOD. In this study, a laboratory scale model of sequencing batch reactor (SBR) was built and used to study the transformation of Ag-NPs in waste water. SBRs operate through four major sequences – Fill, Reaction, Settling and Drawing. Figure 1-9 shows a conceptual schematic of SBR operation in a cycle (Mace and Mata-Alvarez, 2002). In conventional activated sludge process, the aeration and sedimentation process occur in two different tanks, whereas in SBR, aeration and sedimentation happen in the same tank in a sequential manner. SBR tanks are widely preferred in WWTPs because the operating conditions can be modified to manage variation of pollutant loadings.

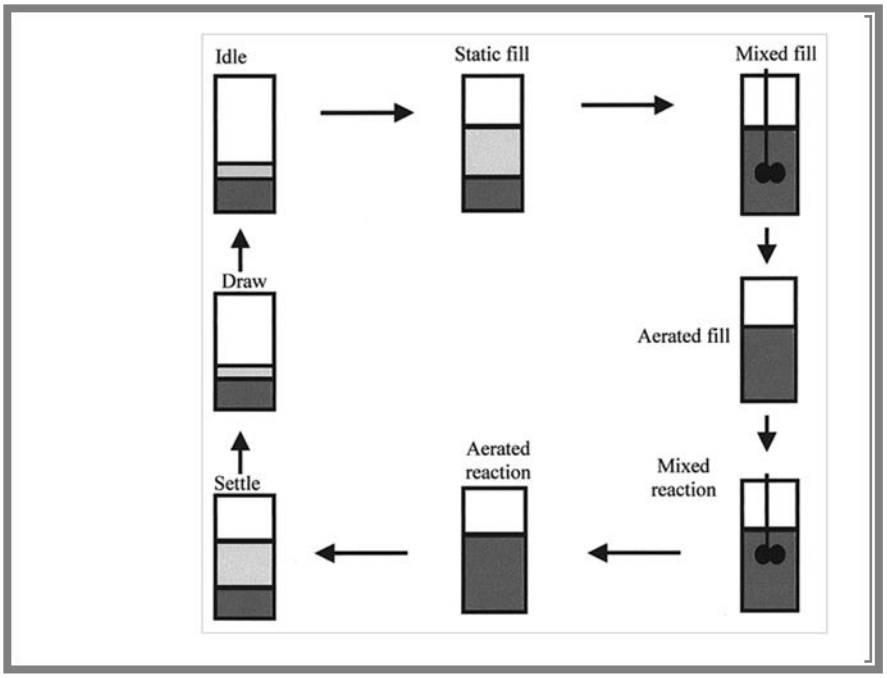

Figure 1-9: Sequential batch reactor phases. Taken from Mace and Mata-Alvarez (2002)

In the WWTP, Ag-NPs can be removed at different treatment steps. The possible fate and removal Ag-NPs in the different units of the WWTP are given in Table 1-8 as hypothesised by Brar et al. (2010). They suggested that removal of Ag-NPs before the secondary treatment stage of wastewater is very poor. Kaegi et al.(2013) used two different sizes (10 nm and 100 nm) of Ag-NPs and Au-NPs and with two different capping agents (citrate and PVP) and TWEEN coated PURE Ag (sourced from a vendor) to explore the transformation and fate of Ag-NP in the sewer networks and WWTP. They found that irrespective of the secondary treatment process, particle type, size and coating, NPs were attached to the flocs which subsequently will get removed in the WWTP sludge.

Table 1-8: Fate of Ag-NPs in each unit of a WWTP as conceptualised by Brar et al. (2010)

Treatment stage	Purpose	Removal Process
Wastewater screening and	Removal of general waste, hair and other debris	Some Ag-NPs may be adsorbed onto the debris
grit removal	Removal of grit	Ag-NPs may be removed via adsorption onto the grit
Primary clarification	Removal of large sludge particulates	Ag-NPs may be removed via sedimentation and settling of sludge
Secondary treatment: sludge aeration	Biological treatment with activated sludge	Ag-NPs may interact with NOM, macromolecules and biomass
Secondary clarification	Settling of the sludge and drawing of the effluent	High proportion of Ag-NPs removed via adsorption onto the sludge through sedimentation and aggregation
Sludge digestion/dewatering the sludge	Sludge is digested and dried before it is disposed of into landfill	Ag-NPs present in the sludge can leak into water stream and groundwater via weathering
Disinfection process	Disinfection of the influent with chlorine	Ag-NPs present in the influent may be removed via oxidation; leaving less chance for any remained particles to enter the water streams

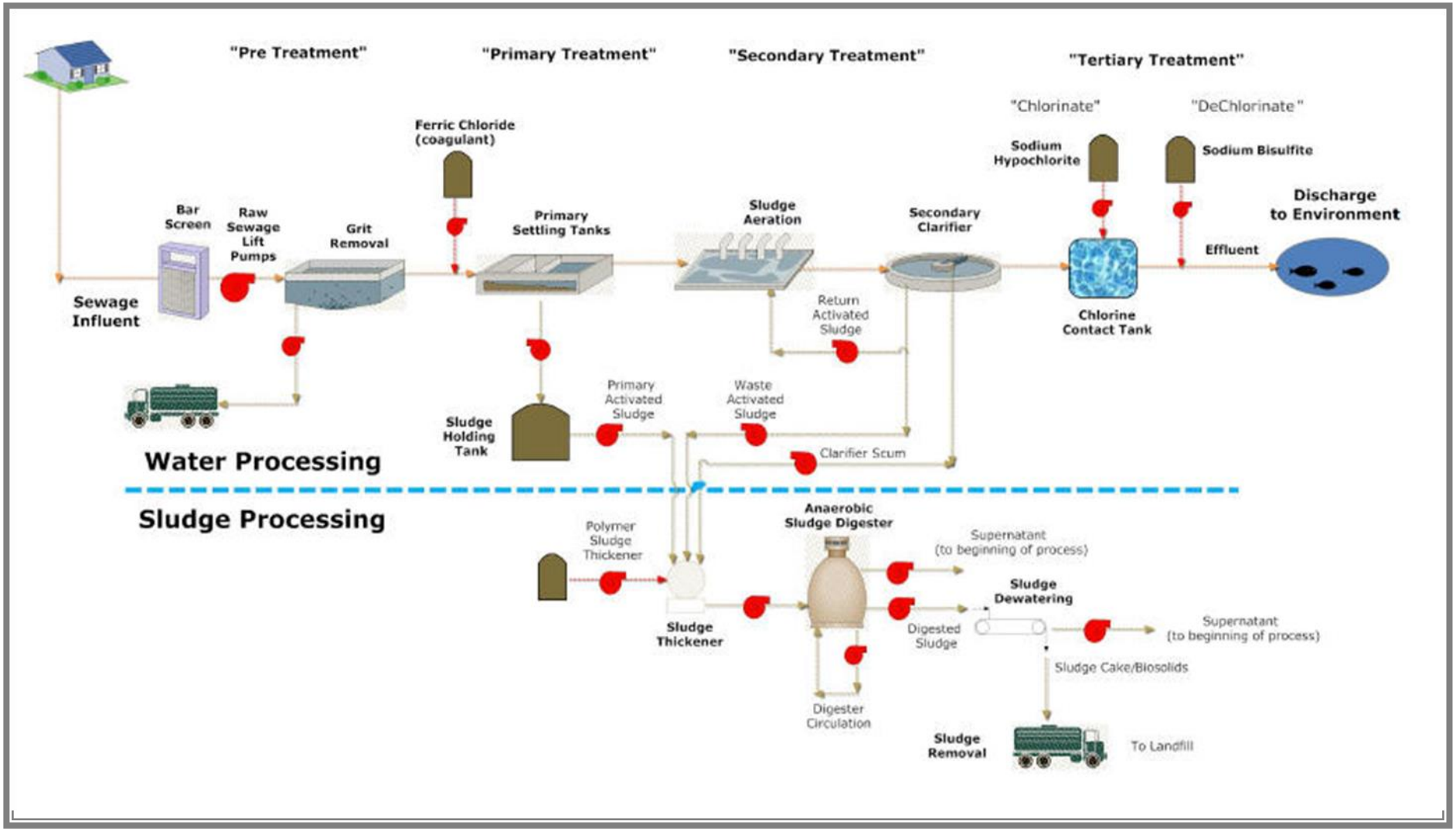

Figure 1-10: Schematic principle of a WWTP. Taken from (https://www.mcilvainecompany.com/generic%20applications/water/mncpl%20wastewater.htm)

1.3.3 Oxidation/dissolution and sulphidation of Ag-NPs in WWTP

The transformation of Ag-NPs into Ag^+, Ag_2O and Ag_2S, is dependent on the NP chemical and physical properties such as size, shape, capping agent and surface area, chemistry and speciation (Kaegi et al., 2013). Figure 1-11shows that Ag_2S NPs can be formed by the reaction of silver ions with oxidation state +1, i.e., Ag(I) via two mechanisms (Liu et al., 2011). First, the Ag-NPs are oxidised with the release of Ag^+ via an oxidation-dissolution phenomenon and these released Ag^+ react with sulphide complexes (e.g.: H_2S/HS^-) by precipitation to form Ag_2S NPs (Liu et al., 2011, Yang et al., 2013c). In the second process, the Ag-NPs sulphidation occurs by direct transformation into Ag_2S NPs via a solid – fluid heterogeneous reaction, also called oxysulphidation(Liu et al., 2011).

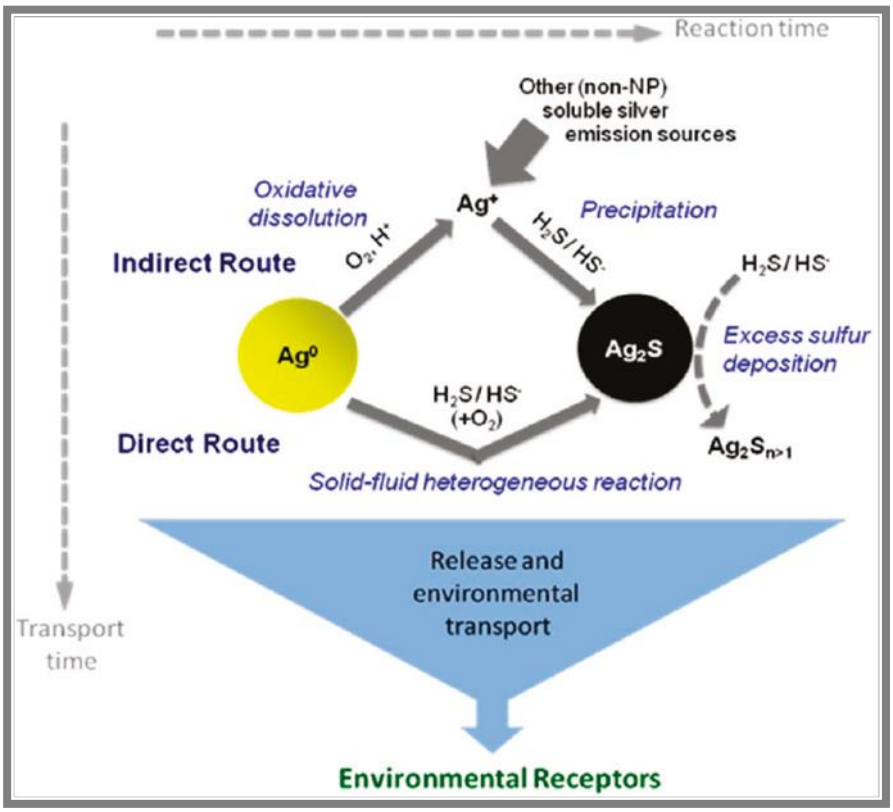

Figure 1-11: Competing chemical and transport pathways of the sulphidation of Ag-NPs and their release to the environment. Taken from (Liu et al., 2011)

Ag_2S NPs form in the environment by the reaction of Ag-NPs with natural sulphide species and this sulphidation is partial when the shell of Ag-NPs is replaced by a layer of Ag_2S forming an Ag^0–Ag_2S core-shell structure (Dale et al., 2013). The degree of Ag-NPs sulphidation is independent of their type of capping agent (Levard et al., 2011). For example, PVP Ag-NPs were found to be very stable from previous studies (Tejamaya et al., 2012, Roh et al., 2013); however, they are not prevented from undergoing agglomeration during sulphidation which is accompanied by the corrosion of the coating (Levard et al., 2011). Also, sulphidation and corrosion processes of citrate and PVP Ag-NPs are not delayed or suppressed by the capping agent, but the presence of a passivating surface layer might reduce the kinetic rate of the corrosion mechanism (Kaegi et al., 2013).

The properties of Ag-NPs are modified during sulphidation with a change in the surface characteristics, formation of agglomerates and reduction of the release of Ag^+ due to the low aqueous solubility of Ag_2S; this may affect the fate, transport and toxicity of Ag-NPs in the WWTPs and in the environment (Levard et al., 2011, Lowry et al., 2012b). In fact, the sulphidation kinetics of Ag-NPs is strongly dependent on their size and occurs at various levels during each stage of the WWTP. Rapid sulphidation of small Ag-NPs occurs in the first 24 hours, while large Ag-NPs are partially sulphidised (Kaegi et al., 2013).

Ag_2S NPs present in WWTP are formed due to the reaction of Ag-NPs and Ag^+ with reduced sulphur ligands (Levard et al., 2011, Kim et al., 2010). Kaegi et al. have demonstrated that 15% of the dispersed Ag-NPs in sewer system are transformed into Ag_2S five hours after their dispersion and 25 to 30% after 24 hours (Kaegi et al., 2013). However, these values were

found to be low, because Ag_2S generally forms before the secondary treatment of the sewage (Kaegi et al., 2013).

In aerated tanks, Ag-NPs can be transformed into Ag_2O NPs that may dissolve or react with inorganic or organics sulphide ligands to form Ag_2S NPs (Lowry et al., 2012b). Ag_2S NPs present in aeration tank are strongly resistant to oxidation and dissolution and are formed before the influent reaches the secondary treatment unit (Doolette et al., 2013). Ag-NPs sulphidation may occur under aerobic conditions before being completed in the anaerobic tank (Doolette et al., 2013). It was found that the sulphidation of Ag-NPs occurring under aerobic conditions may be in the form of weak amorphous crystals of Ag_2S also called partial sulphidation (Kaegi et al., 2013, Dale et al., 2013). Finally, under anaerobic conditions, Ag-NPs are directly transformed into Ag_2S via an oxysulphidation process (Doolette et al., 2013, Kim et al. 2010, Kaegi et al., 2013), see Figure 1-11.

1.4 Research aims and objectives

The previous sections detailed how Ag-NPs enter the various environmental compartments of sediments, agricultural soils, surface water and ground water from many sources, such as disposal of wound and burn dressings and antibacterial wipes containing Ag-NPs, and Ag-NP release from different water disinfection strategies (from water filters- TATA SWACH Nanofilters , Ag-NPs used for fouling control in membrane bioreactors (Zodrow et al., 2009)). Due to their potential toxicity to microorganisms (El Badawy et al., 2011)and widespread use, Ag-NPs have been the key component of campaigns by various environmental activist groups against nanotechnology developments (Pulit-Prociak and Banach, 2016). When this PhD

study was started in late 2010, fate of Ag-NPs in wastewater and mechanisms of its transformation in WWTPs were poorly researched and understood. Elucidation of the fate and transformation mechanisms of Ag-NP can help establish how organisms interact with Ag-NPs in the environment and help shape future public health and environmental regulations with regard to use and disposal Ag-NP enabled products.

The novel contribution of this thesis is towards understanding how different coatings (but same type and size) on NPs effect transformation and fate of NPs in WWTPs. The speciation of silver influences its toxicity and availability to organisms in the environment.

The main purpose of this thesis was to investigate the detailed fate, behaviour and transport of synthesised and well-characterised citrate and PVP stabilised Ag-NPs in OECD synthetic sewage (OECDss) and in sewage (a mix of OECDss and activated sludge) under conditions relevant for WWTPs. The work was divided into four different steps in order to achieve this goal:

- **Aim 1:** To synthesise Ag-NPs of the same size (since settling in WWTP is primarily governed by Stoke's Law) but different capping agents (citrate, PVP and PEG) and characterise Ag-NPs. Multiple approaches to characterisation were adopted to analyse these Ag-NPs before, during and after each step of the WWTP.
- **Aim 2:** To investigate the stability of citrate and PVP Ag-NPs in OECDss[1] under similar conditions as experienced during the treatment of sewage in sequencing batch reactors (SBR). The dissolution, aggregation and changes in surface chemistry and surface charge of Ag-NPs were assessed.

[1] OECD synthetic sewage

- **Aim 3:** To study the fate, behaviour and transport of Ag-NPs in an SBR pilot plant under the following conditions: first, OECDss alone was used as sewage and the different changes of the Ag-NPs were assessed under aerobic and anaerobic conditions. Second, OECDss spiked with Ag-NPs was used as influent and mixed with some activated sludge in order to simulate the environmental conditions of release of Ag-NPs into WWTPs.
- **Aim 4:** To assess the accumulation and removal of Ag-NPs in WWTP under aerobic conditions by using UV-Vis spectroscopy, mass balance properties and a Freundlich isotherm model.

Chapter 2 Materials and Methodology

Chapter Summary

This chapter presents the materials and methods used to provide qualitative and quantitative measurements of the size, amount and form (silver sulphide, silver chloride or silver oxide) of Ag-NPs in an aerobic wastewater treatment pilot plant: before entering the plant and at all stages of the wastewater treatment. Citrate, polyvinylpyrrolidone (PVP) and thiol-polyethylene glycol (PEG-SH) capped Ag-NPs were selected as model particles and were synthesised using methods established in previous work at University of Birmingham (Tejamaya et al., 2014, Römer et al., 2011). For the qualification and quantification of the size, amount and form of Ag-NPs before and after their exposure to the sewage, a multiple techniques approach (Domingos et al., 2009) was needed. The techniques selected include: graphite furnace atomic absorption spectroscopy (GFAAS) for concentration analysis, ultraviolet-visible spectroscopy (UV-Vis) for surface plasmon resonance (SPR) measurements, field-flow fractionation (FFF) and dynamic light scattering (DLS) to determine the hydrodynamic size distribution of particles, transmissions electron microscopy (TEM) for the particles core size and shape factor distributions, energy dispersive X-ray spectroscopy (EDX or EDS) for surface area analysis using scanning electron microscopy (SEM) and TEM, and finally, zeta potential (ZP) for surface charge analysis using DLS. Analytical methods developed for the analysis of the wastewater (Eaton and Franson, 2005) and used to characterise the sewage utilised in this study are also introduced in this chapter. These include the 5-day biological oxygen demand for the oxygen, the total and volatile solid

concentrations, and the dissolved oxygen and pH measurements which help to estimate the efficiency of the treatment plant. The methods used for analysing the OECD synthetic sewage are also presented.

2.1. Silver nanoparticle synthesis

2.1.1. Materials

Ag-NPs can be synthesised by chemical, physical, and electrochemical methods. In this study, the NPs were synthesised using a standard chemical process. The required chemicals were purchased from Sigma-Aldrich: sodium citrate tribasic dihydrate also known as tribasic trisodium citrate ($Na_3C_6H_5O_7.2H_2O$), sodium borohydride ($NaBH_4$), silver nitrate ($AgNO_3$), polyvinylpyrrolidone or PVP10 (with an average molecular weight of 10,000) and thiol-polyethylene glycol (PEG-SH with average molecular weight of 5,000). Equipment used includes 50 and 100 mL volumetric flasks, 500 mL Erlenmeyer flasks, a combined hotplate magnetic stirrer (Bibby Stuart SB162-3 three position) and magnetic stirrer bars. Temperature

2.1.2. Synthesis of citrate capped Ag-NPs

Citrate capped Ag-NPs were synthesised using the method of (Römer et al., 2011, Cumberland and Lead, 2009). Briefly, solutions of 0.31 mM trisodium citrate, 0.25 mM of silver nitrate and 10 mM sodium borohydride were prepared with milli-Q water. The solutions were stored in the fridge for 30 min before synthesis, to lower the temperature of $NaBH_4$ which is a powerful reducing agent, in order to slow down the reduction of Ag-NPs and favour the formation of monodispersed particles (Mavani and Shah, 2013). Having the citrate and $AgNO_3$ solutions at the same temperature as $NaBH_4$, helps maintain the rate of the reduction process.

After refrigerating, the sodium citrate and the silver nitrate solutions were poured together in an Erlenmeyer flask and stirred vigorously while adding 6 mL of the diluted $NaBH_4$ solution (the dilution of 1:3, meaning, 3 part of water (4.5 mL) and 1 part of 10 mM $NaBH_4$ (1.5 mL)) of 0.25 mM. The solution turned yellow instantly signifying the formation of the Ag-NPs via the reduction (by $NaBH_4$) and stabilisation (trisodium citrate) mechanism. The obtained solution was then stirred for 10 min at room temperature to allow the homogeneity of the reduction of Ag^+ and growth to the Ag-NPs nucleus. Because Ag-NPs nuclei were also surrounded citrate molecules, they became partially stable since the citrate molecules are not attached to the particles. This citrate layer was permanently yielded by heating up the solution to 100°C for 1.5 hours. The suspension (Figure 2-1) was left in the dark overnight at room temperature to cool and finally stored in the fridge at 3 to 4 °C.

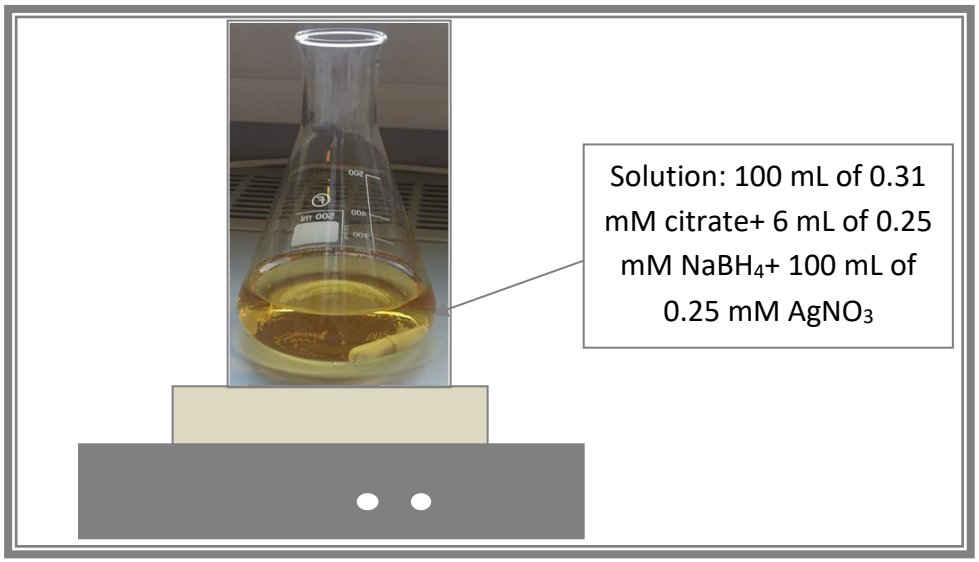

Figure 2-1: Synthesis of citrate Ag-NPs by chemical reduction

The formation of the Ag-NPs consists of a two-step chemical process (Pham Van Dong et al., 2012) and was originally described by Grokhale et al. (2010). The mechanism of formation of the NPs is described as follows:

The first step consists of the interaction between the aqueous solutions of sodium citrate and $AgNO_3$ (Equation 2-1). When added together at room temperature they react to give an Ag-citrate complex and sodium nitrate ($NaNO_3$) in the presence of oxygen and hydrogen ions:

$$4AgNO_3 + C_6H_5O_7Na_3 + 2H_2O \rightarrow 4Ag^+ - C_6H_5O_7H_3 + 3NaNO_3 + H^+ + O_2$$

Equation 2-1

Ag-citrate complex

In the second stage, the solution of 0.25 mM of $NaBH_4$ is added (Equation 2-2). This reduces the Ag-citrate complex by allowing the silver ions to gain an electron and become zerovalent NPs stabilised by citrate. The mechanism for this step is:

$$4Ag^+ - C_6H_5O_7H_3 \xrightarrow{(0.25\ \text{mM}\ NaBH_4)} Ag^0 + \text{by products}$$

Equation 2-2

Ag-citrate complex Ag-NPs

Stirring for 10 min at room temperature and for a further 1.5 hours at 100 °C was applied to yield the citrate coating that surrounded the Ag-NPs. The obtained citrate Ag-NPs have an average core size of 10 nm (Römer et al., 2011) (11.7 nm in our case) and were selected due to their ease of synthesis and high reproducibility. They have been used in numerous research projects within the University of Birmingham Environmental Nanoscience Group (Römer et al., 2011, Tejamaya et al., 2012, Baalousha et al., 2013)

2.1.3. Filtration and ultrafiltration of Ag-NPs

Ultrafiltration was used to remove any excess (unreacted) silver ions from the Ag-NPs suspension after the reaction has finished. This was to prevent the Ag-NPs from continuing to grow slowly and thus become more polydisperse. A 400 mL Millipore Amicon Bioseparations Stirred Cell (Figure 2-2) was used to separate the Ag-NPs from the ions in conjunction with Millipore ultrafiltration membranes (membrane filter Amicon Bioseparations ultrafiltration regenerated cellulose 90 mm diameter 1000 NMWL (or nominal molecular weight limit), with a pore size of around 1 nm). The detailed method used for washing these particles was dependent on their coating.

For the citrate Ag-NPs, the procedure was as follows: 200 mL of the citrate Ag-NPs were transferred to the ultrafiltration cell. The magnetic stirrer bar is placed in the cell before it is sealed with a lid and the latter is connected to a nitrogen gas bottle by a tube; the lid must be locked after it is placed in the cell in order to avoid any gas leakage. The pressure in the cell was kept at 1.2 bars and the liquid in the cell is stirred at a low rate using a stirring plate to facilitate pushing the liquid through the membrane and to prevent the particles from agglomerating (ISO), 2013). If the pressure was too high the membrane would rupture allowing all the liquid to leave the cell rapidly. When the amount of liquid in the cell was reduced by three-quarters (about 50 mL remaining), 150 mL of 0.15 mM sodium citrate solution was added to ensure that the particles remained coated with citrate and the particles were washed again. This process was repeated for a second time using the sodium citrate solution to remove as many ions from the suspension as possible. After a third addition of the sodium citrate solution, 0.15 mM sodium citrate solution was added to the ultrafiltrated Ag-NPs to obtained 200 mL of the initial volume of the NPs. The NPs suspension was filtered with

a Millipore 100 nm membrane, characterised by UV-Vis, DLS and FFF to confirm the formation of Ag-NPs, and size and kept in the fridge until required. The procedure of washing PEG capped Ag-NPs was similar to the citrate-capped Ag-NPs. The difference here was the use of 250 ppm PEG-SH washing solution instead of the citrate.

In the cased of the PVP coated Ag-NPs, the method remained the same with the exception of the washing solution, which consisted of 3% PVP and DI water. The amount of PVP added to the particles was to keep the particles coated with PVP while removing excess Ag ions through washing. The 200 mL citrate Ag-NPs recapped by PVP, were first washed till their volume was reduced to half before adding water and 5 mL of 3% PVP was added to obtain the initial volume of the suspension and the NPs were washed for the second time. After washing the PVP Ag-NPs for a third time, 100 mL of DIW and 5 mL of 3% PVP were added for the last time and the UV-Vis and DLS characterisation were conducted before storing them in the fridge.

Before the NPs were used, they needed to be filtered through a Millipore sterifil filter cell (Figure 2-2) which has a volume capacity of 250 mL, to remove large particulates such as dust. The cell was used in combination with a cellulose nitrate membrane of 47 mm in diameter and 100 nm pore size. Note that, prior to filtration the filter membrane must be washed by passing through 100 mL of deionised water, before the NPs solution.

Figure 2-2: Millipore 400 mL ultrafiltration stirred cell (left image) and the 250 mL Millipore sterifil filter cell (right image, from (FisherScientic), UK)

2.1.4. Recapping of citrate Ag-NPs with polyvinylpyrrolidone (PVP) and thiol-polyethylene glycol (PEG-SH)

100 mL of freshly prepared and washed (sections 2.1.2 and 2.1.3) citrate Ag-NPs, prepared as described above, are recapped with PVP (Tejamaya et al., 2014) or poly(ethylene glycol)-thiol (PEG-SH) (Römer et al., 2011, Tejamaya et al., 2012, Fernandez-Lopez et al., 2009). For PVP, the method consists of adding 4 mL of 3% PVP to the 100 mL citrate Ag-NPs and stirring for 1 hour at room temperature. After stirring, the solution is stored for 24 hrs in the fridge at a temperature of ~4 °C, for the reaction to complete. The next day, the PVP Ag-NPs were characterised by UV-Vis, DLS and FFF to verify recapping and the size measured before they were washed with 3% PVP solution (2.1.3). According to the literature (Tejamaya et al., 2012), the UV-Vis absorbance spectrum of the PVP Ag-NPs shifts to a longer wavelength (MA at around 400 nm) compared to the original citrate-capped Ag-NPs (MA at 390 nm).

For PEG-SH the method consists of adding 8.53 ml of 500 ppm PEG-SH (Mw 5000, purchased from sigma Aldrich) solution to 200 ml of the above-prepared citrate Ag-NPs and stirred for

30 min. The changing of the capping agent on the particles was measured by DLS, FFF and SPR which caused a shift of the UV-Vis absorbance spectrum to longer wavelength – with the MA shifted from 390 nm to 393 nm upon formation of the PEG-SH layer at the particle surface.

After their characterisation, the citrate Ag-NPs with an average core size of 10 nm (Römer et al., 2011), and the PVP-capped Ag-NPs of 11.31 nm core size (Tejamaya et al., 2014) (12.3 nm in our case) were chosen for use in the PhD project; the PVP Ag-NPs were selected in preference to the PEG citrate Ag-NPs due to their enhanced stability in a media (Tejamaya et al., 2012). The PEG-capped Ag-NPs were not investigated in thesis due to workload.

2.2. WWTP pilot and influent

2.2.1. The sequencing batch reactor (SBR) Pilot plant

The treatment pilot plant (Figure 2-3) was developed by Miguel Orbaneja Botija for his PhD degree at the University of Birmingham (Botija, 2006). This scale plant was formed of two sequencing batch reactors (SBRs) (or aeration tanks), with one used for the control sample and the other for the test sample. The two SBRs had a volume of 10 litres each, with a fill and –draw function used for the introduction of the influent to the tank (fill) and the removal of the effluent (draw). Others components include:

- Two automated systems (microprocessor units) to control the SBR cycles. Each system is connected to the flow level electrode device;
- Two solenoid valves (S1) (¾ port, 240 Vac, RS component) used for filling the tanks;
- Two stirrer paddle motors (IKA Labortechnik, RW 16 Basic);

- Two flow metres with aeration supplied by an air pump (RENA air 200); and
- Two solenoid valves (S2) (¾ port, 240 Vac, RS component) for the decantation of the effluent.

The reactors were fully automated and run in parallel for cycles of 24 hours. Unlike how a typical SBR system operates (Figure 2-5), there is no idle phase. The sludge was removed manually from the tanks when required using a stripette pipette or when no longer needed after completing an experiment.

The principle operation of the system was as follows: after the transfer of the activated sludge into the tanks, the influent (which was prepared in 10 L bottles the day before), was transferred to the tank through the operation of the S1 solenoid valve. When the tank was filled to a maximum volume of 10 L, the aeration and stirring started, leading to a homogenous mixture of the activated sludge with the synthetic sewage. The aeration flow was kept at a flow rate between 100 and 200 ($mL*min^{-1}$). The air was distributed from the bottom to the top of the tank using an air stone (generally used to aerate an aquarium) connected to the flow meter through a tube. The SBR cycle was controlled by a flow meter electrode device consisting of three electrodes with different lengths, inserted into the mixed sewage, as follows:

- The shorter electrode (E_1), the fill-level electrode, controls the fill phase;
- The draw phase or removal of the effluent from the tank is controlled by the medium size electrode (E_2);
- The third electrode (E_3) acts as the ground for the automated system and it was required during the whole cycle.

The effluent was discharged from the aeration tank via the solenoid valve (S2).

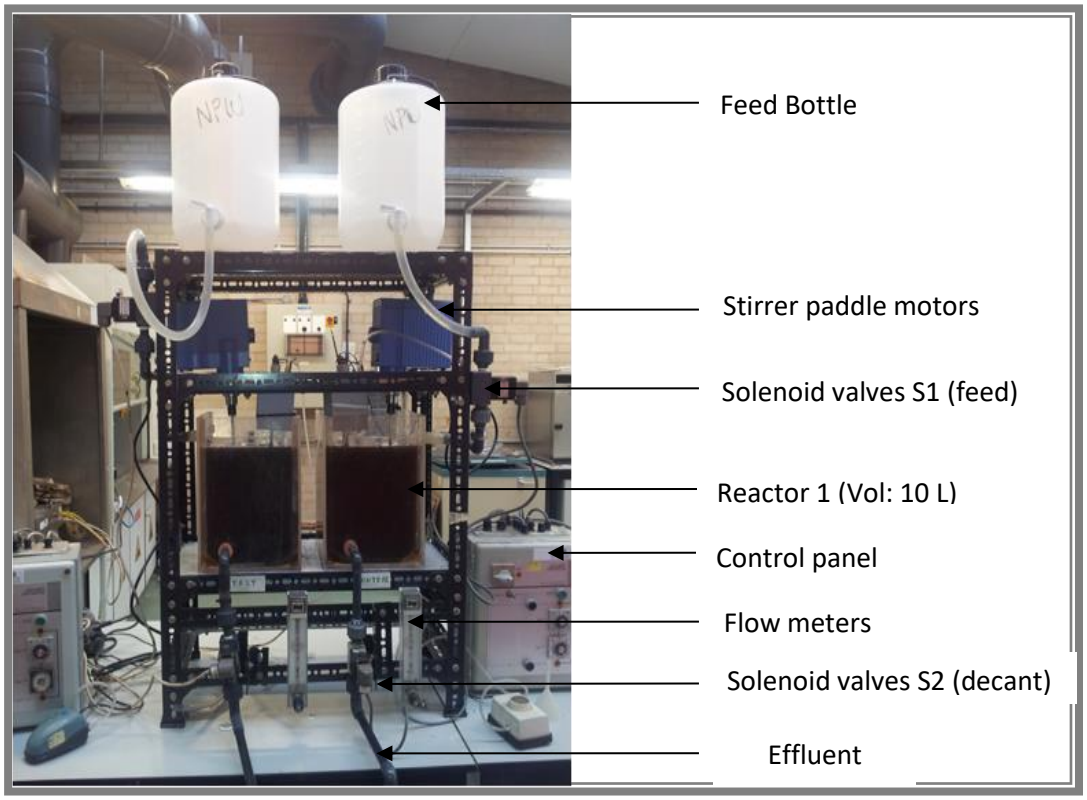

Figure 2-3: The SBR pilot plant designed by Miguel Orbaneja Botija (Botija, 2006)

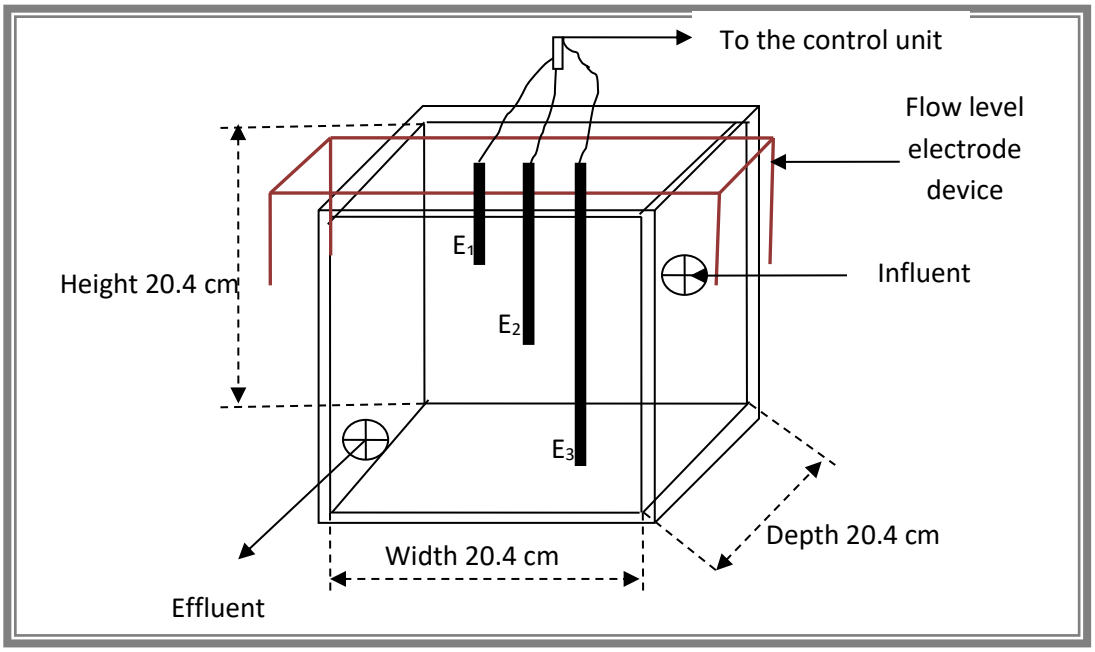

Figure 2-4: Details of the 10 litre SBR tanks (Botija, 2006)

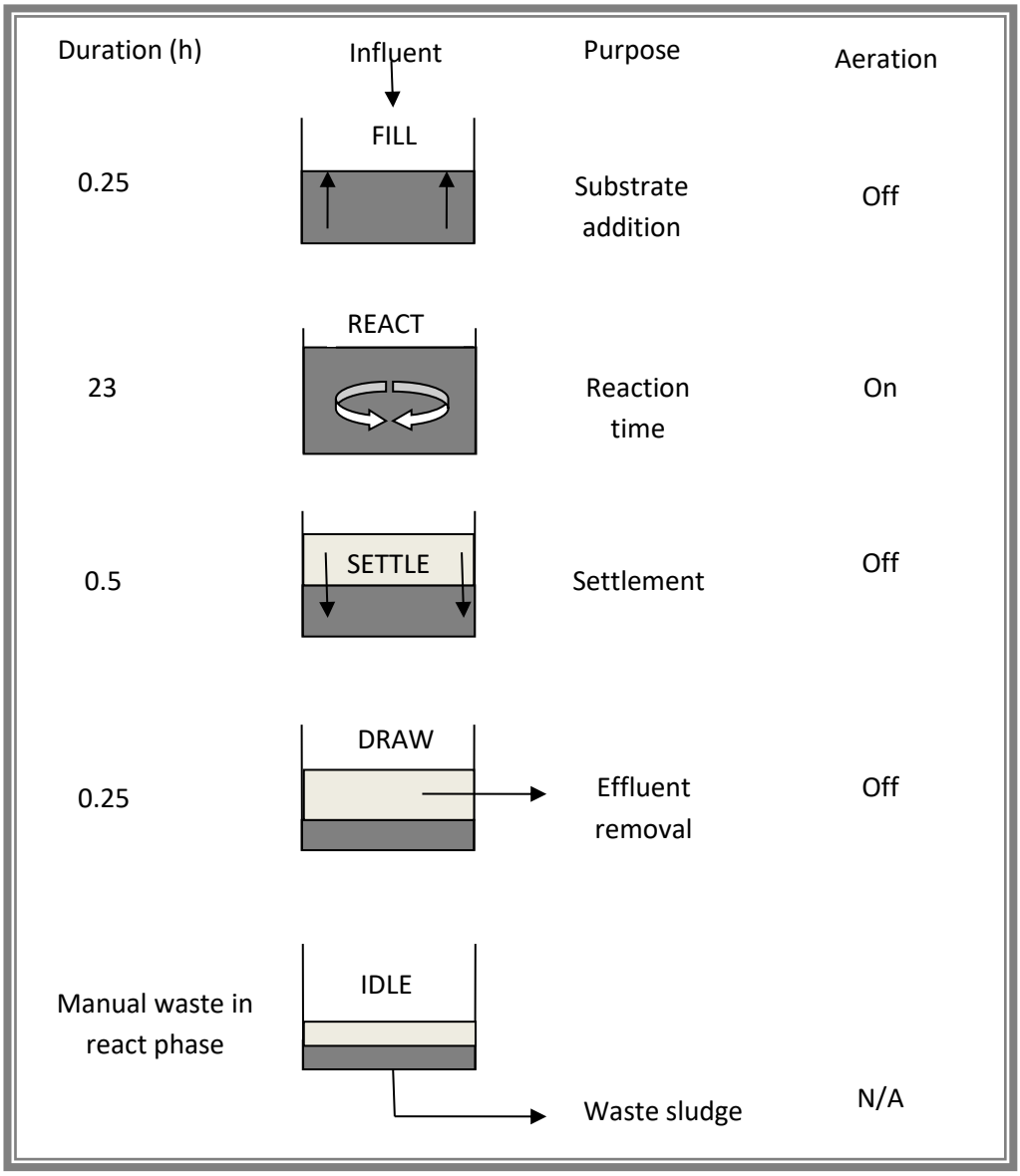

Figure 2-5: Typical operation sequence of the SBRs (Botija, 2006)

2.2.2. Influent wastewater and activated sludge

2.2.2.1. OECD synthetic sewage

OECD synthetic sewage (OECDss) (OECD, 2001) was used as the influent for the main study investigating the fate and behaviour of Ag-NPs in a wastewater treatment pilot plant. The reagents for its preparation were purchased from Sigma-Aldrich, UK. To prepare the synthetic sewage, 1 L of deionised water or DIW (18 MΩ Milli-Q water) was used in place of tap water. Each constituent was added to the DIW at the specified quantity (Table 2-1) as recommended in the literature (OECD, 2001). The information on the total nitrogen and phosphorus content, the molecular weight, the moles of solute and the molarity of the OECDss components are listed in Table A1 - 1, which were obtained from the Sigma-Aldrich UK website.

Table 2-1: chemical composition of the OECDss (OECD, 2001)

OECDss composition	Concentration ($mg*L^{-1}$)
Peptone	160
Meat-extract	110
Urea (CH_4N_2O)	30
Anhydrous dipotassium hydrogen phosphate (K_2HPO_4)	28
Sodium chloride (NaCl, 7 mg)	7
calcium chloride dihydrate ($CaCl_2.2H_2O$)	4
magnesium sulphate heptahydrate ($MgSO_4.7H_2O$)	2

For this work, the content of Nitrogen and phosphate, and the chemical oxygen demand (COD) were determined using AQUANAL-professional wastewater tube tests for all three

respectively. These chemicals where obtained from Sigma Aldrich, UK. The measurements were made using the DRB200 reactor and following the instructions provided by AQUANAL-professional (AQUANAL®-professional, 2012b, AQUANAL®-professional, 2012c, AQUANAL®-professional, 2012a). For the COD testing, two tube tests were needed, one filled was with 2 mL DIW and used as a blank value and another one with 2 mL sewage sample. Both tubes were then sealed and carefully swayed and placed in the oven and heated for two hours at 148°C. After heating, the samples were cooled for 45 min at room temperate while they were shaken with care and finally placed in the reactor for COD reading.

A similar procedure was used for the measurement of nitrogen and phosphate. Two empty tubes were respectively filled with 5 mL DIW and 5 mL sewage sample and shaken with care. 1 level spoonful of digestion reagent were added to the nitrogen tubes and phosphate tubes (black and grey reagent added to the blank and sewage samples respectively). The tubes were then heated at 100°C for a period of 60 min for the nitrogen samples and 30 min for the phosphate ones and let to cool down for 60 and 30 min respectively. Before measuring the nitrogen and phosphate concentrations, a second reagent was added to the samples: one spoonful of grey compensation reagent for the nitrogen samples and one drop of reagent one for the phosphate samples. The phosphate samples were finally analysed after letting them cool at room temperature for 10 min. Whereas, 0.5 mL of each nitrogen sample were placed in a tube test, mixed with care and let 15 min at room temperature before being analysed.
Note that the COD gives similar information for organic carbon and oxygen demand as the total organic carbon (TOC) and the biochemical oxygen demand (BOD_5). In fact, for domestic influent wastewaters, all three parameters are related through the following equations (Dubber and Gray, 2010):

$$\mathrm{COD} = 49.2 + 3.0 * \mathrm{TOC}$$

Equation 2-3

$$\mathrm{COD} = 11.36 + 1.64 * \mathrm{BOD}_5$$

Equation 2-4

According to the OECD (2001), the OECDs has a mean dissolved carbon (DOC) of 100 mg*L^{-1} and allows a better growth of nitrifying organisms at half that value (DOC = 50 mg*L^{-1}). In general, the OECDs was described as a medium with high nitrogen content and low carbon concentration, making it unsatisfactory to mimic the general requirement (of the domestic raw sewage (listed in Table 2-2) (OECD, 2001). This means, OECDss does not satisfy the optimum ratio carbon-nitrogen-phosphorus (C:N:P) criteria of 100:5:1 (i.e.: BOD_5 (or COD) = 100 mg*L^{-1}, total N = 5 mg*L^{-1} and total P = 1 mg*L^{-1}) of the sewage (Gray, 2004). Note that, the ratio C:N:P of raw sewage is about 100:17:5 according to the literature (Gray, 2004), whereas Table 2-2 shows that the ratio C:N:P of the OECDss measured by us was approximately 100:6:10. According to the OECD, nothing better has been proposed to date except to increase the phosphate concentration as buffer and add more peptone (OECD, 2001).

In this thesis, the COD, total P and total N of the OECDss were measured (Table 2-2) using Aquanal-Professional Water testing tubes from Sigma-Aldrich (Appendix 1). We observed that compared to the influent of a municipal WWTP such as Bristol, UK (EGC, 2015), the total nitrogen, and COD were low, whereas the total phosphorus was found to be high, which might help to obtain a better settleability of the activated sludge (OECD, 2001). The settleability of the sludge is a measure representing how well the sludge is able to settle and is dependent on the physicochemical, microbiological and biochemical properties of the sludge – the older

the activated sludge is, the larger are its flocs and the better is the settleability (Gray, 2004). Different studies have shown that the sorption decrease (Berkowitz et al., 2006) and limitation of phosphorus will favour the ageing of the flocs long term (Azimi et al., 2014). So, because the phosphorus is reduced with time by sorption in the flocs, increasing the amount of phosphorus will decrease the ageing of the flocs causing them to increase in size which favours a better settleability of the sludge (Azimi et al., 2014). Note that, one of the consequences of having a high dosage of phosphorus might be the excess flocculation of the sludge as it can overflow over the tank.

Table 2-2: Typical chemical characteristics of OECDss, UK raw sewage (i.e.: untreated domestic sewage)

Characteristics	OECDss only (measured using test tubes)	UK raw sewage(Gray, 2004)
pH	7.17	7.2
BOD_5 ($mg*L^{-1}$)	NA	326
COD ($mg*L^{-1}$)	45.00	650
TOC ($mg*L^{-1}$)	71.07	173
Total N ($mg*L^{-1}$)	2.5	66
Total P ($mg*L^{-1}$)	42.70	15

2.2.2.2. Activated sludge

The sewage used for this work was a mixture of activated sludge and the OECDss. The activated sludge, from an aerated tank, was collected from two different Severn Trent WWTPs in Birmingham, UK (Figure 2-6). However, they cannot be named for confidentiality reasons. The activated sludge of one of the WWTPs was better quality as it was much sticker and settled well during treatment in the pilot plant after three hours, leaving a much clearer

effluent at the top of the tank. Thus, this WWTP activated sludge was chosen for the rest of the work. The activated sludge was collected from the plant on the day of its use and was aerated for at least two hours before it was transferred to the pilot tank.

The total solid material in the activated sludge was determined by filling a metal tray with 50 ml of sludge (note the tray was weighted and the sludge was sieved) (Eaton and Franson, 2005). It was then placed in an oven and heated overnight at a temperature of 105 °C until complete evaporation of the water (or when it appeared completely dry) leaving a dry solid material in the tray. After cooling at room temperature in a desiccator overnight, the tray was weighted and the TS material calculated by deducting the empty tray weight. For the two Birmingham treatment plants, the activated sludge of the first site used has a mean of 14.18 ± 7.07 $g*L^{-1}$ of solid material and the activated sludge of the second site has a mean value of (2419.53 ± 273.20) $g*L^{-1}$.

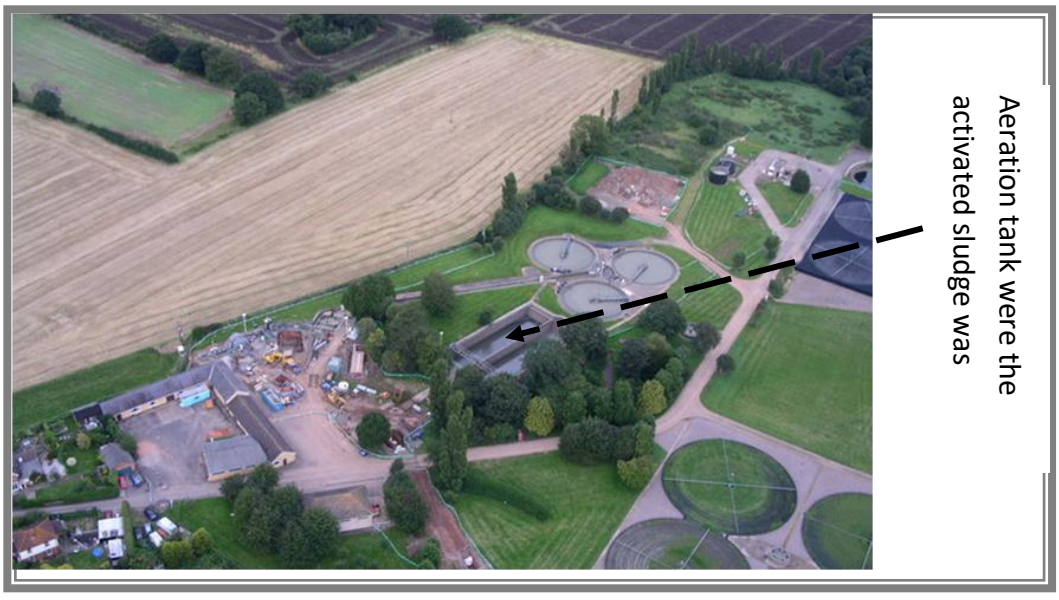

Figure 2-6: Example of WWTP in the UK, Birmingham. (geograph.org.uk)

2.2.3. Analytical methods of the sewage

To analyse the sewage in the pilot plant during the accumulation study (Chapter 6), standard analytical methods were used. These methods were used to determine the following parameters of the sewage:

- 5-day biological oxygen demand (BOD_5): was measured 5 days per weeks for 3 weeks;
- total solids (TS) and volatile solids(VS): was measured at the beginning and end of each experiment;
- potential hydrogen (PH): measured daily;
- and dissolved oxygen (DOC): measured daily.

The analysis of the BOD_5, TS and VS were conducted by Gofetamang Ditalelo in the civil engineering department (University of Birmingham) using analytical standard methods for wastewater (Eaton and Franson, 2005).

2.2.3.1. 5-day biological oxygen demand (BOD_5)

The 5-day biological oxygen demand or BOD_5, is a standardised test set to measure the oxygen consumed by microorganisms during the oxidation of reduced substances in a water sample, within a five day period (Penn et al.). In this study, the BOD_5 of the sewage was investigated during a period of four weeks. The experimental protocol (Figure 2-7) consisted of filling a 300 mL BOD_5 bottle with a mixture (50:50 ratio) of sewage and distilled water which had been aerated overnight (12 hours minimum).

The BOD_5 is also known as the difference between the dissolved oxygen at the initial incubation time (DO_1) and the final incubation time (DO_2). The bottles were incubated for five days at 25 °C in the dark. The BOD_5 was measured using a dissolved oxygen electrode (microprocessor dissolved oxygen meter HI 9146, Hanna instruments (Figure 2-7) and was determined using Equation 2-5:

$$BOD_5(mg/L) = \frac{(DO_1 - DO_2)}{P}$$

Equation 2-5

Where DO_1 is the dissolved oxygen at the initial time of incubation ($mg*L^{-1}$), DO_2 is the dissolved oxygen after five days of incubation ($mg*L^{-1}$) and P is the ratio between the volume of the sewage and the volume of the distilled water (equal one in this case of this study).

Figure 2-7: the 5-day biological oxygen demand measurement (using a microprocessor dissolved oxygen meter, HI 9146, Hanna instruments).

2.2.3.2. Total solids (TS) and volatile solids (VS) (courtesy of Gofetamang Ditalelo)

TS and VS were measured as follow: three nickel tins (or trays) were heated in a furnace at 500 °C for one hour in order to remove any material remaining from previous experiments. The tins were then cooled in a desiccator and weighted prior to use. The laboratory test sieve of 2.36 mm aperture, used to filter the sewage, was washed and dried in an oven at 105 °C for one hour before use.

For the TS measurements, 50.0 mL of the sifted sewage was poured into each tin and placed in an oven at 105 °C for one hour. The tins were then placed in the desiccator to allow them to cool before they were weighted. This whole process of heating and cooling was repeated several times until the weight change of each tin was less than 4% between successive measurements. The TS was determined by calculating the difference in mass between the empty tin and the tin-containing dried sewage. For the measurement of VS, the above sample preparation procedure was also followed, although the method of heating was different. In this case, the sewage samples were ignited once at 500 °C in a furnace for two hours, and then cooled in the desiccator and weighted.

2.2.3.3. Dissolved oxygen (DO) and pH measurements

The dissolved oxygen and the pH of the sewage were measured using a dissolved oxygen electrode (Microprocessor dissolved oxygen meter HI 9146, Hanna instruments (Figure 2-7) and a pre-calibrated pH metre (Mettler Toledo Seven go pro pH meter, pH/ION), respectively.

The DO and pH were measured three times at a specific point in the tank (at the top and/or middle of the tank) in order to produce an average result.

2.3. Method of dispersion of the Ag-NPs in the plant, collection and preparation of the samples for characterisation

2.3.1. Dispersion of the NPs and collection of the synthetic sewage-NPs samples

The 72 hours study was done in two steps. The first step was to study the behaviour of citrate and PVP-capped Ag-NPs in synthetic sewage and the second step was to look at how these NPs would behave when the activated sludge is used in addition to the OECDss. On day 0, 10 L of OECDss was freshly made and placed in an aspiration bottle. Then citrate or PVP Ag-NPs were added to the synthetic sewage to produce a total concentration of 500 $\mu g*L^{-1}$ Ag-NPs. The mean NPs suspension concentration after ultrafiltration was about 11 $mg*L^{-1}$ for both citrate and PVP-capped Ag-NPs (Chapter 3). A volume of 50 mL of the solution (OECDss + Ag-NPs) or influent was then collected from the feed bottle (Figure 2-3) using a pipette stripette and characterised with the following techniques: GFAAS, DLS, UV-Vis and TEM. The prepared mixture of NPs and OECDss was kept at room temperature and was used the following day (day 1) as described below.

On day 1, another sample of the influent was collected for GFAAS, DLS, UV-Vis, TEM, EDS and SEM characterisation before transferring the influent to the pilot plant for treatment. On day 2, during the aeration and at 21 hours into the process, three samples of 50 mL were collected from the top, middle and bottom of the SBR tank for analysis (one sample per location). The

aeration of the sewage stopped after 21 hours, after which the sewage was left to settle for three hours and one sample was again taken from the top, middle and bottom of the tank for analysis of the Ag-NPs using the above methods.

2.3.2. Dispersion of the NPs and collection of the sewage-NPs samples

For this part of the study, the (OECDss + 500 μg*L^{-1} Ag-NPs) was used as influent for the system. The influent was prepared (as described in Section 2.2.2.1) a day before being mixed with activated sludge. The amount of activated sludge used was dependent on how thick the sludge was; an average of 4 L of activated sludge was mixed with the influent for a total volume of 10 L of sewage. The mixture was treated for 24 hours, with 21 hours of aeration and three hours of settling. Samples were collected from the top, middle and bottom of the tank during aeration and after settling and from the effluent (Figure 2-3).

A similar procedure was used for the NP accumulation study, with the exception of the particle concentration and the time length of the treatment. In this part of the work, the accumulation of Ag-NPs in the activated sludge over a period of one month was studied. Influent (OECDss + 10 μg*L^{-1} Ag-NPs) was prepared freshly every other day (day 0) and was transferred into the tank a day after it was made (day 1). The samples were collected 24 hours after the start of the treatment during aeration (day 2) and 24 hours after the completion of aeration during the settling phase (day 3). The effluent was then drawn and the tank was refilled with a day old influent for treatment. This process was repeated ten times in total over the one month period.

2.3.3. Sample preparation for assessment of partitioning of NPs

2.3.3.1. Samples for DLS, UV-Vis characterisations

The samples collected when the influent was treated in the absence of the sludge were filtered twice. First, with a 200 nm pore size membrane filter syringe (hydrophilic polyethersulfone, Acrodisc) was used to remove large particulates or dust and then with a 100 nm pore size membrane filter syringe Millex (Durapore hydrophilic polyvinylidene fluoride, Millipore), to remove any remaining large particulates. After filtration, small quantities of the samples were taken, 1 mL and 5 mL respectively, for DLS and UV-Vis measurements.

Sewage samples with addition of sludge were first centrifuged for 30 min at 5,000 rpm at 10 ˚C to remove large residues from the sludge. The sample supernatant was separated from the sediment and filtered successively with 450, 200 and 100 nm pore size membrane filter syringe. The samples were then characterised by DLS and UV-Vis to assess the NP size and SPR.

2.3.3.2. Samples for TEM characterisation

For TEM, a very small amount of the samples filtered as described above was used. For the TEM, two methods to prepare the samples were used: the ultra-centrifugation (UC) method and the drop method.

For the drop method, a drop of the sample was deposited on the TEM grid, a carbon film (300 meshes), which was held by a pair of tweezers. The ensemble was then covered and let dry at room temperature for approximately two hours. After drying, the grid was dipped in ultrapure deionised water for a couple of seconds, then covered again and let dry for two more hours. All prepared TEM grids were kept in a dry and dark place to reduce the effect of the light and humidity on the NPs prior to imaging.

For the ultracentrifugation preparation method, the TEM grid was placed on a sample holder (Teflon) which is guided into a centrifuge tube using a long and fine screwdriver (Beckman tube) till it touches the bottom of the tube. The screwdriver was then removed and the tube was filled to the top with a much diluted sample (20 $\mu g*L^{-1}$) of OECDss + Ag-NPs. Finally, the tubes were closed with parafilm and placed in the ultracentrifuge rotor and centrifuged for one hour at 30,000 rpm and 10 ˚C. This allowed all the particles to be deposited on the substrate (the TEM grid), with only ions remaining in the supernatant. After centrifugation of the sample, the tubes were carefully removed from the rotor, and the supernatant discharged. The substrate holders were taken out of the tubes, the EM grids were rinsed very quickly (few seconds) in DI water and allowed to dry at room temperature for two hours. They were kept in a grid case and stored in a dry and dark place till they were characterised.

2.3.3.3. Sample preparation for SEM characterisation

Samples for SEM analysis should be in powder form. The sewage sediment obtained after centrifugation of a sample (with or without Ag-NPs) at 5,000 rpm, was kept in a ceramic cup and allowed to dry in the oven at 105 ˚C. The dried sewage was then ground into powder

using a pestle and mortar and transferred into a dry small plastic tube for storage. To prepare the samples for characterisation, a flat SEM specimen (or stub) and double-sided sticky tape were used. A very small amount of each sewage sample (four to six samples maximum) was deposited on the tape and any excess was removed using an air duster in the fume cupboard. The stub was coated with a platinum or carbon film prior to analysis.

2.3.3.4. Sample preparation for GFAAS characterisation

The sample preparation to investigate particle dissolution was done using the ultracentrifuge (UC) method. Samples were prepared according to their composition. For example, samples with OECDss and Ag-NPs only, were directly transferred into UC tubes, and samples with OECDss + Ag-NPs + activated sludge) were centrifuged for 30 min at 5,000 rpm and 10 ˚C and their suspension was collected and transferred into UC tubes. Once in UC tubes, samples were ultra-centrifuged at 35,000 rpm and 10 ˚C for two hours. The first 3 mL of the supernatant were carefully collected and acidified with 70% nitric acid (HNO_3) to a concentration of 20% acid. The 20% acidified samples were diluted with water to 0.2% HNO_3 before characterising them.

For GFAAS analysis, two methods of sample preparations were used: the first for the samples with OECDss sewage only and the second for samples collected when the influent contained some activated sludge. Collected OECDss only samples were acidified with 20% HNO_3, diluted from 70% HNO_3 of general-purpose (GP) quality. However, because the analytical method used for this work was the GFAAS and the element investigated was silver only, the possible effect of impurities from the acid was negligible. After a week, 500 µL of the acidified sample

was diluted to an acidity of 0.2% in order to obtain a pH within the optimum range (between 1 and 3) for GFAAS analysis.

The samples from the SBR reactor in the presence of activated sludge were acid digested using aqua regia. The samples were acid digested using a method described in Standard methods for the examination of water and wastewater (Eaton and Franson, 2005). The procedure of the acid digestion of the sewage was as follow: a solution of the aqua regia was prepared by adding 100 mL of $HN0_3$ to 300 mL of hydrochloric acid (HCl). 1 mL of this aqua regia was transferred into a vial that contained 5 mL of the collected sewage sample. The samples were then placed into the microwave vessels (Figure 2-8) for digestion using the microwave program shown in Table 2-3 Note the vessel has a Teflon liner that prevents the vapour from exiting during the heating process. After the end of the program, the samples were left to cool down at room temperature. Each vessel was then carefully uncapped and allowed to vent in a fume cupboard. The solutions were then filtered with 450 nm filter syringe into plastic containers and stored at room temperature until they are analysed.

Table 2-3: Microwave program for acid digestion of the sewage samples in preparation for GFAAS measurements

Time (min)	Microwave Power (W)
2	250
2	0
5	250
5	400
5	500

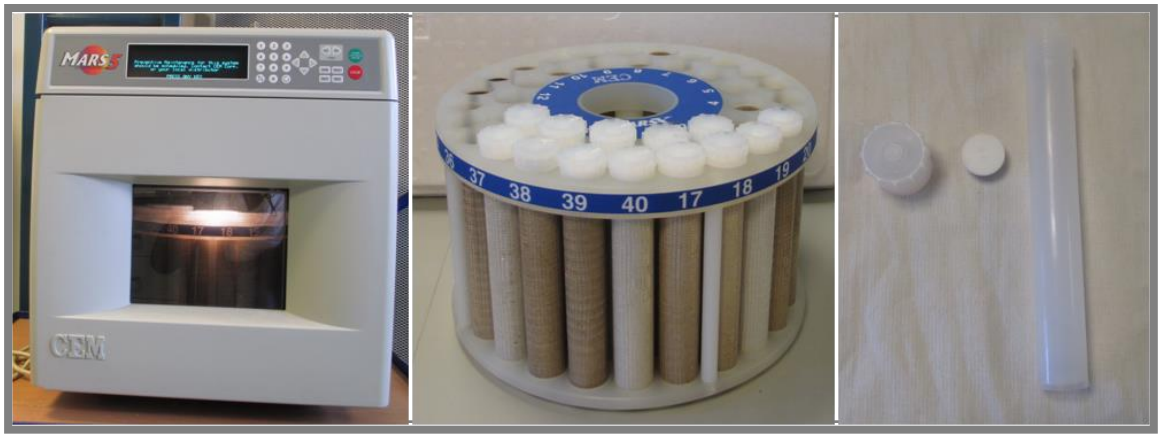

Figure 2-8: CEM Mars 5 microwave digester; microwave vessels and their holder.

2.4. Nanoparticle characterisation techniques

It is of prime importance to characterise the pristine NPs before dispersing and characterising in a particular medium in order to observe how they may change after exposure and to deduct accurate observations and conclusion from the analysis. The characterisation includes the determination of their size, size distribution, their surface plasmon characteristics and their morphology. These parameters were characterized and measured using the following techniques: DLS and FFF: used to investigate the size distribution of the suspended NPs. DLS and FFF give a size distribution of NPs by measuring their light scattering intensity and UV-Vis absorbance respectively plotted against their D_H.

UV-Vis absorbance spectroscopy was used to characterise the surface plasmon resonance of the NPs, giving their absorption spectrum as a function of the applied wavelength in the UV-Vis range (190 nm to 1100 nm). Changes in the UV-visible absorption spectrum can give an indication on the degree of dispersion of the NPs.

The NPs core size distribution was characterised using TEM and SEM. The elemental composition of the NPs can be measured using energy EDS in either SEM or TEM. This was used to investigate the surface chemistry of the NPs in the presence of the sewage. The concentration of the NPs and the amount of dissolution of the NPs was over time depending on the timescale of the study (see Chapter 4, Chapter 5 and Chapter 6) measured using GFAAS which allowed us to investigate the silver concentration in samples from the pilot plant.

2.4.1. Ultraviolet-visible spectroscopy: SPR spectroscopy

2.4.1.1. The principle of UV-Vis absorbance spectroscopy

The principle of SPR spectroscopy is as follows: a monochromatic polarised light is absorbed (Figure 2-9) on the NP surface and transmitted in the form of scattering light to NP neighbours (i.e.: other NPs close by). The absorbed and scattered light are measured as the electrostatic extinction peak shift or change of the NPs (Kazuma and Tatsuma, 2014, Tuchin, 2010) which is calculated using Mie theory (section 2.4.1.2).

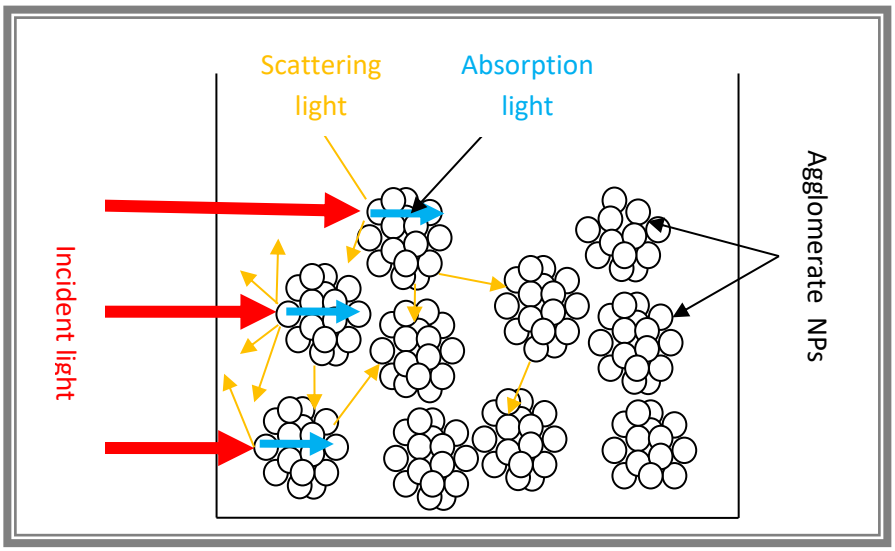

Figure 2-9: Schematic of the transmitted light absorption and light scattering within the particle surface.

For this work, the UV-Vis spectrum of the Ag-NPs is analysed using a double beam 6800 UV-Vis spectrometer Jenway (2012) (Figure 2-10).

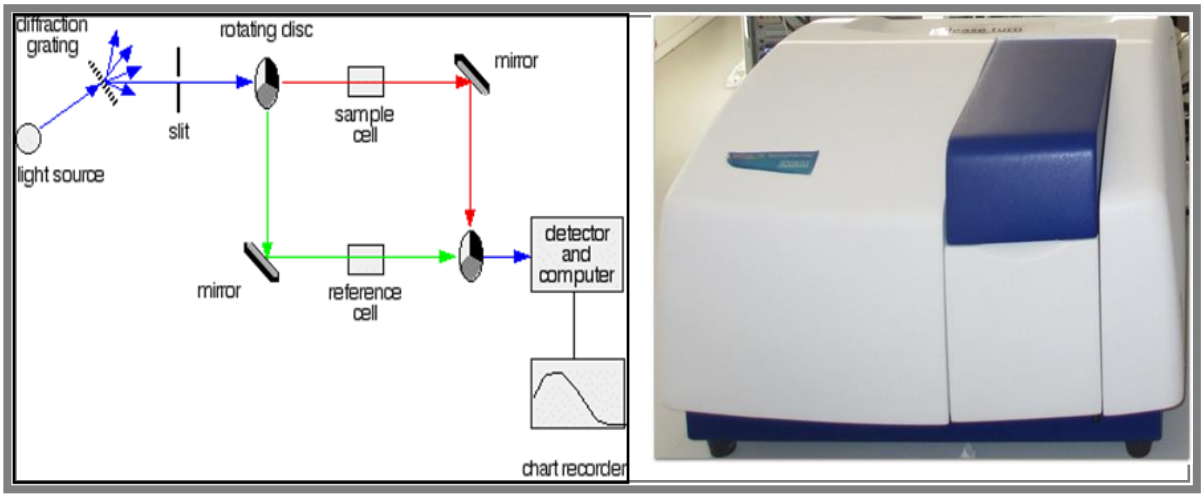

Figure 2-10: Schematic of a simple double UV-Vis spectrometer, taken from (http://www.chemguide.co.uk/analysis/uvvisible/spectrometer.html) and the Jenway 6800 double beam UV-Vis spectrometer (2012 model) used in this work.

2.4.1.2. Surface plasmon resonance: Mie theory and effect on the NPs coating.

One of the most important optical properties for a given metal NP is the formation of optical resonances due to the excitation of electrons at the NP surface, from the interaction of the NPs with an incident light (Englebienne et al., 2003, Noguez, 2007, Biswas et al., 2010). The SPR is a UV-visible band near to the infrared resonance band in which the excited electrons on the NP are maximal (Biswas et al., 2010). The SPR characteristics – spectral location, magnitude, and width are dependent on the size, shape, structure and environment of the NPs (Biswas et al., 2010).

The oscillating electric field resulting from NP–incident light interactions causes the displacement of the conduction NP electrons or electron cloud relative to the NP nuclei (Figure 2-11), due to the Coulomb force (Biswas et al., 2010). These electrons oscillate at a frequency dependent on the NP density, effective mass, shape and charge distribution (Biswas et al., 2010). A higher mode of plasmon excitation appears when the NP is large in size or has a non-spherical shape, half of the electron cloud moves parallel to the electric field, while the other half moves antiparallel to the electric field (Biswas et al., 2010).

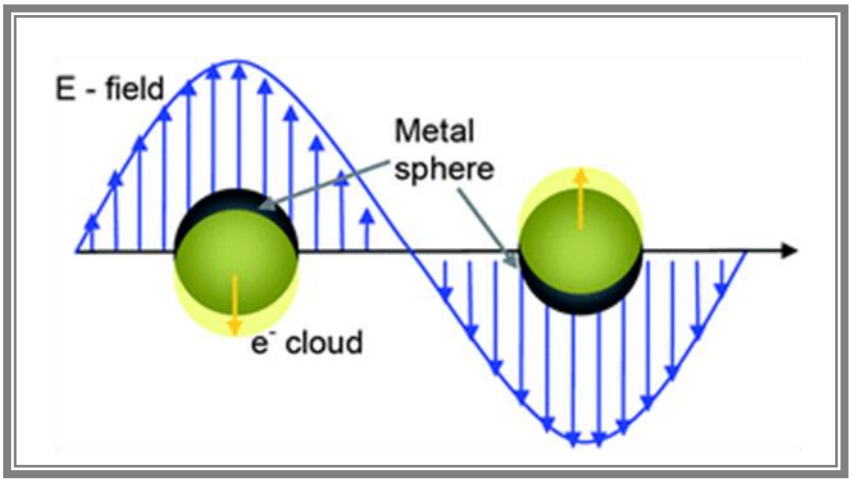

Figure 2-11: Schematic representing the electron cloud oscillation in metal NPs when they are irradiated by light (Biswas et al., 2010)

Gustav Mie described the light scattering by spherical metal NPs using the Maxwell equations (Biswas et al., 2010). According to the Mie theory, a NP of a radius R and absorption cross-section proportional to R^3 has a scattering cross-section smaller than the light wavelength λ ($2\pi R \ll \lambda$) and is proportional to R^6 (Biswas et al., 2010). The detection of NP light scattering is more appropriate when the NP size is smaller than the wavelength of the incident light and the efficiencies of the NP absorption and light scattering are determined by their cross-sections σ_{abs} and σ_{scatt}, respectively (Biswas et al., 2010):

$$\sigma_{abs} = -\frac{8\pi^2}{\lambda} R^3 Im[(\alpha^2 - 1)/(\alpha^2 + 2)]$$

Equation 2-6

And

$$\sigma_{scatt} = \frac{128\pi^5}{3\lambda^4} R^6 |(\alpha^2 - 1)/(\alpha^2 + 2)|^2$$

Equation 2-7

Where α is the complex refractive indices ratio of the NPs and the media, and $\sigma_{abs} + \sigma_{scatt} =$ extinction cross-section of the NPs (Biswas et al., 2010);

$Im[(\alpha^2 - 1)/(\alpha^2 + 2)]$ is the imaginary part (Im) of the complex function $[(\alpha^2 - 1)/(\alpha^2 + 2)]$.

The expressions of the scattering and absorption cross-sections can also be written as functions of the complex dielectric parameter of the NP ($\varepsilon = \varepsilon(\lambda)$) and of the matrix ($\varepsilon_m = \varepsilon_m(\lambda)$) (Biswas et al., 2010).

$$\sigma_{abs} = \frac{\pi^2}{\lambda} R^3 Im[(\varepsilon - \varepsilon_m)/(\varepsilon + 2\varepsilon_m)]$$

Equation 2-8

And

$$\sigma_{scatt} = \frac{2\pi^5}{3\lambda^4} R^6 |(\varepsilon - \varepsilon_m)/(\varepsilon + 2\varepsilon_m)|^2$$

Equation 2-9

From the above equations, one can deduct that the NP absorption and light scattering are maximum at the SPR wavelengths corresponding to $\varepsilon + 2\varepsilon_m = 0$(Biswas et al., 2010).

When the NP size is comparable to λ, the incident light interacts with the particle over a cross-sectional area larger than the geometric cross-section of the particle (Biswas et al., 2010). In the case, according to the general Mie theory, the scattering efficiency parameter Q_{scatt} is given as a function of the scattering cross-section and the cross-sectional area (Biswas et al., 2010).

$$Q_{scatt} = \frac{\sigma_{scatt}}{\pi r^2}$$

Equation 2-10

If the NPs is much smaller than λ, for smaller NPs surface plasmon (SP) oscillation damping or radiative damping effects can be taken into account, the extinction of the particles becomes

a function of the cross-section only while the scattering cross-section is neglected ($\sigma_{ext} = \sigma_{abs}$) (Tuchin, 2010, Madoyan et al., 2012). Please note that in this these, the notion of SP oscillation damping will not be developed as it is not well understood yet, but we believe it is similar to the damping effect occurring during the oscillation of a spring.

SPR is thus used for the characterisation of metal NPs, as well as biological materials in multiple areas such as surface science, biotechnology, medicine, environment and drug and food monitoring (Englebienne et al., 2003, Tao et al., 1999, Pedersen and Duncan, 2005).

2.4.2. Hydrodynamic diameter (D_H) measurements of the NPs

For this, two techniques were used to analyse the NPs D_H in a particular medium. The first technique is DLS which measures the diameter of the particles assuming that they are spheres diffusing at the same speed as the NPs (Malvern, 2013). The DLS instrument used for this work is a Zetasizer Nano from Malvern Instruments (Figure 2-12).

The second technique for measuring the D_H is asymmetric flow field flow fractionation (Fi-FFF), commonly called FFF. FFF is a separation and characterisation technique used to analyse macromolecular and particulate materials such as polymers, powders, emulsions, environmental colloids, geological sediments, biopolymers, bioparticles, and many additional building blocks of modern synthetic and natural materials (Myers, 1997, Chittleborough et al., 2004, Fabrega et al., 2011). The instrument used here is the AF2000 Mid-Temperature, designed by Postnova (Figure 2-15).

2.4.2.1. Dynamic light scattering characterisation

2.4.2.1.1. DLS: principle and theory of NPs size distribution

DLS is a photon correlation spectroscopy (PCS) used to measure Brownian motions by using the intensity fluctuations of the scattering light that occurs when the particles interact with incoming laser light (Malvern, 2013). In principle, the technique can be described as follows (Figure 2-12): an attenuated laser light source illuminates a given sample which is placed in a cell causing the particle to scatter the light. The scattered light is then detected, depending on the detector position (175° or 90°, depending on the DLS model used) (Malvern, 2013). The detected (scattered) light is processed by a correlator which compares time-averaged intensity of the scattered light; the detector information sent to a computer is analysed by the Zetasizer software (Malvern, 2013) and the particle size is given in the form of an average called the Z-average.

The D_H ($= 2r_H$) of a particle is known as the diameter of a hard sphere diffusing with the similar speed as the analysed particles (Shaw, 2014) and it is inversely proportional to the particle diffusion coefficient (D) and this is represented by the Stokes - Einstein equation:

$$D = \frac{k_B T}{6\pi\eta r_H}$$

Equation 2-11

Where r_H is the particle hydrodynamic radius, k_B is the Boltzmann coefficient, T is Temperature η is the Viscosity of the solvent in which the particles are dispersed, and is generally approximated as the viscosity of water (0.01 g*cm^{-}1*s^{-1}).

Based on Rayleigh's approximation the light scattering intensity of NPs is proportional to their radius to the power of 6, i.e. $1/R^6$ (Li et al., 2012b). This means that the presence of a few larger particles or agglomerates in a sample can affect the accuracy of the Z-average. In that case, one might consider the first peak size from the DLS size distribution of the particles as being the "real" NP size.

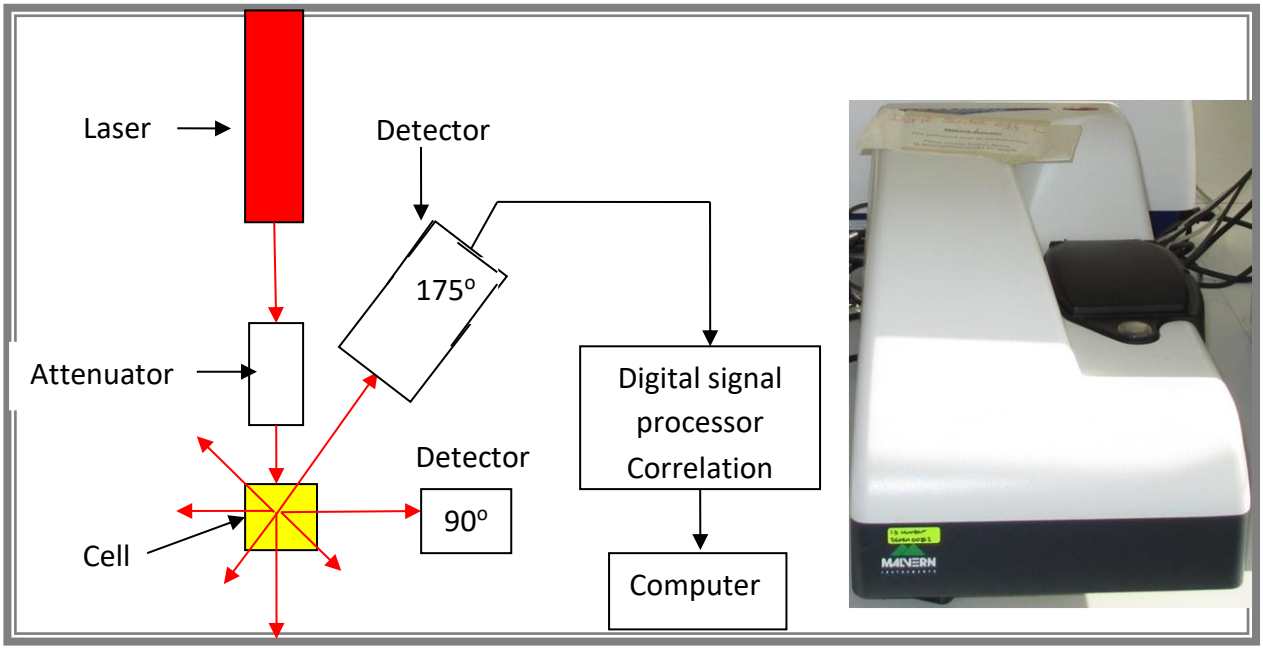

Figure 2-12: Schematic illustrating the principle of the DLS light scattering detection (Azonano.com, 2013) and the DLS Zetasizer nano series, Malvern instruments Ltd. used in this work.

The DLS particle size distribution (PSD) can be obtained in term of intensity, volume or number distribution. The DLS PSD is fundamentally generated as an intensity PSD which can be converted into a volume PSD by using Mie theory that gives the scattering intensity of spherical particles as function of the volume (volume of the sphere is $\frac{4}{3\pi}R^3$, where R is the particle radius) (section 2.4.1.2) (Malvern, 2013). The volume PSD can also be converted to number PSD, but the later has its limits as huge errors might occur if there is a small error on the correlation function's data (Malvern, 2013).

Figure 2-13 presents three graphs showing the number, intensity and volume PSD of a sample containing equal numbers of 5 and 50 nm spherical particles (Malvern, 2013). In the first graph (Figure 2-13, (a)), the PSD is a number distribution constitute of two peaks with equal area due to the (1:1) ratio of the sample composition. In the second graph (Figure 2-13, (b)), in converting the number PSD to a volume PSD, the peak of 50 nm particles becomes 1000 times larger compare to the peak of 5 nm particles and the new ratio is (1:1000) since the 50 nm particles have a volume 1000 times bigger than the 5 nm ones. Finally, in Figure 2-13, (c), the PSD is no converted into an intensity PSD with the area ratio between the two peaks being (1:1000000) due to Rayleigh's approximation of the scattering light intensity.

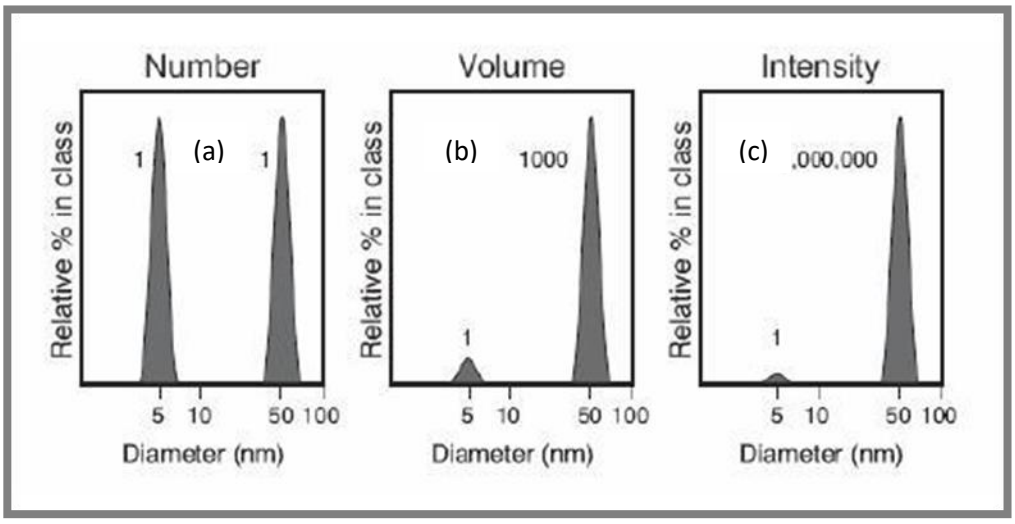

Figure 2-13: DLS measurements of nanoparticle sample constitute of equal numbers of 5 and 50 nm particles: (a) number PSD, volume PSD and (c) intensity PSD (Malvern, 2013, Römer, 2012).

2.4.2.1.2. Zeta potential measurements

With the DLS instrument (Figure 2-12), the ZP (ζ) of NPs in a solution can also be analysed. In general, particles dispersed in a given solution present a surface charge either by ionisation of surface groups, or adsorption of charged molecules/ions (Liese and Hilterhaus, 2013). The ZP comes from the electrical double layer (EDL) that surrounds the particles (Figure 2-14).

The EDL is composed of an inner region (or Stern layer) of the liquid layer that surrounds the particles and an outer layer (or diffuse region). The ionic charge at the Stern layer is opposite to the particle surface charge – for example for a particle with a negative surface charge, the Stern layer will be positive. Within the diffuse layer, the attachment between the ions in the solution and the particle is less strong than within the Stern layer, hence there is a stable entity formed between the ions and the NP with an inside boundary – known as the surface layer of hydrodynamic shear or the slipping plane (Malvern, 2013). The ions at the boundary move with the particle, while the ions beyond the boundary do not follow the particle.

In theory, the ZP is obtained using the theory applied to the electrophoretic mobility (μ_{EP}), in which the mobility of NPs is proportional to both the ZP and radius (r) of the particle (Chun and Lee, 2008). This is described by the Henry equation:

$$\mu_{EP} = \frac{2\zeta\varepsilon}{3\eta} f(kr)$$

Equation 2-12

Where k (m^{-1}) is the Inverse of the EDL thickness, ε (F m^{-1}) is the Dielectric constant or the permittivity of the media and η (kg*m^{-1}*s^{-1} is the Viscosity of the media.

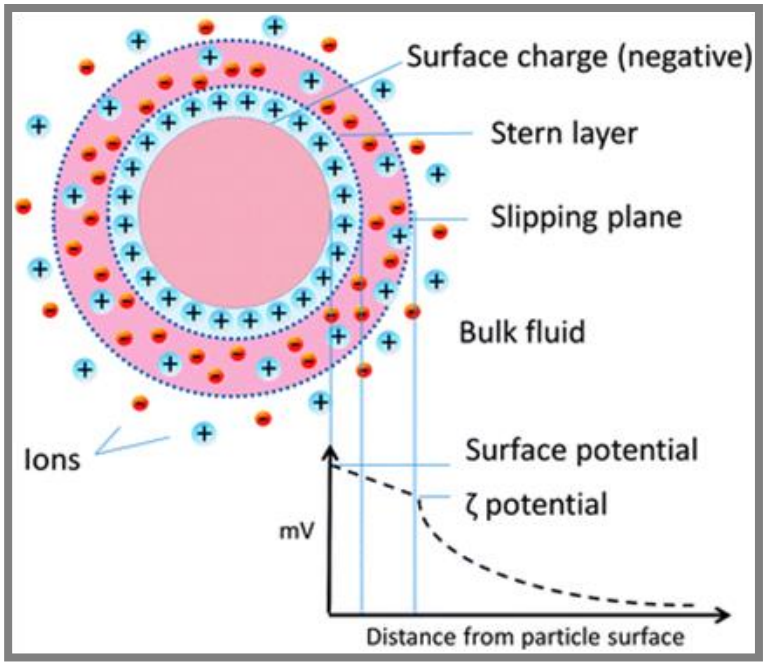

Figure 2-14: Figure 2 12: Schematic representation of ZP (ζ): ionic concentration and potential differences as a function of distance from the charged surface of a particle suspended in a medium (Liese and Hilterhaus, 2013)

2.4.2.2. Asymmetric flow field flow fractionation

FFF is a flow-based chromatography technique used to separate NPs of different sizes in a given sample, using a certain cross flow in the channel and detecting the different size fractions using UV fluorescence (Myers, 1997, Chittleborough et al., 2004, Fabrega et al., 2011).

The FFF particle characterisation is described as follows (Figure 2-15): a given sample of a NP suspension is injected into the FFF channel at a specific volume dependent on the length of the FFF injection loop (a loop of 500 µL volume was used for this thesis). Note that, the lower the concentration of the sample, the longer the loop since a larger volume of the sample is needed to increase the probability of the particles' detection. Once in the channel, the NP

solution mixes with a carrier liquid that drives the solution through to the channel with a constant flow of carrier solution. The application of an external electric field perpendicular to the channel separates the NPs into different specific regions of the channel wall (or accumulation wall) inducing differential retention and separation of the NPs after injection. The NPs are then displaced in the channel at equal velocity to the parabolic flow velocity of the region where they are confined (Schimpf et al., 2000).

In FFF characterisation, NP separation is dependent on the NP size and channel cross flow and their D_H is obtained by UV detection. Assuming one has a solution of NPs which are mainly large, the cross flow should be small in order to have a UV response. Hence the opposite applies to smaller particles for which the cross flow is large. The UV response is a function of the retention time of the particles at a particular location in the channel.

The retention of the particles is defined by a ratio R, Equation 2-13), called retention ratio and is used to relate the retention times t_0 and t_r associated with peak maxima of unretained and retained peaks respectively (Schimpf et al., 2000).

$$R = \frac{t_0}{t_r}$$

Equation 2-13

With:

$$t_0 = \frac{V_0}{F}$$

Equation 2-14

Where V_0 (m^3) is the void volume of the channel corresponding to the unretained or void peak and F (m^3*s^{-1}) is volumetric flow rate.

The particles undergo Brownian motion in the FFF channel, meaning that smaller particles are retained less in the channel longer than larger ones – the smaller particles elute first from the channel followed by the larger particles. The distance between the centre of gravity of the NPs and the accumulation wall, the channel thickness and the characteristics of the NPs – electric field interaction are related to the retention parameter, λ, via the Equation 2-15 (Schimpf et al., 2000):

$$\lambda = \frac{R}{6(1-R)^{1/3}}$$

Equation 2-15

Meaning:

$$R = 6\lambda[coth(1/2\lambda) - 2\lambda]$$

Equation 2-16

In addition the channel thickness (w), and the retention parameter, λ (no SI unit of volume μL), are related by the Equation 2-17:

$$\lambda = \frac{l}{w}$$

Equation 2-17

Where l is the mean layer thickness (in m), defined as:

$$l = \frac{kT}{F}$$

Equation 2-18

Where F is the Electric force applied to the particles.

Because the particles diffuse in the channel with a diffusion coefficient D, the retention parameter, λ, will be dependent not only on the NP size (d_h) but also on their electrophoretic mobility (μ in $m^2*V^{-1}*s^{-1}$) considering that the NPs have a constant charge density. Hence, using Stokes' law or the Nernst-Einstein equation, another equation to determine λ is:

$$\lambda = \frac{D}{\mu E w} = \frac{kT}{3\pi\eta d_h \mu E w} = \frac{kTV_0}{3\pi\eta V_c w^2 d_h}$$

Equation 2-19

Where V_c is the volumetric rate of the crossflow (in m^3*s^{-1}) and E is the electric field (in V m) given by the equation:

$$U = \mu E = \frac{V_c w}{V_0}$$

Equation 2-20

Because FFF is a chromatography technique that separates NPs before they are analysed, the ability of the FFF to separate the particles of an analyte is defined as a measure of the selectivity S_d (Schimpf et al., 2000):

$$S_d = \left|\frac{d(log t_r)}{d(log d_h)}\right|$$

Equation 2-21

Where t_r is the retention time (in s).

The FFF used for this work is an asymmetrical flow-field Flow fractionator (FIFFF) AF2000, from Postnova Analytics (Figure 2-16). The channel accumulation wall is a regenerated cellulose membrane of 1 kDa pore size. The FFF eluent was 10 mM NaCl solution with pH of 7.5 (Römer, 2012), used for the analyte transportation in the channel and to prevent the channel from drying when the machine is not utilised. With a channel flow rate of 1 $mL*min^{-1}$, the cross flow was set depending on the estimated size of the NPs in the analyte and varied from 1 (for citrate Ag-NPs detection) to 2 ml/min (for PEG and PVP Ag-NPs). The amount of sample injected was dependent on how concentrated the sample was (between 0.5 to 3 mL). The obtained UV response, which is a function of the elution time, was used for analyses in which the peak (d_p: Equation 2-22), the number (d_n: Equation 2-23) and the weight (d_w:

Equation 2-24) average D_H and polydispersity of the particles were calculated using the following equations (Baalousha et al., 2008):

$$d_p = \frac{\sum_i C_i X_i}{\sum_i C_i}$$

Equation 2-22

$$d_w = \frac{\sum_i C_i X_i^2}{\sum_i C_i X_i}$$

Equation 2-23

$$d_n = \frac{d_w}{d_p}$$

Equation 2-24

Where C_i is the particle concentration in an FIFFF slice (i) and X_i is the measured characteristic – or D_H in this case (Baalousha et al., 2008).

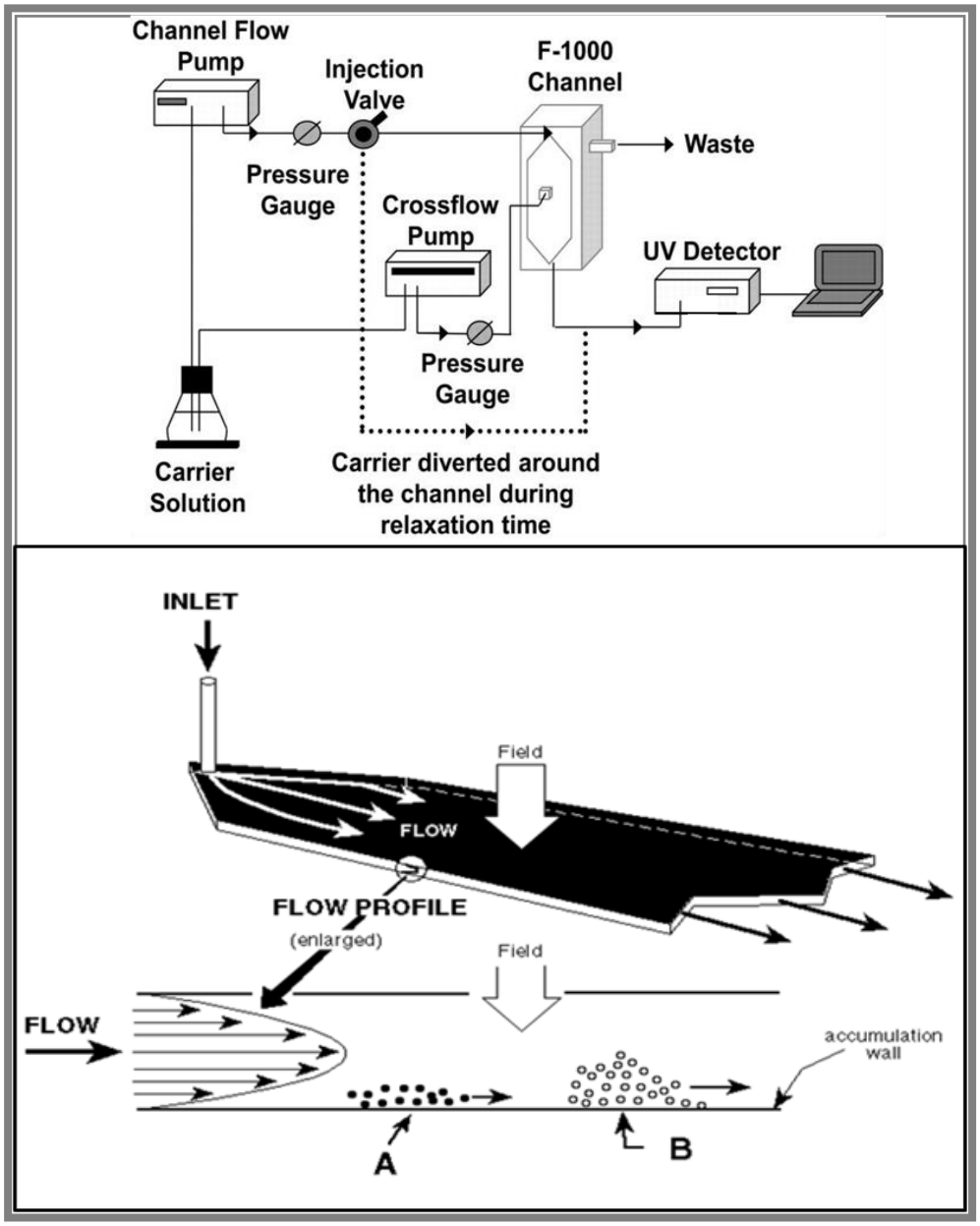

Figure 2-15: Schematic diagram of the FFF (Gimbert et al., 2008) and an illustration of the principle of separation by FFF. Component A is more tightly compressed against the accumulation wall, and is therefore transported more slowly through the channel (Schimpf, 1996).

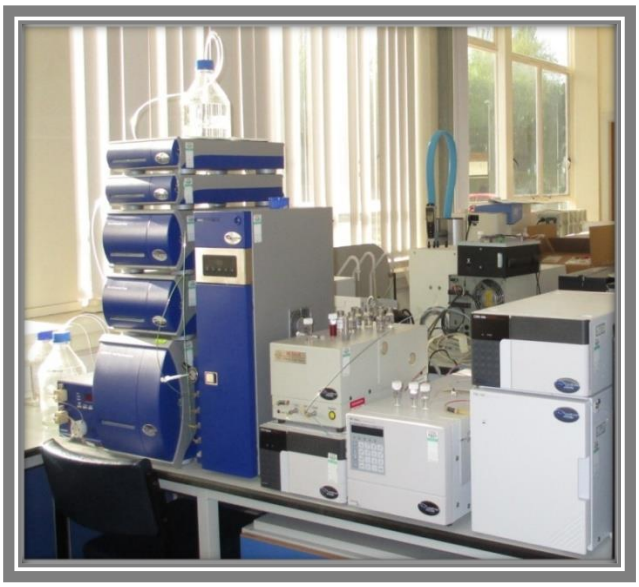

Figure 2-16 : Asymmetrical flow-field Flow fractionator (FIFFF) AF2000, Postnova Analytics.

2.4.3. Electron microscopy (EM)

EM techniques are used for imaging the structure particle size distribution and EDS of the NPs. It allows us to obtain the crystal structure and composition (via EDS) of the samples (Li et al., 2010a, Zhang et al., 2009, Nino-Martinez et al., 2008).

2.4.3.1. Transmission electron microscopy (TEM)

TEM (Wang, 2000) is an imaging technique used to characterise the size and shape of NPs. A TEM instrument is composed of a set of magnetic lenses that manipulate electrons, much in the same way as glass lenses manipulate photons in a light microscope. In TEM, an electron beam of a field emission gun (FEG) passes through the TEM grid and interacts with NPs deposited there (Figure 2-17). The TEM source could be thermionic (Tungsten and lanthanum hexaboride (L_aB_6)), meaning the electrons are emitted from a heated source and accelerated

toward an anode. Or it could be field emitter, in that case, the emission of electrons occurs when an electric field is applied to ignite the source (Lamberti, 2008, Wang, 2000, Bettina Voutou and Stefanaki, 2008).

The electron beam has a small kinetic energy and is accelerated in high-tension through the specimen. According to the particle/wave dualism, for a given electron propagating in the TEM column with charge e, the kinetic energy, E, of the electron is proportional to its accelerating potential, V, and it is described as follow (Elsass, 2006):

$$E = eV$$

Equation 2-25

E can also be written as:

$$E = \frac{1}{2}mv^2 = \frac{1}{2}\frac{h^2}{m\lambda^2}$$

Equation 2-26

With:

$$\lambda = \frac{h}{mv}$$

Equation 2-27

Where m is mass of the electron (in kg), v is the electron velocity (in $m*s^{-1}$), λ is the wavelength associated with the electron ray (in m) and h is the Planck's constant (in $kg*m^2*s^{-1}$).

High resolution with magnitude smaller than the visible range can be obtained with TEM because of the dependence of the wavelength (4 - 0.3 µm) of the electron beam on the acceleration voltage (100 – 1500 kV) (Lamberti, 2008).

The gun deflections are electromagnetic coils (tilts, shifts or stigmators) which help to create a symmetrical and centred beam that passes through the centre of the aperture, C1 (Merrifield, 2008, Hafner, 2011). The TEM has two condenser lenses; the first condenser lens demagnifies the beam and determines the spot size and the second condenser lens controls the focus of the image. The specimen to analyse is placed between the two parts of the objective lenses ensuring the electron beam forms a plane wave when travelling across the sample. The image focused by the objective lenses is projected onto a screen where it can be seen at a human eye because of the deflected beam on the projection lenses. The projected image is recorded by a CCD camera integrated in the TEM and analysed. In addition to the CCD camera, a chemical analysis system can be added to the TEM for electron diffraction characterisation, to give information about the chemical composition of the sample.

The resolution (sub-nanometre level) of the TEM images is related to the C2 aperture size and to the wavelength and spread of the electron beam through the projector screen. Centring the C2 aperture keeps the electron beam around the middle of the projection screen and prevents uneven aberrations (Merrifield, 2008).

The TEMs used for this work are a JEOL 1200 EX II for general TEM imaging and a JEOL 2100 for EDS analysis (Figure 2-18). The JEOL 2100 uses a Tungsten filament as a source, with an energy spread of 1 to 3 keV and operates under a vacuum of 10^{-5} Torr and an acceleration voltage of 80 kV. With these two TEMs, the image contrast of the particles was measured, and the size distribution, shape and surface chemistry of the particles were analysed. The smallest size detected is about 1 nm.

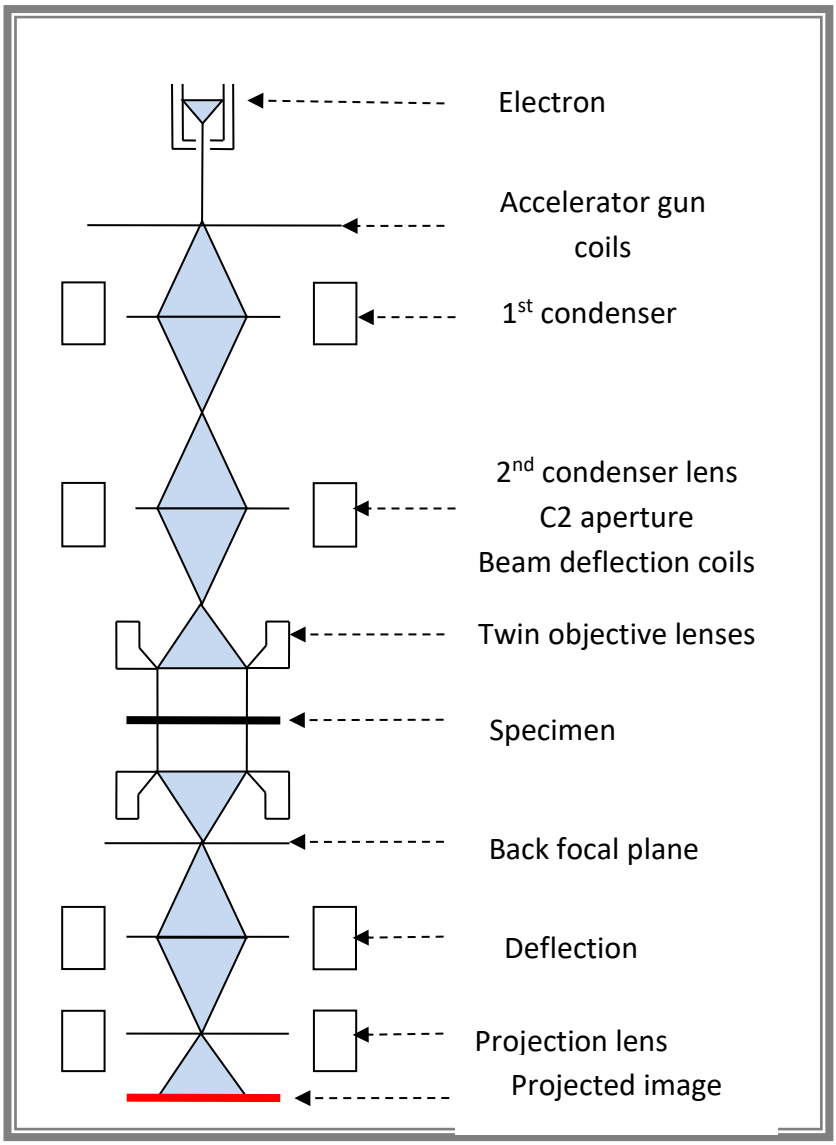

Figure 2-17: principle of image formation in conventional transmission electron microscopy(Williams and Carter, 1996, Merrifield, 2008)

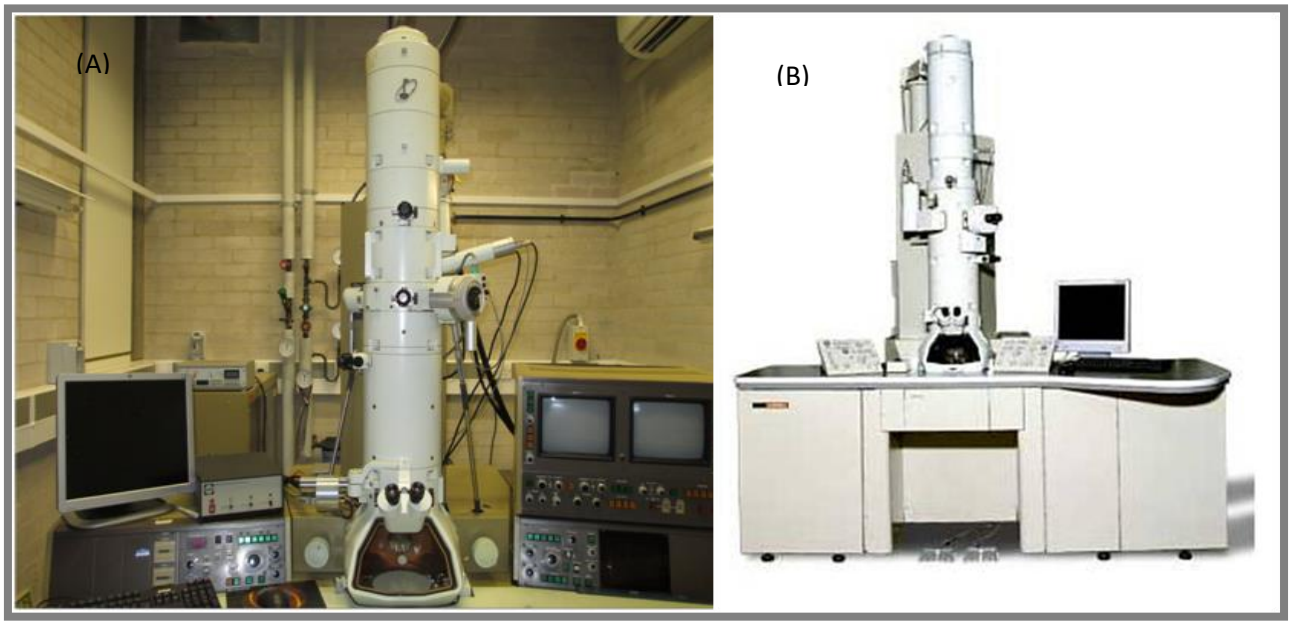

Figure 2-18: Transmission electron microscopes. JEOL 1200 EX II and JEOL 2100 200 kV LaB6 TEM with Oxford INCA EDS. Image (B) was taken from the facility website(UoB, 2014)

2.4.3.2. Energy dispersive spectroscopy: X-ray detection

EDS is a spectroscopy technique integrated into a TEM or SEM and used to detect the X-Ray light emission from the characterised sample. Its principle is based on the excitation of electrons in the inner shell of an atom on the sample by an incident electron of the TEM electron beam which occurs in three steps (Mansfield, Zaluzec, Garratt-Reed and Bell, 2003). The excitation of an inner shell, also known as a K-shell electron, causes the ejection of an electron and formation of a hole in the atom – this primary electron released is accompanied with an inelastic scattering (Figure 2-19). An electron released from the L-shell filled the created hole in the K-shell, but leaves a hole in the L-shell; this process is called distribution – relaxation. The distribution followed by relaxation phase causes an emission of an X-ray photon which can be detected by an X-ray EDS detector for chemical analysis of a particular sample.

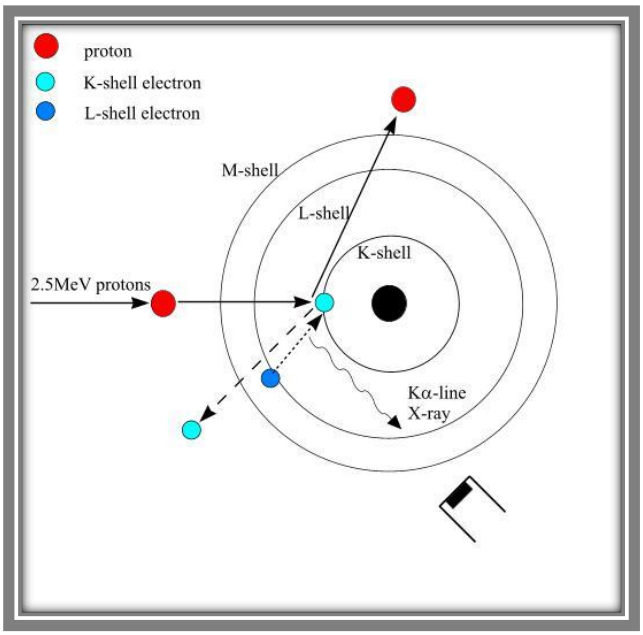

Figure 2-19: X-ray characteristics and EDS detection principle. Taken form (Kernphysik, 2003)

2.4.3.3. Scanning electron microscopy (SEM)

SEM consists of an electron gun (generally a tungsten filament), which generates an electron beam passing through a negative electrode (or anode) under a high voltage of about 15 kV (Figure 2-20). The electromagnetic lenses present between the electrode and the scanning coils help to direct and focus the electron beam at the centre of the sample. The focused beam is a few to tens of nm and is swept through a scanning coil (also called scanning deflector) (Gagnadre et al., 2009). The electron beam is directed through the sample and causes elastic and inelastic collisions with its electrons, producing secondary and backscattered electrons. The two later are detected by two different detectors, and the data are transferred to a monitor for analysis. The SEM used for this work is environmental electron microscope (ESEM) XL30 by Philips which operates at high resolution and under vacuum at a pressure of 10^{-5} Torr.

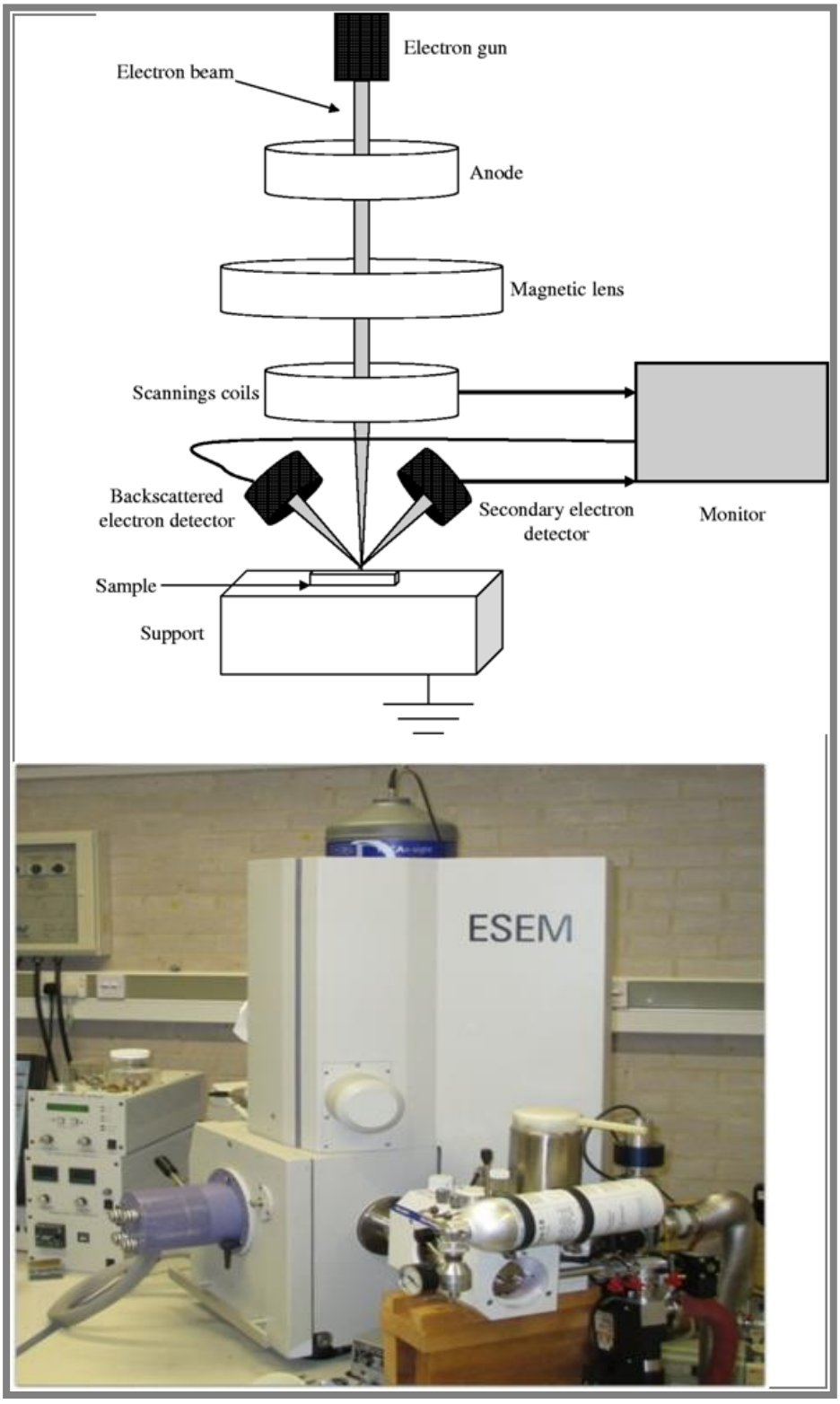

Figure 2-20: Schematic of the basic principle of the scanning electron microscope (Gagnadre et al., 2009) and the Environmental electron microscope (ESEM) XL30 FEG ESEM used in this work

2.4.4. Graphite furnace atomic absorption spectrometry (GFAAS)

GFAAS is used to measure the concentration of a chemical material present in a medium. For our case, it will be silver in sewage. The principle of GFAAS (Figure 2-21) is straightforward and described as follows: analyte solution is dispensed into a cuvette then placed in the autosampler, transferred inside the GFAAS atomisation chamber (or graphite furnace) by auto-sampling. Note the sample to analyse should have the property to absorb an emitted light in the ultraviolet – visible range to be detected (R. García and Báez). The sample is then heated to a very high temperature (of about 2500 °C) and vaporised.

An incident light emission from a lamp source is directed through the displaced sample and interacted with the analyte atoms – silver atoms or ions in this case. The analyte atoms absorb the ultraviolet – visible wavelengths of the emitted light, causing their excitation. As a result, a photon of an energy E is released, due to the removal of an electron from one energy level of the atom to another energy level. The emitted photons passed through a monochromator prism which has pre-selected wavelengths in the UV-Vis range before detection. The data from the detector are read and analysed using the AA Winlab software. The concentration is calculated based on the Beer-Lambert Law (R. García and Báez) that links light absorbance intensity to the analyte concentration (Hardesty and Bassam, 2010):

$$A = \varepsilon \times l \times C$$

Equation 2-28

Where l is the path length of the light (in cm), C is the measured concentration (in mol*L^{-1}) and ε is the molar absorbance coefficient (in L*mol^{-1}*cm^{-1}).

In practice, however, it is difficult to apply the Beer –Lambert law directly to the GFAAS due to variations in atomization efficiency from the analyte matrix, non-uniformity of concentration and path length of the sample atoms (R. García and Báez). Thus, a calibration curve is needed. For our case, we used a solution of 25 ppb of silver ions, acidified with 70% HNO_3 at a concentration of 0.2% as the calibration standard. Seven calibration points were chosen, 0, 1, 2.5, 5.0, 7.5, 10.0, 12.5, and 25.0 with a correlation coefficient of 0.995. Hence, for good analysis results, the sample must be at very low concentration (below 25 ppb). The sample should also have a very low pH ($1 \leq pH \geq 3$) and can be acidified with 0.2% with HNO_3 to achieve this.

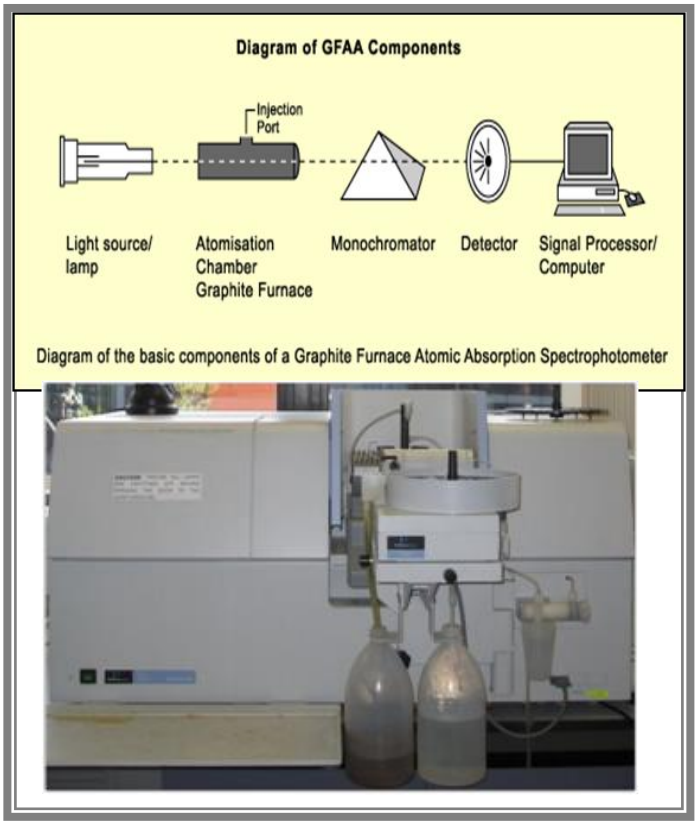

Figure 2-21: Diagram of a graphite absorption spectrophotometer taken from (toolboxes.flexiblelearning.net.au) and photo of the GFAAS used in this work.

Chapter 3 Silver nanoparticles synthesis and characterisation

Chapter Summary

Citrate, PVP) and PEG-SH Ag-NPs were synthesised using the methods described in section 2.1. Their characteristic properties in term of concentration, size, shape, SPR, surface area and surface chemistry were measured using a multiple method approaches applying a range of characterisation techniques (Domingos et al., 2009). These Ag-NPs were used in chapters 4, 5, and 6 investigating their behaviour, accumulation and removal in a SBR plant pilot.

3.1. Introduction

Nanotechnology applied to the environment includes aspects such as fate and transformation of released NPs in the environment from commercial product (Lombi et al., 2014, Keller et al., 2014) and remediation (Araujo et al., 2015, Ni et al., 2016). Hence, the importance of starting with well characterised NPs is crucial for tracking their transformations in the environment. One is required to accurately define the properties of any given particle in term of concentration, size, shape, density and surface chemistry. These properties can then be used to describe the fate, behaviour and toxicity of NPs in the environment.

In this chapter, we described the characterisation of Ag-NPs with similar core size but different capping agents. The Ag-NPs were synthesised chemically in a 'bottom-up' fashion, as described in Chapter 2. In brief, the citrate-capped Ag-NPs were made by reducing silver nitrate with sodium borohydride ($NaBH_4$) and particle growth is stopped and stabilisation effected with sodium citrate (Römer et al., 2011). The PEG-SH and PVP Ag-NPs were obtained by recapping the citrate Ag-NPs respectively with PEG-SH and PVP (Tejamaya et al., 2014); these processes are described in detail in section 2.1.2. The characteristics of the Ag-NPs were measured including: concentration (GFAAS analysis), D_H of the NPs (using DLS and FFF), their core size and shape factor (by TEM), their chemical characteristics (by EDS for chemical composition) and the surface charge (or ZP using DLS). All Ag-NP solutions were filtered with a 100 nm pore size membrane (section 2.1.3) before any characterisation was performed.
The sample preparation was dependent to the characterisation used. For UV-Vis and DLS samples respectively, 1 and 5 mL of Ag-NP filtrated solution were carefully placed in the DLS or UV-Vis cuvette for analysis. For TEM and EDS measurements, the samples were prepared

by using the drop method (section 2.3.3.2). For FFF characterisation, 0.5 to 3 mL of each Ag-NP filtrated solution was injected into the FFF channel (section 2.4.2.2). Finally, GFAAS samples were obtained using the method described in section 2.3.3.4.

3.2. Analysis of concentration of Ag in the Ag-NPs

The Ag-NPs were made and purified as described in section 2.1.2. The yield from each NP synthesis/re-capping process was measured by estimating of the total silver concentration in the Ag-NPs' suspension before and after the Ag-NPs were washed (see below).

The citrate Ag-NPs were synthesised with 100 mL of $AgNO_3$ (42.47 $mg*L^{-1}$), 100 mL of sodium citrate (80 $mg*L^{-1}$) and 6 mL of $NaBH_4$ (378.4 $mg*L^{-1}$). The PVP and PEG-SH Ag-NPs (Tejamaya et al., 2012) were obtained by recapping the later with 3% PVP and 500 PEG-SH respectively. According to the values above, the expected Ag-NP concentration is 26.97 $mg*L^{-1}$ after synthesis and ultrafiltration (section 2.1.3) of the NPs, since the atomic mass of Ag is known to be 107.87 $g*mol^{-1}$ (Housecroft and Constable, 2010). However, Table 3-1 shows that not all Ag^+ was reduced into Ag-NPs and that some ions may have remained after synthesis and were removed during the washing process.

The concentration of the Ag-NPs was measured using GFAAS, and the corresponded sample preparation method described in section 2.4.4, and the concentration of Ag-NPs was found to be 11.58 $mg*L^{-1}$ for the citrate Ag-NPs, 10.93 $mg*L^{-1}$ for PVP Ag-NPs and 10.31 $mg*L^{-1}$ for PEG Ag-NPs (Table 3-1). Thus, many silver ions (14.24 $mg*L^{-1}$) did not transform into Ag-NPs during synthesis of the citrate NPs and further losses occur when the Ag-NPs were recapped

with PVP and PEG-SH. Thus, the Ag-NPs may undergo some dissolution during recapping as the citrate capping agent left to make place for a new one. Ag-NPs became ionised first, then stabilised with the new capping agent. Both processes occur very quickly. Also, because Ag has the tendency to adhere to any surface material such as glass (Schneid et al., 2015) it comes into contact with; these losses may be related to the Ag-NPs binding to the ultrafiltration cell's wall, the magnetic stirrer and the filter during the washing process.

Table 3-1: Ag concentration (in Ag-NPs) ($mg*L^{-1}$) after synthesis and recapping, as determined by GFAAS

Ag-NPs	Concentration ($mg*L^{-1}$)	% yield
Citrate Ag-NPs	11.58 ± 1.06	42.94 ± 3.93
PEG Ag-NPS	10.31 ± 0.97	38.23 ± 3.59
PVP Ag-NPS	10.93 ± 1.15	40.53 ± 4.26

3.3. UV-Vis spectroscopy: SPR characterisation on the NPs

Most metallic NPs possess the unique feature of a SPR which causes absorption of light in the UV-visible part of the electromagnetic spectrum giving them colours that are distinctive. These absorption bands are only attributed to NPs and do not show up in larger metal particle dispersions or in metal salt solutions (Lead and Smith, 2009). Ag-NPs have a sharp characteristic absorption band in the 350-500 nm range (Lead and Smith, 2009) and the appearance of the UV-Vis peak of Maximum Absorbance (MA) is determined by the size and coating of the NPs(Manikandan et al., 2003, Bastus et al., 2014).

The UV-Vis spectra of the NPs (Figure 3-1) were measured in the wavelength range 290 – 600 nm. The citrate-capped Ag-NPs exhibit a maximum absorption at 386 nm (Table 3-2). Their recapping with PVP or PEG-SH causes a red shift (Tejamaya et al., 2014) in the absorption peak

to 392 and 396 nm for PVP Ag-NPs and PEG Ag-NPs respectively (Table 3-2), probably due to their increase in size (Ashkarran and Bayat, 2013) since the large PVP and PEG-SH molecules are now attached to the particles surface.

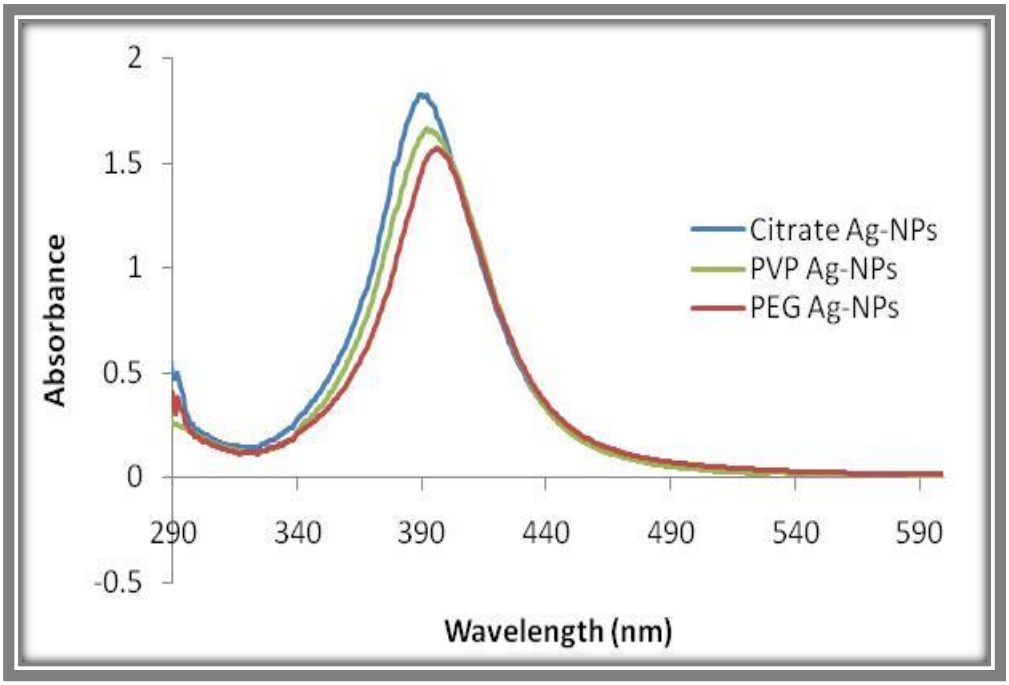

Figure 3-1: UV-Vis absorbance spectrum of citrate (blue curve), PVP (green curve) and PEG (red curve) capped Ag-NPs.

The full width at half maxima (FWHM) of the spectra were determined for all three Ag-NPs and are 49 nm, 51 nm and 48 nm for citrate, PVP and PEG respectively. Based on Mie's theory in which the absorption coefficient of a spherical particle is a function of the refractive index, volume and SPR wavelength of the particles (Manikandan et al., 2003), it was demonstrated in the literature that the average size of the particles is linked to the FWHM by the Equation A2 - 1. In this equation, the FWHM is inversely proportional to the particle size, meaning it is expected to be wider or narrower if the particle size decreases or increases, relative to the initial particles (i.e. to the citrate-capped Ag-NPs in this case).

Using the citrate Ag-NPs as the reference, the percentage of peak shift between of the PVP Ag-NPs was 1.55 % and 2.59 % for PEG-SH Ag-NPs:

$$Percentage of the peak shift = \frac{\lambda_{max}(given\ Ag-NPs) - \lambda_{max}(citrate\ Ag-NPs)}{\lambda_{max}(citrate\ Ag-NPs)} \times 100$$

Equation 3-1

The maximum absorbance (MA) it is related to the concentration of the NPs and its decrease reflects the loss of Ag-NPs that occurred during the recapping process. In fact, the reduction of the NPs MA is a characteristic of the NP size reduction due to their dissolution (Peng et al., 2010). With citrate Ag-NPs used as reference Equation 3-2, the percentage of the MA decreased (%MAD) between citrate and PVP Ag-NPs was 5.14 % and between citrate and PEG-SH Ag-NPs was found to be 10.28 %.

$$\%MAD = \frac{MA(given\ Ag-NPs) - MA(citrate\ Ag-NPs)}{MA(citrate\ Ag-NPs)} \times 100$$

Equation 3-2

Table 3-2: Surface plasmon properties of citrate, PVP and PEG capped Ag-NPs results

	Citrate capped Ag-NPs	PVP capped Ag-NPs	PEG capped Ag-NPs
λ_{max} (nm)	386	392	396
MA	1.75	1.66	1.57
MAD (%)	0	5.14	10.28
FWHM (nm)	49	51	48
Percentage of the peak shift (%)	0	1.55	2.59

3.4. Ag-NPs Hydrodynamic diameter

3.4.1. Dynamic light scattering measurements

DLS measurements present the D_H (section 2.4.2.1.1) distribution of the NPs against their scattering light intensity. The average diameter or Z-average of the three Ag-NPs is shown in Figure 3-2. The citrate-capped NPs have a Z-average of 20.3 ± 0.3 nm and are mono-dispersed due to their low polydispersity index (PDI) (Table 3-3). By recapping these Ag-NPs with PVP or PEG-SH, their D_H increased to 30.4 ± 0.5 nm and 39.3 ± 1.3 nm for PVP and PEG-SH, respectively, with a slight increase of the PDI.

DLS measures the D_H by utilising the Rayleigh scattering diffraction pattern from each NP when illuminated with coherent light. Series of these patterns are taken over a period of time and compared. Because of the Brownian motion of the NPs, each diffraction will be slightly different from the previous one. From this, the D_H of the NPs can be deduced using the Stoke-Einstein equation (Equation 2-11). This technique has some drawbacks:

(1) it is assumed that each NP is a spherical hard object (Shaw, 2014);

(2) larger NPs scatter significantly more than smaller ones since the intensity of light scattering is proportional to the radius: $I \propto R^6$(Li et al., 2012b);

(3) it is assumed that the temperature is stable and there are no currents due to temperature gradients;

(4) all NPs are small enough to undergo Brownian motion, and no NPs are settling;

(5) the D_H is dependent on the core size of the particle, its surface structure (or coating) and on the ionic concentration of the media surrounding it (Shaw, 2014);

(6) also, in the case of a polydisperse sample where the intensity distribution of the particles has more than one distinct peak, the Z-average value does not represent the average size of the NPs since even a smaller number of larger NPs can overpower the intensity of smaller NPs. So, in addition to the intensity distribution, the volume distribution and the number distribution of the particles are also considered(Tomaszewska et al., 2013).

In this study, the first condition does not apply fully, in the case of the PVP capped Ag-NPs since the change of particle coating affected their diffusion speed, hence their apparent size was also affected (Shaw, 2014). Therefore the D_H was overestimated because of their soft external shell, which can also be highly hydrated, and hence polydispersity increases.

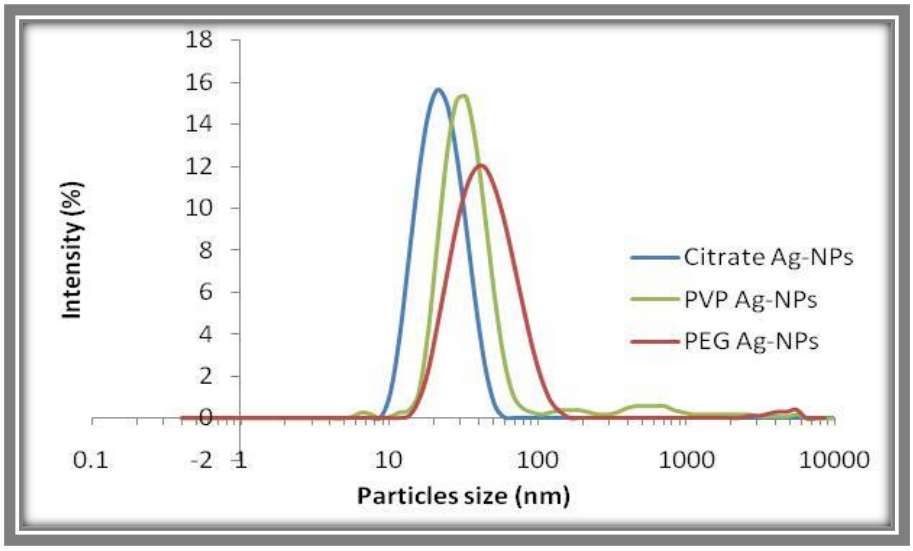

Figure 3-2: Particle size distribution (diameters) of citrate (blue curve), PVP (green curve) and PEG (red curve) capped Ag-NPs plotted as a function of their scattering intensity measured by DLS.

Table 3-3: Average diameter of citrate, PVP and PEG capped Ag-NPs, measured by DLS

	Citrate capped Ag-NPs	PVP capped Ag-NPs	PEG capped Ag-NPs
Z-Average (nm)	20.3 ± 0.3	30.4 ± 0.5	39.3 ± 1.3
PDI	0.12 ± 0.01	0.25 ± 0.01	0.20 ± 0.02
Peak size (nm)	23.1 ± 0.6	33.5 ± 2.5	47.2 ± 2.2

In addition, because the intensity distribution of PVP Ag-NPs has more than one peak, we applied the sixth condition by looking at their volume and number distributions instead of the z-average in order to estimate their average D_H. Table 3-4 shows that a volume of about 98% of PVP Ag-NPs had average diameter of 33.5 ± 2.5 nm, with a scattering intensity of about 91%. Since the intensity distribution had more than one peak, the diameter at maximum intensity in peak 1 was chosen as the average diameter of the PVP Ag-NPs instead of their z-average.

Table 3-4: PVP capped Ag-NPs: Average D_H, percentage of intensity, volume and number of particles corresponding to each peak particle distribution measured by DLS.

	D_H (nm)	% Intensity	% Volume	% Number
Peak 1 (nm)	33.5 ± 2.5	91.16 ± 5.16	97.75 ± 1.67	100.0 ± 0.0
Peak 2 (nm)	1285.1 ± 1674.6	8.56 ± 5.42	1.79 ± 1.70	0.0 ± 0.0
Peak 3 (nm)	510.7 ± 1444.6	0.28 ± 0.78	0.48 ± 1.34	0.0 ± 0.0

3.4.2. Field flow fractionation (FFF) characterisation

The D_H of the NPs obtained by FFF is shown in Table 3-5. The Ag-NPs capped with citrate, PVP and PEG-SH have an average diameter of 11.2, 42.0 and 28.9 nm respectively. The peak size (or particle diameter) at MA was 10.4, 27.9 and 19.4 nm for the citrate, PVP and PEG Ag-NPs.

The difference in diameter was related to the changes of NPs surface during recapping, which affect their diffusion speed – hence the D_H will also change (Shaw, 2014). Also, the way PVP molecules lay on Ag-NP surface will decrease or increase the diffusion speed of the particles whether they were lying flat or straight (Shaw, 2014) (Figure 3-3). So in our case, because the average diameter of PVP Ag-NPs was bigger than the average diameter PEG-SH Ag-NPs, of we may suggest that PVP molecules lay straight on the Ag-NP surface, while PEG-SH molecule may lay flat. All three have a very low polydispersity (between 1.20 and 1.3) meaning there was little to no agglomeration (Table 3-5).

Table 3-5: Average diameter of Ag-NPs capped citrate, PVP and PEG-SH measured by FFF

	Citrate capped Ag-NPs	PVP capped Ag-NPs	PEG capped Ag-NPs
Average diameter (nm)	11.2 ± 4.9	42.0 ± 3.4	28.9 ± 3.7
Peak size (nm)	10.4 ± 0.4	27.9 ± 1.5	19.4 ± 0.2
PDI	1.25 ± 0.00	1.27 ± 0.01	1.31 ± 0.02

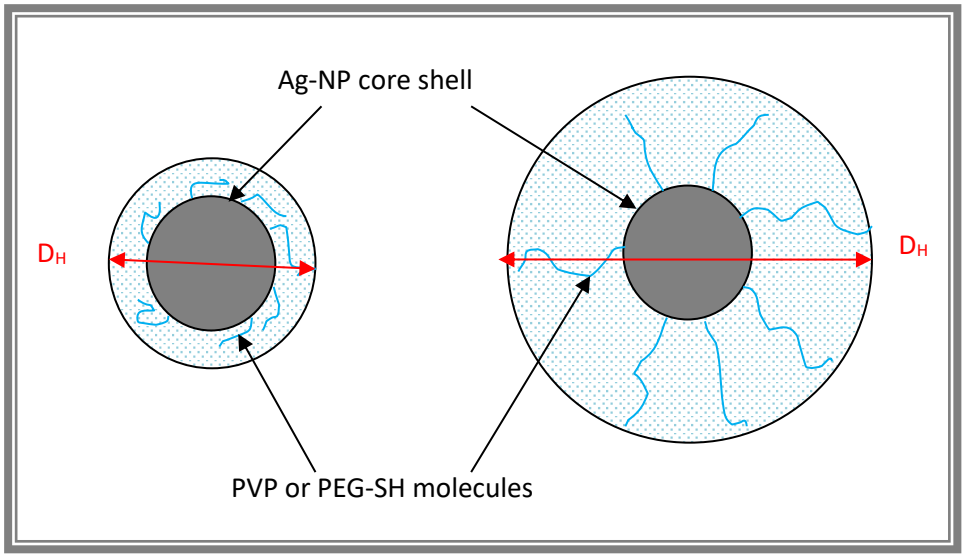

Figure 3-3: illustration of the D_H of PVP and PEG –SH Ag-NPs depending to their surface structure (Shaw, 2014).

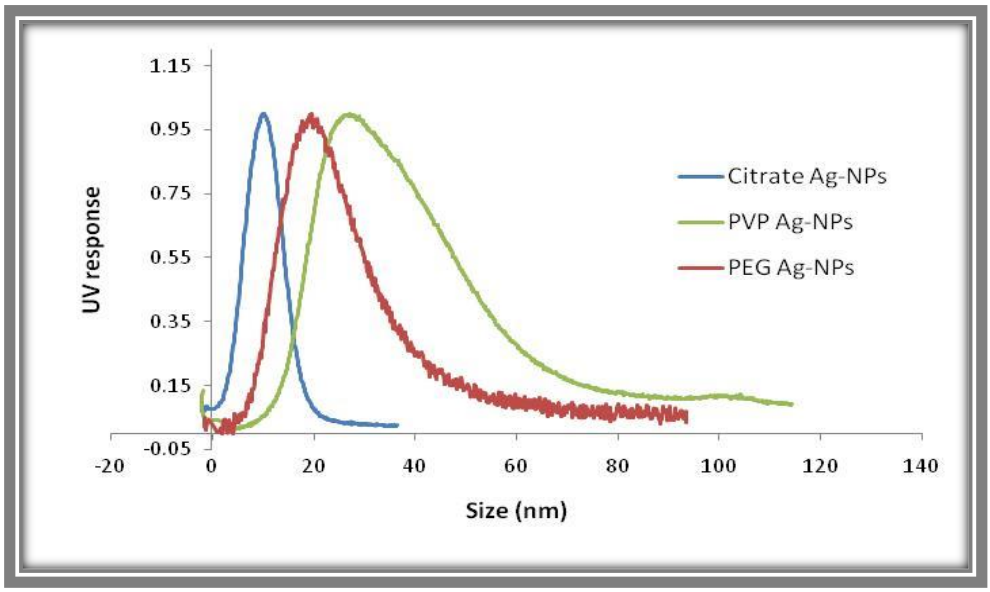

Figure 3-4: Particle size distribution (diameters) of citrate (blue curve), PVP (green curve) and PEG (red curve) capped Ag-NPs as a function of their UV-response (or UV absorbance), measured by the FFF.

3.5. Determination of the particles core-shell size distribution

3.5.1. Transmission electron microscope characterisation

The Ag-NPs were characterised using a JEOL 1200 transmission electron microscope (TEM). Representative images of the Ag-NPs their associated size distributions (base on > 200 NPs) are shown in Figure 3-4. The particle core size does not significantly change with either capping agent. This is confirmed by measuring about 200 Ag-NPs of each type of capped Ag-NPs and giving their shortest and longest lengths (Table 3-6). The values shown in the table were obtained using ImageJ to analyse the TEM images. ImageJ gives the NP shortest and longest lengths, along with their specific surface area and circularity or shape factor. The diameter (D) of the NPs is related to the area (A) by the Equation 3-3(DuneSciences, 2011):

$$D = 2\sqrt{\frac{A}{\pi}}$$

Equation 3-3

The diameter values show that recapping the Ag-NPs with PEG and citrate does influence their overall size.

Table 3-6: TEM mean diameter of citrate, PVP and PEG-SH capped Ag-NPs

	Citrate Ag-NPs	PVP Ag-NPs	PEG Ag-NPs
Shortest length (nm)	8.8 ± 4.8	9.9 ± 4.0	9.6 ± 4.6
Longest length (nm)	11.7 ± 6.4	12.3 ± 5.4	12.4 ± 6.2
Diameter (nm)	9.4 ± 4.9	10.6 ± 4.4	10.4 ± 5.0

3.5.2. Shape factor

The shape factor (α) is the surface area ratio of a non-spherical NP (S') to a spherical NP (S) with same volume (Qi and Wang, 2005):

$$\alpha = \frac{S'}{S} and S = 4\pi R^2$$

Equation 3-4

Where R is the particle radius (in nm).

According to the Equation 3-4, a perfect spherical particle will have a shape α = 1 and for a non-spherical particle 1< α > 1 (Qi and Wang, 2005). In this study, all three Ag-NPs can be considered as mostly spherical with their average shape factor being above 0.8 (Table 3-7). The histogram of the NP shape factor distribution is illustrated in Figure 3-6 with more than

80% of citrate Ag-NPs having $\alpha \geq 0.8$, and at least 90% of PVP Ag-NPs or PEG-SH NPs have their shape factor equal 1.

Table 3-7: Shape factor of the Ag-NPs capped with citrate, PVP or PEG-SH

Ag-NPs	Shape factor
Citrate Ag-NPs	0.81 ± 0.16
PVP Ag-NPS	0.96 ± 0.05
PEG Ag-NPS	0.96 ± 0.06

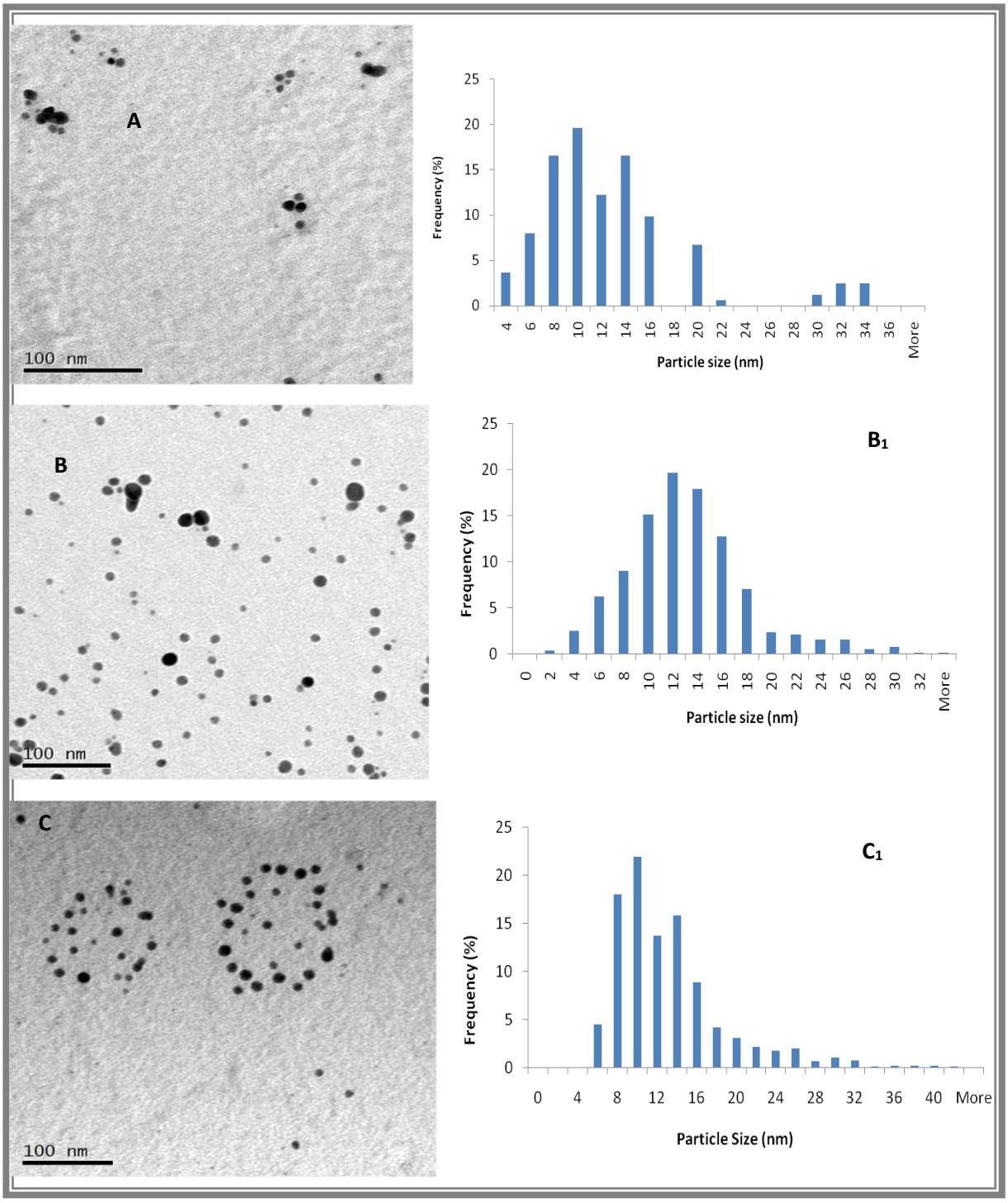

Figure 3-5: (A), (B) and (C) TEM images of citrate, PVP and PEG capped Ag-NPs; (A_1), (B_1) and (C_1) are the particle size distributions (diameters) of the corresponding Ag-NPs when their longest length it is measured (based on > 200 NPs).

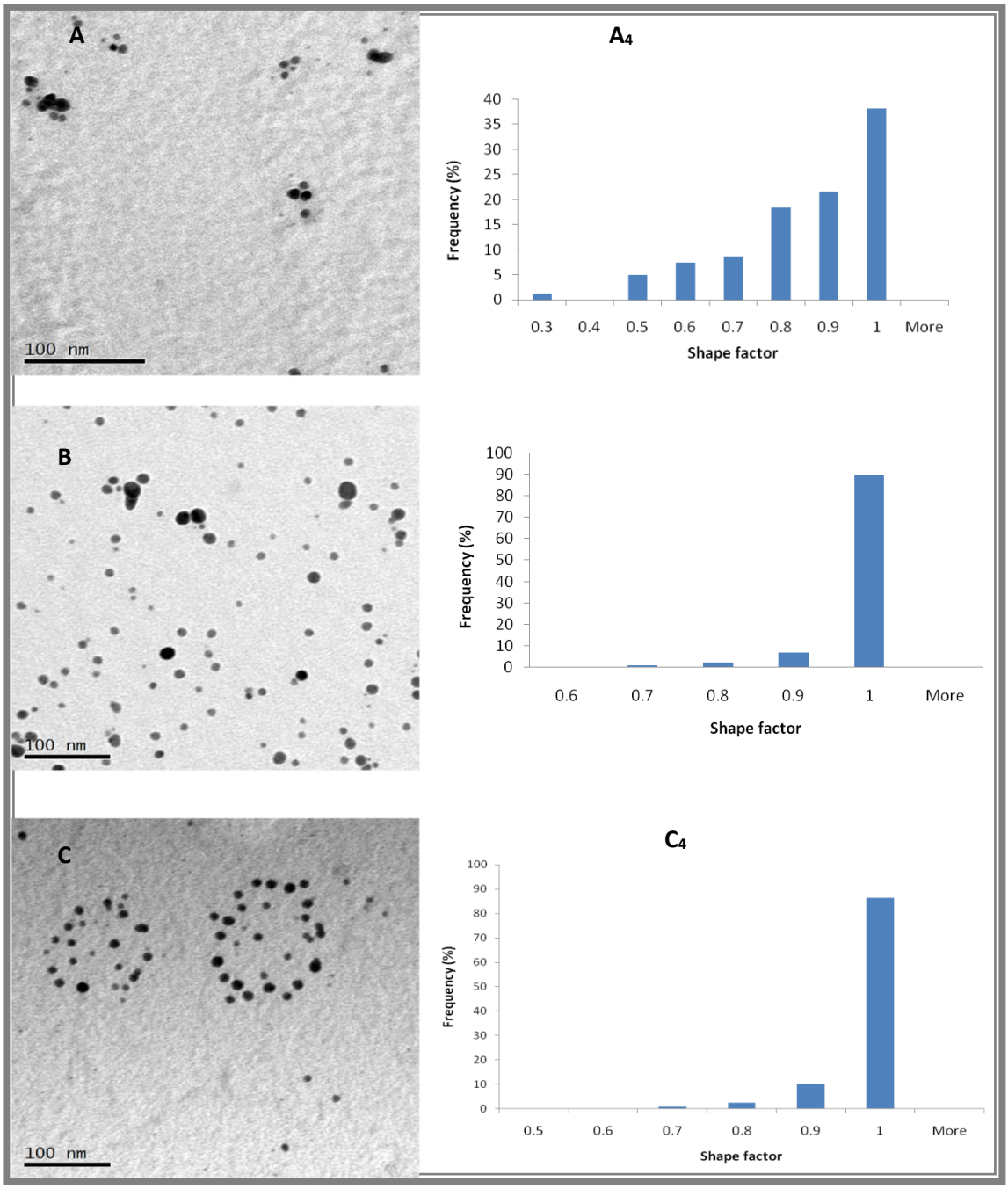

Figure 3-6: (A), (B) and (C) TEM images of citrate, PVP and PEG capped Ag-NPs; (A_4), (B_4) and (C_4) are the shape factor distributions of the corresponding particles (based on > 200 NPs).

3.6. Surface analysis of Ag-NPs

3.6.1. Zeta potential (ZP) analysis of surface charge

The ZP (section 2.4.2.1.2) is a parameter representing the particle charge and indicates their stability in the solution in which they are suspended (Singh et al., 2014). ZP is the name given to the potential at the hydrodynamic slipping plane and represents the magnitude of the electrostatic interactions between the particle surface charge (or Helmholtz layer) and the surface charge of the medium surrounding the particle (Lead and Smith, 2009, Salgin et al., 2012, Singh et al., 2014). The distance between the surface of the ionic layer and the particles surface is limited by a boundary (or slipping plane) beyond which ionic charges in the medium do not diffuse with the particle (Escubed, 2011).

The ZP value of the citrate, PVP and PEG Ag-NPs were -37.80 ± 1.42 mV, -8.57 ± 0.88 mV and -13.2 ± 1.5 mV respectively (Table 3-8). Based on the definition of the ZP, the above results show that citrate capped Ag-NPs which are known to be electrostatically stabilised (El Badawy et al., 2010) were highly stable as their ZP was less than -25 mV (nanoComposix, 2012). However, the high values of PVP and PEG-SH Ag-NP ZP does not mean that they were less stable than the citrate Ag-NPs since the ZP is not significant for sterically stabilised NPs (El Badawy et al., 2010). The polymer surrounding the particle cores prevent them from coming into contact with one another. Hence the stability related ZP of NPs is dependent on the type of capping. Tejamaya et al., (2012) have shown that PVP and PEG-SH Ag-NPs were found to be more stable than citrate ones when dispersed in medium with different ionic strength or pH.

Table 3-8: ZP of the various Ag-NPs

Ag-NPs	ZP (mV)
Citrate capped Ag-NPs	-37.8 ± 1.4
PVP capped Ag-NPs	-8.6 ± 0.9
PEG capped Ag-NPs	-13.2 ± 1.5

3.6.2. EDS characterisation

EDS analysis was conducted on the various Ag-NPs to confirm their chemical composition. Figure 3-7 shows the EDS spectrum of citrate, PEG-SH, and PVP-capped Ag-NPs with the corresponding TEM images. Silver was the most predominant element present in all 3 spectra with a high-intensity peak. The elements C, Cu, (Fe) and Si were from the TEM grid itself, with carbon (C) coming from the support, copper (Cu) because of the TEM grid was in copper and silica (Si) is a common contaminant in microscopes from the vacuum grease. The presence of iron (Fe) was also most likely due to cross-contamination from previous samples of other users of the TEM.

It is important to note that the PEG-SH Ag-NPs spectrum has a prominent peak of sulphide which comes from PEG-SH: whose structure is shown in Figure 3-8.

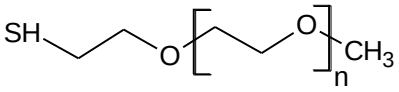

Figure 3-7: molecular structure of poly(ethylene glycol) methyl ether thiol (PEG-SH)

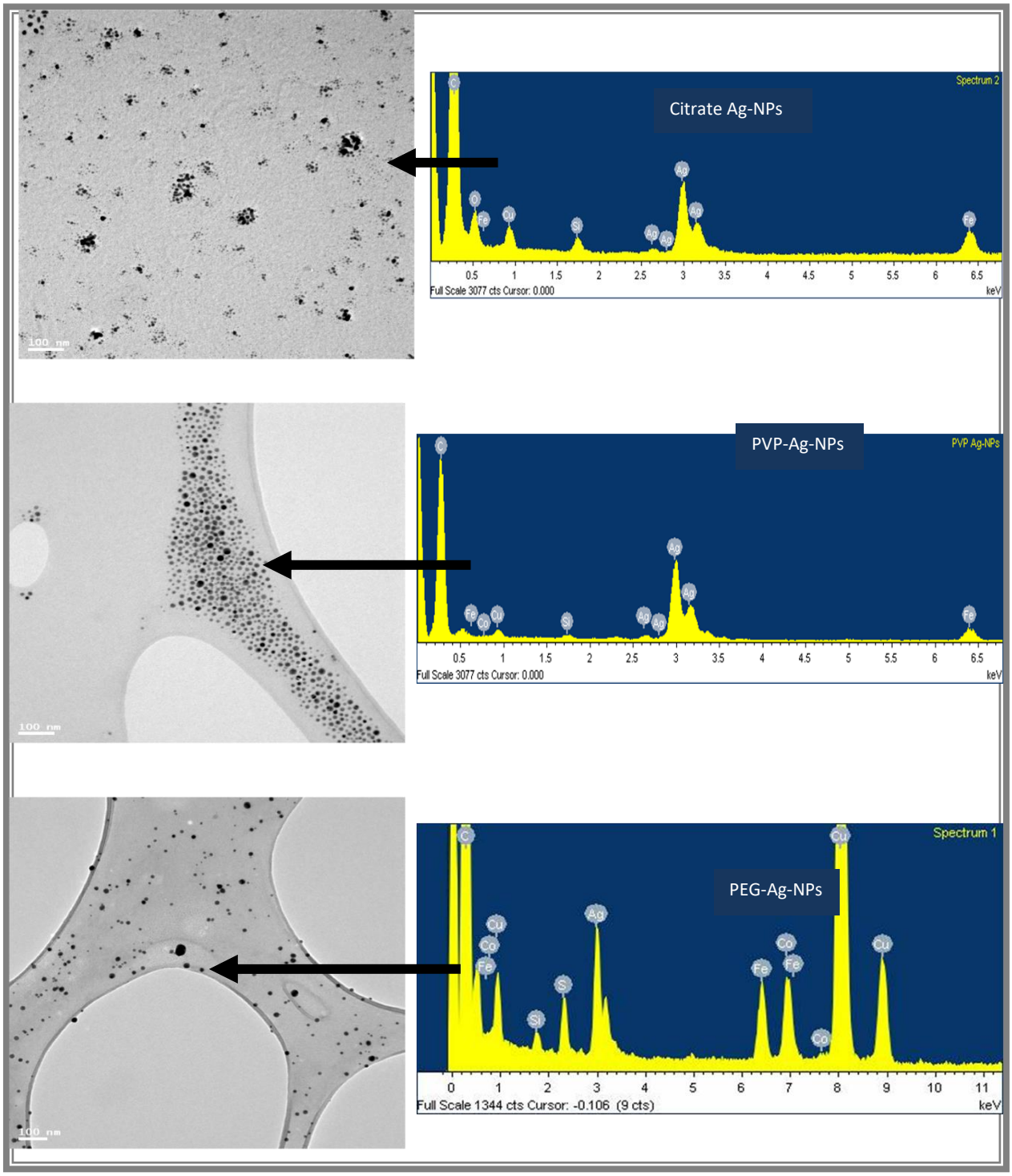

Figure 3-8: EDS results of Ag-NPs capped with citrate, PVP or PEG-SH

3.7. Discussion and conclusion

In this chapter, it has been shown that the total silver concentrations of the Ag-NPs capped by citrate, PEG-SH or PVP are 11.8, 10.2 and 10.6 $mg*L^{-1}$, respectively. The lower Ag values of PEG-SH and PVP Ag-NPs may be due to the recapping process that includes washing the citrate NPs by ultrafiltration for the removal of ions and ultrafiltration of the Ag-NPs again after the recapping. So the loss in silver after the recapping was 12.92% for PEG-SH Ag-NPs and 9.52% for the PVP ones.

The D_H(z-average) measured by DLS in Milli-Q water of citrate Ag-NPs, was 20.3 nm with a very low PDI (0.12), suggests there was no aggregation and are stable because their ZP was high (-37.8 mV) indicating good electrostatic stabilisation (nanoComposix, 2012). By recapping (Tejamaya et al., 2012) these Ag-NPs with PEG-SH or PVP, the average diameter increased to 39.3 nm for PEG-SH Ag-NPs and 33.5 nm for the PVP, confirming the presence of a hydrated polymer shell around NPs. The Ag-NPs remained relatively stable with little to no aggregation or agglomeration during the recapping as demonstrated by their low PDI. Thus, the PEG-SH (-13.2 mV) and PVP (-8.6 mV) Ag-NPs were sterically stabilised and display very low surface charge.

The D_H was also measured using FFF. The resulting data were different to the DLS results. For citrate Ag-NPs, the FFF average diameter (11.2 nm) was similar to the TEM average diameter of the Ag-NPs. For the PEG-SH Ag-NPs, the FFF average diameter (28.9 nm) was a bit lower than their DLS Z-average and considerably high in comparison with the citrate Ag-NPs FFF average diameter. This was the result of the large polymer coating of the particle as shown in

Figure 3-3. Similar conclusions could be made for the PVP Ag-NPs (Table 3-9). The FFF average diameter of PVP Ag-NPs was higher than the DLS D_H, which was different to what was expected. This might be due to the instrument not working properly at the time of the measurement, and the poor retention flow may have affected the UV response of the particles. Indeed, the FFF average diameter of PVP Ag-NPs (42.0 nm) may have corresponded to the average diameter of Ag-NPs dimers. However, this was not detected by the DLS or TEM.

The TEM results show that all three particle types have similar core size; this means that the recapping of the citrate Ag-NPs with PVP or PEG-SH does not have a particular effect on their core size. Also, all three particle types tend to remain spherical with a shape factor above 0.8 (based on counting > 200 NPs per NP type).

Table 3-9: Summary of the optical, physical and chemical characteristics of the citrate, PVP and PEG-SH capped Ag-NPs

	Citrate Ag-NPs	PVP Ag-NPs	PEG Ag-NPs
Ag-NPs concentration ($mg*L^{-1}$)	11.76	10.64	10.24
λ_{max} (nm)	392	393	396
DLS Z-Average diameter (nm)	20.3 ± 0.3	33.5 ± 2.5	39.3 ± 1.3
PDI	0.12 ± 0.01	0.25 ± 0.01	0.2 ± 0.02
FFF diameter (nm)	11.2 ± 4.9	42.0 ± 3.4	28.9 ± 3.7
TEM Average diameter (nm)	11.7 ± 6.4	12.3 ± 5.4	12.4 ± 6.2
ZP (mV)	-37.8 ± 1.4	-8.6 ± 0.9	-13.2 ± 1.5
Shape factor	0.81 ± 0.16	0.96 ± 0.05	0.96 ± 0.06

In conclusion, one could note that the recapping of citrate Ag-NPs with PEG-SH or PVP has no effect on their core size and shape, but has affected their surface chemistry and charge in the diffuse layer (or ZP) (Table 3-9).

For further work in this thesis, citrate and PVP were chosen for the investigation of the behaviour, fate and transformation of Ag-NPs in a sewage treatment plant. PVP capped Ag-NPs were chosen over PEG capped Ag-NPs because they were used the most in the scientific literature and due to their high stability level (Tejamaya et al., 2012).

Chapter 4 Stability of Ag-NPs in OECD SYNTHETIC SEWAGE (OECDSS)

Chapter Summary

In this chapter, the effect of the individual components of the OECDss (OECD, 2001) on the physical and chemical behaviour of Ag-NPs capped with citrate and PVP were investigated, to provide baseline understanding prior to the study in the complete OECD synthetic sewage (Chapter 5). The Ag-NPs were described in Chapter 3, where their synthesis and characterisation was given.

The OECDss was analysed using several standard testing methods that are usually applied to testing domestic sewage water (section 2.2.3) and was used to simulate the properties of domestic wastewater. The stability of the particles in each individual component of the OECDss was observed using DLS and TEM for Ag-NPs size distribution, UV-Vis for SPR and average size analysis and ZP and concentration measurements by GFAAS for chemical compositions. The obtained results show specific changes of Ag-NPs in individual OECDss and help to make assumptions on how the Ag-NPs react in the more complex sewage system used in later chapters.

4.1. Introduction

Understanding the behaviour of Ag-NPs in sewage has been of great interest in recent years due to their increased production and application utilising their antibacterial properties (Morones et al., 2005). Fate and behaviour research has focussed on their ability to transform into silver sulphide(Kim et al., 2010) and their toxicity in the pristine and modified states (Fabrega et al., 2011). Moreover, the presence of Ag-NPs in a multitude of consumer products including textiles (Benn and Westerhoff, 2008a), washing machines (Farkas et al., 2011) and cosmetic products (Kokura et al., 2010) plays a significant role in their release into sewer systems. The instability of citrate and PVP Ag-NPs in wastewater systems has been well established in a recent study (Kaegi et al., 2013). Kaegi et al. (2013) have shown that citrate and PVP Ag-NPs with an average core size of 10 and 100 nm were transformed into AgCl and Ag_2S depending on the environmental conditions of the treatment plant. Their 10 nm Ag-NPs citrate and PVP particles had the same size range and coating as the particles used in our case. According to Navarro et al. (2008) and Xiu et al. (2011), amorphous carbon coated Ag-NPs (of about 35 and 25 nm respectively in size) were found to dissolve with a continuous release of silver ions (Ag^+) under aerobic condition (Yang et al., 2012, Xiu et al., 2012).

In recent years several studies on the stability of Ag-NPs in media such as standard OECD media for Daphnia species toxicity, in stock solution (i.e. .during storage) and in carrier solutions such as acetone, ethanol, deionised water (DIW) have been reported (Tejamaya et al., 2012, Tilaki et al., 2006, Pinto et al., 2010). In all these studies, the media were chosen in order to look at the optical and physical properties and aggregation, agglomeration and sedimentation of Ag-NPs. Other studies include the stability of Ag-NPs in $CaCl_2$ and NaCl media

(DIW supplemented with these salts) (Huynh and Chen, 2011, Li et al., 2012a), in $MgSO_4$ media (DIW supplemented with that salt) (Baalousha et al., 2013) and proteins (Tai et al., 2014, Martin et al., 2014). In these studies, changes in the size and shape (aggregation and dissolution), kinetic, surface charge and plasmon resonance of the Ag-NPs were reported and the dissolved Ag ions toxicity (Li et al., 2010a, Fabrega et al., 2011) was observed. Since observation of the physicochemistry and optical properties when assessing Ag-NPs stability are crucial, it has also been suggested that there is a lack of knowledge of the complex mechanisms of Ag-NPs behaviour in colloidal systems (Tai et al., 2014) which this chapter addresses.

4.1.1. Aims and objectives

The complexity of the OECDss medium makes it difficult to understand the physical and chemical mechanisms that occur when spiked with citrate or PVP-capped Ag-NPs. Hence, we have chosen to look at the stability of both Ag-NPs in each constituent of the OECDss (peptone, meat-extract, urea, K_2HPO_4, NaCl, $CaCl_2$ and $MgSO_4$) individually in order to understand their impact on the Ag-NPs. The experimental conditions considered include the aeration and settling steps, which are similar to the SBR treatment plant functions (section 2.3.1). The objectives of the work presented in this chapter were to:

- Characterise samples collected from the various media spiked with Ag-NPs after 0 and 24 hrs before aeration, at 45 hrs during aeration and finally at 48 hrs during settling, using GFAAS, UV-Vis, DLS and TEM to determine interactions/drivers of Ag-NP change.

- ❖ Analyse changes in Ag-NP concentration, size, and surface chemistry of the citrate and PVP Ag-NPs in the media and determine whether the observed effects were the result of agglomeration or dissolution.

4.2. Materials and Methodology

4.2.1. OECD synthetic sewage components and their ionic strength

The OECDss composition is given in Section 2.2.2.1. For this study, 500 mL of each medium (i.e. peptone, meat-extract, urea, K_2HPO_4, NaCl, $CaCl_2$ and $MgSO_4$) was prepared with the weight of each chemical being proportional to 1/20 of if their weight needed to make 10 L of the OECDss (Table 2-1). The ionic strength of the synthetic sewage salt components was calculated using the Equation 4-1 (Solomon, 2001):

$$I = \mu = \frac{1}{2}\sum C_i Z_i^2$$

Equation 4-1

Where C_i (in mol*L^{-1}) and Z_i are the ionic concentration and the valency on the ion respectively. The ionic strength is described in units that are the same as concentration (in mol*L^{-1}). Table 4-1 shows the ionic strength of the salts in OECDss.

Table 4-1: Values of ionic strength of the salts in the OECDss

Chemical compound	Concentration C_i (mM)	Ionic strength I (mM)
K_2HPO_4	0.161	0.482
NaCl	0.120	0.120
$CaCl_2$	0.036	0.108
$MgSO_4$	0.017	0.066

The concentrations of the components are all relatively low with K_2HPO_4 having the highest ionic strength and $MgSO_4$ being the lowest. Due to the variation in ionic strength of the salts, the Ag-NPs may remain stable, agglomerate or dissolve. These possible stated of the NPs were investigated in this chapter.

4.2.2. Dispersion of the particles in OECD synthetic sewage (OECDss) and its constituents

500 $\mu g*L^{-1}$ Ag-NPs capped with citrate or PVP were spiked into 500 mL of the OECDss medium and its individual constituent solutions. The suspensions were kept at room temperature for 24 hours and then aerated for 21 hours. Finally, the aeration was switched off, and they were allowed to settle for 3 hours. This mimics the sewage treatment conditions used in a SBR plant (Morgenroth et al., 1998). A small amount of each sample was collected and characterised from each suspension at 0, 24, 45 and 48 hours to trace the changes of the Ag-NPs during each stage. Figure 4-1 and Figure 4-2 show the experimental setup used, for citrate and PVP-capped Ag-NPs, respectively. Pictures were taken on day 1 after 24 hrs stored at room temperature (A_1, A_3 for citrate Ag-NPs, A_5 and A_7 for PVP Ag-NPs) and at 45 hrs, before the end of the aeration (A_2, A_4 for citrate Ag-NPs, A_6 and A_8 for PVP Ag-NPs). The suspensions were analysed using UV-Vis, DLS and ZP, and TEM.

To measure the total silver concentration in the media through time, 5 ml of each medium containing Ag-NPs was collected and acidified with 20% nitric acid. Samples collected at 0 hrs, 24 hrs, 45 hrs and 48 hrs were measured using GFAAS. To trace the dissolved silver concentration ((Kreibig and Genzel, 1985)) in the media, 7 ml of each solution was ultrafiltrated at 50,000 rpm and 10 °C for two hours using an ultracentrifuge angle rotor (rotor

70Ti) from Beckman Coulter. The ultrafiltrated samples were acidified with 2 % HNO_3 as it assumed no Ag-NPs remains in the solution. Thus, a concentration of 2% acid was enough to acidify the samples prior their analysis and then diluted to 0.2% according to the measurement criteria of the GFAAS (section 2.4.4).

Please note that no replicate was conducted during this work, making it impossible to assess the recovery of Ag concentration using the GFAAS. Loss of Ag that occurred during the centrifugation, because of Ag-NPs sticking property, could have been measured by GFAAS. To do so, every material that was used should have been rinsed with 20% HNO_3 at the end and the total Ag content determined by diluting the obtained solution to 2% HNO_3. Additionally, a silver nitrate control could have been run to assess the % recovery following centrifugation. To overcome this, we estimate the possible loss of Ag-NPs by subtracting each measurement of the total Ag concentration from the initial one (total Ag concentration at 0 hrs).

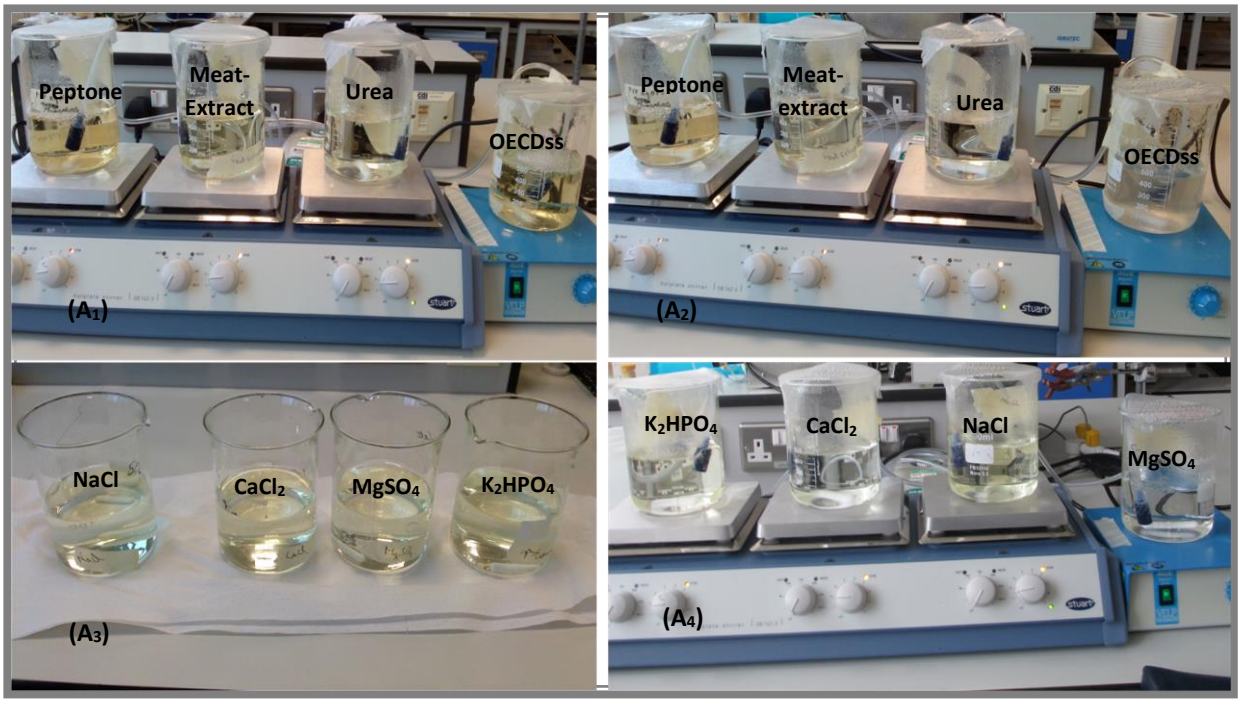

Figure 4-1: Photos of the experimental set-up: (A1) and (A2) – Citrate Ag-NPs in OECDss, peptone, meat-extract and urea respectively at 24 hrs and 45 hrs; (A3) and (A4) – citrate Ag-NP in K_2HPO_4, NaCl, $CaCl_2$, $MgSO_4$ and urea respectively at 24 hrs and 45 hrs.

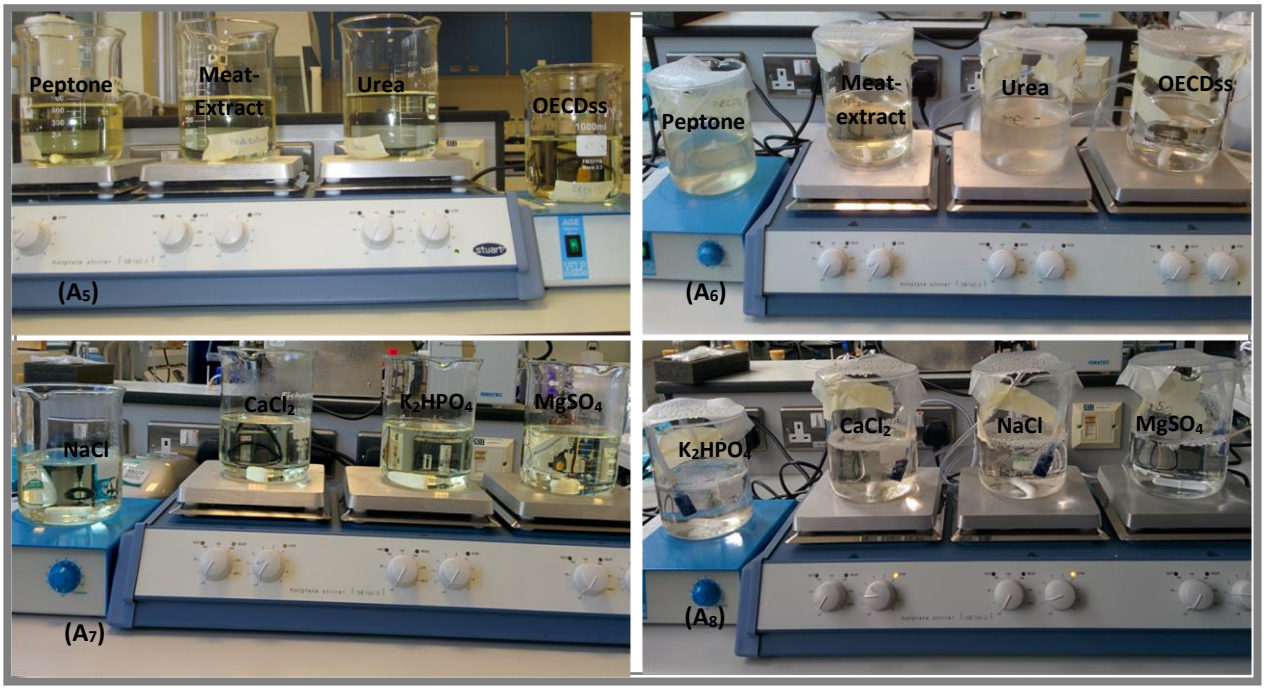

Figure 4-2: Photos of the experimental set-up: (A_5) and (A_6) – PVP Ag-NPs in OECDss, peptone, meat-extract and urea respectively at 24 hrs and 45 hrs; (A_7) and (A_8) – PVP Ag-NPs in K_2HPO_4, NaCl, $CaCl_2$, $MgSO_4$ and urea respectively at 24 hrs and 45 hrs.

4.2.3. Measurement of the Particles by UV-Vis (see Appendix A3-1)

The average diameter of the particle (D) was determined using three equations deducted from Mie theory and the Drude model (section 2.4.1.2 and appendix 0). The UV-Vis particle size was obtained using $Model_1$ (Equation A2 - 1), $model_2$ (Equation A2 - 3) and $model_3$ (Equation A2 - 7) and associated results are given and discussed in the (appendix A3-1).

4.2.4. DLS measurements

Because of the existence of the multiple peaks in the DLS NPs size distribution for all media, the z-average measurement would not be considered, and the NPS D_H would be represented by the average size of the scattering signal primary peak size.

4.2.5. Settling velocity of the Particles

To describe the settling velocity or settling time of the Ag-NPs, Stokes' law equation (Chakraborti and Kaur, 2014) as written below was used.

$$V_s = \frac{g}{18}\left(\frac{\rho_s - \rho_w}{\mu}\right) D^2$$

Equation 4-2

Where ρ_s is the density of the Ag-NPs (10490 kg*m^{-3}), ρ_w is the density of water (1000 kg*m^{-3}), g is the gravity (9.81 m*s^{-2}), μ is the dynamic viscosity of water (1.14*10^{-3} kg*m^{-1}*s^{-1}) and D the diameter of the Ag-Nps (m).

The settling time of the NPs in each media was deducted, knowing that NPs can settle over a distance of 7 cm in the beaker.

4.2.6. ZP of the Particles

The ZP of NPs is defined as the magnitude of the electrostatic interactions between the particle charges and the ionic charges of the solution (Salgin et al., 2012). Note that variation of pH is influenced by the dissociation of existing functional groups in media, associated with ion absorption (Salgin et al., 2012), which can affect the ZP of the Ag-NPs. The ZP potential can be calculated using Equation 4-3:

$$\lambda_D = \sqrt{\frac{\varepsilon_0 \varepsilon_r k_B T}{2\rho e^2}} = \frac{1}{\sqrt{8\pi\lambda_B \rho}} = \frac{0.308}{\sqrt{I}}$$

Equation 4-3

Where I is the Ionic strength of the medium (mol*L^{-1}), λ_B is the Bjerrum length (in m), ε_r Dielectric constant of the water, ε_0 is the dielectric constant of the vacuum (8.85 *10^{-12} F*m^{-1}), k_B is the Boltzmann constant (J*K^{-1}), T is the absolute temperature (in K), ρ is the density of the added salt in the media 9 in kg*$^{-1}$) and e is the electrical charge of an electron (in C).

4.2.7. Statistical analysis

To identify statistically the differences existing between citrate and PVP-capped Ag-NPs in each medium; the statistical two-way analysis of variance (ANOVA) without replica was used to compare the mean values of the particle concentration, DLS size, TEM size and ZP. The details of the one-way ANOVA are given in Appendix A3-3, and the same principles are applied to the two-way analysis.

4.3. Results and discussions

4.3.1. Citrate and PVP Ag-NPs in peptone medium

The peptone used in the study is a milk type protein purchased from Sigma-Aldrich (SigmaAldrich). Milk peptone or proteose-peptone (PP) is a complex mixture of peptides which are mostly produced by the action of indigenous plasmin (also known as indigenous proteinases) and indigenous milk (Fox et al., 2015). Bovine proteose peptone 3 (PP3) is a heat-stable, acid soluble and indigenous milk protein (phosphoglycoproteine) and is synthesised in the mammary gland (Fox et al., 2015). The bovine PP3 structure is formed of 135 amino acids and has hydrophobic behaviour due to its amphiphillic α-helix structure formed by peptide bonds, with one side being hydrophilic and the other side hydrophobic (Fox et al., 2015).

Figure 4-3 illustrates the possible interactions of peptone proteins with the Ag-NPs. Due to their amphiphillic structure, peptone molecules might be bound to citrate and PVP Ag-NPs forming surface activity or a corona layer (Livney, 2010) on their surface. Another possibility is to have the peptone proteins covering the particles through binding hydrophobic caused by hydrophobic interaction and Van Der Waals attractions (Livney, 2010).

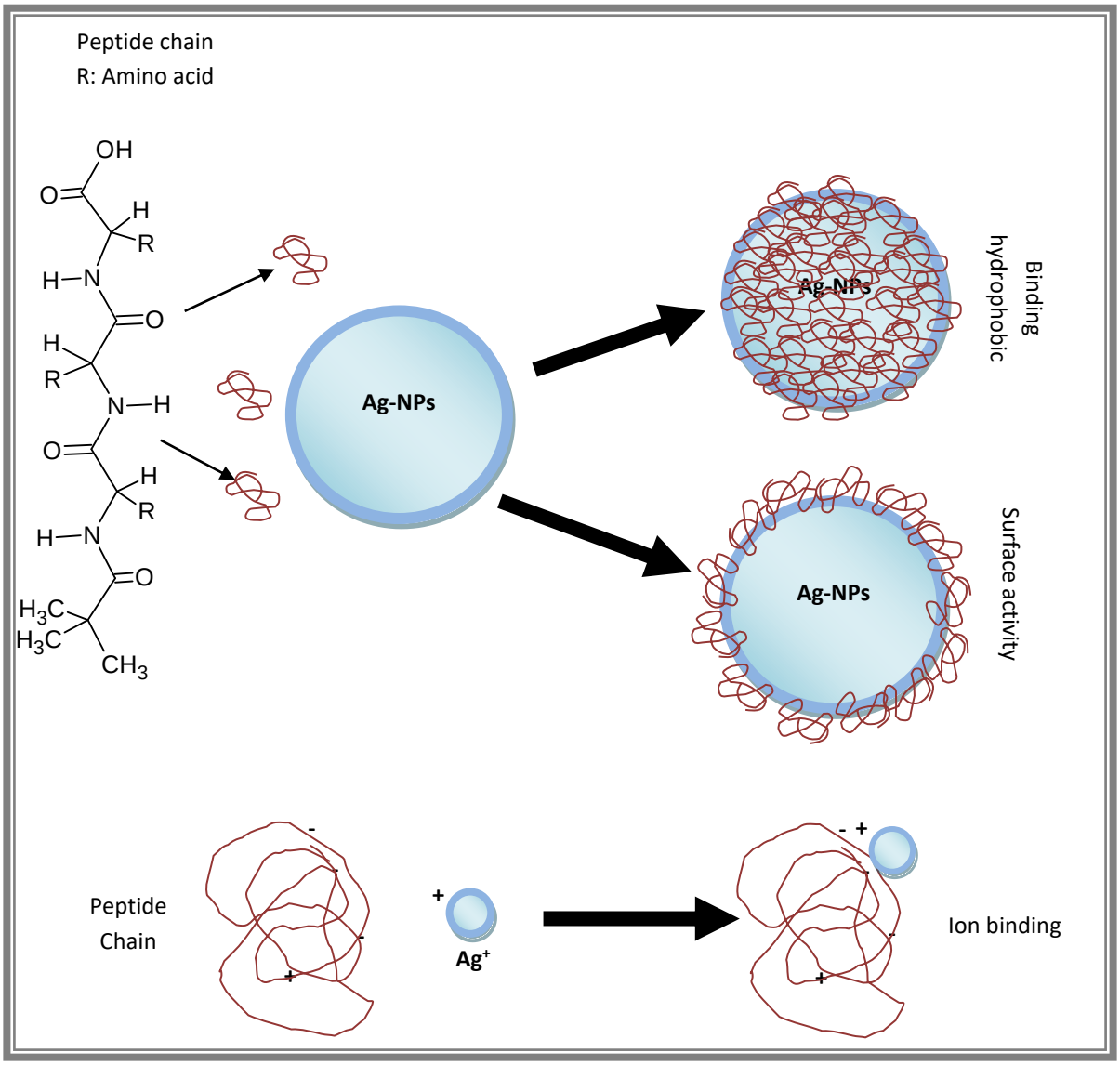

Figure 4-3: Illustration of the Ag-NPs with milk peptone proteins: binding hydrophobic molecules (through hydrophobic interactions, Van Der Waals attractions or hydrogen bond), surface activity (due to the protein amphiphilic structure) and ion binding (Livney, 2010, Milkfacts.info, 2016).

4.3.1.4. Dissolution study: silver concentration in peptone

Table 4-2 shows the variation in silver concentration ((Saha et al.)) as well as the percentage of dissolved silver (Ag^+) when citrate or PVP Ag-NPs were dispersed in 160 $mg*L^{-1}$ of peptone medium. At 0 hrs, the total concentration of Ag in peptone for both citrate and PVP Ag-NPs were similar. There was a significant reduction in the total Ag concentration of PVP Ag-NPs with time which may not have been a consequence of their dissolution but caused by their

sorption onto the glass surface and aeration tube. The percentage of the unrecovered particles was 7% for the citrate particles versus 12.57% for the PVP particles (Table 4-2). Also, the dissolved percentage Ag of PVP Ag-NPs was increased with time, reaching a percentage of 46.60% at the end of the experiment; whereas only about 6.28% of the total citrate Ag-NPs concentration was Ag^+ ions. Meaning, in the presence of peptone, citrate Ag-NPs were more stable in peptone medium and due to their lower sensitivity to dissolution and sorption than the PVP Ag-NPs.

There was no significant difference between the variations of Ag concentration, %dissolved Ag (%diss. Ag) and %unrecovered (%unr. Ag) of citrate and PVP Ag-NPs overtime and at a specific time point (STP) **(**Table A3 - 18). Thus, the changes in the concentration of Ag-NPs in peptone were independent to their coating. From the above results, we may observe that PVP particles were the most affected by the exposure with nearly half of their corresponded total Ag at 48 hrs being Ag^+ (Table 4-2), while only 6.28% of the citrate total Ag was Ag^+. Thus we may conclude that the behaviour of Ag-NPs in the peptone media in terms of dissolution is independent of their coating and to the aeration flow.

Table 4-2: Changes in Ag concentration when citrate and Ag-NPs were dispersed in 160 mg*L^{-1} peptone at 0 hrs, 24 hrs, 45 hrs (during aeration) and 8 hrs (during) settling as measured by GFAAS.

	Citrate Ag-NPs in peptone			PVP Ag-NPs in peptone		
	$C_{Total\ Ag}$ (µg*L^{-1})	%Diss. Ag	%Unr. Ag	$C_{Total\ Ag}$ (µg*L^{-1})	%Diss. Ag	%Unr. Ag
0 hrs	616.7 ± 19.1	3.8 ± 0.1	0	613.2 ± 5.5	1.1 ± 0.1	0
24 hrs	612.1 ± 30.3	5.1 ± 0.2	0.75	425.0 ± 51.5	23.3 ± 0.9	14.57
45 hrs	600.3 ± 58.2	5.8 ± 0.3	2.70	373.4 ± 3.9	40.5 ± 2.1	14.42
48 hrs	573.6 ± 41.4	6.3 ± 0.5	7.00	365.7 ± 10.4	46.6 ± 1.3	12.57

4.3.1.5. UV-Vis characterisation of citrate and PVP Ag-NPs in peptone

When citrate (Figure 4-4 (B_{1a})) and PVP (Figure 4-4 (B_{1a})) were first dispersed in peptone (at 0 hrs) a red shift of the spectrum occurred (compared to the pristine particles) and the MA (λ_{max}) in both cases was 398 nm (Table 4-3). Citrate and PVP Ag-NPs might have their surface chemistry changed with a similar mechanism as they were coated with peptone proteins. At 24 hrs, λ_{max} remained constant in both cases, but the MA of the Ag-NPs was decreased with a spreading in the PVP Ag-NPs FWHM, possibly due to their interaction with peptone molecules which might be bind to the particle surface. As for the citrate Ag-NPs, they seemed to have been affected mostly by their dissolution which was lower compared to the PVP Ag-NPs ones (Table 4-3) and may not have agglomerated or bound with the peptone. There may have been a reaction between the PVP and peptone in the PVP Ag-NPs suspension such as the formation a surface activity (or corona layer) or hydrophobic binding at the NPs surface (Figure 4-3), that suppressed the agglomeration or dissolution effect of the NPs (Tai et al., 2014). And as a consequence, there was a spreading of the UV-Vis peak.

During aeration at 45 hrs, the MA of citrate Ag-NPs decreased, and a red shift (λ_{max} = 402 nm) and spreading of the corresponded UV-Vis spectrum was observed. Meaning, the aeration process may have caused the agglomeration of citrate Ag-NPs and changed their surface chemistry. For the PVP Ag-NPs however, λ_{max} (= 399 nm) was constant, meaning that after the initial alteration during the first stage, their surface chemistry was essentially unaffected by the aeration. Also, there was little to no agglomeration of the PVP Ag-NPs occurring during that phase since the FWHM of the UV-Vis signal was constant, as expected due to the steric stabilisation by PVP.

After the settling phase (at 48 hrs), the λ_{max} and the FWHM of citrate Ag-NPs UV-Vis signal remained constant. Hence, in the presence of peptone and aeration, citrate-capped Ag-NPs may have gone through two transformations. First, they could have agglomerated as well as having a corona of proteins from the peptone formed at their surface (Shannahan et al., 2013), which might have changed their surface chemistry and second, they may have oxidised and dissolved when the aeration flow was applied. For the PVP Ag-NPs, it can be deduced that their surface chemistry went through similar changes as the citrate Ag-NPs when they were first introduced in the peptone solution and no further changes were observed on their surface chemistry throughout the process.

There was a significant difference of the MA changes overtime between of citrate and PVP Ag-NPs, but not at a STP; also no significant difference was found in λ_{max} variations overtime or at a STP between citrate and PVP Ag-NPs (Table A3 - 19). Thus the changes in the MA of Ag-NPs in peptone were dependent to their coating. However, the variations of λ_{max} between both particles were not.

Table 4-3: UV-Vis parameters (extracted from curves in Figure 4-3) from citrate and PVP Ag-NPs in 160 mg*L^{-1} peptone at 0 hrs, 24 hrs, 45 hrs (during aeration) and at 48 hrs (during settling).

	Citrate Ag-NPs in peptone				PVP Ag-NPs in peptone			
	0 hrs	**24 hrs**	**45 hrs**	**48 hrs**	**0 hrs**	**24 hrs**	**45 hrs**	**48 hrs**
λ_{max} (nm)	398	399	402	401	398	398	399	399
MA	0.067	0.062	0.054	0.052	0.062	0.040	0.042	0.039
Absorbance Decreased (%)	0	7.46	19.40	22.39	0	55.00	47.62	58.97
FWHM (nm)	69	76	133	131	55	110	109	127
Peak shift (%)	0	0.25	1.00	0.75	0	0	0.25	0.25

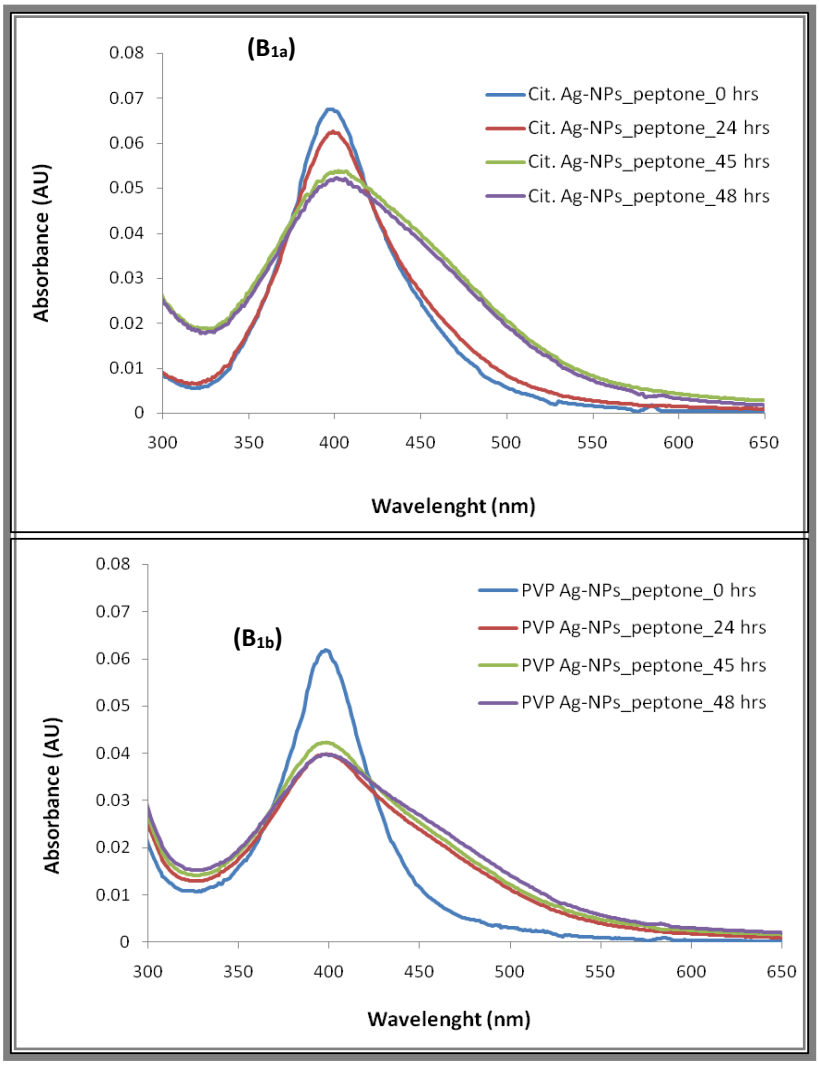

Figure 4-4: UV-Vis spectra of citrate (B1a) and PVP (B1b) Ag-NPs in 160 mg*L^{-1} peptone (at 0 hrs, 24 hrs, 45 hrs (during aeration) and at 48 hrs (during settling)).

4.3.1.6. DLS characterisation of citrate and PVP Ag-NPs in peptone

The DLS size distributions of the citrate and PVP Ag-NPs in peptone are shown in Figure 4-5 and the corresponding data summarised in Table 4-4. When first dispersed in the peptone solution (at 0 hrs), the citrate and PVP Ag-NPs showed an increase in size which could be due to slight agglomeration (e.g. formation of particle dimers or trimers) and their D_H was 34.6 ± 1.6 and 39.0 ± 16.8 nm, respectively. Table 4-4 shows that the agglomeration of the Ag-NPs increased with time in all stages of the experiment; except in the case of the citrate Ag-NPs where there was a reduction in D_H during the settling stage (at 48 hrs). There was no significant difference between citrate and PVP Ag-NPs behaviour overtime or at a STP; while the variation of their PDI was significantly different overtime (Table A3 - 9). Thus, the changes of the average D_H of Ag-NPs in peptone were not dependent to their coating; but the variations of their PDI were significantly dependent on their capping agent.

Table 4-4: DLS data extracted from the curves in Figure 4-4 of citrate and PVP Ag-NPs in 160 mg*L^{-1} peptone (at 0 hrs, 24 hrs, 45 hrs (during aeration) and at 48 hrs (during settling)).

	Citrate Ag-NPs in peptone		PVP Ag-NPs in peptone	
	Primary peak (D_H) (nm)	**PDI**	**Primary peak (D_H) (nm)**	**PDI**
0 hrs	34.6 ± 1.6	0.27 ± 0.03	39.0 ± 16.8	0.36 ± 0.04
24 hrs	35.5 ± 4.2	0.31 ± 0.07	45.5 ± 7.5	0.36 ± 0.04
45 hrs	84.5 ± 10.9	0.30 ± 0.07	53.5 ± 1.9	0.24 ± 0.02
48 hrs	47.9 ± 1.1	0.20 ± 0.01	60.8 ± 4.2	0.30 ± 0.04

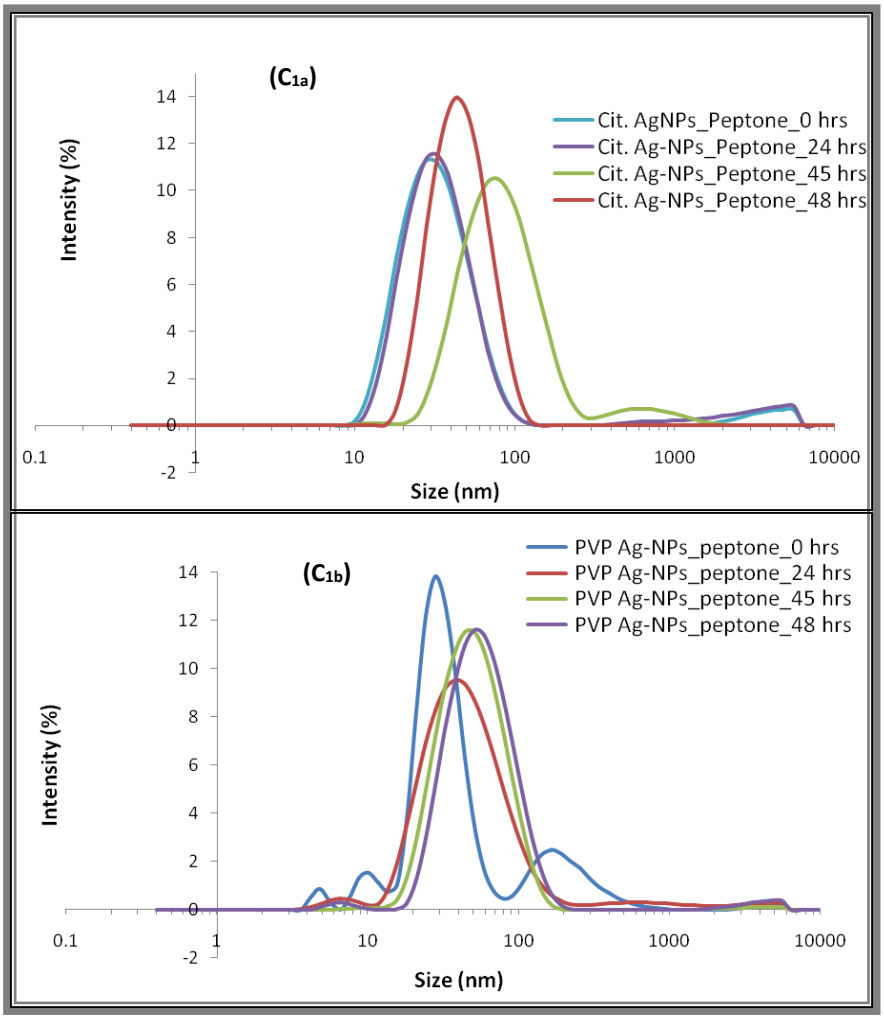

Figure 4-5: D_H distribution of the citrate (C1a) and PVP (C1b) Ag-NPs in 160 mg*L^{-1} peptone (at 0 hrs, 24 hrs, 45 hrs (during aeration) and at 48 hrs (during settling)).

Table 4-5 shows the calculated values of the particle settling velocities of each particle in the peptone media after three hours of settling. Because the velocity is proportional to the D_H (Equation 4-2), PVP Ag-NPs had a faster settling rate than citrate Ag-NPs. Also, the settling time values show that three hours were probably not sufficient to have at least half of the Ag-NPs present in the medium settled at the bottom of the beaker. However, in WWTP, the settling time of the Ag-NPs would be dependent on the settling time of the sludge due to their uptake into the sewage flocs.

Table 4-5: Settling velocity of citrate and PVP Ag-NPs in 160 mg*L^{-1} peptone (at 48 hrs during settling).

	D_H (nm) At 48 hrs	Settling velocity (nm*s^{-1})	Settling time (weeks)
Citrate Ag-NPs in peptone	47.9 ± 1.1	10.41	11.12
PVP Ag-NPs in peptone	60.8 ± 4.2	16.77	6.90

4.3.1.7. TEM characterisation of citrate and PVP Ag-NPs in peptone

The TEM results (Table 4-6 and Figure 4-6 and Figure 4-7) show that citrate Ag-NPs dispersed in peptone initially (at 0 hrs) showed agglomeration while the PVP Ag-NPs average size remained generally unchanged. After 24 hours, no further agglomeration was observed in either case since the Ag-NP average size was constant. The aeration of the solution for 24 hours might have caused the NPs to dissolve because their size at 45 hrs decreased in both cases. However, after the settling phase, the Ag-NPs size significantly increased, with the citrate Ag-NPs being considerably larger than the PVP Ag-NPs. There was a significant difference between citrate and PVP Ag-NPs size behaviour overtime and no significant difference was observed for the average size of both particles at a STP (Table A3 - 22).Thus, the changes of the average core size of Ag-NPs in peptone were dependent on their coating.

Table 4-6: TEM average size and shape factor of citrate and PVP Ag-NPs in 160 mg*L^{-1} peptone (at 0 hrs, 24 hrs, 45 hrs (during aeration) and at 48 hrs (during settling)).

	Citrate Ag-NPs in Peptone			PVP Ag-NPs in Peptone		
	Longest length (nm)	**Shortest length (nm)**	**Shape factor**	**Longest length (nm)**	**Shortest length (nm)**	**Shape factor**
0 hrs	16.3 ± 8.0	12.4 ± 5.9	0.93 ± 0.07	11.2 ± 4.9	8.6 ± 3.7	0.97 ± 0.05
24 hrs	16.4 ± 9.9	12.1 ± 7.0	0.90 ± 0.09	12.6 ± 6.4	9.8 ± 4.8	0.96 ± 0.06
45 hrs	13.3 ± 8.4	10.0 ± 6.5	0.92 ± 0.08	10.6 ± 4.5	8.1 ± 3.2	0.97 ± 0.05
48 hrs	22.5 ± 10.9	15.5 ± 7.1	0.85 ± 0.11	14.2 ± 7.6	10.5 ± 5.3	0.93 ± 0.07

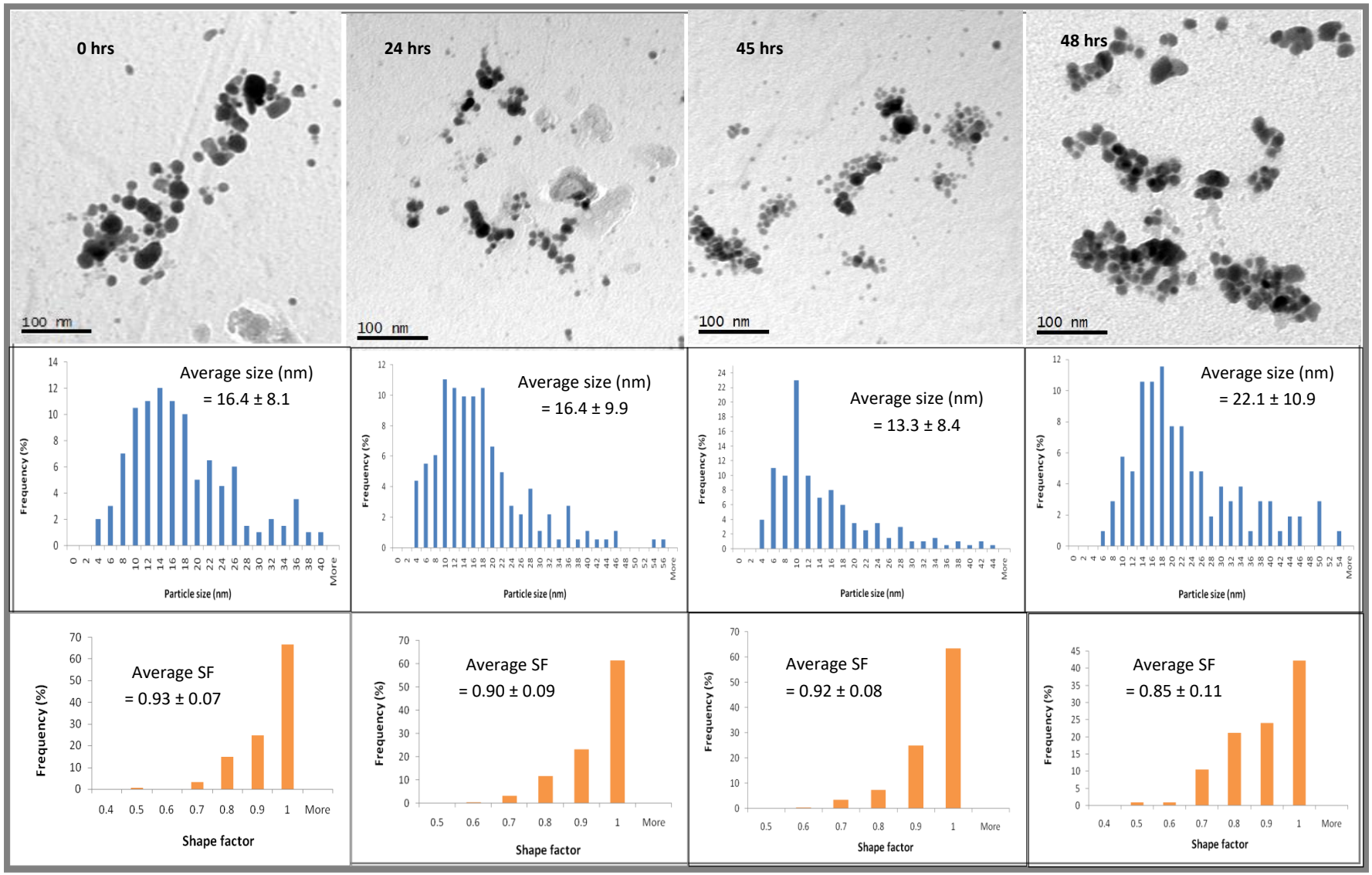

Figure 4-6: Primary particle size distribution of citrate Ag-NPs in 160 mg*L^{-1} peptone (at 0 hrs, 24 hrs, 45 hrs (during aeration) and at 48 hrs (during settling)). Based on the count of 200, 181, 200 and 104 NPs for the 0 hrs, 24 hrs, 45 hrs and 48 hrs sample respectively.

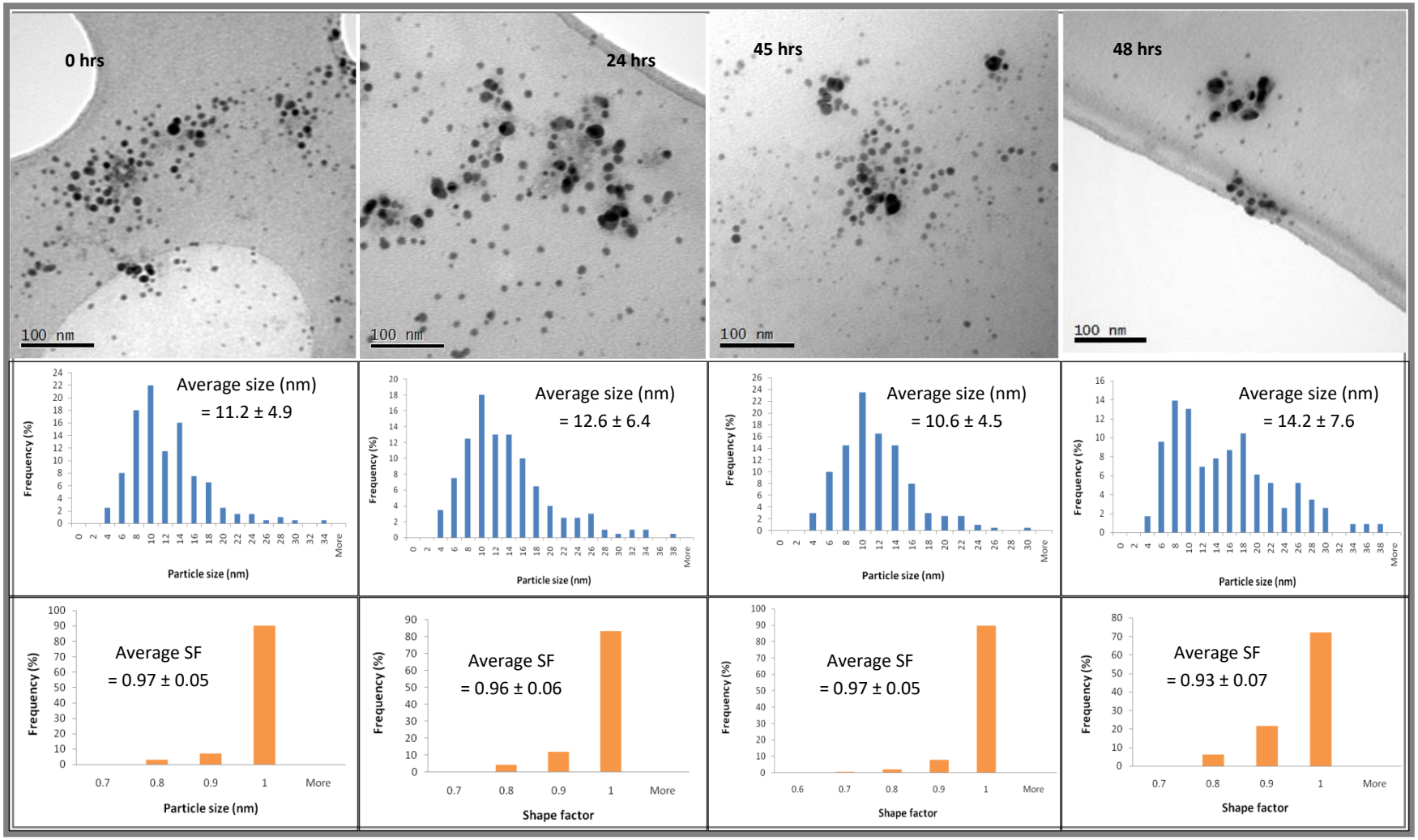

Figure 4-7: TEM primary particle size distribution of PVP Ag-NPs in 160 mg*L^{-1} peptone (at 0 hrs, 24 hrs, 45 hrs (during aeration) and at 48 hrs (during settling)). Based respectively on the count of 200 NPs for the 0 hrs, 24 hrs, and 45 hrs sample and 115 NPs for the 48 hrs sample

4.3.1.8. Surface chemistry analysis: ZP of citrate and PVP Ag-NPs in peptone

Figure 4-8 shows the variation of the ZP of citrate and PVP Ag-NPs in peptone and pH solution at a STP during the experiment, with the corresponding data summarised in Table 4-7. At 0 hrs, the ZP of citrate and PVP Ag-NPs was -8.49 ± 0.63 and -3.64 ± 0.52 mV, respectively. In both cases, the Ag-NPs were immediately less negative compared to the pristine particle ZP, which is indicative of binding of peptone to the NPs and formation of a "corona" (Dell'Orco et al., 2014). These ZP values potentially reflect the Ag-NPs being surrounded by the proteins, which could affect their surface charge, stability in solution, and potential for dissolution.

After 24 hours, both Ag-NPs ZP were increasingly negatively charges due to the formation of a corona layer on their surfaces (Duran et al., 2015, Shannahan et al., 2013); with citrate Ag-NPs exhibiting more negative ZP than the PVP Ag-NPs. Shannahan et al. (2013) had investigated the behaviour of stabilised citrate and PVP Ag-NPs (20 and 110 nm) in water and cell culture media with 10% foetal bovine serum and measured their DLS size and ZP after one hour of incubation. They found that the total number of proteins bound to each Ag-NP was related to the ZP and the more negative it was, the more proteins were attached to them. They also found that smaller particles were more sensitive to hydrophobic interactions with proteins than large ones because of the higher number of hydrophobic particles bound as they were receptive to curvature-induced folding and crowding in an aqueous environment (Shannahan et al., 2013). Thus, due to the small size of both citrate and PVP Ag-NPs in this study a protein corona was formed on their surface through hydrophobic interactions with the hydrophobic peptone proteins (Livney, 2010, Fox et al., 2015). Finally, although the pH of

the PVP Ag-NPs varied much more widely than that of citrate particles (which itself provides a buffering effect), the ZP of the citrate particles was much more variable than that of PVP.

During aeration, both citrate and PVP were more negatively charged. While in the settling phase, the citrate Ag-NPs became less negatively charged and the pH of the solution remained constant; but the opposite was observed for the PVP Ag-NPs with a reduction of their ZP. There was no significant difference between citrate and PVP Ag-NPs size behaviour overtime, and at a STP (Table A3 - 21). Thus, the changes of in ZP between the particles were significantly independent to their coating; which correlated with the ZP variations prior and during aeration.

After settling at 48 hrs, the pH of the solution for the citrate Ag-NPs remained constant while it increased for the PVP Ag-NPs, due to the buffering property of citrate itself as it can mop up H^+ ions and prevent fluctuations of the pH. Whereas, PVP may cause steric interference with counter-ion binding because of its polymer nature. Hence, in the presence of citrate Ag-NPs the pH of the peptone medium was unchanged after aeration and the solution remained slightly acidic. In the presence of PVP Ag-NPs the solution became acidic after aeration, with the pH reaching 6.38.

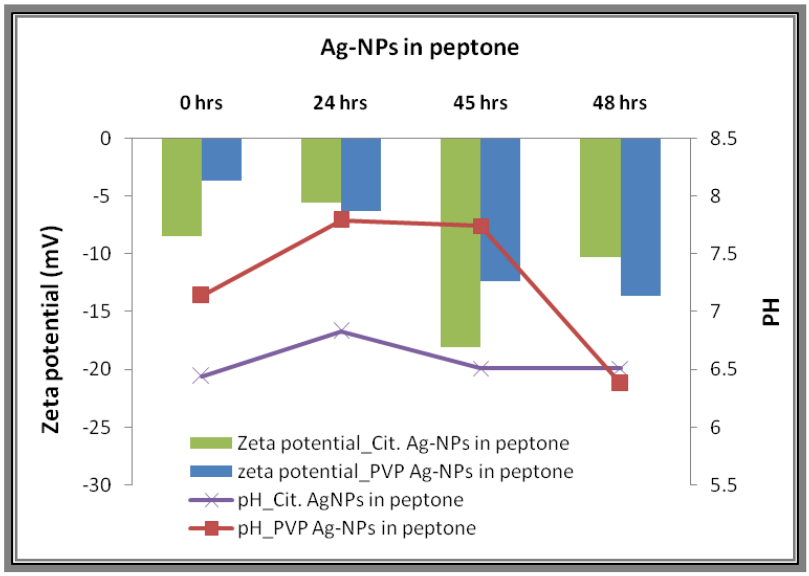

Figure 4-8: Variation of the citrate capped Ag-NPs ZP in combination with the associated pH when dispersed in 160 mg*L^{-1} peptone (at 0 hrs, 24 hrs, 45 hrs (during aeration) and at 48 hrs (during settling))

Table 4-7: ZP and pH of citrate and PVP Ag-NPs in 160 mg*L^{-1} peptone (at 0 hrs, 24 hrs, 45 hrs (during aeration) and at 48 hrs (during settling)) summarised from Figure 4-7.

	Citrate Ag-NPs in peptone		PVP Ag-NPs in peptone	
	pH	**ZP (mV)**	**pH**	**ZP (mV)**
0 hrs	6.44	-8.49 ± 0.63	7.14	-3.64 ± 0.52
24 hrs	6.83	-5.54 ± 0.64	7.79	-6.27 ± 0.85
45 hrs	6.51	-18.1 ± 0.30	7.74	-12.4 ± 0.70
48 hrs	6.51	-10.30 ± 0.79	6.38	-13.6 ± 0.86

4.3.2. Citrate and PVP Ag-NPs in meat-extract

The meat-extract used in the study was purchased from Sigma Aldrich and used to complement to nutritive property of peptone which lacks minerals and phosphates (Aldrich). The chemical composition of meat-extract (Table 4-8) is constituted of organic matter such as proteins (amino acids and peptides), nitrogen compounds and pigments, minerals and moisture (Belitz et al., 2009). Dispersed Ag-NPs in meat-extract will interact with the proteins

and the lipids through hydrophobic interactions with the formation of a corona layer (similar to Figure 4-3) and lipid layer (Lin and Gu, 2014, Bothun, 2008) on the particles surface (Figure 4-9). Other interactions of the Ag-NPs with the meat-extract might include the formation of the AgCl precipitates formed by the Cl^- (from NaCl) and Ag^+ interactions (Loza et al., 2014). The Ag^+ might occur if some Ag-NPs undergo oxidation/dissolution after their dispersion in the medium; however, this could be stopped or reduced by proteins and lipids binding on the particles surface.

Table 4-8: Chemical composition of meat-extract (Belitz et al., 2009)

compounds	Concentration (%)
Organic matter	**56 – 64**
Amino acids, peptides	15 – 20
Other N-compounds	10 – 15
Total creatinine	5.4 – 8.2
Ammonia	0.2 – 0.4
urea	0.1 – 0.3
N-free compounds	10 – 15
Total lipids	> 1.5
Pigments	10 – 20
Minerals	18 – 24
Sodium Chloride (NaCl)	2.5 – 5
Moisture	15 – 23

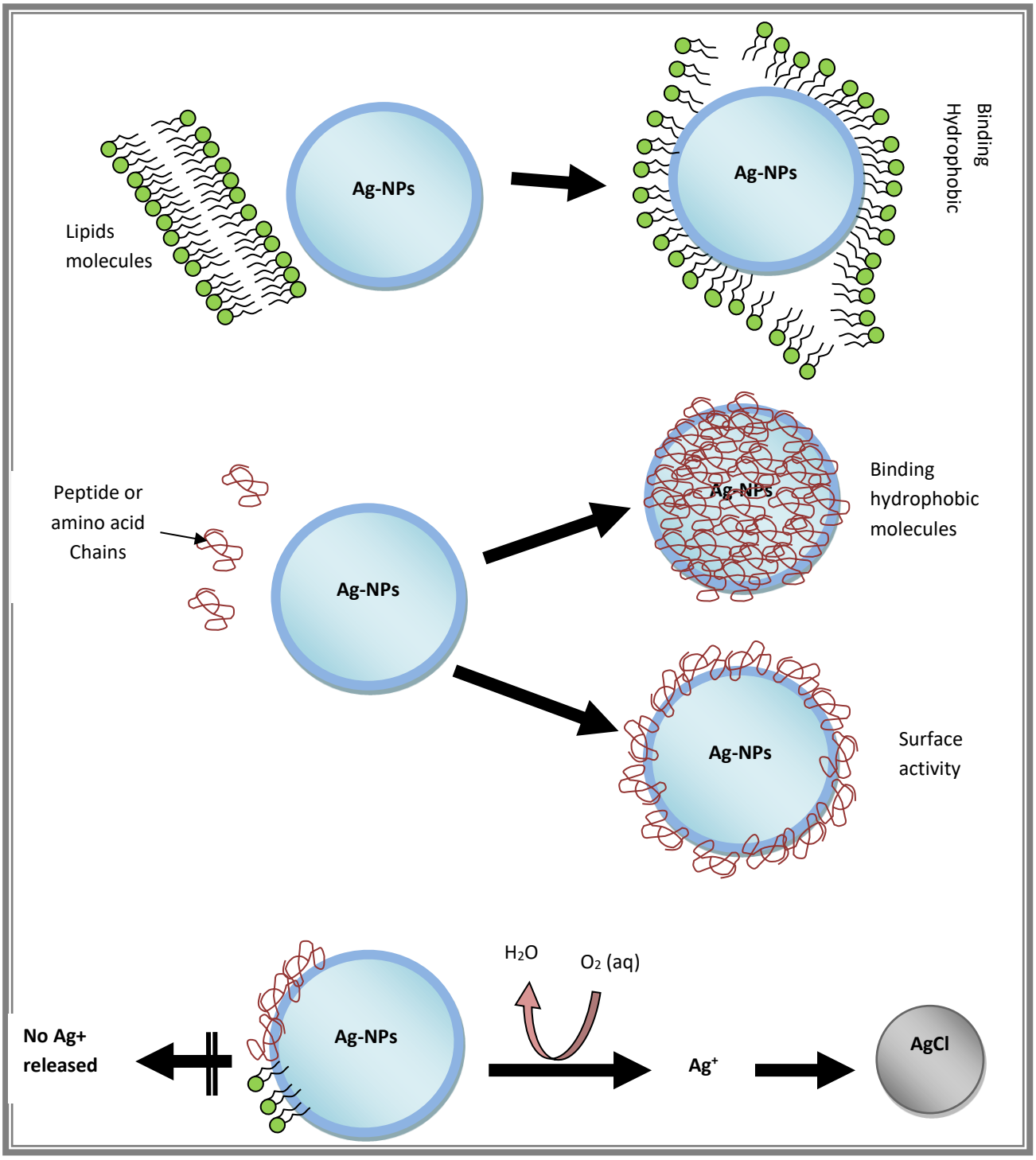

Figure 4-9: Illustration of Ag-NPs reactions with the meat-extract components. Formation of lipids/protein's hydrophobic binding and protein corona (via surface activity interaction) formation of AgCl precipitates via oxidation dissolution mechanism. (Bothun, 2008, Livney, 2010, Loza et al., 2014)

4.3.2.1. Dissolution study: silver concentration in meat-extract

The dispersion of citrate and PVP Ag-NPs in 110 mg*L^{-1} meat-extract medium showed a rapid dissolution of the citrate Ag-NPs at 0 hrs, while the concentration of PVP Ag-NPs remained constant indicated by the low level of Ag^+ (Table 4-9). Within 24 hours and in the absence of aeration, we could note that the $C_{Total\ Ag}$ (citrate) remained practically constant while the $C_{Total\ Ag}$ (PVP) decreased to nearly 1/3. Citrate and PVP Ag-NPs in meat extract continued to dissolve during the aeration (at 45 hrs) and settling (48 hrs) stages. However, the degree of dissolution of PVP Ag-NPs was higher because in their case, 75.30% of Ag in the medium was Ag^+ at 45 hrs, while there was 25.09% of Ag^+ in the citrate case, hence citrate Ag-NPs were relatively more stable in meat-extract.

There was no significant difference between the variations of Ag concentration, %dissolved Ag and %unrecovered of citrate and PVP Ag-NPs overtime and at a specific time point (STP) (Table A3 - 18). Thus, the changes in the concentration of Ag-NPs in peptone were independent of their coating.

Table 4-9: Changes in Ag concentration when citrate and Ag-NPs were dispersed in 110 mg*L^{-1} meat-extract (at 0 hrs, 24 hrs, 45 hrs (during aeration) and at 48 hrs (during settling)) as measured by GFAAS.

	Citrate Ag-NPs in meat-extract			PVP Ag-NPs in meat-extract		
	$C_{Total\ Ag}$ (µg*L^{-1})	%Diss. Ag	%Unr. Ag	$C_{Total\ Ag}$ (µg*L^{-1})	%Diss. Ag	%Unr. Ag
0 hrs	614.8 ± 3.6	6.2 ± 0.1	0	629.3 ± 44.8	1.03 ± 0.5	0
24 hrs	600.9 ± 9.2	8.4 ± 0.3	2.27	424.4 ± 17.2	12.6 ± 0.8	32.56
45 hrs	526.9 ± 19.4	11.8 ± 0.2	14.30	308.7 ± 8.9	53.6 ± 0.5	50.94
48 hrs	472.4 ± 8.9	25.1 ± 0.5	23.17	194.9 ± 4.1	75.3 ± 2.4	69.03

4.3.2.2. UV-Vis characterisation of citrate and PVP Ag-NPs in meat-extract

In 110 mg*L^{-1} meat-extract, the UV-Vis spectrum of citrate (Figure 4-10(B_{2a})) and PVP Ag-NPs (Figure 4-10 (B_{2b})) was initially red shifted at 0 hrs with MA occurring at 401 and 399 nm, respectively (Table 4-10). It is likely that their surface chemistry might have changed while reacting with the meat-extract components (lipids, proteins or Cl^-). At 24 hrs, the MA in both cases decreased with a spreading in the FWHM; the λ_{max} of citrate Ag-NPs remained constant while the λ_{max} of PVP Ag-NPs was slightly increased.

At 45 hrs, the Ag-NPs shell may have increased in size or changed shape due to the formation of lipids/proteins corona on their surface and precipitation of Ag^+ into AgCl (Figure 4-9), causing the spreading of the UV-Vis peak (Loza et al., 2014). This explains the red-shift of the citrate Ag-NPs UV-Vis peak, caused by their increased size as they may have interacted with the proteins (or lipids); while, a blue-shift of the PVP peak may be a consequence of their size decreasing due to dissolution (Desai et al., 2012). With aeration, the MA of the citrate and PVP Ag-NPs was further reduced and it was also observed that the FWHM of the UV-Vis signal for both particles increased. Baalousha et al. (Baalousha et al., 2013, Baalousha et al., 2015) have shown that variations of λ_{max} could be associated with NP dissolution or aggregation (Afshinnia et al., 2016). Thus in this study, the citrate and PVP Ag-NPs had probably experienced continuous aggregation and dissolution respectively under aeration. As a consequence, their size and shape may be affected and lead to the spreading of their UV-Vis peak.

During settling (at 48 hrs), the λ_{max} of the citrate and PVP Ag-NPs were respectively 399 nm and 406 nm and their MA was reduced with a spreading in the UV-Vis spectra. Based on these results, we can conclude that both citrate and PVP Ag-NPs have gone through three transformations. Firstly, they may have got a protein or a lipid corona formed on their surface by binding with the proteins and lipids present in meat-extract (Table 4-10). Secondly they may have undergone dissolution during aeration (Yang et al., 2013c) and/or aggregation based on the changes of λ_{max}. Finally, the dissolved Ag may have reacted with the Cl^- ions, forming AgCl precipitates as illustrated in Figure 4-9.

There was a significant difference on the MA changes between both particles (Table A3 - 19). This correlates with the GFAAS results showing that PVP Ag-NPs were more sensitive to dissolution than citrate particles as shown in Table 4-10 and their UV-Vis MA decreased being a consequence of this dissolution. However, there was no significant difference found in λ_{max} variations overtime.

Table 4-10: UV-Vis parameters (extracted from curves in Figure 4-8) for citrate and PVP Ag-NPs dispersed in 110 mg/L meat-extract (at 0 hrs, at 24 hrs, at 45 hrs (during aeration) and at 48 hrs (during settling))

	Citrate Ag-NPs in meat-extract				PVP Ag-NPs in meat-extract			
	0 hrs	**24 hrs**	**45 hrs**	**48 hrs**	**0 hrs**	**24 hrs**	**45 hrs**	**48 hrs**
λ_{max} (nm)	401	400	404	399	399	401	399	406
MA	0.079	0.057	0.037	0.051	0.056	0.038	0.012	0.024
Absorbance Decreased (%)	0	32.83	62.68	41.79	0	47.37	366.70	133.33
FWHM (nm)	60	78	111	132	58	90	NA	NA
Peak shift (%)	0	0.25	0.74	0.50	0	0.50	0	1.72

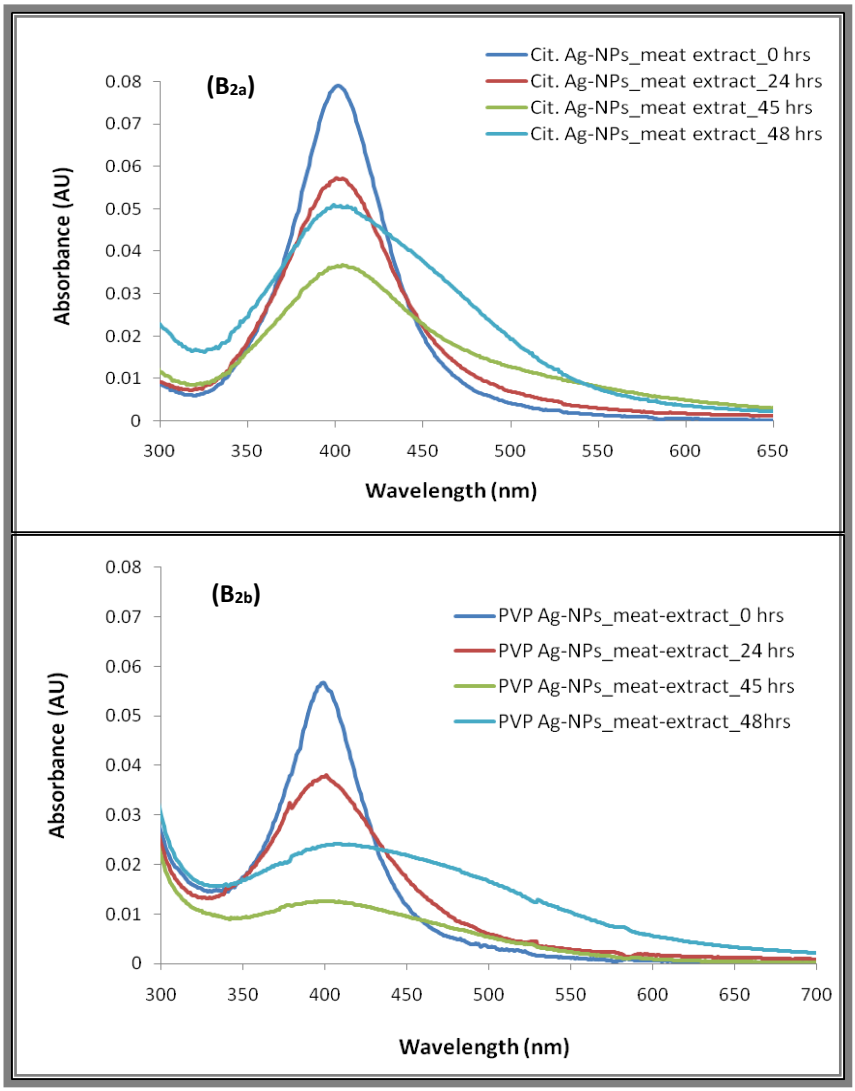

Figure 4-10: UV-Vis spectra of citrate (B_{2a}) and PVP (B_{2b}) Ag-NPs dispersed in 110 mg/L meat-extract (at 0 hrs, 24 hrs, 45 hrs (during aeration) and at 48 hrs (during settling)).

4.3.2.3. DLS characterisation of citrate and PVP Ag-NPs in meat-extract

The D_H distributions of citrate and PVP Ag-NPs in meat-extract are shown in Figure and the corresponding data summarised in Table 4-11. Initially, both citrate and PVP Ag-NPs may have undergone slight agglomeration with an average D_H of 39.9 ± 5.4 and 37.3 ± 13.7 nm, respectively indicative of the presence of particle dimers or trimers. After 24 hours, citrate Ag-NPs appeared to be more agglomerated and polydisperse (PDI >0.4 traditionally taken as indicative of polydisperse solutions) while PVP Ag-NPs may have re-dispersed with transient

agglomerates breaking before aeration due to the reduction in their D_H. At 45 hrs and 48 hrs, the agglomeration citrate particles seemed to have increased under and after aeration, causing the spreading of their scattering size distribution. PVP particles, however, appeared to have dissolved under aerobic conditions, this could be observed by disappearing off the scattering peak of the NPs with D_H< 10 nm.

There was a significant difference between citrate and PVP Ag-NPs average D_H behaviour at a STP (Table A3 - 21). Thus, the size of citrate Ag-NPs in meat-extract and under aerobic conditions might have been affected by their interaction with the chemical components (proteins, lipids and Cl^- ions). However, PVP Ag-NPs were likely affected by the aeration of the medium, as they underwent dissolution. Finally, no different was found in the variations of their PDI overtime.

Table 4-11: DLS data (extracted from Figure 4-9) of citrate and PVP Ag-NPs 110 mg*L^{-1} meat-extract (at 0 hrs, 24 hrs, 45 hrs (during aeration) and at 48 hrs (during settling)).

	Citrate Ag-NPs in meat-extract		PVP Ag-NPs in meat-extract	
	Primary peak (D_H) (nm)	**PDI**	**Primary peak (D_H) (nm)**	**PDI**
0 hrs	39.9 ± 5.4	0.32 ± 0.06	37.3 ± 13.7	0.52 ± 0.12
24 hrs	34.2 ± 5.0	0.44 ± 0.12	31.8 ± 0.4	0.39 ± 0.01
45 hrs	85.0 ± 12.3	0.39 ± 0.02	99.7 ± 5.9	0.24 ± 0.01
48 hrs	174.1 ± 27.1	0.48 ± 0.01	122.4 ± 11.5	0.34 ± 0.04

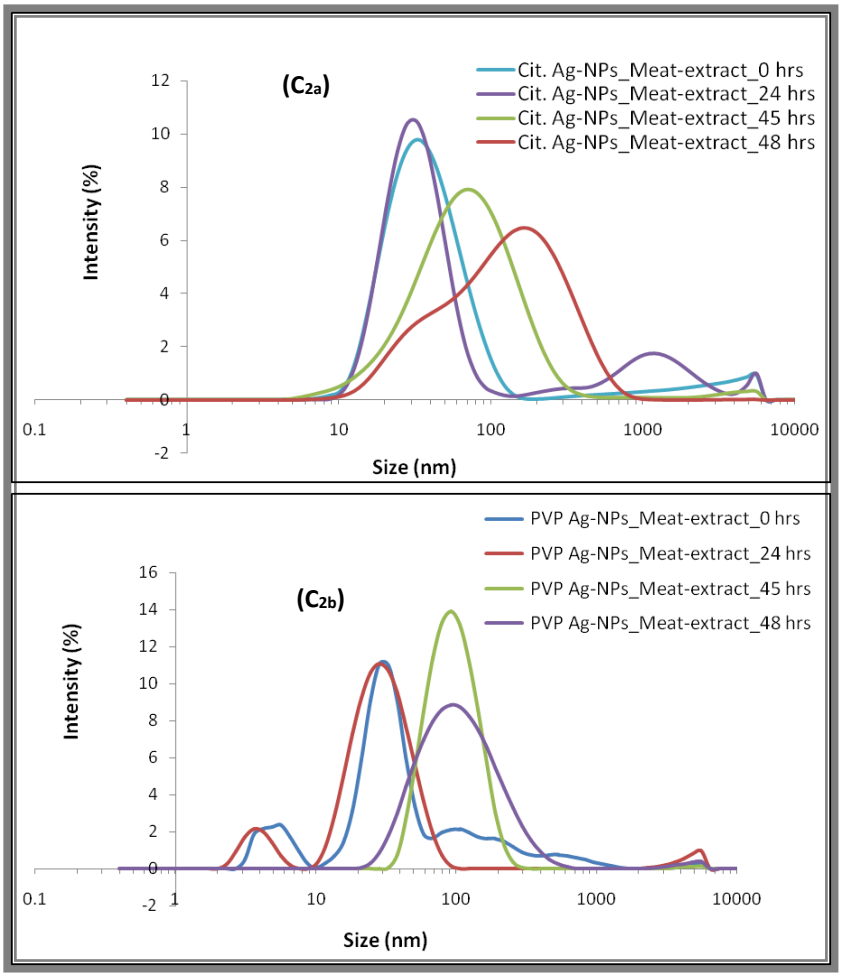

Figure 4-11: D_H distribution of the citrate (C2a) and PVP (C2b) Ag-NPs dispersed in 110 mg*L^{-1} meat-extract (at 0 hrs, 24 hrs, 45 hrs (during aeration) and at 48 hrs (during settling)).

Regarding the settling phase, Table 4-14 shows that both citrate and PVP Ag-NPs settled at a similar rate in meat extract solution. However, the three hours settling time set for this experiment was insufficient to have Ag-NPs fully settled at the bottom of the beaker. Please note that these times were much shorter than the peptone's settling time (Table 4-5). Thus the meat-extract in OECDss might help to accelerate the overall settling rate of the particles in the SBR pilot plant.

Table 4-12: Settling velocity with the corresponding size (D_H) of citrate and PVP Ag-NPs in 110 mg*L^{-1} meat-extract (at 0 hrs, 24 hrs, 45 hrs (during aeration) and at 48 hrs (during settling)).

	D_H (nm) At 48 hrs	Settling velocity (nm*s^{-1})	Settling time (weeks)
Citrate Ag-NPs in meat-extract	122.4 ± 11.5	137.51	0.84
PVP Ag-NPs in meat-extract	174.1 ± 27.1	67.97	1.70

4.3.2.4. TEM characterisation of citrate and PVP Ag-NPs in meat-extract

TEM results (Table 4-13 and Figure 4-12 and Figure 4-13) show that citrate Ag-NPs dispersed in meat-extract at 0 hrs agglomerated while little to no agglomeration was observed for the PVP Ag-NPs. After 24 hours, PVP Ag-NPs may have dissolved/re-precipitated as the NPs became smaller and very polydisperse; while citrate Ag-NPs showed agglomeration. It could be observed that the degree of agglomeration of the citrate Ag-NPs increased throughout the aeration and the settling stages. The PVP Ag-NPs, However, had no significant changes in their average size beyond the initial apparent dissolution by 24 hrs. There was no significant difference statistically between citrate and PVP Ag-NPs size behaviour overtime and at a STP (Table A3 - 22).

Table 4-13: TEM average size and shape factor of citrate and PVP Ag-NPs dispersed in 110 mg*L^{-1} meat-extract (at 0 hrs, 24 hrs, 45 hrs (during aeration) and at 48 hrs (during settling)).

	Citrate Ag-NPs in meat-extract			PVP Ag-NPs in meat-extract		
	Longest length (nm)	**Shortest length (nm)**	**Shape factor**	**Longest length (nm)**	**Shortest length (nm)**	**Shape factor**
0 hrs	14.9 ± 8.0	11.6 ± 5.9	0.93 ± 0.07	14.5 ±5.0	11.6 ± 4.0	0.96 ± 0.04
24 hrs	18.1 ± 10.5	13.4 ± 7.1	0.89 ± 0.11	11.4 ± 5.1	9.1 ± 4.4	0.97 ± 0.03
45 hrs	22.1 ± 12.7	16.0 ± 8.7	0.87 ± 0.09	12.3 ± 5.6	9.7 ± 4.5	0.96 ± 0.05
48 hrs	21.7 ± 14.7	15.8 ± 10.03	0.87 ± 0.12	14.3 ± 6.5	11.3 ± 5.3	0.94 ± 0.07

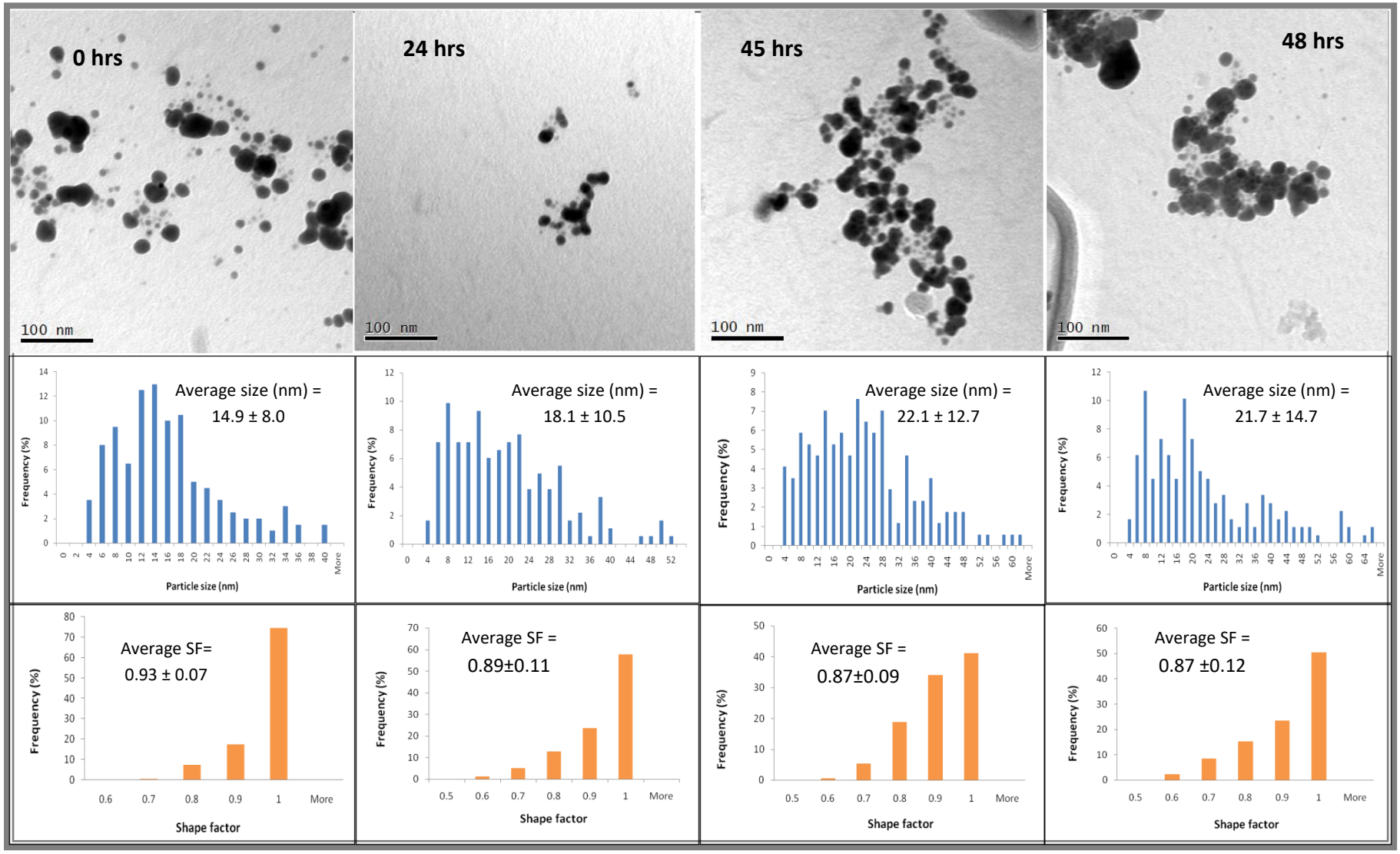

Figure 4-12: TEM primary particle size distribution of citrate Ag-NPs in meat-extract (at 0 hrs, 24 hrs, 45 hrs (during aeration) and at 48 hrs (during settling)).Based on the count of 200, 182, 170 and 178 NPs for the 0 hrs, 24 hrs, 45 hrs and 48 hrs sample respectively.

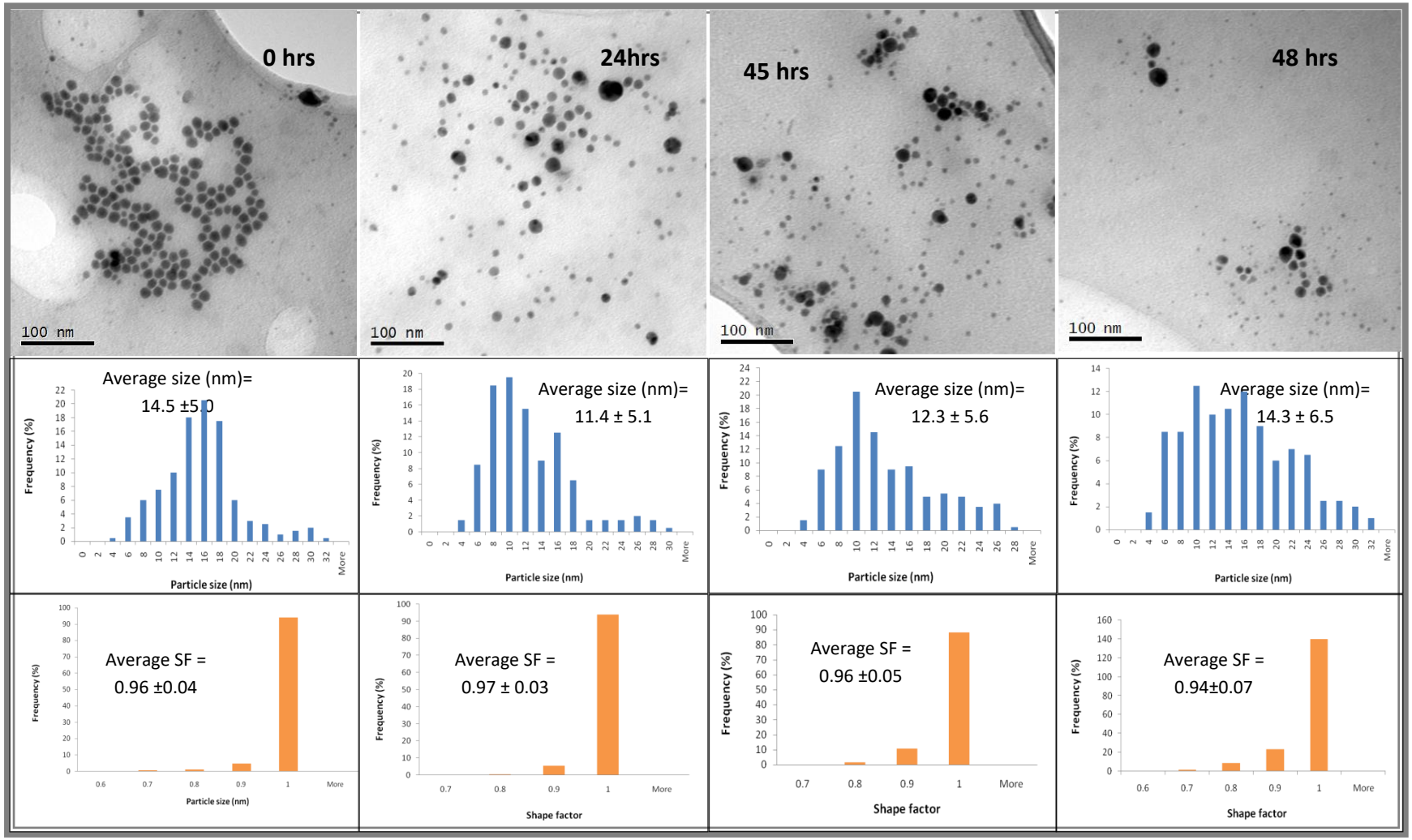

Figure 4-13: TEM primary particle size distribution of PVP Ag-NPs in meat-extract (at 0 hrs, 24 hrs, 45 hrs (during aeration) and at 48 hrs (during settling)).Based on the count of 200 NPs for the 0 hrs, 24 hrs, 45 hrs and 48 hrs sample.

4.3.2.5. Surface chemistry analysis: ZP of citrate and PVP Ag-NPs in meat-extract

The ZP changes of the citrate and PVP Ag-NPs in 110 $mg*L^{-1}$ meat-extract solution and the variations of the pH medium are shown in Figure 4-14 and Table 4-14. At 0 hrs, both citrate and PVP Ag-NPs were less stable since they were less negatively charged compare to the pristine particles (Table 3-9). During aeration, the Ag-NPs charge was strongly negative in both cases; however, during the settling stage, their ZP decreased to less negative values, especially for the PVP Ag-NPs. There was no significant difference statistically between citrate and PVP Ag-NPs size behaviour overtime and at a STP (Table A3 - 21).

We can note that the pH of the meat-extract (Figure 4-14) solution with citrate Ag-NPs was more variable than the pH of the peptone medium (with citrate Ag-NPs) (Figure 4-8). However, with dispersed PVP Ag-NPs, the pH of the meat-extract solution was more stable than the pH of the peptone. The pH increased with time before aeration and then decreased under aerobic conditions for both particles; and after aeration, the pH decreased for the PVP Ag-NPs, but increased for the citrate Ag-NPs due to the oxygen interfering with the buffering capacity of the citrate agent. In fact, the addition of oxygen to a buffer solution will affect its efficiency or buffering capacity causing fluctuations of the pH (Slatter, 2003).

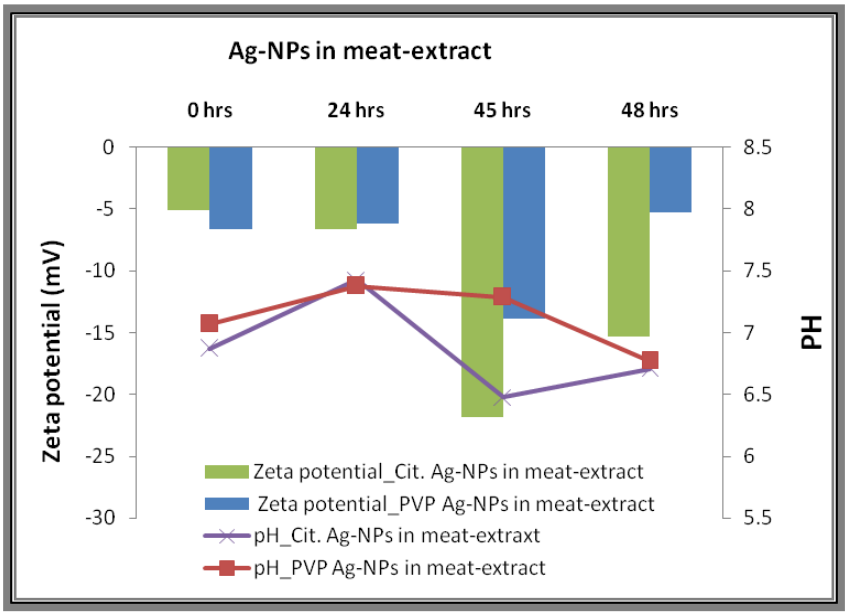

Figure 4-14: Variation of the citrate and PVP capped Ag-NPs ZP when dispersed in meat-extract (at 0 hrs, 24 hrs, 45 hrs (during aeration) and at 48 hrs (during settling)) and the associated variation in solution pH.

Table 4-14: ZP and pH of citrate and PVP Ag-NPs 110 mg*L^{-1} dispersed in meat-extract (at 0 hrs, 24 hrs, 45 hrs (during aeration) and at 48 hrs (during settling)) summarised from Figure 4-12.

	Citrate Ag-NPs in meat-extract		PVP Ag-NPs in meat-extract	
	pH	**ZP (mV)**	**pH**	**ZP (mV)**
0 hrs	6.87	-5.05 ± 0.43	7.07	-6.64 ± 0.09
24 hrs	7.43	-6.62 ± 1.51	7.38	-6.18 ± 1.24
45 hrs	6.48	-21.80 ± 0.51	7.29	-13.9 ± 0.52
48 hrs	6.71	-15.3 ± 0.94	6.77	-5.23 ± 0.16

4.3.3. Citrate and PVP Ag-NPs in urea

Urea is a chemical compound first artificially synthesized by Friedrich Wöhler in 1828 as a result of a chemical reaction between silver cyanate (AgNCO) and ammonium chloride (NH_4Cl) (Meessen, 2014):

$$AgNCO + NH_4Cl \rightarrow (NH_2)CO + AgCl$$

Equation 4-4

However, the Basaroz reaction is the one used today in production of urea ($CO(NH_2)_2$) formed by the dehydration of ammonium carbamate (NH_2COONH_4) at high temperature (170 – 220 ˚C) and pressure (125 – 250 bar) (Meessen, 2014, Meessen, 2010):

$$NH_2COONH_4 \rightarrow (NH_2)_2CO + HO_2$$

Equation 4-5

Urea decomposes into ammonia (NH_3) and carbon dioxide (CO_2) if exposed to temperature of 132.7 ˚C (Equation 4-6) or to water at lower temperatures – including temperatures between 20 – 25 ˚C (Equation 4-7) (Nakamura et al., 2014, Simka et al., 2009)

$$(NH_2)_2CO \rightarrow NH_3 + CO_2$$

Equation 4-6

$$(NH_2)_2CO + H_2O \rightarrow 2NH_3 + CO_2$$

Equation 4-7

Mumper et al. (2013) found that the dissolution of dispersed citrate Ag-NPs (20 nm) was enhanced with increased NH_3 and the released Ag^+ reacted with NH_3 forming soluble silver amine ($Ag(NH_3)_2^+$) (Peard and Pflaum, 1958). According to Gorup et al. (2011), the addition of ammonia to a suspension citrate Ag-NPs (2 nm average size) generated rapid formation of $Ag(NH_3)_2^+$ (Figure 4-15), removing non-reduced Ag^+, preventing new nuclei from forming and

thus preventing growth of citrate Ag-NPs. They found that with no more Ag^+ in the suspension, the particles state remained unchanged and the particles were virtually monodispersed.

$$Ag^+ + 2NH_3 \longrightarrow 4Ag(NH_3)_2^+ + 4OH^-$$

Equation 4-8

The presence of NH_3 can also cause the release Ag^+ from Ag-NPs by puncturing the passivation layer; leading to the formation of $Ag(NH_3)_2^+$ (Le Ouay and Stellacci, 2015). In the presence of oxygen and water, the reaction between Ag^+ and NH_3 forms $Ag(NH_3)_2^+$ and hydroxide anions (Mumper et al., 2013):

$$4Ag^+ + 8NH_3 + O_2 + 2H_2O \longrightarrow 4Ag(NH_3)_2^+ + 4OH^-$$

Equation 4-9

In the presence of PVP, $Ag(NH_3)_2^+$ might be reduced to zero valent Ag/PVP under UV exposure (Montazer et al., 2012), leading to the growth of PVP Ag-NPs due to the deposition of Ag/PVP on their surface (Figure 4-15).

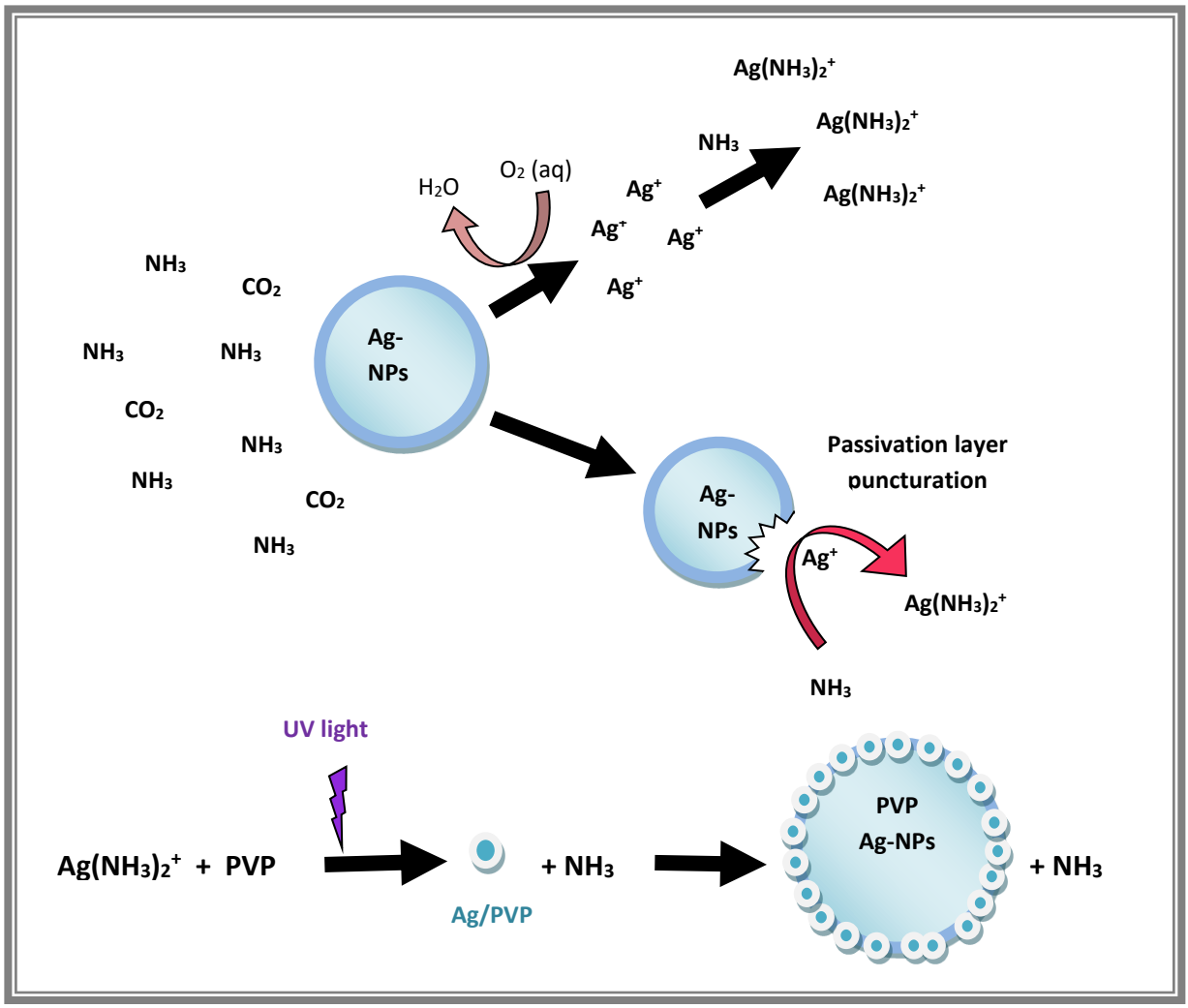

Figure 4-15: Illustration of Ag-NPs reactions with urea ($CO(NH_2)_2$). Urea in water ($CO(NH_2)_2$) decomposes into ammonia (NH_3) and carbon dioxide (CO_2) (Nakamura et al., 2014, Simka et al., 2009). Formation of soluble silver amine ($Ag(NH_3)_2^+$) via Ag^+ and NH_3 (Mumper et al., 2013). With Ag^+ released through oxidation/dissolution or puncture of the passivation layer by NH_3 (Le Ouay and Stellacci, 2015). In the presence of a polymer such as PVP, $Ag(NH_3)_2^+$) can be reduced onto Ag/PVP atoms under the exposure of UV light (Montazer et al., 2012) causing the grow of the PVP Ag-NPs.

4.3.3.1. Dissolution study: silver concentration in urea

In 30 $mg*L^{-1}$ urea solution, dissolution of citrate and PVP Ag-NPs was nearly undetectable at 0 hrs, given the low percentage of dissolved Ag (Table 4-15). However, after 24 hours, there was a significant decrease in total Ag concentration for the PVP Ag-NPs, while $C_{Total\ Ag}$(citrate) did not change much suggesting either loss to container walls or settling although during the stirring phases (up to 45 hrs) this is less likely. At 45 hrs, PVP Ag-NPs were highly dissolved

with nearly 76% of the total Ag being ions; while for the citrate Ag-NPs, slight dissolution was observed, but the dissolved Ag concentration was very low with only about 13% of Ag^+ present at 45 hrs. During the settling phase, although both citrate and PVP Ag-NPs continued to dissolve, the dissolution rate of PVP Ag-NPs after aeration was lower than that of the citrate particles. Meaning, the rate of dissolution for the PVP Ag-NPs was probably caused by the addition of an oxygen flow. There was no significant difference between both particles overtime and at a particular time point regarding their $C_{Total\ Ag}$, %dissolved Ag and %unrecovered Ag (Table A3 - 18).

Table 4-15: Changes in Ag concentration when citrate and PVP Ag-NPs were dispersed in 30 mg/L urea (at 0 hrs, 24 hrs, 45 hrs (during aeration) and at 48 hrs (during settling)) as measured by GFAAS.

	Citrate Ag-NPs in urea			PVP Ag-NPs in urea		
	$C_{Total\ Ag}$ (µg/L)	%Diss. Ag	%Unr. Ag	$C_{Total\ Ag}$ (µg/L)	%Diss. Ag	%Unr. Ag
0 hrs	681.6 ± 9.2	1.9 ± 0.4	0	635.2 ± 14.6	1.6 ± 0.3	0
24 hrs	592.3 ± 15.8	2.9 ± 0.2	13.10	491.3 ± 6.1	13.6 ± 2.1	22.65
45 hrs	520.7 ± 9.0	13.0 ± 0.6	23.60	226.7 ± 19.9	75.8 ± 2.8	64.42
48 hrs	363.2 ± 22.4	37.9 ± 0.6	46.71	223.0 ± 18.3	81.8 ± 0.8	64.90

4.3.3.2. UV-Vis characterisation of citrate and PVP Ag-NPs in urea

At 0 hrs, the UV-Vis spectra of the citrate and PVP Ag-NPs were red shifted (Figure 4-16) with their λ_{max} being respectively 395 and 398 nm (Table 4-16). This implies that the core size of citrate and PVP Ag-NPs increased due to aggregation through binding caused by the surface charge reduction (Baalousha et al., 2013) or through continued growth of the particles caused by the reduction of $Ag(NH_3)_2^+$ via exposure of the PVP particle solution to the UV light according to Montazer et al. (2012) (Figure 4-15). At 24 hrs, the λ_{max} slightly increased for

both PVP and citrate Ag-NPs, and the FWHM was reduced for citrate Ag-NPs while it remained constant for PVP Ag-NPs. Also, the MA of citrate Ag-NPs decreased, whereas the PVP Ag-NPs MA remained constant. Hence in urea, PVP Ag-NPs stabilised with time in the absence of aeration with no agglomeration observed; while citrate Ag-NPs may react with urea causing agglomeration.

In the presence of aeration at 45 hrs, the UV-Vis spectra of citrate and PVP particles red shifted, and their corresponding λ_{max} were 402 and 424 nm, respectively. There was a slight decrease in the FWHM of the citrate Ag-NPs; while the FWHM of the PVP Ag-NPs increased a lot, due to agglomeration or formation of precipitated Ag/PVP on the particle surface (Figure 4-15). During the settling phase, the MA and λ_{max} of both Ag-NPs remained constant (relative to the 45 hrs time point) and the FWHM of the spectra slightly increased. Thus in the presence of urea, citrate Ag-NPs may have agglomerated due the decreased of their surface charge (Baalousha et al., 2013), while and PVP Ag-NPs may have agglomerated but also grown as a consequence of deposition of zero valent Ag/PVP on their surface (Figure 4-15). The oxidation/dissolution mechanism of both particles was amplified by the addition of oxygen with higher dissolution observed for the PVP Ag-NPs (Table 4-15). This might explain the spreading of the PVP peak at 45 and 48 hrs as more dissolved Ag might have led to a higher content of $Ag(NH_3)_2^+$ reduced onto the PVP Ag-NPs surface at 48 hrs and caused their size to increase. There was no significant difference in the MA and λ_{max} changes between both particles overtime and at a STP (Table A3 - 19). Thus, the optical properties of Ag-NPs in urea were statically independent of their capping agent and the conditions of the experiment. However, the results described in this section show the opposite.

Table 4-16: UV-Vis parameters (extracted from Figure 4-13) for citrate Ag-NPs and PVP in 30 mg*L^{-1} urea (at 0 hrs, at 24 hrs, at 45 hrs (during aeration) and at 48 hrs (during settling)).

	Citrate Ag-NPs in urea				PVP Ag-NPs in urea			
	0 hrs	**24 hrs**	**45 hrs**	**48 hrs**	**0 hrs**	**24 hrs**	**45 hrs**	**48 hrs**
λ_{max} (nm)	395	397	402	402	398	400	424	425
MA	0.071	0.065	0.068	0.064	0.065	0.064	0.012	0.013
Absorbance Decrease (%)	0	8.95	4.48	10.45	0	1.56	441.7	400
FWHM (nm)	70	66	55	70	48	49	192	202
Peak shift (%)	0	0.50	1.74	1.74	0	0.50	6.13	6.35

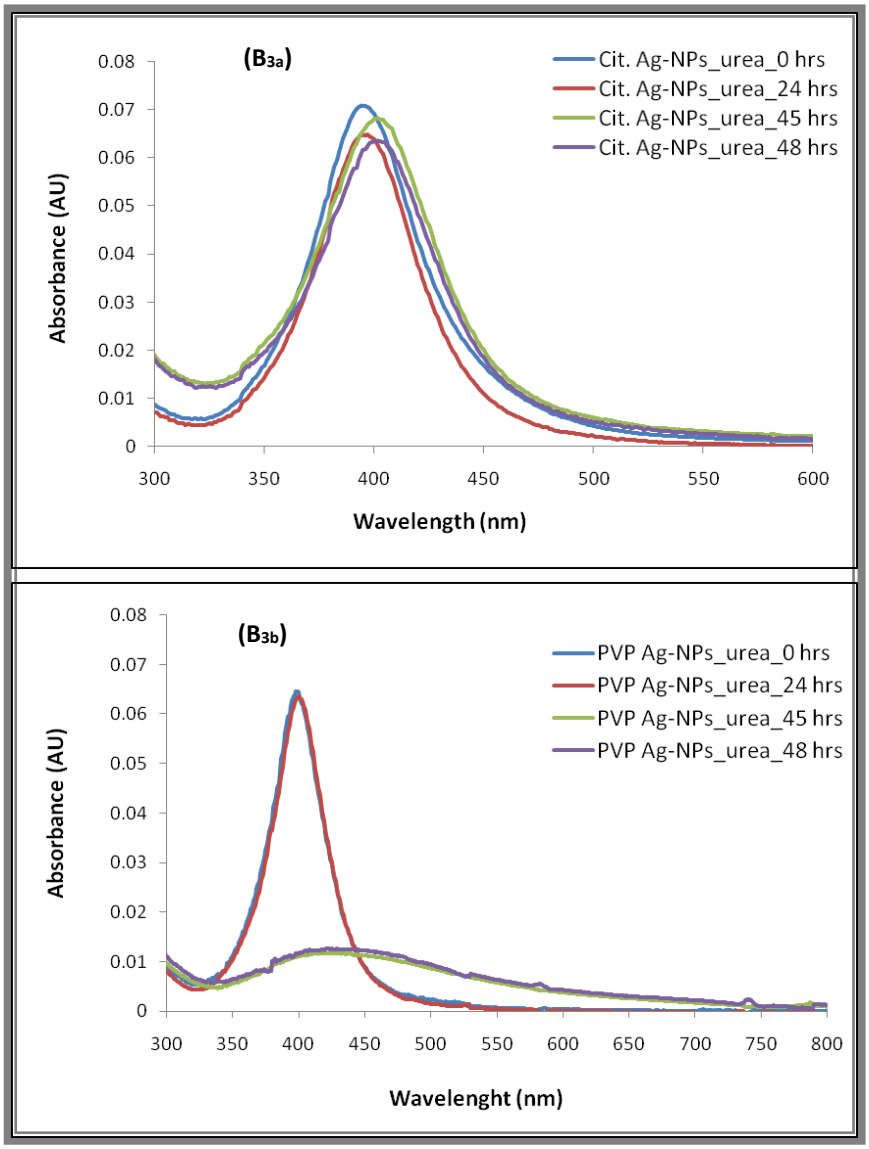

Figure 4-16: UV-Vis spectra of citrate (B_{3a}) and PVP (B_{3b}) Ag-NPs in 30 mg*L^{-1} urea (at 0 hrs, 24 hrs, 45 hrs (during aeration) and at 48 hrs (during settling)).

4.3.3.3. DLS characterisation of citrate and PVP Ag-NPs in urea

The D_H data for the citrate and PVP Ag-NPs in urea is shown in Figure 4-17 and Table 4-17. At 0 hrs, both citrate and especially PVP Ag-NPs may have agglomerated having a D_H diameter of 24.9 ± 2.9 and 30.6 ± 4.5 nm, respectively. However, the PVP Ag-NPs' D_H might have been affected by the presence of large particulate or by excess PVP. At 24 hrs, it is believed that

citrate Ag-NPs were more agglomerated because of the significant increase in their D_H; while the PVP Ag-NPs may have dissolved or stayed stable prior to aeration. With aeration, the D_H of the citrate Ag-NPs increased because of the aeration flow, which may have caused them to dissolve. As a result, the citrate particles were unstable due to the reduction of their electrostatic stability; hence the formation of agglomerate particles (dimers or trimers). For PVP Ag-NPs, the effect of aeration was significant with D_H being about 167 nm -this was probably due to their high degree of dissolution causing the reduction of their steric stability. Thus, the agglomeration of PVP NPs might have increased and led to the formation of dimers, trimers or tetramers. At 48 hrs, the D_H of citrate Ag-NPs significantly reduced due to continuous dissolution after the aeration flow stopped (Table 4-15). The D_H of PVP Ag-NPs was slightly increased, meaning that after their partial dissolution, PVP particles may have grown via the reduction of $Ag(NH_3)_2^+$ by the UV light (Montazer et al., 2012) on the NPs surface (Figure 4-15).

The higher value of PVP Ag-NPs PDI at 45 hrs was probably a consequence of their high-level of dissolution during the aeration phase, causing the particles to agglomerate due to the reduction of their steric hindrance. Also at 48 hrs, the possible deposition of reduced Ag/PVP atoms on the particles surface during the settling phase might have increased not only the size of the particles but also the passivation of their surface, hence a slight reduction of their polydispersity. There was no significant difference between the citrate and PVP Ag-NPs average D_H and PDI behaviours overtime and at a STP **(**Table A3 - 21**).**

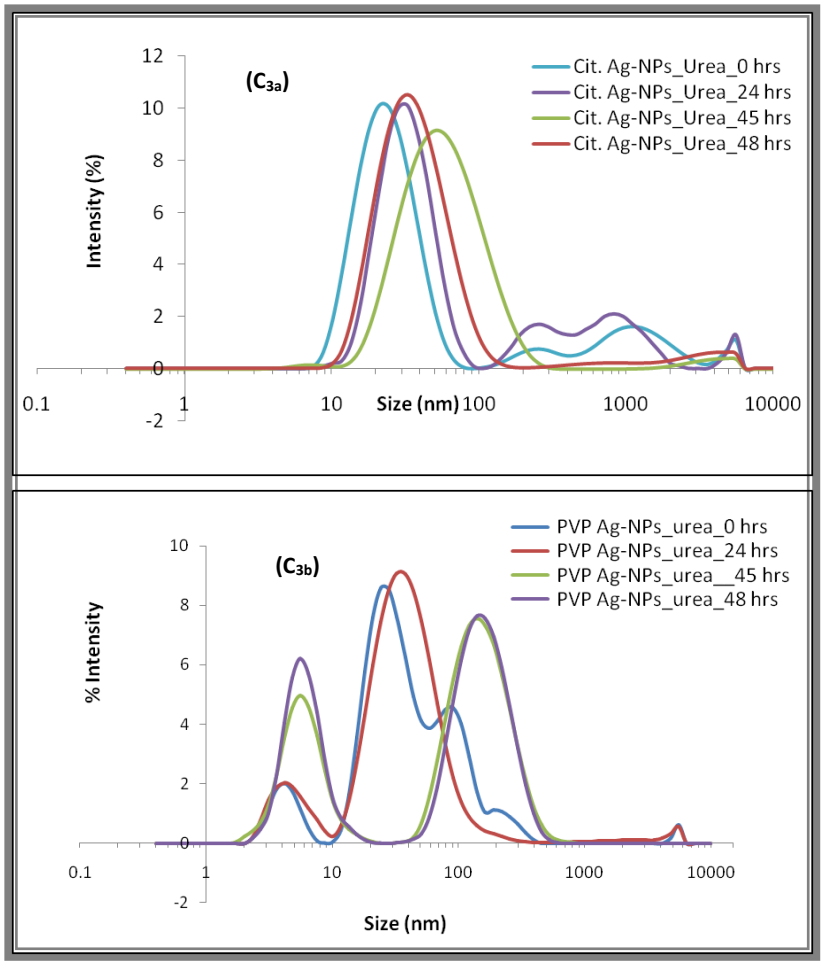

Figure 4-17: D_H distribution of the citrate (C_{3a}) and PVP (C_{3b}) Ag-NPs in 30 mg*L^{-1} urea (at 0 hrs, 24 hrs, 45 hrs (during aeration) and at 48 hrs (during settling)).

Table 4-17: DLS data (relating to Figure 4-14) for citrate Ag-NPs in 30 mg*L^{-1} urea (at 0 hrs, 24 hrs, 45 hrs (during aeration) and at 48 hrs (during settling))

	Citrate Ag-NPs in urea		PVP Ag-NPs in urea	
	Primary peak (D_H) (nm)	**PDI**	**Primary peak (D_H) (nm)**	**PDI**
0 hrs	24.9 ± 2.9	0.50 ± 0.05	30.6 ± 4.5	0.18 ± 0.01
24 hrs	33.1 ± 2.5	0.37 ± 0.25	44.6 ± 10.0	0.48 ± 0.02
45 hrs	64.5 ± 3.2	0.33 ± 0.01	166.7 ± 13.7	0.97 ± 0.04
48 hrs	38.8 ± 3.4	0.32 ± 0.02	168.6 ± 8.3	0.89 ± 0.06

The settling velocity of the Ag-NPs at 48 hrs was calculated and Table 4-18 shows that citrate Ag-NPs had a faster settling rate than PVP Ag-NPs when dispersed in 30 mg*L^{-1} urea solution.

However, similar to the peptone and meat-extract cases, the three hours settling time was not sufficient to have most, or all the Ag-NPs settled at the bottom of the beaker.

Table 4-18: Settling velocity with the corresponding DH size of citrate and PVP Ag-NPs in 30 mg/L urea (at 0 hrs, 24 hrs, 45 hrs (during aeration) and at 48 hrs (during settling))

	D_H (nm) At 48 hrs	Settling velocity ($nm*s^{-1}$)	Settling time (weeks)
Citrate Ag-NPs in urea	38.8 ± 3.4	6.83	16.94
PVP Ag-NPs in urea	5.8 ± 0.8	0.15	758.35

4.3.3.4. TEM characterisation of citrate and PVP Ag-NPs in urea

The TEM data and images (Table 4-19 and Figure 4-18 and Figure 4-19) show that citrate Ag-NPs dispersed in urea initially agglomerated while no agglomeration was observed for the PVP Ag-NPs. Over time, including and during the aeration phase, the citrate Ag-NPs dissolved while the PVP Ag-NPs remained mostly unchanged. However, at 48 hrs, both citrate and PVP Ag-NPs showed agglomeration, with the PVP agglomerates being significantly larger than the citrate agglomerates. There was no significant difference between citrate and PVP Ag-NPs size behaviour overtime and at a STP (Table A3 - 22).

Table 4-19: TEM average size and shape factor of citrate and PVP Ag-NPs in 30 $mg*L^{-1}$ urea (at 0 hrs, 24 hrs, 45 hrs (during aeration) and at 48 hrs (during settling)).

	Citrate Ag-NPs in urea			PVP Ag-NPs in urea		
	Longest length (nm)	**Shortest length (nm)**	**Shape factor**	**Longest length (nm)**	**Shortest length (nm)**	**Shape factor**
0 hrs	20.3 ± 12.7	14.5 ± 8.9	0.88 ± 0.10	11.6 ± 4.9	9.2 ± 3.6	0.97 ± 0.04
24 hrs	12.5 ± 7.3	8.7 ± 4.9	0.93 ± 0.09	12.8 ± 6.3	9.9 ± 4.7	0.96 ± 0.06
45 hrs	11.4 ± 6.3	8.0 ± 4.3	0.91 ± 0.12	13.2 ± 6.2	10.4 ± 5.1	0.96 ± 0.06
48 hrs	13.7 ± 5.5	9.5 ± 3.3	0.90 ± 0.10	18.3 ± 11.7	13.5 ± 8.4	0.91 ± 0.09

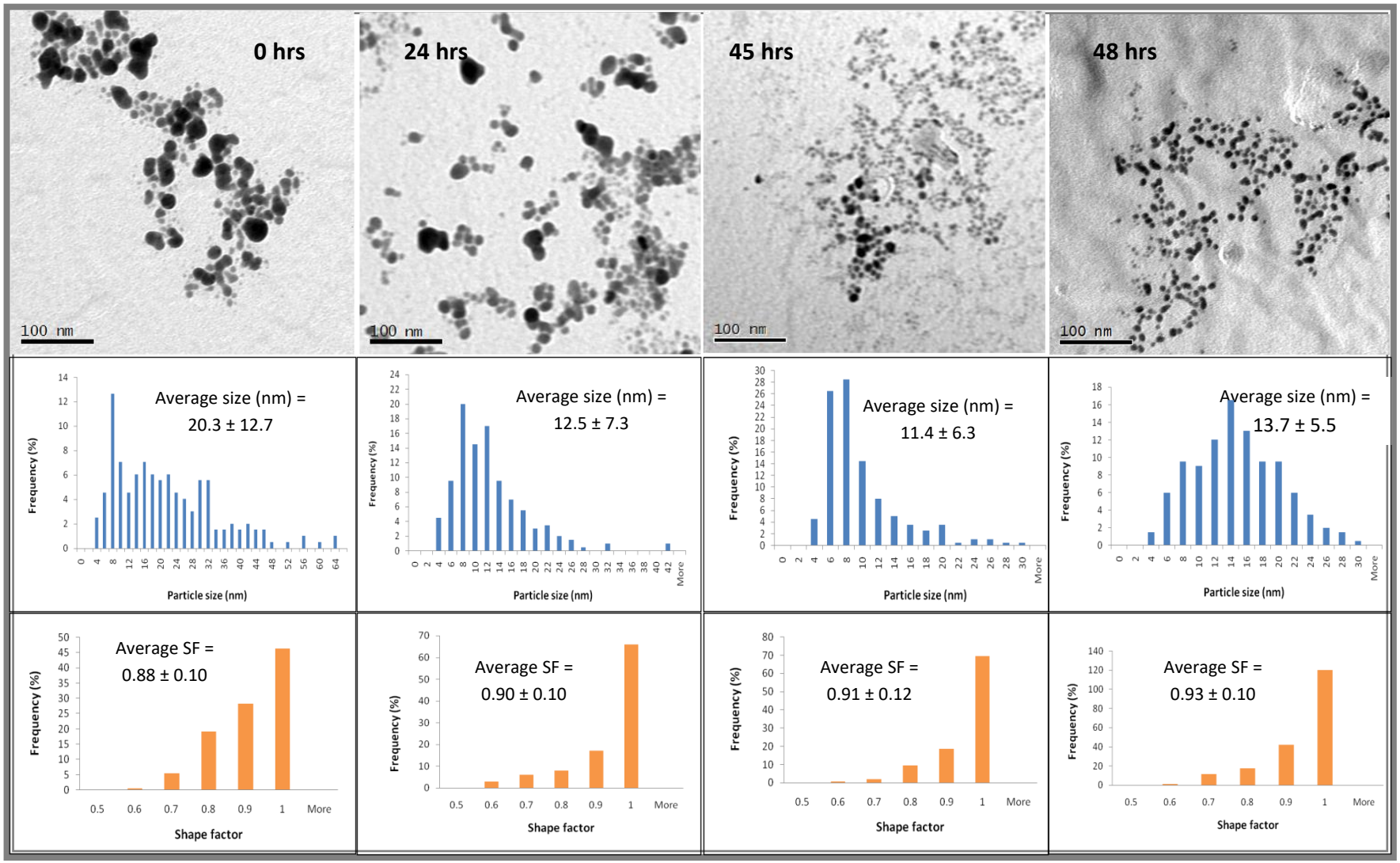

Figure 4-18: TEM primary particle size distribution of citrate Ag-NPs in 30 mg/L urea (at 0 hrs, 24 hrs, 45 hrs (during aeration) and at 48 hrs (during settling)).Based on the count of 198 NPs for the 0 hrs and 200 NPs for the 24 hrs, 45 hrs and 48 hrs samples

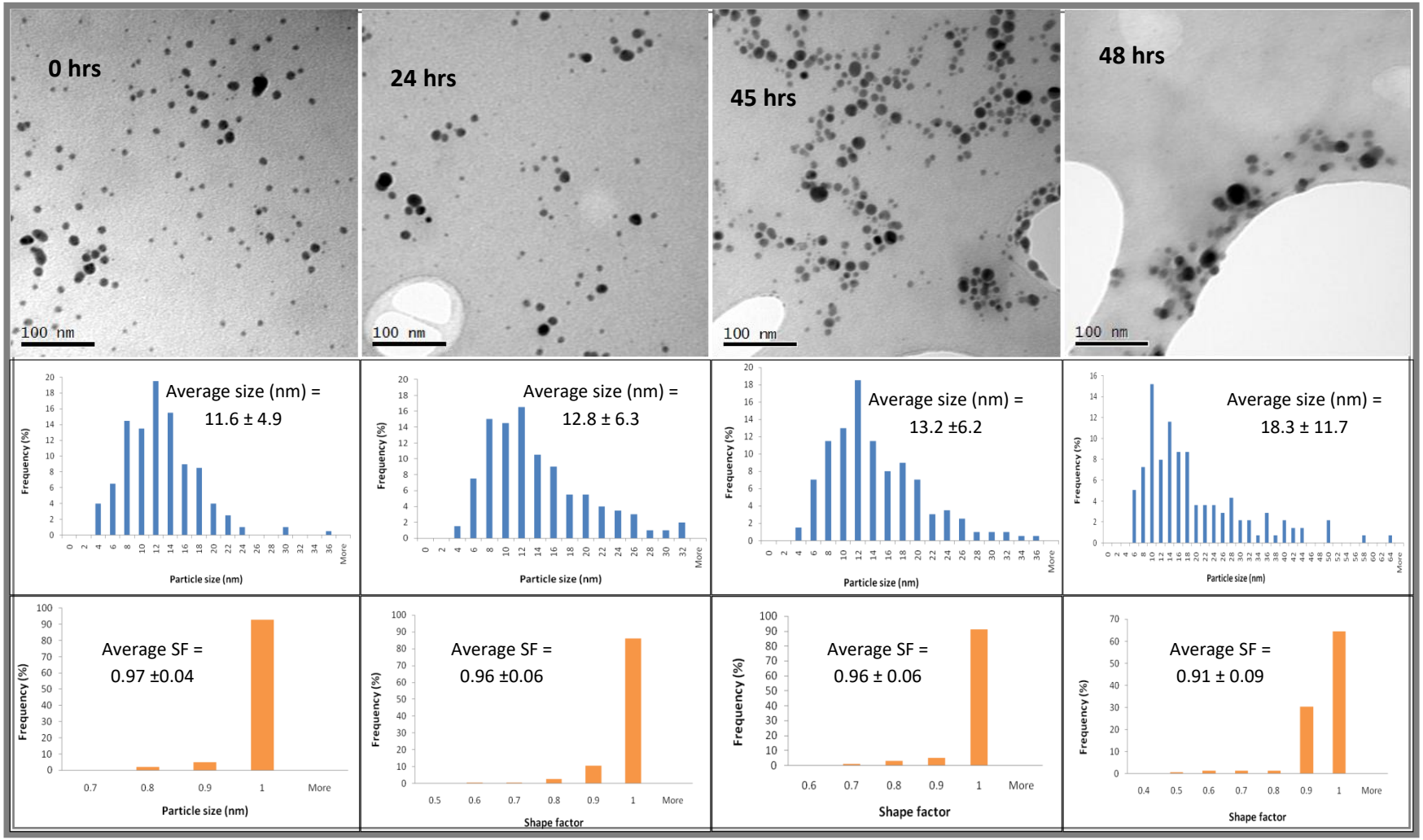

Figure 4-19: TEM primary particle size distribution of PVP Ag-NPs in 30 mg/L urea (at 0 hrs, 24 hrs, 45 hrs (during aeration) and at 48 hrs (during settling)). Based on the count of 200 NPs for the 0 hrs, 24 hrs, and 45 hrs samples and 138 NPs for the 48 hrs sample

4.3.3.5. Surface chemistry analysis: ZP of citrate and PVP Ag-NPs in urea

In 30 mg*L^{-1} urea, the ZP of the citrate and PVP Ag-NPs became more negative at 0 hrs (Table 4-20and Figure 4-20), and their average values were both in the same range. Because the ZP of the pristine PVP Ag-NPs was found to be -8.57 ± 0.88 mV (Table 3-8) it can be concluded that PVP Ag-NPs dispersed in urea were mostly stable, and this stability may have been maintained throughout the entire experiment based on the ZP values at the different time points. For the citrate Ag-NPs However, although they were more negative at 24 hrs, aeration of the solution caused an increase of their ZP making them more unstable and which was also the case during the settling stage. There was no significant difference between citrate and PVP Ag-NPs size behaviour overtime and at a STP (Table A3 - 21).

We can note that the pH of the meat-extract (Figure 4-14) solution has a similar trend as the peptone medium (Figure 4-8) for both citrate and PVP Ag-NPs. Also, the pH increased with time before aeration and decreased during and after aeration for the PVP Ag-NPs, but increased (very slightly) after aeration for the citrate Ag-NPs. A study conducted by Tai et al. (2014) on the dissolution and aggregation kinetics of 20 nm citrate Ag-NPs in acidic media (HNO3; pH in 2.9 – 6.4 range) over 19 hours, found the aggregation rate of Ag-NPs increased with the acidity of the medium within the first 10 min of their exposure (Axson et al., 2015). Because of the buffering nature of the sodium citrate, the dispersion of citrate-capped Ag-NPs in urea lowered it pH from 7 – 9.5 (SigmaAldrich) to a more acidic pH (< 7). Thus, the citrate coating may have corroded causing a reduction of the electrostatic stabilisation of the particles and leading to Van der Waal's interactions between them. As a consequence, dispersed citrate Ag-NPs agglomerated within the first hour of their exposure in urea as

shown by the TEM images (Figure 4-18). This may explain the significant reduction in the negativity of their ZP from -37.8 ± 1.4 mV before exposure (Table 3-9) to -10.5 ± 3.74 mV at 0 hrs of their exposure.

Table 4-20: ZP and pH of citrate and PVP Ag-NPs in30 mg/L urea (at 0 hrs, 24 hrs, 45 hrs (during aeration) and at 48 hrs (during settling)) extracted from Figure 4-17.

	Citrate Ag-NPs in meat-extract		PVP Ag-NPs in meat-extract	
	pH	**ZP (mV)**	**pH**	**ZP (mV)**
0 hrs	6.94	-10.5 ± 3.74	7.75	-10.3 ± 1.46
24 hrs	6.57	-13.00 ± 0.32	7.78	-11.2 ± 0.46
45 hrs	6.78	-6.07 ± 1.9	8.13	-19.6 ± 1.04
48 hrs	6.74	-4.62 ± 0.90	7.75	12.6 ± 0.86

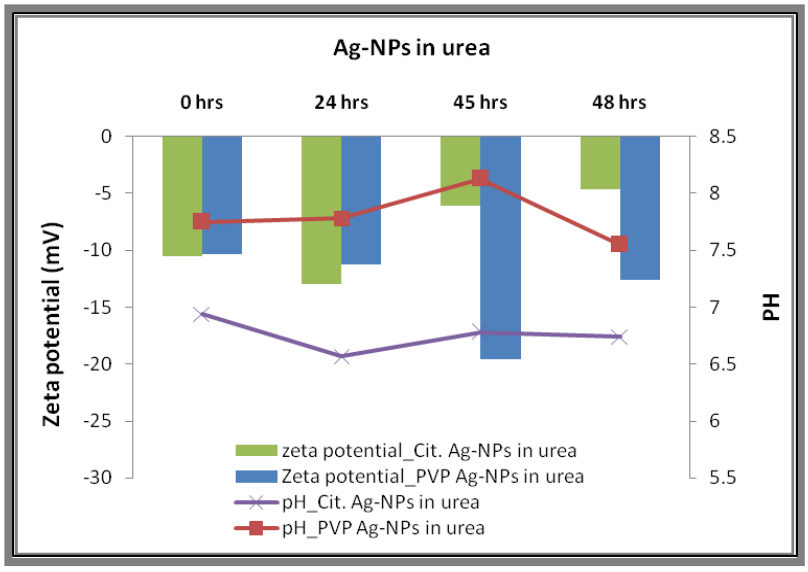

Figure 4-20: Variation of the citrate and PVP capped Ag-NPs ZP dispersed in 30 mg/L urea (at 0 hrs, 24 hrs, 45 hrs (during aeration) and at 48 hrs (during settling)) and the corresponding changes in solution pH.

4.3.4. Citrate and PVP Ag-NPs in K_2HPO_4

Ag-NPs in K_2HPO_4 released Ag^+ ions as the particles dissolved under the oxidation mechanism. It was observed by Yu et al. (2015) that, when exposed to Ag^+ (from $AgNO_3$) solution, Ba_3PO_4 nanosheets formed through precipitation of Na_3PO_4 and barium chloride (BaCl) had their surface covered with Ag_3PO_4 cubes formed by the precipitation of released PO_4^{3-} ions from the Ba_3PO_4 nanosheets with Ag^+ ions. As a result, they obtained Ba-doped (barium-doped) Ag_3PO_4 hollow nanosheets. Thus, for this study, it may be assumed that dissolved Ag^+ ions from the Ag-NPs will react with the PO_4^{3-} ions (from K_2HPO_4) via formation of Ag_3PO_4 through precipitation onto the NPs surface.

As a consequence, the surface of the NPs may be passivated, leaving the NPs subject to agglomeration. In fact, the passivation of the NP surfaces reduces the electrostatic (citrate Ag-NPs) and steric (PVP Ag-NPs) forces existing between them, leaving place for the existence of Van der Waal's attraction between the NPs. And, with time, the agglomerated particles may aggregate and form Ag_3PO_4 NPs as (Figure 4-21).

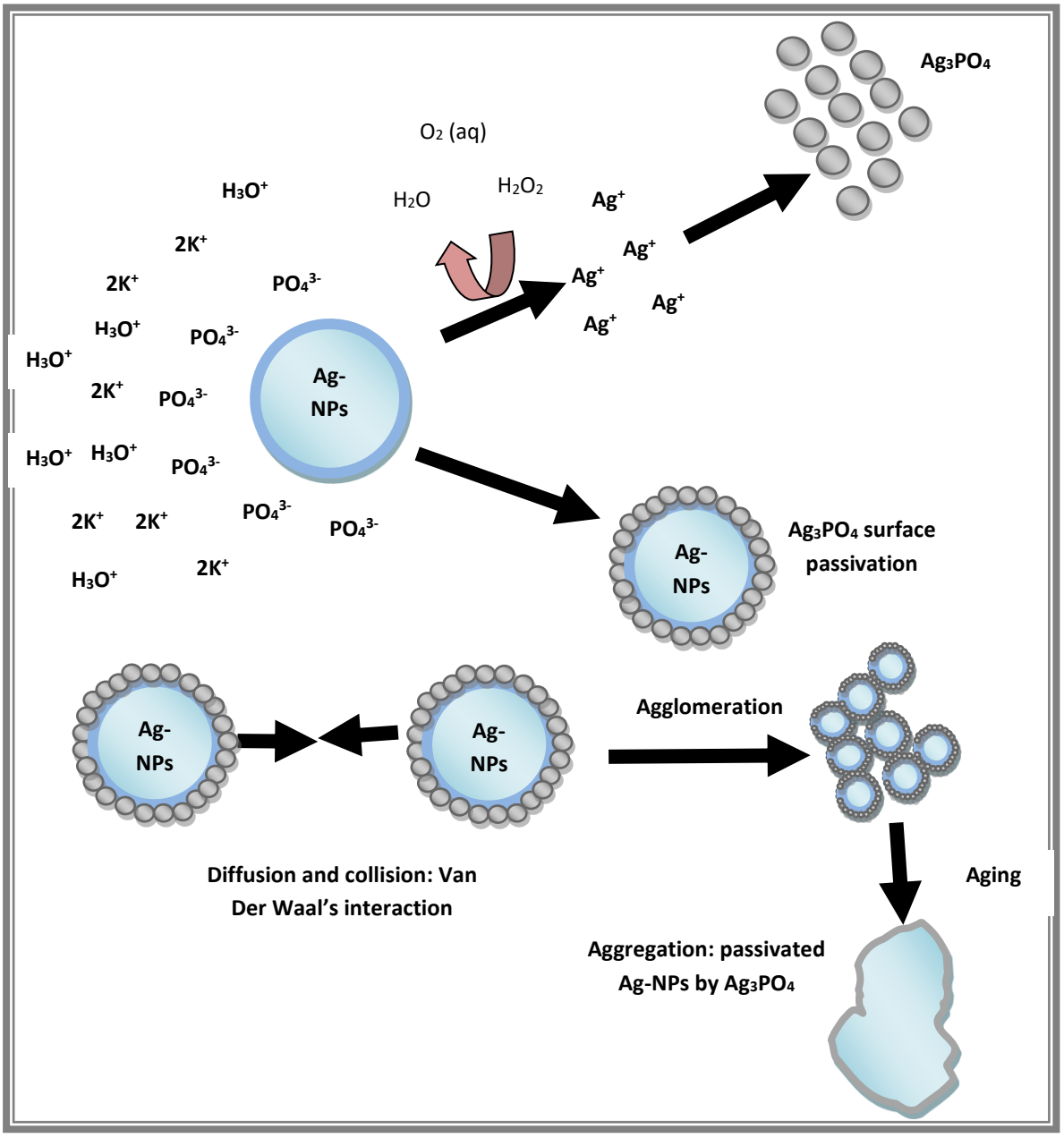

Figure 4-21: Illustration of dispersed citrate Ag-NPs in dissolved K_2HPO_4 solution. Ag-NPs dissolved through oxidation/dissolution mechanism, Ag^+ precipitation into Ag_3PO_4; agglomeration of passivate

4.3.4.1. Dissolution study: silver concentration in K_2HPO_4

A rapid dissolution of both Ag-NPs was observed initially (at 0 hours), although the rate of subsequent dissolution was low for the first 24 hours (Table 4-21). During aeration (at 45 hrs) However, the amount of Ag^+ for the PVP Ag-NPs increased greatly and more than half of the

PVP Ag-NPs dissolved compared with 10.61% for the citrate Ag-NPs. In the settling stage, both citrate and PVP Ag-NPs continued to dissolve. However, at the end of the experiment (at 48 hrs), only 14% of total Ag in the medium spiked with PVP Ag-NPs were not dissolved, versus 85% for the citrate Ag-NPs (based on the total recovered Ag concentration). Hence, when looking at their dissolution in 28 mg*L^{-1} of K_2HPO_4 medium, citrate Ag-NPs were more stable than the PVP Ag-NPs. There was no significant difference between both particles overtime or at a STP regarding their $C_{Total\ Ag}$, %dissolved Ag and %unrecovered Ag variations (Table A3 - 18).

Table 4-21: Changes in Ag concentration when citrate and Ag-NPs were dispersed into of 28 mg*L^{-1} K_2HPO_4 (at 0 hrs, 24 hrs, 45 hrs (during aeration) and at 48 hrs (during settling)). Measured by GFAAS

	Citrate Ag-NPs in K_2HPO_4			PVP Ag-NPs in K_2HPO_4		
	$C_{Total\ Ag}$ (µg*L^{-1})	%Diss. Ag	%Unr. Ag	$C_{Total\ Ag}$ (µg*L^{-1})	%Diss. Ag	%Unr. Ag
0 hrs	669.3 ± 15.9	7.6 ± 0.1	0	601.5 ± 15.3	6.1 ± 0.7	0
24 hrs	628.7 ± 19.3	9.2 ± 0.5	6.10	560.1 ± 20.9	10.8 ± 0.7	6.90
45 hrs	568.8 ± 4.5	10.6 ± 0.8	15.02	296.1 ± 10.6	54.2 ± 1.0	38.70
48 hrs	535.8 ± 31.2	15.3 ± 1.2	19.94	200.9 ± 17.9	83.7 ± 2.6	42.19

4.3.4.2. UV-Vis characterisation of citrate and PVP Ag-NPs in K_2HPO_4

In the presence of 28 mg*L^{-1} K_2HPO_4 (Figure 4-22), the MA of citrate and PVP Ag-NPs was observed at a similar wavelength (λ_{max} = 392 nm) as the pristine Ag-NPs suspension. After 24 hours, the λ_{max} (Table 4-22) remained constant in both cases as well as the FWHM of the UV-Vis spectra. During aeration at 45 hrs, the UV-Vis spectrum of citrate Ag-NPs underwent a blue-shift to λ_{max} = 390 nm while a red shift (λ_{max} = 440 nm) was observed for the PVP Ag-NPs.

The spectra were also much wider and the MA highly reduced. At 48 hrs after settling, a red shift was observed for the citrate Ag-NPs with λ_{max} = 397 nm while the MA for PVP Ag-NPs was constant (from the 45 hr value). Also, there was no change regarding the FWHM of both Ag-NPs UV-Vis peaks, meaning that, their average size which is inversely proportional (Manikandan et al., 2003, Ashkarran and Bayat, 2013, Picciotto et al., 2010) to the FWHM did not vary.

Based on these results, how the Ag-NPs might have reacted in the media during their exposure in K_2HPO_4 as illustrated in Figure 4-21, in which it could be assumed that citrate and PVP Ag-NPs underwent two transformations: dissolution through oxidation and agglomeration. Before aeration of the media (at 0 and 24 hrs), both citrate and PVP Ag-NPs had low dissolution levels with about 10% of Ag^+ present after 24 hrs of exposure (Table 4-21) which can be associated with the slight reduction of their MA in the UV-Vis spectrum Table 4-22.

In the absence of aeration during the first 24 hours, they may not agglomerate or have their surface chemistry changed, but they could oxidise and dissolve in the presence of aeration. Second, after aeration, their surface chemistry may change which caused a red shift in the UV-Vis spectrum. PVP Ag-NPs may not undergo further changes, and as a consequence, the FWHM and the MA of the UV-Vis spectrum did not significantly change during the first 24 hours. In fact, these changes occurred during aeration as their surface chemistry might be modified due to oxidation and dissolution. There was no significant difference in the MA changes between both particles overtime. There was a significant difference in the MA at a STP. But, the variations of λ_{max} at a STP for both particles were not significantly different (Table A3 - 19)

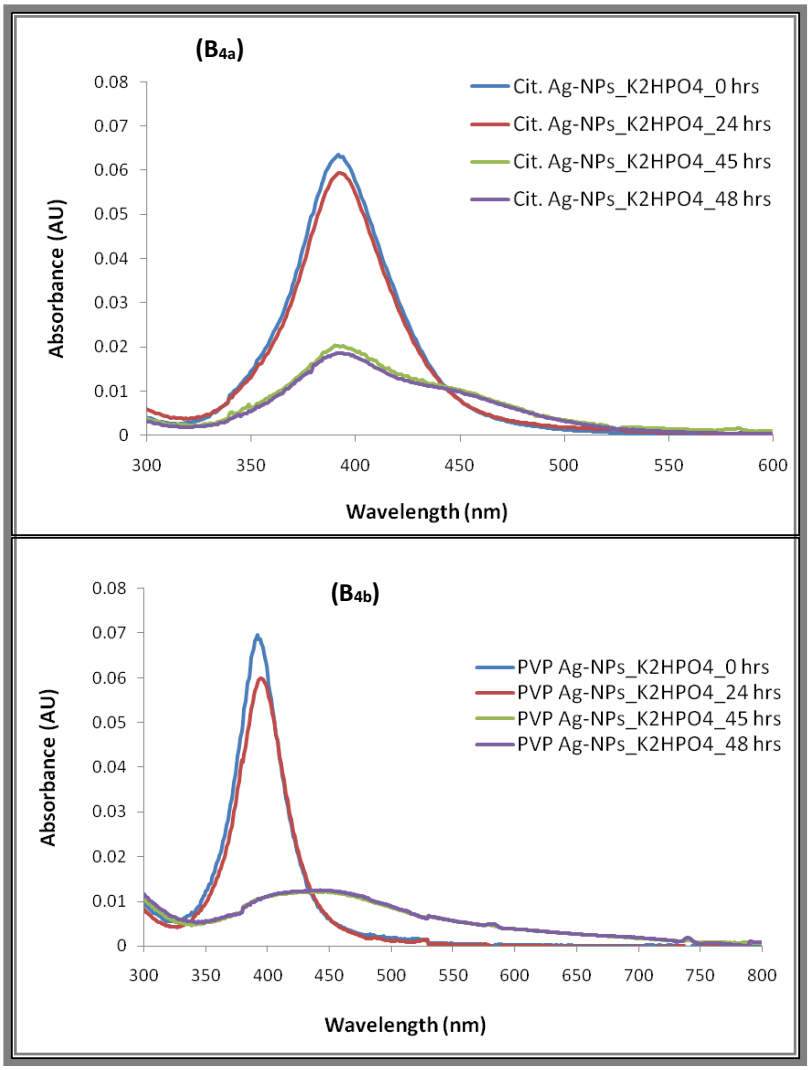

Figure 4-22: UV-Vis spectra of citrate (B_{4a}) and PVP (B_{4b}) Ag-NPs in 28 mg*L^{-1} K_2HPO_4 (at 0 hrs, 24 hrs, 45 hrs (during aeration) and at 48 hrs (during settling)).

Table 4-22: UV-Vis parameters (extracted from Figure 4-18) for citrate and PVP particles dispersed in 28 mg*L^{-1} K_2HPO_4 (at 0 hrs, 24 hrs, 45 hrs (during aeration) and at 48 hrs (during settling)).

	Citrate Ag-NPs in K_2HPO_4				PVP Ag-NPs in K_2HPO_4			
	0 hrs	**24 hrs**	**45 hrs**	**48 hrs**	**0 hrs**	**24 hrs**	**45 hrs**	**48 hrs**
λ_{max} (nm)	392	393	390	397	392	394	440	440
MA	0.063	0.059	0.020	0.019	0.070	0.060	0.012	0.013
Absorbance Decrease (%)	0	5.97	64.18	65.67	0	16.67	483.3	438.3
FWHM (nm)	51	51	83	89	42	45	179	178
Peak shift (%)	0	0.25	0.51	1.26	0	0.51	10.91	10.91

4.3.4.3. DLS characterisation of citrate and PVP Ag-NPs in K_2HPO_4

The DLS size distributions of citrate and PVP Ag-NPs dispersed in 28 mg*L^{-1} K_2HPO_4 are given in Figure 4-23 and Table 4-23. At 0 hrs, both citrate and PVP Ag-NPs appear to have agglomerated with D_H of 45.6 ± 3.7 and 30.0 ± 0.5 nm, respectively. However, due to the very high D_H value for the PVP Ag-NPs which could have been affected by the presence of large particulates, the average size (29.9 ± 0.46 nm) of the primary peak should be considered more representative. At 24 hrs, since the citrate NPs slightly dissolved (Table 4-21) the reduction of their D_H was certainly not related to their dissolution but probably caused by the reduced agglomeration. However, the increase of PDI from 0.43 at 0 hrs to 0.47 at 24 hrs suggested that some agglomeration of citrate Ag-NPs might have occurred indicated by the presence of a second peak at around 200 nm (Figure 4-23). The PVP Ag-NPs may have agglomerated by forming dimers after 24 hrs as D_H had doubled reaching a value of 63.2 ± 7.4 nm; as a consequence, their PDI was significantly higher.

During the aeration and the settling phases, both citrate and PVP Ag-NPs were highly agglomerated and polydisperse; their D_H at 45 hrs was in the 211 nm range. However, the D_H of the PVP Ag-NPs at 48 hrs was significantly reduced, although their degree of agglomeration might have been maintained because of their high polydispersity (PDI =1.00 ± 0.00) during that stage. There was no significant difference between the citrate and PVP Ag-NPs average D_H behaviour overtime and at a STP (Table A3 - 21). Also, no significant difference was observed for the variation of the PDI of both particles over time or at a STP.

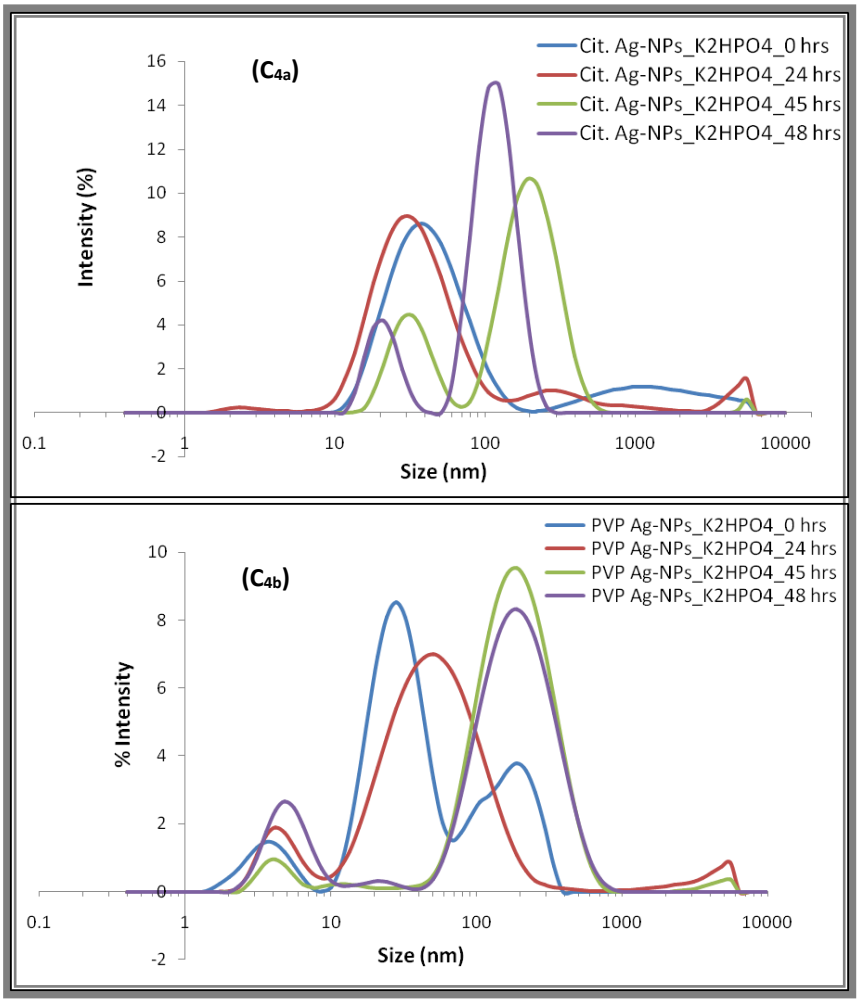

Figure 4-23: D_H distribution of the citrate (C_{4a}) and PVP (C_{4b}) Ag-NPs in 28 mg*L^{-1} K_2HPO_4 (at 0 hrs, 24 hrs, 45 hrs (during aeration) and at 48 hrs (during settling)).

Table 4-23: DLS data (extracted from Figure 4-19) of citrate and PVP Ag-NPs in 28 mg*L^{-1} K_2HPO_4 (at 0 hrs, 24 hrs, 45 hrs (during aeration) and at 48 hrs (during settling)).

	Citrate Ag-NPs in K_2HPO_4		PVP Ag-NPs in K_2HPO_4	
	Primary peak (D_H) (nm)	**PDI**	**Primary peak (D_H) (nm)**	**PDI**
0 hrs	45.6 ± 3.7	0.43 ± 0.1	29.9 ± 0.46	0.20 ± 0.06
24 hrs	37.3 ± 2.2	0.47 ± 0.10	63.2 ± 7.4	0.52 ± 0.14
45 hrs	33.1 ± 2.9	0.43 ± 0.19	211.3 ± 10.1	0.50 ± 0.09
48 hrs	21.3 ± 1.6	0.18 ± 0.01	218.4 ± 10.9	1.00 ± 0.00

An evaluation of the settling velocity of the Ag-NPs at 48 hrs Table 4-24) showed that citrate Ag-NPs had a higher velocity than PVP Ag-NPs when dispersed in 28 $mg*L^{-1}$ K_2HPO_4 solution. But, nearly two weeks or more would be needed to complete sedimentation of the Ag-NPs in both cases.

Table 4-24: Settling velocity with the corresponded D_H of citrate and PVP Ag-NPs in 28 $mg*L^{-1}$ K_2HPO_4 (at 48 hrs (during settling))

	D_H (nm) At 48 hrs	Settling velocity ($nm*s^{-1}$)	Settling time (weeks)
Citrate Ag-NPs in K_2HPO_4	21.3 ± 1.6	2.06	56.23
PVP Ag-NPs in K_2HPO_4	218.4 ± 10.9	21.64	0.53

4.3.4.4. TEM characterisation of citrate and PVP Ag-NPs in K_2HPO_4

The TEM data (Table 4-25, Figure 4-24and Figure 4-25) show that at 0 hrs citrate Ag-NPs dispersed in 28 $mg*L^{-1}$ K_2HPO_4 slightly agglomerated while there was no agglomeration observed for the PVP Ag-NPs. After 24 hrs, the citrate Ag-NPs might have slightly dissolved because of the reduction in their average size; while PVP Ag-NPs might have gone through dissolution and re-precipitation of Ag^+ as Ag_3PO_4 (Figure 4-21) on their surfaces, leading to increased polydispersity with no change in average size.

However during the aeration phase (at 45 hrs), the TEM images show the citrate Ag-NPs were agglomerated probably due to dissolution and re-precipitation Ag^+ into Ag_3PO_4onto their surfaces (Figure 4-21), leading to their passivation. Thus, as a consequence, the electrostatic forces existing between the citrate Ag-NPs were reduced, causing increased of agglomeration through Van der Waal's interactions (Figure 4-21) and increased polydispersity of the

particles. But at 48 hrs (settling phase), the agglomeration of citrate Ag-NPs was non-existent, and the average size of the particles was slightly reduced (Table 4-2) due to a low degree of dissolution as shown in Table 4-21 with only 15.3% of total Ag in the solution being Ag^+.

For PVP Ag-NPs, their continuous average size increase over the time might have been not only caused dissolution and re-precipitation of Ag^+ as attested above. It could have also been associated with the re-precipitation of smaller dissolved NPs (silver phosphate NPs (AgP NPs)) onto the large ones - this is known as Ostwald ripening (Wu et al., 2016). There was no significant difference between citrate and PVP Ag-NPs size behaviour overtime and at a STP (Table A3 - 22).

Table 4-25: TEM average primary particle size and shape factor of citrate Ag-NPs in 28 mg*L^{-1} K_2HPO_4 (at 0 hrs, 24 hrs, 45 hrs (during aeration) and at 48 hrs (during settling)). Data extracted from Figures 4-20 and 4-21.

	Citrate Ag-NPs in K_2HPO_4			PVP Ag-NPs in K_2HPO_4		
	Longest length (nm)	**Shortest length (nm)**	**Shape factor**	**Longest length (nm)**	**Shortest length (nm)**	**Shape factor**
0 hrs	15.2 ± 9.9	10.7 ± 5.9	0.86 ± 0.11	11.9 ± 4.3	9.8 ± 3.9	0.98 ± 0.03
24 hrs	11.2 ± 6.7	8.5 ± 4.8	0.91 ± 0.09	12.3 ± 5.8	9.7 ± 4.6	0.96 ± 0.07
45 hrs	14.9 ± 7.9	10.6 ± 5.3	0.89 ± 0.11	14.3 ± 9.6	10.8 ± 7.0	0.94 ± 0.08
48 hrs	12.1 ± 4.7	9.3 ± 3.5	0.95 ± 0.07	17.8 ± 9.2	13.4 ± 6.8	0.92 ± 0.08

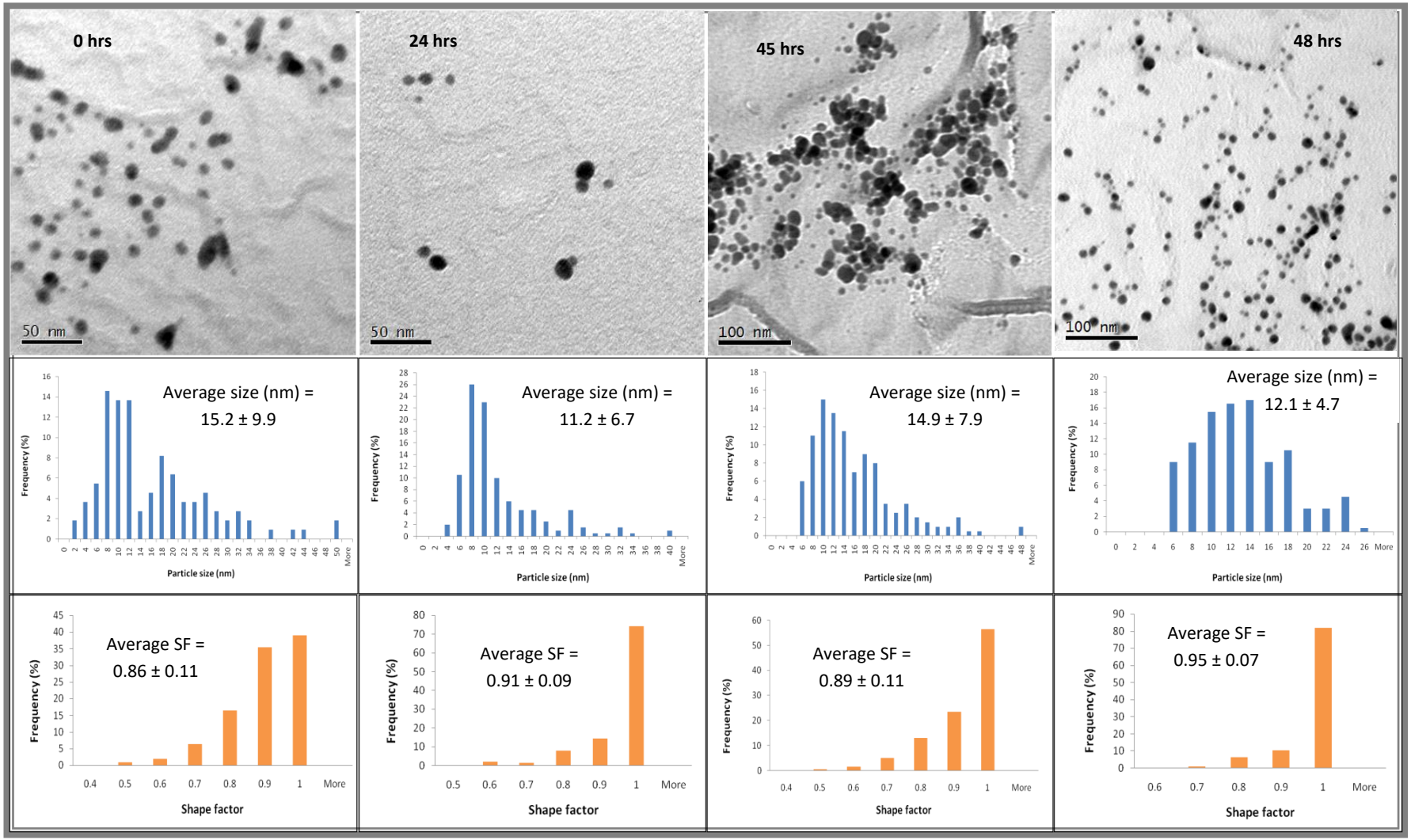

Figure 4-24: TEM primary particle size distribution of citrate Ag-NPs in 28 mg*L^{-1} K_2HPO_4 (at 0 hrs, 24 hrs, 45 hrs (during aeration) and at 48 hrs (during settling)). Based on the count of 110 NPs for the 0 hrs and 200 NPs for the 24 hrs, 45 hrs and 48 hrs samples

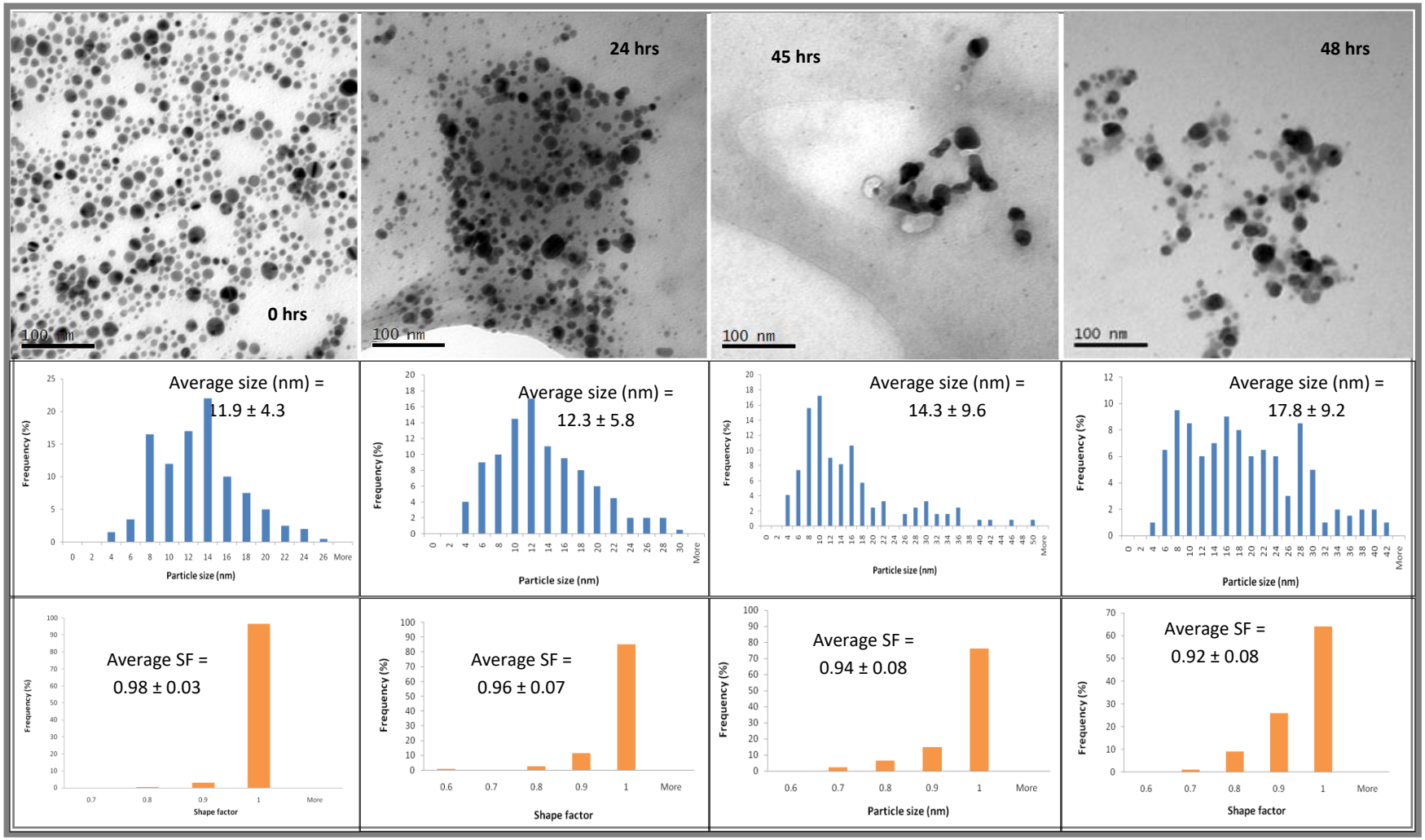

Figure 4-25: TEM primary particle size distribution of PVP Ag-NPs in 28 mg*L^{-1} K_2HPO_4 (at 0 hrs, 24 hrs, 45 hrs (during aeration) and at 48 hrs (during settling)). Based on the count of 200 NPs for the 0 hrs, 24 hrs and 48 hrs samples and 122 NPs for the 45 hrs sample

4.3.4.5. Surface chemical analysis: ZP of citrate and PVP Ag-NPs in K_2HPO_4

Citrate Ag-NPs were less negative (ZP = -8.76 ± 0.96 mV) when they were initially exposed to 28 $mg*L^{-1}$ K_2HPO_4, and the ZP remained unchanged during the first twenty-four hours and before aeration (Table 4-26). For the PVP Ag-NPs, the negative value of charge was increased at 0 hrs following their dispersions in the medium (Figure 4-26), meaning they were less sensitive to agglomeration. However, after 24 hours, their surface charge was reduced probably due to the limitation of the steric forces between the particles due to the precipitation of Ag^+ in the form of Ag_3PO_4 onto the NP surfaces (Figure 4-21). As a result, the particles were slightly agglomerated as shown in Figure 4-25.

The aeration of the solution in both cases affected the surface charge of the Ag-NPs by increasing their negative charge. At this stage, the agglomerated PVP Ag-NPs were stabilised, and their surface charge stayed constant even after the settling stage. The removal of the aeration flow in the citrate Ag-NPs may have caused a decrease in the negative charge of the NPs making them dissolve as found by the GFAAS (Table 4-21). The dissolution of the particles after aeration could be due to the oxidation mechanism (Figure 4-21) caused by excess O_2 in the solution. There was no significant difference between citrate and PVP Ag-NPs size behaviour overtime or at a STP (Table A3 - 21).

The K_2HPO_4 can be used a buffer solution with a pH of about 7.0 (Klecka and Gonsior, 1984). It is important to note that the pH of the solution spiked with PVP Ag-NPs mostly stayed constant and in the case of the citrate Ag-NPs, it decreased (Figure 4-26) – with a noticeable change occurring at 24 hrs and 48 hrs. In fact, the changes in the surface chemistry of the

citrate Ag-NPs might affect the pH of the medium because of the buffering nature of citrate (section 4.3.4.5); while for the PVP Ag-NPs these changes may have no effects on the pH.

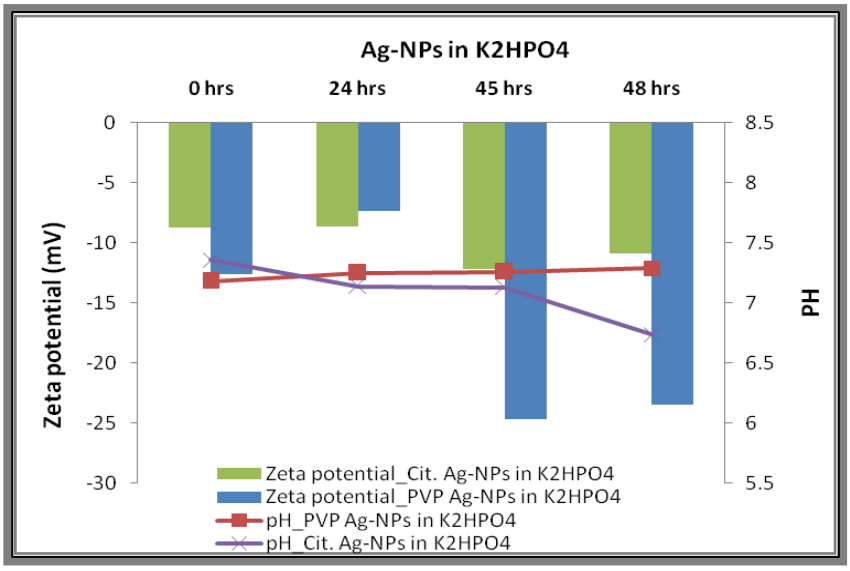

Figure 4-26: Variation of the citrate and PVP capped Ag-NPs ZP when dispersed in 28 mg*L^{-1} K_2HPO_4 (at 0 hrs, 24 hrs, 45 hrs (during aeration) and at 48 hrs (during settling)) and the consequent changes in pH.

Table 4-26 : ZP and pH of citrate and PVP Ag-NPs in 28 mg*L^{-1} K_2HPO_4 (at 0 hrs, 24 hrs, 45 hrs (during aeration) and at 48 hrs (during settling)) extracted from Figure 4-17.

	Citrate Ag-NPs in K_2HPO_4		PVP Ag-NPs in K_2HPO_4	
	pH	**ZP (mV)**	**pH**	**ZP (mV)**
0 hrs	7.36	-8.76 ± 0.96	7.18	-12.6 ± 0.78
24 hrs	7.14	-8.65 ± 3.10	7.25	-7.33 ± 1.56
45 hrs	7.13	-12.20 ± 0.58	7.26	-24.7 ± 0.61
48 hrs	6.74	-10.9 ± 0.78	7.29	-23.5 ± 0.96

4.3.5. Citrate and PVP Ag-NPs in NaCl

In the presence of NaCl aqueous solution, Ag-NPs will oxidise and dissolved by releasing Ag^+ ions which rapidly precipitate into AgCl (Loza et al., 2014, Fargasova et al., 2015). AgCl can

also slow down the dissolution of the particles by passivating their surface, which leads to growth in size; this causes the collision of the particles through Van Der Waal's interactions (Figure 4-27) (Loza et al., 2014, Axson et al., 2015). Particles will then agglomerate through ageing due to the decreased of the electrostatic repulsion in the solution (Axson et al., 2015).

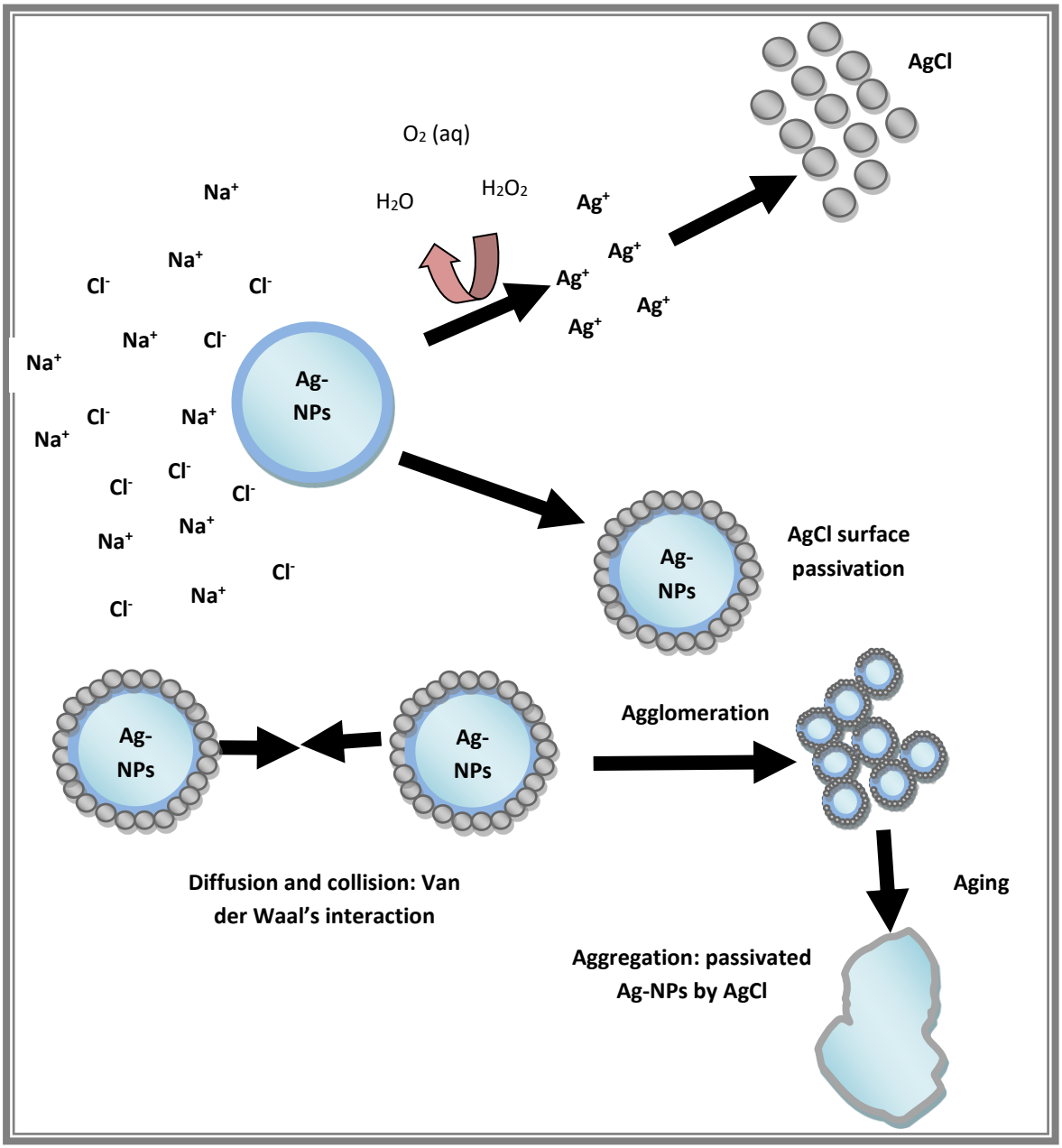

Figure 4-27: illustration of dispersed citrate Ag-NPs in dissolved NaCl solution. Ag-NPs dissolved through oxidation/dissolution mechanism, Ag^+ precipitation into AgCl; agglomeration of passivated Ag-NPs by Van der Waal's interactions following aggregation through aging. (Loza et al., 2014, Axson et al., 2015).

4.3.5.1. Dissolution study: silver concentration in NaCl

In 7 mg*L^{-1} NaCl medium, citrate and PVP Ag-NPs had similar degrees of dissolution at 0 hrs, as shown in Table 4-31. But after 24 hrs, dissolution increased with citrate Ag-NPs whereby the dissolved Ag fraction doubled, whereas in the PVP case, the dissolution was very low. However, in the presence of aeration (at 45 hrs), PVP Ag-NPs were highly dissolved with only about 25% of the total Ag occurring as particles as opposed to the 58% of Ag-NPs in the medium containing the citrate Ag-NPs. Hence, PVP Ag-NPs were more sensitive to aeration than citrate Ag-NPs.

More than 50% of the initial concentration of both Ag-NPs was not recovered, probably due to the particles sticking to the glass or aeration tube. There was no significant difference between both particles overtime regarding their $C_{Total\ Ag}$, %dissolved Ag and %unrecovered Ag with their respective ANOVA parameters (Table A3 - 18). However, the ANOVA analysis comparing the changes in $C_{Total\ Ag}$, %dissolved Ag and %unrecovered Ag between citrate and PVP Ag-NPs at a STP were significantly different. Thus, we may conclude that addition of oxygen in the NaCl solution will significantly accelerate the dissolution of PVP Ag-NPs.

Table 4-27: Changes in Ag concentration when citrate and Ag-NPs were dispersed into 7 mg*L^{-1} NaCl (at 0 hrs, 24 hrs, 45 hrs (during aeration) and at 48 hrs (during settling)). Measured by GFAAS

	Citrate Ag-NPs in NaCl			PVP Ag-NPs in NaCl		
	$C_{Total\ Ag}$ (µg*L^{-1})	%Diss. Ag	%Unr. Ag	$C_{Total\ Ag}$ (µg*L^{-1})	%Diss. Ag	%Unr. Ag
0 hrs	573.6 ± 3.4	6.0 ± 0.5	0	600.6 ± 33.0	5.1 ± 0.5	0
24 hrs	412.4 ± 4.4	11.9 ± 2.2	26.53	583.8 ± 3.1	6.8 ± 1.2	30.12
45 hrs	321.0 ± 10.0	32.1 ± 0.7	44.03	368.2 ± 32.1	63.9 ± 1.3	43.25
48 hrs	259.8 ± 2.0	41.5 ± 2.7	54.70	347.2 ± 23.0	76.5 ± 2.3	67.71

4.3.5.2. UV-Vis characterisation of citrate and PVP Ag-NPs in NaCl

In 7 mg*L^{-1} NaCl, the UV-Vis spectra of citrate and PVP Ag-NPs (Figure 4-28) were initially red-shifted, and their MA occurred at 394 nm and 400 nm (Table 4-28), respectively. After 24 hrs, the λ_{max} of the citrate Ag-NPs slightly increased while for the PVP Ag-NPs the MA occurred at a constant wavelength. Also, the λ_{max} of the citrate Ag-NPs decreased while remaining constant for PVP Ag-NPs and the FWHM of the UV-Vis spectrum did not significantly change in both cases. After aeration (45 hrs), the UV-Vis spectra further red-shifted, and their MA occurred at 399 nm for the citrate Ag-NPs and 410 nm for the PVP Ag-NPs. Thus, the aeration of the NaCl solution might have caused the NPs size to increased (red shift). At 48 hrs, after settling, there was no significant change in the Ag-NPs UV-Vis spectra since their MA and corresponding λ_{max} remained constant.

In 7 mg*L^{-1} NaCl medium, citrate and PVP Ag-NPs undergo two processes. Initially, the formation of AgCl on their surface may have slowed down their dissolution through surface passivation. As a consequence, both citrate and PVP Ag-NPs did not change significantly in size or suffer from agglomeration or dissolution prior to aeration. Subsequently, the introduction of aeration might have altered the surface of the Ag-NPs increasing their oxidation/dissolution due to the addition of oxygen. This explains the red-shift of the UV-Vis spectrum as a result of modification their surface chemistry through AgCl passivation (Figure 4-27). There was no significant difference in the MA of both particles overtime or at a STP (Table A3 - 19). While the variation of λ_{max} overtime of citrate and PVP particles were significantly different, no significant difference was found in λ_{max} changes at a STP.

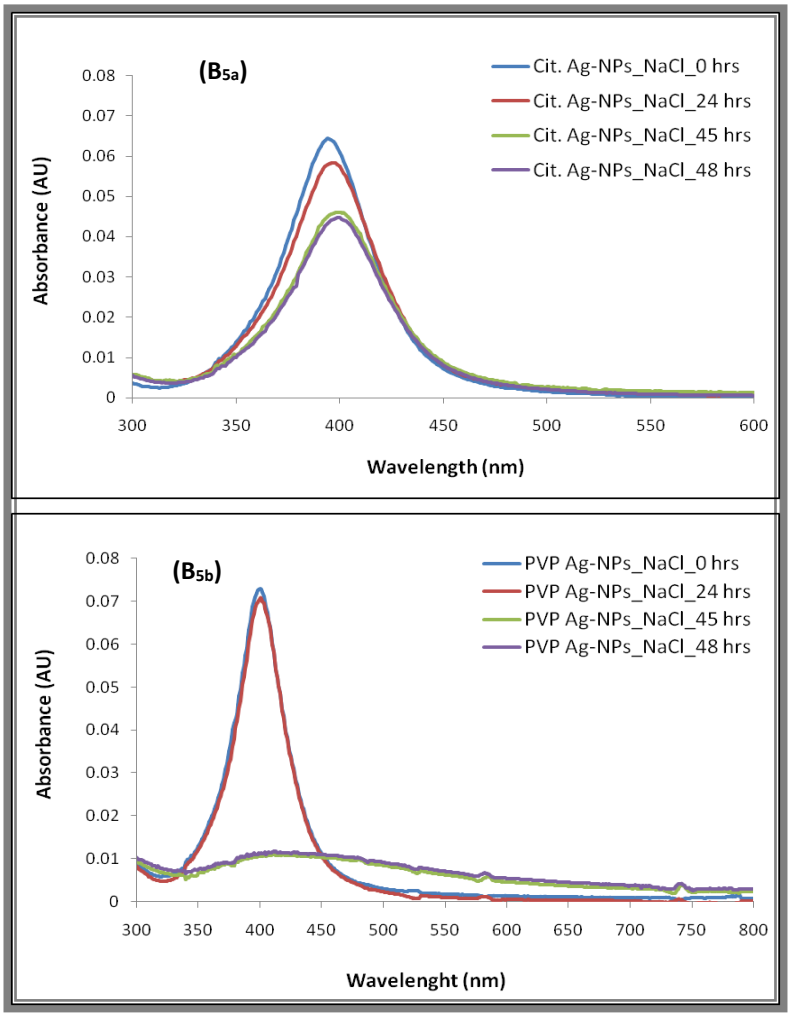

Figure 4-28: UV-Vis spectra of citrate (B_{5a}) and PVP (B_{5b}) Ag-NPs in 7 mg*L^{-1} NaCl (at 0 hrs, 24 hrs, 45 hrs (during aeration) and at 48 hrs (during settling)).

Table 4-28: UV-Vis data (from Figure 2-23) of citrate and PVP Ag-NPs 7 mg*L^{-1} NaCl (at 0 hrs, 24 hrs, 45 hrs (during aeration) and at 48 hrs (during settling)).

Citrate Ag-NPs in NaCl					PVP Ag-NPs in NaCl			
	0 hrs	**24 hrs**	**45 hrs**	**48 hrs**	**0 hrs**	**24 hrs**	**45 hrs**	**48 hrs**
λ_{max} (nm)	394	396	399	399	400	400	410	411
MA	0.064	0.058	0.046	0.045	0.073	0.071	0.011	0.012
Absorbance Decrease (%)	0	8.95	26.86	28.36	0	2.82	563.6	508.3
FWHM (nm)	48	50	55	54	47	47	226	233
Peak shift (%)	0.00	0.50	1.25	1.25	0	0	2.44	2.67

4.3.5.3. DLS characterisation of citrate and PVP Ag-NPs in NaCl

The DLS size distributions of citrate and PVP Ag-NPs in 7 $mg*L^{-1}$ NaCl are shown in Figure 4-29 and Table 4-29. Both citrate and PVP Ag-NPs may have had their capping agents partially stripped off, leading to the release of Ag^+ through oxidation/dissolution process (Figure 4-27). These Ag^+ ions rapidly precipitated onto the NP surfaces, causing the formation of a passivation layer that increasing their D_H to 43.0 ± 3.8 and 43.9 ± 4.2 nm, respectively. At 24 hrs, the size of citrate particles may have continued to grow as more AgCl formed on their surface, while, the average size of PVP Ag-NPs was reduced due to more corrosion of the PVP coating with time, leading to their dissolution. Both particles were quite polydisperse within the first 24 hours, and the average PDI was about 0.4 at 24 hrs time point.

During aeration, the average size of the citrate Ag-NPs decreased to an average of 34.3 ± 3.6 nm, certainly due to the addition of the oxygen which might have affected the AgCl layer on their surface and caused the release of more Ag^+. PVP Ag-NPs may have agglomerated into tetramers, reaching an average size of 155.6 ± 7.8 nm. After aeration, the average size of both particles was slightly decreased, likely due to continuous dissolution of citrate Ag-NPs and agglomeration of the PVP particles.

There was no significant difference between the citrate and PVP Ag-NPs average D_H behaviour over time or at a STP (Table A3 - 21). Also, no significant different was observed for the variation of the PDI of both particles overtime and at a STP. These results suggest that the behaviour Ag-NPs in NaCl medium under aerobic conditions was independent of their coating. However, the above data clearly show that, although citrate and PVP Ag-NPs may have gone

through a similar transformation as illustrated in Figure 4-27, their exposure to an oxygen flow might have led to their dissolution and agglomeration respectively.

Table 4-29: DLS data of citrate Ag-NPs in 7 mg*L^{-1} NaCl (at 0 hrs, 24 hrs, 45 hrs (during aeration) and at 48 hrs (during settling))

	Citrate Ag-NPs in NaCl		PVP Ag-NPs in NaCl	
	Primary peak (D_H) (nm)	**PDI**	**Primary peak (D_H) (nm)**	**PDI**
0 hrs	43.0 ± 3.8	0.40 ± 0.1	43.9 ± 3.3	0.56 ± 0.07
24 hrs	48.8 ± 3.6	0.38 ± 0.07	35.8 ± 6.7	0.44 ± 0.15
45 hrs	34.3 ± 3.6	0.56 ± 0.10	155.6 ± 7.8	0.25 ± 0.02
48 hrs	32.1 ± 0.7	0.57 ± 0.02	147.0 ± 29.2	0.24 ± 0.02

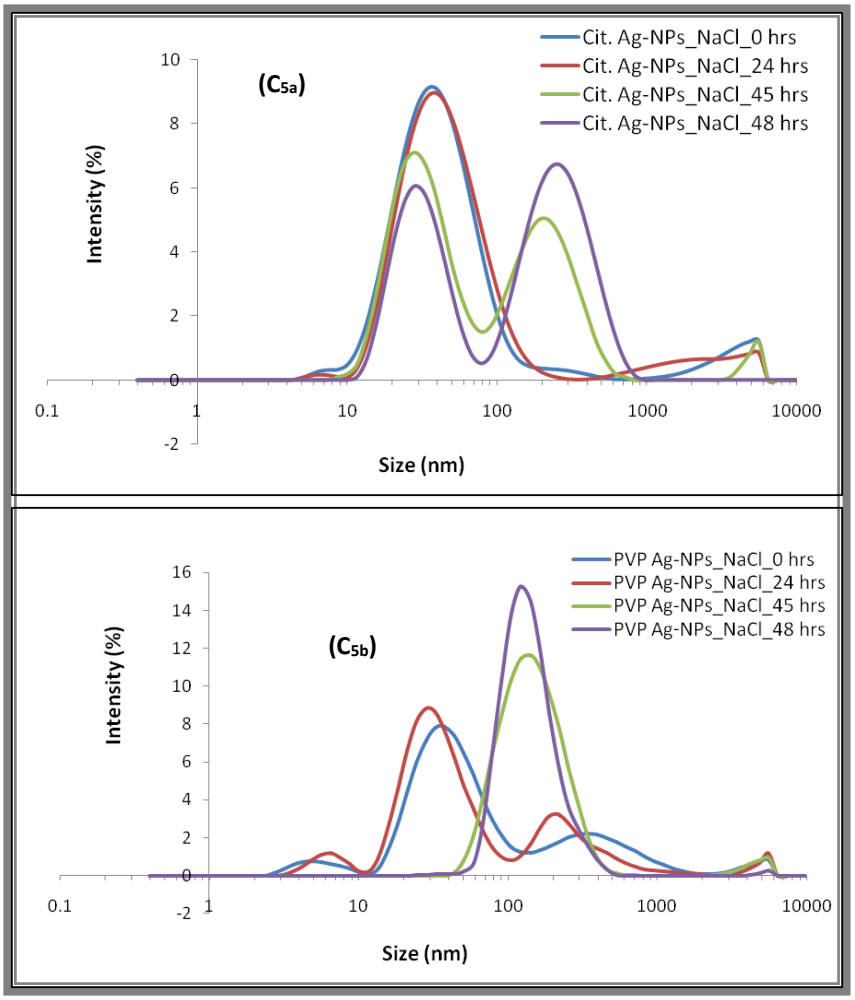

Figure 4-29: D_H distribution of the citrate (C_{5a}) and PVP (C_{5b}) Ag-NPs in 7 mg*L^{-1} NaCl (at 0 hrs, 24 hrs, 45 hrs (during aeration) and at 48 hrs (during settling)).

The calculated values of the settling velocity at 48 hrs (Table 4-30) show that the PVP Ag-NPs had a higher velocity than the citrate Ag-NPs when in a 7 mg*L^{-1} NaCl solution. It should be noted that three hours settling time was not sufficient to expect complete sedimentation of the Ag-NPs in both cases.

Table 4-30: Settling velocity with the corresponded D_H of citrate and PVP Ag-NPs 7 mg*L^{-1} NaCl (at 0 hrs, 24 hrs, 45 hrs (during aeration) and at 48 hrs (during settling)).

	D_H (nm) At 48 hrs	Settling velocity (nm*s^{-1})	Settling time (weeks)
Citrate Ag-NPs in NaCl	32.1 ± 0.7	4.67	24.76
PVP Ag-NPs in NaCl	147.0 ± 29.2	98.04	1.18

4.3.5.4. TEM characterisation of citrate and PVP Ag-NPs in NaCl

The TEM data (Table 4-31) and images (Figure 4-30 and Figure 4-31) show that at 0 hrs the citrate Ag-NPs in 7 mg*L^{-1} NaCl were slightly agglomerated while there was no agglomeration observed for the PVP Ag-NPs. At 24 hrs, both citrate and PVP Ag-NPs might have slightly dissolved because their average size decreased. However, in the presence of aeration loose agglomerates of NPs were formed in both cases, and during the settling phase the level of agglomeration remained constant in the case of the citrate Ag-NPs and increased in the case of the PVP Ag-NPs. There was no significant difference between citrate and PVP Ag-NPs size behaviour over time or at a STP (Table A3 - 22). Thus similar to the DLS results (section 4.3.5.3), the changes in size of Ag-NPs in NaCl were found to be independent of their coating, which was contrary to our observations.

Table 4-31: TEM average primary particle size and shape factor of citrate Ag-NPs 7 mg*L^{-1} NaCl (at 0 hrs, 24 hrs, 45 hrs (during aeration) and at 48 hrs (during settling)).

	Citrate Ag-NPs in NaCl			PVP Ag-NPs in NaCl		
	Longest length (nm)	**Shortest length (nm)**	**Shape factor**	**Longest length (nm)**	**Shortest length (nm)**	**Shape factor**
0 hrs	13.5 ± 5.6	10.2 ± 3.7	0.94 ± 0.06	12.5 ± 3.6	9.4 ± 2.3	0.96 ± 0.05
24 hrs	12.0 ± 7.5	8.8 ± 5.2	0.88 ± 0.09	10.3 ± 4.2	8.4 ± 3.4	0.95 ± 0.04
45 hrs	14.5 ± 8.7	10.9 ± 6.8	0.88 ± 0.08	13.2 ± 6.2	10.3 ± 4.4	0.93 ± 0.08
48 hrs	14.8 ± 12.5	10.8 ± 9.2	0.92 ± 0.09	19.2 ±11.8	15.3 ± 8.3	0.93 ± 0.06

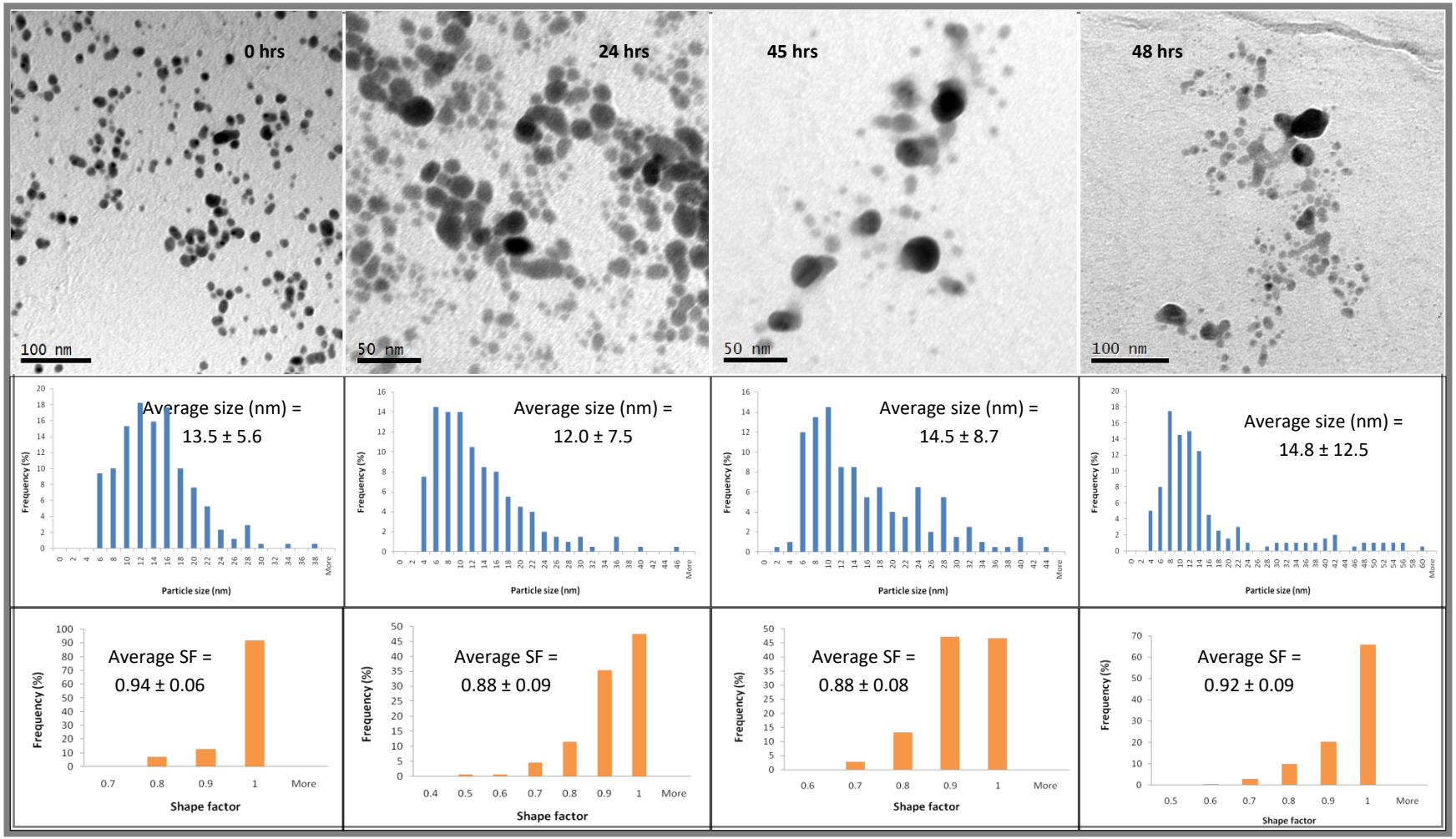

Figure 4-30: TEM primarily particle size distribution of citrate Ag-NPs in 7 mg*L^{-1} NaCl (at 0 hrs, 24 hrs, 45 hrs (during aeration) and at 48 hrs (during settling)). Based on the count of 200 NPs for all four samples

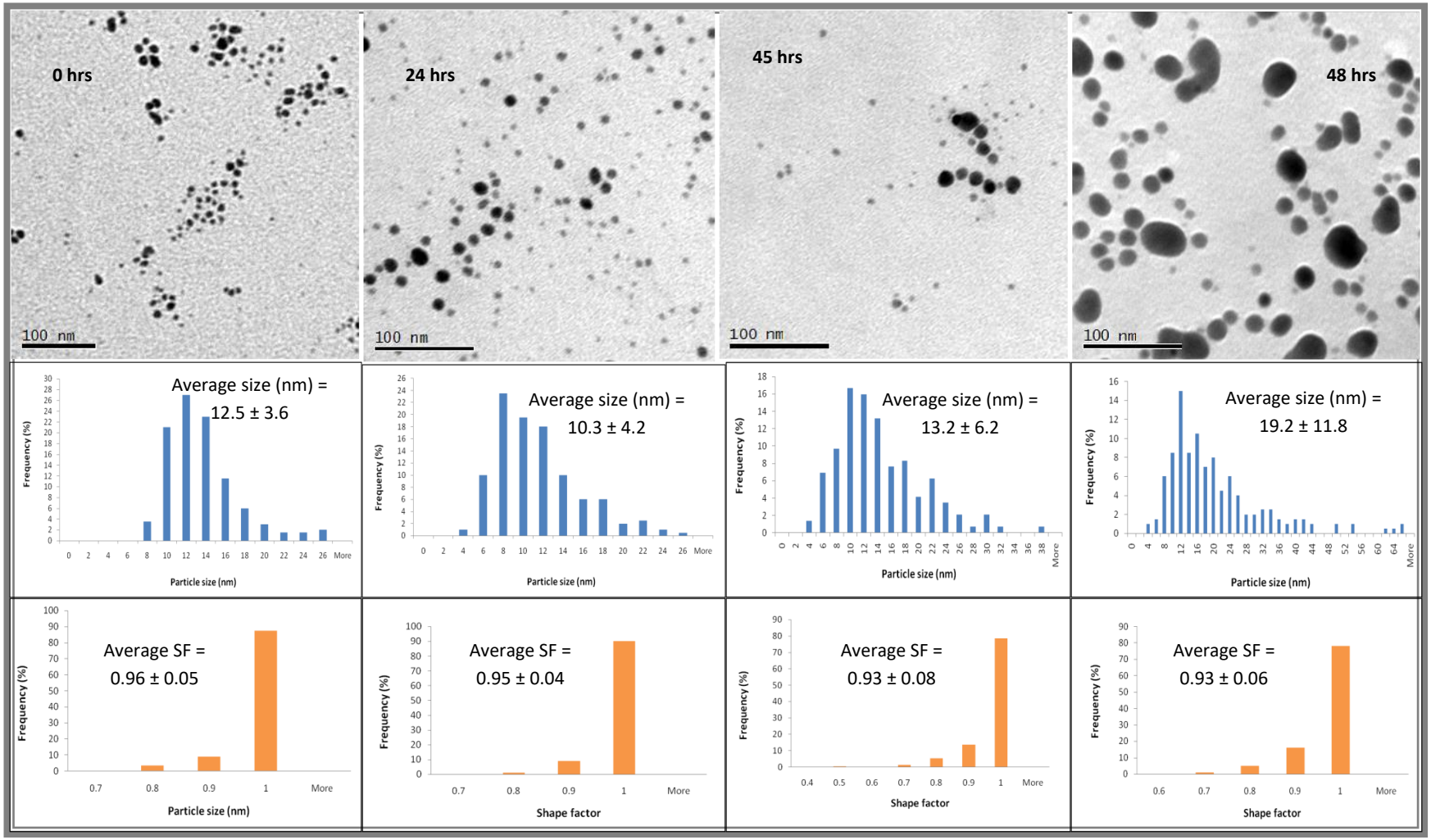

Figure 4-31: TEM primary particle size distribution of PVP Ag-NPs in mg*L^{-1} NaCl (at 0 hrs, 24 hrs, 45 hrs (during aeration) and at 48 hrs (during settling)). Based on the count of 200 NPs for the 0 hrs, 24 hrs and 48 hrs samples and 144 NPs for the 45 hrs sample

4.3.5.5. Surface chemistry analysis: ZP of citrate and PVP Ag-NPs in NaCl

When initially dispersed in 7 mg*L^{-1} of NaCl, the ZP of the citrate Ag-NPs was significantly reduced with an average value of -11.6 ± 1.04 mV and further reductions were observed over time and during each stage of the experiment (Table 4-32and Figure 4-32). Thus, the surface charge of citrate Ag-NPs was affected in the absence and presence of aeration, due to the exchange of counterions with the medium leading to the reduction of the Debye layer, with more counterions condensed on the NP surface (Lowe et al., 2017). In fact, the presence of chloride ion (Cl^-) causes a rapid formation of AgCl (with a solubility product K_{sp} = 1.56 * 10^{-10} at room 25 ˚C) onto the surface of the particles (Figure 4-27), leading to the attraction of the particles to one another (Axson et al., 2015). The solubility product of AgCl at 25 ˚C (or room temperature) is K_{sp} = 1.56 * 10^{-10}, thus it is insoluble in water (Römer et al., 2011). However, for a concentration of 1.25 * 10^{-5} mol*L^{-1}, AgCl can be dissolved in water at saturation (Römer et al., 2011, Myerson, 2002).

PVP Ag-NPs in NaCl were initially more negatively charged. However, after 24 hours, their electrical charge significantly increased, and they might have become unstable. But, during the aeration phase, the charge of the PVP Ag-NPs raised in negativity, and the ZP value remained constant during the settling phase. Thus, the surface chemistry of the Ag-NPs might have been altered by partial formation of AgCl on their surface (Figure 4-27) during the dispersion at 0 hrs as a result of the particles being slightly stripped of their PVP coating (Axson et al., 2015). The decrease in negativity of the ZP suggested that there was not enough AgCl to passivate the PVP particle surface and help to slow down their dissolution if were exposed to more oxygen. Thus, with the addition of oxygen the dissolution of the particles was

accelerated based on the GFAAS data (Table 4-27) and significantly increasing the amount AgCl on their surface. Hence, the increase in the negativity of the ZP to -16.6 ± 0.84 mV, meant that the particles were less prone to aggregation. However, Van Der Waal's forces led the NPs to agglomerate and then aggregate (Axson et al., 2015). There was no significant difference between citrate and PVP Ag-NPs size behaviour overtime and at a STP (Table A3 - 21). Thus, the surface chemistry transformations of dispersed Ag-NPs in NaCl were independent to their coating under aerobic conditions.

Also, there is little to no variation of the pH when the NaCl solution was added to PVP Ag-NPs; this implies that the pH in that case has, not influenced the ZP. Thus, because the ZP is influenced not only by the pH of the medium, but also by its ionic strength and the counterion valence, the changes in ZP were due to the compression of the diffuse layer between the particles and the electrolyte solution (French et al., 2009). As a consequence, the repulsion between the particles was diminished, leading to their agglomeration follow by their aggregation (French et al., 2009) (Figure 4-31).

For the citrate Ag-NPs, the pH of the media fluctuates with the variation of ZP – which was not significant in this case probably because of the basic nature of the medium. Their ZP was less variable over the course of their exposure, showing a higher decreased in negativity compare ZP to the pristine particles. Thus, citrate particles were more prone to agglomeration compared to the PVP particles.

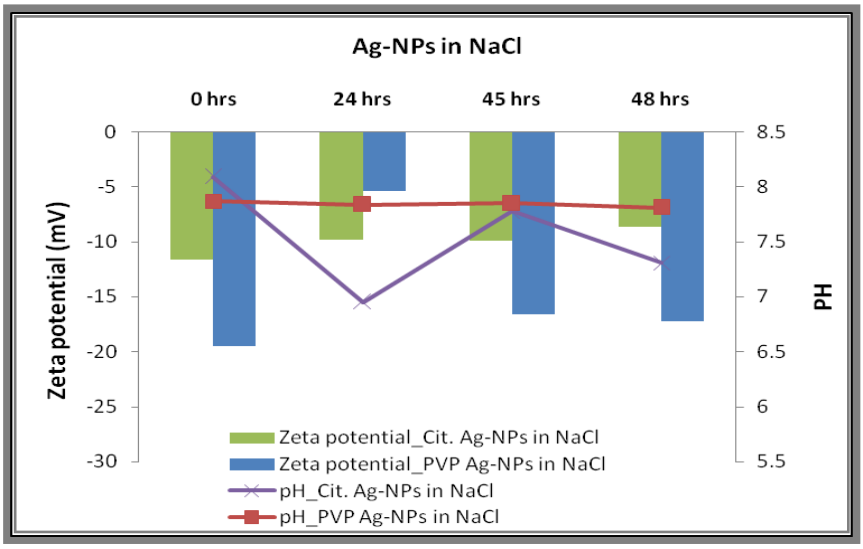

Figure 4-32: Variation of the citrate and PVP capped Ag-NPs ZP dispersed 7 mg*L^{-1} NaCl (at 0 hrs, 24 hrs, 45 hrs (during aeration) and at 48 hrs (during settling)) and the corresponding variation in pH.

Table 4-32: ZP and pH of citrate and PVP Ag-NPs 7 mg*L^{-1} NaCl (at 0 hrs, 24 hrs, 45 hrs (during aeration) and at 48 hrs (during settling)) extracted from Figure 4-27.

	Citrate Ag-NPs in NaCl		PVP Ag-NPs in NaCl	
	pH	**ZP (mV)**	**pH**	**ZP (mV)**
0 hrs	8.09	-11.6 ± 1.04	7.87	-19.5 ± 2.12
24 hrs	6.95	-9.83 ± 2.55	7.84	-5.38 ± 0.72
45 hrs	7.78	-9.87 ± 1.05	7.85	-16.6 ± 0.84
48 hrs	7.31	-8.65 ± 0.58	7.81	-17.2 ± 0.57

4.3.6. Citrate and PVP Ag-NPs in $CaCl_2$

Dispersed Ag-NPs in $CaCl_2$ behaved similarly to Ag-NPs in NaCl (Figure 4-33). They oxidised and dissolved by releasing Ag^+ ions as counterions onto their surface, which lead to a rapid precipitation into AgCl (Loza et al., 2014, Fargasova et al., 2015). The passivation of the Ag-NP surface by the AgCl can also slow down the dissolution and lead to the growth of the particles, and agglomeration through Van Der Waal's interactions followed by aggregations (Loza et al.,

2014, Axson et al., 2015). Baalousha et al., (2013) found that upon dispersing citrate Ag-NPs (TEM average size of 17 ± 6.0 nm) in $CaCl_2$ and NaCl, the divalent nature of the calcium cation (Ca^{2+}) strongly influenced the particles aggregation compared to monovalent sodium cation (Na^+).

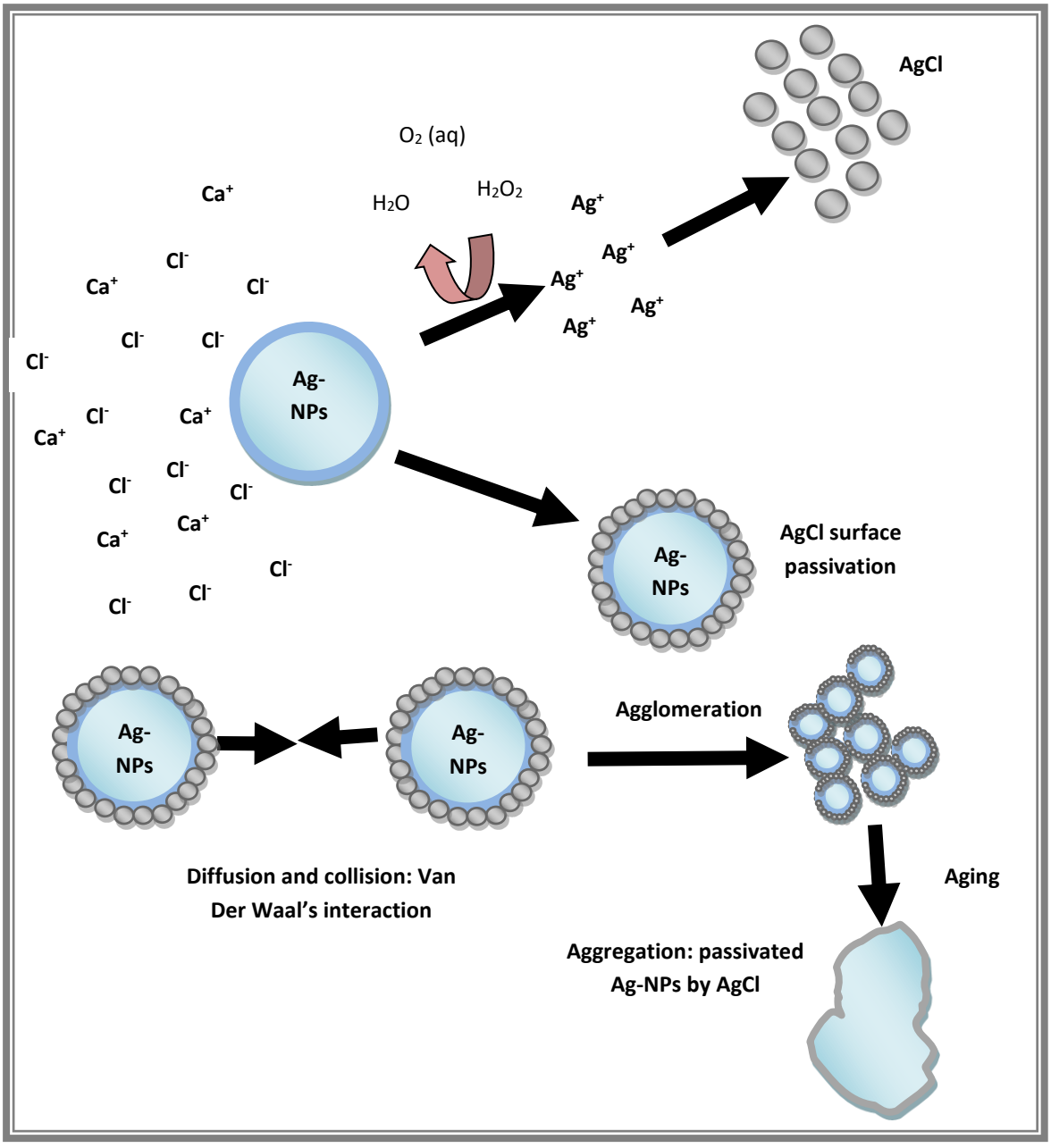

Figure 4-33: Illustration of dispersed citrate Ag-NPs in dissolved CaCl2 solution. Ag-NPs dissolved through oxidation/dissolution mechanism, Ag+ precipitation into AgCl; agglomeration of passivated Ag-NPs by Van Der Waal's interactions following aggregation through (Loza et al., 2014, Axson et al., 2015).

4.3.6.1. Dissolution study: silver concentration in $CaCl_2$

In a 2 mg*L^{-1} of $CaCl_2$, citrate Ag-NPs showed a faster dissolution at 0 hrs than the PVP Ag-NPs (Table 4-38). But after 24 hours, more Ag-NPs dissolved in the case of PVP Ag-NPs and the rate of dissolution was accelerated during aeration with about 86% of the PVP Ag-NPs dissolved at 45 hrs as opposed to 50% for the citrate Ag-NPs. After settling, nearly 94% of Ag was Ag^+ for the PVP Ag-NPs against 60% for the citrate Ag-NPs case; it could be concluded that the PVP Ag-NPs were more unstable than the citrate Ag-NPs in $CaCl_2$.

There was no significant difference between both particles overtime regarding their $C_{Total\ Ag}$, %dissolved Ag and %unrecovered Ag (Table A3 - 18). However, the ANOVA analysis comparing the changes in $C_{Total\ Ag}$, %dissolved Ag and %unrecovered Ag between citrate and PVP Ag-NPs at a STP were significantly different. Thus, the dissolution of Ag-NPs in $CaCl_2$ and under aerobic condition was dependent to their coating agent; in this case, PVP particles were more affected by the dissolution than the citrate particles.

Table 4-33: Changes in Ag concentration when citrate and PVP Ag-NPs were dispersed into 4 mg*L^{-1} $CaCl_2$ (at 0 hrs, 24 hrs, 45 hrs (during aeration) and at 48 hrs (during settling)). Measured by GFAAS

	Citrate Ag-NPs in $CaCl_2$			PVP Ag-NPs in $CaCl_2$		
	$C_{Total\ Ag}$ (µg*L^{-1})	%Diss. Ag	%Unr. Ag	$C_{Total\ Ag}$ (µg*L-1)	%Diss. Ag	%Unr. Ag
0 hrs	549.5 ± 67.5	6.6 ± 1.3	0	581.0 ± 24.2	2.1 ± 0.2	0
24 hrs	378.7 ± 3.6	28.1 ± 0.2	31.10	406.0 ± 14.1	36.8 ± 1.1	30.12
45 hrs	228.2 ± 39.7	49.3 ± 3.1	58.47	329.7 ± 16.9	85.6 ± 1.5	43.25
48 hrs	216.4 ± 48.6	60.2 ± 1.2	60.62	187.6 ± 50.0	93.7 ± 2.3	67.71

4.3.6.2. UV-Vis characterisation of citrate and PVP Ag-NPs in $CaCl_2$

The UV-Vis spectra of the citrate and PVP Ag-NPs in $CaCl_2$ (Figure 4-34) initially redshifted with their maximum wavelength occurring at λ_{max} = 394 nm (Table 4-34) due to their coating being partially stripped, leading to oxidation and dissolution and the increase of counterions (Ag^+) on their surfaces (as see seen section 4.3.6.1). The reaction between Ag^+ and Cl^- ions led to a rapid formation of AgCl on the particles surface through precipitation and creating a layer of AgCl on the NP surface, which increased the size of the particles (Figure 4-33); hence, the shifting of citrate and PVP Ag-NPs UV-Vis spectra to higher wavelengths. After 24 hours, the UV-Vis of citrate and PVP Ag-NPs MA was decreased as the more dissolution occurred, which may have increased the AgCl precipitates on the particles surface. Thus, the UV-Vis speaks of the particles were further shifted to higher wavelength as their size grew. The spreading of the UV-Vis peak was likely associated to the diminution of the particles monodispersity.

The application of an aeration flow caused further changes in the Ag-NPs absorbance as the λ_{max} for both citrate and PVP Ag-NPs was respectively 400 nm and 479 nm at 45 hrs, due to the particles getting bigger. Also, the MA of the citrate Ag-NPs was reduced and a significant spread in the UV-Vis spectra width was observed. However, for the PVP Ag-NPs, the MA was very low, and high spreading of the UV-Vis peak was observed. This significant reduction of the MA could be associated with the high level of dissolution observed in section 4.3.6.1 at 45 hrs. Also, the larger spreading of the UV-Vis was indeed caused by the aggregation of the particles from their agglomeration state of the 24 hrs time point.

Three hours after the settling phase (at 48 hrs), the MA and corresponding λ_{max}, as well as the FWHM of the UV-vis of the citrate Ag-NPs were constant. While for the PVP Ag-NPs, λ_{max} was

452 nm and the MA stayed the same. Meaning, citrate Ag-NPs size and concentration mostly remained in the same state as at 45 hrs time point. As for the PVP particles, the blue-shift of the absorbance peak is a consequence of their reduction in size. These results corroborated with the GFAAS data Table 4-33) which showed that dissolved Ag percentage of citrate Ag-NPs was constant during and after aeration, while PVP Ag-NPs further dissolved after aeration.

These results demonstrate that when dispersed in $CaCl_2$, citrate and PVP Ag-NPs may undergo a two and three stage process, respectively. First, they both dissolved within the first hour of their dispersion in the medium. By 24 hrs, the particles underwent further dissolution associated with some agglomeration, causing respectively the reduction of their MA and the spreading of the UV-Vis peak. The addition of oxygen led to both particles having increased in size and aggregated as their UV-Vis peaks were further red-shifted and spread. There was no significant difference in the MA changes between both particles overtime or at a STP (Table A3 - 19). Also, no significant difference was found in λ_{max} variations overtime and at a STP. Although no significant difference was found between the citrate and PVP Ag-NPs in MA and λ_{max}, the results of Figure 4-34 and Table 4-34 show that although both citrate and PVP particle may have gone through similar changes, PVP particles were more affected by the aeration.

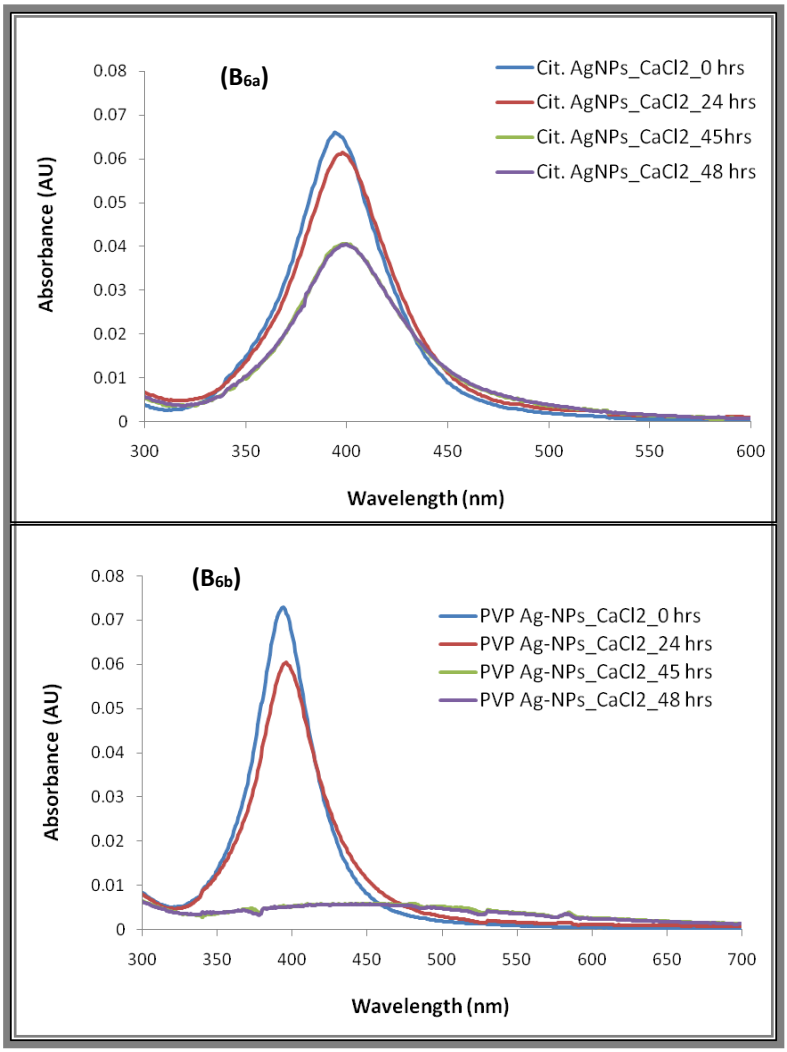

Figure 4-34: UV-Vis spectra of citrate (B_{6a}) and PVP (B_{6b}) Ag-NPs in 7 $CaCl_2$ mg*L^{-1} (at 0 hrs, 24 hrs, 45 hrs (during aeration) and at 48 hrs (during settling))

Table 4-34: UV-Vis data of citrate and PVP Ag-NPs in 4 mg*L^{-1} $CaCl_2$ (at 0 hrs, 24 hrs, 45 hrs (during aeration) and at 48 hrs (during settling))

	Citrate Ag-NPs in $CaCl_2$				PVP Ag-NPs in $CaCl_2$			
	0 hrs	**24 hrs**	**45 hrs**	**48 hrs**	**0 hrs**	**24 hrs**	**45 hrs**	**48 hrs**
λ_{max} (nm)	394	398	400	400	394	396	479	452
MA	0.066	0.061	0.041	0.040	0.073	0.060	0.006	0.006
Absorbance Decrease (%)	0	7.46	37.31	38.80	0	21.67	25.86	25.86
FWHM (nm)	51	55	64	64	44	49	233	236
Peak shift (%)	0.00	1.00	1.50	1.50	0	0.50	17.74	12.83

4.3.6.3. DLS characterisation of citrate and PVP Ag-NPs in $CaCl_2$

The DLS data for the citrate and PVP Ag-NPs in 4 $mg*L^{-1}$ $CaCl_2$ are shown in Figure 4-35 and Table 4-35. Both citrate and PVP Ag-NPs initially grew in size as we saw in section 4.3.6.2 and their D_H at 0 hrs was 31.7 ± 3.7 and 39.0 ± 4.6 nm, respectively. The D_H increased with time and in all phases of the experiment, except its reduction at 48 hrs. Thus we believe that the degree of the NP agglomeration the PVP Ag-NPs may have also increased with the formation of dimers or trimers. But, citrate Ag-NPs seemed to have not be affected by the agglomeration, but by more dissolution and increased in polydispersity as seen in Table 4-35. The size reduction of citrate at 48 hrs was likely caused by continuous released of the Ag+ three hours stopping the aeration of the medium. As for PVP particles, they were likely to have aggregated into larger particles Ag-NP, with stabilised AgCl coating (Figure 4-33).

There was no significant difference between the citrate and PVP Ag-NPs average D_H behaviour and variations of the PDI overtime or at a STP (Table A3 - 21). This shows that the changes in size of the Ag-NPs in CaCl2 were independent of their coating. However, the DLS characteristics of both citrate and PVP Ag-NPs (Figure 4-35and Table 4-35) showed that under aerobic conditions, dispersed citrate Ag-NPs were continually dissolved, while PVP Ag-NPs were agglomerated by forming dimers or trimers particles under aeration, and then aggregated during the settling phase.

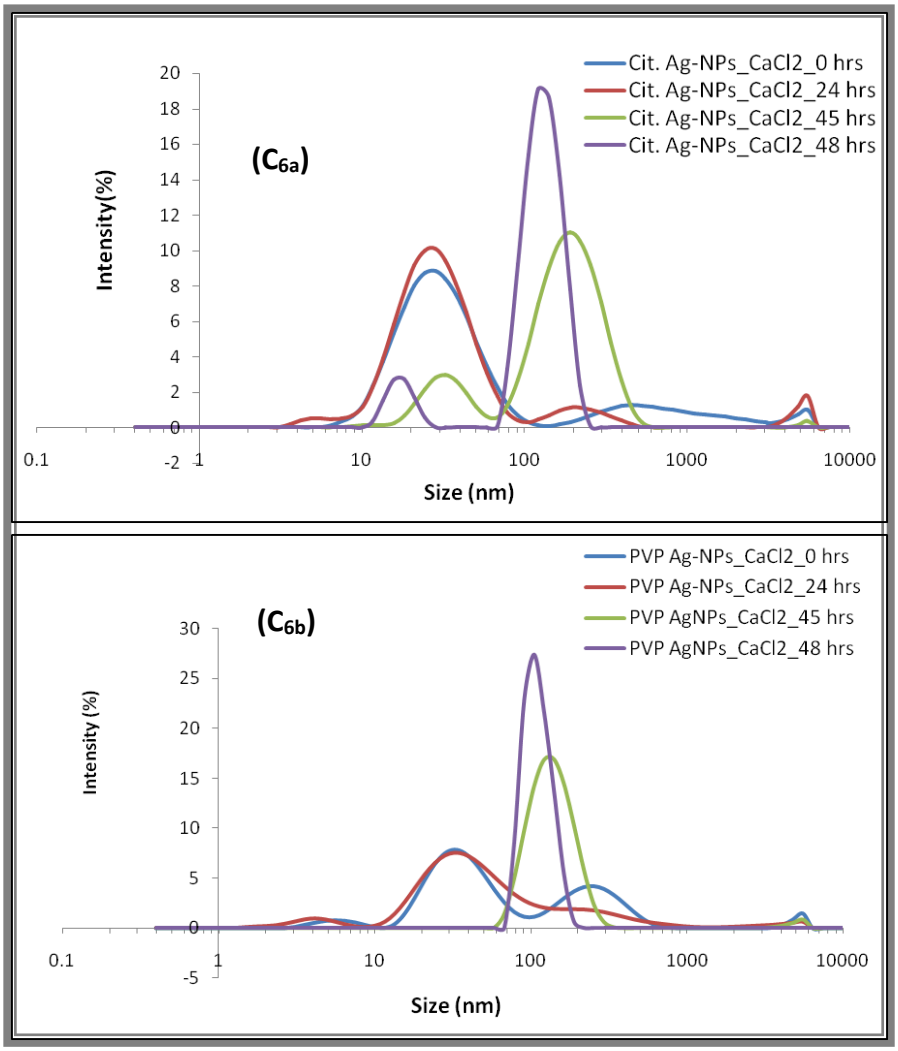

Figure 4-35: D_H distribution of the citrate (C_{6a}) and PVP (C_{6b}) Ag-NPs in 4 mg*L^{-1} $CaCl_2$ (at 0 hrs, 24 hrs, 45 hrs (during aeration) and at 48 hrs (during settling))

Table 4-35: DLS data of citrate Ag-NPs in 4 mg*L^{-1} $CaCl_2$ (at 0 hrs, 24 hrs, 45 hrs (during aeration) and at 48 hrs (during settling))

	Citrate Ag-NPs in $CaCl_2$		PVP Ag-NPs in $CaCl_2$	
	Primary peak (D_H) (nm)	**PDI**	**Primary peak (D_H) (nm)**	**PDI**
0 hrs	31.7 ± 3.7	0.47 ± 0.07	39.0 ± 4.6	0.58 ± 0.16
24 hrs	30.1 ± 2.8	0.31 ± 0.21	59.7 ± 33.6	0.51 ± 0.2
45 hrs	33.3 ± 18.9	0.52 ± 0.03	140.7 ± 4.6	0.26 ± 0.03
48 hrs	17.4 ± 1.4	0.22 ± 0.01	112.0 ± 14.0	0.3 ± 0.09

The calculated values of the settling velocity of the Ag-NPs at 48 hrs (Table 4-36) show that the PVP Ag-NPs had the highest velocity when exposed to 4 $mg*L^{-1}$ $CaCl_2$solution. As previously seen, three hours were not sufficient to have most of the Ag-NPs sediment at the bottom of the glass container in both cases.

Table 4-36: Settling velocity with the corresponded D_H of citrate and PVP Ag-NPs in 4 $mg*L^{-1}$ $CaCl_2$ (at 0 hrs, 24 hrs, 45 hrs (during aeration) and at 48 hrs (during settling))

	D_H (nm) At 48 hrs	Settling velocity ($nm*s^{-1}$)	Settling time (weeks)
Citrate Ag-NPs in $CaCl_2$	17.4 ± 1.4	1.37	84.26
PVP Ag-NPs in $CaCl_2$	112.0 ± 14.0	56.91	2.03

4.3.6.4. TEM characterisation of citrate and PVP Ag-NPs in $CaCl_2$

The TEM data (Table 4-37) and images (Figure 4-36 and Figure 4-37) show that at 0 hrs the PVP Ag-NPs might have slightly dissolved because their average size decreased. While citrate Ag-NPs were agglomerated and the presence of aeration might have caused their dissolution. The TEM images of PVP Ag-NPs (Figure 4-37) show that their level of agglomeration increased with time and during each stage of the experiment, causing their average size to increase. There was no significant difference between citrate and PVP Ag-NPs size behaviour overtime and at a STP (Table A3 - 22).

Table 4-37: TEM average size and shape factor of citrate Ag-NPs in 4 $CaCl_2$ mg*L^{-1} (at 0 hrs, 24 hrs, 45 hrs (during aeration) and at 48 hrs (during settling))

	Citrate Ag-NPs in $CaCl_2$			PVP Ag-NPs in $CaCl_2$		
	Longest length (nm)	**Shortest length (nm)**	**Shape factor**	**Longest length (nm)**	**Shortest length (nm)**	**Shape factor**
0 hrs	11.2 ± 5.4	8.3 ± 4.1	0.88 ± 0.08	9.7 ± 4.6	7.7 ± 3.6	0.97 ± 0.04
24 hrs	12.4 ± 10.3	8.7 ± 6.6	0.80 ± 0.11	14.2 ± 7.7	11.0 ± 5.7	0.94 ± 0.07
45 hrs	11.9 ± 7.0	9.0 ± 5.5	0.89 ± 0.08	14.8 ± 7.7	11.7 ± 6.1	0.92 ± 0.07
48 hrs	7.2 ± 2.9	5.2 ± 2.1	0.95 ± 0.08	42.7 ± 27.1	30.5 ± 16.4	0.87 ± 0.10

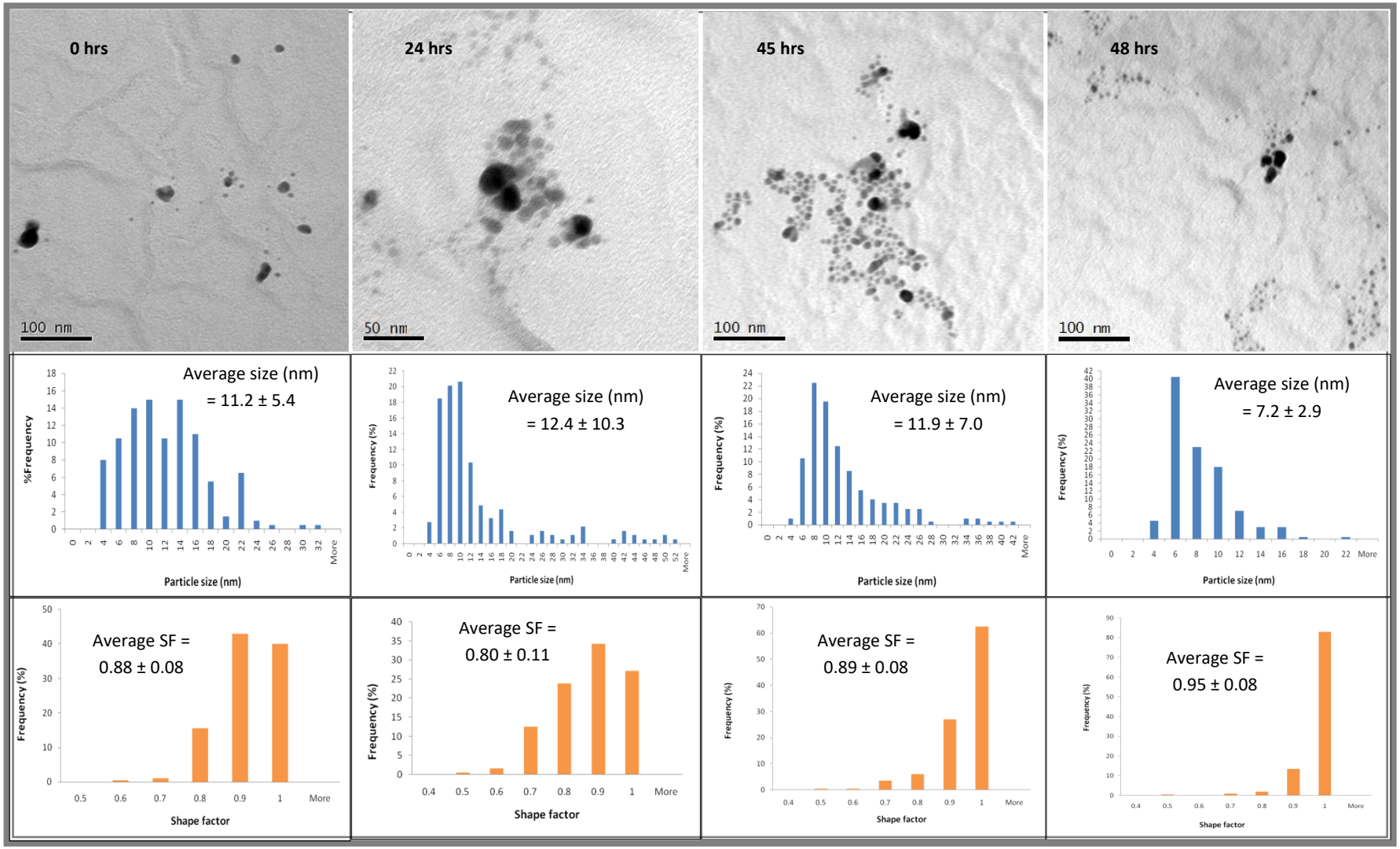

Figure 4-36: TEM size distribution of citrate Ag-NPs in 4 mg*L^{-1} $CaCl_2$ (at 0 hrs, 24 hrs, 45 hrs (during aeration) and at 48 hrs (during settling)). Based on the count of 200 NPs for the 0 hrs, 45 hrs and 48 hrs samples and 184 for 24 hrs sample

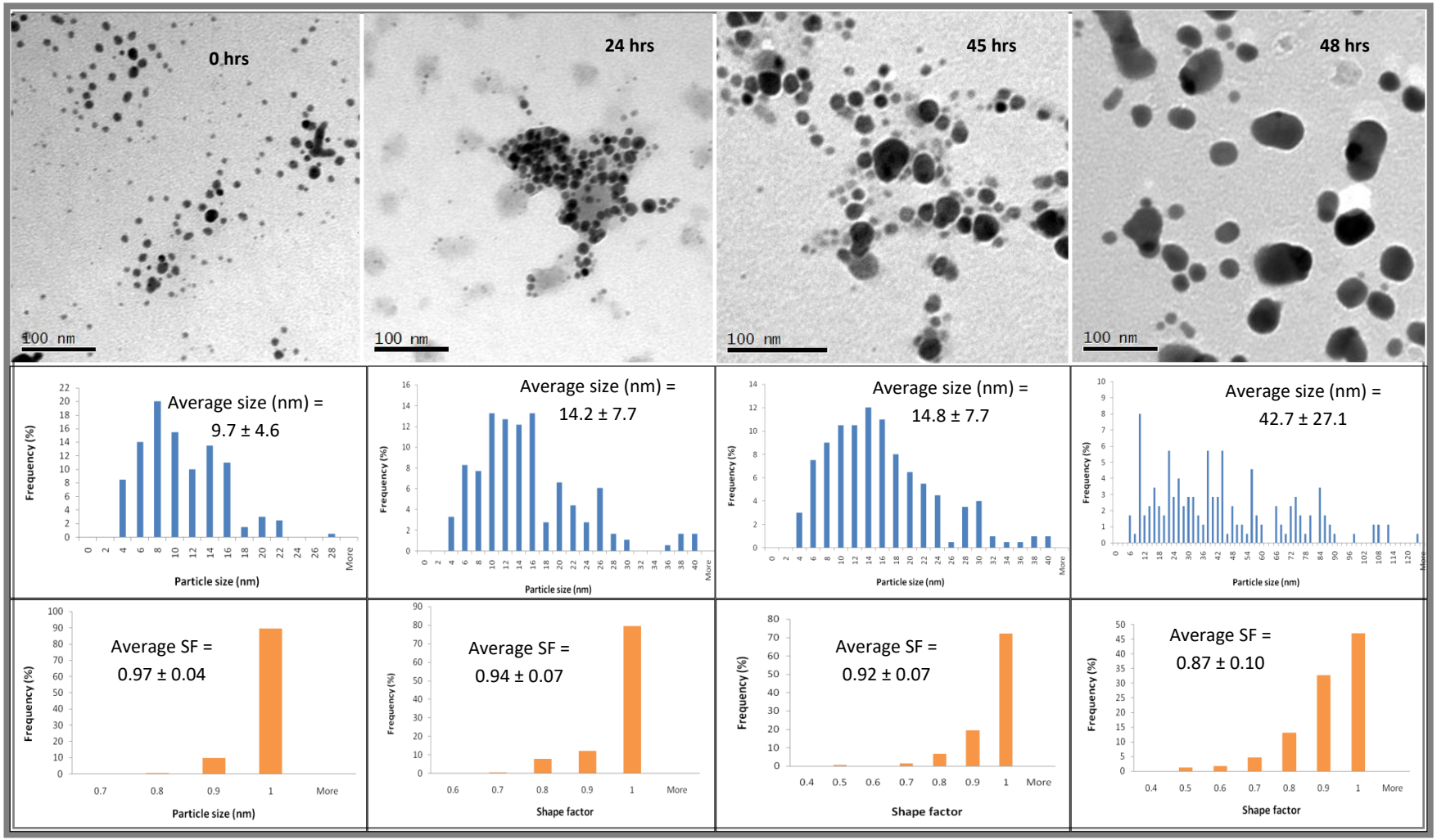

Figure 4-37: TEM size distribution of PVP Ag-NPs in 4 mg*L^{-1} $CaCl_2$ (at 0 hrs, 24 hrs, 45 hrs (during aeration) and at 48 hrs (during settling)). Based on the count of 200, 181, 200 and 175 NPs for the 0 hrs, 24 hrs, 45 hrs and 48 hrs sample respectively.

4.3.6.5. Surface chemistry analysis: ZP of citrate and PVP Ag-NPs in $CaCl_2$

The dispersion of citrate Ag-NPs in 4 mg*L-1 $CaCl_2$ solution at 0 hrs led to a decrease in the negativity of the ZP to an average value of -3.50 ± 0.62 mV (Table 4-38 and Figure 4-38). This was likely due oxidation/dissolution mechanism leading a rapid formation of AgCl on the particle surface (Figure 4-33). After 24 hrs of exposure the ZP was increased in negativity, but this state was maintained during the aeration phase (at 45 hrs) and the ZP was dropped to an average value of -6.05 ± 1.33 mV. Thus at 24 hrs, the citrate particles were likely agglomerated (Figure 4-33) as a consequence to the AgCl precipitating on their surface, leading to the reduction of the electrostatic repulsive forces between the particles which are induced by the citrate coating of the NPs (Gutierrez et al., 2015). This agglomeration of citrate Ag-NPs is common in solutions with high ionic strength containing divalent cations (Ca^{2+}) (Römer et al., 2011). The reduction of the ZP at 45 hrs was likely caused by further dissolution of the particles (Table 4-33), and the particles might have been transformed into aggregated Ag-NPs with an AgCl corona on their surface.

The ZP of PVP Ag-NPs (Table 4-38) at 0 hrs (- 8.66 ± 0.47 mV) was similar to the ZP of the pristine particles (3.6.1). Thus, the initial dispersion of the PVP particles in the $CaCl_2$ solution did not affect the PVP coating generally; hence the low percentage of Ag^+ concentration measured by GFAAS (Table 4-33). But after twenty-four hours, the ZP was less negative, which suggest that the PVP coating might have been stripped, causing the particles to oxidise and dissolve. This also leads to a rapid formation of AgCl precipitated onto the surface of the NPs and their agglomeration (Figure 4-33). The addition of oxygen seemed to have accelerated the dissolution of the particles according to the GFAAS in Table 4-33. This might have

contributed to the increase of counterions, leading to surface modification of the particles as more AgCl precipitated onto them. At 48 hrs as the ZP slightly decreased in negativity, the PVP particles might have undergone aggregation with an AgCl passivated layer, as evidenced by the average size increase observed by the TEM (Figure 4-37). There was no significant difference between citrate and PVP Ag-NPs size behaviour overtime or at a STP (Table A3 - 21). Thus, the variations of citrate and PVP Ag-NPs ZP in 4 $mg*L^{-1}$ $CaCl_2$ were independent of their coating.

Similar to the NaCl, there were no significant changes in the pH of the $CaCl_2$ solution with PVP Ag-NPs. Thus, for the PVP particles, the ZP was not only influenced by the pH but also by its ionic strength and the counterion valence as these cause compression of the diffuse layer between the particles and the electrolyte solution (French et al., 2009). Hence more agglomeration occurs due to the reduction of the steric repulsive force repulsion between the particles (French et al., 2009).

For the citrate Ag-NPs, the pH of the media changed in opposition with the variation of ZP – but was not significant because of the basic nature of the medium. Their ZP was highly variable with a high decrease in negativity compared to the ZP of the pristine particles. Thus, citrate particles were more prone to not only aggregation but also dissolution as shown in section 4.3.6.4 compared to the PVP particles.

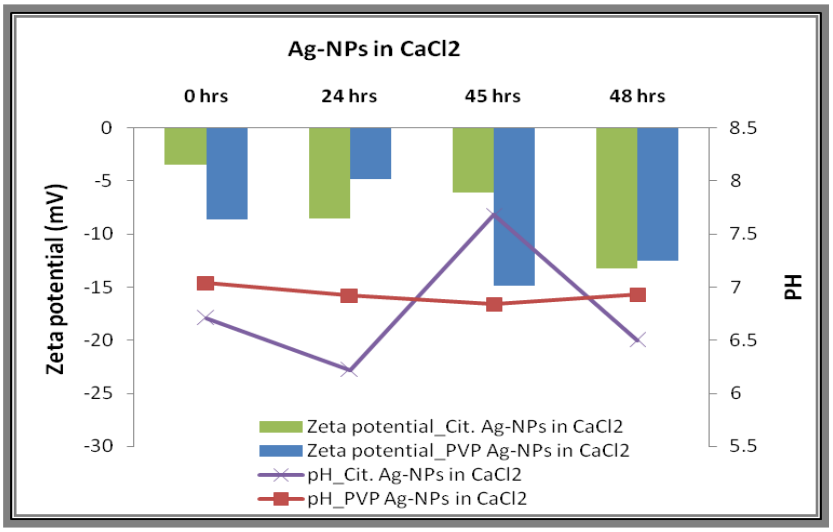

Figure 4-38: variation of the citrate and PVP capped Ag-NPs ZP in combination with the associate pH when dispersed in 4 mg*L^{-1} $CaCl_2$ (at 0 hrs, 24 hrs, 45 hrs (during aeration) and at 48 hrs (during settling))

Table 4-38: ZP and pH of citrate and PVP Ag-NPs in 4 mg*L^{-1} $CaCl_2$ (at 0 hrs, 24 hrs, 45 hrs (during aeration) and at 48 hrs (during settling)).

	Citrate Ag-NPs in $CaCl_2$		PVP Ag-NPs in $CaCl_2$	
	pH	**ZP (mV)**	**pH**	**ZP (mV)**
0 hrs	6.71	-3.50 ± 0.62	7.04	-8.66 ± 0.47
24 hrs	6.22	-8.49 ± 1.18	6.92	-4.86 ± 0.18
45 hrs	7.68	-6.05 ± 1.33	6.84	-14.9 ± 0.41
48 hrs	6.5	-13.20 ± 1.70	6.93	-12.5 ± 0.58

4.3.7. Citrate and PVP Ag-NPs in $MgSO_4$

The behaviour of dispersed Ag-NPs in $MgSO_4$ is illustrated in Figure 4-39. The oxidation of Ag-NPs generates the release of Ag^+ ions as counter ions on their surface. The dissolved Ag will rapidly precipitate as Ag_2S onto the particle surface, and this could stabilise the particle by reducing or stopping their dissolution completely (Loza et al., 2014, Fargasova et al., 2015). This passivation of the particle surface might reduce the steric and electrostatic repulsion

forces existing between citrate and PVP particles respectively, and this can cause the agglomeration through Van Der Waal's attractions (Loza et al., 2014, Axson et al., 2015).

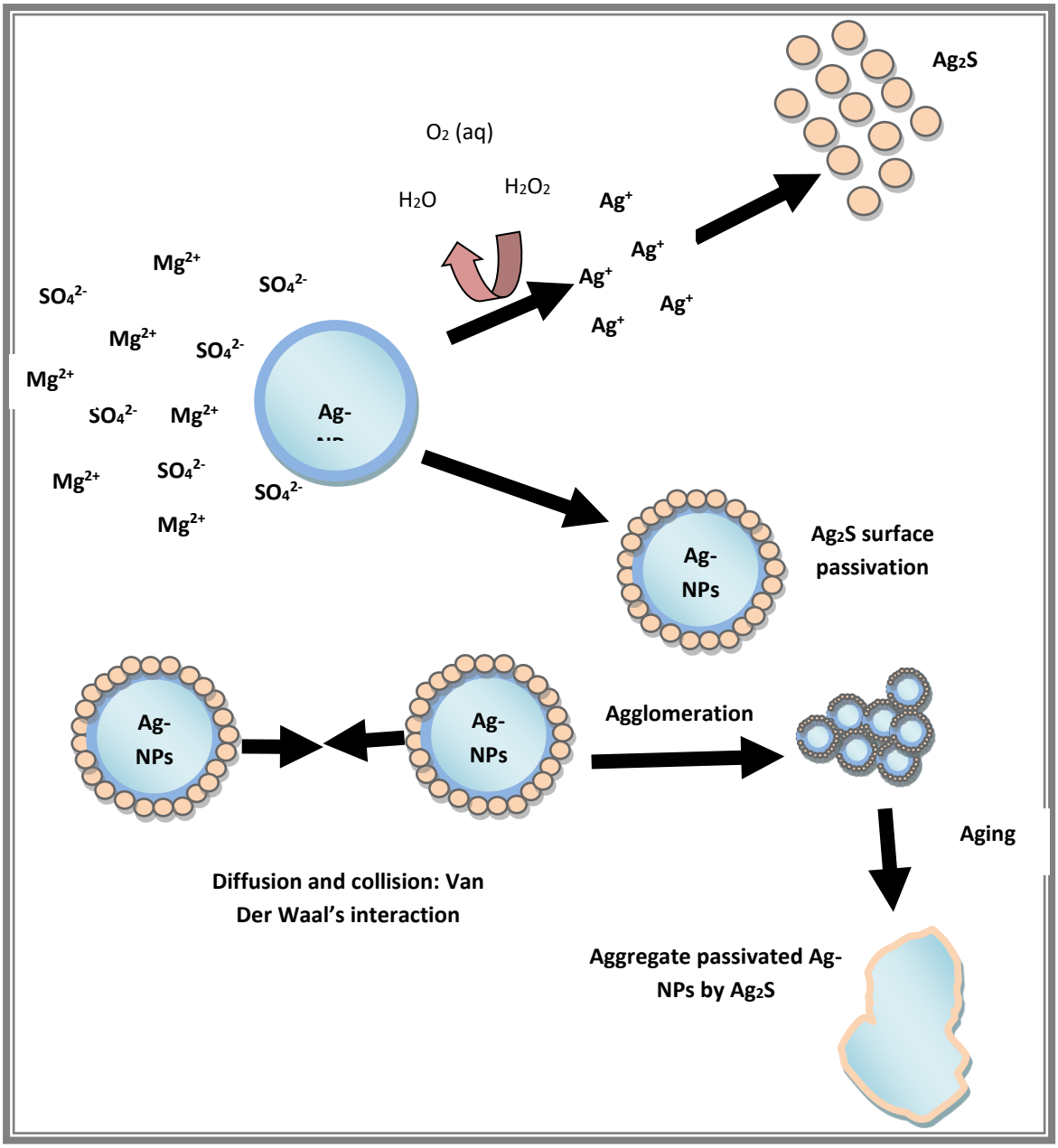

Figure 4-39: Illustration of dispersed citrate Ag-NPs in dissolved $MgSO_4$ solution. Ag-NPs dissolved through oxidation/dissolution mechanism, Ag^+ precipitation into Ag_2S; agglomeration of passivated Ag-NPs by Van der Waal's interactions following aggregation.

4.3.7.1. Dissolution study: silver concentration in $MgSO_4$

In 2 $mg*L^{-1}$ of $MgSO_4$, dispersed citrate and PVP Ag-NPs were not stable in terms of dissolution, with nearly 17 and 26% (Table 4-39) of Ag^+ generated within 24 hours in the medium and in absence of aeration. The aeration process highly accelerated the dissolution of PVP Ag-NPs, and less so in the case of the citrate Ag-NPs. However, after the aeration was stopped the amount Ag^+ generated between the aeration step and the settling stage was higher for the citrate Ag-NPs. Based on these results, both citrate and PVP Ag-NPs were unstable in 2 $mg*L^{-1}$ of $MgSO_4$ solution. Also the strong decrease in total Ag concentration over time in both cases was most likely due to agglomeration, sedimentation or adsorption on to the glass container or the aeration system (tube + stone).

There was no significant difference between both particles overtime regarding their $C_{Total\ Ag}$, %dissolved Ag and %unrecovered Ag (Table A3 - 18)**.** However, the ANOVA analysis comparing the changes in $C_{Total\ Ag}$, %dissolved Ag and %unrecovered Ag between citrate and PVP Ag-NPs at a STP were significantly different. Thus, aeration of the medium affected the dissolution of citrate and PVP Ag-NPs differently and based on the GFAAS results in Table 4-39 PVP particles were the most affected by the aeration.

Table 4-39: Changes in Ag concentration when citrate and Ag-NPs were dispersed into of 2 mg*L^{-1} $MgSO_4$ (at 0 hrs, 24 hrs, 45 hrs (during aeration) and at 48 hrs (during settling)). Measured by GFAAS

	Citrate Ag-NPs in $MgSO_4$			PVP Ag-NPs in $MgSO_4$		
	$C_{Total\ Ag}$ (µg*L^{-1})	%Diss. Ag	%Unr. Ag	$C_{Total\ Ag}$ (µg*L^{-1})	%Diss. Ag	%Unr. Ag
0 hrs	576.8 ± 2.1	5.4 ± 0.8	0	519.4 ± 1.8	7.8 ± 0.2	0
24 hrs	443.5 ± 15.8	16.7 ± 0.6	23.11	395.0 ± 19.8	26.3 ± 0.3	23.95
45 hrs	316.5 ± 6.9	33.9 ± 2.9	45.13	257.6 ± 13.0	80.5 ± 1.5	50.40
48 hrs	179.9 ± 3.6	59.8 ± 2.1	68.18	200.8 ± 35.2	86.6 ± 1.7	61.35

4.3.7.2. UV-Vis characterisation of citrate and PVP Ag-NPs in $MgSO_4$

In 2 mg*L^{-1} $MgSO_4$, the UV-Vis spectrum (Figure 4-40) of the dispersed PVP Ag-NPs was redshifted at 0 hrs with λ_{max} = 398 nm (Table 4-40), while for the citrate Ag-NPs the MA occurred at a similar wavelength (λ_{max} = 392 nm) as the pristine Ag-NPs. At 24 hrs, no further shifting for both Ag-NPs spectra was observed, even though the MA reduced. However, the aeration of the solution caused the UV-Vis spectrum of the citrate Ag-NPs to shift toward lower wavelengths (λ_{max} = 390 nm) while the spectrum of the PVP Ag-NPs shifted toward a higher wavelength (λ_{max} = 403 nm).

In addition, the FWHM of the UV-Vis spectrum increased in both cases. In the settling phase, the UV-Vis spectrum of the citrate Ag-NPs redshifted for the second time with λ_{max} = 397 nm; but their MA and the corresponding FWHM remained unchanged. In the case of the PVP Ag-NPs, both λ_{max} and FWHM were constant.

From the above results, it could be observed that although citrate Ag-NPs might have agglomerated when they were first dispersed in the $MgSO_4$ medium, their surface chemistry may not have been modified by the Ag_2S precipitate because the λ_{max} remained constant.

Also, in the presence of aeration flow, the citrate Ag-NPs may have oxidised and dissolved with changes in their surface chemistry. In the settling phase, further agglomeration may have caused the redshift implying a modification of their surface chemistry.

PVP Ag-NPs however, may have partially dissolved initially, and the released Ag^{+} would have precipitated onto their surface (Figure 4-39), leading to the modification of the surface chemistry of the particles. This state of the Ag-NPs was maintained during the first 24 hours. The application of aeration may have caused not only their oxidation and dissolution but also further changes such the increase of Ag_2S precipitates on the particle surface, associated with more agglomeration during the settling phase. There was a significant difference in the MA changes between both particles over time and at a STP (Table A3 - 19). Also, the variations of λ_{max} of citrate and PVP Ag-NPs were significantly different overtime, but not at a STP. These data show that the absorbance of Ag-NPs in Mg_2SO_4 solution was significantly dependent on their capping.

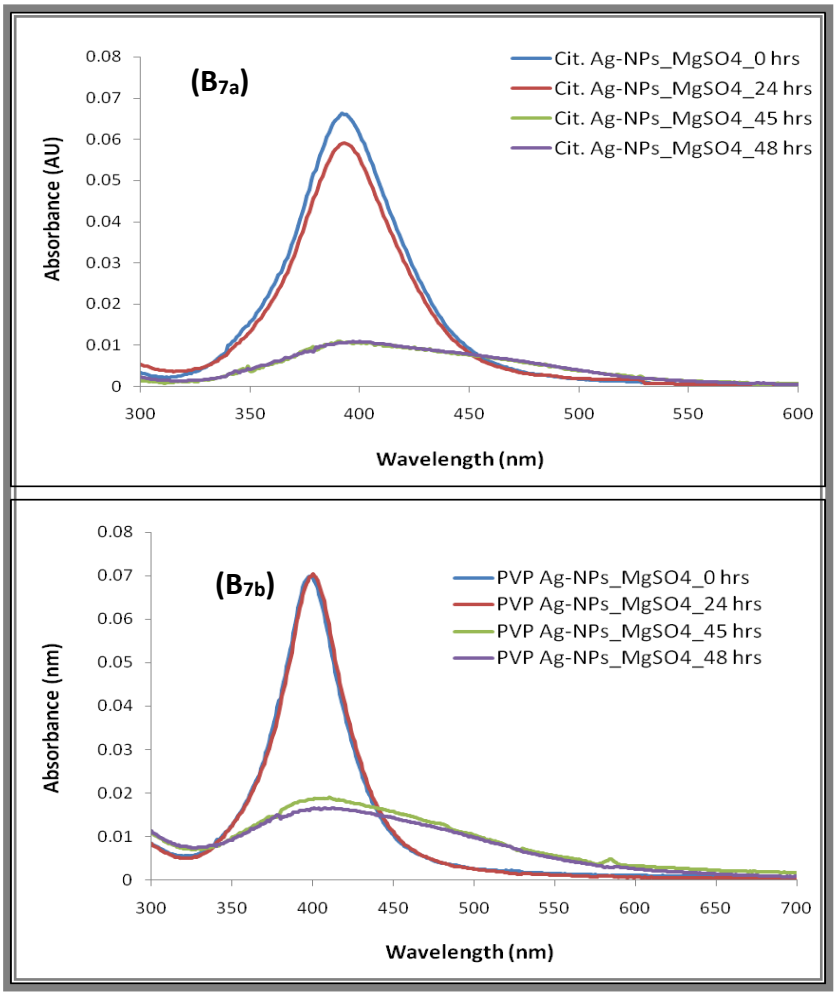

Figure 4-40: UV-Vis spectra of citrate (B_{7a}) and PVP (B_{7b}) Ag-NPs in 2 mg*L^{-1} $MgSO_4$ (at 0 hrs, 24 hrs, 45 hrs (during aeration) and at 48 hrs (during settling))

Table 4-40: UV-Vis data of citrate and PVP Ag-NPs in 2 mg*L^{-1} $MgSO_4$ (at 0 hrs, 24 hrs, 45 hrs (during aeration) and at 48 hrs (during settling))

	Citrate Ag-NPs in $MgSO_4$				PVP Ag-NPs in $MgSO_4$			
	0 hrs	**24 hrs**	**45 hrs**	**48 hrs**	**0 hrs**	**24 hrs**	**45 hrs**	**48 hrs**
λ_{max} (nm)	392	393	390	397	398	400	403	404
MA	0.062	0.059	0.011	0.011	0.069	0.070	0.019	0.017
Absorbance decrease (%)	0	4.48	76.12	76.27	0	1.43	263.2	305.9
FWHM (nm)	53	53	122	124	47	46	158	170
Peak shift (%)	0.00	0.25	0.51	1.26	0	0.5	1.24	1.48

4.3.7.3. DLS characterisation of citrate and PVP Ag-NPs in $MgSO_4$

The DLS size distributions of the citrate and PVP Ag-NPs in $MgSO_4$ are given in Figure 4-41 and Table 4-41. At 0 hrs, both citrate and PVP Ag-NPs might have agglomerated with a D_H of 44.2 ± 4.2 and 35.6 ± 4.5 nm, respectively. At 24 hrs, the level of agglomeration remained unchanged in both cases because there was no significant change in the D_H. During the aeration and the settling phases, both citrate and PVP Ag-NPs were highly agglomerated and polydisperse. There was no significant difference between the citrate and PVP Ag-NPs average D_H behaviour and the variations of the PDI overtime and at a STP (Table A3 - 21); meaning that the average D_H of Ag-NPs in $MgSO_4$ solution was independent to their coating.

Table 4-41: DLS data of citrate Ag-NPs in 2 mg*L^{-1} $MgSO_4$ (at 0 hrs, 24 hrs, 45 hrs (during aeration) and at 48 hrs (during settling))

	Citrate Ag-NPs in $MgSO_4$		PVP Ag-NPs in $MgSO_4$	
	Primary peak (D_H) (nm)	**PDI**	**Primary peak (D_H) (nm)**	**PDI**
0 hrs	44.2 ± 4.2	0.42 ± 0.11	35.6 ± 4.5	0.47 ± 0.11
24 hrs	42.2 ± 3.3	0.44 ± 0.18	38.1 ± 1.7	0.52 ± 0.09
45 hrs	32.0 ± 1.1	0.57 ± 0.02	174.3 ± 50.2	0.26 ± 0.02
48 hrs	25.1 ± 4.3	0.21 ± 0.02	136.1 ± 11.6	0.27 ± 0.02

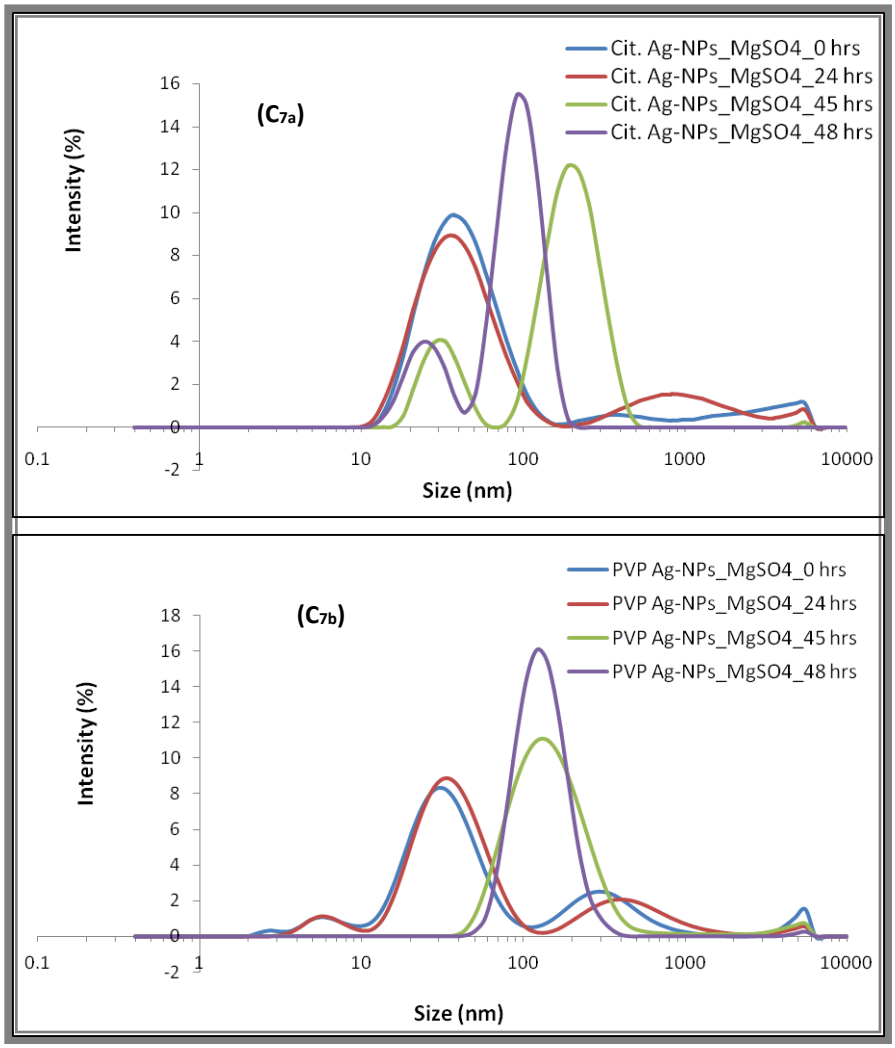

Figure 4-41: D_H distribution of the citrate (C_{7a}) and PVP (C_{7b}) Ag-NPs in 2 mg*L^{-1} $MgSO_4$ (at 0 hrs, 24 hrs, 45 hrs (during aeration) and at 48 hrs (during settling))

An estimate of the settling velocity of the NPs at 48 hrs (Table 4-42) shows that the citrate Ag-NPs had a higher velocity than the PVP Ag-NPs when exposed in $MgSO_4$ solution. But, nearly a week would be needed to expect the completed sedimentation of the NPs in both cases.

Table 4-42: Settling velocity with the corresponded D_H of citrate and PVP Ag-NPs in 2 mg*L^{-1} $MgSO_4$ (at 0 hrs, 24 hrs, 45 hrs (during aeration) and at 48 hrs (during settling))

	D_H (nm) at 48 hrs	Settling velocity (nm*s^{-1})	Settling time (weeks)
Citrate Ag-NPs in $MgSO_4$	25.1 ± 4.3	2.86	40.49
PVP Ag-NPs in $MgSO_4$	136.1 ± 11.6	84.04	1.38

4.3.7.4. TEM characterisation of citrate and PVP Ag-NPs in $MgSO_4$

The TEM data (Table 4-43) and images (Figure 4-42 and Figure 4-43) show that at 0 hrs both citrate and PVP Ag-NPs were agglomerated, as their average size was respectively 27.5 ± 19.1 and 15.2 ± 8.5 nm. At 24 hrs, the size of the NPs decreased, and the level of agglomeration was relatively high for the citrate Ag-NPs. Although in the presence of aeration the Ag-NPs might oxidise and dissolve, the size of both Ag-NPs during that stage increased with probably no dissolution in either case. After leaving the sample to settle for three hours, the 48 hrs images show that the PVP Ag-NPs might have grown into large individual particles or aggregates from agglomerating (Figure 4-39) while the citrate Ag-NPs significantly dissolved. There was no significant difference between citrate and PVP Ag-NPs size behaviour overtime and at a STP (Table A3 - 22); confirming that the variation of the average size of the particles in $MgSO_4$ was independent to their coating.

Table 4-43: TEM average size and shape factor of citrate Ag-NPs in 2 mg*L^{-1} $MgSO_4$ (at 0 hrs, 24 hrs, 45 hrs (during aeration) and at 48 hrs (during settling))

	Citrate Ag-NPs in $MgSO_4$			PVP Ag-NPs in $MgSO_4$		
	Longest length (nm)	**Shortest length (nm)**	**Shape factor**	**Longest length (nm)**	**Shortest length (nm)**	**Shape factor**
0 hrs	27.5 ± 19.1	20.0 ± 13.9	0.85 ± 0.10	15.2 ± 8.5	11.7 ± 6.4	0.94 ± 0.07
24 hrs	15.1 ± 10.2	10.9 ± 7.5	0.86 ± 0.11	10.3 ± 5.2	8.2 ± 4.1	0.95 ± 0.06
45 hrs	20.8 ± 11.8	14.8 ± 8.4	0.86 ± 0.11	13.9 ± 6.4	11.3 ± 5.2	0.97 ± 0.04
48 hrs	12.9 ± 7.5	9.4 ± 5.3	0.92 ± 0.09	20.3 ± 12.6	16.9 ± 10.1	0.95 ± 0.05

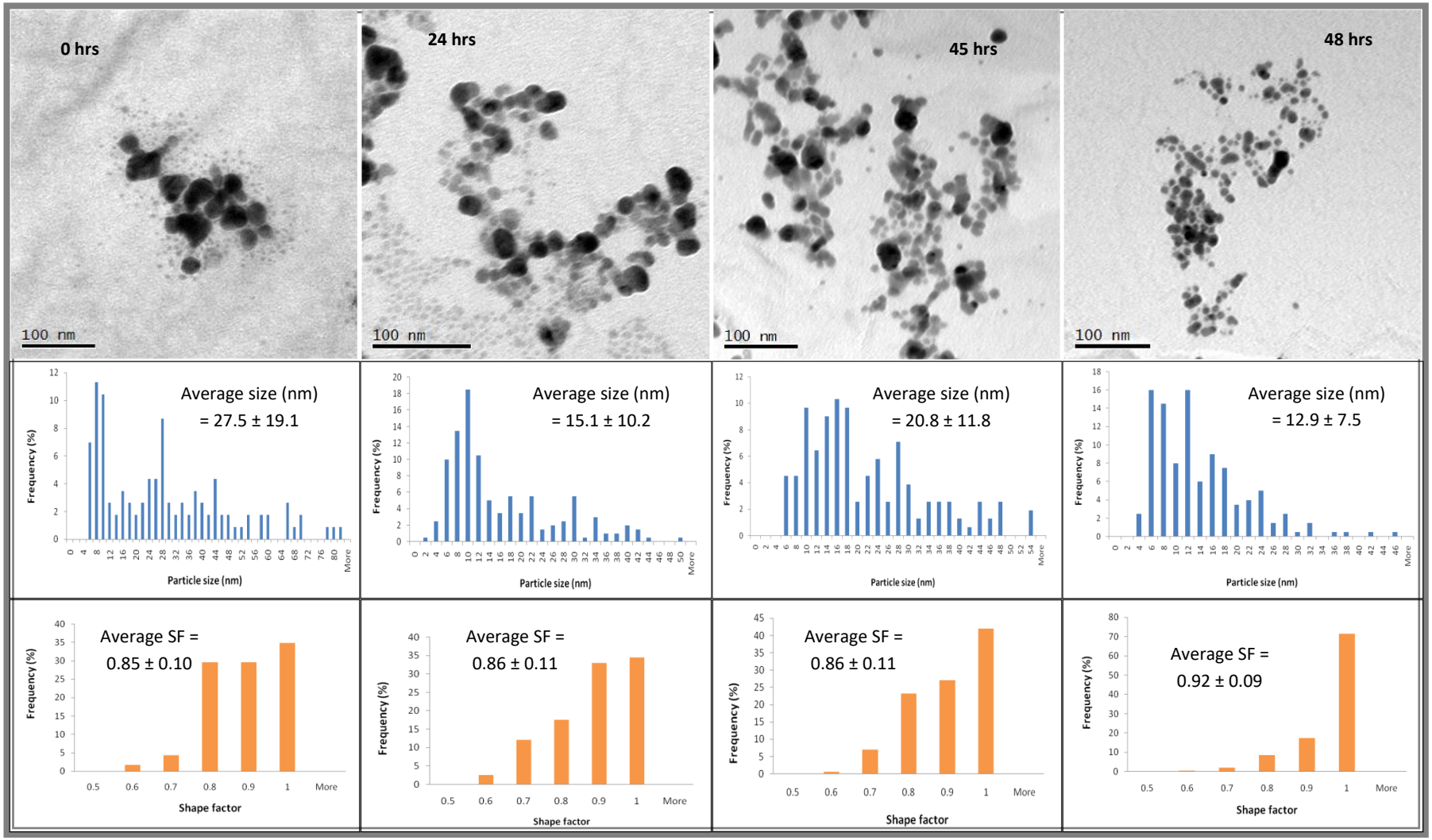

Figure 4-42: TEM size distribution of citrate Ag-NPs in 2 mg*L^{-1} $MgSO_4$ (at 0 hrs, 24 hrs, 45 hrs (during aeration) and at 48 hrs (during settling)). Based on the count of 115, 200, 155 and 200 NPs for the 0 hrs, 24 hrs, 45 hrs and 48 hrs sample respectively.

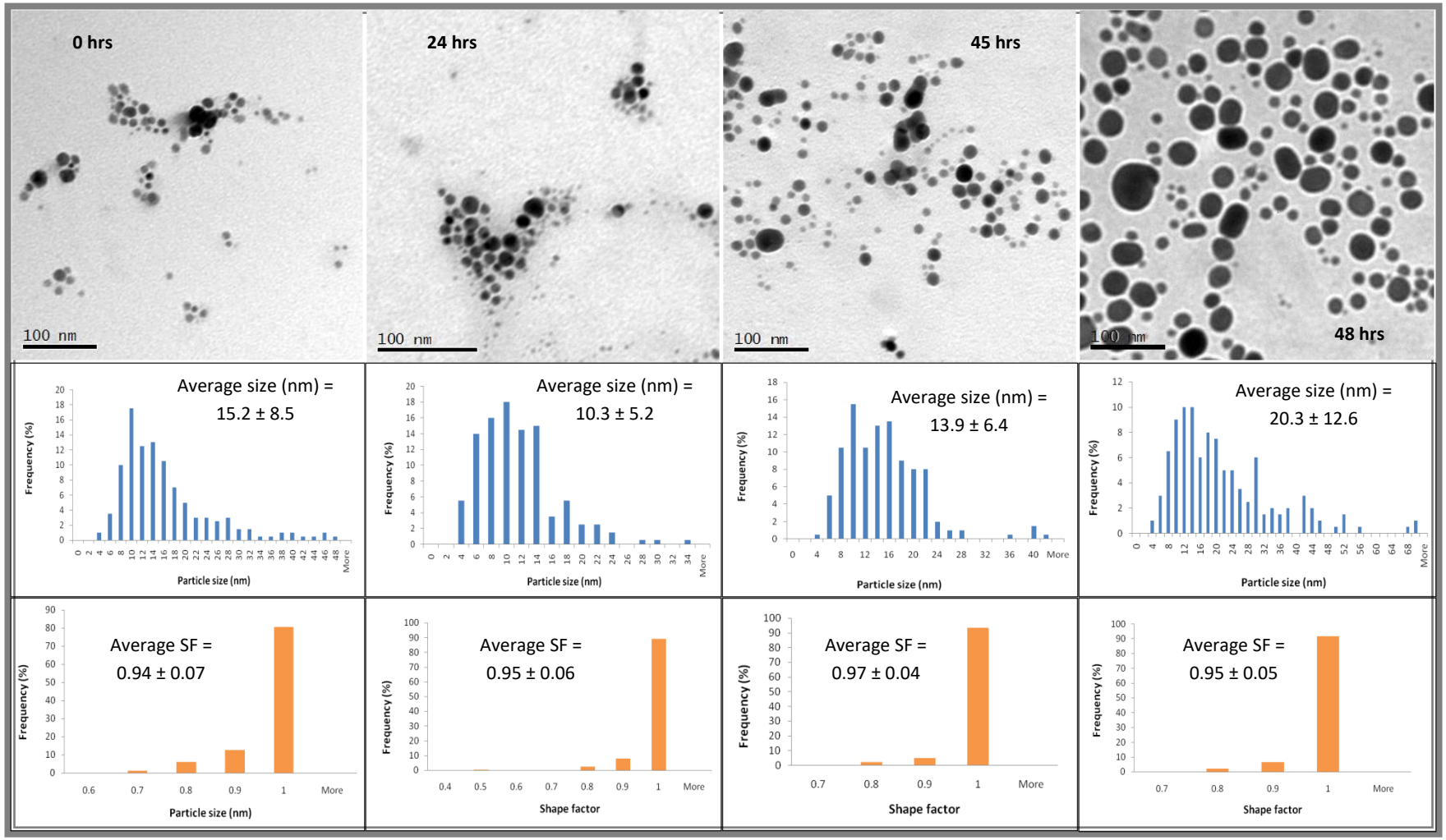

Figure 4-43: TEM size distribution of PVP Ag-NPs in 2 mg*L^{-1} $MgSO_4$ (at 0 hrs, 24 hrs, 45 hrs (during aeration) and at 48 hrs (during settling)). Based on the count of 200 NPs for all four samples.

4.3.7.5. Surface chemistry analysis: ZP of citrate and PVP Ag-NPs in $MgSO_4$

In 2 $mg*L^{-1}$ $MgSO_4$, the surface charge of the citrate and PVP Ag-NPs was less negative at 0 hrs (Table 4-44 and Figure 4-44), meaning the exposure of the NPs in the $MgSO_4$ might have affected their surface chemistry and made them unstable. This instability was maintained over time as indicated by the fluctuation of the NP properties. The citrate Ag-NPs were unstable during each stage of the experiment due to their high ZP value. The ZP of the PVP Ag-NPs continuously decreased over time.

It is therefore likely that the initial surface charge of both NPs might have favoured their transformation into Ag_2S particles. In the case of the citrate Ag-NPs, the surface chemistry was not stable because they agglomerated over time and significantly dissolved during the settling phase (see TEM images Figure 4-42). For the PVP Ag-NPs however, the increase in negativity after 24 hours and during each step of the experiment might mean that their surface chemistry was transformed by three processes. Firstly, the PVP Ag-NPs might have changed into Ag_2S NPs, and this state was stabilised over the first twenty-four hours. Second, they were oxidised during the aeration process for twenty-one hours. The ZP after settling (at 48 hrs) showed that the transformed PVP Ag-NPs were more stable than their initial suspension. There was no significant difference between citrate and PVP Ag-NPs size behaviour over time and in the STP when comparing the ZP of both particles in $MgSO_4$ (Table A3 - 21).

Finally, the pH of the $MgSO_4$ medium containing citrate Ag-NPs might have been affected by the aeration, evidenced by a significant increase of pH during that stage, which was then reduced to its previous value. The pH of the PVP Ag-NPs was relatively constant over time.

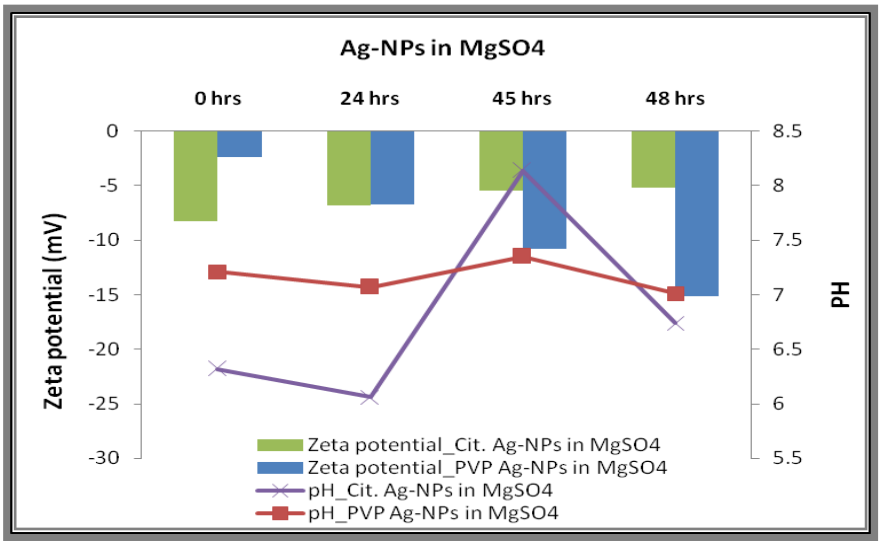

Figure 4-44: Variation of the citrate and PVP capped Ag-NPs ZP in combination with the associate pH when dispersed in 2 mg/L $MgSO_4$ (at 0 hrs, 24 hrs, 45 hrs (during aeration) and at 48 hrs (during settling))

Table 4-44: ZP and pH of citrate and PVP Ag-NPs in 2 mg*L^{-1} MgSO4 (at 0 hrs, 24 hrs, 45 hrs (during aeration) and at 48 hrs (during settling))

	Citrate Ag-NPs in $MgSO_4$		PVP Ag-NPs in $MgSO_4$	
	pH	**ZP (mV)**	**pH**	**ZP (mV)**
0 hrs	6.32	-8.26 ± 1.03	7.21	-2.40 ± 0.89
24 hrs	6.06	-6.78 ± 2.00	7.07	-6.76 ± 0.57
45 hrs	8.14	-5.44 ± 0.29	7.35	-10.8 ± 1.03
48 hrs	6.74	-5.15 ± 1.05	7.01	-15.1 ± 1.88

4.3.8. Citrate and PVP Ag-NPs in OECDss

4.3.8.1. Dissolution study: silver concentration in OECDss

The dispersion of the PVP Ag-NPs in OECDss itself caused rapid dissolution of the Ag-NPs in the first 24 hours (Table 4-45), with approximately 42% of the total Ag (a 24 hrs) being Ag^+. For the citrate Ag-NPs the dissolution was not significant prior to aeration, with only 5% of the Ag-NPs dissolved at 24 hrs as the particles might have been surrounded by proteins or lipids that prevented them from dissolving, as illustrated in Figure 4-3 and Figure 4-9.As for PVP Ag-NPs, they might have been partially covered by the proteins and lipids (Figure 4-9), leaving place to the oxidation mechanism to occur, leading to a high level of dissolution. 43.60% of the initial concentration of the PVP Ag-NPs total Ag was unrecovered, probably due to the capacity of Ag^+ to stick to the glass container; versus 6% for citrate Ag-NPs.

The application of an aeration flow did not have a strong effect on the dissolution due to the small increase of dissolved Ag at 45 hrs in both cases. However, after settling, the dissolved Ag from the citrate Ag-NPs had more than doubled while the PVP Ag-NPs remained unchanged. This shows that during the aeration phase changes in the Ag-NPs may be due to dissolution/oxidation which occurs in a typical aerobic WWTP (Yang et al., 2013c). It is also possible that new Ag compounds may had been formed, such Ag_2S, AgCl or $Ag3PO_4$ before, during and after aeration, since the medium contained sulphide, chloride and phosphate. Also, as PVP Ag-NPs might have been partially covered with proteins, lipids or Ag precipitates before aeration, the low degree of released Ag^+ during and after aeration means that their surface was protected from dissolution and very few ions were released.

There was no significant difference between both particles overtime regarding their $C_{Total\ Ag}$, %dissolved Ag and %unrecovered Ag, as shown in Table A3 - 18**.** However, the ANOVA analysis comparing the changes in $C_{Total\ Ag}$, and %unrecovered Ag between citrate and PVP Ag-NPs at a STP were significantly different; but, there was no significant difference on %dissolved Ag between both particles.

Table 4-45: Changes in Ag concentration when citrate and Ag-NPs were dispersed into of OECDss (at 0 hrs, 24 hrs, 45 hrs (during aeration) and at 48 hrs (during settling)). Measured by GFAAS

	Citrate Ag-NPs in OECDss			PVP Ag-NPs in OECDss		
	$C_{Total\ Ag}$ ($\mu g*L^{-1}$)	%Diss. Ag	%Unr. Ag	$C_{Total\ Ag}$ ($\mu g*L^{-1}$)	%Diss. Ag	%Unr. Ag
0 hrs	587.1 ± 11.6	2.3 ± 1.1	0	554.5 ± 8.7	6.7 ± 1.2	0
24 hrs	551.0 ± 6.4	5.2 ± 0.2	6.14	312.8 ± 5.5	41.8 ± 1.0	43.60
45 hrs	429.5 ± 6.4	16.6 ± 4.7	26.84	295.4 ± 4.1	45.0 ± 2.1	46.73
48 hrs	289.4 ± 12.0	41.3 ± 1.6	50.71	205.2 ± 3.9	47.5 ± 7.3	63.00

4.3.8.2. UV-Vis characterisation of citrate and PVP Ag-NPs in OECDss

The characterisation by UV-Vis (Figure 4-45) of the dispersed citrate and PVP Ag-NPs in OECDss shows that the spectra for both Ag-NPs were initially red-shifted with the MA occurring at λ_{max} = 398 nm (Table 4-46). After 24 hrs, the Ag-NPs MA reduced and the FWHM of the UV-Vis spectrum was significantly larger in both cases. However, the UV-Vis spectrum of the PVP Ag-NPs shifted toward the lower wavelengths with a λ_{max} = 395 nm, while for the citrate Ag-NPs the λ_{max} was constant.

The aeration of the synthetic sewage caused further shifting of the UV-Vis spectra of both the citrate and PVP Ag-NPs toward the lower wavelength and their λ_{max} at 45 hrs were respectively 397 and 390 nm. Also, the UV-Vis peaks of both citrate and PVP Ag-NPs were not real Gaussians and showed an exponential decrease in slope for the value of $\lambda > \lambda_{max}$. After settling at 48 hrs, the UV-Vis spectrum of both citrate and PVP-NPs were blue shifted with their MA occurring at λ_{max} = 379 nm.

In conclusion, the UV-Vis results show that at 0 hrs, citrate and PVP Ag-NPs might have their surface chemistry modified via a similar process, likely bound to media proteins (peptone, meat-extract). Although both Ag-NPs may have agglomerated within 24 hours, the surface area of the PVP Ag-NPs might have changed for a second time while citrate particle surface chemistry stabilised. However, there might be further transformations of the surface chemistry occurring with the application of aeration due to oxidation and dissolution of Ag- (Yang et al., 2013c). During the settling phase, the citrate and PVP Ag-NPs might have undergone a similar process with further agglomeration and changes in surface chemistry. There was a significant difference of the MA changes between both particles overtime and at a STP **(**Table A3 - 19**).** Also, the variations of λ_{max} of citrate and PVP Ag-NPs were significantly different at an STP, but not overtime.

Table 4-46: UV-Vis data of citrate and PVP Ag-NPs in OECDss (at 0 hrs, 24 hrs, 45 hrs (during aeration) and at 48 hrs (during settling))

	Citrate Ag-NPs in OECDss				PVP Ag-NPs in OECDss			
	0 hrs	**24 hrs**	**45 hrs**	**48 hrs**	**0 hrs**	**24 hrs**	**45 hrs**	**48 hrs**
λ_{max} (nm)	398	399	397	379	398	395	390	379
MA	0.071	0.044	0.049	0.063	0.062	0.035	0.039	0.049
Absorbance decrease (%)	0	40.29	32.83	11.94	0	77.14	58.97	26.53
FWHM (nm)	59	97	NA	NA	46	59	NA	NA
Peak shift (%)	0	0.25	0.25	5.01	0	0.76	2.05	5.01

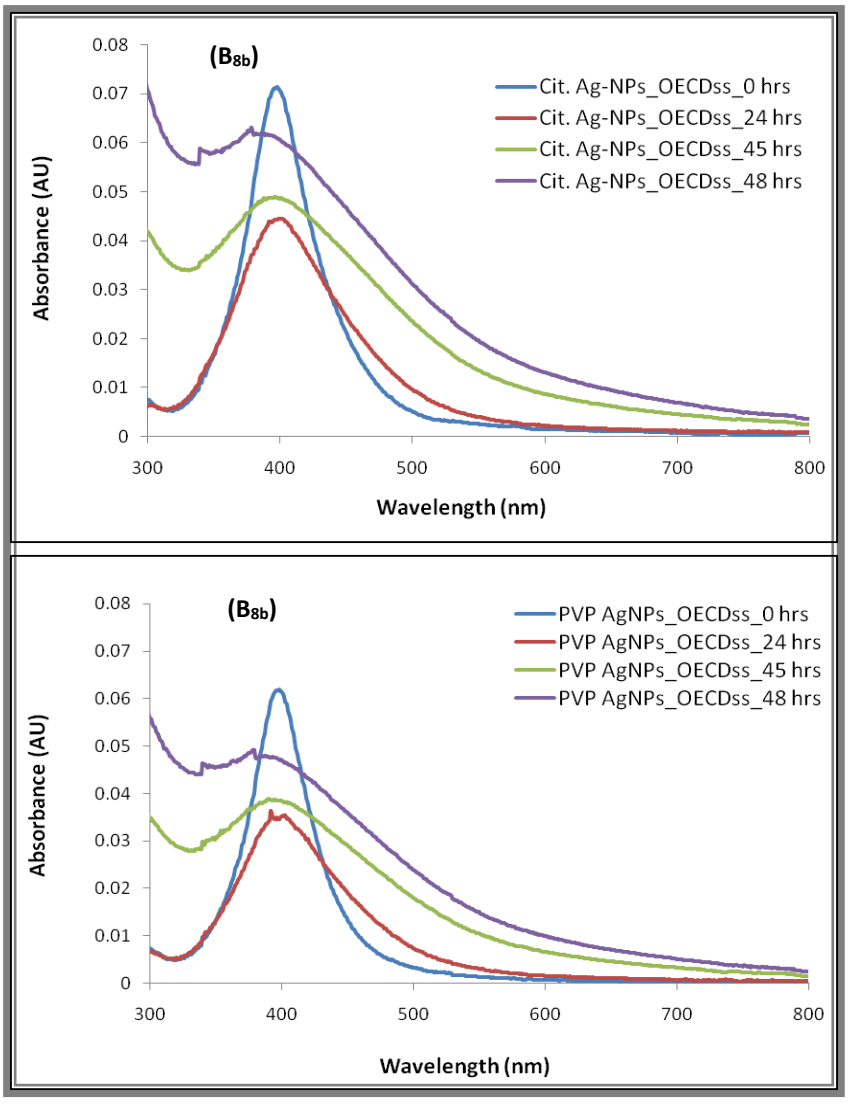

Figure 4-45: UV-Vis spectra of citrate (B_{7a}) and PVP (B_{7b}) Ag-NPs in OECDss (at 0 hrs, 24 hrs, 45 hrs (during aeration) and at 48 hrs (during settling))

4.3.8.3. DLS characterisation of citrate and PVP Ag-NPs in OECDss

Based on the DLS results (Figure 4-46and Table 4-47), despite the high D_H value, citrate Ag-NPs added to OECDss might not have agglomerated right after their exposure due to the low PDI. Meaning, the organic materials (proteins and urea) surrounding the Ag-NPs might have affected their D_H measured by DLS. After the particles were exposed to OECDss at room temperature for 24 hrs, the D_H and the PDI were relatively constant. The aeration of the solution might have caused further agglomeration of the Ag-NPs because of the increase in both D_H and PDI. The citrate Ag-NPs were generally stable over the settling phase.

In addition, the low PDI value shows that the PVP Ag-NPs may not have agglomerated when they were first exposed to the OECDss. But after 24 hours, the Ag-NPs agglomerated based on the increase of their D_H and PDI values, the Ag-NPs then remained stable during the aeration and settling. There was no significant difference between the citrate and PVP Ag-NPs average D_H behaviour and on the variation of the PDI overtime and at a STP (Table A3 - 21).

Table 4-47: DLS data of citrate Ag-NPs in OECDss (at 0 hrs, 24 hrs, 45 hrs (during aeration) and at 48 hrs (during settling))

	Citrate Ag-NPs in OECDss		PVP Ag-NPs in OECDss	
	Primary peak (D_H) (nm)	**PDI**	**Primary peak (D_H) (nm)**	**PDI**
0 hrs	36.0 ± 9.2	0.24 ± 0.14	28.1 ± 0.1	0.16 ± 0.04
24 hrs	33.3 ± 3.6	0.29 ± 0.03	42.7 ± 6.8	0.43 ±0.08
45 hrs	69.2 ± 13.2	0.39 ± 0.03	61.5 ± 5.6	0.30 ± 0.05
48 hrs	63.2 ± 7.7	0.37 ± 0.04	41.5 ± 2.9	0.34 ± 0.01

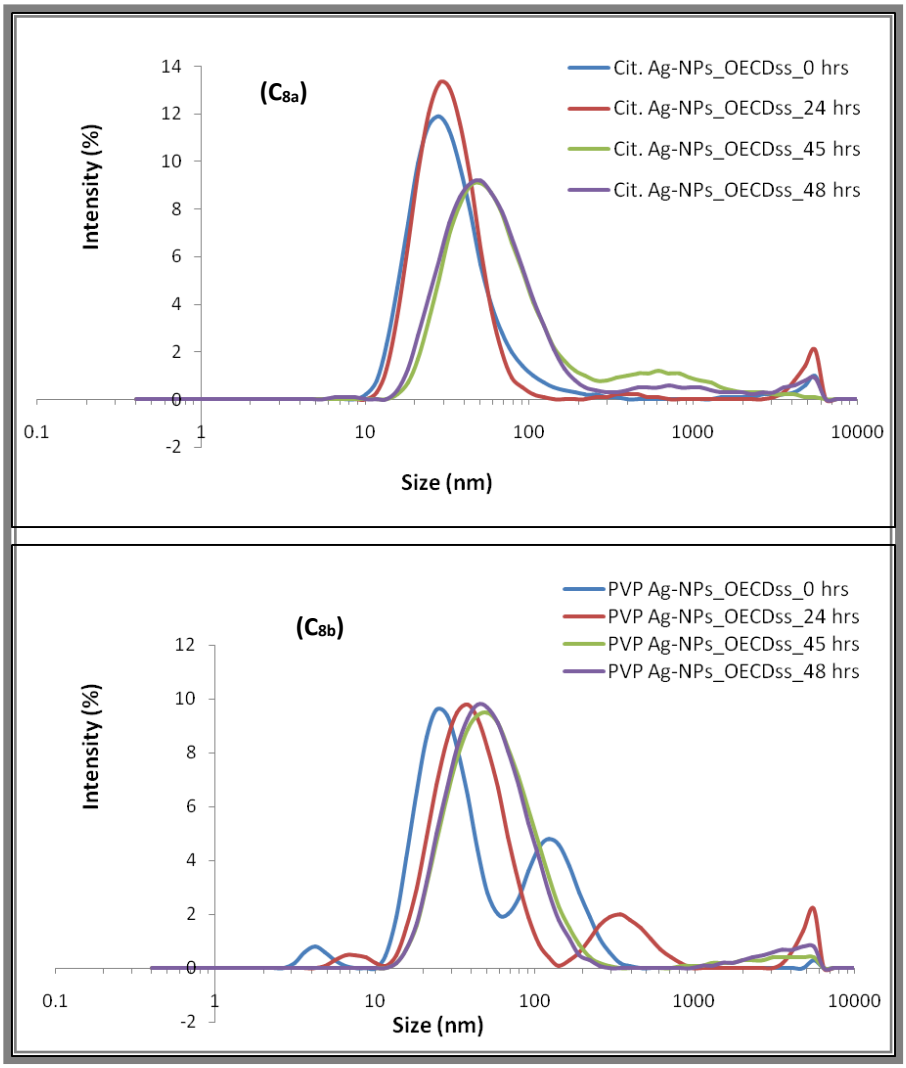

Figure 4-46: D_H distribution of the citrate (C_{8a}) and PVP (C_{8b}) Ag-NPs in OECDss (at 0 hrs, 24 hrs, 45 hrs (during aeration) and at 48 hrs (during settling))

Table 4-48 indicates that although the citrate Ag-NPs showed the highest velocity compared to the PVP Ag-NPs when they were exposed in OECDss, more than two weeks would be necessary instead of three hours to expect a complete sedimentation of the Ag-NPs in both cases.

Table 4-48: Settling velocity with the corresponded DH of citrate and PVP Ag-NPs in OECDss (at 0 hrs, 24 hrs, 45 hrs (during aeration) and at 48 hrs (during settling)).

	D_H (nm) At 48 hrs	Settling velocity ($nm*s^{-1}$)	Settling time (weeks)
Citrate Ag-NPs in OECDss	63.2 ± 7.7	18.12	6.39
PVP Ag-NPs in OECDss	41.5 ± 2.9	7.81	14.81

4.3.8.4. TEM characterisation of citrate and PVP Ag-NPs in OECDss

In OECDss, at 0 hrs the citrate (Figure 4-47) and PVP (Figure 4-48) Ag-NPs were stable in size and shape and their average size was respectively 11.7 ± 5.0 and 12.2 ± 5.1 nm (Table 4-49). After 24 hours, both Ag-NPs agglomerated and their average size increased.

The aeration of the synthetic sewage spiked with citrate Ag-NPs, might have not increased the agglomeration of the Ag-NPs, but may have caused their agglomeration. While for the PVP Ag-NPs, there was an average size reduction, indicating they might have dissolved during aeration. After aeration and settling, the TEM images of the samples collected at 45 hrs show that further dissolution may have occurred in both case. There was no significant difference between citrate and PVP Ag-NPs size behaviour overtime and at a STP (Table A3 - 22).

Table 4-49: TEM average size and shape factor of citrate Ag-NPs in OECDss (at 0 hrs, 24 hrs, 45 hrs (during aeration) and at 48 hrs (during settling))

	Citrate Ag-NPs in OECDss			PVP Ag-NPs in OECDss		
	Longest length (nm)	**Shortest length (nm)**	**Shape factor**	**Longest length (nm)**	**Shortest length (nm)**	**Shape factor**
0 hrs	11.7 ± 5.0	9.02 ± 3.9	0.96 ± 0.06	12.2 ± 5.1	9.3 ± 3.8	0.96 ±0.06
24 hrs	17.5 ± 10.4	13.1 ± 7.8	0.93 ± 0.08	19.5 ± 8.5	15.1 ± 6.3	0.91 ±0.07
45 hrs	18.4 ± 10.0	13.3 ± 7.1	0.89 ± 0.09	14.0 ± 7.3	10.9 ± 5.8	0.94 ±0.07
48 hrs	16.0 ± 8.5	12.1 ± 6.4	0.92 ± 0.08	12.6 ± 6.5	9.7 ± 4.9	0.94 ±0.08

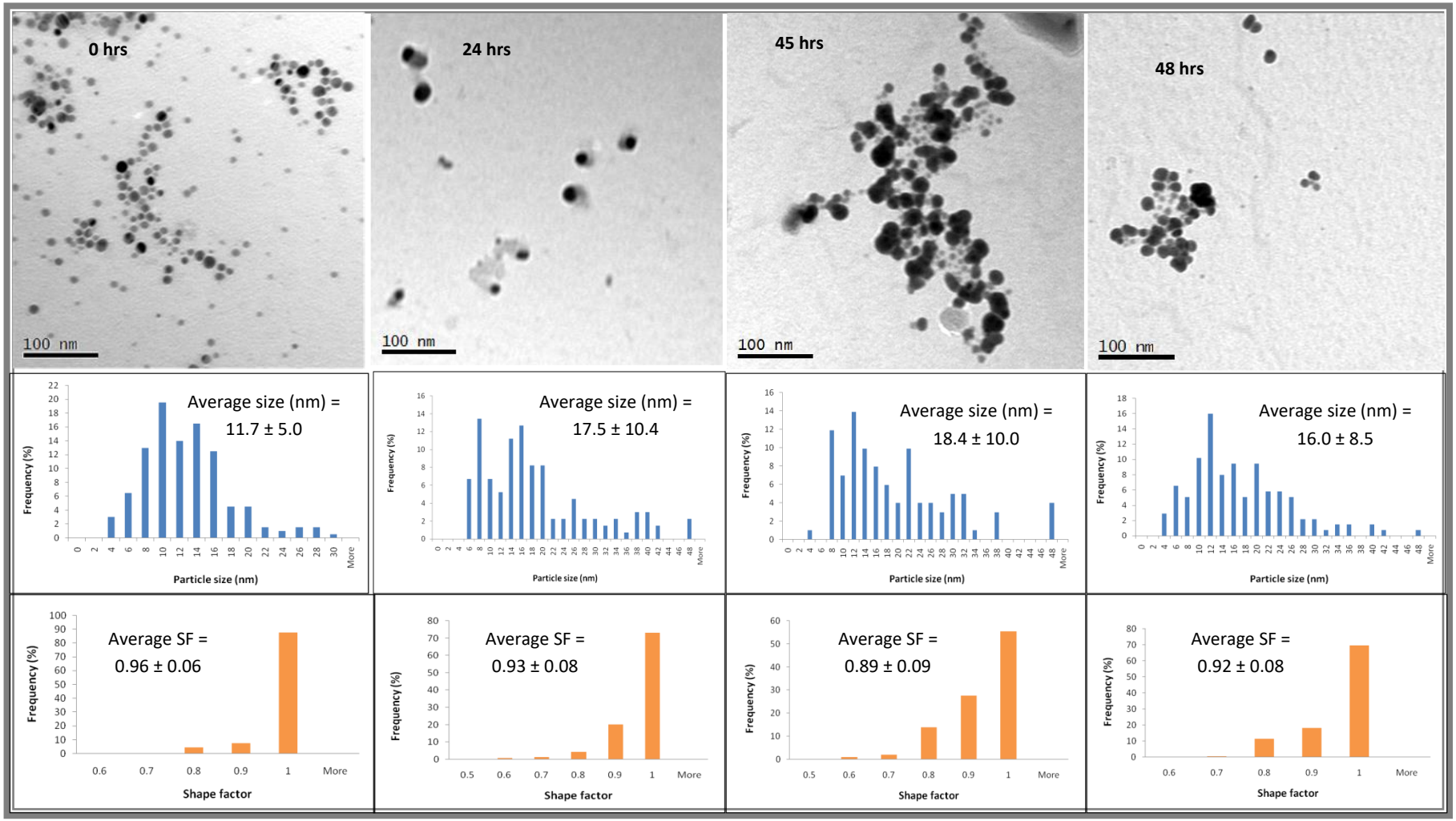

Figure 4-47: TEM size distribution of citrate Ag-NPs in OECDss (at 0 hrs, 24 hrs, 45 hrs (during aeration) and at 48 hrs (during settling)). Based on the count of 200, 134, 101 and 138 NPs for the 0 hrs, 24 hrs, 45 hrs and 48 hrs sample respectively.

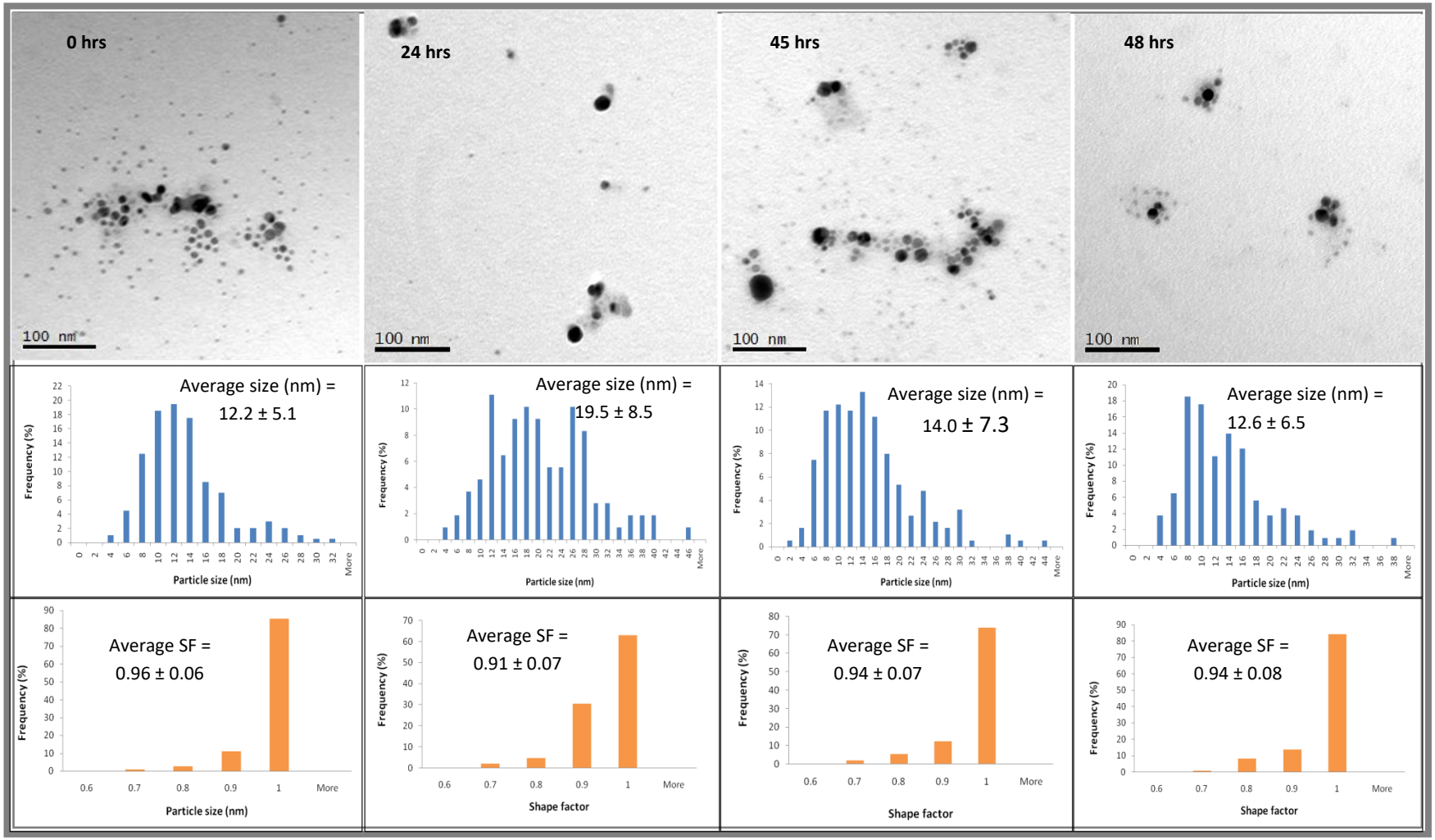

Figure 4-48: TEM size distribution of PVP Ag-NPs in OECDss (at 0 hrs, 24 hrs, 45 hrs (during aeration) and at 48 hrs (during settling)). Based on the count of 200, 108, 188 and 116 NPs for the 0 hrs, 24 hrs, 45 hrs and 48 hrs sample respectively.

4.3.8.5. Chemical surface analysis: ZP of citrate and PVP Ag-NPs in OECDss

When the Ag-NPs were initially dispersed in OECDss, the ZP of the citrate Ag-NPs became more negative (Figure 4-49and Table 4-50), and the opposite was observed for the PVP Ag-NPs. These changes in surface charge might have affected their surface chemistry and favour their transformation into AgCl or Ag_2S. At 24 hrs, the agglomeration of the Ag-NPs (see Figure 4-47 and Figure 4-48) might have been a consequence of their change in surface charge.

During aeration, the surface charge was more negative in both cases since more oxygen ions may have reacted with the Ag-NPs and caused their oxidation and dissolution. At 48 hrs, the ZP was reduced in both cases, and the surface chemistry of the Ag-NPs may have been modified. Thus, Ag_2O NPs formed by oxidation of the Ag-NPs during aeration might have been sulphidised by precipitating during the settling stage (Yang et al., 2013c, Liu et al., 2011). The two-way ANOVA without replication (with $\alpha = 0.05$) comparing the ZP of both particles in OECDss (Table A3 - 21) shows that there was no significant difference between citrate and PVP Ag-NPs size behaviour overtime (P-value =0.466 and $F = 0.69 < F_{critical} = 10.13$) and at a STP (P-value = 0.0.42 and $F = 3.84 < F_{critical} = 1.27$).

Table 4-50: ZP and pH of citrate and PVP Ag-NPs in OECDss (at 0 hrs, 24 hrs, 45 hrs (during aeration) and at 48 hrs (during settling))

	Citrate Ag-NPs in $CaCl_2$		PVP Ag-NPs in $CaCl_2$	
	pH	**ZP (mV)**	**pH**	**ZP (mV)**
0 hrs	6.52	-9.51 ± 3.88	7.2	-11.9 ± 1.67
24 hrs	6.97	-10.6 ± 0.46	7.59	-7.02 ± 1.33
45 hrs	7.96	-12.3 ± 0.78	7.43	-14.6 ± 1.10
48 hrs	7.18	-6.47 ± 0.56	7.12	-11.7 ± 0.63

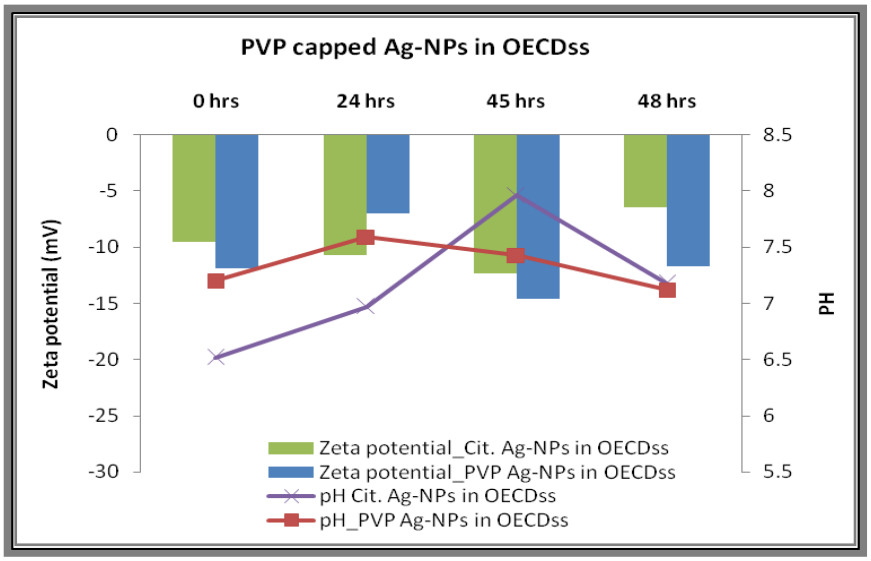

Figure 4-49: variation of the citrate and PVP capped Ag-NPs ZP in combination with the associate pH when dispersed in OECDss (at 0 hrs, 24 hrs, 45 hrs (during aeration) and at 48 hrs (during settling))

4.4. Discussion and conclusion

The stability of fully characterised citrate and PVP Ag-NPs (Chapter 3) in OECDss and its chemical components was considered in the above results. The properties of the Ag-NPs, precisely their dissolution, agglomeration, size, shape and surface chemistry, when considered together helped to establish their stability in a particular medium. In our case, we have assessed these properties of the dispersed Ag-NPs in OECDss and its constituents (peptone, meat-extract, and urea, K_2HPO_4, NaCl, $CaCl_2$ and $MgSO_4$) under experimental conditions that simulate the treatment of sewage in SBR pilot plant.

Based on the results presented in this chapter, we could conclude that the NPs are generally not stable in OECDss or its constituents irrespective of their coating. Each media had a significant impact on both the citrate and PVP Ag-NPs stability and was further compounded by the addition of oxygen using aeration flow, leading to a partial dissolution of the particles. This was followed by the rapid precipitation of AgCl, Ag_2S, Ag_3PO_4 or SP-NPs (silver phosphate NPs) when the particles were dispersed in NaCl, $CaCl_2$, K_2PHO_4 or $MgSO_4$ (as shown in Table Y below). Other transformations include the interaction of Ag-NPs with proteins and lipids (from meat-extract) that may have led to the formation of a corona layer on the particles surface through hydrophobic bonding (Livney, 2010). Also, in urea solution, the urea molecules might behave like proteins and form a corona layer or the particles surface may dissolve, by exposing Ag-NPs to ammonia NH_3 if the urea breaks down.

These mechanisms would affect, to a certain degree, the surface chemistry of the particles through passivation, as precipitated molecules, proteins, lipids or urea accumulate onto the

surface of the particles. The passivation of the particles would reduce the electrostatic repulsion forces that prevent citrate and PVP particles from agglomeration, although might provide some steric repulsion. Hence, in OECDss and it components of the citrate and PVP particles were subject to a certain degree of agglomeration depending on the media and it ionic strength which influenced the ZP. Also, the addition of the oxygen seems to accelerate the agglomeration/aggregation mechanism occurring when Ag-NPs are dispersed into the NaCl, $CaCl_2$, K_2PHO_4 and $MgSO_4$; as it was observed by UV-Vis, DLS and TEM results. All three techniques suggested an increase of the average size of the particles, as evidenced by the red-shift of the UV-Vis spectra, and the presence of dimers, trimers or tetramers by DLS. And there was also a significant increase of the average core size of the particles determined from TEM.

According to these results, PVP particles were highly subject to agglomeration and aggregation in NaCl, $CaCl_2$, K_2PHO_4 and $MgSO_4$, while their exposure to peptone, meat-extract and urea did not affect much their surface chemistry. Citrate Ag-NPs however, were less dissolved in peptone and meat-extract solution after their exposure to oxygen; which means that, the protein binding onto their surface and formation of a corona provided some protection against dissolution. In other media (without biomolecules available to form a corona), the dissolution of citrate Ag-NPs was accentuated under aeration.

Finally, we may conclude that exposure of citrate and PVP Ag-NPs in OECDss might lead to the above transformations. Ag-NPs in this particular media and under aeration will be highly dissolved and the release of Ag^+ will give rise to the rapid formation of AgCl, Ag_2S or SP precipitates onto their surface. The presence of proteins and lipids might slow down

dissolution especially for citrate Ag-NPs. However, the urea in OECDss could weaken the hydrophobic bonds between the particles and proteins (as urea is known to unfold proteins) and leave the particles exposed to oxygen; hence they will dissolve more. Alternatively, the Cl^-, SO_4^- and HPO_4^- ions might partially stabilise the particles as they precipitated onto their surface, leading to the formation Ag-NPs with passivated layers of AgCl, Ag_2S or SP. These particles were more likely to agglomerate according to the TEM results. Thus in a real WWTP, Ag-NPs would indeed be transformed into the AgCl, Ag_2S or SP particles as found in the literature (Kaegi et al., 2013).

Chapter 5 Physical and chemical transformation of silver nanoparticles in sequencing batch reactor pilot plant

Chapter Summary

This chapter investigates the behaviour of dispersed Ag-NPs during the treatment of sewage in a SBR pilot plant. OECD synthetic sewage (OECDss) was spiked with 10 nm citrate and PVP-capped Ag-NPs and used as influent for the wastewater treatment in an SBR pilot plant (Botija, 2006). The activated sludge to be treated was collected from an aerated reactor of the Severn Trent WWTP in Birmingham, UK. The research was divided into two parts. The first part was to investigate the chemical and physical transformation Ag-NPs in OECDss when the influent was treated without activated sludge and in this section of the study, the influence of aeration was also explored in the case of citrate Ag-NPs by looking at their changes in the presence or absence of oxygen flow. For the second part of the work, the behaviour of Ag-NPs was examined when the influent was treated using activated sludge. Samples were collected at 0 and 24 hrs after the dispersion of the Ag-NPs in OECDss and at 45 hrs during the aeration (or non-aeration), 48 hrs settling phases of the treatment. After centrifugation and filtration, the samples were characterised by GFAAS, UV-Vis, DLS, TEM and SEM to assess any changes from the pristine characteristics.

5.1. Introduction

In recent years, several studies (Kaegi et al., 2012, Kaegi et al., 2011b, Kim et al., 2010) have been conducted to investigate the behaviour and fate of Ag-NPs in WWTPs (section 1.2.3). A range of commercial applications utilise Ag-NPs (section 1.1.3.6), and as a result, Ag-NPs are commonly found in consumer products such as cosmetics, clothing, paints, plastics and optical devices (Kaegi et al., 2013, Yang et al., 2013c, Kumar et al., 2014). Investigations of the fate, behaviour and toxicity of Ag-NPs in freshwaters (Kumar et al., 2014, Lowry et al., 2012a) and landfills (Yang et al., 2013b) have raised concerns about their release into the environment via WWTPs (Gottschalk and Nowack, 2011). In fact, due to their presence in consumer products, the majority of Ag-NPs entering sewage treatment systems are derived from discharge/release into wastewater and general waste disposal into landfill (Benn and Westerhoff, 2008b, Kaegi et al., 2013).

Despite more than 85% of Ag-NPs in the WWTP being captured in the activated sludge biosolids (Doolette et al., 2013), much of the research has focused on the Ag-NPs remaining in the effluent that is ultimately released into freshwaters (Benn and Westerhoff, 2008a, Kaegi et al., 2013). In the UK (DEFRA, 2012), the 85% of the Ag-NPs captured in the sludge are most likely re-distributed to agriculture soil since 80% of the sludge is discharged to soil, while 18% is incinerated and the rest (about 2%) is reused or disposed of in the landfill. These sludge-associated Ag-NPs are anticipated to be mainly silver sulphide (Ag_2S) NPs (Kim et al., 2010) which are found to have a very stable surface chemistry, making them less susceptible to oxidation and dissolution than metallic Ag-NPs (Dale et al., 2013, Jacobson et al., 2005). The amount of Ag-NPs in the WWTP can be estimated by assessing their release from consumer

products into wastewater (Doolette et al., 2013, Whiteley et al., 2013a, Yang et al., 2012). The concentration ultimately released into the freshwater environment will depend on the efficiency of Ag-NPs removal by the sewage system (Li et al., 2013) which is likely to be influenced by the NP surface properties (King et al., 2015, Kaegi et al., 2013).

5.1.1. Oxidation of Ag-NPs in an aerated WWTP

In a WWTP, the surface properties of Ag-NPs may be modified by the presence of even low concentrations of oxygen in the reactor (Doolette et al., 2013), which may react with Ag-NPs by oxidising them (Yang et al., 2013c). The formation of Ag_2O in a treatment plant is due to the interaction of dissolved Ag (Ag^+ ions) and the oxygen atoms in the sewage through precipitation (Choi et al., 2009). Yang et al. (2013c) have established that the presence of dissolved oxygen in an aerobic WWTP is the leading cause of Ag-NPs oxidative dissolution, which generates silver oxide Ag_2O. However, because of their low stability, Ag_2O dissolved living placed to the formation of Ag_2S and AgCl through Ag^+ binding with chloride and sulphate (Doolette et al., 2013). The oxidative dissolution of Ag-NPs in the plant is represented by the following equations in the case where there is both zero valent Ag-NPs (Equation 5-1) and Ag_2S NPs (Equation 5-2) present (Dale et al., 2013):

$$2Ag^0 + {}^1/_2\, O_2 + 2H^+ \rightarrow 2Ag^+ + H_2O$$

Equation 5-1

$$Ag_2S(NP) + 2O_2 \rightarrow 2Ag^+ + SO_4^{2-}$$

Equation 5-2

The silver ions may then be transformed into Ag_2S NPs through their reaction with sulphide ligand (S^{2-}) (Choi et al., 2009). Kaegi et al. (2011a) found, for concentration as low as 0.5 $mg*L^{-1}$ of Ag-NPs, there was a nearly complete transformation of the particles (> 90%) intoAg_2S

within two hours of their dispersion in the a non-aerated WWTP reactor containing activated sludge. But at a higher concentration (5 mg*L^{-1}), only approximately 60% the dispersed Ag-NPs were precipitated into Ag_2S after two hours and this fraction remained unchanged as the saturation of the solution with Ag^+ was reached. Also, the degree of sulphidation of Ag-NPs was found to be of size dependent (Kaegi et al., 2013) with 100% of 10 nm Ag-NP sulphidising at 24 hrs, while only 10 % of 100 nm Ag-NPs were sulphidised at 24 hrs.

Although most of the Ag-NPs present in WWTP is transformed into Ag_2S, the other species (Kaegi et al., 2013, Kaegi et al., 2011a)of Ag in WWTP might include Ag^+, AgO_2, $AgNO_3$, Ag – CuS (proxy of Ag_2S or Ag^+ absorbed on the surface of a metal sulphide other than Ag), metallic Ag(0) and AgCl.

5.1.2. Sulphidation of Ag-NPs in an aerated WWTP

The sulphidation of Ag-NPs, which only occurs under anaerobic conditions (Kaegi et al., 2013, Kaegi et al., 2011b), obeys two distinctive mechanisms (Liu et al., 2011). The first reaction occurs when Ag^+ ions released from the oxidative dissolution of Ag-NPs are sulphidised (Equation 5-3) while the second reaction is a solid-fluid heterogeneous reaction which occurs through direct sulphidation of Ag-NP surfaces (Liu et al., 2011).

$$Reaction(1): \quad 2Ag^+ + H_2S(aq) \leftrightarrow Ag_2S + 2H^+$$

Equation 5-3

$$Reaction(2): \quad 2Ag^0 + H_2S + {}^1/_2\, O_2 \leftrightarrow Ag_2S + H_2O$$

Equation 5-4

Choi et al. (2009) found that the oxidation ofsulphide species (H_2S and HS^-) into (S^{2-}) in nitrifying organisms is inversely proportional to the dissolved oxygen (DO) concentration – hence reducing Ag-NPs toxicity, as they will precipitate into Ag_2S via after undergoing oxidation/dissolution transformations. Also, in presence and absence of DO, Ag_2S undergo little to no dissolution in reducing conditions and finally the release of Ag^+ from Ag-NPs was dependent on thesulphide (S^{2-}) or sulphate (SO_4^{2-}) ligand associated with Ag_2S formation. They concluded that Ag_2S NPs formed from Ag-NP –sulphide complexes were more stable than the Ag-NP – sulphate complex.

In addition, Ag-NPs' coating and size play a significant role in their sulphidation state. Smaller Ag-NPs have a faster sulphidation rate than large ones (Kaegi et al., 2013), and PVP coated Ag-NPs have a rapid sulphidation with more than 50% of the particles sulphidising within five days of the treatment (Ma et al., 2014).

5.1.3. Fate and behaviour of Ag-NPs in WWTP

Until recently, the fate and behaviour of Ag-NPs in WWTP were unknown. However, recent research has reported that not only do Ag-NPs sulphidise, but that sulphidation process occurs primarily in the sewer system in the WWTP (Kim et al., 2010, Kaegi et al., 2013). Under aeration, a dual reaction occurs with Ag-NPs oxidising or sulphidising instantly as shown in Equation 5-1 and Equation 5-3. After the aeration, most or nearly all of the initial Ag-NPs have been converted to Ag_2S NPs which accumulate in the activated sludge (Kim et al., 2010, Kaegi et al., 2011b, King et al., 2015). With multiple complex materials present in the sewage, it is

likely that in addition to the Ag_2S NPs, other silver complexes are found in the wastewater and this could include metallic Ag, AgCl, Ag_2O and Ag^+ (Kaegi et al., 2013).

5.1.4. Aims and objectives

The aim of this chapter was to investigate and compare the behaviour of citrate and PVP coated Ag-NPs; first, when dispersed in OECDss and second, when the OECDss was used as the influent for the SBR pilot plant. The objectives were to:

1) Characterise samples collected from the influent before treatment in the SBR at 0 and 24 hrs using GFAAS, UV-Vis, DLS, TEM and SEM/EDS.
2) Characterise collected samples from the SBR (at 45 and 48 hrs respectively) during the two treatment phases: aeration phase (from the 24 hrs to 45 hrs time point of the experiment) and settling phase (from the 45 hrs to 48 hrs time point of the experiment). And examine the changes that have occurred to the NPs and their physicochemical properties during the treatment process such as dissolution, aggregation, and changes in surface chemistry, size and shape.

5.2. Materials and method

For this part of the work, 10 nm pristine citrate (Römer et al., 2011) and PVP (Tejamaya et al., 2014) Ag-NPs were synthesised and characterised as described in Chapter 3. Table 5-1shows the chemical and physical characteristics measured for these particles as synthesised (pristine).

Table 5-1: Characterisation results of citrate and PVP pristine particles

	Ag-NPs ($mg*L^{-1}$)	λ_{max} (nm)	DLS Average diameter (nm)	PDI	TEM Average size (nm)	ZP (mV)	Shape factor
Citrate Ag-NPs	11.76	392	20.3 ± 0.3	0.12 ± 0.01	11.7 ± 6.4	-37.8 ± 1.4	0.81 ± 0.16
PVP Ag-NPs	10.64	393	33.4 ± 2.5	0.25 ± 0.01	12.3 ± 5.4	-8.6 ± 0.9	0.96 ± 0.05

5.2.1. The synthetic sewage (OECDss) experiment

The first part of the experiment covered the investigation of the fate and transformations of citrate, and PVP-capped Ag-NPs spiked into OECD synthetic sewage (OECDss) and during treatment in the SBR pilot plant. The composition and characteristics of the OECDss are discussed in section 2.2.2.1. The experiment was set-up for forty-eight hours and was divided into four phases corresponding to the 0, 24, 45, and 48 hr time points. The influent was prepared by dispersing 500 $\mu g*L^{-1}$ of Ag-NPs into 9.5 mL of OECDss at 0 hrs, and the samples were analysed using GFAAS, UV-Vis, DLS, and TEM.

The influent was left at room temperature for 24 hours and samples were taken for analysis before starting the treatment. It was then transferred to the SBR pilot plant, where it was aerated for twenty-one hours (45 hr sampling point) and was left to settle for three hours (48 hr sampling point). During this treatment, three samples were collected from the top, middle and bottom of the reactor during the aeration (TTA = Test Top Aeration, TMA = Test Middle Aeration and TBA = Test Bottom Aeration) and settling (TTS = Test Top Settling, TMS = Test Middle Settling, TBS = Test Bottom Settling and TES = Test Effluent Settling) phases at 45 hrs and 48 hrs, respectively.

The SEM samples for EDS analysis were obtained by leaving the rest of the synthetic sewage (about four litres) in the reactor for forty-eight hours after the effluent removal. After 48 hours, the left-in synthetic sewage had formed a thick layer on the surface, and very large clumps were sedimented at the bottom of the reactor. This layer and the clumped materials were collected by sifting the sewage, and these samples were subsequently dried in the oven for over 24 hours at 25 °C. The samples were then ground up and stored in microtubes. Note that the methods used to prepare the aqueous samples for each specific characterisation technique were described in section2.3.

5.2.2. The real sewage (OECDss + activated sludge) experiment

For this part of the work, the influent made 24 hours earlier was used to fill the reactor containing 4 L of activated sludge from a Severn Trent WWTP, UK (Chapter 2). The obtained sewage was then aerated for twenty-one hours (45 hr sampling point) and then left to settle for three hours (48 hr sampling point). Samples were collected from the top, middle and bottom of the reactor during aeration (at 45 hrs) and settling (at 48 hrs). Figure 5-1shows the state of the sewage after three hours of settling.

Figure 5-1: Sewage treatment in the SBR pilot WWTP after completion of the settlement phase.

5 ml of each collected sample was acid digested for GFAAS characterisation, and the rest of the sample was centrifuged at 5000 rpm and 10 °C for 30 min to remove any solid material larger than 500 µm. The remaining particles greater than 100 nm were removed by filtering the samples through 450, 200 and 100 nm pore size syringe filters. Finally, the filtered solution from each sewage sample was characterised using the various characterization techniques.

5.2.3. GFAAS analysis

The concentration of Ag^+ and Ag-NPs of the samples collected at a particular period and phase of the experiment (0 hrs, 24 hrs, 45 hrs (TTA_45 hrs, TMA_45 hrs and TBA_45 hrs), 48 hrs (TTS_48 hrs, TMS_48 hrs and TBS_48 hrs), were measured by GFAAS (session 2.4.4) after their preparation (section 2.3.3.4). Because the experiment was done three times, the obtained three sets of data were used to determine the average concentrations ((Henglein and Giersig), (Vodnik et al.), dissolved Ag percentage and unrecovered Ag-NPs percentage)along with the

associated standard deviations. Unrecovered Ag was assumed to be Ag-NPs or ions that may have stuck to the influent bottle, to the SBR reactor or to stirring paddle.

Basic calculations were used to estimate the concentration of Ag-NPs (Equation 5-5) and percentage of Ag^+ (Equation 5-6) and unrecovered Ag-NPs (Equation 5-7) for each set of data and their averages and standard deviations were deducted:

$$\mathrm{C}_{Ag-NPs}(\mathrm{i\ hrs}) = \mathrm{C}_{Total\ Ag}(\mathrm{i\ hrs}) - \mathrm{C}_{Ag^+}(\mathrm{i\ hrs})$$

Equation 5-5

$$Dissolved\ Ag_{ihrs}(\%) = \left(\frac{\mathrm{C}_{Ag^+}(\mathrm{i\ hrs})}{\mathrm{C}_{Total\ Ag}(\mathrm{i\ hrs})}\right) * 100$$

Equation 5-6

$$Unrecovered\ Ag - NPs_{ihrs}(\%) = \left(\frac{\mathrm{C}_{Ag-NPs}(0\ \mathrm{hrs}) - \mathrm{C}_{Ag-NPs}(\mathrm{i\ hrs})}{\mathrm{C}_{Ag-NPs}(0\ \mathrm{hrs})}\right) * 100$$

Equation 5-7

Where $\mathrm{C}_{Total\ Ag}(\mathrm{i\ hrs})$ is the measured total Ag concentration (in $\mu g*L^{-1}$) of a collected sample a at specific period and phase of the experiment (i hrs), $\mathrm{C}_{Ag^+}(\mathrm{i\ hrs})$ ist the measured total Ag concentration (in $\mu g*L^{-1}$) of a collected sample a at specific period and phase of the experiment (i hrs) and $\mathrm{C}_{Ag-NPs}(\mathrm{i\ hrs})$ is the estimated Ag-NPs concentration (in $\mu g*L^{-1}$) of a collected sample at specific period and phase of the experiment (i hrs).

5.2.4. UV-Vis average size of the particles

The average size of the particles given by UV-Vis was estimated using the Drude and Mie models (Appendix 0) and the associated results and discussion are given in the Appendix A4-1.

5.2.5. Statistical analysis: one-way ANOVA(Wackerly et al., 2002, Rasmussen, 1992)

The analysis of variance is applied to analyse to variation in a set of observations and give portions of this modification to each of a set of independent variables (Wackerly et al., 2002). In a single variable experiment with several independent random samples, the ANOVA observations can be used to make interference about the set of samples (Rasmussen, 1992).

5.3. Results and discussions

We have seen from Chapter 4that, the TEM size (Table 4-49) of citrate and PVP Ag-NPs in OECDss increased with time before aeration due to aggregation. In addition, the dissolution of citrate and PVP Ag-NPs was also observed by GFAAS with PVP Ag-NPs having the highest percentage of dissolved Ag prior aeration (Table 4-45). Finally, according to the ZP measurements (Table 4-50), the surface chemistry of both citrate and PVP Ag-NPs also changed over time and during treatment. In fact, in OECDss, citrate and PVP Ag-NPs might interact with the peptone and meat-extract proteins or transform into AgCl, Ag_2S or Ag_2O. The results below help to investigate these transformations further by using an SBR plant pilot instead of the experimental set-up that was used in Chapter 4. This set-up also allows examination of a more complex environment when the activated sludge was added to influent.

5.3.1. Characteristics of Ag-NPs dispersed in OECDss: treatment with aeration and absence of activated sludge

This work was completed using multiple characterisation techniques in order to understand the behaviour of Ag-NPs in OECDss before and during treatment in the SBR pilot plant in the presence of aeration, i.e. in an oxidising environment. The influent alone was used during the treatment, i.e., the mixture of both OECDss and Ag-NPs was treated on its own without usage of the activated sludge. Samples were collected at 0 hrs, 24 hrs, 45 hrs (TTA_45 hrs, TMA_45 hrs and TBA_45 hrs), 48 hrs (TTS_48 hrs, TMS_48 hrs and TBS_48 hrs) and from the effluent (TES_48 hrs), filtered and characterised.

5.3.1.1. Dissolution study: determination of silver concentration

The concentration of total Ag, Ag^+ ions and Ag-NPs in OECDss before and during treatment, are summarized in Table 5-2 and Table 5-3 for citrate and PVP-capped Ag-NPs respectively. The initial concentration of citrate and PVP Ag-NPs was 566.32 ± 17.63 and 527.07 ± 78.73 mg/L respectively. Citrate and PVP Ag-NPs dissolved over time in the OECDss before treatment with 14.30 ± 2.86 and 15.75 ± 1.20 % dissolved Ag at 24 hrs, respectively. Because of the low dissolution, the concentration of Ag-NPs in OECDss could be considered relatively constant before treatment.

The one-way ANOVA for the critical value of α = 0.05 (Table A4 - 23) was calculated by comparing the concentration of total Ag, Ag^+ ions and Ag-NPs (respectively $C_{Total\ Ag}$, C_{Ag+} and $C_{Ag\text{-}NPs}$) in OECDss of the citrate and PVP Ag-NPs at 0 and 24 hrs. There was no significant difference in the variations of $C_{Total\ Ag}$, C_{Ag+} and $C_{Ag\text{-}NPs}$ between citrate and PVP Ag-NPs influents over twenty-four hours since $F < F_{critical}$ in each case. So, there is no significant difference between the dissolution level of dispersed citrate and PVP Ag-NPs in OECDss.

The application of an aeration flow (100 to 120 cm^3/min) caused further dissolution of the Ag-NPs because of the oxidative dissolution mechanism occurring during that phase (Yang et al., 2013c). However, this form of dissolution was predominant for the citrate Ag-NPs (Figure 5-2) compared to the PVP particles (Table A4 - 23); likely as a result of the PVP coating shielding the Ag-NP surface from exposure to oxygen. For the citrate Ag-NPs, there was less Ag^+ ions at the top and middle of the reactor by 45 hours, whereas for the PVP particles, the lowest percentage of Ag^+ ions was found at the bottom of the reactor. At 45 hrs, the concentration of Ag-NPs was fluctuating between 272.70 ± 22.51 and 335.86 ± 33.27 $\mu g*L^{-1}$ for citrate Ag-NPs and 398.50 ± 73.84 and 433.10 ± 14.41 $\mu g*L^{-1}$ for PVP Ag-NPs, which shows that citrate Ag-NPs might have been less stable than PVP Ag-NPs in presence of aeration.

The calculation of the one-way ANOVA (Table A4 - 23) for the critical value of $\alpha = 0.05$ was obtained from the statistical analysis between $C_{Total\ Ag}$, C_{Ag+} and $C_{Ag\text{-}NPs}$ in OECDss of the citrate and PVP Ag-NPs at 45 hrs. The results show a significant difference in both $C_{Total\ Ag}$ and $C_{Ag\text{-}NPs}$ between citrate and PVP Ag-NPs because their corresponded F-test value is higher than $F_{critical}$ ($F > F_{critical}$). Thus, the mean value of $C_{Total\ Ag}$ and $C_{Ag\text{-}NPs}$ observations during the aeration of the synthetic sewage were not equal for both citrate and PVP Ag-NPs. However, the ANOVA between C_{Ag+}(citrate) and C_{Ag+}(PVP) shows that the null hypothesis cannot be rejected since $F < F_{critical}$, so the means of C_{Ag+}(citrate) and C_{Ag+}(PVP) are similar during aeration.

From the above results, we may conclude that the difference between $C_{Total\ Ag}$ and $C_{Ag\text{-}NPs}$ of citrate and PVP Ag-NPs in OECDss was due to the high concentration of unrecovered Ag (about 17 to 26% (Table 5-2)) than PVP Ag-NPs (about 1 to 6% (Table 5-3)) at 45 hrs. This shows that citrate Ag-NPs were more likely to adhere to any surface they might have come into contact

with; which in this study may have been the proteins in the OECDss, the SBR reactor and the paddle of the stirrer surfaces.

At 48 hrs, the dissolution of citrate Ag-NPs reached about 49% (Table 5-2) and 37% for the PVP particles (Table 5-3). Also at the end of the process, there were about 26 and 15% unrecovered of Ag from the citrate and PVP Ag-NP samples, respectively, that were not recovered due to the well-known problem of Ag sticking to surfaces, in this case to one or more of the influent container, the reactor or on the stirrer.

At 48 hrs (Table A4 - 23), the ANOVA test for $\alpha = 0.05$ for the samples collected during the settling phase shows that there was a significant difference in the variation in concentration of the total Ag, Ag^+ and Ag-NPs because their corresponding F value was beyond $F_{critical}$. Thus, there was a significant difference between the means of all three factors for both citrate and PVP Ag-NPs. With the above observations and the results of Table 5-2 and Table 5-3, as well as in Figure 5-2and Figure 5-3, we may conclude that dispersed citrate Ag-NPs in OECDss had a high level of dissolution and a high tendency to adhere to any surface they come into contact with.

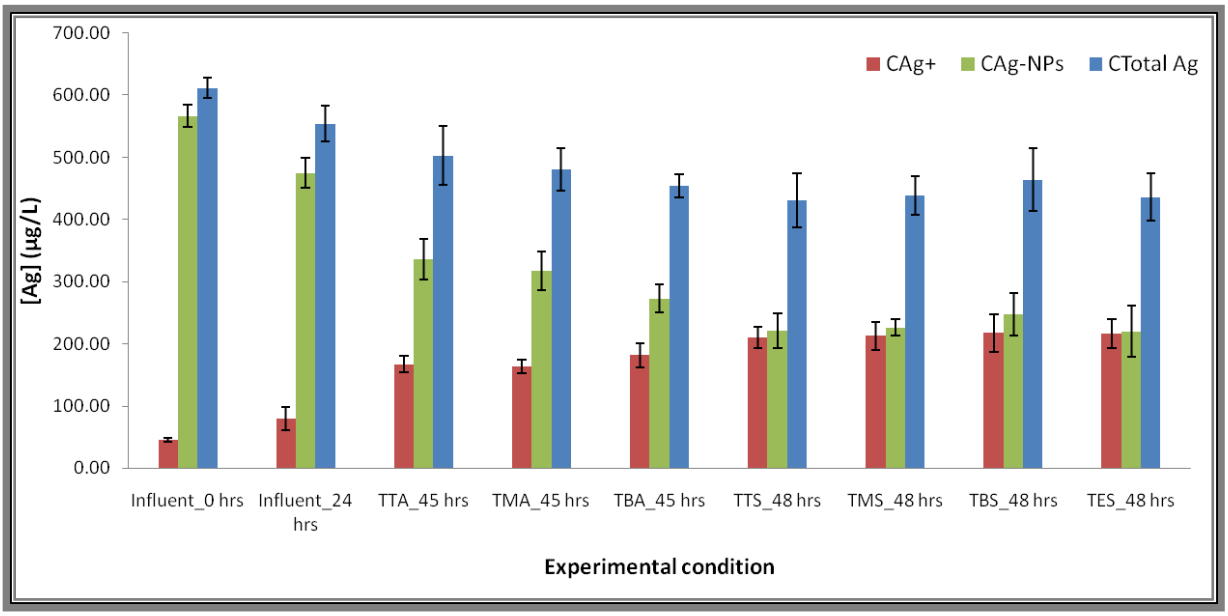

Figure 5-2: Citrate Ag-NPs in OECDss – Analysis of Ag concentration and distribution between ionic and NP form before and during treatment.

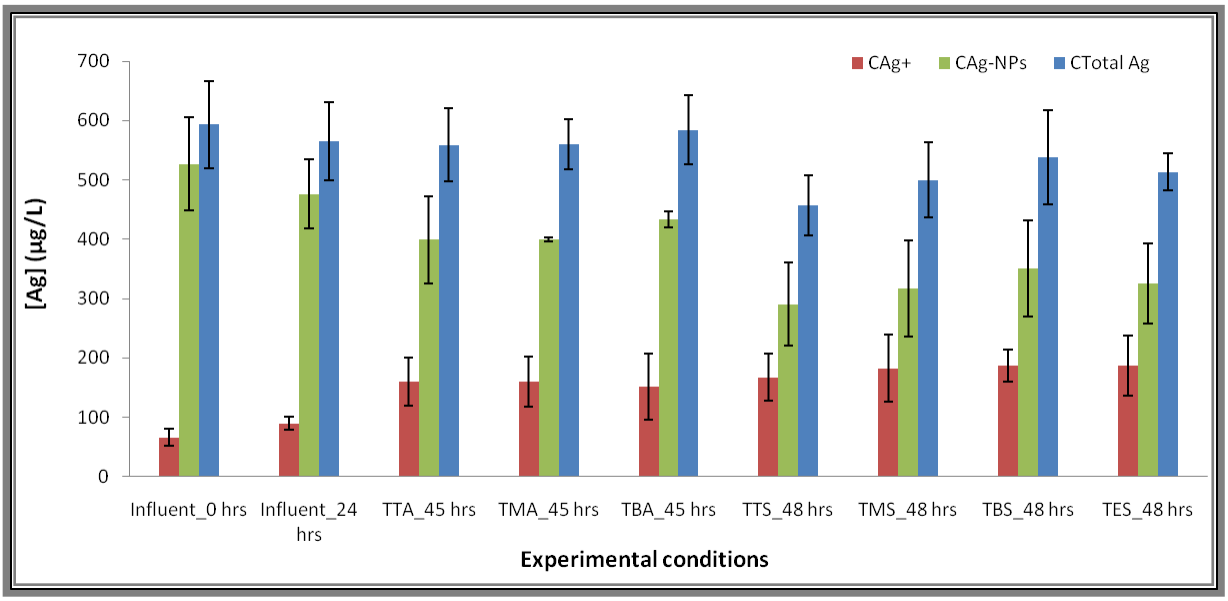

Figure 5-3: PVP Ag-NPs in OECDss – Analysis of Ag concentration and distribution between ionic and NP form before and during treatment.

Table 5-2: Citrate-capped Ag-NPs in OECDss – Total Ag concentration ($C_{Total\ Ag}$), dissolved Ag concentration (C_{Ag+}), estimated Ag-NPs concentration ($C_{Ag\text{-}NPs}$), percentage of dissolved Ag and losses in Ag-NPs before (at 0 and 24 hrs) and during treatment in the SBR pilot plant with samples collected from the top, middle and bottom of the reactor at 45 hrs (aeration stage) and 48 hrs (settling stage).

	$C_{Total\ Ag}$(citrate) ($\mu g*L^{-1}$)	C_{Ag+}(citrate) ($\mu g*L^{-1}$)	$C_{Ag\text{-}NPs}$(citrate) ($\mu g*L^{-1}$)	%Diss. Ag (Citrate) (%)	Unr. Ag (citrate) (%)
0 hrs	612.07 ± 16.17	45.76 ± 2.51	566.32 ± 17.63	7.48 ± 0.54	0.00 ± 0.00
24 hrs	554.53 ± 28.84	79.49 ± 11.18	475.04 ± 23.95	14.30 ± 2.86	9.29 ± 6.79
TTA_45 hrs	502.65 ± 46.51	166.79 ± 13.30	335.86 ± 33.27	33.21 ± 0.49	17.75± 9.10
TMA_45 hrs	479.95 ± 33.83	163.11 ± 11.40	316.85 ± 31.39	34.06 ± 2.75	21.57± 5.58
TBA_45 hrs	453.94 ± 18.21	181.24 ± 20.08	272.70 ± 22.51	39.93 ± 4.13	25.82 ± 2.84
TTS_48 hrs	430.95 ± 44.08	210.74 ± 16.51	220.21 ± 27.58	48.98 ± 1.22	29.57 ± 7.33
TMS_48 hrs	438.28 ± 30.63	212.35 ± 22.93	225.93 ± 12.68	48.38 ± 2.53	28.45 ± 3.13
TBS_48 hrs	463.96 ± 51.16	217.10 ± 31.13	246.86 ± 34.43	46.80 ± 4.71	24.09 ± 9.49
TES_48 hrs	436.01 ± 37.93	216.34 ± 24.31	219.67 ± 41.11	49.79 ± 2.27	28.72 ± 6.77

Table 5-3: PVP-capped Ag-NPs in OECDss – Total Ag concentration ($C_{Total\ Ag}$), dissolved Ag concentration (C_{Ag+}), estimated Ag-NPs concentration ($C_{Ag\text{-}NPs}$), percentage of dissolved Ag and losses in Ag-NPs before (at 0 and 24 hrs) and during treatment in the SBR pilot plant with samples collected from the top, middle and bottom of the reactor at 45 hrs (aeration stage) and 48 hrs (settling stage).

	$C_{Total\ Ag}$ (PVP) ($\mu g*L^{-1}$)	C_{Ag+} (PVP) ($\mu g*L^{-1}$)	$C_{Ag\text{-}NPs}$ (PVP) ($\mu g*L^{-1}$)	%Diss. Ag (PVP) (%)	Unr. Ag (PVP) (%)
0 hrs	593.00 ± 73.17	65.93 ± 15.07	527.07 ± 78.73	11.31 ± 3.2	0.00 ± 0.00
24 hrs	565.30 ± 65.74	88.90 ± 10.73	476.40 ± 57.94	15.75 ± 1.20	4.60 ± 1.77
TTA_45 hrs	558.53 ± 62.26	160.03 ± 39.7	398.50 ± 73.84	28.86 ± 7.39	5.67 ± 5.36
TMA_45 hrs	560.53 ± 41.82	160.13 ± 42.06	400.40 ± 3.40	28.29 ± 5.62	5.05 ± 5.32
TBA_45 hrs	583.67 ± 57.57	150.57 ± 56.01	433.10 ± 14.41	25.32 ± 7.50	1.34 ± 3.35
TTS_48 hrs	456.83 ± 50.65	167.27 ± 39.88	289.57 ± 70.35	37.01 ± 9.73	21.44 ± 18.71
TMS_48 hrs	500.13 ± 64.19	183.00 ± 56.82	317.13 ± 80.60	36.81 ± 11.82	15.55 ± 5.47
TBS_48 hrs	538.03 ± 79.67	186.57 ± 27.40	351.47 ± 81.47	35.11 ± 6.37	9.43 ± 3.52
TES_48 hrs	512.63 ± 31.4	187.43 ± 50.37	325.20 ± 66.94	36.77 ± 10.36	13.06 ± 6.03

5.3.1.2. UV-Vis characterisation of the particles

The UV-Vis spectra of the citrate and PVP Ag-NPs during each phase are represented respectively by Figure 5-4 and Figure 5-5. The wavelengths at MA (λ_{max}) for the pristine particles were 393 and 392 nm respectively for citrate and PVP Ag-NPs. Their dispersion in the OECDss at 0 hrs caused a red-shift of the UV-Vis spectrum, with the magnitude of the red-shift of citrate Ag-NPs being slightly higher (1.52%) than the magnitude of PVP Ag-NPs red-shift (1.27%). The corresponded new values of λ_{max} for both citrate and PVP Ag-NPs were found to be 399 and 397 nm respectively. With these results, we may suggest that, either the surface chemistry of the NPs was modified or that the particles might have agglomerated and increased in size (Hussain et al., 2014).

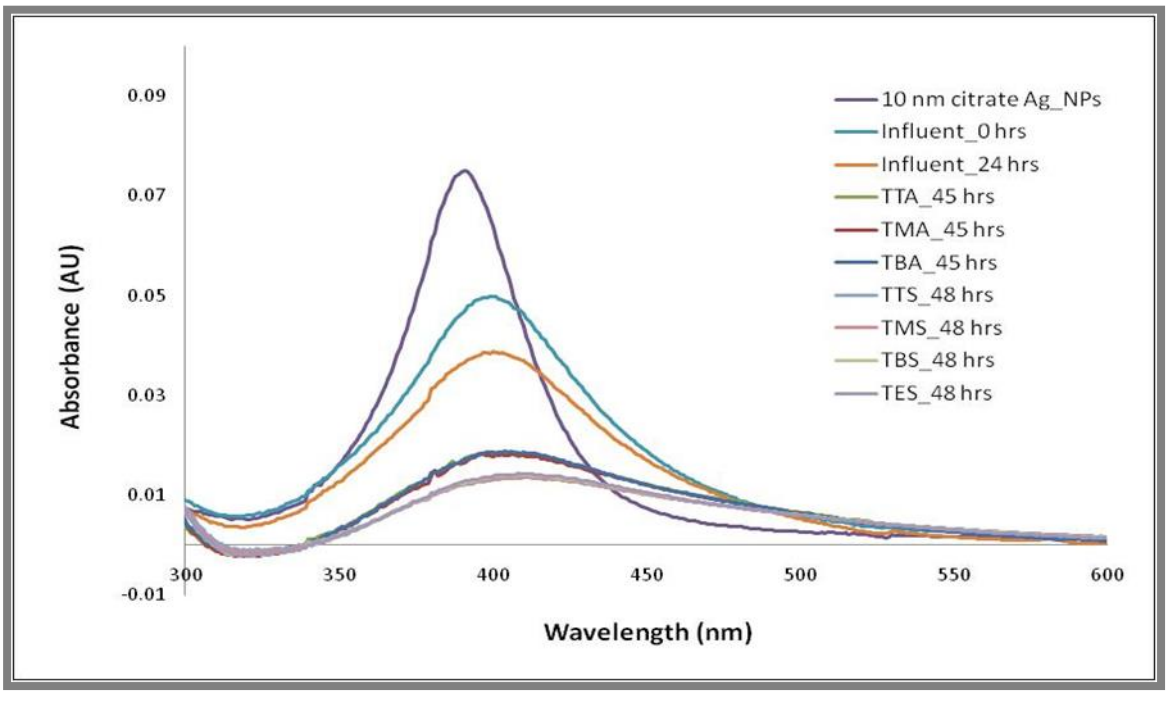

Figure 5-4: UV-Vis spectrum of the citrate Ag-NPs in OECDss before and during treatment. Note the initial red-shift by 6 nm upon introduction to the influent, and the gradual loss of absorbance over time.

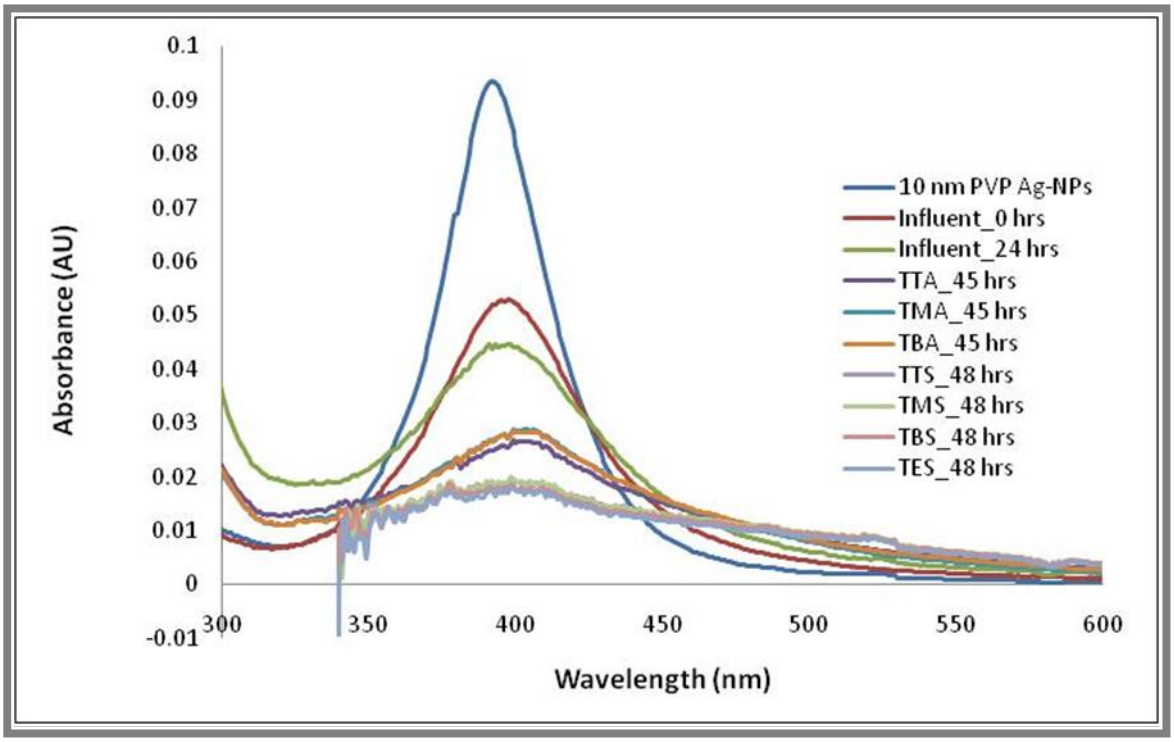

Figure 5-5: UV-Vis spectrum of the PVP Ag-NPs in OECDss before and during treatment. Note the initial redshift by 5 nm upon introduction to the influent, and the gradual loss of absorbance over time.

It is also possible that proteins present in the influent could have affected the surface chemistry of the particles (Anouar et al., 2014) through binding or adsorption on the particle surface forming a corona layer (Tai et al., 2014). In fact, the SPR of the particles is also characterised by their dielectric function (ε) and the dielectric constant of the medium surrounding them. The interaction between Ag-NPs and proteins affects ε, which causes a red-shift of the UV-Vis peak (Podila et al., 2012). In addition, the MA of the Ag-NPs was decreased to 40.5% and 43.0% for citrate (Table 5-4) and PVP Ag-NPs (Table 5-5), respectively, most likely due to NP dissolution (Zook et al., 2011).

Table 5-4: UV-Vis data of citrate Ag-NPs in OECDss before and during treatment – Wave length at the MA (λ_{max}), MA, percentage of the shifting of the spectrum (peak shift) and its magnitude decreased (absorbance reduction) and the full width at half maximum of the spectra (FWHM)

	λ_{max} (nm)	MA (AU)	Peak shift (%)	Absorbance reduction (%)	FWHM (nm)
Citrate Ag-NPs	393.0	0.084	0	0	45.0
Influent_0 hrs	399.0	0.050	1.53	40.5	74.0
Influent_24 hrs	400.3	0.040	1.86	52.4	81.0
TTA_45 hrs	406.0	0.018	3.31	78.6	105.0
TMA_45 hrs	406.0	0.018	3.31	78.6	105.0
TBA_45 hrs	404.0	0.019	2.80	77.4	103.0
TTS_48 hrs	408.0	0.014	3.82	83.3	121.0
TMS_48 hrs	411.0	0.036	4.58	57.1	120.0
TBS_48 hrs	408.0	0.014	3.82	83.3	119.0
TES_48 hrs	408.0	0.014	3.82	83.3	115.0

Table 5-5: UV-Vis data of PVP Ag-NPs in OECDss before and during treatment – Wave length at the MA (λ_{max}), MA, percentage of the shifting of the spectrum (peak shift) and its magnitude decreased (absorbance reduction) and the full width at half maximum of the spectra (FWHM)

	λ_{max} (nm)	MA (AU)	Peak shift (%)	Absorbance reduction (%)	FWHM (nm)
PVP Ag-NPs	392.0	0.094	0.00	0.0	44.0
Influent_0 hrs	397.0	0.053	1.27	43.6	63.0
Influent_24 hrs	397.0	0.045	1.27	52.1	86.0
TTA_45 hrs	399.0	0.027	1.79	71.3	135.0
TMA_45 hrs	399.0	0.029	1.79	69.1	109.0
TBA_45 hrs	399.0	0.029	1.79	69.1	109.0
TTS_48 hrs	398.0	0.020	1.53	78.7	144.0
TMS_48 hrs	398.0	0.020	1.53	78.7	145.0
TBS_48 hrs	398.0	0.018	1.53	80.8	154.0
TES_48 hrs	398.0	0.018	1.53	80.8	151.0

The FWHM of the UV-Vis spectra of the citrate and PVP Ag-NPs was increased due to their possible aggregation (Prathna et al., 2011) or formation of complex organic-Ag-NPs – species, with large molecules such as proteins (peptone and meat-extract are known to be present in the synthetic sewage). Indeed, the increase of the FWHM might not be associated with particle agglomeration, but to the corona effect of the protein – Ag-NPs interaction which can increase the particle size slightly (Bolea et al., 2014). After 24 hours, the absorbance was decreased, and the λ_{max} remained constant in both cases; the absorbance reduction was due to the increase of the dissolved Ag in the influent over time as show in session 5.3.1.1.

During the aeration and settling phases, the UV-Vis absorbance was further reduced as a consequence of the aeration flow application. In the literature, it has been reported that in an aerated WWTP, Ag-NPs present in the sewage can dissolve by releasing silver ions (Ag^{+}) (Yang et al., 2013c). Therefore, the decrease in absorbance may have been caused by the oxygen flowing into the reactor for twenty-one hours. Also, for citrate Ag-NPs, the UV-Vis spectrums were shifted further towards higher wavelengths and the average of λ_{max} was about 405 nm during aeration and 409 nm during settling. However, λ_{max} of PVP Ag-NPs remained generally constant. In fact, the dispersed citrate Ag-NPs might have their surface chemistry modified twice as they may have undergone dissolution and oxidation during the aeration phase and finally sulphidised (Doolette et al., 2013). The sulphidation phase was possibly continuing through settling. The presence of the PVP coating likely prevented significant sulphidation of the PVP Ag-NPs.

The broadening of the FWHM increased with time, suggesting an increase in the polydispersity of the NPs with time (Agnihotri et al., 2014). This might be due to fact that the

Ag-NPs become smaller as a result of dissolution, but end up with a much broader size distribution (Pal and Mohan, 2014). The shape of the SPR might be related to the formation of Ag_2O NPs, which have an MA at 650 nm according to Gallardo et al. (2012) which could be accelerated by the application of an aeration flow. However, the broadening of the UV-Vis peak might also be a result of formation of a different Ag species.

5.3.1.3. DLS measurements: Hydrodynamic size distribution of the NPs

The DLS characteristic of the NPs through measurement of their Z-average must only be used to provide the average D_H of the particles if the analyse suspension is monomodal – meaning the only peak it observes by the DLS and constitutes of monodispersed spherical particles (Lim et al., 2013). However, in our case, the DLS characteristics of the particles given in Figure 5-6 show that scattering signal of most samples had more than one peak, making it impossible to use their z-average as a representation of D_H. To overcome this, we determined the D_H of the particles using the average diameter of the particles distribution of the main peak (or peak 1) of the DLS spectra. We considered the average diameter of peak 1 to be DH compared to peak 2 and peak 3 because of its high percentage of particles per intensity, volume and number (Shaw, 2014). The broadening of the measurements is represented by the variations of the PDI (PDI) (Figure 5-10).

Figure 5-6 shows the scattered light intensity of the Ag-NPs as a function of D_H measured by the DLS. At 0 hrs, the D_H distribution of citrate Ag-NPs (Figure 5-6 (A)), was shifted toward higher values (compared to the size in water) and its width had slightly increased due to possible agglomeration of the NPs in the OECDss medium. For the PVP Ag-NPs (Figure 5-6(B)),

there was no significant change in the D_H distribution of the particles and the fluctuations appearing in the signal could come from excess PVP or Ag-NP – protein interaction.

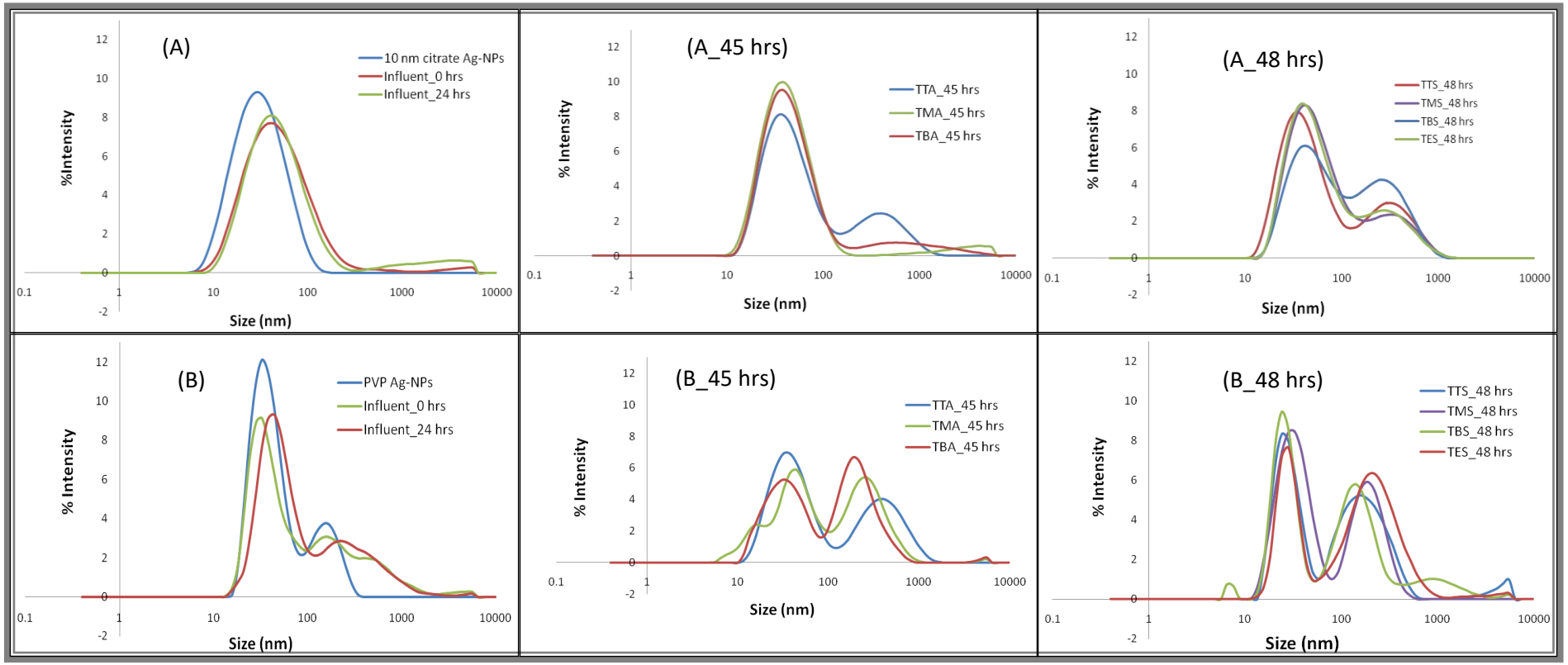

Figure 5-6: DLS spectra of Ag-NPs in OECDss before and during treatment. Figures (A) and (B) represent the citrate and PVP Ag-NPs respectively before treatment and Figures (A_45 hrs) and (A_48 hrs), (B_45 hrs) and (B_48 hrs) represent the citrate and PVP Ag-NPs in OECDss during the aeration phase at 45 hrs and settling phase at 48 hrs. At 45 hrs, samples were from the top middle and bottom of the reactor (respectively TTA_45 hrs, TMA_45 hrs, TBA_45 hrs). At 48 hrs, samples were collected from the top, middle and bottom of reactor and from the effluent (respectively TTS_48 hrs, TMS_48 hrs, TBS_48 hrs and TTE_48 hrs).

Figure 5-7 shows that the average D_H of citrate Ag-NPs had increased from 34.9 ± 0.7 to 55.6 ± 5.7 nm; the PVP Ag-NP diameter remained constant with a D_H before exposure being equal to 38.9 ± 1.6 nm and 38.7 ± 9.0 nm after exposure in OECDss at 0 hrs. After 24 hrs of exposure at room temperature in the synthetic sewage, the average DH of citrate Ag-NPs was slightly lower than it value at 0 hrs: 53.3 ± 7.6 nm; whereas the average D_H of PVP Ag-NPs had increased to 49.5 ± 6.7 nm. Thus, citrate-capped Ag-NPs agglomerated within the first hour of their dispersion in the OECDss and remained in that state after twenty hours of exposure with slight dissolution due to the decreasing of their average D_H.

The changes in average D_H of PVP Ag-NPs show that when first exposed to the media, the diameter of PVP particles was not affected; however, after twenty-first hours, the particle diameter considerably increased due to agglomeration as for the citrate particles. But, because PVP Ag-NPs are known to be more stable than citrate Ag-NPs (Tejamaya et al., 2012), we may assume that the increasing in diameter of PVP Ag-NPs may have been associated with the proteins absorbing onto the particle surface.

The ANOVA for the critical value of $\alpha = 0.05$ was done by comparing the average DH of Ag-NPs of the citrate and PVP Ag-NPs in OECDss at 0 and 24 hrs. There was no significant difference between the citrate and PVP Ag-NPs regarding the changes of their z-average, since the ANOVA parameter F (= 0.56) < F_{critic} (7.71) and P-Value (= 0.497) > 0.05.

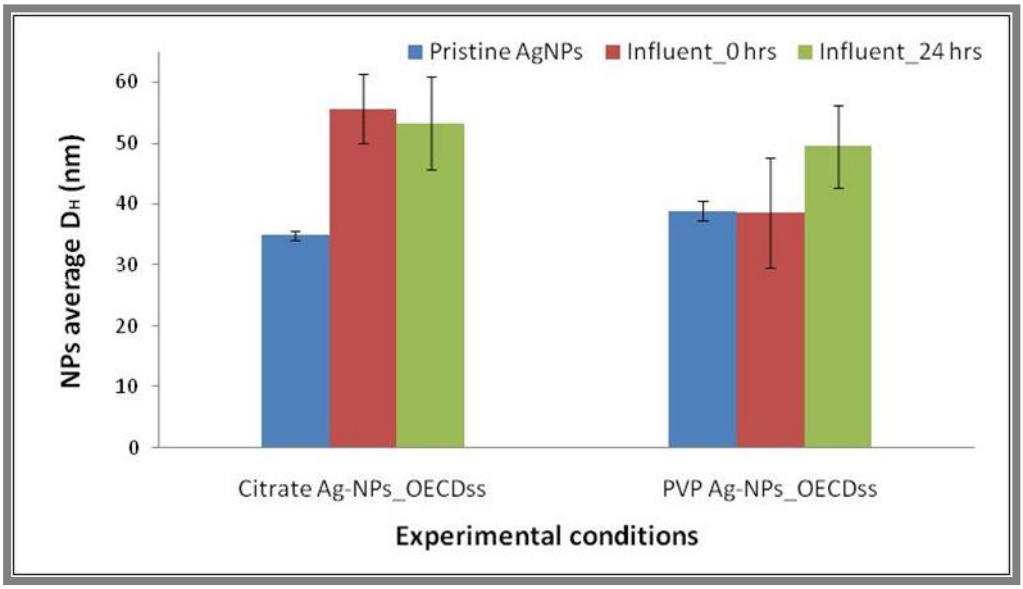

Figure 5-7: Variations of peak one size of citrate and PVP capped Ag-NPs in OECDss before (Pristine NPs, at 0 hrs and 24 hrs) given by DLS: also known as average size distribution of the first peak (or peak representing a distribution off Ag-NPs with a maximum percentage of volume and number of particles.

At 45 hrs, the average diameter of the particles was generally in the same range for citrate Ag-NPs despite the collecting point: top sample (TTA_45 hrs), middle sample (TMA_45 hrs) and bottom sample (TBA_45 hrs); with the average D_H fluctuating between 48 nm and 45 nm (Figure 5-8). While for PVP Ag-NPs, the average D_H was the same at the top and bottom of the reactor (about 42 nm) but was very low in the middle of the reactor (about 29 nm). The reduction of the average DH of the particles might be associated with the oxidation/dissolution phase occurring under aerobic conditions.

Also, based on our results, the rate of oxidative dissolution phenomena might be dependent on how close the particles are to the aeration flow source (located at the bottom of the reactor) and to their capping agent. Indeed, for both citrate and PVP Ag-NPs, the closer they were to the oxygen source the smaller was their average diameter D_H (Figure 5-6). Although we expected the average diameter PVP-capped Ag-NPs to remain mostly constant, their diameter significantly decreased to 28.9 ± 6.2 nm in the presence of a high oxygen

environment. This may indicate that their PVP surface functionalisation may be lying flat instead of straight on the particle surface, causing their diameter to shrink (Shaw, 2014) as described in Figure 3-3. However, this may have given them more protection from oxidation and dissolution by slowing their access to oxygen (Jia and Schuth, 2011).

The above results corroborate with the GFAAS, and UV-Vis observed in sections 5.3.1.1 and 5.3.1.2 showing that the presence of aeration may have accelerated the dissolution (Yang et al., 2013c) of Ag-NPs as the average particle diameter was decreased due to possible dissolution.

The ANOVA for the critical value of $\alpha = 0.05$ was done by comparing average D_H of citrate and PVP Ag-NPs in OECDss during aeration (at 45 hrs). There was no significant difference between the citrate and PVP Ag-NPs regarding the changes of their average D_H, since the ANOVA parameter F (= 4.04) < F_{critic} (7.71) and P-Value (= 0.115) > 0.05.

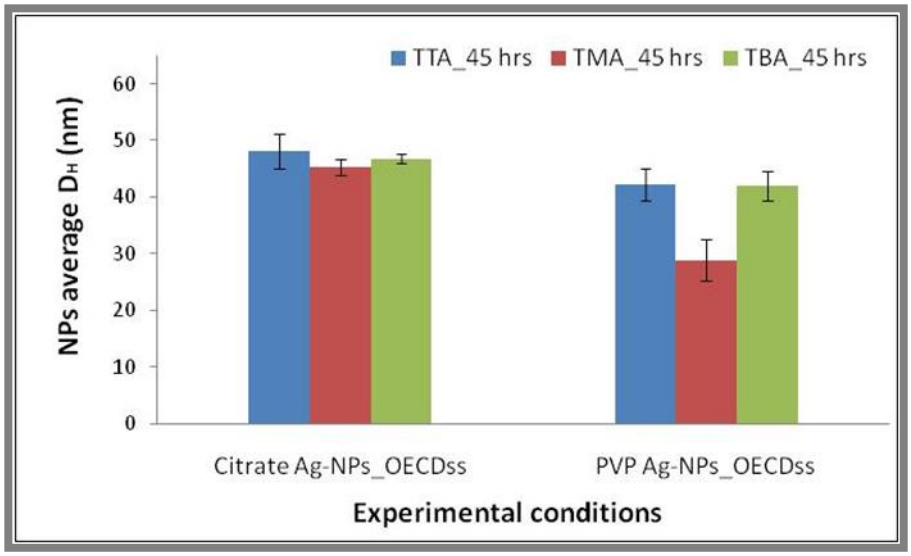

Figure 5-8: Variations of peak one size of citrate and PVP capped Ag-NPs in OECDss during aeration (at 45 hrs) given by DLS: also known as average size distribution of the first peak (or peak representing a distribution off Ag-NPs with a maximum percentage of volume and number of particles.

At 48 hrs (Figure 5-9), the average D_H of the Ag-NPs increased as a function of the collecting point of the sample from the reactor: top sample (TTS_48 hrs), middle sample (TMS_48 hrs), and bottom sample (TBS_48 hrs). Ag-NPs from the top part (TTS_48 hrs) might have been affected by ambient oxygen since the SBR was open to the air. And have caused oxidation and dissolution of the particles, hence their decrease in size. However, because of the low level of oxygen in the middle (TMS_48 hrs) and the bottom (TBS_48 hrs) of the reactor, the aggregation of citrate Ag-NPs level was increased, and so was their average D_H. Besides, larger particles or aggregates were found to be in the middle of the reactor with an average D_H of 59.2 ± 2.6 nm for the citrate Ag-NPs and 34.5 ± 4.8 nm for the PVP Ag-NPs. The Z-average of the collected effluent (TES_48 hrs) samples for citrate and PVP particles cases which was 53.9 ± 5.9 nm and 28.3 ± 3.2 nm respectively confirmed these assumptions

The ANOVA for the critical value of $\alpha = 0.05$ was done by comparing the average D_H of Ag-NPs of the citrate and PVP Ag-NPs in OECDss during settling (at 48 hrs). There was a significant difference between the citrate and PVP Ag-NPs regarding the changes of average D_H since the ANOVA parameter F (= 44.64) > F_{critic} (5.99) and P-Value (= 0.0005) < 0.05. Thus, PVP Ag-NPs in SBR treatment plant go through very little to no aggregation or agglomeration during treatment, while citrate Ag-NPs aggregated.

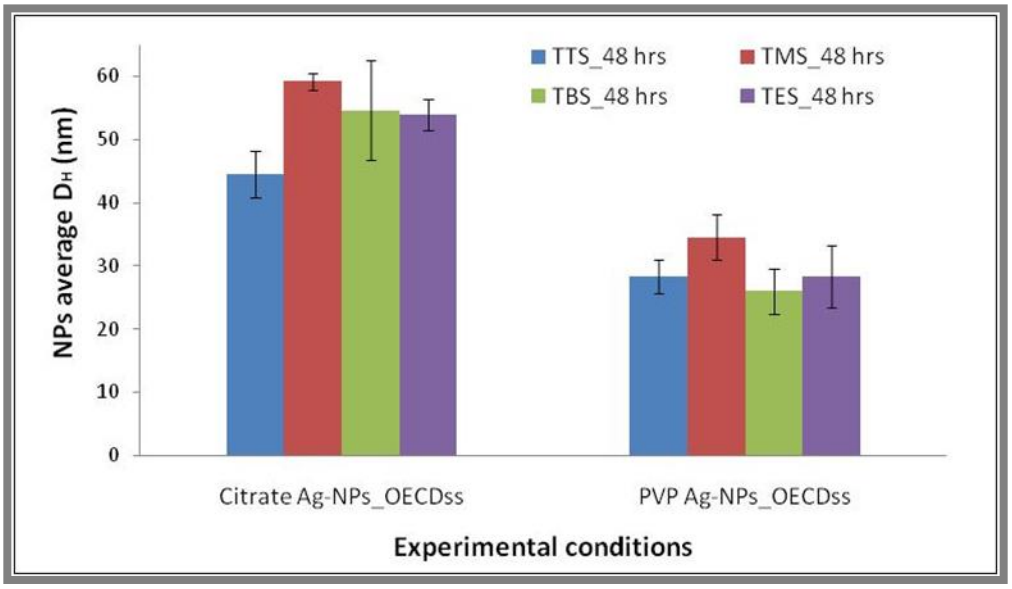

Figure 5-9: Variations of peak one size of citrate and PVP capped Ag-NPs in OECDss during settling (at 48 hrs) given by DLS: also known as average size distribution of the first peak (or peak representing a distribution off Ag-NPs with a maximum percentage of volume and number of articles.

The PDI trends (Figure 5-10) show the fluctuations of polydispersity of the particles over time. The PDI was relatively higher for the PVP Ag-NPs than for the citrate Ag-NP for each step of the experimental process. This could be due to the nature of the PVP lying flat or straight as shown Figure 3-3, or could be the result of larger molecules such a meat-extract or peptone being attached to the particles. The PDI was ≥ 0.30 for most samples, indicating that citrate and PVP Ag-NPs had become quite polydisperse over time.

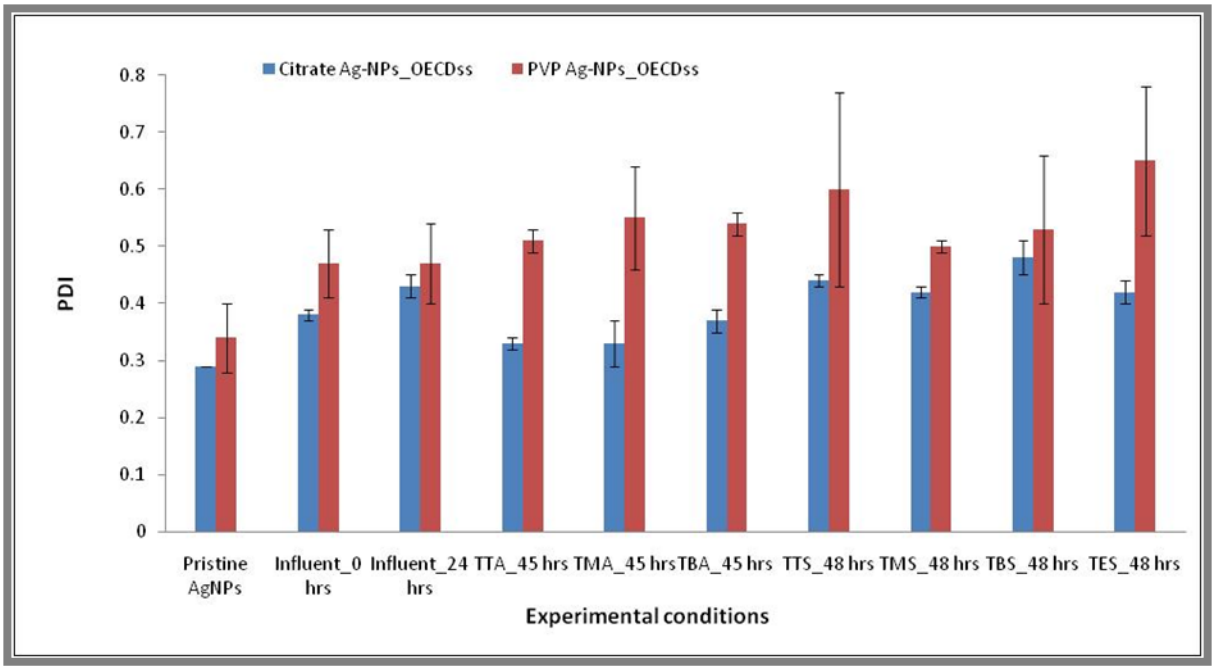

Figure 5-10: Variations of Ag-NPs PDI in OECDss before and during treatment before (Pristine NPs, at 0 hrs and 24 hrs) and during treatment (at 45 hrs and 48 hrs) given by DLS.

5.3.1.4. TEM characterisation of citrate and PVP Ag-NPs in OECDss before and during treatment: at 0, 24, 45 and 48 hrs of their exposure in the media

The TEM characterisation for the samples collected at 0 hrs and 24 hrs (Figure 5-11 and Figure 5-12) shows that the average size of Ag-NPs initially remained mostly constant compared to the pristine particles (Table 5-1). At 0 hrs, the degree of agglomeration of citrate Ag-NPs (Figure 5-11 (A_0 hrs)) was relatively high, and the agglomeration of PVP Ag-NPs (Figure 5-12 (B_0 hrs)) was non-existent. Also, the average size of the citrate Ag-NPs (10.0 ± 5.2 nm, based on the counting of 473 NPs) was slightly lower than the mean size of the pristine particles (11.7 ± 6.7 nm), due to a possible dissolution. This was consistent with the UV-Vis data that showed a reduction of the absorbance of dispersed citrate Ag-NPs in OECDss compared to the pristine particles (Figure 5-4). As for the PVP particles, the average size remained in the same range (12.7 ± 7.0 nm, based on the counting of 466 NPs) as the pristine particle average

size (12.3 ± 5.4 nm), because of their surface functionalisation which prevented them from dissolution due to the PVP layer hindering access of the oxygen as stated earlier in section 5.3.1.3.

The reduction of the particles core size is associated with the dissolution effects that cause Ag^+ ion release from the NPs. Based on the above DLS results, the average D_H of the citrate Ag-NPs at 0 hrs may have suggested the agglomeration of the particles after their dispersion in the OECDss. However, the TEM results confirmed that spiked citrate Ag-NPs not only dissolved but also agglomeration within the first minutes of their exposure in the OECDss. Based on this reduction in size, we could assume that the citrate Ag-NPs undergo dissolution within the first hour of the exposure in this media and then re-precipitation in the form of AgS_2 or AgCl.

At 24 hrs, the re-precipitation of the particles after dissolution had caused the formation of larger particles for both citrate (Figure 5-11 (A_24 hrs)) and PVP (Figure 5-12 (A_24 hrs)) particles, with their average size increasing to 14.2 ± 8.6 (based on the counting of 159 particles) and 13.4 ± 7.7 nm (based on the counting of 165 particles) respectively. The images also show some interaction with the OECDss and indicate some corona-type layer surrounding a few particles. This shows that citrate and PVP Ag-NPs were unstable in the OECDss medium regarding their size and shape because of their sensitivity to re-precipitation, with PVP Ag-NPs showing less re-precipitation than the citrate Ag-NPs. Both Ag-NPs have their surface chemistry modified and tend to re-precipitate through time, as was observed from the UV-Vis data.

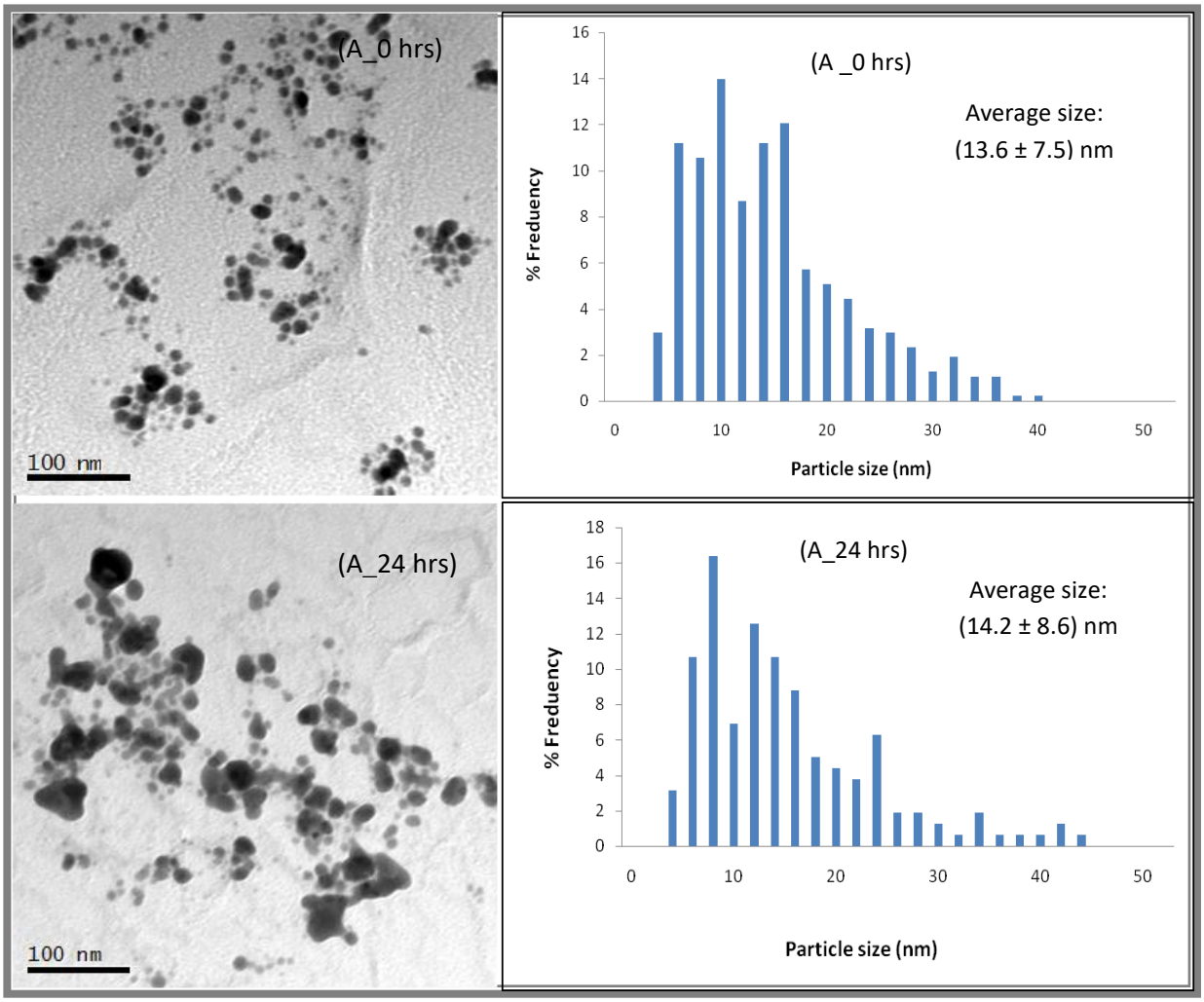

Figure 5-11: TEM images and size distribution of the citrate (A) in OECDss at 0 and 24 hrs, based on the counting of 473 particles for sample A_0 hrs, 159 particles for sample A_24 hrs. Citrate Ag-NPs (A_0 hrs) were going through dissolution at 0 hrs and re-precipitate with formation of larger particles or aggregates (A_24 hrs).

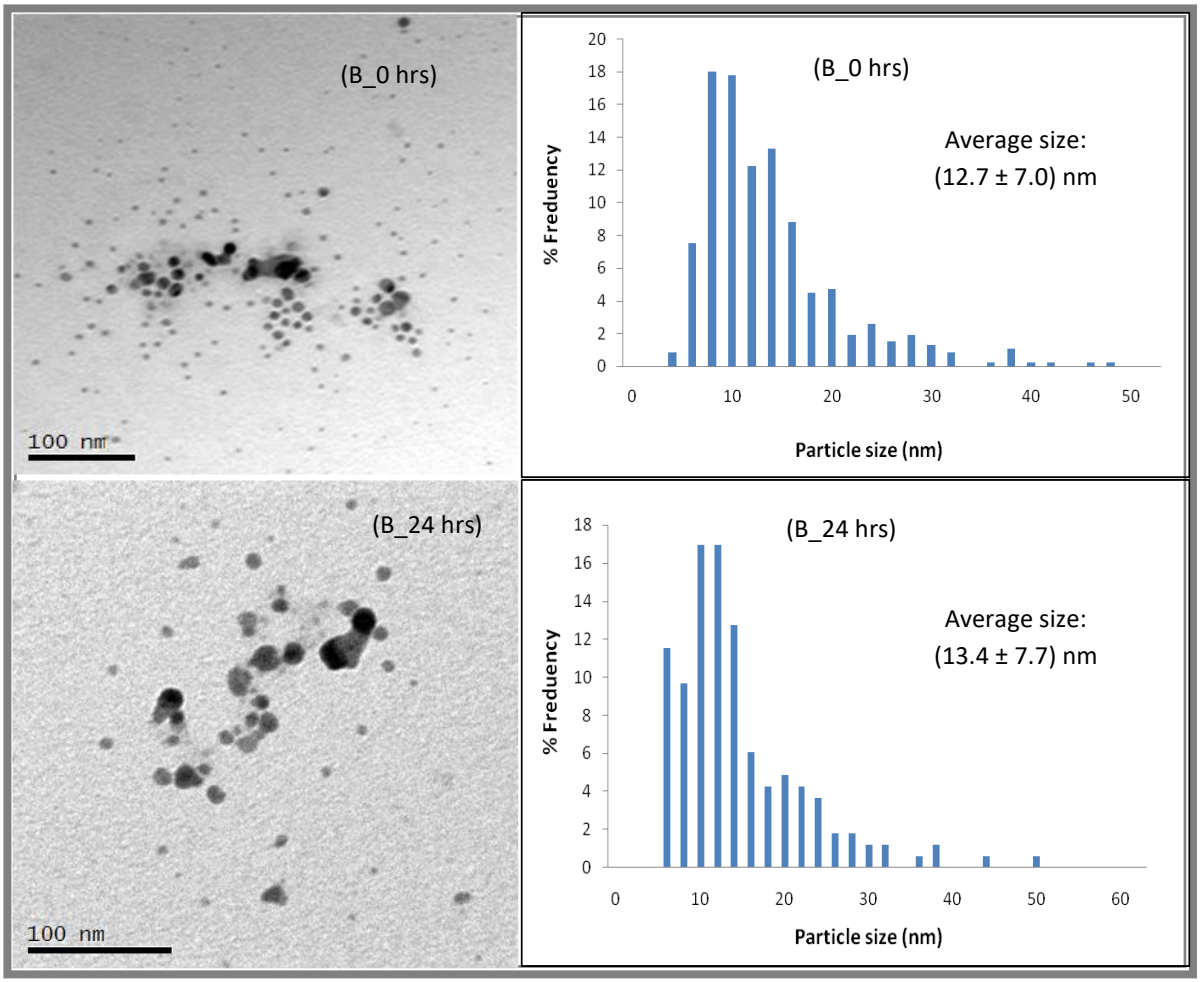

Figure 5-12: TEM images and size distribution of the PVP (B) Ag-NPs in OECDss at 0 and 24 hrs, based on the counting of 466 particles for sample B_0 hrs and 165 particles for sample B_24 hrs. PVP Ag-NPs were stable at 0 hrs (B_0 hrs) and underwent dissolution with time then re-precipitate (B_24 hrs), hence their increased in average size.

The TEM images of the citrate particles shown in Figure 5-13are for the samples collected from the bottom of the reactor during aeration (Figure 5-13 (A_45 hrs)) and settling Figure 5-13 (A_45 hrs)). These images show that the re-precipitation of citrate Ag-NPs increased in the presence of oxygen and their average size was 18.8 ± 11.9 nm. Also at 48 hrs, there was a further increase of the particle size and their average size distribution was found to be 21.6 ± 11.0 nm.

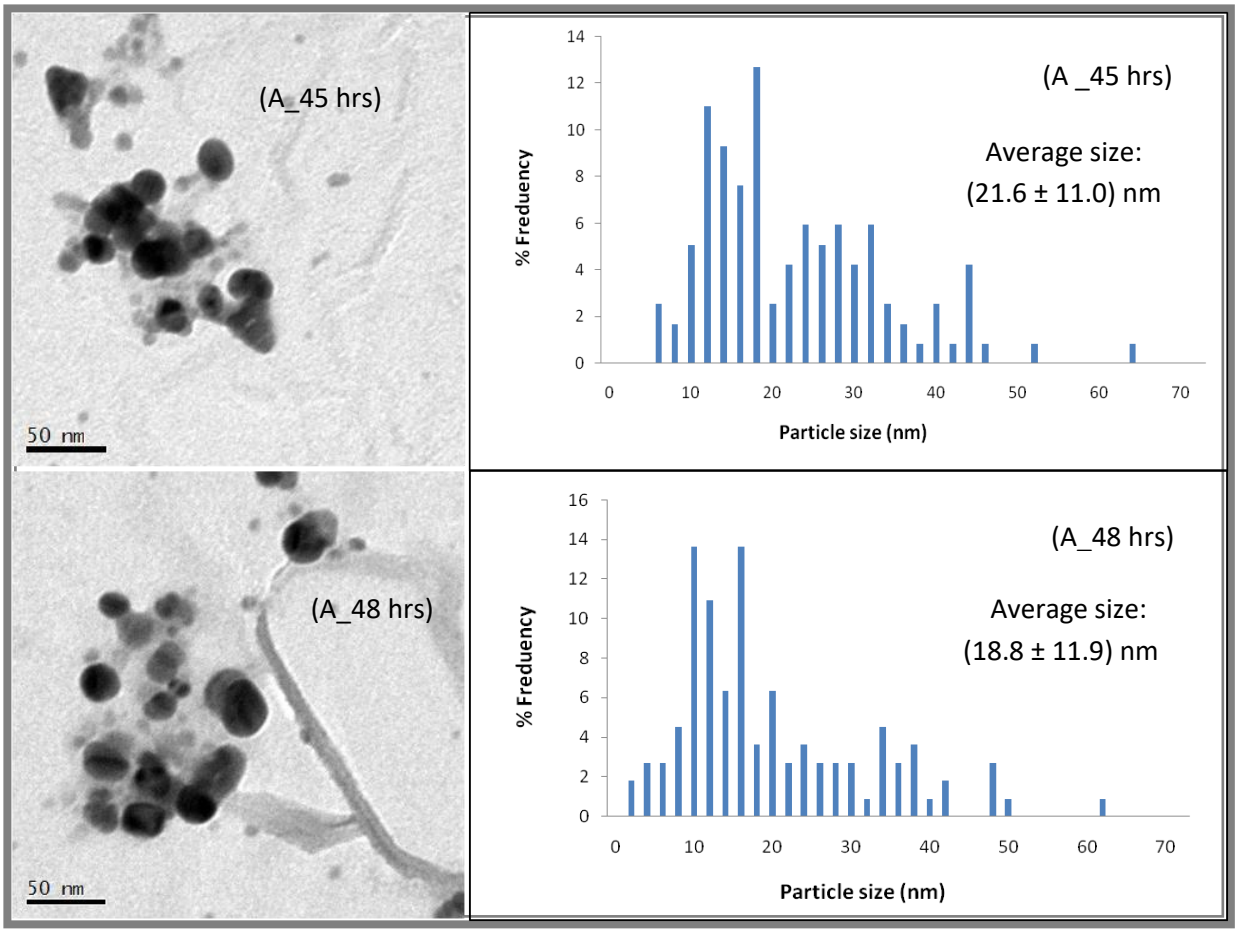

Figure 5-13: TEM images of citrate Ag-NPs in OECDss and their corresponding size distribution during the aeration phase (A_45 hrs) and the settling phase (A_48 hrs). Particles sampled from the bottom of the reactor. This was based on the counting of 117 particles for sample A_45 hrs and 110 particles for sample A_48 hrs.

For PVP Ag-NPs Figure 5-14, there was little to no aggregation during the aeration phase (Figure 5-14 (B_45 hrs)). However, the particles may have dissolved because of the reduction of their average size (10.0 ± 5.2 nm) which is nearly 1/4 lower compared to the average size of Ag-NPs of influent_24 hrs (Figure 5-12 (B-24 hrs)). During settling, the ionic silver formed during the aeration phase may have re-precipitated (Figure 5-14 (B_48 hrs)), causing the augmentation of the particle size was to 14.2 ± 8.6 nm. Also, the less dense material around PVP particles might be a consequence of biomolecules such as excess PVP or molecules from the OECDss; but, it this could also be two particles trapped together. Either way, this might

explain the agglomeration (or high polydispersity) observed in DLS data, meaning the particles may have been held together by biomolecules, and thus appear agglomerated. Finally, the actual size of the PVP particles did not change as much citrate particles core size; meaning their degree of dissolution might have been considerably lower.

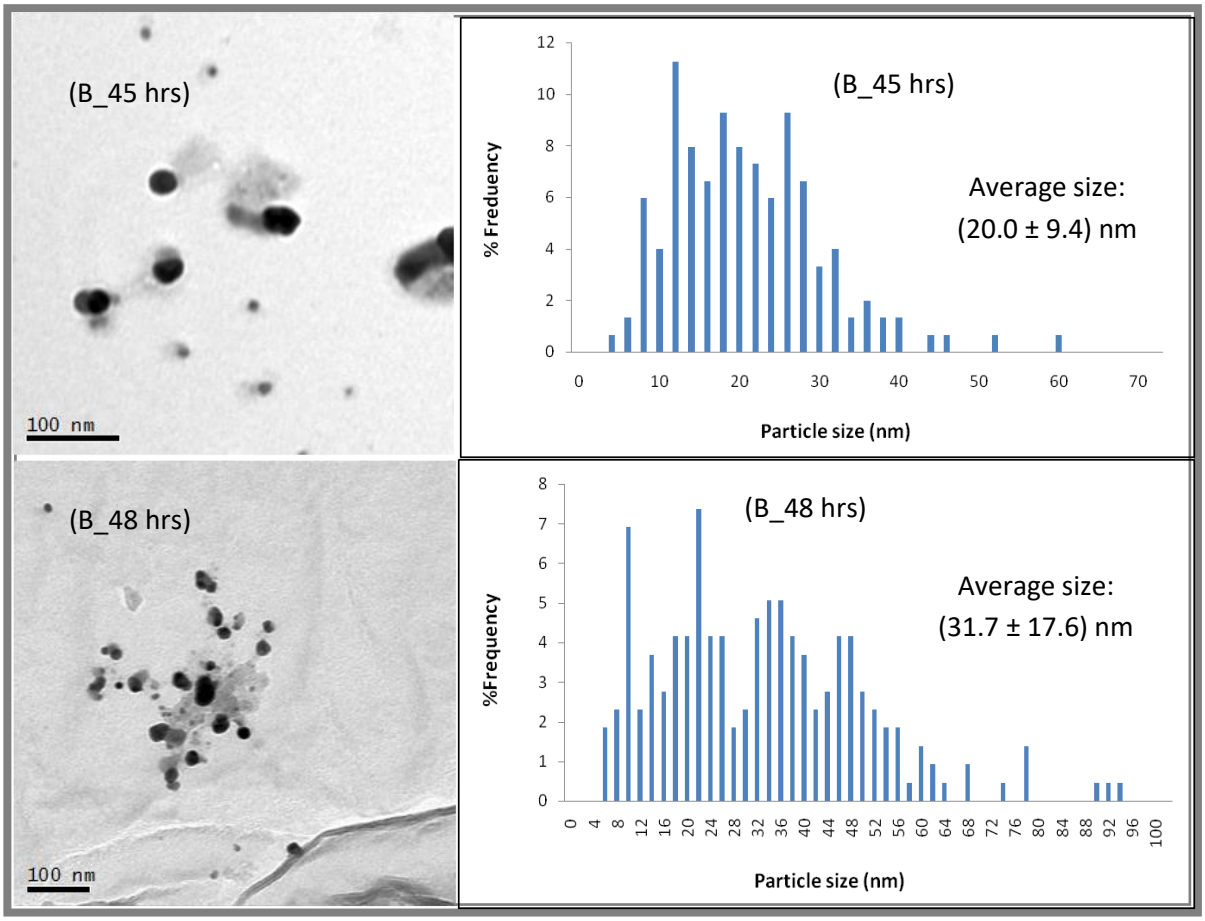

Figure 5-14: TEM images of PVP Ag-NPs in OECDss and their corresponding size distribution during the aeration phase (B_45 hrs) and the settling phase (B_48 hrs): based on the counting of 151 particles for sample B_45 hrs and 217 particles for sample A_48 hrs.

The ANOVA for the critical value of $\alpha = 0.05$ was done by comparing the TEM average core size of Ag-NPs of the citrate and PVP Ag-NPs in OECDss during treatment in SBR plant pilot. There was no significant difference between the citrate and PVP Ag-NPs regarding the

changes of their average core size, since the ANOVA parameter F (= 1.737) < F_{critic} (5.987) and P-Value (= 0.236) > 0.05.

5.3.1.5. Chemical surface analysis: EDS analysis

The samples were collected 48 hours after the synthetic sewage treatment was completed and the effluent was drawn out of the reactor. The samples were analysed using SEM-EDS, and in the images, the dark area is representative of non-metal materials, (i.e. different salts and proteins present in OECDss in this case) and lighter areas of the image represent the presence of metal: Ag. From the SEM analysis of the OECDss spiked with citrate Ag-NPs (Figure 5-15), large particles with sizes above the micron level were observed. These results show that the size increase of the citrate particles may not only have been caused by their re-precipitation after they were dissolved, but also might have also been due to the OECDss biomolecules trapped on their surface.

The performance of EDS analysis on one of these lighter areas gave a general chemical composition of the synthetic sewage sample as seen in the EDS spectrum (Appendix A4-1). In addition to the presence of silver (Ag) in the spectrum, salts and non-metals materials from the OECDss were also detected. The high content of the sulphur (S: from sulphide) and phosphorus (P: from phosphate) suggested that there was a direct ageing or dissolution/re-precipitation mechanism of particles as silver sulphide (Ag_2S) particles or silver phosphate particles (SP-NPs). The spectrum was also found to contain silica (Si) and aluminium (Al), which can be attributed to sewage contamination such as from the glass vessels or to residues from the SEM itself.

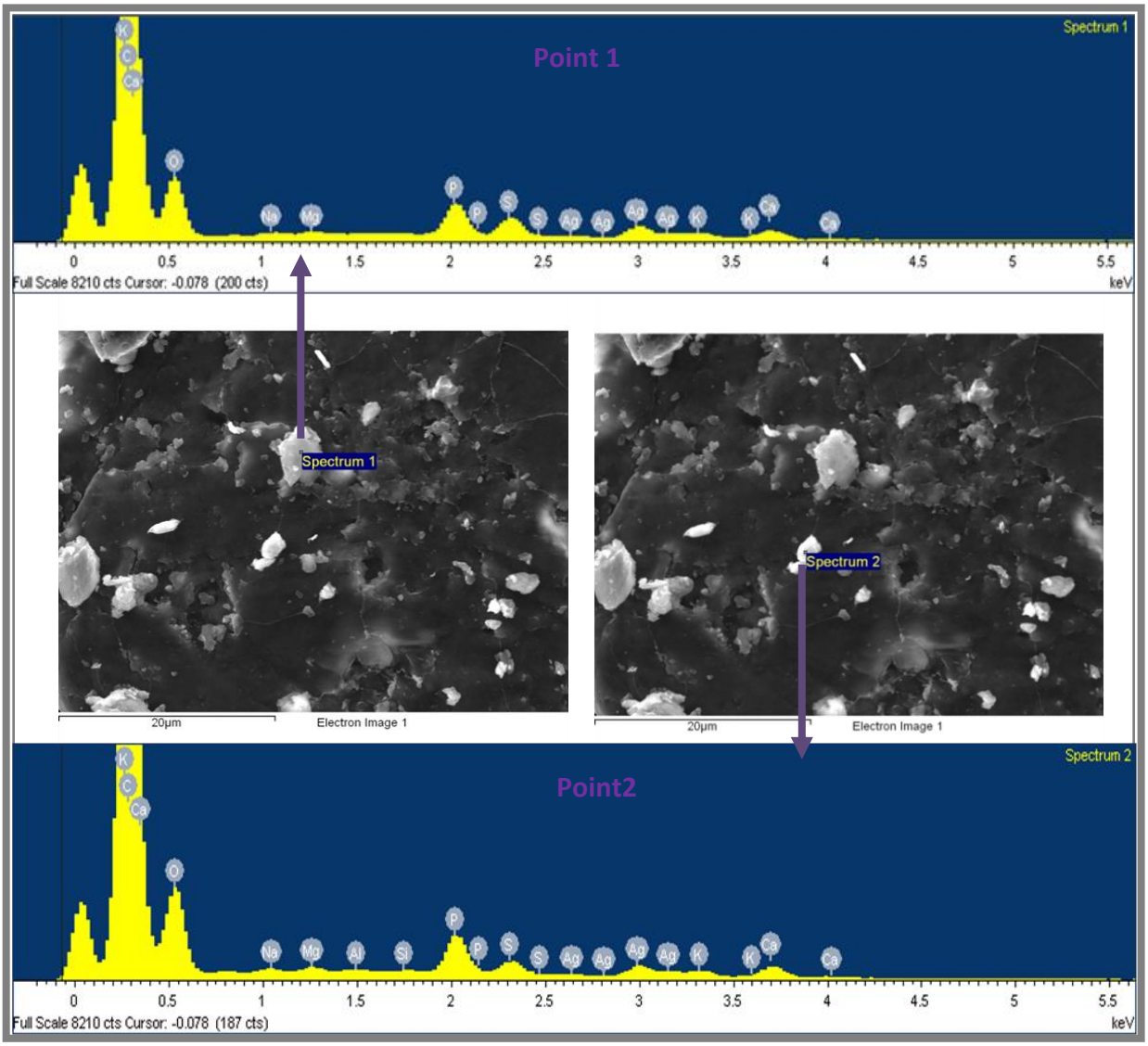

Figure 5-15: SEM and EDS characterisation of effluent from OECDss sludge treatment in the pilot plant containing 10 nm citrate capped Ag-NPs. Sample collected 48 hours after the settling phase.

A mapping analysis was also conducted for the samples, and the results (Figure 5-16) show that Ag (Figure 5-16 (A_6), and S Figure 5-16 (A_4), were everywhere on the surface of the analysed dispersed citrate Ag-NPs in OECDss. Although the chloride peak (from NaCl and $CaCl_2$) did not appear in the EDS spectrum, the mapping analysis showed that while chlorine was present, the concentration was much lower than sulphate. Note that EDS results are only semi-quantitative.

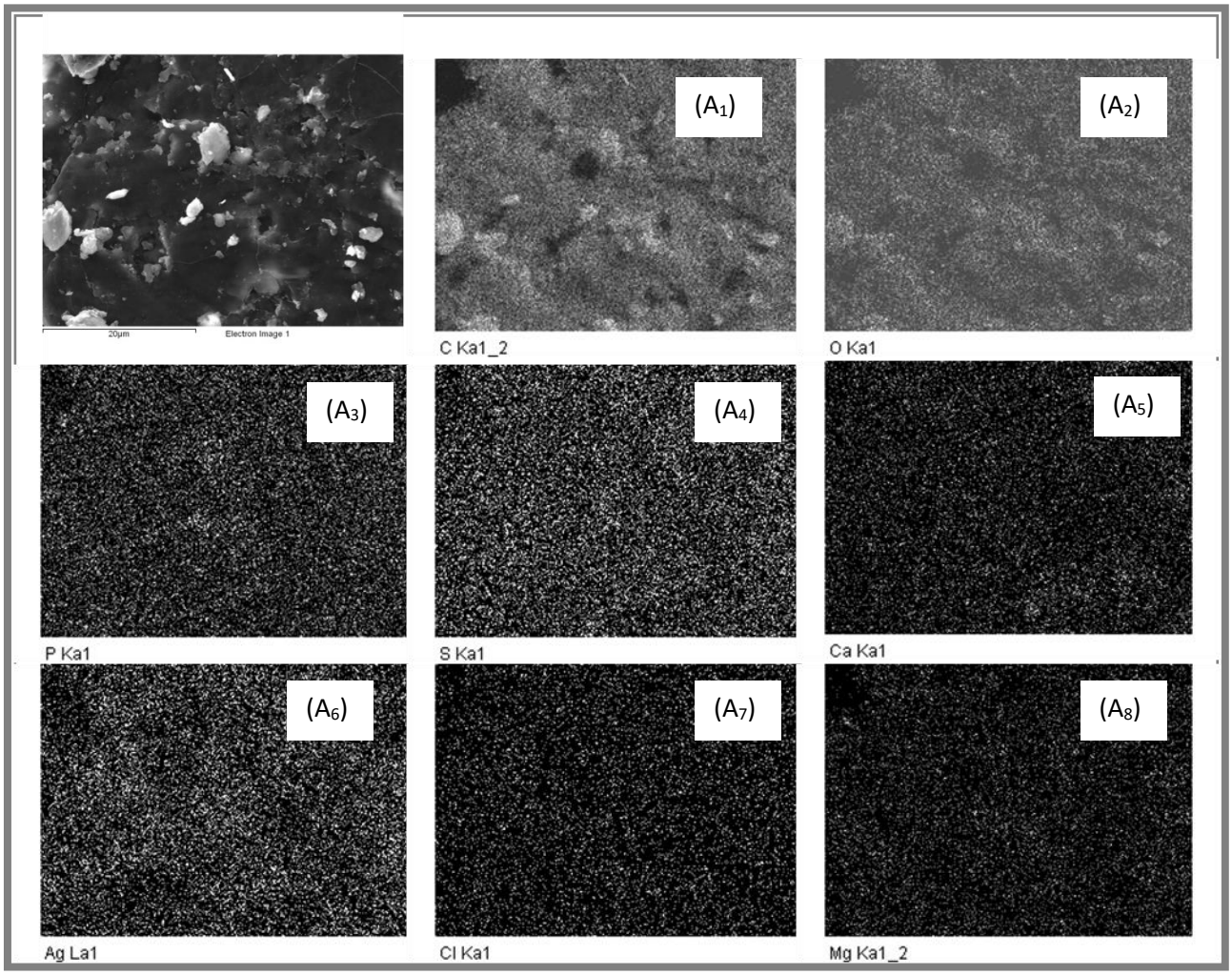

Figure 5-16: EDS mapping analysis of (OECDss + citrate Ag-NPs) dried sample acquired via SEM. The following elements carbon (C, (A_1)), oxygen (O, (A_2)), phosphorus (P: from phosphate, (A_3)), sulphur (S: from Sulphide, (A_4)), calcium (Ca, (A_5)), silver (Ag, (A_6)), chloride (Cl, (A_7)) and magnesium (Mg, (A_8)) were detected on the dry particulates.

The weight and atomic percentages of the chemical elements present in the SEM sample of the OECDss spiked citrate Ag-NPs are listed in Table 5-6. The electrons L in the shell for Ag were detected instead of the K-shell electrons due to the fact that the photon (or X-rays) energy absorbed by the Ag atoms was sufficient enough to release an electron from their L shell. An electron of the K-shell will be more difficult to release since it is closer to the nucleus, and the energy needed to release an electron from a K-shell of Ag atom must be at least equal to 21.99 keV (Poole, 2015). Thus, the emission of an X-ray by Ag atom is the energy needed by an electron of its outer shell to fill the hole left in the L shell (section 2.4.3.2).

The elements with the largest percentages of C were from the SEM sample's substrate, and the proteins and O were from water, K_2HPO_4 and $MgSO_4$. The weight % of Ag was found to be slightly more than double that of sulphide suggesting there was sulphidation (Ag_2S) of the Ag-NPs.

Table 5-6: Chemical composition in term of weight % and atomic % of the element present in OECDss spiked with citrate Ag-NPs. Sample collected 48 hours after treatment. Note results are semi-quantitative.

	Point 1		Point 2	
Element	**Weight%**	**Atomic%**	**Weight%**	**Atomic%**
O K	58.49	78.87	63.57	81.19
Na K	1.12	1.05	1.27	1.13
Mg K	0.81	0.72	1.23	1.03
Al K	11.10	7.73	0.51	0.39
Si K	7.16	4.82	0.94	0.69
P K	2.26	1.25	11.15	7.36
S K	5.20	2.80	4.17	2.66
K K	13.87	2.77	1.93	1.01
Ca K	5.20	2.80	5.22	2.66
Ag L	13.87	2.77	10.00	1.89
Totals	100.00	100.00	**100.00**	**100.00**

Figure 5-17 represents the composition of the OECDss in the presence of 10 nm PVP Ag-NPs. The EDS spectrum is similar to the spectrum of the OECDss sample with citrate Ag-NPs. However, it is important to note that in the case of the PVP particles a chloride signal was detected (shown in conjunction with Ag signal for the peaks corresponding to the 26.5 and 28 keV (or 42.4 and $44.8*10^{-16}$ J) energies).

The mapping gives an equal distribution of Ag (Figure 5-18 (B_1)) and S (Figure 5-18(B_2)) with a respective weight percentage of 1.76% and 0.71%. Also, the chloride mapping shows that there is more chloride (Figure 5-18 (B_3)) on the surface of the particles compared to the sample of citrate Ag-NPs OECDss. However, the weight percentage of Cl is the same in both cases (0.20 %). It therefore, appears that the concentration of AgCl particles in the OECDss + PVP Ag-NPs medium might be higher than in OECDss + citrate Ag-NPs, although we note again that these results can only be considered semi-quantitative.

Note that, although we have no further evidence that there may have been a formation of Ag_2O precipitate during the process, the detection of oxygen by EDS suggests the possibility that Ag-NP dissolution/re-precipitation into Ag_2O had occurred.

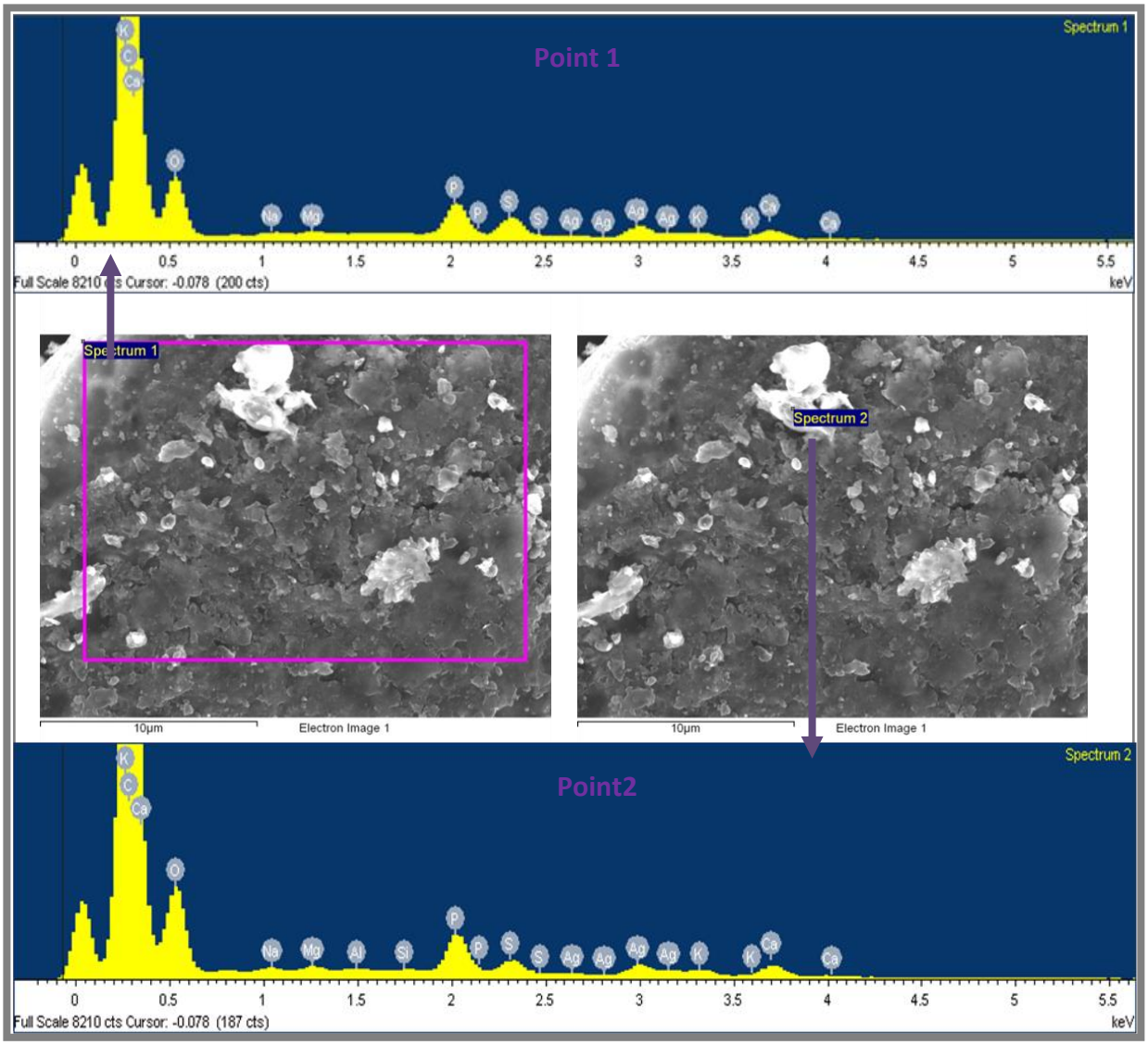

Figure 5-17: SEM and EDS characterisation of a residue from OECDss spiked with 10 nm PVP capped Ag-NPs. Sample collected 48 hours after the settling phase.

Table 5-7: Chemical composition in terms of weight % and the atomic % of the elements present in OECDss spiked with PVP Ag-NPs. Sample collected 48 hours after treatment. Note results are semi-quantitative.

	Point 1		Point 2	
Element	**Weight%**	**Atomic%**	**Weight%**	**Atomic%**
C K	61.12	75.66	69.60	80.89
O K	15.04	13.97	14.83	12.94
Na K	0.94	0.61	0.73	0.44
Mg K	0.19	0.12	0.19	0.11
Si K	0.53	0.28	0.33	0.16
P K	12.17	5.84	7.33	3.30
S K	0.92	0.43	0.71	0.31
Cl K	0.41	0.17	0.20	0.08
K K	6.13	2.33	3.24	1.16
Ca K	1.04	0.39	1.07	0.37
Ag L	1.51	0.21	1.76	0.23
Totals	**100.00**	**100.00**	**100.00**	**100.00**

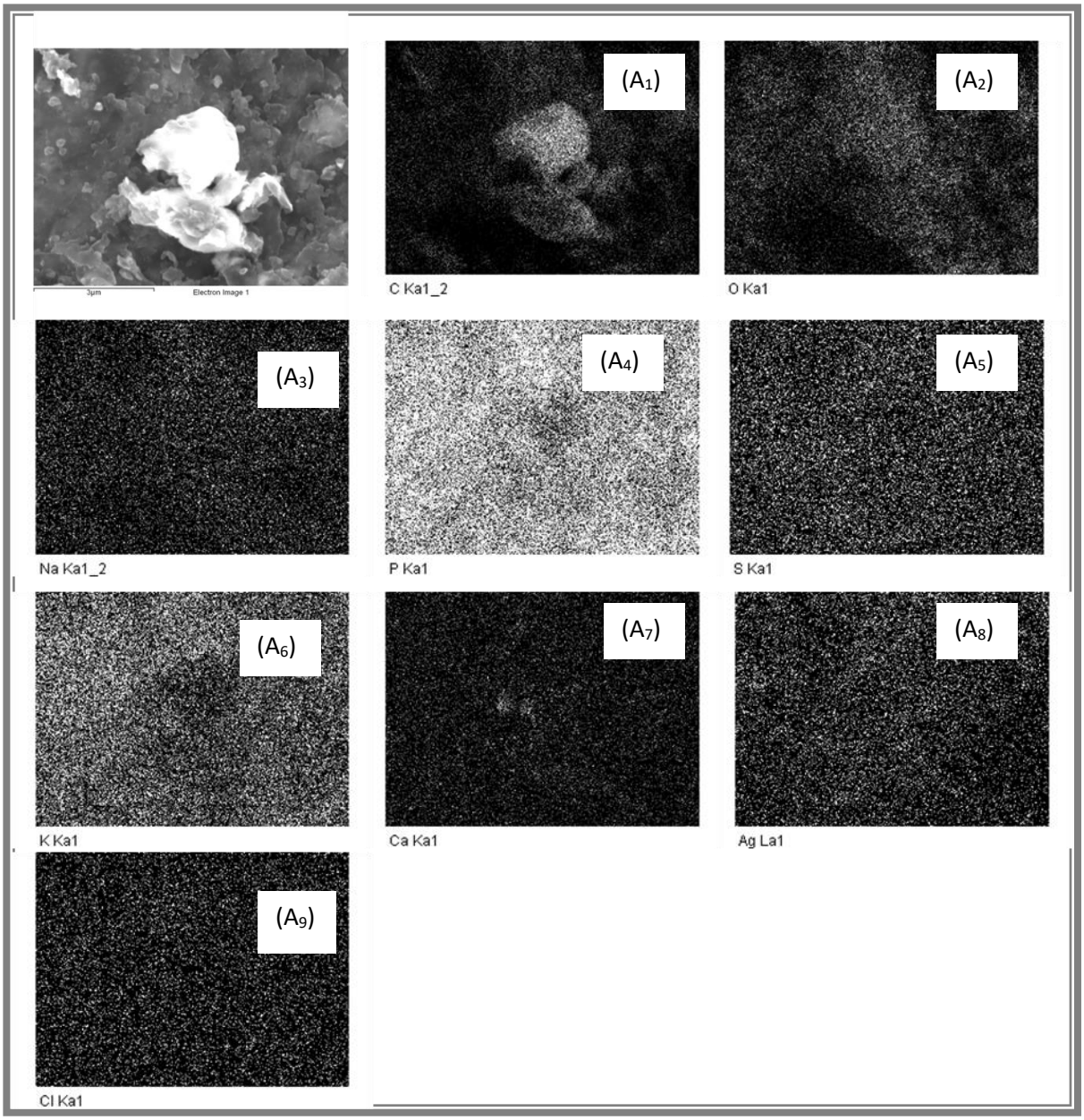

Figure 5-18: EDS mapping analysis of (OECDss + citrate Ag-NPs) dried sample acquired from SEM. The elements carbon (C, (A_1)), oxygen (O, (A_2)), sodium (Na, (A_3)), phosphorus (P, (A_4)), sulphur (S, (A_5)), potassium (K, (A_6)), calcium (Ca, (A_7)), silver (Ag, (A_8)), and chloride (Cl, (A_9)) were detected on the dry particulates.

5.3.2. Ag-NPs in OECDss during treatment without aeration flow at 45 hrs (non-aeration phase) and 48 hrs (settling phase)

This section discusses the behaviour of citrate Ag-NPs in synthetic sewage, when the influent was treated in the SBR plant pilot without aeration, to assess the role of oxygen in the observed behaviours reported in section 5.3.1. We have seen above that Ag-NPs go through chemical and physical changes by oxidising and dissolving in the sewage media in the presence of oxygen. If the aeration flow is not applied, a lower degree of dissolution and formation of larger particles via re-precipitation into Ag_2S, SP-NPs, AgCl or even Ag_2O is expected. Please note that a similar study was not conducted on the PVP-Ag-NPs due to lack of time. But this can be investigated to have a complete idea of how both types of particles might be affected if present in an aerated treatment plant.

5.3.2.1. Dissolution study: determination of silver concentration

The concentration of the particles before treatment at 24 hrs was found to 466.5 µg/L (Table 5-8 and Figure 5-19). The treatment in the SBR plant pilot in the absence of aeration (0A) was conducted by stirring for twenty-one hours. The samples were collected the top, middle and bottom of the reactors at 45 hrs during the stirring phase (TT0A_45 hrs, TM0A_45 hrs and TB0A_45 hrs) and at 48 hrs during the settling phase (TTS_48 hrs, TMS_48 hrs and TBS_48 hrs).

At 45 hrs, the dissolution rate of citrate Ag-NPs was relatively low in the absence of aeration compare to when the late was applied (section 5.3.1.1). The concentration of Ag-NPs in the

reactor with aeration was approximately 300 µg*L^{-1} (Table 5-2) and 420 µg/L without aeration (Table 5-8). There was very low dissolved Ag produced overtime when there no aeration (TBS_48 (without aeration) = 86.65 µg*L^{-1}) compared to case with aeration (TBS_48 (with aeration) = 181.24 µg*L^{-1}). Also, the total Ag concentration was slightly slower compared to the concentration measured at 24 hrs, and there was less unrecovered silver which might have stuck to the SBR vessel or stirrer paddle.

Through the different phases of treatment, the percentage of Ag^+ and the percentage of Ag loss were in the same range meaning that the decrease in particle concentration observed was mainly due to dissolution. Also, due to the lack of aeration flow, the variable dissolution of the citrate Ag-NPs during treatment was not significant, which probably meant the Ag-NPs oxidation was very low or did not occur in the absence of aeration.

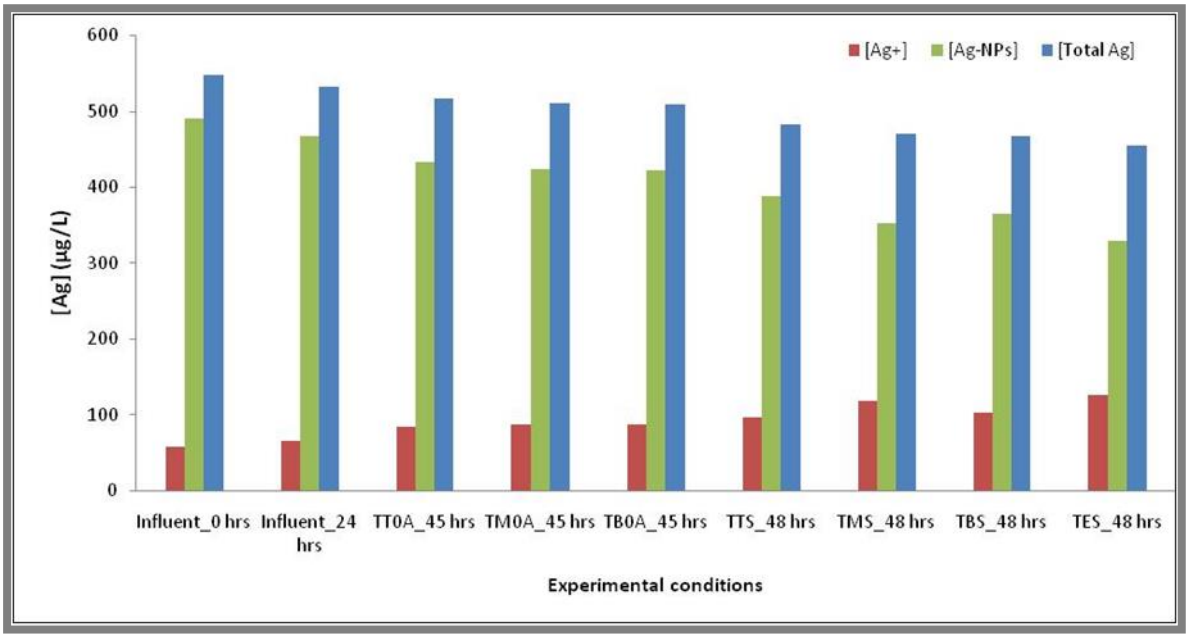

Figure 5-19: Characterisation data of GFAAS citrate Ag-NPs in OECDss: concentration of total Ag, Ag+ and Ag-NPs before) and during treatment in SBR pilot plant in absence of aeration. Samples collected before treatment: influent_0 hrs and influent_24 hrs. Samples collected during treatment: after twenty-one hours stirring with zero aeration (0A) (top sample (TT0A_45 hrs), top sample (TM0A_45 hrs), top sample (TB0A_45) hrs)) and after three hours settling

The analysis of the one-way ANOVA for the critical value of α = 0.05 comparing the concentration of total Ag, Ag^+ ions and Ag-NPs in OECDss of the citrate Ag-NPs during treatment with the aeration flow and without aeration is given in Table A4 - 25. There was no significant difference on the variations of $C_{Total\ Ag}$, C_{Ag+} and $C_{Ag\text{-}NPs}$ between both cases for their influents before treatment since $F < F_{critical} = 18.51$ and P-value > α in all three cases; which is normal since the same type of particles were used.

The calculated one way ANOVA for the concentration of total Ag, Ag^+ ions and Ag-NPs at 45 hrs (Table A4 - 25) shows that there was no significant difference between the total Ag concentration of the treatment with aeration and the treatment without it, as the corresponding$F < F_{critical} = 7.71$ and P-value > α. However, there a significant difference in the variation of Ag^+ and Ag-NPs concentration between the treatment with aeration and without because$F > F_{critical} = 7.71$ and P-value < α. So, the application of an aeration flow accelerated the dissolution of the Ag-NPs – hence increasing their precipitation.

Finally, the one-way ANOVA for the concentration of total Ag, Ag^+ ions and Ag-NPs at 48 hrs (Table A4 - 25), shows that there was a significant difference in concentration for all three cases between the treatment with aeration and the treat without aeration with $F > F_{critical} = 5.99$ and P-value < α. Thus, in the presence on aeration, citrate Ag-NPs highly oxidised and dissolved.

Table 5-8: Concentration of Ag (from citrate Ag-NPs) in OECDss during and after treatment in the absence of aeration

	$C_{Total\ Ag}$ (µg*L^{-1})	C_{Ag+} (µg*L^{-1})	$C_{Ag\text{-}NPs}$ (µg*L^{-1})	%Diss. Ag (%)	Unr. Ag (%)
0 hrs	546.84	56.90	489.95	10.40	0
24 hrs	531.20	64.60	466.59	12.16	2.86
TTA_45 hrs	516.90	83.60	433.30	16.17	5.50
TMA_45 hrs	509.50	86.96	422.52	17.07	6.83
TBA_45 hrs	507.96	86.65	421.31	17.06	7.11
TTS_48 hrs	482.80	95.46	387.33	19.80	11.70
TMS_48 hrs	470.45	118.56	351.90	25.20	13.97
TBS_48 hrs	466.55	102.11	364.44	21.90	14.70
TES_48 hrs	455.02	126.20	328.90	27.73	16.80

5.3.2.2. UV-Vis characterisation

With no oxygen added in the SBR plant pilot, the slope present at 45 hrs in the UV-Vis spectrum at $\lambda > \lambda_{max}$ was generally nonexistent (Figure 5-20). Throughout the non-aeration process, λ_{max} (=398 nm at 0 hrs) remained constant (Table 5-9) irrespective of the sample collection protocol (i.e. top/middle/bottom of the reactor). Despite λ_{max} generally being constant, the Ag-NP absorbance was decreased because of the dissolution, and the UV-Vis peak width had become larger which can be a consequence of agglomeration or precipitation due to their interaction with the proteins, sulfur, phosphorus or chloride present in the OECDss, as seen earlier. However, because of the low degree of dissolution (Table 5-8) compared to when the aeration was used (Table 5-2); the amount of Ag^+ lost by each Ag-NP via oxidation was probably been lower than when more oxygen was added. Hence, the amount or size of precipitated particles was certainly smaller than in the presence of aeration.

At 48 hrs, the SPR peak was redshifted and λ_{max} was found to be 401 nm; which could be caused by the changing surface chemistry as more particle precipitation occurred. Although, the width of the UV-Vis signal was similar as at 45 hrs, the MA was slightly decreased as a result of further dissolution (Table 5-8); consistent with the higher percentage of dissolved Ag found in the effluent (TTE_48 hrs (%dissolved Ag) = 20%). However, this was still lower than in presence of aeration where about 50% of the total Ag was from the dissolved Ag (Table 5-2). So, after settling the size of precipitated particles might have stayed constant or slightly increased in the absence of aeration.

With these results, we may conclude that in the absence of oxygen, the dissolution rate of Ag-NPs was lower, evidenced by their absorbance being higher than when the aeration was present (Figure 5-4). Thus, their surface chemistry was kept stable compared to their state before treatment (at 24 hrs).

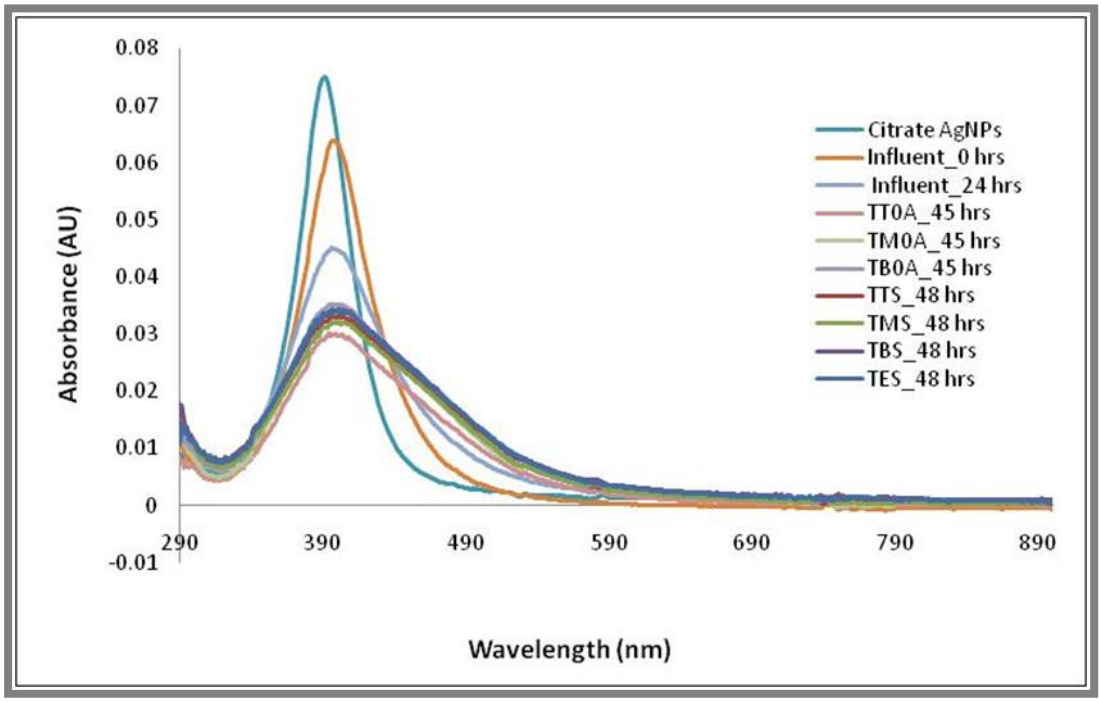

Figure 5-20: UV-Vis spectrum of the citrate Ag-NPs in OECDss before treatment with no aeration applied.

Table 5-9: UV-Vis results of citrate Ag-NPs in OECDss and during treatment in the absence of aeration

	λ_{max} (nm)	MA (AU)	Peak shift (%)	Absorbance reduction (%)	FWHM (nm)
Citrate Ag-NPs	393.0	0.084	0	0	45.0
Influent_0 hrs	398.0	0.064	1.27	23.81	59
Influent_24 hrs	399.0	0.045	1.52	46.43	85
TTA_45 hrs	398.0	0.030	1.27	64.3	116.0
TMA_45 hrs	399.0	0.034	1.53	59.5	117.0
TBA_45 hrs	399.0	0.035	0.76	58.3	119.0
TTS_48 hrs	401.0	0.033	2.04	60.7	130.0
TMS_48 hrs	401.0	0.032	2.04	6.2	126.0
TBS_48 hrs	401.0	0.034	2.04	59.5	130.0
TES_48 hrs	401.0	0.034	2.04	59.5	129.0

5.3.2.3. DLS measurements: Hydrodynamic size distribution of the NPs

Figure 5-21 shows the DLS size distribution (D_H) of Ag-NPs in OECDss before (at 0 and 24 hrs) and after treatment (at 45 and 48 hrs) in SBR pilot plant without aeration. Before treatment, the size of the particles was increased within the first twenty-four hours, causing the DLS signal to sift toward higher diameters as a consequence. The average D_H of the citrate Ag-NPs was 18.7 ± 0.3 nm before their dispersion in the media, but was significantly increased at 0 and 24 hrs after their exposure with the average DH becoming equal to 24.5 ± 1.2 nm and 34.5 ± 2.7 nm. These changes in size might be related to the agglomeration and precipitation of the particles rather than their aggregation.

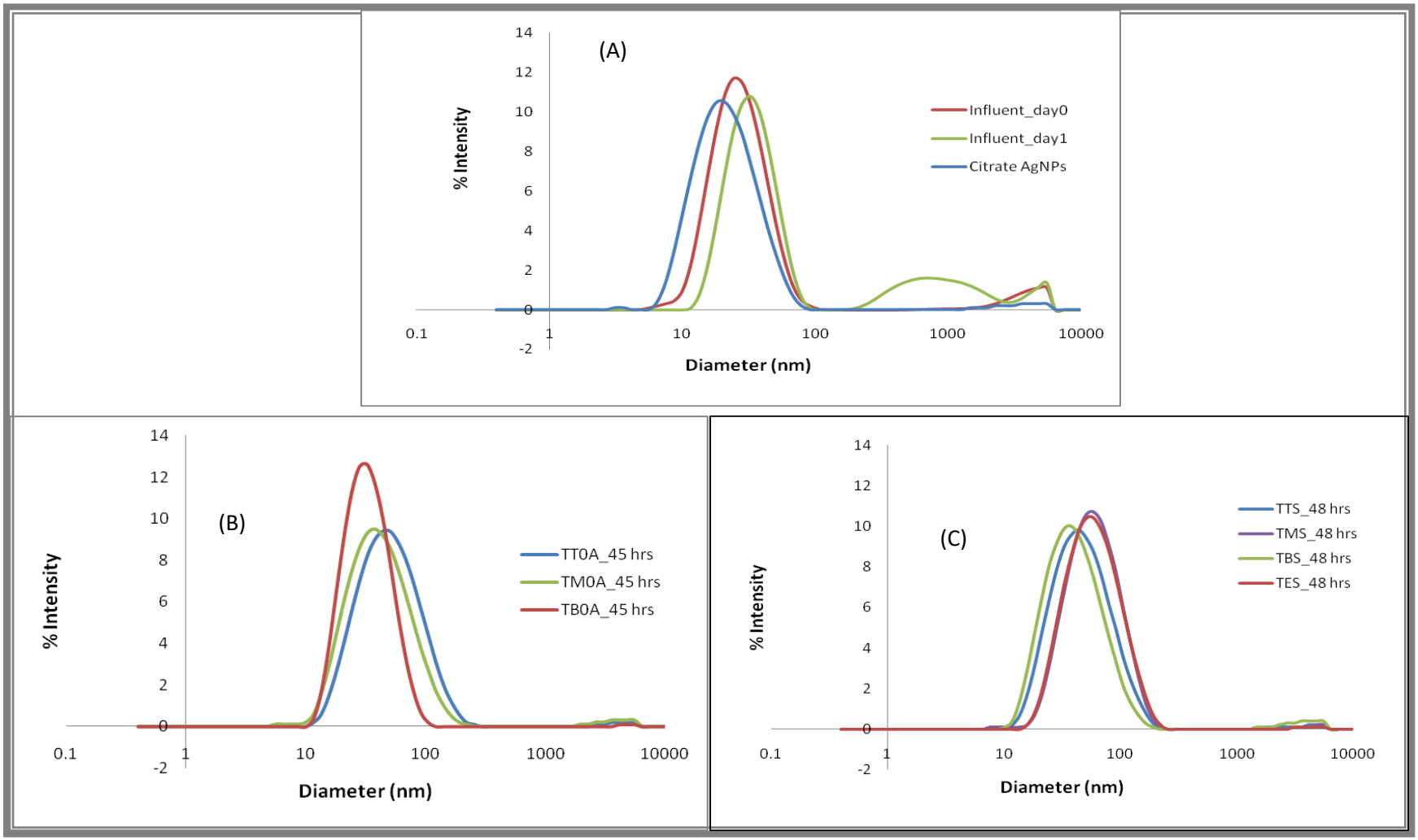

Figure 5-21: DLS measurement of Ag-NPs in OECDss (influent) before treatment (at 0 and 24 hrs) and during treatment with zero aeration (0A) at 45 hrs and during settling at 48 hrs. Samples collected from the influent at 0 and 24 hrs (figure (A)): influent_0 hrs and influent_24 hrs; from the top middle and bottom of the reactor at 45 hrs while stirring (figure (B)): TT0A_45 hrs, TM0A_45 hrs and TB0A_45 hrs; from the top middle and bottom of the reactor and the effluent at 48 hrs (figure (C)): TTS_45 hrs, TMS_48 hrs, TBS_48 hrs and TES_48 hrs.

The variations of the Ag-NP average D_H and PDI during the experimental process are illustrated in Figure 5-22 and Figure 5-23 respectively. The average D_H was found to be decreased or increased at 45 hrs depending on the collection point of the analysed samples from the reactor. Larger particles were found at the top of the reactor, and their average D_H was 40 ± 2.1 nm, and the particles located in the bottom of the reactor seemed to have dissolved; while those in the middle had similar average size as the influent_24 hrs sample. Dissolution of the particles is a non-equilibrium event; thus, if the region around the Ag-NPs is saturated with Ag^+, no further dissolution would occur. So, the presence of smaller particles in the bottom of the reactor than in the top may be caused their diffusion through stirring to the bottom and thus localised particle concentration may have been reduced, and more dissolution occurred. This might justify why there was less dissolved Ag at the top of the reactor than in the middle and the bottom at 45 hrs (Table 5-8)

The ANOVA for the critical value of $\alpha = 0.05$ was done by comparing the average D_H of citrate Ag-NPs in OECDss at 45 hrs in presence (case 1) and absence (case 2) of aeration. There was a significant difference between (case 1) and (case 2) regarding the changes in Ag-NPs average D_H since the ANOVA parameter F (= 9.83) < F_{critic} (7.71) and P-Value (=0.04) < 0.05. This suggests that the presence of the aeration in the plant will affect the size of the particles via agglomeration and/or dissolution and re-precipitation process.

At 48 hrs (or three hours after the stirring was stopped), the particles may have dissolved due to the oxygen present at the surface of the reactor, causing the decrease in their average D_H. From the middle to the bottom of the reactor, the average D_H was increased with larger particles found in the middle of the reactor and the effluent. The ANOVA for the critical value

of α = 0.05 was done by comparing the average D_H of Ag-NPs of the citrate in OECDss at 48 hrs in presence and absence (case 1) of aeration (case 2). There was no significant difference between (case 1) and (case 2) regarding the changes in Ag-NPs average D_H, since the ANOVA parameter F (= 4.90) < F_{critic} (6.00) and P-Value (=0.07) > 0.05.

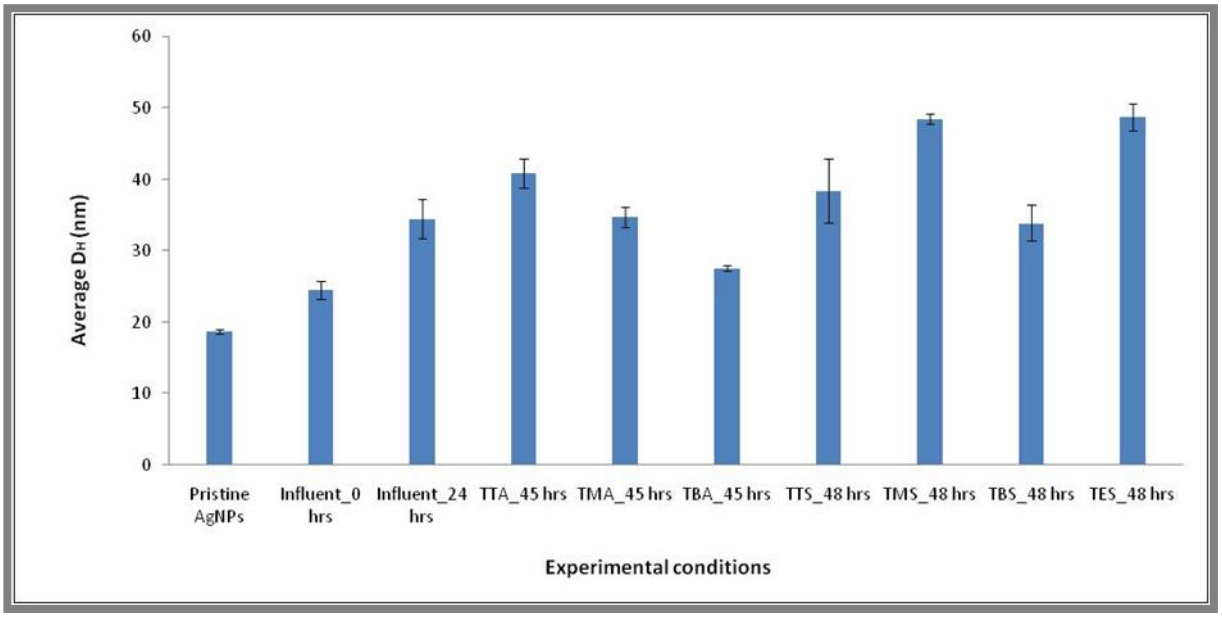

Figure 5-22: Average D_H of the citrate Ag-NPs in OECDss during treatment in the absence of aeration.

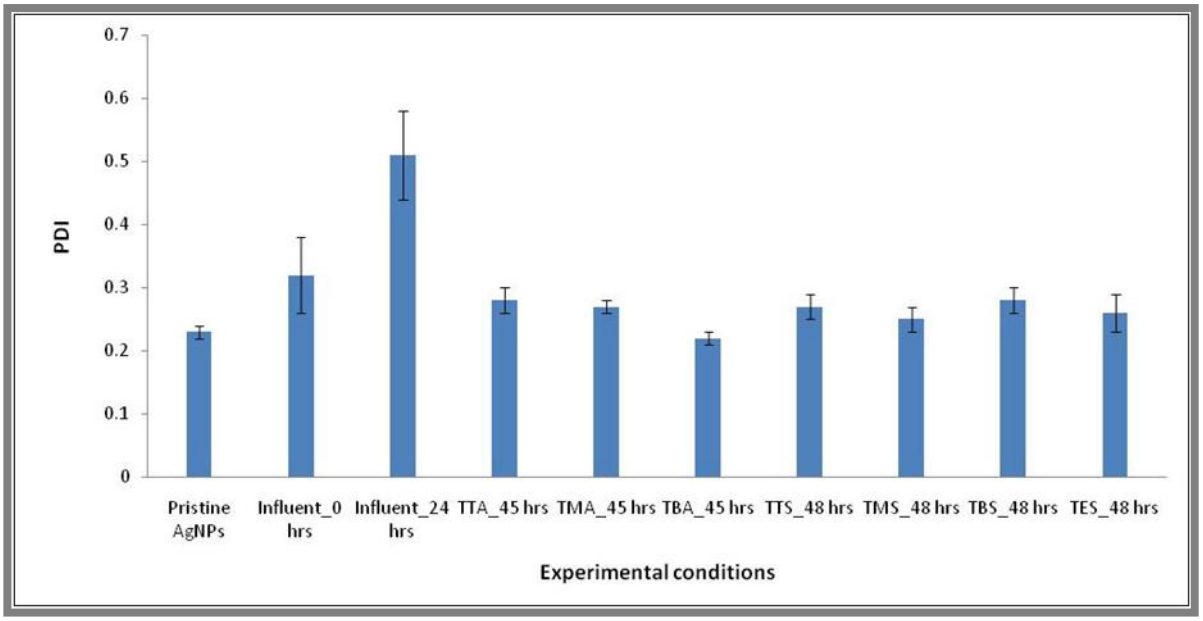

Figure 5-23: PDI of the citrate Ag-NPs in OECDss during treatment in the absence of aeration.

5.3.3. Ag-NPs characteristics dispersed sewage (OECDss + activated sludge) treated in SBR plant pilot

Since the behaviour of Ag-NPs in the influent at 0 and 24 hrs has already been discussed, this section focuses on how Ag-NPs behave in the SBR pilot plant when the activated sludge was used. By using the activated sludge, we investigate how efficiently the SBR pilot plant was in retaining most of the Ag in the activated sludge and thus significantly reducing the amount of ions and NPs in the effluent. Also, agglomeration and precipitation by dissolution of the particles due to their interaction with the organic and inorganic ligands were observed, as well as their plausible transformation into Ag_2S, SP-NPs, AgCl and Ag_2O.

5.3.3.1. Dissolution study: determination of silver concentration

The changes in concentration of citrate and PVP Ag-NPs in sewage (OECDss + Ag-NPs + activated sludge) which were treated in the SBR batch reactor are illustrated in Figure 5-24 and Figure 5-25 respectively. In both cases, samples collected from the bottom were found to have the highest concentration of Ag-NPs.

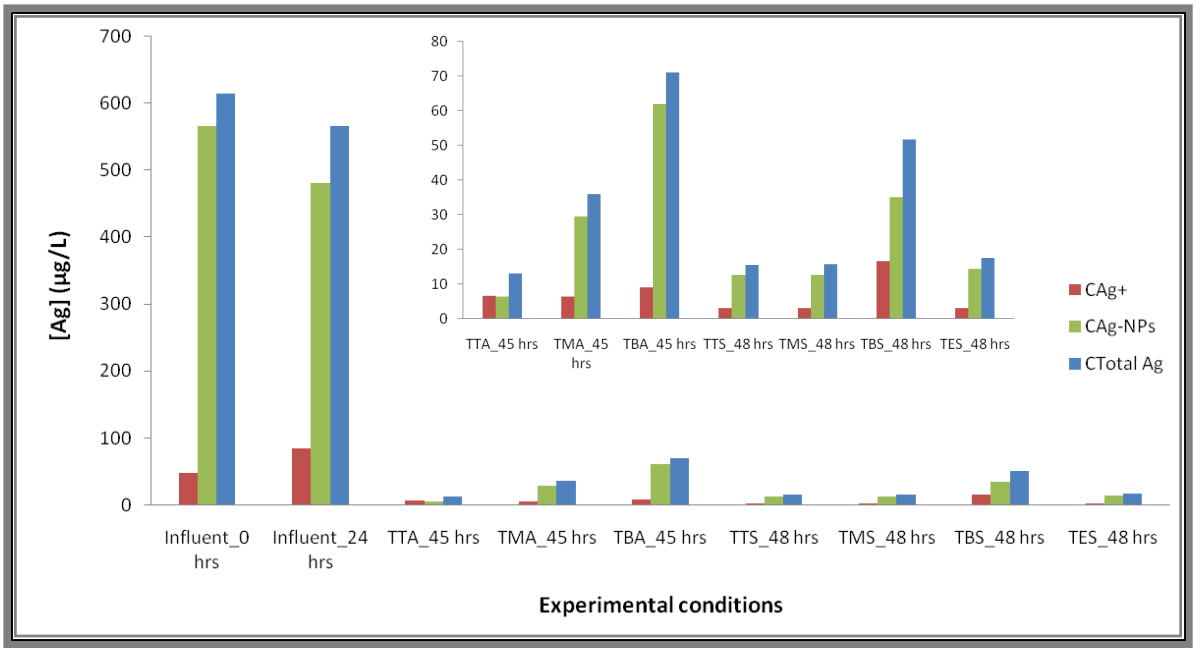

Figure 5-24: Ag concentration in sewage (OECDss + activated sludge) spiked with citrate capped Ag-NPs during treatment in SBR batch reactor and presence of an aeration flow Inset shows the 45 and 48 hour sampling points with a zoomed in y-axis.

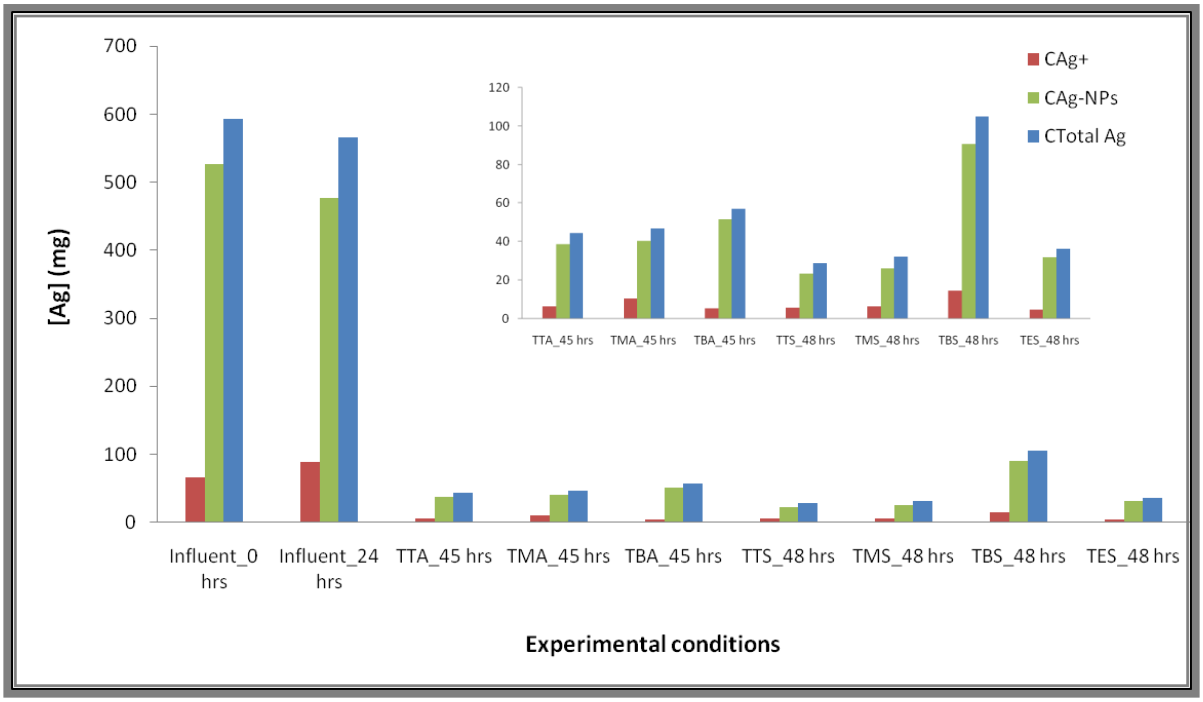

Figure 5-25: Ag concentration in sewage (OECDss + activated sludge) spiked with PVP capped Ag-NPs during treatment in SBR batch reactor and in presence of the aeration flow. Inset shows the 45 and 48 hour sampling points with a zoomed in y-axis.

Table 5-10summarises the percentage of Ag^+ (or dissolved Ag) as well as the percentage of the Ag losses due to their binding to the feed's bottles, reactor walls stirrer pallets and sludge. It can be seen that at 45 hrs, there was 87.36% loss of citrate Ag-NPs on average, while for the PVP Ag-NPs, this loss was 92.55%. These losses indicate that near half of the particles may have dissolved in sewage treatment plant in the presence of aeration as we found in 5.3.1.1, while the other half was captured in the biosolids. Hence, the very low concentration of Ag-NPs presents in the effluent. A similar observation has been reported in the literature (Doolette et al., 2013, Kaegi et al., 2011b).

The ANOVA test for $\alpha = 0.05$ for the samples collected during aeration are given in Table A4 - 27. There was no significant difference on the variation in concentration of the total Ag, Ag^+ and Ag-NPs at 45 hrs between the citrate and PVP Ag-NPs cases.

After settling, the estimated percentage of Ag-NPs from the effluent sample (TES_48 hrs) was lower for the citrate particles (2.56%) compared to the PVP Ag-NPs (5.99%). Also, the samples collected from the bottom of the reactor were found to have the lowest losses of Ag-NPs, although these were still above 80% for both citrate and PVP Ag-NPs. This indicates that the removal of Ag-NPs in the SBR pilot plant was slightly more efficient than 85 and 88% of Ag-NPs removal found in the literature (Doolette et al., 2013, Wang et al., 2012)

The ANOVA test for $\alpha = 0.05$ for the samples collected after settling are given in the Table A4 - 26. There was a significant difference on the variation in concentration of the total Ag, Ag^+ and Ag-NPs at 48 hrs between the citrate and the PVP particles. Thus, dissolution of the particles in SBR pilot plant in the presence of activated sludge was independent to their coating.

Table 5-10: Citrate-capped Ag-NPs in OECDss – Total Ag concentration ($C_{Total\ Ag}$), dissolved Ag concentration (C_{Ag+}), estimated Ag-NPs concentration ($C_{Ag\text{-}NPs}$), percentage of dissolved Ag and losses in Ag-NPs before (at 0 and 24 hrs) and during treatment in the SBR pilot plant with samples collected from the top, middle and bottom of the reactor at 45 hrs (aeration stage) and 48 hrs (settling stage).

	$C_{Total\ Ag}$ (citrate) ($\mu g*L^{-1}$)	C_{Ag+} (citrate) ($\mu g*L^{-1}$)	$C_{Ag\text{-}NPs}$ (citrate) ($\mu g*L^{-1}$)	%Diss. Ag (Citrate) (%)	Unr. Ag (citrate) (%)
0 hrs	614.44 ± 14.29	48.45 ± 4.29	566.00 ± 17.88	7.90 ± 0.84	0.00 ± 0.00
24 hrs	565.87 ± 35.79	84.85 ± 12.19	481.02 ± 31.84	15.00 ± 1.83	7.79 ± 7.80
TTA_45 hrs	13.08 ± 2.69	6.65 ± 2.79	6.43 ± 4.99	54.91 ± 33.16	97.87 ± 0.41
TMA_45 hrs	36.04 ± 8.09	6.51 ± 3.44	29.53 ± 10.87	23.54 ± 5.16	94.12 ± 1.41
TBA_45 hrs	71.07 ± 15.14	9.17 ± 3.82	61.89 ± 18.95	14.05 ± 8.05	88.40 ± 2.63
TTS_48 hrs	15.63 ± 4.3	3.03 ± 1.92	12.59 ± 2.97	18.70 ± 7.45	97.46 ± 0.70
TMS_48 hrs	15.81 ± 15.81	3.10 ± 1.69	12.70 ± 3.1	18.93 ± 5.24	97.44 ± 0.69
TBS_48 hrs	51.72 ± 13.15	16.67 ± 11.43	35.06 ± 23.07	36.22 ± 26.18	91.60 ± 2.27
TES_48 hrs	17.64 ± 5.46	3.17 ± 1.47	14.47 ± 5.62	19.50 ± 10.20	97.14 ± 0.85

Table 5-11: PVP-capped Ag-NPs in OECDss – Total Ag concentration ($C_{Total\ Ag}$), dissolved Ag concentration (C_{Ag+}), estimated Ag-NPs concentration ($C_{Ag\text{-}NPs}$), percentage of dissolved Ag and losses in Ag-NPs before (at 0 and 24 hrs) and during treatment in the SBR pilot plant with samples collected from the top, middle and bottom of the reactor at 45 hrs (aeration stage) and 48 hrs (settling stage).

	$C_{Total\ Ag}$ (PVP) ($\mu g*L^{-1}$)	C_{Ag+} (PVP) ($\mu g*L^{-1}$)	$C_{Ag\text{-}NPs}$ (PVP) ($\mu g*L^{-1}$)	%Diss. Ag (PVP) (%)	Unr. Ag (PVP) (%)
0 hrs	593.00 ± 73.17	65.93 ± 15.07	527.07 ± 78.73	11.31 ± 3.32	0.00 ± 0.00
24 hrs	565.3 ± 65.74	88.90 ± 10.73	476.40 ± 57.94	15.75 ± 1.20	4.60 ± 1.77
TTA_45 hrs	44.46 ± 6.89	6.01 ± 3.12	38.45 ± 5.93	13.40 ± 5.73	92.34 ± 2.07
TMA_45 hrs	46.62 ± 14.69	10.10 ± 2.77	40.21 ± 8.99	21.80 ± 1.31	91.84 ± 3.7
TBA_45 hrs	56.85 ± 15.45	5.23 ± 0.68	51.62 ± 15.64	9.70 ± 2.72	90.10 ± 4.04
TTS_48 hrs	28.64 ± 3.39	5.47 ± 2.13	23.17 ± 1.85	17.96 ± 14.86	95.15 ± 0.50
TMS_48 hrs	32.08 ± 14.42	6.02 ± 3.78	26.06 ± 10.77	17.33 ± 5.14	94.43 ± 2.86
TBS_48 hrs	105.17 ± 17.93	14.44 ± 9.29	90.72 ± 9.46	12.97 ± 7.42	81.90 ± 5.24
TES_48 hrs	36.17 ± 6.31	4.55 ± 2.52	31.55 ± 3.83	11.99 ± 5.45	93.82 1.50

5.3.3.2. UV-Vis characterisation

The UV-Vis spectrum of Ag-NPs in sewage during the aeration (at 45 hrs) and the settling (48 hrs) phases are shown in Figure 5-27. At 45 hrs, the citrate Ag-NPs were highly dissolved compared to the PVP Ag-NPs because of their lower absorbance values. The corresponding λ_{max} for citrate and PVP Ag-NPs during that phase was 402 nm, whether the measured samples were collected from the top, middle or bottom of the reactor. Hence, the spiked citrate and PVP Ag-NPs had their surface chemistry modified due to the oxidation-dissolution mechanism occurring in an aerated WWTP (Yang et al., 2013c) or due to re-precipitation.

At 48 hrs, the UV-Vis signal of TTS_48 hrs, TMS_48 hrs and TES_48 hrs, show an exponential decay curve shape. These spectrums were similar to UV-Vis signals obtained from the control samples with no particles added to sewage (Figure 5-26) and these spectra from the control samples are corresponding to the UV-Vis of wastewater given by in the literature (M. Hochedlinger et al., 2007, Brito et al., 2014). Hence in the citrate case, Ag-NPs were low in concentration or may have completely dissolved in the sewage. The sample from the bottom part of the reactor however shows the opposite situation, with its UV-Vis absorbance being negative with an exponential increased shape.

For the PVP Ag-NPs, the sample collected at 48 hrs have λ_{max} showing a dependence to their collection point and which is respectively 414, 418, 410 and 412 nm for the top, middle, bottom and effluent sample. Also the fact that the Ag-NPs were detected by UV-Vis with little to no loss in absorbance intensity in the PVP case, may have confirmed that they were not completely dissolved or sedimented in the sludge.

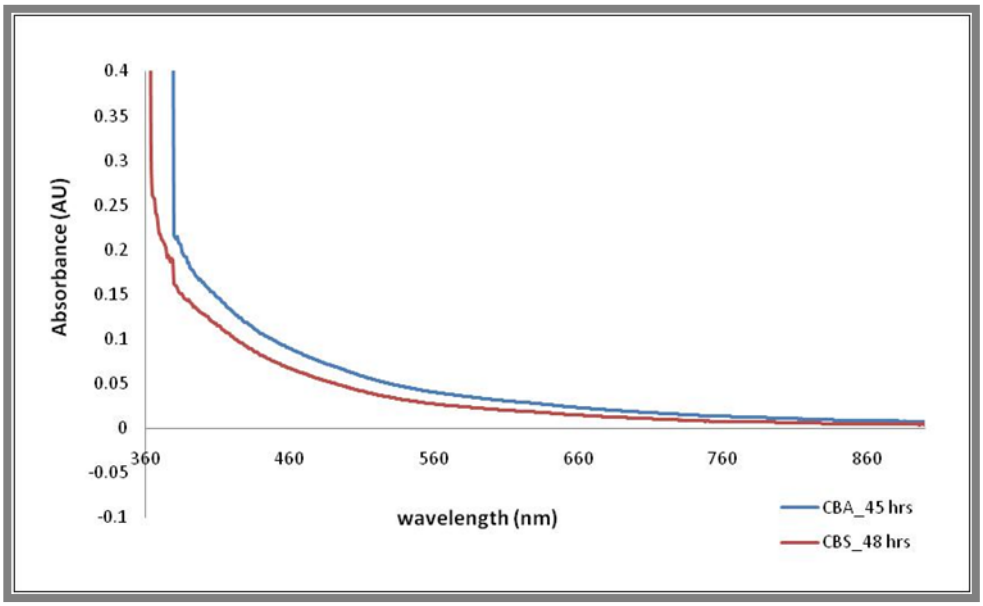

Figure 5-26: UV-Vis spectra of the control sample during the aeration and settling, when the (OECDss + Activated sludge) medium is used without addition of Ag-NPs

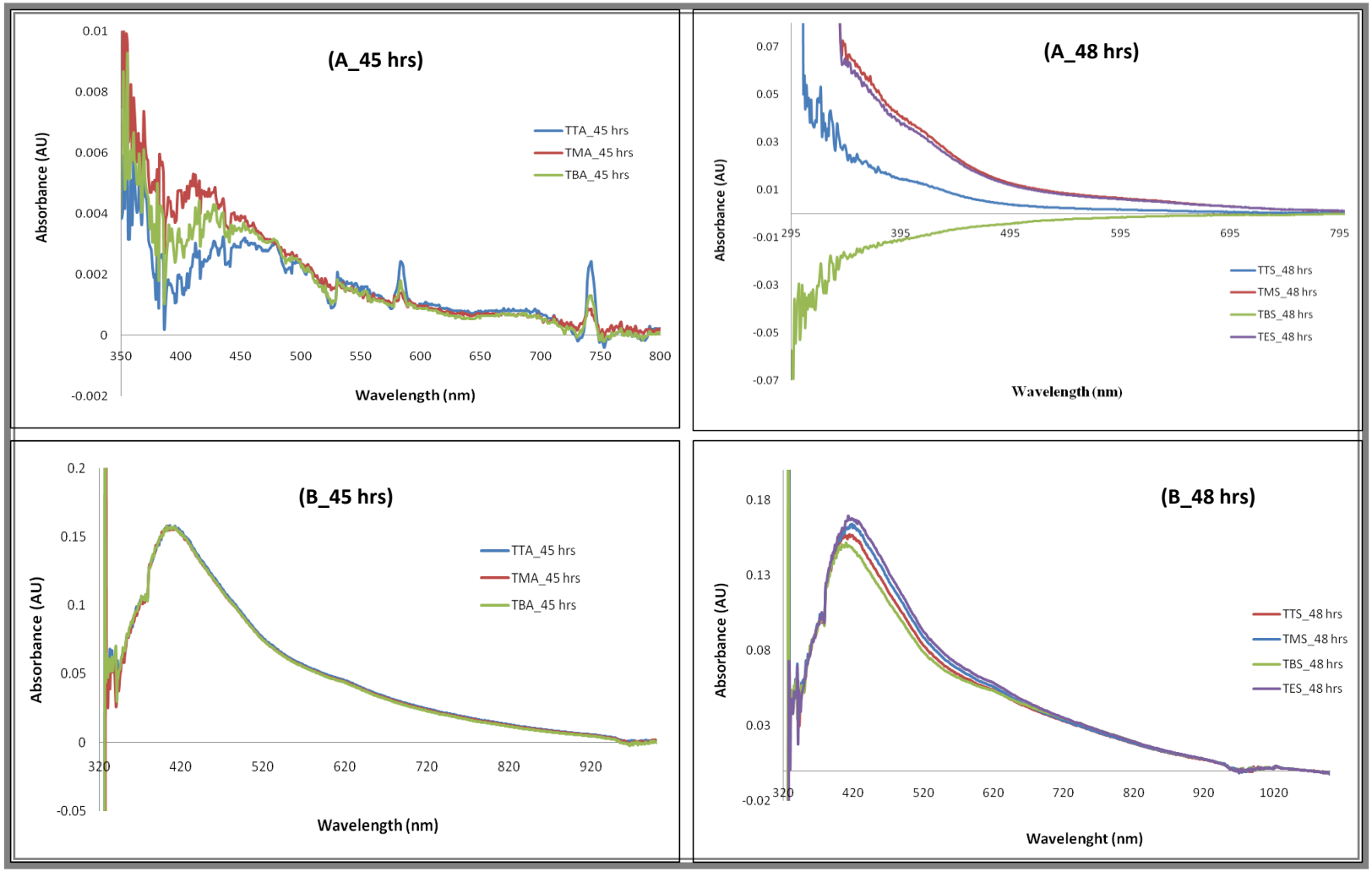

Figure 5-27: UV-Vis spectra of spiked citrate (A) and PVP (B) Ag-NPs in sewage during aeration (A_45 hrs) and after settling (B_48 h)

5.3.3.3. DLS measurements: Hydrodynamic size distribution of the NPs

From the DLS results, it was impossible to deduct whether the measured scattering D_H corresponded to the Ag-NPs size, due to the multitude of other particles present in the activated sludge. The figure below (Figure 5-28) describes this by showing the similarity between the control sample without Ag-NPs added (Figure 5-28(a)) and the test samples with spiked citrate Ag-NPs (Figure 5-28(b)). For both test (TBA, TBS and TES) and control (CBA, CBS and CES) the scattering intensity signal covers X-axis in the range {10, 4000} nm approximately and the average D_H is between 150 nm to 200 nm.

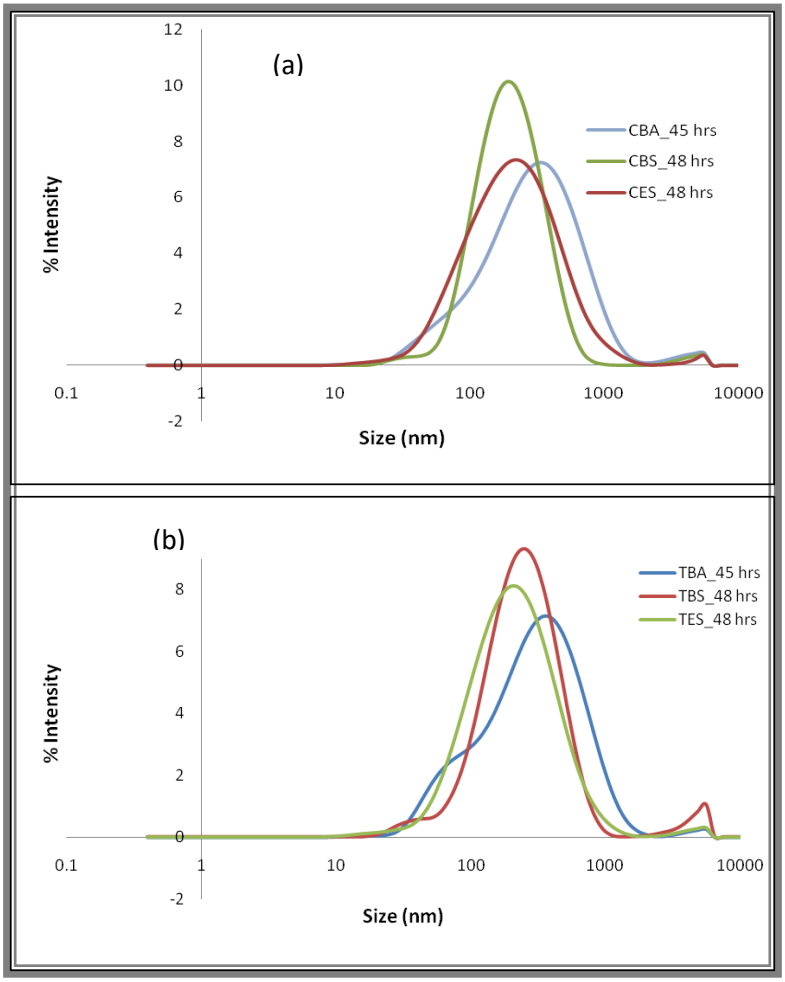

Figure 5-28: DLS size distribution of particulates in sewage without Ag-NPs added (a) and with Ag-NPs added (b)

5.3.3.4. TEM characterisation

Using the TEM JEOL 1200, identification of Ag-NPs was not possible in either the test or the control sewage medium. Figure 5-29 represents the TEM images of sewage spiked with citrate Ag-NPs (A_TBS 48 hrs) and PVP Ag-NPs (B_TBS 48 hrs) and of the sewage without particles (control sample: C_CBS 48 hrs). The analysed samples were collected from the bottom of the reactor and during the settling phase. The images show the presence of large aggregates particles, but we were unable to tell if they were Ag-NPs based on these pictures, since several other metals may be present in the activated sludge (e.g.: Fe, Co, Cu, Ag, Zn, Si, Ti).

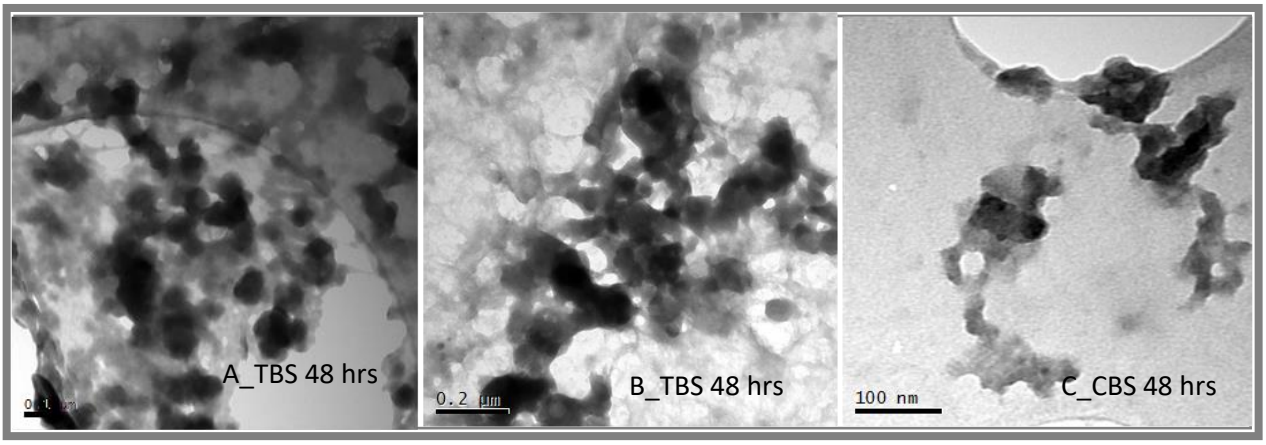

Figure 5-29: TEM images of the sewage samples collected from the bottom of the test reactor containing citrate Ag-NPs (A_TBS 48 hrs) and PVP Ag-NPs (B_TBS 48 hrs) and the sample collected from the control sample with no particles (C-CBS 48 hrs).

5.3.3.5. SEM and TEM Chemical surface characterisation: EDS analysis

Figure 5-30showsthe SEM analysis of a dried sewage sample containing citrate Ag-NPs and collected from the bottom of reactor after redrawing the effluent; this sample was ground up before characterisation. In the EDS spectrum, there was no Ag signal found while other metals (Fe, Ti, Al and Si) were detected. In fact, the concentration of Ag particles dispersed in the

influent was insufficient for the EDS characterisation. Indeed, previous studies on the Ag-NPs transport, behaviour and fate in WWTP were conducted with a concentration of Ag-NPs higher than 10 ppm (Kim et al., 2010, Kaegi et al., 2013). In this case, the concentration of Ag-NPs in the influent at 24 hrs was about 480 ppb for both citrate and PVP Ag-NPs (Table 5-2 and Table 5-3). Thus, this might justify the lack of Ag detection due to the high density of biosolids; so, looking to detect the Ag, in this case would the equivalent of looking for a needle in a haystack.

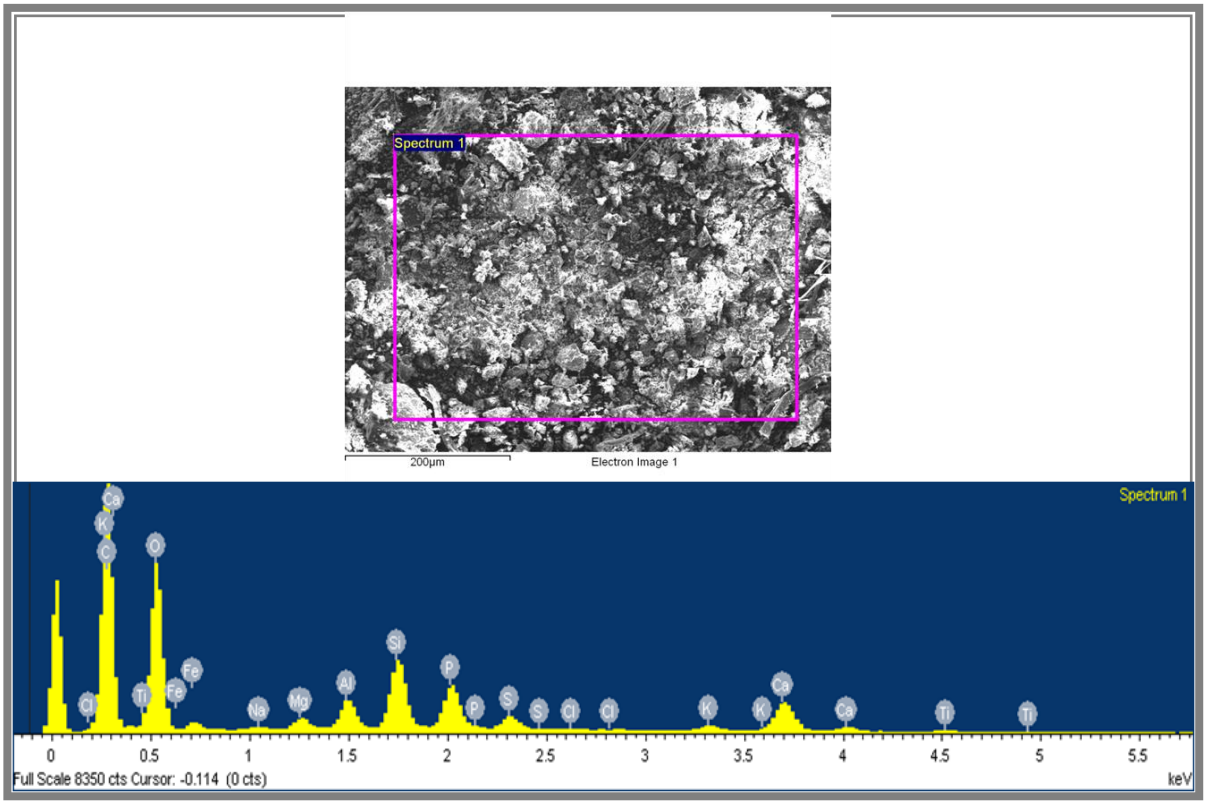

Figure 5-30: SEM and EDS characterisation of the Ag-NPs in sewage spiked with 500 ppb citrate capped Ag-NPs. Activated sludge sample at 48 hrs in the treatment process.

The TEM characterisation obtained using the JEOL 2100 of the sewage sample collected during the aeration period are given in Figure 5-31. The EDS spectrum shows similar results as the one obtained with SEM, with no Ag peak, implying this element was not detectable by EDS. However, other metals (Fe, Co and Si) from the sewage were found. The copper (Cu) signal was from the TEM grid itself.

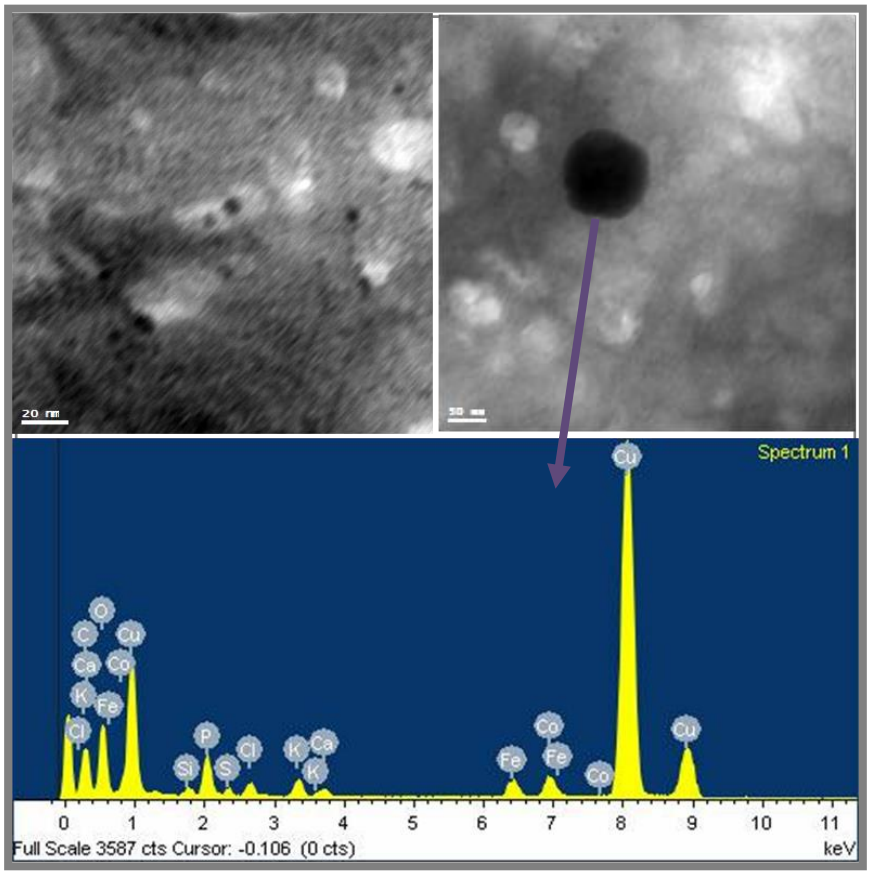

Figure 5-31: TEM and EDS characterisation of the Ag-NPs in sewage spiked with 500 ppb citrate capped Ag-NPs. Sample Collected the selling phase at 48 hrs in the treatment process.

5.4. Discussion and conclusion

In this chapter, it has been demonstrated that dispersed citrate and PVP Ag-NPs in OECDss (influent) were not stable before and after treatment in the SBR pilot plant. The results from treatment of the influent in the presence of aeration and in the absence of activate sludge (section 5.3.1) demonstrated that citrate and PVP Ag-NPs underwent several changes throughout the treatment process. Indeed, when comparing the changes in concentration, it was observed that citrate Ag-NPs had a higher dissolution rate than PVP-capped Ag-NPs and more losses were observed in the case of citrate Ag-NPs compared to the PVP Ag-NPs. These losses were not chemical, but physical and the particles may have been absorbed through the reactor walls, or they may have settled at the bottom of the reactor.

It was also demonstrated that in absence of aeration, the dissolution rate of Ag-NPs in an SBR pilot plant was low as it was occurring without an additional flow. Finally, when the activated sludge was used, nearly 80% or more Ag-NPs from the influent were absorbed by the sludge. The results have also shown that the changes in the total concentration of Ag, Ag^+ and Ag-NPs were dependent on the capping agent of the Ag-NPs, with citrate Ag-NPs leading to a higher dissolution and losses than PVP Ag-NPs.

The SPR results revealed some evidence regarding the change in size through aggregation and dissolution of citrate and PVP Ag-NPs in OECDss only with or without aeration and real sewage. Both citrate and PVP Ag-NPs may have initially undergone similar modifications following their dispersion in OECDss. In the presence of aeration without activated sludge, aggregation and dissolution of the particles was observed for both citrate and PVP Ag-NPs.

Also, the red-shift of SPR peak of Ag-NPs was more significant for the citrate NPs during the aeration and the settling phase, which suggests a potential transformation of the particles surface through binding of a chemical element present in media such as proteins on the NPs surface or aggregation of the NPs. In fact, as it is known that the SPR spectrum of the NPs is dependent on their size, shape and to the dielectric function of the exposed medium (Podila et al., 2012). So, we may suggest that the red-shift of the Ag-NPs SPR spectrum was caused by the interaction of the chemical elements present in the OECDss with the Ag-NPs, affecting their size and (or) shape. On the other hand, for PVP particles, λ_{max} remained generally constant in both stages of the treatment. Two assumptions might be made:

- First PVP Ag-NPs might have been protected from oxidation due to their surface functionalisation property as they are sterically stabilised (Tejamaya et al., 2012);
- Second, their surface chemistry might have transformed into a different state (Ag_2S, AgCl or Ag_2O) through dissolution which may cause the Ag speciation by OECDss chemical components (Ma et al., 2014), preventing further transformation (size and shape of the NPs). Similar observations were made for the citrate Ag-NPs case in the absence of aeration since λ_{max} was generally constant in that case (section 5.3.2.2).

In the presence of activated sludge in the sewage (section 5.3.3.2), citrate and PVP Ag-NPs may have been transformed by a similar oxidation mechanism during the aeration phase because they show a similar value of λ_{max} at 45 hrs. Finally, the Ag-NPs were not detected by UV-Vis for citrate during the settling phase. However, for PVP Ag-NPs the SPR peak was redshifted to a higher λ_{max} similar to the citrate Ag-NPs case when the activated sludge was not used (Table 5-5). This suggested that in the presence of the activated sludge, PVP Ag-NPs might have been oxidised and transformed into Ag_2S during the settling phase.

TEM and DLS results in the presence of aeration and in of absence activated sludge revealed that the size of the Ag-NPs increased over time and in all stages of the treatment in both citrate and PVP Ag-NPs; with citrate particles having the higher degree of aggregation (sections 5.3.1.3 and 5.3.1.4). No detection of Ag-NPs by TEM and DLS was observed in presence of the activated sludge, from the filtered sewage samples collected from the bottom of the reactor after treatment, due to the low amount of Ag-NPs that was dispersed in the influent. Statistically, the TEM and DLS results show that no significant difference in size was found between both citrate and PVP Ag-NPs during aeration and settling of the OECDss. Meaning, the changes in the size of Ag-NPs in an aerobic waste water treatment plant were independent to their capping agent. However, this was in contradiction with the estimated average size of the particles from the UV-Vis characteristic, which show the opposite (Table A4 - 1 and Table A4 - 2).

Finally, the EDS results have indicated that when the activated sludge was not used, citrate Ag-NPs transformed into Ag_2S while PVP Ag-NPs changed into AgCl. No silver peak was detected from the activated sludge samples due to the low concentration Ag-NPs in the influent. Indeed, similar studies on Ag-NPs behaviour in WWTP were conducted using much higher concentrations of Ag-NPs, about 2 to 3 $g*L^{-1}$ (Kaegi et al., 2011b, Kaegi et al., 2013).

Chapter 6 Accumulation and removal of silver nanoparticles in an aerobic wastewater treatment plant pilot

Chapter Summary

10 nm citrate and PVP Ag-NPs were exposed to sewage made with OECDss and activated sludge from a Seven Trent WWTP, UK. This sewage was then treated over a twenty-one day period, by adding 6 L of a one-day old influent solution (OECDss + 10 $\mu g*L^{-1}$ pristine particles) every two days, after the drawing of the effluent while the settled activated sludge was kept in the tank. The total amount of citrate and PVP Ag-NPs added in the reactor was respectively 36 and 55.1 $\mu g*L^{-1}$. Following 21-days of exposure, 44% and 47% respectively of the added citrate and PVP Ag-NPs remained in the activated sludge. The test (sewage with particles) and control (sewage without particles) samples collected during aeration and settling phases were characterised by UV-Vis, dynamic light scattering and atomic absorption spectroscopy. This chapter looks at the accumulation of the Ag-NPs under these experimental conditions, representing an aerated WWTP and their removal by the activated sludge.

6.1. Introduction

Ag-NPs are currently found in consumer products such as cosmetics, soaps, paints, optical devices, clothing, medical and home appliances and they are also used as food preservatives (Kumar et al., 2014, Park et al., 2013). Their popularity is primarily due to their unique optical, electrical, thermal and antimicrobial properties (Geertsma et al., 2009, Park et al., 2013). The use of Ag-NPs in commercial products has significantly increased in recent years, with more than 30% of nanoproducts made with Ag-NPs (Geertsma et al., 2009). And this in turn has increased the release of Ag-NPs in the sewerage and wastewater treatment systems (Yang et al., 2012).

Recent studies have shown that the wastewater treatment process plays a significant role in NPs uptake by the sludge over the different stages of treatment (Hou et al., 2012, Doolette et al., 2013, Kaegi et al., 2013). In fact, more than 85% to 95% of Ag-NPs that enter the sewerage system are retained by the sewage biomass as a result of settling, implying their low presence in the effluent (Kaegi et al., 2011b, Park et al., 2013, King et al., 2015, Doolette et al., 2013). Similar behaviours were expected for this present study.

The aim of this chapter was to investigate the accumulation and removal mechanism of citrate and PVP Ag-NPs in an aerated wastewater treatment pilot plant. The objectives were to:

(1) Characterise the influent and the collected sewage and effluent samples using UV-Vis, DLS, and GFAAS to assess and quantify the presence of Ag NPs over time,

(2) Calculate the percentage removal of Ag-NPs using mass concentration and application of the Freundlich isotherm model for the adsorption of Ag-NPs by the sludge as it settled (as the NPs come into contact with the sludge).

6.2. Materials and Method

For this study, the influent of the SBR pilot plant was prepared by dispersing freshly synthesised and washed 10 nm citrate or PVP Ag-NPs (Chapter 4) in fresh OECDss (Figure 5-2) for a total concentration and volume of 10 $\mu g*L^{-1}$ and 10 L respectively. Ten samples were collected from the influent medium at 0 hrs (Influent_day 0) and analysed using GFAAS, DLS and UV-Vis, before storing the influent at room temperature for twenty-four hours. At day 1 and after a second round (Influent_day 1) of characterisation (GFAAS, DLS and UV-Vis), the influent was transferred into the sequence batch reactor (SBR) which was filled with 4 L of the activated sludge (Figure 6-1). The obtained sewage was aerated for twenty-four hours with an aeration flow rate of 100 to 150 m^3/L, and the samples were collected from the middle and bottom of the tank (TMA and TBA respectively), on day 2 before the aeration was stopped at 48 hrs. After aeration, the sewage was left to settle for another twenty-four hours and samples were taken from the top, middle and bottom of the tank (TTS, TMS and TBS respectively) and also from the effluent (TES) after it was withdrawn from the tank.

After the settling phase was completed and the effluent was removed on day 3, the second batch of a day old influent containing Ag-NPs was discharged into the tank for a second series of the sewage treatment. This was done ten times in total over a twenty-one day period with

the transfer of the influent in the tank done every other day, from day 1 until day 19 (Table 6-1).

5 ml of each sewage sample collected from the tank was acid digested using aqua regia acid which was constituted of 1:3 ratio of nitric (70% HNO_3) and hydrochloric (30% HCl) acids. The digestion method is discussed in chapter 3. These digested samples were diluted to 0.2% with deionised water prior to their characterisation by GFAAS. The undigested sewage samples were centrifuged at 5000 rpm at 10 °C and then filtered with 450, 200 and 100 nm filtered syringes. The filtrate samples were then analysed using UV-Vis to detect the accumulation of Ag-NPs in the sewage and for the ultracentrifuged samples for the traceability of the dissolved Ag.

Table 6-1: list of the collected samples from: the influent test and control (in the day of its preparation and 24 hrs after), the test tank during aeration (TMA and TBA), test tank during settling (TTS, TMS and TBS), the effluent – test (TES), the control tank during aeration (CMA and CBA), control tank during settling (CTS, CMS and CBS) and the effluent – control (CES).

	Test samples			Control samples		
	Influent samples	**Aeration samples**	**Settling samples**	**Influent samples**	**Aeration samples**	**Settling samples**
Day 0	fresh Influent			fresh Influent		
Day 1	A day old Influent			A day old Influent		
Day 2	fresh Influent	TMA and TBA		fresh Influent	CMA and CBA	
Day 3	A day old Influent		TTS, TMS, TBS and TES	A day old Influent		CTS, CMS, CBS and CES
Day 4	fresh Influent	TMA and TBA		fresh Influent	CMA and CBA	
Day 5	A day old Influent		TTS, TMS, TBS and TES	A day old Influent		CTS, CMS, CBS and CES
Day 6	fresh Influent	TMA and TBA		fresh Influent	CMA and CBA	
Day 7	A day old Influent		TTS, TMS, TBS and TES	A day old Influent		CTS, CMS, CBS and CES
Day 8	fresh Influent	TMA and TBA		fresh Influent	CMA and CBA	
Day 9	A day old Influent		TTS, TMS, TBS and TES	A day old Influent		CTS, CMS, CBS and CES
Day 10	fresh Influent	TMA and TBA		fresh Influent	CMA and CBA	
Day 11	A day old Influent		TTS, TMS, TBS and TES	A day old Influent		CTS, CMS, CBS and CES
Day 12	fresh Influent	TMA and TBA		fresh Influent	CMA and CBA	
Day 13	A day old Influent		TTS, TMS, TBS and TES	A day old Influent		CTS, CMS, CBS and CES
Day 14	fresh Influent	TMA and TBA		fresh Influent	CMA and CBA	
Day 15	A day old Influent		TTS, TMS, TBS and TES	A day old Influent		CTS, CMS, CBS and CES
Day 16	fresh Influent	TMA and TBA		fresh Influent	CMA and CBA	
Day 17	A day old Influent		TTS, TMS, TBS and TES	A day old Influent		CTS, CMS, CBS and CES
Day 18	fresh Influent	TMA and TBA		fresh Influent	CMA and CBA	
Day 19	A day old Influent		TTS, TMS, TBS and TES	A day old Influent		CTS, CMS, CBS and CES
Day 20		TMA and TBA			CMA and CBA	
Day 21			TTS, TMS, TBS and TES			CTS, CMS, CBS and CES

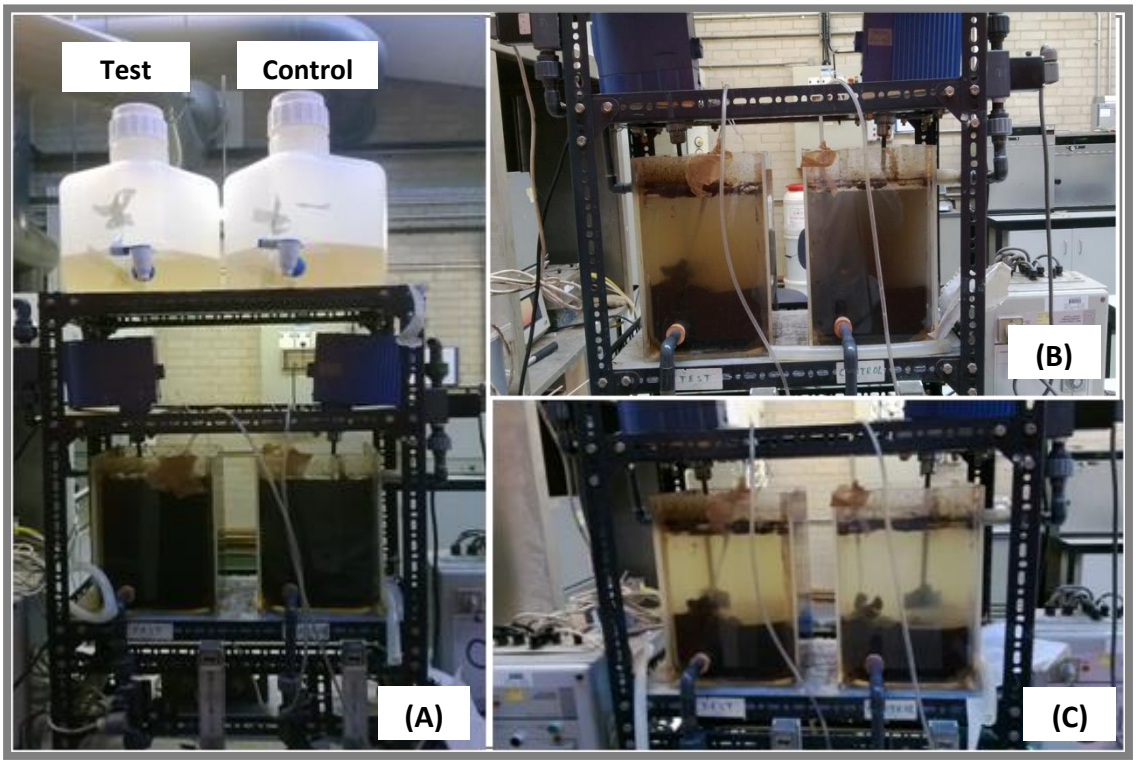

Figure 6-1: Appearance of sludge throughout the 21 days of the treatment: at the start of experiment in week 1 (A), in week 2 (B) and at the end of the experiment in week 3 (C)

The activated sludge was collected from a Seven Trent WWTP in Birmingham, UK. The efficiency of the sewage treatment was investigated on a laboratory scale pilot treatment unit courtesy of Dr. Gofetamang Ditalelo from the University of Birmingham Civil Engineering department. Key sludge characteristics including the 5-day oxygen biological demand (BOD_5) (Figure 6-2), and the total and TS of the test and control sewage were determined. In addition, the dissolved oxygen of the sewage was measured during aeration over the 21 days period (daily). The analytical methods of these measurements are described in the methodology chapter (section 2.2.3).

Figure 6-2: (A) - BOD5 measurement experiment; (B) – test and control (without NPs or Ag^{+}) samples for BOD measurements in week 2 after incubation, test samples more clear than the control samples due the increase in settlement of the test sewage.

6.3. Results and discussions

6.3.1. Efficiency of the sewage treatment in the SBR pilot plant

The treatment efficiency of the SBR pilot plant was investigated by observing the change in solid concentration ($g*mL^{-1}$) of the effluent at the end of the treatment period as compared to the start of the treatment (Spellman, 2009, Eaton and Franson, 2005). This was coupled with the changes in BOD_5 exerted by the effluent at various periods of the treatment (Eaton and Franson, 2005). Observation of these parameters showed similar treatment efficiency of the control (sewage with no Ag-NPs) and the test tank (supplemented with Ag-NPs).

During the early stages (week 2) the test tank (with Ag-NPs) showed better settlement of the sludge (Figure 6-1 (B)) than the untreated control. The effluent from the test tank also exerted a smaller BOD_5 in week 2; which can tentatively be associated with reduced microorganisms in the effluent due to their increased settling ability (Figure 6-4 (A)). At the end of the treatment, the test tank had 99% reduction in TS content, while the control tank

had 97% reduction in TS (Figure 6-3). This is the range of the percentage of the settleable solid (90 to 99%) accepted to quantify the efficient removal of solids from the effluent (Spellman, 2009). TS in the effluent were not measured at end of the experiment as TS were not enough to enable that.

The increase in BOD_5 exerted by the effluent from the control tank was mostly associated with an observed increase in the amount of floating sludge (that previously had settled). The cause of this sudden floatation of sludge is unknown, but the onset of anaerobic conditions leading to biogas production at the bottom of the tank was suspected. Figure 8.0 shows the weekly percentage BOD_5 reduction.

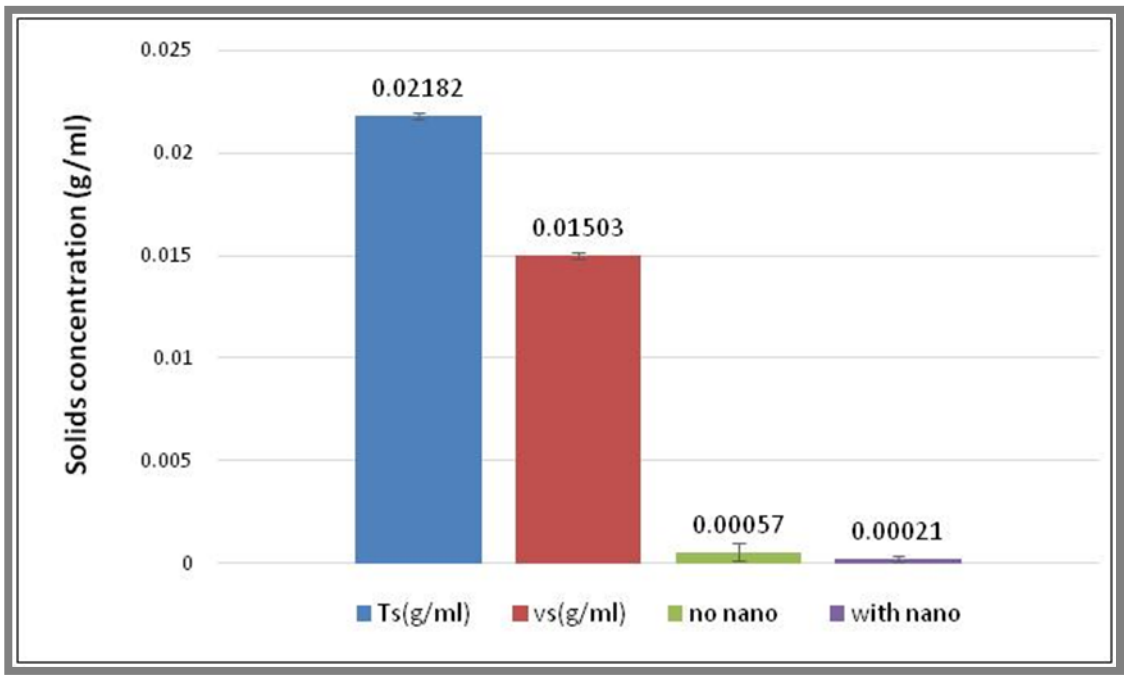

Figure 6-3: The concentration of the Total solids (TS) and volatile solid (VS) content in the effluent in week 1 (blue and red column respectively) and the total solid content in the test tank effluent (with nano) and the control tank effluent (no nano) after 21 days

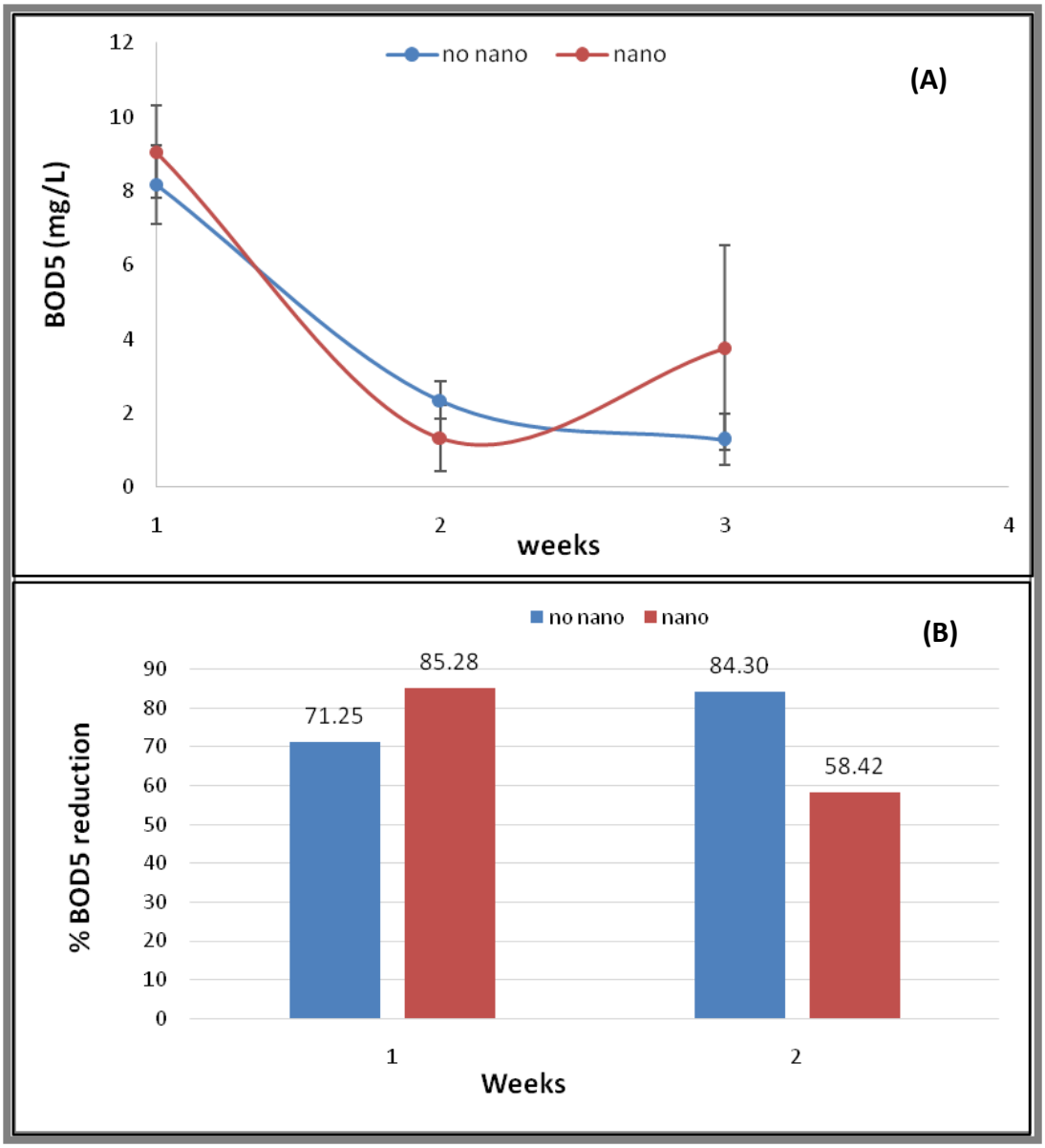

Figure 6-4: (A) BOD5 exertion curve 8% reduction in BOD5 from start of experiment of the test tank (nano) and the tank sewage (no nano); (B) percentage – reduction of the BOD5 in week 1 and week 2

6.3.2. GFAAS, UV-Vis and DLS characterisations of Ag-NPs in the influent

A freshly made solution of OECDss was prepared and spiked with 10 nm citrate or PVP Ag-NPs for a total concentration and volume of 10 µg*L^{-1} and 10 L respectively. This concentration was chosen in order to be close to the environmental range but still detectable by the GFAAS with a limit of detection of Ag of 0.005 µg*L^{-1} (PerkinElme, 2013) as opposed to the higher

concentrations used in previous research (Kaegi et al., 2011c, Kaegi et al., 2013). The GFAAS, UV-Vis and DLS characterisation results of the Ag-NPs in the synthetic sewage are presented and discussed in this session.

The average concentration of Ag-NPs and dissolved silver in the influent are summarised in Table 6-2. Although both citrate and PVP Ag-NPs had an average concentration in the 11 $\mu g*L^{-1}$ range; dissolution occurred over twenty-four hours period, and was predominant for the citrate particles (with a %dissolved Ag of 47.84%), for which only 6.30 ± 1.68 $\mu g*L^{-1}$ NPs remained by day 1 compared to 8.68 ± 1.54 $\mu g*L^{-1}$ for the PVP Ag-NPs (%dissolved Ag = 24.0%).

Table 6-2: Ag concentration in OECDss (or influent) on day 0 and day 1

	Ag-NPs concentration day 0	**Ag^+ Day 0**	**Ag-NPs concentration day 1**	**Ag^+ Day 1**
Influent spiked with citrate Ag-NPs	11.06 ± 1.26	0.47 ± 0.16	6.30 ± 1.68	5.29 ± 0.86
Influent spiked with PVP Ag-NPs	11.90 ± 2.10	0.32 ± 0.03	8.68 ± 1.54	2.88 ± 1.01

The UV-vis spectra of Ag-NPs in the influent are shown in Figure 6-5. On day 0, the MA occurred at the corresponding maximum wavelength (λ_{max}) of 398 nm for both the citrate and PVP Ag-NPs. However, unlike the PVP Ag-NPs, λ_{max} of citrate Ag-NPs did not remain constant after 24 hrs (Table 6-2), exhibiting a redshift of the UV-Vis spectrum to 408 nm. Also, there was a significant decrease in the intensity of the citrate Ag-NPs compared to the Influent_day 0 of the citrate Ag-NPs; the UV-Vis absorbance of influent sample of the PVP Ag-NPs showed a minimal change in absorbance intensity at day 1 compared to day 0.

Together, the redshift and the decreased intensity indicated that citrate-capped Ag-NPs were more prone to dissolution over time compared to the PVP-capped Ag NPs.

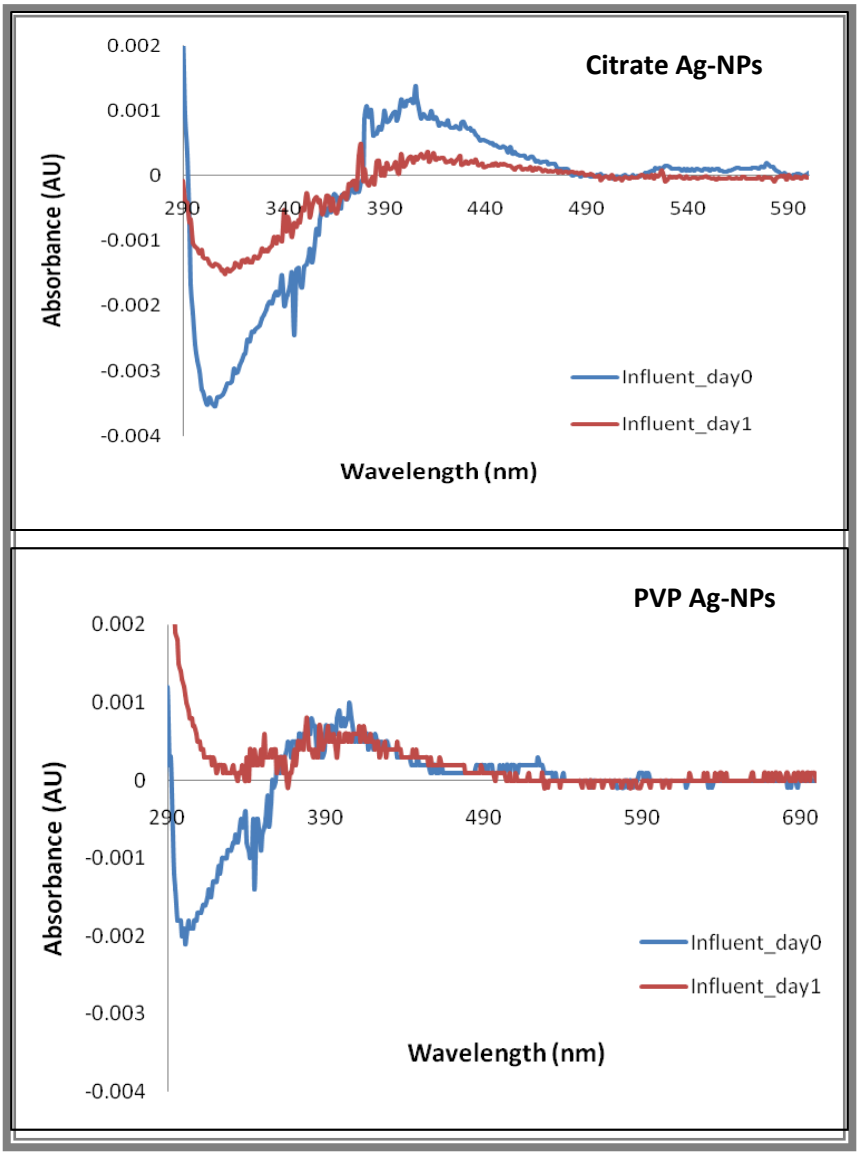

Figure 6-5: UV-Vis characterisation of 10 µg/L citrate and PVP Ag-NPs in the influent (OECDss) initially upon addition, and after 24 hrs, prior to treatment in the SBR plant pilot.

The DLS size distributions of the particles (Figure 6-6 and Table 6-3) show that Ag-NPs aggregated in the synthetic sewage with PDI averaging 0.45 in both cases. Since the Z-average

does not mean much due to the presence of the multiple peaks (see Chapter 3), the average size of the first peak might be considered for the description on the NPs D_H.

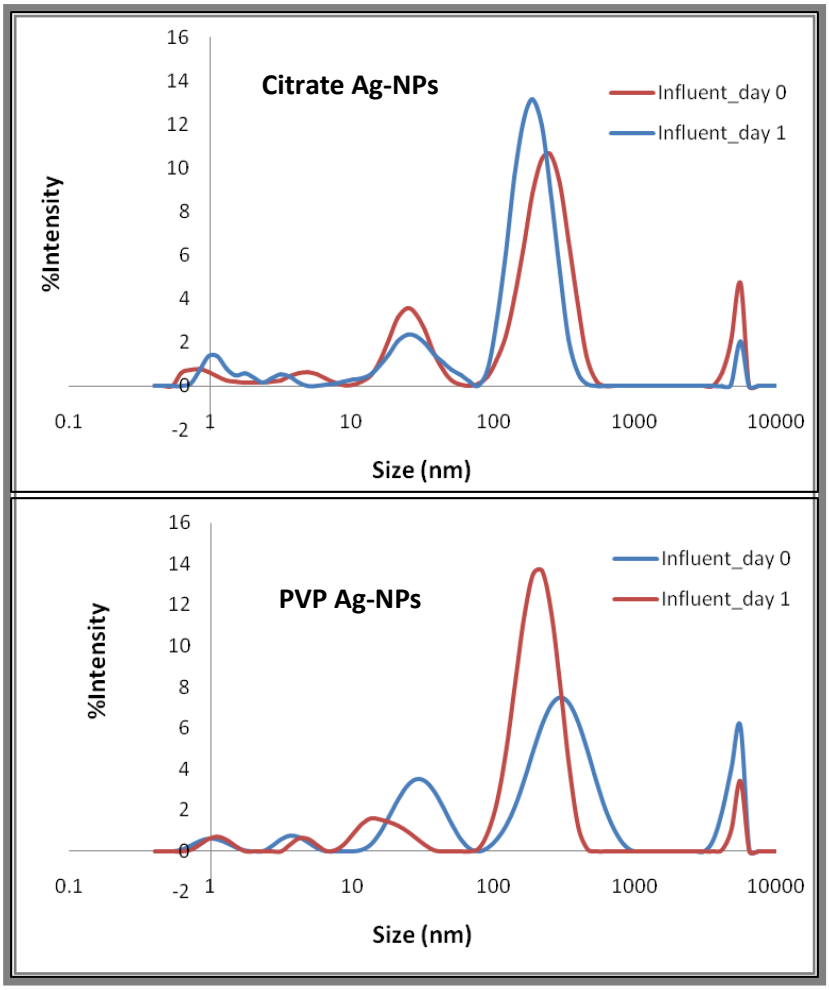

Figure 6-6: DLS size distribution of 10 µg*L^{-1} citrate and PVP Ag-NPs in the influent (OECDss) prior to treatment in the SBR pilot plant

Table 6-3: UV-Vis maximum wavelength absorbance (λ_{max}) and DLS data of Ag-NPs in the influent

	λmax (nm) day0	λmax (nm) day1	Z-average (nm) Day0	Z-average (nm) Day1	Peak 1 Day0	Peak 2 Day1
Influent spiked with citrate Ag-NPs	398	408	267.0 ± 72.4	285.9 ± 52.5	26.9 ± 4.7	23.9 ± 16.6
Influent spiked with PVP Ag-NPs	398	398	227.1 ± 63.0	284.9 ± 58.2	31.1 ± 3.6	18.4 ± 6.1

6.3.3. Detection of Ag-NPs accumulation in aerated wastewater treatment pilot plant over 21 days

Here, the UV-Vis data of the sewage over the twenty-one day period are described. The characterised samples were collected during aeration from the middle and bottom of the tank (TMA and TBA respectively), during settling from the top, middle and bottom (TTS, TMS and TBS) and from the effluent (TES) every second day. The experiment was replicated using two different reference solutions. A control sewage sample without addition of Ag-NPs, or silver ions (Ag^+) (Figure 6-7 and Figure 6-8) and a control sewage sample made with an influent medium spiked with 10 $\mu g*L^{-1}$ of Ag^+ (Figure 6-9and Figure 6-10). The maximum wavelengths of the UV-Vis spectra are given in Table 6-4 and Table 6-5.

From these results, it was observed that the detection of silver was better using a background sewage sample containing Ag^+ of a concentration similar to the Ag-NPs concentration in order to improve the detection limit of the UV-Vis. The background sewage sample was collected from the control tank that was filled with an influent containing 10 $\mu g*L^{-1}$ of Ag^+. Table 6-5 shows that during aeration, detection of Ag-NPs by UV-Vis was obtained from day 12 for the citrate and from day 16 the PVP Ag-NPs; the characterised samples were the samples collected from the bottom of the tank (TBA). Also, during the settling phase, the presence of Ag-NPs was observed from day 11. Although there were few samples for which λ_{max} ranged between 384 and 404 nm, the rest of the samples had their MA occurring at λ_{max} between 348 and 361 nm. Thus UV-Vis spectrum of Ag-NPs was blue-shifted for both citrate and PVP Ag-NPs, which we propose is related to a change in the surface chemistry. According to Kumar and Anthony (2014), the presence of both nitrite (NO_2^-) and nitrate (NO_3^-) ions causes the

appearance of a silver peak at 360 nm and a disappearance of the peak at 426 nm and the colour of Ag-NPs solution to change from yellow to grey. Therefore, the detected UV-Vis peak λ_{max} ranging between 348 and 361 nm might be due to the high level of NO_2^- and NO_3^- in the sewage that might have caused the formation of Ag-NPs and AgCl precipitates.

Table 6-4: UV-Vis measurement of sewage medium spiked with 6 µg*L^{-1} of 10 nm citrate or PVP Ag-NPs every other day. The measurements were conducted using a control sewage sample with no addition of Ag-NPs or Ag+ ions.

Aeration phase	λ_{max} (nm) during aeration citrate Ag-NPs	λ_{max} (nm) during aeration PVP Ag-NPs	Settling phase	λ_{max} (nm) during settling citrate Ag-NPs	λ_{max} (nm) during Effluent citrate Ag-NPs	λ_{max} (nm) during settling PVP Ag-NPs	λ_{max} (nm) during Effluent PVP Ag-NPs
Day 2	NA	NA	Day 3	457	NA	NA	NA
Day 4	NA	NA	Day 5	NA	395	NA	386
Day 6	NA	NA	Day 7	NA	NA	NA	NA
Day 8	NA	NA	Day 9	NA	NA	NA	NA
Day 10	NA	NA	Day 11	NA	359	NA	NA
Day 12	387	NA	Day 13	NA	403	NA	NA
Day 14	354	NA	Day 15	NA	358	NA	NA
Day 16	357	NA	Day 17	NA	357	NA	NA
Day 18	NA	NA	Day 19	407	391	303	NA
Day 20	NA	NA	Day 20	NA	NA	318	NA

Table 6-5: UV-Vis measurement of sewage medium spiked with 6 µg*L^{-1} of 10 nm citrate or PVP Ag-NPs every other day. The measurements conducted using a control sewage sample spiked with Ag+ ions.

Aeration phase	λ_{max} (nm) during aeration citrate Ag-NPs	λ_{max} (nm) during aeration PVP Ag-NPs	Settling phase	λ_{max} (nm) during settling citrate Ag-NPs	λ_{max} (nm) during Effluent citrate Ag-NPs	λ_{max} (nm) during settling PVP Ag-NPs	λ_{max} (nm) during Effluent PVP Ag-NPs
Day 2	NA	NA	Day 3	NA	NA	NA	NA
Day 4	NA	NA	Day 5	NA	NA	NA	NA
Day 6	NA	NA	Day 7	NA	NA	NA	NA
Day 8	NA	NA	Day 9	NA	NA	NA	NA
Day 10	351	NA	Day 11	348	358	346	345
Day 12	384	NA	Day 13	394	389	NA	NA
Day 14	393	NA	Day 15	397	358	394	NA
Day 16	357	354	Day 17	404	353	404	354
Day 18	361	361	Day 19	NA	361	361	361
Day 20	358	361	Day 20	NA	361	361	361

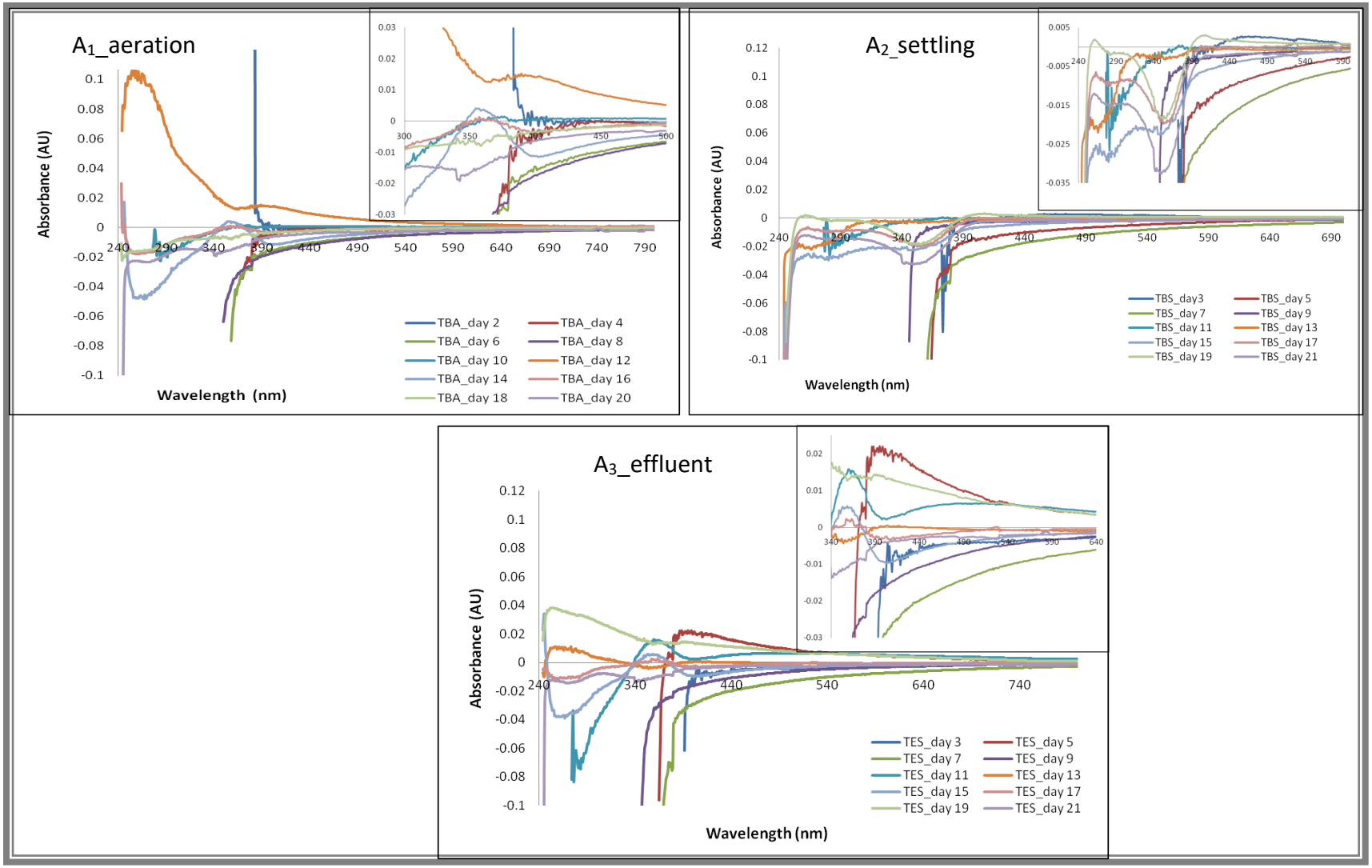

Figure 6-7: UV-Vis spectra of Ag-NPs in sewage spiked with 6 µg*L^{-1} of 10 nm citrate every other day. Measurements were conducted with a background control of filtered effluent without Ag^+ added. With this background, UV-Vis absorbance of most aeration and settling samples was negative, meaning nothing was detected for most samples with the exception of the some effluent samples. Samples collected respectively from the bottom of the tank during aeration (A_1_aeration), from bottom of the tank during settling (A_2_settling) and from the effluent (A_3_effluent).

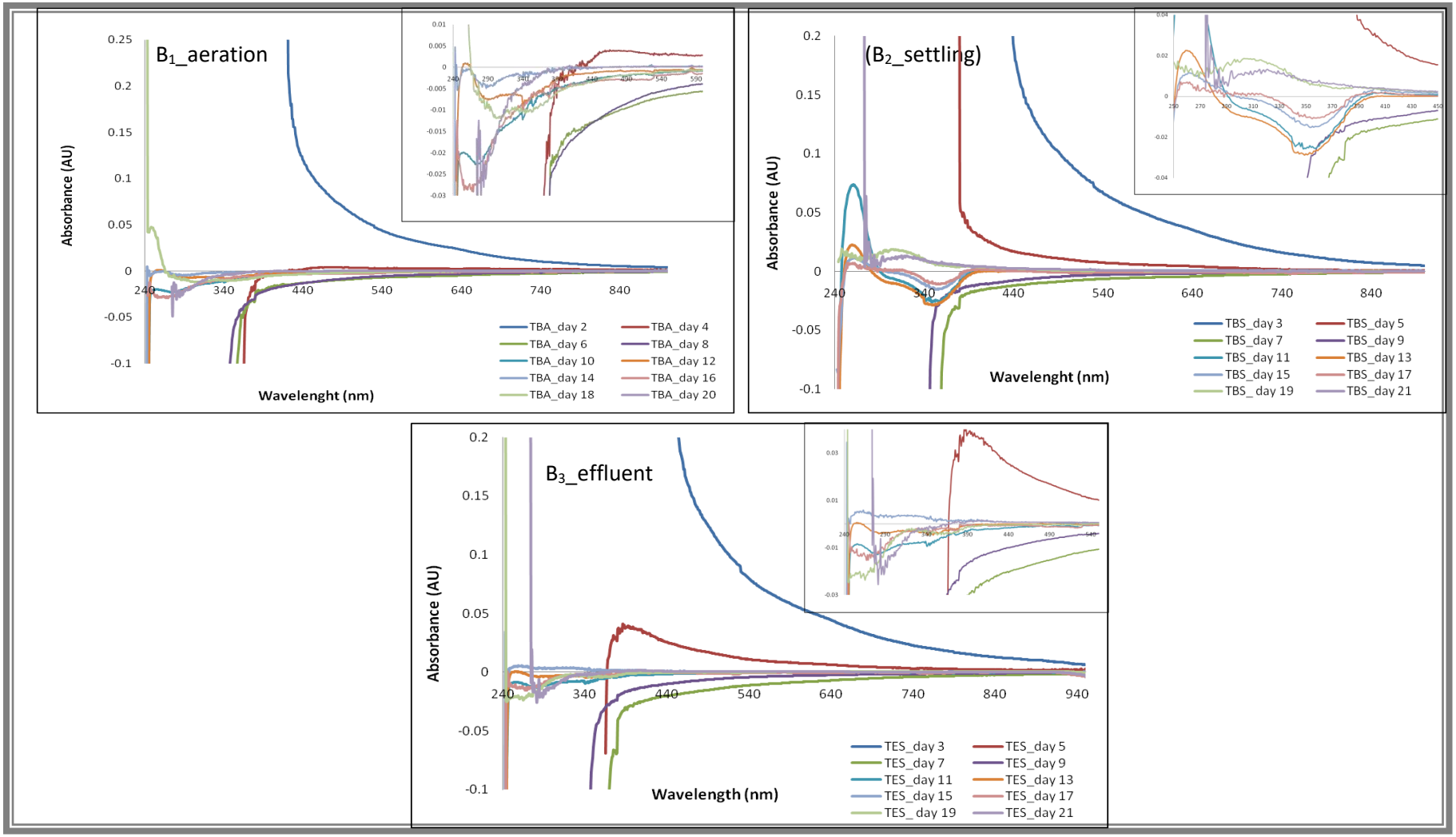

Figure 6-8: UV-Vis absorbance of Ag-NPs in sewage spiked with 6 µg*L^{-1} of 10 nm PVP Ag-NPs every other day. Measurements were conducted with a background control of filtered effluent without Ag^{+} added. With this background, Ag-NPs UV-Vis absorbance of most aeration, settling and effluent samples was negative, meaning nothing was detected. Samples collected respectively from the bottom of the tank during aeration (B_1_aeration), from bottom of the tank during settling (B_2_settling) and from the effluent (B_3_effluent).

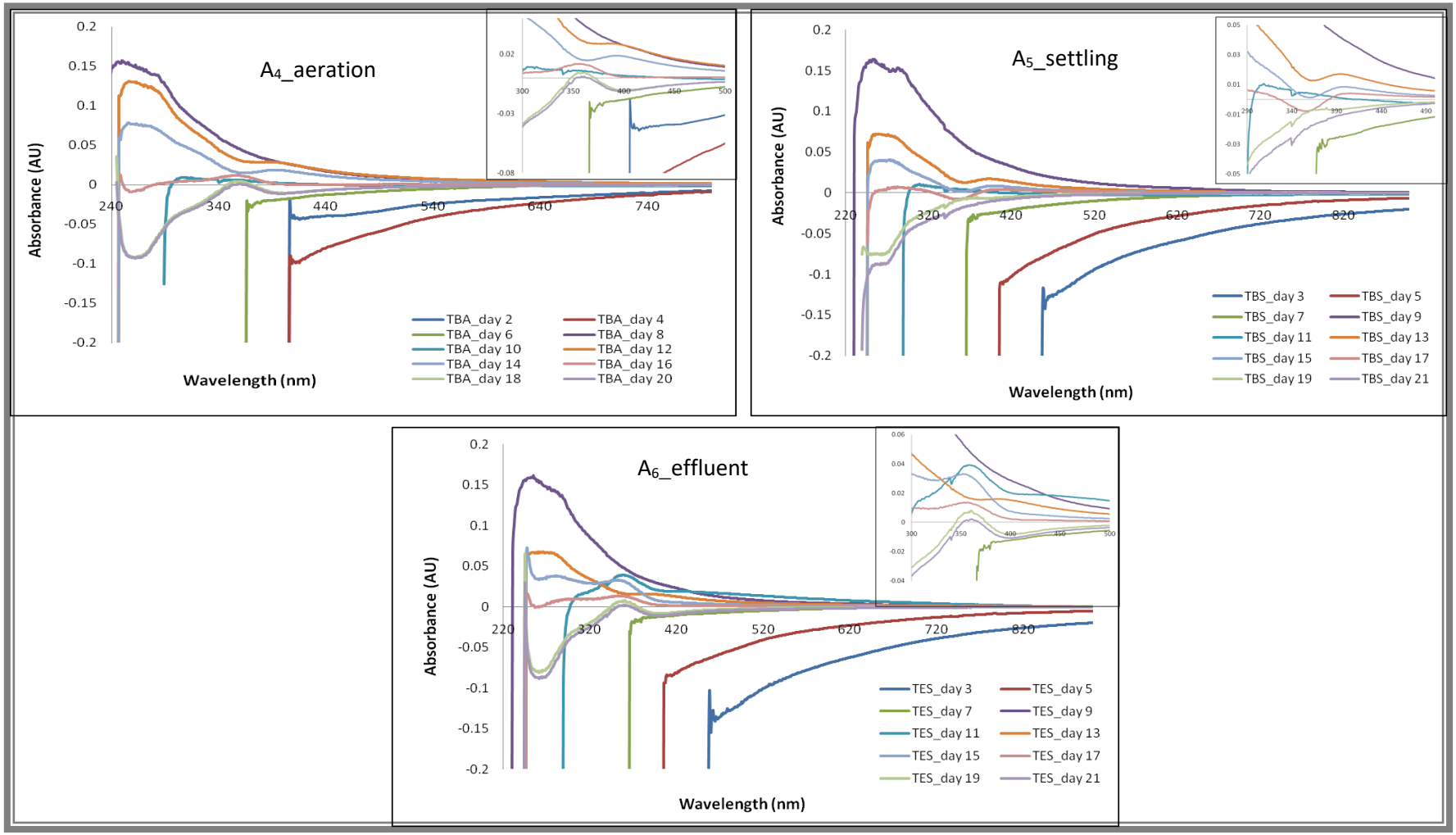

Figure 6-9: UV-Vis spectrums of Ag-NPs in sewage spiked with 6 µg*L^{-1} of 10 nm citrate Ag-NPs every other day. Measurements were conducted with a background control of filtered effluent of the control tank spiked with 6 µg*L^{-1} Ag^+ every other day. With this background, the detection of Ag-NPs by UV-Vis occurred from day 10 during aeration and from 11 day settling and in the effluent. Samples collected respectively from the bottom of the tank during aeration (A_4_aeration), from bottom of the tank during settling (A_5_settling) and from the effluent (A_6_effluent).

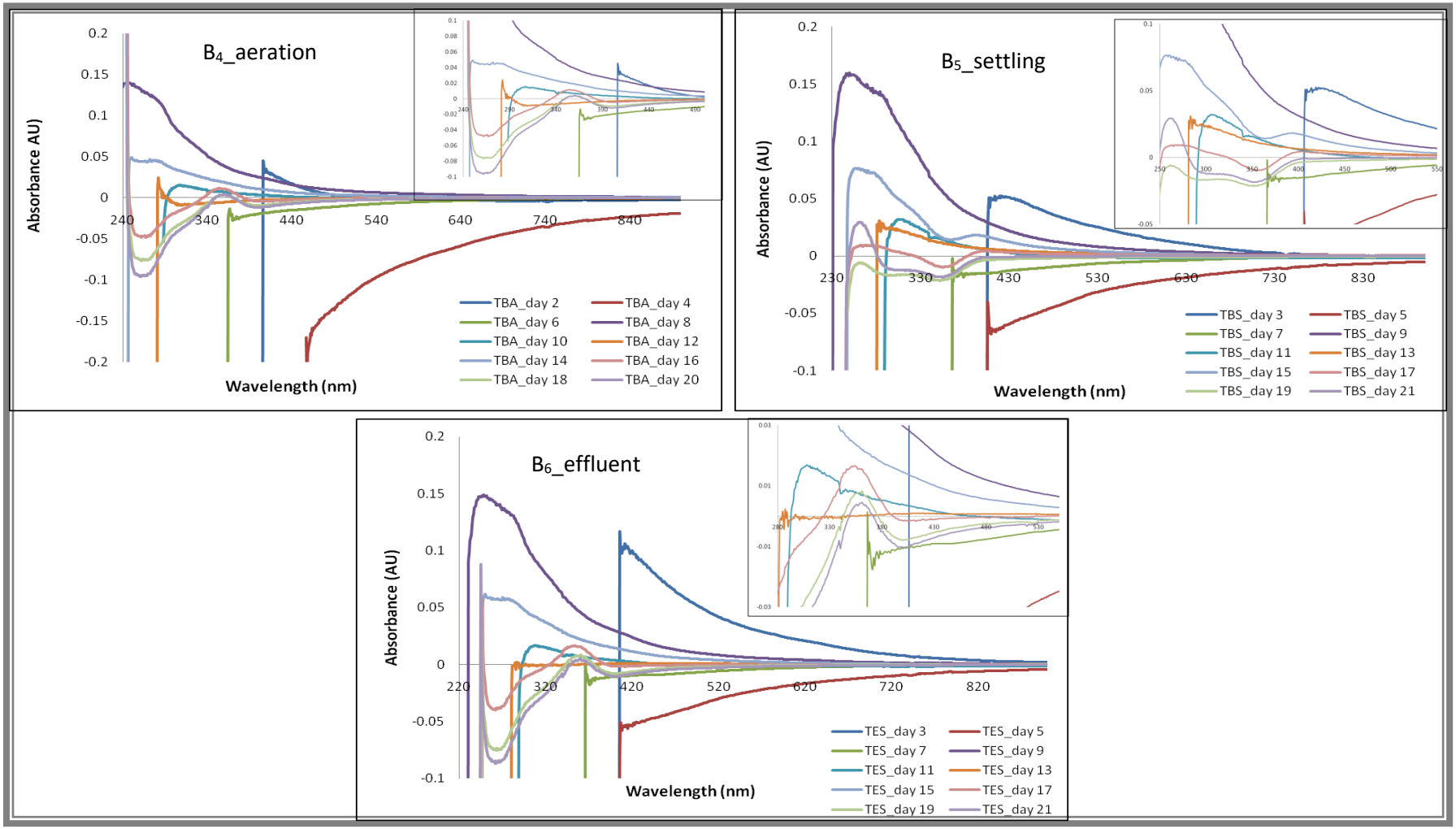

Figure 6-10: UV-Vis spectra of Ag-NPs in sewage spiked with 6 µg*L^{-1} of 10 nm PVP Ag-NPs every other day. Measurements were conducted with a background control of filtered effluent spiked of the control tank spiked with 6 µg*L^{-1} Ag^+ every other day. With this background, the detection of Ag-NPs by UV-Vis occurred from day 16 during aeration and from 11 day settling and in the effluent. Samples collected respectively from the bottom of the tank during aeration (B_4_aeration), from bottom of the tank during settling (B_5_settling) and from the effluent (B_6_effluent).

6.3.4. Ag concentration in aerated wastewater treatment pilot plant over 21 days period

In this section, the changes in concentration as more Ag-NPs were added to the sewage through time are discussed. The Ag-NPs concentration was estimated as follows:

- The total Ag and the dissolved Ag concentration of each p collected test (T_p (total Ag) and T_p (Ag^+)) and control sample (C_p (total Ag) and C_p (Ag^+)) was measured;
- Then the amount of Ag-NPs of each p collected was calculated:
  - Test sample: $T_p(Ag - NPs) = T_p(totalAg) - T_p(Ag^+)$
  - and control sample: $C_p(Ag - NPs) = C_p(totalAg) - C_p(Ag^+)$
- Thus, we then estimate the amount of dispersed Ag-NPs in each p test sample using the following equation: $T_{p_{dispersed}}(Ag - NPs) = T_p(Ag - NPs) - C_p(Ag - NPs)$

The results are divided into three subsections:

(1) The concentration of Ag-NPs in the sewage during aeration; samples were taken from the middle and bottom of the reactor at day l (where l is a natural number and $1 \leq l \leq 10$) (Figure 6-11). The concentration of Ag-NPs in the tank during aeration at day 2l was the average concentration of Ag-NPs between the two collected samples.

(2) The concentration of Ag-NPs in the effluent; samples were collected at day 2l + 1 from the top and middle parts of the reactor and also from the effluent after its removal from the plant. The average concentration of Ag-NPs in the effluent was represented by the average concentration of the Ag-NP between TTS, TMS and TES.

(3) Concentration of Ag-NPs in the sludge. This was measured from the samples collected from the bottom of the reactor after removal of the effluent.

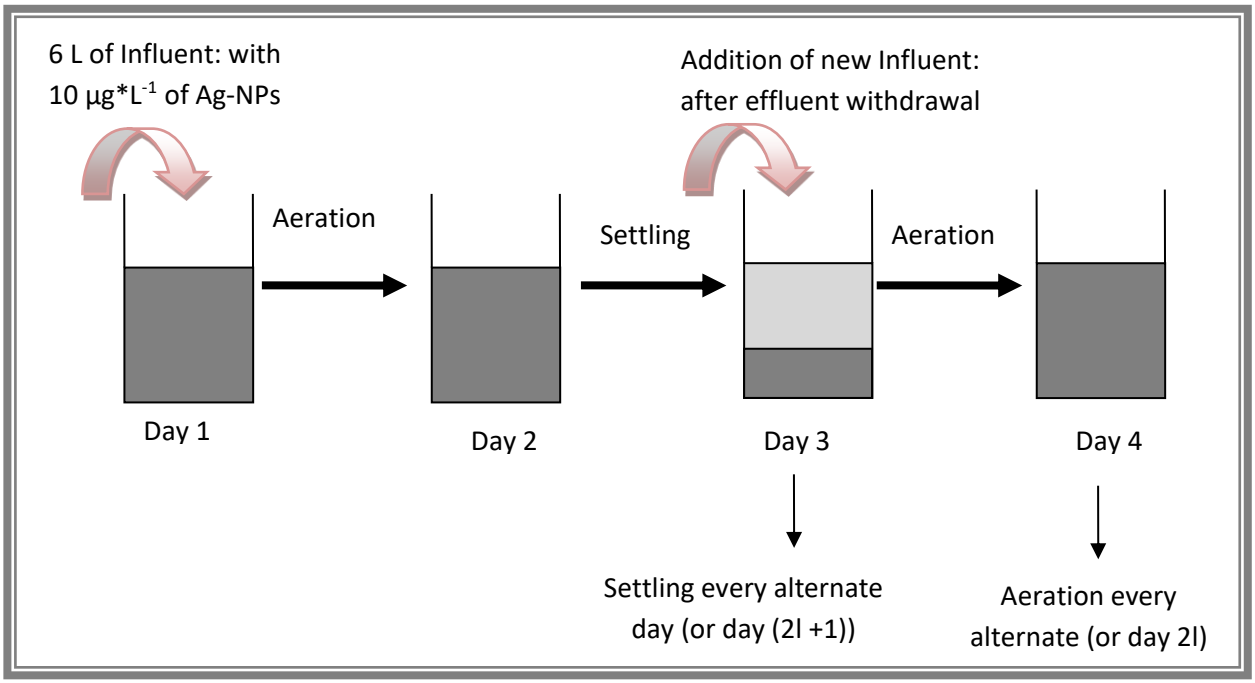

Figure 6-11: Illustration of the experiment showing the different steps taking place during this study

The unpaired t-test was used to investigate the changes in the concentration of citrate and PVP Ag-NPs in the sewage during aeration and the effluent and sludge during the settling phase. Because the chemical state of the silver retained in sludge for this work was unknown; hence it was qualified as Ag-colloids for the rest of the chapter.

The concentration of Ag-colloids in the sewage during aeration and over the twenty-one day period is shown in Figure 6-12. From this figure, it was observed that the Ag-colloids were accumulating with time. Since the plant was filled ten times with an influent OECDss spiked with 10 µg*L^{-1} citrate or PVP Ag-NPs, the total concentration of Ag-NPs transferred into the reactor at the end of the experiment was expected to be 100 µg*L^{-1}. However, because the particles were partially dissolved within 24 hrs of their dispersion in OECDss, total Ag-NPs concentration of citrate and PVP Ag-NPs that entered the plant by the end of the experiment was 60.3 and 86.8 µg*L^{-1} respectively. However, only 6 L of the influent was discharged on

day 21, meaning that the total citrate and PVP Ag-NPs exposed to the sewage in the tank was about 36 and 55.1 $\mu g*L^{-1}$ respectively. Based on these values and the results shown in Figure 6-12, it could be assumed that about 70 and 44% of citrate and PVP Ag-NPs respectively were absorbed in the sludge by day 20.

The application of an unpaired t-test on the measured Ag-colloids concentration, in the presence of an aeration flow, shows that there was no difference in the level of Ag accumulation in the SBR plant pilot between the citrate and PVP particles (P-Value = 0.48). This leads us to conclude that the level of adsorption of Ag-colloids in the sludge was independent of their capping agent.

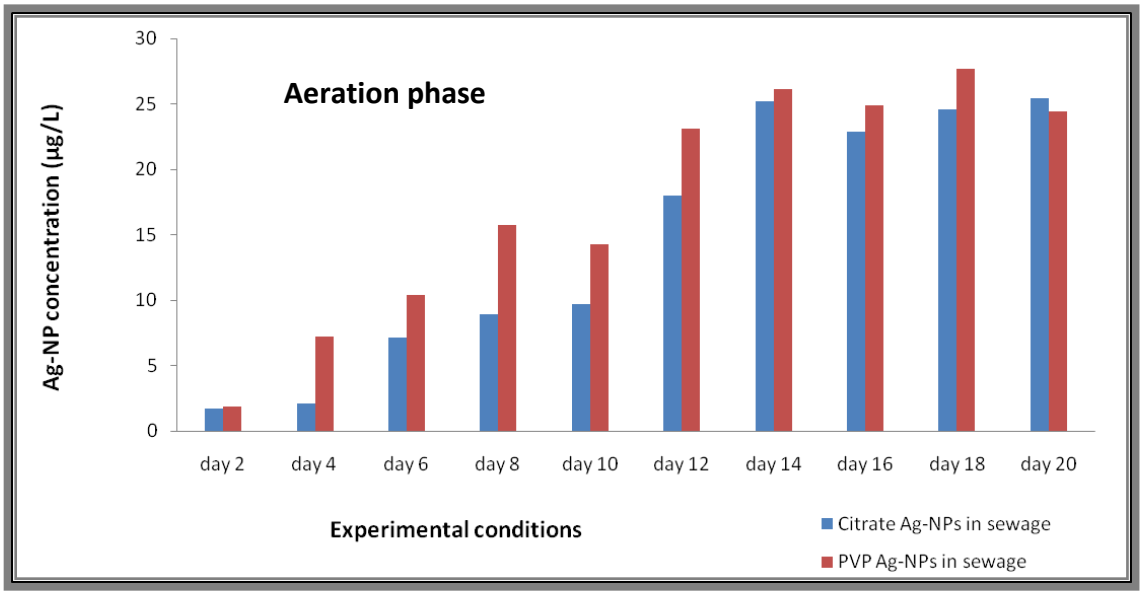

Figure 6-12: Ag-NP concentration in the sewage over twenty-one day period with 6 $\mu g*L^{-1}$ spiked influent added every 2 days. Samples collected during aeration as measured by GFAAS

During the settling phase, the presence of Ag-colloids in the effluent for both citrate and PVP particles was low or nearly non-existent, as seen in Figure 6-13. The application of an unpaired t-test on the two sets of data shows that there was no significant difference regarding the

concentration of Ag-colloids present in the effluent (P-value = 0.078). Hence, the capping agent had no influence on the amount of the Ag-colloids remaining in the effluent.

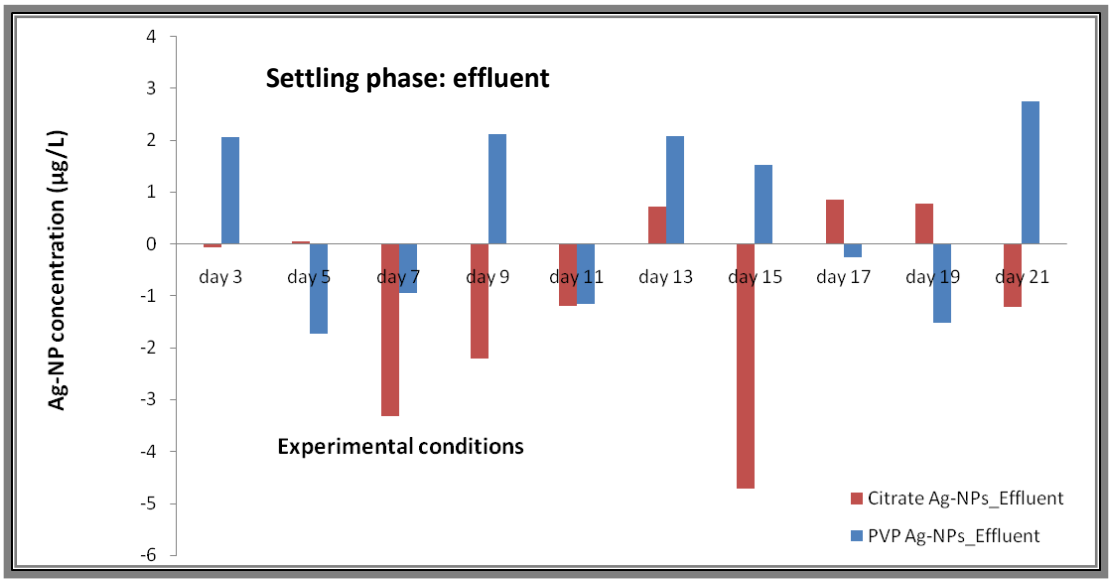

Figure 6-13: Ag-NP concentration in the effluent over twenty-one day period as measured by GFAAS.

The changes in the concentration of Ag-colloids in the activated sludge over the twenty-one day period are illustrated in Figure 6-14, and it can be seen that the amount of Ag-colloids in the activated sludge had increased with time for both citrate and PVP Ag-NPs. Also, about 70 and 55% of Ag-colloids respectively from citrate and PVP Ag-NPs were absorbed by the sludge. A t-test (P-value of 0.37) shows that removal of Ag-NPs was independent of the capping agent during settling.

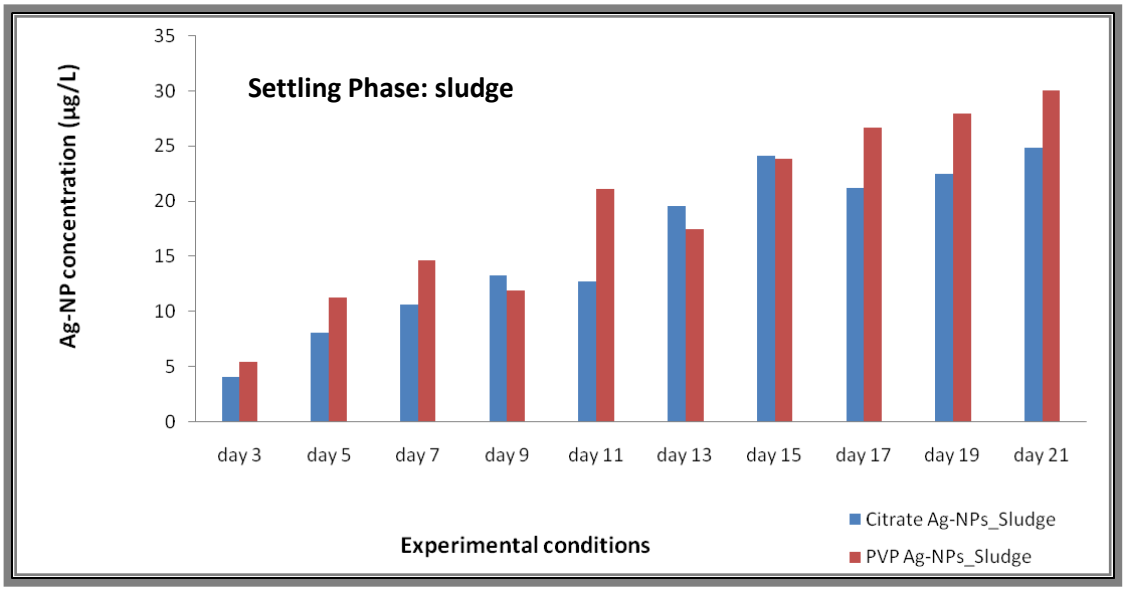

Figure 6-14: Ag-NP concentration in the activated sludge measured over twenty-one day period as measured by GFAAS.

6.3.5. Estimation of Ag-NPs removal in the SBR plant pilot

Kang et al. (2014) used the adsorption isotherm model to estimate the removal of heavy metal in a sewage treatment plant based on the adsorption mechanism of the metals by the inorganic materials and the activated sludge. A similar model was applied in this study. However, instead of a WWTP with three step processes including a primary clarification, aeration and secondary clarification stage, there was only one step in our case, namely aeration. In fact, for an SBR treatment plant, the primary clarification and aeration occur in the same tank, and there is no secondary clarification (Aziz et al., 2011). The removal of Ag-NPs from the sewage was determined using the batch sorption experiment (Desta, 2013) by assuming that the full amount of Ag-NPs that were mixed in the tank were incorporated all at once in volume V of the sewage. The schematic of the model could be represented as follows (Figure 6-15):

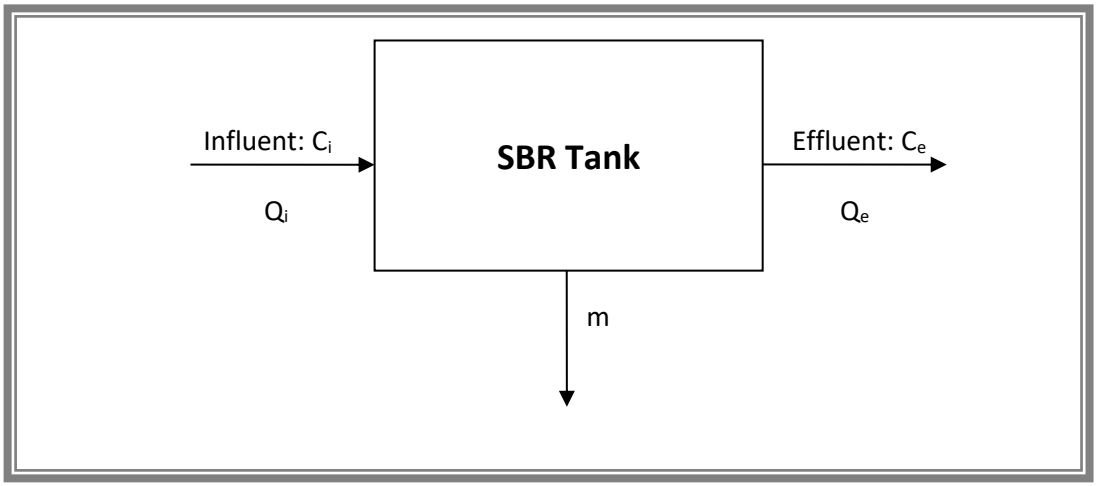

Figure 6-15: The mass balance schematic of the flow through the SBR pilot plant. Qi and Qe (L/day) are respectively the inflow and outflow of the tank, m is the mass rate of Ag-NPs, C_i and C_e ($g*L^{-1}$) are the Ag-NPs concentrations.

The mass balance of the system is written as follows:

$$Q_i C_i - Q_i C_i = m$$

Equation 6-1

Where Q_i is the inflow of the tank (in $L*d^{-1} = L*day^{-1}$), Q_e is the outflow of the tank (in $L*d^{-1} = L*day^{-1}$), C_i is the Ag-colloids concentrations of the influent (in $g*L^{-1}$), C_e is the Ag-colloids concentrations the effluent (in $g*L^{-1}$) and M is the mass rate of Ag-colloids removal in the tank (in g);

It is assumed here that the removal of Ag-colloids occurred by their adsorption in the sludge, the mass rate could be written as a function of the activated sludge mass M_s (in $g*d^{-1}$) and the coefficient partition of Ag-colloids in the tank K_s (in $L*g^{-1}$).

$$m = M_s K_s C_e$$

Equation 6-2

By combining Equation 6-1 and Equation 6-2 and assuming conservation of mass (i.e. that inflow and outflow are equal), the equation can be written as:

$$\frac{M_s K_s}{M_s K_s + Q_i} = \frac{C_i - C_e}{C_i} = R$$

Equation 6-3

Where R is the removal coefficient of Ag-colloids by adsorption to the sludge (generally given in percentage).

The variation of Ag-colloids removal over time for both citrate and PVP case is presented in Figure 6-16 where it is shown that the average percentage removal of the particles over 21 days was 44% and 47.7% for citrate and PVP Ag-colloids respectively. The unpaired t-test analysis gave a P-value of 0.68, indicating that there was no difference in the uptake of citrate Ag-colloids compared to the PVP Ag-colloids.

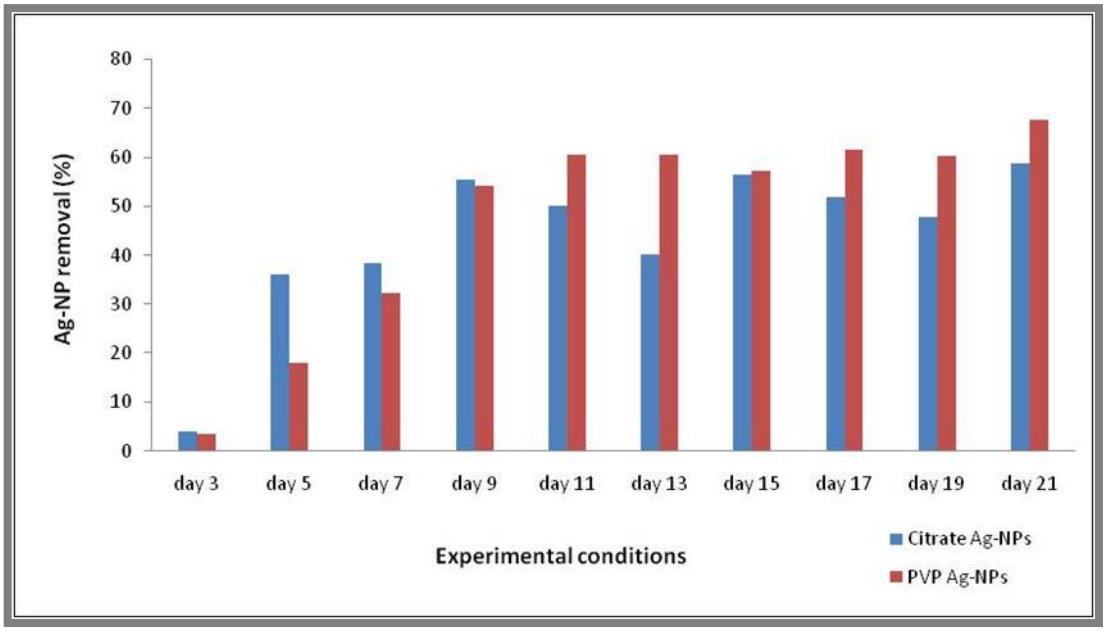

Figure 6-16: Removal coefficient in percentage of Ag-colloids in the sludge over time.

6.3.6. Batch adsorption operation: Freundlich isotherm

The description of Ag-colloids adsorption in the sludge or inorganic material particulates present in the sewage is given here. The Freundlich isotherm was used based on the assumption that the surface of the adsorbent was heterogeneous (Amuda et al., 2007, Desta, 2013). The Freudlich isotherm is an empirical model represented by Equation 6-4 :

$$q = K_f C^{1/n}$$

Equation 6-4

Where q is the Amount of Ag-adsorbed per g of activated sludge (in $\mu g*g^{-1}$), C = Measured concentration of Ag-in the activated sludge after settling ($\mu g*L^{-1}$), K_f are the Freundlich constant and n (n > 0) are the Freundlich constants representing respectively, the adsorption capacity and intensity and are determined by linearisation of the Freundlich equation (Equation 6-4) (Desta, 2013).

$$\ln q = \ln K_f + \frac{1}{n} \ln C$$

Equation 6-5

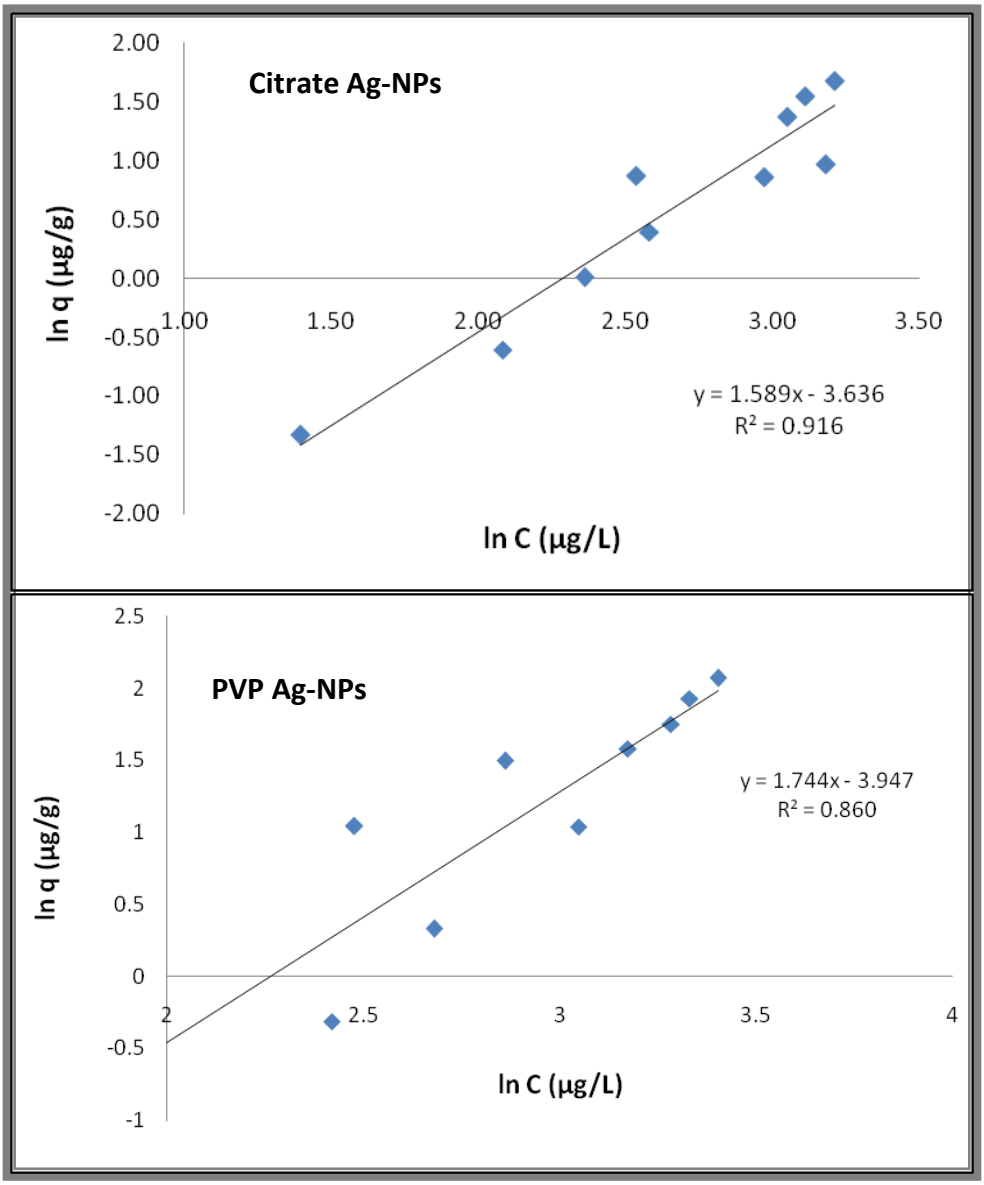

Figure 6-17: Linearisation of the Freundlich isotherm model, representing logarithmic variation of the amount of Ag-colloids adsorbed to the activated sludge with respect to their corresponding logarithm concentration over 21 days.

The uptake, q, of Ag-colloids in the activated sludge was determined from the mass balance (Equation 6-1) which is formulated as follows (Desta, 2013):

$$q = \frac{(C_i - C_e)}{m} V_i$$

Equation 6-6

Where V is the volume of the influent used during the treatment (in L) and m the activated sludge mass (in g).

From the analysis of the sewage given in section 6.2, TS in the activated sludge prior to treatment, was found to be 22 ± 0.16 mg*mL^{-1}. For 4 L of the active sludge transferred into the tank, the mass of solids in the SBR plant pilot was approximately equal to 88 g on day 1. However, this mass was found to reduce each day because of the collection of the samples during the aeration phase, on day 21and the settling phase, on day 21 + 1 with l varying between 1 and 10. In fact, about 200 mL of sewage was collected in total during both phases with an estimates solid mass of:

$$m_r(2i) = \frac{m_{2p}}{V} 0.26.26.2$$

Equation 6-7

Where m_r is the mass of solids removed on day 2l (in g) and V is the total sewage volume (V = 10 L)

Hence the mass of TS on day 2l+ 1 during the settling phase was:

$$m_{2p+1} = m_{2p} * \frac{(V - 0.2)}{V}$$

Equation 6-8

and

$$q_{2p+1} = \frac{(C_i - C_e)}{m_{2p+1}} Vi$$

Equation 6-9

Hence in this study, the Freundlich isotherm was represented by the equation:

$$\ln q_{2p+1} = \ln K_f + \frac{1}{n} \ln C_{2p+1}$$

Equation 6-10

Figure 6-17 shows the Freundlich isotherm applied to the batch experiment with Ag^+ released from the Ag-colloids being the adsorbates and the activated sludge being the adsorbent. The Freundlich constants and the correlation coefficient of the citrate and PVP Ag-NP isotherms are given in Table 6-6. The constant n represents the degree of nonlinearity between the concentration of Ag-colloids in the sewage and their adsorption in the activated sludge (Desta, 2013).

Table 6-6: Freundlich isotherm coefficient for the adsorption of Ag-NPs in the activated sludge

	n	Kf	R^2
Citrate Ag-NPs	0.629	0.026	0.916
PVP Ag-NPs	0.573	0.019	0.860

Depending on its value, n gives the information on the type of adsorption occurring for the Ag-colloids at the surface of the activated sludge particulates. The ranges of n values for comparison are listed in Table 6-7.

Table 6-7: Ranges of n comparing the type of adsorption that may occur during the process

	Type of Freundlich isotherm
n > 1	Chemical process adsorption
n = 1	Linear adsorption
n >1	Physical process adsorption

The Freundlich isotherms of the adsorption of citrate and PVP Ag-NPs by the activated sludge have the constant n < 1, meaning the adsorption of the Ag-colloids through the sludge particles was physical.

6.4. Discussion and Conclusion

The accumulation and removal of Ag-NPs in the SBR pilot plant were demonstrated in this chapter. The results of section 6.3.1 have shown that by using OECDss + Ag-NPs as the influent, the treatment of the sewage in an SBR plant pilot over a 21 day period was relatively efficient with 97 to 99% of total solids removed from the effluent by day 21. The characterisation of the influent by DLS, UV-Vis, and GFAAS (section 6.3.2) demonstrated that the dispersed citrate and PVP Ag-NPs in OECDss were aggregated and partially dissolved before treatment; with 47.8% and 24.2% dissolved Ag percentage for citrate and PVP Ag-NPs respectively.

The accumulation of the Ag-NPs in the activated sludge over the twenty-one day period was detected by UV-Vis (section 6.3.3), and it was observed that the Ag-NPs were accumulated in the sludge through time. However, the surface chemistry of Ag-NPs might have changed through precipitation mechanism for both citrate and PVP Ag-NPs, due to a blue-shift of their UV-Vis peak compared to the pristine particles observed for both (Chapter 4). The values of the wavelength at MA (Table 6-4 and Table 6-5) which correspond to the wavelength associated with Ag-NPs dissolution through oxidation by NO_2^- (Kumar and Anthony, 2014) present in the sewage. In fact, Kumar and Anthony (2014) had shown that in the presence of NO_2^-, Ag-NPs dissolved via NO_2^- oxidation causing discoloration of the pristine Ag-NPs solution from yellow to clear, hence the shifting of the absorbance peak from around 400 nm to around 360 nm. However, the dissolved silver immediately precipitated into AgCl due to the presence of NaCl in the solution (Figure 6-18).

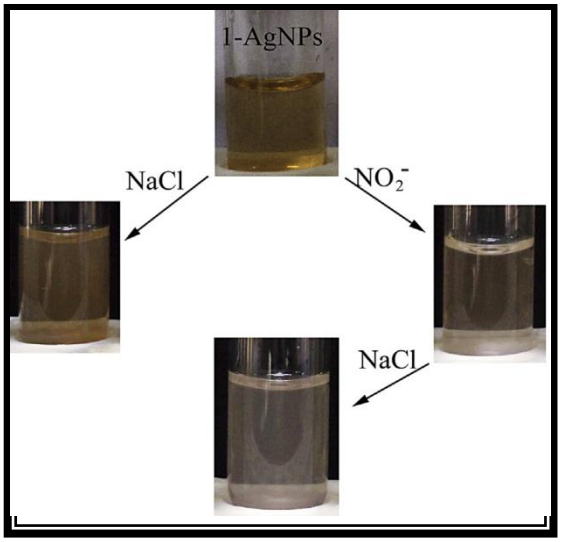

Figure 6-18: AgCl precipitates formed from released functionalised Ag-NPs by NO_2^- oxidation (Kumar and Anthony, 2014).

In our case, the blue-shift of Ag-NPs might have been due to the release of Ag^+ via NO_2^- oxidation; with NO_2^- formed through ammonia-oxidising bacteria (Michels et al., 2015) present in the sludge. The resulting Ag^+ had likely precipitated to Ag_2S and (or) AgCl which settled into the sludge biosolids and bound there. So, the release of Ag-NPs in the SWTP might have caused their dissolution by NO_2^- oxidation, causing a temporary formation of nitrous oxide (N_2O also known as the greenhouse gas) which can be detrimental to the environment concerning air pollution (Michels et al., 2015).

The GFAAS results showed that about 44 and 48% of the citrate and PVP Ag-NPs were removed by the activated sludge. This percentage is lower than what was observed in the literature (Hou et al., 2012, Kaegi et al., 2013), and may suggest that the remaining Ag-NPs were present in a dissolved form or adsorbed to the influent bottle, tank walls or the stirrer paddle. This could have been verified by filling the influent bottle and the tank with a diluted

20% NHO_3 acid solution; the paddle should also be left in the tank. The 20% NHO_3 acid obtained solution can be diluted to 0.2% the next day and analysed by GFAAS.

The statistical analysis of the data has shown that the removal of Ag-NPs was independent of their capping agent. Finally, the application of the Freundlich isotherm model demonstrated that the adsorption of Ag-NPs in the activated sludge was physical.

Chapter 7 Conclusions and further work

Chapter Summary

The increase of Ag-NPs usage in consumer products in recent years has brought with it a need to understand the implications of their release into the environment through the sewer and wastewater systems. In fact, these Ag-NPs might be discharged into natural waters through the treated effluent released from WWTPs if they dissolve during the treatment process and release Ag^+. Ionic Ag is known to be toxic to freshwater biota. A further route into the environment may be through Ag-NP remaining in particulate form and accumulating in sewage sludge, if this is subsequently used as fertiliser that releases Ag NPs into the soil. For these reasons, the behaviour, fate and transportation of Ag-NPs in the sewage and aerated WWTP or SBR plant pilot are investigated in this thesis. This last chapter gives conclusions drawn from the results and discussions of chapters 4 to 6. Future research interests that might help to fully understand how Ag-NPs, along with other NPs, might behave in a completed lab scale WWTP will be of prime importance.

7.1. Conclusions

In this section, we present the conclusions on the different case studies based on the synthesis and characterisation of Ag-NPs, along with their stability in OECDss and their accumulation and removal in an SBR pilot plant.

7.1.1. Aim 1: Ag-NPs synthesis and characterisation

In this part of the work, freshly synthesised citrate Ag-NPs were recapped with PVP and PEG-thiol in order to produce three types of Ag-NPs, which have different capping agents and similar concentration and core size distribution. All three Ag-NPs were fully characterised using a range of characterisation techniques.

It was found that, despite the shared core properties citrate, PVP and PEG capped Ag-NPs were significantly different in surface chemistry and surface area.

Citrate and PVP-capped Ag-NPs were chosen between the three for the next step of the work which included a study of their stability and behaviour in sewage and consideration of their accumulation and removal in the sewage system.

7.1.2. Aim 2: Stability study of Ag-NPs in OECD synthetic sewage (OECDss)

The stability results of the citrate and PVP Ag-NPs in OECDss and its constituents under similar conditions as the treatment of the sewage in the SBR pilot plant have shown that neither type

of NPs was stable in these media. In fact, citrate and PVP Ag-NPs were aggregated and dissolved at different levels over the time and within each stage of the experiment with similar treatment step as for sewage in the SBR pilot plant. It was observed that the presence of an aeration flow affected the surface chemistry of both Ag-NPs in all media. However, the citrate Ag-NPs were prone to dissolution after the aeration stage, while the PVP Ag-NPs were aggregated. Finally, the transformation into AgCl, SP-NPs and Ag_2S of the Ag-NPs exposed to NaCl, $CaCl_2$, K_2HPO_4, $MgSO_4$ and OECDss might have taken place prior the aeration of the media.

7.1.3. Aim 3: Physical and chemical transformation of Ag-NPs in an aerobic WWTP pilot

The results have revealed that Ag-NPs present in the OCEDss influent may be primarily transformed in size, shape, surface area and surface chemistry through aggregation and dissolution. Also, under aeration, the surface chemistry of the NPs was through oxidative dissolution phenomena (Yang et al., 2013c), which caused them the dissolved or aggregate depending on their capping agent and this state, and remain in that state after the aeration was completed.

The EDS results have shown that, in the absence of activated sludge, citrate Ag-NPs may transform into Ag_2S NPS while PVP may transform into AgCl NPs. Uptake of Ag-NPs into activated sludge was about 80% for both citrate and PVP Ag-NPs; which was close the what was found in the literature (Kaegi et al., 2013). Ag-NPs could not be identified by DLS, TEM and EDS when the activated sludge was used, due to the low concentration of the pristine Ag-NPs dispersed in the influences (500 $\mu g*L^{-1}$). Indeed, recent studies reporting the behaviour

of Ag-NPs in WWTP were only possible by using high concentrations of Ag-NPs, enabling their detection by EM characterisations (Kaegi et al., 2011b, Kim et al., 2010, Doolette et al., 2013).

7.1.4.Aim 4: Accumulation and removal of Ag-NPs in an aerobic WWTP

It was revealed in this part of the work that, the dispersion of Ag-NPs in sewage over a relatively long period of time (twenty days in this case) via the influent induced their accumulation in the activated sludge over that time. It was also found from the UV-Vis characterisation that Ag-NPs may have reacted with nitrite (NO_2^-) and nitrate (NO_3^-) causing them to precipitate and have their surface chemistry changed (Kumar and Anthony, 2014). Hence, the appearance of SPR peak at around 360 nm.

The uptake of Ag-NPs by the activated sludge increased over the time of the experiment and the calculation of the mass balance concentration had shown that about 44 and 48% of respectively citrate and PVP Ag-NPs were removed at the end of the treatment cycle. Finally, fitting a Freundlich isotherm on the data showed that the adsorption of Ag-NPs by the activated sludge was physical.

7.2. Further work

For future work, the concentration Ag NPs in the influent can be increase to facilitate detection of NPs using electron microscopy characterisation. Also, characterisation of the chemical structure of Ag-NPs can be carried out by electron energy loss spectroscopy (EELs).

Other characterisation techniques such as the X-ray adsorption near edge spectroscopy structure (XANES) would benefit an in depth understanding of particle transformations.

A model, on the transportation of Ag-NPs in WWTP, could be generated from the GFAAS data and inductively coupled plasma spectroscopy (ICP-MS) results.

Further complementary work could be conducted by using dye or stable isotope labelled Ag-NPs synthesised as citrate, PVP or PEG capped Ag-NPs, similarly to those used in this thesis. This might enable traceability of Ag-NPs in WWTP by using fluorescence confocal microscopy or ICP-MS respectively and operating at low concentrations.

Appendix

A1 Appendix 1: wastewater testing

Table A1 - 1: OECDss chemical components - concentration (mg/L) and molecular weight (g/mol).

OECDss composition	Concentration ($mg*L^{-1}$)	Molecular weight ($g*mol^{-1}$)	Moles of solute (mol)	Molarity (mM)
Peptone	160	NA	NA	NA
Meat-extract	110	NA	NA	NA
Urea (CH_4N_2O)	30	60.06	0.0005	0.5
Anhydrous dipotassium hydrogen phosphate (K_2HPO_4)	28	174.18	0.00016	0.516
Sodium chloride (NaCl, 7 mg)	7	58.44	0.00012	0.12
calcium chloride dihydrate ($CaCl_2.2H_2O$)	4	147.01	0.00027	0.27
magnesium sulphate heptahydrate ($MgSO_4.7H_2O$)	2	246.47	0.0000081	0.0081

A1-1 COD testing: Aquanal –plus Chemical Oxygen Demand (Sigma-Aldrich)

- For the blank value, 2 ml of distilled water is filled into a cuvette. For the measured value, 2 ml sewage sample is filled into another cuvette. Close both cuvettes tightly and mix by careful swaying
- Samples are then digested in a heating system for 2 hours at 148 °C. After heating, the samples are mix again by careful swaying and permit to cool down to room temperature for at least 45 minutes. Stop shaking!
- To read the COD of the samples, a spectrometer is used.

A1-2 Nitrogen testing: Aquanal – professional Nitrogen Cuvette Test (Sigma Aldrich)

❖ Digestion for the analysis of total nitrogen:

- Fill a 5 ml sample into an empty cuvette, close the cuvette and mix by swaying. Add one black level spoonful of digestion reagent, close the cuvette again and mix.
- Digest in a heating block for 60 minutes at 100 °C.
- After 60 minutes are over, remove the cuvette from the heating block, sway it and allow it to cool down to room temperature.

❖ Testing:

- After digestion, add 1 grey spoonful of compensation reagent to the digested sample, close the cuvette and mix.
- Fill 0.5 ml of this solution into a test cuvette, close it and mix. Add 0.2 ml of reagent 1, close the cuvette and mix. Wait 15 minutes until the reaction time is over.
- The total nitrogen is measured with a spectrometer. A blank test is required for calibration.

A1-3 Phosphorus testing:

❖ Digestion for the analysis of total nitrogen:

- Fill a 5 ml sample into an empty cuvette, close the cuvette and mix by swaying. Add 1 grey level spoonful of digestion reagent, close the cuvette again and mix.
- Digest in a heating block for 30 minutes at 100 °C.
- After 30 minutes are over, remove the cuvette from the heating block and allow it to cool down to room temperature.

❖ Testing:

- To analyse the orthophosphate either use the cuvette treated (digested sample) or fill a 1 ml sample into the cuvette (untreated).
- Add 2 drops of reagent 1, close the cuvette and mix. Wait 10 minutes until the reaction if over.

The total phosphorus is measured with a spectrometer. A blank test is required for calibration.

A2 Appendix 2: UV-Vis particles size and statistical analysis theory

A2-1 Determination of the NP size by UV-Vis analysis

UV-Vis characterisation can give information on the NP properties such as agglomeration or polydispersity, size, dissolution and surface chemistry changes. Measuring the full width at half maximum (FWHM), the MA and the degree of shift of the SPR peak toward lower λ (blueshift) or higher λ (redshift), helps to compare the recapped citrate Ag-NPs to the non-recapped ones as well as to analyse the changes of the particles in a media.

The size distribution of the particles can be determined using the method used in previous literature (Baset et al., 2011, Tuchin, 2010, Biswas et al., 2010). Three models can be used to estimate the average size of the particles by UV-Vis.

In the first equation ($model_1$), the particle size is proportional to λ_{max} and inversely proportional to the FWHM (Manikandan et al., 2003, Ashkarran and Bayat, 2013, Picciotto et al., 2010):

$$R = \frac{v_F \lambda_{max}^2}{2\pi C \Delta\lambda} \beta$$

Equation A2 - 1

and

$$\lambda_{max} = 382.6 + 1.18D$$

Equation A2 - 2

Where R is the particle radius (in m), D is the average particle diameter (in m), Δλ is the FWHM (full width at half maximum) of the UV-Vis peak (in m), C is the velocity of light in vacuum (C = 3*108 m*s-1), v_F is the Fermi velocity of an electron gas for the Ag-NPs (v_F = 1.39*106 m*s-1) and β is the proportionality constant depending on the particle core composition and shape.

The second model (model$_2$) is Drude's model relating the dielectric complex (given in Mie's theory in section 2.4.1.2) to the plasmon frequency (Kreibig and Genzel, 1985, Baset et al., 2011, Van Hoonacker and Englebienne, 2006):

$$\Gamma_{PL} = \Gamma_{bulk} + \frac{\beta}{D} = \Gamma_{bulk} + \frac{\hbar . v_F . g(v)}{D}$$

Equation A2 - 3

Where Γ_{PL} is the band width of the capped NPs and is equal to the FWHM (in eV), v_F is the Fermi velocity of the NPs (v_F = 1.39 *10^6 m*s-1), Γ_{bulk} is the scattering velocity of the bulk ($\Gamma_{bulk} = 5 * 10^{12} s^{-1}$ for silver), D is the average diameter of particles (in m), β is the theoretical slope of the linear relationship predicted by Mie theory and $g(v)$ is the complex function defined by the following equation (Kreibig, 1974):

$$g(v) = \frac{(1+v)^{3/2} - (1-v)^{3/2}}{3v^3} - \frac{(2+v)(1+v)^{1/2} - (2-V)(1-v)^{1/2}}{8v^2} + ln\frac{\frac{2+v+(1+v)^{1/2}}{2-v+(1-v)^{1/2}}}{16}$$

Equation A2 - 4

With

$$v = \frac{\hbar\omega_{PL}}{E_F} = \frac{2\pi c\hbar}{E_F\lambda_{max}}$$

Equation A2 - 5

Where ω_{PL} is the plasmon frequency (in s^{-1}), $E_F(=\frac{1}{2}m_e v_F^2)$ in the Fermi energy (E_F = 5.49 eV for silver), $\hbar = \frac{h}{2\pi} = 6.58 * 10^{-16} eV.s$ (with $h = 4.136 * 10^{-15} eV.s$ being Planck's constant).

Finally, $model_3$ consists of using an empirical equation given by Kreibig and Genzel (1985) derived from the expanded version of Mie theory or Drude's model relating the mean free-path of the electron in the bulk material to its frequency damping (Kreibig and Genzel, 1985, Baset et al., 2011):

$$\Gamma_{bulk} = \frac{v_F}{L_\infty}$$

Equation A2 - 6

Where v_F is the Fermi velocity of the NPs (v_F = 1.39 *10^6 m*s^{-1}) and L_∞ is the mean free-path of an electron in the bulk material (in m).

If the particles have an average size approximately in the L_∞ range, the frequency damping is written as a function of the particle radius (R):

$$\Gamma(R) = \Gamma_{bulk} + \frac{Av_F}{R}$$

Equation A2 - 7

Where A is the slope parameter due to the electron damping or scattering process (A = 0.5 for Ag-NPs).

An increase of the FWHM and the intensity of the SPR peak (e.g. over time or compared to a reference NP) is related to an increase of the NP size via agglomeration or attachment of polymer ligands onto the NP surface causing a redshift of the SPR peak (Ashkarran and Bayat, 2013, Peng et al., 2010). By contrast, a decrease of the NP size, e.g. via dissolution, causes a blueshift of the SPR spectrum.

A2-2 Statistical analysis: one-way ANOVA(Wackerly et al., 2002, Rasmussen, 1992)

Let say we have k independent random groups and n_1 through n_i observations within each group. We assume that for classical analysis, each group follow a Gaussian distribution and all k groups of these Gaussian distributions have the same variance σ^2, the one-way ANOVA approach use to test the null hypothesis that there is no difference between the means of each group in a single factor experiment (Rasmussen, 1992).

Table A2 - 1shows a basic data set of our k groups. Although Microsoft Excel was used in our case to compare the population means using the F-test, the analysis can be done manually using the following steps.

Table A2 - 1: Random set of data for the statistics analysis constitutes for k group with each having n_i observations.

Group 1	Group 2	...	Group k
n_1	n_1	n_1	n_1
...	...	...	...
n_i	n_i	n_i	n_i

- **Step 1: state the hypothesis of test statistic**

We state the hypothesis of the one-way ANOVA and specify the α level we plan to use in the analysis: the null hypothesis (H_0) and the alternative hypothesis (H_a). In this study we chose $\alpha = 0.05$, meaning estimated $P - value \leq \alpha$ indicates a significant difference with 95 % confidence levels. So, we have:

- Null hypothesis (H_0): nothing is happening, and there is no difference between the means of each group ($\mu_1, \mu_2 \dots \mu_k$). Meaning:

$$\mu_1 = \mu_2 = \cdots = \mu_k$$

Equation A2 - 8

- Alternative hypothesis (H_a): depending on the number of groups we have, we might have several alternative outcomes; hence we are going to simplify by hypothesising that there is at least one difference amount the means.

- **Step 2: determination of the degrees of freedom and $F_{critical}$**

In step 2, we analyse the degrees of freedom (D.F.) to estimate the critical value in which we will compare the test statistic to by using an F-distribution (Table A2 - 1). To do so, we first

calculate the degree of freedom between groups (D.F.$_{Between}$) and the degree of freedom within groups (D.F. $_{Within}$) in order determine the critical F value (F$_{critical}$). Thus:

$$D.F._{Between} = k - 1$$

Equation A2 - 9

$$D.F._{Within} = N - k$$

Equation A2 - 10

Where k is the number of groups in the study and

$$N = \text{ the total number of observations in all groups}$$
$$= number\ observations\ in\ group\ 1 + \cdots$$
$$+ number\ observations\ in\ group\ k$$

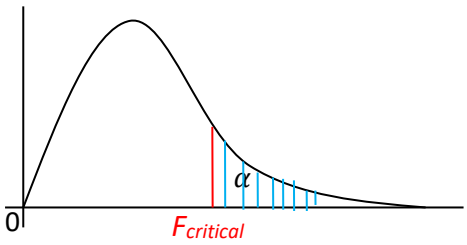

Figure A2 - 1: F-distribution curve

The total degree of freedom is given by the equation below:

$$D.F._{Total} = D.F._{Between} + D.F._{Within}$$

Equation A2 - 11

Finally, $F_{critical}$ is determined by using the F-distribution table (see statistic books e.g.: Rasmussen (1992)), where for each calculated value of $D.F._{Between}$ against a calculated value of $D.F._{Within}$ there is a corresponded $F_{critical}$ value.

- **Step 3: first step of the analysis of variance**

In this step, we analyse the sum of square or the sum of square deviation from the mean for each observation and the total sum of squares which is a combined sum of squares between and within the groups. To start, we calculate a mean value for each group or condition and call them $\overline{X}_1, \bar{X}_2 \ldots \bar{X}_k$.

With:

$$\bar{X}_i = \frac{\sum_{j=1}^{n_i} X_{ij}}{N_k}$$

Equation A2 - 12

Where, N_k is the number of observations in a k group and X is an n_i observation.

The next step is the determination of the grand mean or mean of the means ($\bar{\bar{X}}$):

$$\bar{\bar{X}} = \frac{G}{N}$$

Equation A2 - 13

Where G is the total sum of the observations of the set groups.

Finally, the total sum of square (SS_{Total}) is calculated by putting together all availabilities across the conditions, meaning:

$$SS_{Total} = \sum_{i=1}^{k} \sum_{j=i}^{n_i} \left(X_{ij} + \bar{\bar{X}}\right)^2$$

Equation A2 - 14

Where X_{ij} is the observation on an experimental unit J in a group i.

In similar analysis, we can calculate the sum of square within the groups by putting together all availability within the groups; meaning:

$$SS_{Within} = \sum_{i=1}^{k} \sum_{j=i}^{n_i} \left(X_{ij} + \bar{X}_i\right)^2$$

Equation A2 - 15

Finally the sum of square between the groups can be given as the subtraction between the total sum of squares and the sum of squares within the groups.

So:

$$SS_{Between} = SS_{Total} - SS_{Within} = \sum_{i=1}^{k} n_i \left(\bar{X}_i - \bar{\bar{X}}\right)$$

Equation A2 - 16

- **Step 4: calculation of the variance within and the variance between the groups**

The mean squares between and within respectively $MS_{Between}\ and\ MS_{Within}$ also known as variances between and within are determined by the equation below:

$$MS_{Between} = \frac{SS_{Between}}{D.F._{.between}}$$

Equation A2 - 17

And

$$MS_{Within} = \frac{SS_{within}}{D.F._{.within}}$$

Equation A2 - 18

- **Step 5: Calculation of the F-statistics**

The F-statistics is the ration between the mean squares between and mean squares within:

$$F = \frac{MS_{Between}}{MS_{Within}}$$

Equation A2 - 19

If $F < F_{critical}$, we can assume that base on the dataset, we did not go into the critical region for the rejection of the hypothesis. Meaning, in that case, we fail to reject the null hypothesis (H_0): $\mu_1 = \mu_2 = \cdots = \mu_k$. In other words, we can conclude that there is no significant difference between the groups. On the other side, if $F > F_{critical}$, the null hypothesis is rejected and this implies that there is a significant difference between the groups.

The above results are summarised in Table A2 - 2 also known the ANOVA table for one-way layout.

Table A2 - 2: Random set of data for the statistics analysis constitutes for k group with each having n_i observations

Source	D.F.	SS	MS	F
Between	$k-1$	$SS_{Between}$	$MS_{Between} = \frac{SST}{k-1}$	$\frac{MS_{Between}}{MS_{Within}}$
Within	$N-k$	SS_{Within}	$MS_{Within} = \frac{SSE}{n-k}$	
Total	$N-1$	$\sum_{i=1}^{k}\sum_{j=1}^{n_i}\left(X_{ij}-\bar{\bar{X}}\right)^2$		

A3 Appendix3: Chapter 4 supplement

A3-1 UV-Vis particles size of citrate and PVP Ag-NPs in OECDss and its components and data statistical analysis

A3-3.1 UV-Vis particles size of citrate and PVP Ag-NPs in peptone

The average size of the citrate and PVP Ag-NPs in 160 mg*L^{-1} peptone was calculated as a function of λ_{max}, ω_{PL}, or FWHM (Table A3 - 1). For $model_1$, the average diameter of the NPs (D) fluctuated mostly with λ_{max}. This is noticeable for the citrate Ag-NPs in peptone which had a significant change in λ_{max} at 45 hrs: from D (24 hrs) = 13.90 nm to D (45 hrs) = 16.44 nm. And Whereas for PVP-capped Ag-NPs, the average size of the NPs remained generally constant (D ≈ 13 to 14 nm) even though their frequency damping increased with time. The increase in size of citrate Ag-NPs during aeration was too limited to suggest that the particles agglomerated to any significant degree and as D decreased slightly again at 48 hrs, the NPs seemed not to be affected by dissolution which could have been caused by the aeration. Thus, the small increase in size of the particles may be caused by peptone molecules binding at their surface. Contrary to $model_1$ which shows that the aeration of the solution caused aggregation and slight increase in size of citrate Ag-NPs. While the size of PVP Ag-NPs stayed the same, using $model_2$ and $model_3$ to calculate D shows a strong reduction of its value during aeration (at 45 hrs) for citrate Ag-NPs and this state of the particles was unchanged even after the settling phase (at 48 hrs). Using $model_2$ and $model_3$ to calculate the average size of the PVP Ag-NPs shows that PVP Ag-NPs dispersed in peptone considerably dissolved during the first twenty-four hours of the of their exposure to the media with D dropping a little bit more than 50%

from its initial value. Also, similar to model$_1$, the aeration of the PVP Ag-NPs in peptone media did not affect their size since the value of D stayed in the same range till the end of the experiment.

There was no significant difference between citrate and PVP Ag-NPs size behaviour overtime and at a STP (Table A3 - 20) using respectively model$_1$ (Equation A2 - 1) model$_2$ (Equation A2 - 3), and model$_3$ (Equation A2 - 7). Thus the changes in MA of Ag-NPs in peptone were dependent to their coating. However the variations of λ_{max} between both particles were not.

Table A3 - 1: calculated average size of the particle (D) as a function of the MA and the FWHM of the UV-Vis spectrum of citrate and PVP Ag-NPs (from Figure 4-3) in 160 mg*L^{-1} peptone (at 0 hrs, 24 hrs, 45 hrs (during aeration) and at 48 hrs (during settling)).

	Citrate Ag-NPs in peptone				PVP Ag-NPs in peptone			
	0 hrs	**24 hrs**	**45 hrs**	**48 hrs**	**0 hrs**	**24 hrs**	**45 hrs**	**48 hrs**
λ_{max} (nm)	398	399	402	401	398	398	399	399
ω_{PL} (*10^{15} s^{-1})	4.74	4.72	4.69	4.70	4.74	4.73	4.72	4.72
FWHM (nm)	69	76	133	131	55	110	109	127
FWHM (*10^{14} s^{-1})	1.29	1.41	2.36	2.32	1.04	1.99	1.98	2.27
FWHM (eV)	0.54	0.58	0.98	0.96	0.43	0.83	0.82	0.94
D (nm): model$_1$	13.05	13.90	16.44	15.60	13.05	13.05	13.90	13.90
D (nm): model$_2$	7.87	7.24	4.34	4.40	9.84	5.02	5.09	4.43
D (nm): model$_3$	11.20	10.20	6.02	6.12	14.00	7.13	7.18	6.26

A3-3.2 UV-Vis particles size of citrate and PVP Ag-NPs in meat-extract

For the citrate and PVP Ag-NPs in 110 mg*L^{-1} meat-extract, the calculation of the average NPs size using $model_2$ and $model_3$ shows that the NPs had partially dissolved in the first twenty-four hours of their dispersion (Table A3 - 2). However, the D-values calculated using $model_1$ show that citrate Ag-NPs in meat-extract did not change in size within the first twenty-four hours of their exposure. However, a different behaviour was observed for the PVP-Ag-NPs as their average size increased from 13.90 nm (at 0 hrs) to 15.59 nm (at 24 hrs), indicative of a small percentage of the particles forming dimers or trimers (for example). Finally, $model_1$ gave a high value of D at 45 hrs for the citrate Ag-NPs, suggesting that they had agglomerated. But this estimated D value was not stabilised after the aeration was stopped, because the Ag-NPs had reduced to 13.90 nm at 48 hrs, suggesting only transient agglomeration. Note we were not able to calculate the size of the PVP Ag-NPs NPs at 45 and 48 hrs due to the inability to determine the FWHM of their corresponding UV-Vis spectrum. Statistical analysis was not done to compare the changes in size of citrate and PVP Ag-NPs in meat-extract because we were unable to measure accurately the FWHM of PVP Ag-NPs ate 45 and 48 hrs time points.

Table A3 - 2: calculated average size of the particles (D) as a function of the MA and the FWHM from the UV-Vis spectrum (Figure 4-8) of citrate and PVP Ag-NPs in 110 mg*L^{-1} meat-extract (at 0 hrs, 24 hrs, 45 hrs (during aeration) and at 48 hrs (during settling)).

	Citrate Ag-NPs in meat-extract				PVP Ag-NPs in meat-extract			
	0 hrs	**24 hrs**	**45 hrs**	**48 hrs**	**0 hrs**	**24 hrs**	**45 hrs**	**48 hrs**
λ_{max} (nm)	401	400	404	399	399	401	399	406
ω_{max} (*10^{15} s^{-1})	4.70	4.71	4.67	4.72	4.72	4.70	4.72	4.64
FWHM (nm)	60	78	111	132	58	90	NA	NA
FWHM (*10^{14} s^{-1})	1.12	1.46	2.01	2.33	1.10	1.71	NA	NA
FWHM (eV)	0.46	0.61	0.83	0.97	0.46	0.71	NA	NA
D (nm): model$_1$	15.60	14.74	18.14	13.90	13.90	15.59	NA	NA
D (nm): model$_2$	9.31	7.02	5.17	4.31	9.33	6.00	NA	NA
D (nm): model$_3$	13.00	9.85	7.08	6.08	13.20	8.38	NA	NA

A3-3.3 UV-Vis particles size of citrate and PVP Ag-NPs in urea

The average size of citrate Ag-NPs in 30 mg*L^{-1} urea had slightly increased within the first twenty-four hours (Table A3 - 3) of their exposure. The aeration of the solution caused dissolution of particles since their average size, D, calculated using model$_2$ (Equation A2 - 3) and model$_3$ (Equation A2 - 7) had reduced. However, when the first model is used, D increased from 12.20 nm (at 24 hrs) to 16.44 nm (at 45 hrs). Meaning the citrate Ag-NPs may have agglomerated during aeration and this state of the particles size stayed the same even after three hours of settling (D (48 hrs) = 16.44 nm).

For PVP particles, the calculated average was constant between 0 hrs and 24 hrs for all three models. But, while the calculated D with $model_1$ had considerably increased at 45 hrs (during aeration) due to agglomeration, D calculated using models 2 and 3 showed the opposite as the particle size had dropped significantly in both cases. Based on these observations, we may conclude that aeration of PVP Ag-NPs caused their agglomeration and (or) dissolution in urea media and led to the formation of particle dimers or trimers. There was no significant statistical (Table A3 - 20) difference between the variation of citrate and PVP Ag-NPs average size (D) when exposed to urea overtime using $model_1$ (Equation A2 - 1) $model_2$ (Equation A2 - 3), and $model_3$ (Equation A2 - 7). Thus, the change of the UV-Vis size of Ag-NPs in urea was independent of their coating.

Table A3 - 3: calculated average size of the particles (D) as a function of the MA and the FWHM of UV-Vis spectra (Figure 4-13) of citrate and PVP Ag-NPs in 30 mg*L^{-1} urea (at 0 hrs, 24 hrs, 45 hrs (during aeration) and at 48 hrs (during settling)).

	Citrate Ag-NPs in urea				PVP Ag-NPs in urea			
	0 hrs	**24 hrs**	**45 hrs**	**48 hrs**	**0 hrs**	**24 hrs**	**45 hrs**	**48 hrs**
λ_{max} (nm)	395	397	402	402	398	400	424	425
ω_{max} (*10^{15} s^{-1})	1.24	1.05	1.33	1.24	4.74	4.71	4.44	4.43
FWHM (nm)	70	66	55	70	48	49	192	202
FWHM (*10^{14} s^{-1})	4.77	4.75	4.69	4.69	9.08	0.92	2.97	3.15
FWHM (eV)	0.52	0.44	0.550	0.513	0.37	0.38	1.23	1.30
D (nm): $model_1$	10.51	12.20	16.44	16.44	13.05	14.74	35.08	35.93
D (nm): $model_2$	8.04	9.68	7.84	8.42	11.41	11.38	3.90	3.69
D (nm): $model_3$	11.60	13.80	10.90	11.70	16.20	16.00	4.77	4.48

A3-3.4 UV-Vis particles size of citrate and PVP Ag-NPs in K_2HPO_4

Determination of the average size (D) of citrate and PVP Ag-NPs in 28 $mg*L^{-1}$ K_2HPO_4 by UV-Vis (Table A3 - 4) shows that D was constant during the first 24 hrs of the NP exposure. The highest values of D (D (0 hrs) = 14.80 nm) obtained using $model_1$ (Equation A2 - 1) and $model_3$ (Equation A2 - 7) gave the lowest value (D (0 hrs) = 7.96 nm). At 45 and 48 hrs, the particle size had dramatically decreased (from D = 14.80 nm to D ≈ 9 nm for citrate Ag-NPs and from D = 18.1 0 nm to about D ≈ 5 nm for PVP Ag-NPs) when using $model_2$ (Equation A2 - 3), and $model_3$ (Equation A2 - 7) due to dissolution. But, the opposite was found using $model_1$ with the size of the particles being about five times larger than their initial size for PVP Ag-NPs. However, for citrate Ag-NPs, $model_1$ shows a slight dissolution of the NPs at 45 hrs as D had decreased (D (45 hrs) = 6.30 nm), followed probably by some agglomeration of the particles as they had apparently doubled in size at 48 hrs.

There was no significant statistical difference between the variation of citrate and PVP Ag-NPs average size (D) in K_2HPO_4 overtime with D calculated using $model_1$ $model_2$ and $model_3$ (Table A3 - 20). However, for the ANOVA of D changes at a STP, the citrate and PVP Ag-NPs were significantly different in average size when using $model_2$. But when looking at the variations of D calculated using $model_1$ and $model_3$ at a STP between both particles, no significant difference was observed between both citrate and PVP Ag-NPs since their corresponded P-value were higher than 0.05 and $F < F_{critical} = 9.28$.

Table A3 - 4: calculated average size of the particle (D) as a function of the MA and the FWHM from the UV-Vis spectra (Figure 4-18) of citrate and PVP Ag-NPs dispersed in 280 mg*L^{-1} K_2HPO_4 (at 0 hrs, 24 hrs, 45 hrs (during aeration) and at 48 hrs (during settling)).

	Citrate Ag-NPs in K_2HPO_4				PVP Ag-NPs in K_2HPO_4			
	0 hrs	**24 hrs**	**45 hrs**	**48 hrs**	**0 hrs**	**24 hrs**	**45 hrs**	**48 hrs**
λ_{max} (nm)	392	393	390	397	392	394	440	440
ω_{max} (*10^{15} s^{-1})	4.81	4.79	4.83	4.75	4.81	4.78	4.28	4.28
FWHM (nm)	51	51	83	89	42	45	179	178
FWHM (*10^{14} s^{-1})	0.99	0.99	1.53	1.62	0.82	0.87	2.74	2.73
FWHM (eV)	0.41	0.41	0.63	0.67	0.34	0.36	1.14	1.13
D (nm): $model_1$	7.96	8.81	6.27	12.20	7.97	9.70	48.64	48.64
D (nm): $model_2$	10.07	10.13	6.30	6.20	12.28	11.71	4.61	4.63
D (nm): $model_3$	14.80	14.80	9.39	8.86	18.10	17.00	5.16	5.18

A3-3.5 UV-Vis particles size of citrate and PVP Ag-NPs in NaCl

The calculated average diameters (D) of the citrate and PVP Ag-NPs in 7 mg*L^{-1} NaCl are shown in Table A3 - 5. The D values obtained using $model_1$ (Equation A2 - 1) show a slight increase in size of citrate particles with time before aeration from initially 9.70 nm to 11.35 nm in the first twenty- hours, whereas the average size of PVP Ag-NPs (14.74 nm) was constant before aeration. The introduction of the aeration flow in the media caused further increase in the average size of citrate Ag-NPs to 13.90 nm, But, PVP Ag-NPs seemed to be considerably affected with the size increasing to 23.22 nm. The effects caused by aeration of the media on the Ag-NP size were maintained even three hours after the settling phase with the average particle size staying constant for both particle types.

When using $model_2$ (Equation A2 - 3) and $model_3$ (Equation A2 - 7) the average size of Ag-NPs was constant before aerating the solutions for both citrate and PVP Ag-NPs. At 45 and 48 hrs, the calculated D values show that citrate Ag-NPs do not change in size in the presence or absence of aeration. However, PVP Ag-NPs had highly dissolved with an average size of about 4 and 3 nm respectively using models 2 and 3 by 45 and 48 hrs. The results showed that the average size of citrate and PVP Ag-NPs was significantly different overtime when using $model_1$ to calculate D (Table A3 - 20); but there was no difference using $model_2$ and $model_3$. Finally, significant difference in the variation of D at STP was observed between both particles

Table A3 - 5: calculated average size of the particles (D) as a function the MA and the FWHM of UV-Vis spectrum of citrate and PVP Ag-NPs in 7 mg*L^{-1} NaCl (at 0 hrs, 24 hrs, 45 hrs (during aeration) and at 48 hrs (during settling)) using parameters extracted from Figure 4-23.

	Citrate Ag-NPs in NaCl				PVP Ag-NPs in NaCl			
	0 hrs	**24 hrs**	**45 hrs**	**48 hrs**	**0 hrs**	**24 hrs**	**45 hrs**	**48 hrs**
λ_{max} (nm)	394	396	399	399	400	400	410	411
ω_{max} (*10^{15} s^{-1})	4.78	4.76	4.72	4.72	4.71	4.71	4.60	4.59
FWHM (nm)	48	50	55	54	47	47	226	233
FWHM (*10^{14} s^{-1})	0.93	0.96	1.04	1.02	0.89	0.88	3.47	3.59
FWHM (eV)	0.34	0.35	0.38	0.37	0.37	0.36	1.44	1.49
D (nm): $model_1$	9.70	11.35	13.90	13.90	14.74	14.74	23.22	24.07
D (nm): $model_2$	12.40	12.20	11.46	11.68	11.84	11.90	3.07	2.98
D (nm): $model_3$	15.90	15.40	14.00	14.30	16.6	16.7	4.06	3.93

A3-3.6 UV-Vis particles size of citrate and PVP Ag-NPs in $CaCl_2$

The average size of citrate and PVP Ag-NPs in 4 $mg*L^{-1}$ $CaCl_2$ calculated as a function of λmax, FWHM and ω_{max} depending on the model used are given in Table A3 - 5. Similar to other media, the first model (Equation A2 - 1) shows that before aeration, citrate and PVP Ag-NPs were the same size at 0 hrs (9.70 nm). But twenty-four hours after their exposure in the media, they had increased in size from 9.70 nm to 13.05 nm for citrate Ag-NPs and 11.36 nm for PVP Ag-NPs. With the aeration of the media, the size of citrate Ag-NPs reached 14.75 nm at 45 hrs as the particles might have agglomerated, and this state of the particles is maintained even three hours after the aeration was completed. As for the PVP Ag-NPs, they had strongly agglomerated during aeration with their average size reaching 81.70 nm at 45 hrs, but at 48 hrs, the particles had partially dissolved with D (48 hrs) = 58.81 nm).

With $model_2$ (Equation A2 - 3) and $model_3$ (Equation A2 - 7) the average size of citrate Ag-NPs slightly had decreased with time but was still in the same range even under the aeration conditions. For PVP Ag-NPs However, the aeration had caused the particles to dissolve, and their average had reduced to approximately 4 nm with both models. After dissolution, the calculated D-values at the end of the settling phase were in the same range as the D values of to the aeration phase. There was no significant difference between both particles size behaviour overtime and at a STP (Table A3 - 20) when using respectively $model_1$, $model_2$ and $model_3$. Thus, the variation of the Ag-NPs size in $CaCl_2$ under aerobic condition was independent to their coating.

Table A3 - 6: calculated average size of the particle (D) as a function the MA and the FWHM of UV-Vis spectrum of citrate and PVP Ag-NPs in $CaCl_2$ (at 0 hrs, 24 hrs, 45 hrs (during aeration) and at 48 hrs (during settling)).

	Citrate Ag-NPs in $CaCl_2$				PVP Ag-NPs in $CaCl_2$			
	0 hrs	**24 hrs**	**45 hrs**	**48 hrs**	**0 hrs**	**24 hrs**	**45 hrs**	**48 hrs**
λ_{max} (nm)	394	398	400	400	394	396	479	452
ω_{max} ($*10^{15}$ s^{-1})	4.78	4.74	4.71	4.71	4.78	4.76	3.94	4.17
FWHM (nm)	51	55	64	64	44	49	233	236
FWHM ($*10^{14}$ s^{-1})	0.98	1.04	1.19	1.19	0.85	0.93	3.59	3.68
FWHM (eV)	0.41	0.43	0.49	0.49	0.35	0.39	1.49	1.53
D (nm): $model_1$	9.70	13.05	14.75	14.75	9.70	11.36	81.70	58.81
D (nm): $model_2$	10.25	9.84	8.64	8.64	11.90	10.94	4.27	3.64
D (nm): $model_3$	14.90	14.00	12.10	12.1	17.30	15.70	3.93	3.83

A3-3.7 UV-Vis particles size of citrate and PVP Ag-NPs in $MgSO_4$

The calculated the average size of citrate and PVP-capped Ag-NPs in 2 $mg*L^{-1}$ $MgSO_4$ are shown in Table A3 - 7. When using the first model, citrate and PVP Ag-NPs had slightly increased in size over 24 hour period, and their initial size at 0 hrs were 7.97 and 13.05 nm respectively. However, the application of an aeration flow seemed to have favoured the partial dissolution of citrate Ag-NPs while PVP Ag-NPs had agglomerated. Three hours after the aeration was stopped (at 48 hrs), citrate Ag-NPs had double in size by reaching an average size of 12.20 nm and no further agglomeration was observed for PVP Ag-NPs since their average size at 45 hrs and 48 hrs were in the same range.

The calculated average size of citrate and PVP Ag-NPs were respectively 9.70 and 11.64 nm at 0 hrs when using the second model and but with the third model, the obtained values were

14.20 and 16.50 nm. After storing the solution at room temperature for twenty-four hours, the particles size had remained constant. But, by aerating the samples for twenty-one hours, both models showed that citrate and PVP were affected by dissolving, and their average size at 45 hrs was approximately 4 to 7 nm range. The NPs size stayed unchanged even three hours after stopping the aeration. The average size of the citrate and PVP Ag-NPs was significantly different overtime when using $model_1$ to calculate D; also no significant difference was found for the variations of D calculated using $model_2$ and $model_3$ (Table A3 - 20). But, the opposite was observed by for the changes at a STP of D, with the average size of the citrate and PVP-capped particles being not significantly different when using $model_1$ and significant different when using $model_2$ and $model_3$. Thus, the changes in size of the Ag-NPs in $MgSO_4$ solution and under aerobic condition were dependent on their coating.

Table A3 - 7: calculated average size of the particle (D) as a function the MA and the FWHM of UV-Vis spectrum of citrate and PVP Ag-NPs in 2 mg*L^{-1} $MgSO_4$ (at 0 hrs, 24 hrs, 45 hrs (during aeration) and at 48 hrs (during settling)).

	Citrate Ag-NPs in $MgSO_4$				PVP Ag-NPs in $MgSO_4$			
	0 hrs	**24 hrs**	**45 hrs**	**48 hrs**	**0 hrs**	**24 hrs**	**45 hrs**	**48 hrs**
λ_{max} (nm)	392	393	390	397	398	400	403	404
ω_{max} (*10^{15} s^{-1})	4.81	4.79	4.83	4.75	4.74	4.71	4.68	4.67
FWHM (nm)	53	53	122	124	47	46	158	170
FWHM (*10^{14} s^{-1})	1.03	1.03	2.12	2.16	0.89	0.87	2.68	2.88
FWHM (eV)	0.42	0.42	0.88	0.89	0.37	0.36	1.11	1.19
D (nm): $model_1$	7.97	8.81	6.27	12.20	13.05	14.74	17.30	18.14
D (nm): $model_2$	9.70	9.72	4.50	4.62	11.64	12.15	3.84	3.60
D (nm): $model_3$	14.20	14.20	6.72	6.60	16.50	17.00	5.29	4.90

A3-3.8 UV-Vis particles size of citrate and PVP Ag-NPs in OECDss

The average size of citrate and PVP Ag-NPs in OECDss calculated from the UV-Vis data are given in Table A3 - 8, but please note that we were unable to estimate the size of Ag-NPs during the aeration and the settling phase because of the corresponded UV-Vis spectrums were not completed Gaussians. So, only the calculated D values before aerating the solution were given, meaning at 0 and 24 hrs. According to the results obtained using $model_1$, the average of size of citrate particles had stayed constant (D ≈ 13 nm) for the first twenty-four hours, while PVP Ag-NPs had slightly dissolved from 13.05 nm at 0 hrs to 10.51 nm at 24 hrs.

However, the results given by the models 2 and 3 show a similar behaviour of the NPs during these first twenty-four hours, in fact, it can be observed that the average size of the particles had decreased with time as the particles might have dissolved. And this is in concordance to what was observed in section 4.3.8.2 regarding the reduction of the absorbance of citrate and PVP Ag-NPs with time and in the absence of aeration. The two-way ANOVA without replicate was not determined relating the difference changes in size of citrate and PVP Ag-NPs in OECDss as it was not possible to give the exact FWHM of the NPs spectrums at 45 and 48 hrs measurements (Table A3 - 8).

Table A3 - 8: calculated average size of the particle (D) as a function the MA and the FWHM of UV-Vis spectrum of citrate and PVP Ag-NPs in OECDss (at 0 hrs, 24 hrs, 45 hrs (during aeration) and at 48 hrs (during settling)).

	Citrate Ag-NPs in OECDss				PVP Ag-NPs in OECDss			
	0 hrs	**24 hrs**	**45 hrs**	**48 hrs**	**0 hrs**	**24 hrs**	**45 hrs**	**48 hrs**
λ_{max} (nm)	398	399	397	379	398	395	390	379
ω_{max} (*10^{15} s^{-1})	4.74	4.72	4.75	4.97	4.74	4.77	4.83	4.97
FWHM (nm)	59	97	NA	NA	46	59	NA	NA
FWHM (*10^{14} s^{-1})	1.11	1.78	NA	NA	0.87	1.18	NA	NA
FWHM (eV)	0.46	0.76	NA	NA	0.37	0.49	NA	NA
D (nm): $model_1$	13.05	13.90	NA	NA	13.05	10.51	NA	NA
D (nm): $model_2$	9.24	5.70	NA	NA	11.68	8.51	NA	NA
D (nm): $model_3$	13.10	8.05	NA	NA	16.60	12.30	NA	NA

A3-2 DLS Average size of citrate and PVP Ag-NPs dispersed in OECDss and its constituents and data statistical analysis

Table A3 - 9: DLS data of Citrate and PVP Ag-NPs spiked in 160 mg*L^{-1} peptone: before aeration (at 0 and 24 hrs), during aeration (at 45 hrs) and after settling (at 48 hrs).

	Citrate pristine Ag-NPs in peptone at 0 hrs: Z-average (nm) = 28.6 ± 0.7 and PDI = 0.27 ± 0.03				**PVP pristine Ag-NPs in peptone at 0 hrs:** Z-average (nm) = 31.9 ± 4.7 and PDI = 0.44 ± 0.08			
	D_H (nm)	**% Intensity**	**%Volume**	**% Number**	**D_H (nm)**	**% Intensity**	**%Volume**	**% Number**
Peak 1	34.6 ± 1.6	96.0	95.8	100.0	39.0 ± 16.8	72.9	49.9	45.3
Peak 2	3888.0 ± 326.0	4.0	4.2	0.0	195.7 ± 109.2	20.4	0.5	0.0
Peak 3	0.0	0.0	0.0	0.0	10.5 ± 1.9	4.3	28.8	34.4
	Citrate pristine Ag-NPs in peptone at 24 hrs: Z-average (nm) = 31.4 ± 4.4 and PDI = 0.31 ± 0.07				**PVP pristine Ag-NPs in peptone at 24 hrs:** Z-average (nm) = 34.8 ± 2.5 and PDI = 0.36 ± 0.04			
	D_H (nm)	**% Intensity**	**%Volume**	**% Number**	**D_H (nm)**	**% Intensity**	**%Volume**	**% Number**
Peak 1	35.6 ± 4.2	92.6	92.6	100.0	45.5 ± 7.5	92.9	62.8	60.8
Peak 2	2502 ± 1696	7.4	7.4	0.0	793.6 ± 470.0	3.3	0.3	0.0
Peak 3	0.0	0.0	0.0	0.0	6.8 ± 1.6	2.1	34.6	39.2
	Citrate pristine Ag-NPs in peptone at 45 hrs: Z-average (nm) = 66.9 ± 4.5 and PDI = 0.30 ± 0.07				**PVP pristine Ag-NPs in peptone at 45 hrs:** Z-average (nm) = 40.9 ± 1.3 and PDI = 0.24 ± 0.02			
	D_H (nm)	**% Intensity**	**%Volume**	**% Number**	**D_H (nm)**	**% Intensity**	**%Volume**	**% Number**
Peak 1	84.5 ± 10.9	93.5	81.0	81.4	53.5 ± 1.9	99.4	88.8	81.4
Peak 2	142.6 ± 297.6	6.0	2.2	0.0	3859 ± 1128	0.6	2.3	0.0
Peak 3	13.4 ± 3.0	0.4	13.6	18.6	0.0	0.0	9.0	18.6
	Citrate pristine Ag-NPs in peptone at 48 hrs: Z-average (nm) = 38.9 ± 0.5 and PDI = 0.20 ± 0.01				**PVP pristine Ag-NPs in peptone at 48 hrs:** Z-average (nm) = 45.2 ± 2.0 and PDI = 0.30 ± 0.04			
	D_H (nm)	**% Intensity**	**%Volume**	**% Number**	**D_H (nm)**	**% Intensity**	**%Volume**	**% Number**
Peak 1	39.9 ± 5.4	91.1	93.1	80.6	37.3 ± 13.7	68.9	95.5	52.5
Peak 2	2677 ± 1692	8.9	6.9	19.4	5.9 ±2.0	12.4	4.4	47.5
Peak 3	0.0	0.0	0.0	0.0	122.4 ± 25.3	7.7	0.0	0.0

Table A3 - 10: DLS data of Citrate and PVP Ag-NPs spiked in 110 mg*L^{-1} meat-extract: before aeration (at 0 and 24 hrs), during aeration (at 45 hrs) and after settling (at 48 hrs).

	Citrate pristine Ag-NPs in meat-extract at 0 hrs: Z-average (nm) = ± and PDI = ±				**PVP pristine Ag-NPs in meat-extract at 0 hrs:** Z-average (nm) = ± and PDI = ±			
	D_H (nm)	**% Intensity**	**%Volume**	**% Number**	**D_H (nm)**	**% Intensity**	**%Volume**	**% Number**
Peak 1	39.9 ± 5.4	91.1	93.1	80.6	37.3 ± 13.7	68.9	95.5	52.5
Peak 2	2677 ± 1692	8.9	6.9	19.4	5.9 ±2.0	12.4	4.4	47.5
Peak 3	0.0	0.0	0.0	0.0	122.4 ± 25.3	7.7	0.0	0.0
	Citrate pristine Ag-NPs in meat-extract at 24 hrs: Z-average (nm) = ± and PDI = ±				**PVP pristine Ag-NPs in meat-extract at 24 hrs:** Z-average (nm) = ± and PDI = ±			
	D_H (nm)	**% Intensity**	**%Volume**	**% Number**	**D_H (nm)**	**% Intensity**	**%Volume**	**% Number**
Peak 1	34.2 ± 5.0	79.8	87.0	90.2	31.8 ± 0.4	87.5	96.6	100.0
Peak 2	1189 ± 725.5	18.2	5.0	0	3.9 ± 0.4	9.5	3.2	0.0
Peak 3	4954 ±696.0	2.0	3.8	0	4509.0 ± 966.3	3.0	0.1	0.0
	Citrate pristine Ag-NPs in meat-extract at 45 hrs: Z-average (nm) = ± and PDI = ±				**PVP pristine Ag-NPs in meat-extract at 45 hrs:** Z-average (nm) = ± and PDI = ±			
	D_H (nm)	**% Intensity**	**%Volume**	**% Number**	**D_H (nm)**	**% Intensity**	**%Volume**	**% Number**
Peak 1	85.0 ± 12.35	97.8	96.0	100	99.7 ± 5.9	99.5	88.8	100.0
Peak 2	3912 ± 1165	1.7	3.4	0	4633.0 ± 812.0	0.5	11.2	0.0
Peak 3	1216 ± 302.3	0.4	0.6	0	0.0	0.0	0.0	0.0
	Citrate pristine Ag-NPs in meat-extract at 48 hrs: Z-average (nm) = ± and PDI = ±				**PVP pristine Ag-NPs in meat-extract at 48 hrs:** Z-average (nm) = ± and PDI = ±			
	D_H (nm)	**% Intensity**	**%Volume**	**% Number**	**D_H (nm)**	**% Intensity**	**%Volume**	**% Number**
Peak 1	174.1 ± 27.1	99.9	91.1	100.0	122.4 ± 11.5	98.5	60.7	100
Peak 2	4172 ± 1018	0.1	0.4	0.0	4365.0 ± 979.6	1.5	24.4	0
Peak 3	0.0	0.0	8.4	0.0	0.0	0.0	15.2	0

Table A3 - 11: DLS data of Citrate and PVP Ag-NPs spiked in 30 mg*L^{-1} urea: before aeration (at 0 and 24 hrs), during aeration (at 45 hrs) and after settling (at 48 hrs).

	Citrate pristine Ag-NPs in urea at 0 hrs: Z-average (nm) = 26.4 ± 1.3 and PDI = 0.50 ± 0.05				**PVP pristine Ag-NPs in urea at 0 hrs:** Z-average (nm) = 100.5 ± 37.3 and PDI = 0.18 ± 0.01			
	D_H (nm)	**% Intensity**	**%Volume**	**% Number**	**D_H (nm)**	**% Intensity**	**%Volume**	**% Number**
Peak 1	25.0 ± 2.9	78.4	96.6	100.0	30.6 ± 4.5	66.8	96.6	100.0
Peak 2	1243.0 ± 644.5	14.7	1.9	0.0	121 ± 63.5	22.9	3.3	0.0
Peak 3	255.0 ± 77.7	4.6	1.4	0.0	4.2 ± 0.7	8.0	0.0	0.0
	Citrate pristine Ag-NPs in urea at 24 hrs: Z-average (nm) = 57.0 ± 15.5 and PDI = 0.37 ± 0.25				**PVP pristine Ag-NPs in urea at 24 hrs:** Z-average (nm) = 24.6 ± 0.5 and PDI = 0.48 ± 0.02			
	D_H (nm)	**% Intensity**	**%Volume**	**% Number**	**D_H (nm)**	**% Intensity**	**%Volume**	**% Number**
Peak 1	33.3 ± 2.5	71.1	84.9	84.3	44.6 ± 10.0	85.5	97.7	100.0
Peak 2	875.5 ± 375.8	16.5	6.7	15.7	4.5 ± 1.2	12.3	2.2	0.0
Peak 3	263.9 ± 75.6	10.2	0.8	0.0	4976 ± 665.0	1.2	0.1	0.0
	Citrate pristine Ag-NPs in urea at 45 hrs: Z-average (nm) = 45.2 ± 1.7 and PDI = 0.33 ± 0.01				**PVP pristine Ag-NPs in urea at 45 hrs:** Z-average (nm) = 21.1 ± 1.0 and PDI = 0.97 ± 0.04			
	D_H (nm)	**% Intensity**	**%Volume**	**% Number**	**D_H (nm)**	**% Intensity**	**%Volume**	**% Number**
Peak 1	64.5 ± 3.2	96.8	68.7	70.6	166.7 ± 13.7	86.2	100.0	100.0
Peak 2	3768 ± 1190	2.5	7.4	0.0	5.5 ± 1.1	31.8	0.0	0.0
Peak 3	7.2	0.8	23.9	29.4	0.0	0.0	0.0	0
	Citrate pristine Ag-NPs in urea at 48 hrs: Z-average (nm) = 31.3 ± 1.3 and PDI = 0.32 ± 0.02				**PVP pristine Ag-NPs in urea at 48 hrs:** Z-average (nm) = 18.7 ± 1.7 and PDI = 0.89 ± 0.06			
	D_H (nm)	**% Intensity**	**%Volume**	**% Number**	**D_H (nm)**	**% Intensity**	**%Volume**	**% Number**
Peak 1	38.8 ± 3.4	93.4	94.6	100	168.6 ± 8.3	64.1	100.0	100.0
Peak 2	3422 ± 1300	4.7	5.4	0	5.8 ± 0.8	35.9	0.0	0.0
Peak 3	737.5 ± 306.4	1.9	0.0	0	0.0	0.0	0.0	0.0

Table A3 - 12: DLS data of Citrate and PVP Ag-NPs spiked in 28 mg*L^{-1} K_2HPO_4: before aeration (at 0 and 24 hrs), during aeration (at 45 hrs) and after settling (at 48 hrs).

	Citrate capped Ag-NPs in K_2HPO_4 at 0 hrs: Z-average (nm) = 41.2 ± 2.2 and PDI = 0.43 ± 0.10				**PVP capped Ag-NPs in K_2HPO_4 at 0 hrs:** Z-average (nm) = 122.8 ± 60.1 and PDI = 0.20 ± 0.06			
	D_H (nm)	**% Intensity**	**%Volume**	**% Number**	**D_H (nm)**	**% Intensity**	**%Volume**	**% Number**
Peak 1	45.6 ± 3.7	82.5	89.0	100.0	30.0 ± 0.5	61.0	98.2	100.0
Peak 2	1746 ± 1333	17.5	11.0	0.0	169.1 ± 69.5	30.1	0.0	0.0
Peak 3	0.0	0.0	0.0	0.0	3.8 ± 1.3	8.9	1.8	2.5
	Citrate capped Ag-NPs in K_2HPO_4 at 24 hrs: Z-average (nm) = 30.4 ± 3.7 and PDI = 0.5 ± 0.1				**PVP capped Ag-NPs in K_2HPO_4 at 24 hrs:** Z-average (nm) = 32.7 ± 1.3 and PDI = 0.52 ± 0.14			
	D_H (nm)	**% Intensity**	**%Volume**	**% Number**	**D_H (nm)**	**% Intensity**	**%Volume**	**% Number**
Peak 1	37.2 ± 2.1	84.8	69.7	75.0	63.2 ± 7.4	86.1	97.7	100.0
Peak 2	478.7 ± 421.4	9.8	0.3	0	4.7 ± 1.5	10.1	2.1	0.0
Peak 3	4742 ± 778.3	4.1	0	0	3848 ± 1405	3.9	0.2	0.0
	Citrate capped Ag-NPs in K_2HPO_4 at 45 hrs: Z-average (nm) = 117.7 ± 16.5 and PDI = 0.43 ± 0.20				**PVP capped Ag-NPs in K_2HPO_4 at 45 hrs:** Z-average (nm) = 126.8 ± 10.1 and PDI = 0.50 ± 0.09			
	D_H (nm)	**% Intensity**	**%Volume**	**% Number**	**D_H (nm)**	**% Intensity**	**%Volume**	**% Number**
Peak 1	214.2 ± 16.5	74.9	13.1	0.0	211.3 ± 10.1	93.3	79.7	80.0
Peak 2	33.1 ± 2.9	24.4	80.0	100.0	4.4 ± 1.1	4.2	9.2	20.0
Peak 3	5446. ± 270.9	0.7	6.9	0.0	13.7 ± 4.7	1.4	0.0	0.0
	Citrate capped Ag-NPs in K_2HPO_4 at 48 hrs: Z-average (nm) = 119.5 ± 9.3 and PDI = 0.18 ± 0.01				**PVP capped Ag-NPs in K_2HPO_4 at 48 hrs:** Z-average (nm) = 49.0 ± 6.3 and PDI = 1.0 ± 0.00			
	D_H (nm)	**% Intensity**	**%Volume**	**% Number**	**D_H (nm)**	**% Intensity**	**%Volume**	**% Number**
Peak 1	120.6 ± 10.7	82..2	3.7	0.0	218.4 ± 10.9	83.0	99.9	100.0
Peak 2	21.3 ± 1.6	17.8	96.3	100.0	5.4 ±0.6	15.4	0.1	0.0
Peak 3	0.0	0.0	0.0	0.0	12.2 ± 14.4	1.6	0.0	0.0

Table A3 - 13: DLS data of Citrate and PVP Ag-NPs spiked in 7 mg*L^{-1} NaCl: before aeration (at 0 and 24 hrs), during aeration (at 45 hrs) and after settling (at 48 hrs).

	Citrate capped Ag-NPs in NaCl at 0 hrs: Z-average (nm) = 34.8 ± 2.0 and PDI = 0.40 ± 0.1				**PVP capped Ag-NPs in NaCl at 0 hrs:** Z-average (nm) = 40.9 ± 4.2 and PDI = 0.56± 0.07			
	D_H (nm)	**% Intensity**	**%Volume**	**% Number**	**D_H (nm)**	**% Intensity**	**%Volume**	**% Number**
Peak 1	43.0 ± 3.8	92.8	68.4	59.9	43.9 ± 3.3	68.4	70.5	74.9
Peak 2	3729.0 ± 1302	7.2	0.1	0.0	459.1 ± 319.5	23.8	1.0	0.0
Peak 3	0.0	0.0	0.0	0.0	5.6 ± 2.0	4.8	26.5	25.1
	Citrate capped Ag-NPs in NaCl at 24 hrs: Z-average (nm) = 38.0 ± 1.6 and PDI = 0.38± 0.07				**PVP capped Ag-NPs in NaCl at 24 hrs:** Z-average (nm) = 49.4 ± 12.5 and PDI = 0.44 ± 0.15			
	D_H (nm)	**% Intensity**	**%Volume**	**% Number**	**D_H (nm)**	**% Intensity**	**%Volume**	**% Number**
Peak 1	48.8 ± 3.6	89.3	76.4	79.8	35.8 ± 6.7	67.5	72.5	79.6
Peak 2	1578.0 ± 659.6	5.5	0.0	0.0	320.5 ± 263.6	24.6	0.7	0.0
Peak 3	4071 ± 998.7	4.5	8.2	0.0	6.3 ± 1.6	5.5	23.3	20.4
	Citrate capped Ag-NPs in NaCl at 45 hrs: Z-average (nm) = 46.8 ± 1.7 and PDI = 0.57 ± 0.10				**PVP capped Ag-NPs in NaCl at 45 hrs:** Z-average (nm) = 131.9 ± 6.4 and PDI = 0.25± 0.02			
	D_H (nm)	**% Intensity**	**%Volume**	**% Number**	**D_H (nm)**	**% Intensity**	**%Volume**	**% Number**
Peak 1	34.3 ± 3.6	55.0	90.8	100.0	155.6 ± 7.8	97.0	55.3	100.0
Peak 2	222.1 ± 106.4	42.4	2.2	0.0	4595 ± 836.5	3.0	12.4	0.0
Peak 3	4967.0 ± 643.1	2.6	7.1	0.0	0.0	0.0	0.0	0.0
	Citrate capped Ag-NPs in NaCl at 48 hrs: Z-average (nm) = 62.1± 2.6 and PDI = 0.57 ± 0.02				**PVP capped Ag-NPs in NaCl at 48 hrs:** Z-average (nm) = 145.4 ± 9.5 and PDI = 0.24 ± 0.02			
	D_H (nm)	**% Intensity**	**%Volume**	**% Number**	**D_H (nm)**	**% Intensity**	**%Volume**	**% Number**
Peak 1	278.9 ± 13.0	58.1	6.4	0.0	147.0 ± 29.2	99.6	85.5	81.3
Peak 2	32.1 ± 0.7	41.9	93.6	100.0	5254.0 ± 440.2	0.4	11.6	18.7
Peak 3	0.0	0.0	0.0	0.0	0.0	0.0	0.0	0.0

Table A3 - 14: DLS data of Citrate and PVP Ag-NPs spiked in 4 mg*L^{-1} $CaCl_2$: before aeration (at 0 and 24 hrs), during aeration (at 45 hrs) and after settling (at 48 hrs).

	Citrate capped Ag-NPs in $CaCl_2$ at 0 hrs: Z-average (nm) = 29.9 ± 3.2 and PDI = 0.47 ± 0.07				**PVP capped Ag-NPs in $CaCl_2$ at 0 hrs:** Z-average (nm) = 44.5 ± 4.8 and PDI = 0.59 ± 0.16			
	D_H (nm)	**% Intensity**	**%Volume**	**% Number**	**D_H (nm)**	**% Intensity**	**%Volume**	**% Number**
Peak 1	31.7 ± 3.7	81.2	95.8	100.0	39.0 ± 4.6	60.4	74.0	79.8
Peak 2	854.2 ± 660.7	16.0	0.5	0.0	264.5 ± 20.3	32.4	0.9	0.0
Peak 3	4648 ± 841.0	2.8	3.7	0.0	5.9 ± 1.8	4.5	22.8	20.2
	Citrate capped Ag-NPs in $CaCl_2$ at 24 hrs: Z-average (nm) = 38.8 ± 17.1 and PDI = 0.31 ± 0.21				**PVP capped Ag-NPs in $CaCl_2$ at 24 hrs:** Z-average (nm) = 35.6 ± 4.7 and PDI = 0.51 ± 0.18			
	D_H (nm)	**% Intensity**	**%Volume**	**% Number**	**D_H (nm)**	**% Intensity**	**%Volume**	**% Number**
Peak 1	30.1 ± 2.8	86.4	53.6	33.0	59.7 ± 33.6	91.7	96.6	72.5
Peak 2	230.4 ± 85.8	7.8	0.1	0.0	4.2 ± 1.5	5.6	0.1	27.5
Peak 3	4978 ± 640.2	3.8	2.8	0.0	4004 ± 1229	2.7	0.0	0.0
	Citrate capped Ag-NPs in $CaCl_2$ at 45 hrs: Z-average (nm) = 108 ± 1.8 and PDI = 0.52 ± 0.00				**PVP capped Ag-NPs in $CaCl_2$ at 45 hrs:** Z-average (nm) = 137.7 ± 5.9 and PDI = 0.36 ± 0.03			
	D_H (nm)	**% Intensity**	**%Volume**	**% Number**	**D_H (nm)**	**% Intensity**	**%Volume**	**% Number**
Peak 1	205.8 ± 18.9	81.9	15.5	0.0	140.7 ± 4.6	98.2	55.6	100
Peak 2	33.3 ± 5.7	17.6	60.9	68.2	4946.0 ± 691.3	1.8	44.4	0.0
Peak 3	5307 ± 397.4	0.5	0.0	0.0	0.0	0.0	0.0	0.0
	Citrate capped Ag-NPs in $CaCl_2$ at 48 hrs: Z-average (nm) = 131.4 ± 5.2 and PDI = 0.22 ± 0.01				**PVP capped Ag-NPs in $CaCl_2$ at 48 hrs:** Z-average (nm) = 231.0 ± 69.2 and PDI = 0.30 ± 0.09			
	D_H (nm)	**% Intensity**	**%Volume**	**% Number**	**D_H (nm)**	**% Intensity**	**%Volume**	**% Number**
Peak 1	133.8 ± 2.5	90.4	4.2	0.0	112.0 ± 14.0	100.0	100.0	100.0
Peak 2	17.4 ± 1.4	9.6	95.8	100.0	0.0	0.0	0.0	0.0
Peak 3	0.0	0.0	0.0	0.0	0.0	0.0	0.0	0.0

Table A3 - 15: DLS data of Citrate and PVP Ag-NPs spiked in 2 mg*L^{-1} $MgSO_4$: before aeration (at 0 and 24 hrs), during aeration (at 45 hrs) and after settling (at 48 hrs).

	Citrate capped Ag-NPs in $MgSO_4$ at 0 hrs: Z-average (nm) = 39.15 ± 0.9 and PDI = 0.42 ± 0.11				**PVP capped Ag-NPs in $MgSO_4$ at 0 hrs:** Z-average (nm) = 36.7 ± 4.5 and PDI = 0.47 ± 0.11			
	D_H (nm)	**% Intensity**	**%Volume**	**% Number**	**D_H (nm)**	**% Intensity**	**%Volume**	**% Number**
Peak 1	44.2 ± 4.2	86.0	85.0	100.0	35.6 ± 4.5	67.2	80.9	79.2
Peak 2	3110 ± 1484	9.4	14.5	0.0	364.8 ± 232.8	22.0	0.3	0.0
Peak 3	436.5 ± 181.5	4.6	0.5	0.0	6.3 ± 1.9	6.2	18.1	20.8
	Citrate capped Ag-NPs in $MgSO_4$ at 24 hrs: Z-average (nm) = 41.9 ± 3.3 and PDI = 0.44 ± 0.18				**PVP capped Ag-NPs in $MgSO_4$ at 24 hrs:** Z-average (nm) = 33.8 ± 2.5 and PDI = 0.52 ± 0.09			
	D_H (nm)	**% Intensity**	**%Volume**	**% Number**	**D_H (nm)**	**% Intensity**	**%Volume**	**% Number**
Peak 1	42.2 ± 3.3	79.6	89.9	100.0	38.1 ± 1.7	72.4	70.7	79.6
Peak 2	1134 ± 762.5	18.0	0.0	0.0	540.5 ± 378.9	20.4	0.9	0.0
Peak 3	4708.0 ± 732.3	2.4	10.1	0.0	6.2 ± 1.7	5.5	28.0	20.4
	Citrate capped Ag-NPs in $MgSO_4$ at 45 hrs: Z-average (nm) = 115.3 ± 5.7 and PDI = 0.57 ± 0.02				**PVP capped Ag-NPs in $MgSO_4$ at 45 hrs:** Z-average (nm) = 125.9 ± 1.8 and PDI = 0.26 ± 0.02			
	D_H (nm)	**% Intensity**	**%Volume**	**% Number**	**D_H (nm)**	**% Intensity**	**%Volume**	**% Number**
Peak 1	211.4 ± 11.8	80.1	17.0	0.0	174.3 ± 50.2	97.6	54.7	100
Peak 2	32.0 ± 1.1	19.7	79.7	100.0	4430 ± 977.2	2.4	14.0	0.0
Peak 3	5378 ± 323.7	0.3	3.2	0.0	0.0	0.0	31.3	0.0
	Citrate capped Ag-NPs in $MgSO_4$ at 48 hrs: Z-average (nm) = 156.6 ± 16.1 and PDI = 0.21 ± 0.02				**PVP capped Ag-NPs in $MgSO_4$ at 48 hrs:** Z-average (nm) = 132.3 ± 3.7 and PDI = 0.27 ± 0.02			
	D_H (nm)	**% Intensity**	**%Volume**	**% Number**	**D_H (nm)**	**% Intensity**	**%Volume**	**% Number**
Peak 1	98.4 ± 6.9	80.0	5.8	0.0	136.1 ± 11.6	99.5	87.1	100.0
Peak 2	25.1 ± 4.3	20.0	94.2	100.0	5183.0 ± 483.6	0.5	12.9	0.0
Peak 3	0.0	0.0	0.0	0.0	0.0	0.0	0.0	0.0

Table A3 - 16: DLS data of Citrate and PVP Ag-NPs spiked in OECDss: before aeration (at 0 and 24 hrs), during aeration (at 45 hrs) and after settling (at 48 hrs).

	Citrate capped Ag-NPs in OECDss at 0 hrs: Z-average (nm) = 34.8 ± 2.7 and PDI = 0.24 ± 0.14				**PVP capped Ag-NPs in OECDss at 0 hrs:** Z-average (nm) = 86.1 ± 4.6 and PDI = 0.13 ± 0.01			
	D_H (nm)	**% Intensity**	**%Volume**	**% Number**	**D_H (nm)**	**% Intensity**	**%Volume**	**% Number**
Peak 1	36.3 ± 9.2	97.1	95.7	100.0	28.1 ± 0.5	65.2	53.4	50.1
Peak 2	4192 ± 1364	2.9	4.2	0.0	138.8 ± 55.3	32.0	0.2	0.0
Peak 3	0.0	0.0	0.1	0.0	4.3 ± 0.8	2.5	46.2	49.9
	Citrate capped Ag-NPs in OECDss at 24 hrs: Z-average (nm) = 22.8 ± 0.1 and PDI = 0.30 ± 0.00				**PVP capped Ag-NPs in OECDss at 24 hrs:** Z-average (nm) = 42.2 ± 4.3 and PDI = 0.43 ± 0.08			
	D_H (nm)	**% Intensity**	**%Volume**	**% Number**	**D_H (nm)**	**% Intensity**	**%Volume**	**% Number**
Peak 1	33.3 ± 3.6	94.3	91.1	100.0	42.5 ± 6.8	80.1	50.0	50.6
Peak 2	4924 ± 689.1	4.7	8.8	0.0	370.5 ± 143.2	13.2	0.7	0.0
Peak 3	422.9 ± 113.1	1.0	0.1	0.0	4994 ± 632.2	4.5	7.8	0.0
	Citrate capped Ag-NPs in OECDss at 45 hrs: Z-average (nm) = 53.4 ± 4.3 and PDI = 0.39 ± 0.03				**PVP capped Ag-NPs in OECDss at 45 hrs:** Z-average (nm) = 45.5 ± 4.3 and PDI = 0.30 ± 0.05			
	D_H (nm)	**% Intensity**	**%Volume**	**% Number**	**D_H (nm)**	**% Intensity**	**%Volume**	**% Number**
Peak 1	69.2 ± 13.2	86.8	87.9	100.0	61.5 ± 5.6	96.1	80.1	100
Peak 2	1038 ± 942.8	13.2	3.8	0.0	365 ± 76.9	3.9	13.2	0.0
Peak 3	0.0	0.0	3.5	0.0	0.0	0.0	0.0	0.0
	Citrate capped Ag-NPs in OECDss at 48 hrs: Z-average (nm) = 50.0 ± 5.4 and PDI = 0.37 ± 0.04				**PVP capped Ag-NPs in OECDss at 48 hrs:** Z-average (nm) = 44.3 ± 0.8 and PDI = 0.34 ± 0.01			
	D_H (nm)	**% Intensity**	**%Volume**	**% Number**	**D_H (nm)**	**% Intensity**	**%Volume**	**% Number**
Peak 1	63.2 ± 7.7	90.0	73.1	80.4	41.5 ± 2.9	94.7	84.5	100.0
Peak 2	907.7 ± 527.2	6.1	0.6	19.6	3558 ± 1293	5.3	15.5	0.0
Peak 3	4224 ± 1045	3.5	13.3	0.0	0.0	0.0	0.0	0.0

Table A3 - 17: DLS data of pristine citrate and PVP particles.

	Citrate pristine Ag-NPs Z-average (nm) = 22.8 ± 0.1 and PDI = 0.30 ± 0.00				**PVP pristine Ag-NPs** Z-average (nm) = 26.5 ± 0.7 and PDI = 0.43 ± 0.01			
	Average D_H (nm)	**% Intensity**	**%Volume**	**% Number**	**Average D_H (nm)**	**% Intensity**	**%Volume**	**% Number**
Peak 1	26.6 ± 12.75	95.7	97.4	100	44.09 ± 24.9	90.0	88.8	89.2
Peak 2	4043 ± 1262	3.0	2.6	0	4.2 ± 1.4	8.9	9.1	10.8
Peak 3	541.8 ± 174.0	0.8	0.0	0	4904.0 ± 989.9	1.1	0.7	0.0

A3-3 GFAAS, UV-Vis, DLS and TEM data statistical analysis of the citrate and PVP Ag-NPs in OECDss and its constituents.

A3-3.1 Two-way ANOVA test without replicate (α = 0.05) of GFAAS of citrate and PVP Ag-NPs in OECDss and is components; samples collected at 0 hrs and 24 hrs (left at room temperature), 45 hrs (during aeration) and 48 hrs (during settling)

Table A3 - 18: Two way ANOVA without replicate (α = 0.05), comparing the total Ag, the dissolved Ag, the unrecovered Ag of citrate and PVP Ag-NPs in peptone, meat-extract, urea, K_2HPO_4, NaCl $CaCl_2$, $MgSO_4$ and OECDss media: before aeration (at 0 and 24 hrs), during aeration (at 45 hrs) and after settling (at 48 hrs)

ANOVA comparing GFAAS data of citrate and PVP Ag-NPs in peptone						
	Overtime ANOVA			ANOVA for specific time point (STP)		
	$C_{Total\ Ag}$ (µg*L^{-1})	%diss. Ag	%unr. Ag	$C_{Total\ Ag}$ (µg*L^{-1})	%diss. Ag	%unr. Ag
F	9.183	5.490	6.182	1.581	1.237	1.997
P-value	0.056	0.101	0.089	0.358	0.433	0.292
$F_{critical}$	10.128	10.128	10.128	9.277	9.277	9.277
ANOVA comparing GFAAS data of citrate and PVP Ag-NPs in meat-extract						
	Overtime ANOVA			ANOVA for STP		
	$C_{Total\ Ag}$ (µg*L^{-1})	%diss. Ag	%unr. Ag	$C_{Total\ Ag}$ (µg*L^{-1})	%diss. Ag	%unr. Ag
F	6.782	2.780	8.070	3.870	2.440	4.000
P-value	0.080	0.194	0.066	0.148	0.242	0.142
$F_{critical}$	10.128	10.128	10.128	9.277	9.277	9.277
ANOVA comparing GFAAS data of citrate and PVP Ag-NPs in urea						
	Overtime ANOVA			ANOVA for STP		
	$C_{Total\ Ag}$ (µg*L^{-1})	%diss. Ag	%unr. Ag	$C_{Total\ Ag}$ (µg*L^{-1})	%diss. Ag	%unr. Ag
F	7.460	3.945	3.861	9.532	3.680	8.355
P-value	0.072	0.141	0.144	0.048	0.156	0.057
$F_{critical}$	10.128	10.128	10.128	9.277	9.277	9.277
ANOVA comparing GFAAS data of citrate and PVP Ag-NPs in K_2HPO_4						
	Overtime ANOVA			ANOVA for STP		
	$C_{Total\ Ag}$ (µg*L^{-1})	%diss. Ag	%unr. Ag	$C_{Total\ Ag}$ (µg*L^{-1})	%diss. Ag	%unr. Ag
F	7.230	2.740	3.208	3.406	1.404	5.415
P-value	0.074	0.197	0.171	0.170	0.393	0.099
$F_{critical}$	10.128	10.128	10.128	9.277	9.277	9.277
ANOVA comparing GFAAS data of citrate and PVP Ag-NPs in NaCl						

	Overtime ANOVA			ANOVA for STP		
	$C_{Total\ Ag}$ (µg*L^{-1})	%diss. Ag	%unr. Ag	$C_{Total\ Ag}$ (µg*L^{-1})	%diss. Ag	%unr. Ag
F	7.341	2.083	1.562	19.829	6.542	67.203
P-value	0.073	0.245	0.300	0.018	0.079	0.003
$F_{critical}$	10.128	10.128	10.128	9.277	9.277	9.277
ANOVA comparing GFAAS data of citrate and PVP Ag-NPs in $CaCl_2$						
	Overtime ANOVA			ANOVA for STP		
	$C_{Total\ Ag}$ (µg/L)	%diss. Ag	%unr. Ag	$C_{Total\ Ag}$ (µg*L^{-1})	%diss. Ag	%unr. Ag
F	1.517	3.520	0.232	34.970	11.430	35.644
P-value	0.306	0.160	0.662	0.007	0.038	0.008
$F_{critical}$	10.128	10.128	10.128	9.277	9.277	9.277
ANOVA comparing GFAAS data of citrate and PVP Ag-NPs in $MgSO_4$						
	Overtime ANOVA			ANOVA for STP		
	$C_{Total\ Ag}$ (µg*L^{-1})	%diss. Ag	%unr. Ag	$C_{Total\ Ag}$ (µg*L^{-1})	%diss. Ag	%unr. Ag
F	3.550	4.700	0.005	66.714	9.808	128.090
P-value	0.156	0.119	0.947	0.003	0.046	0.001
$F_{critical}$	10.128	10.128	10.128	9.277	9.277	9.277
ANOVA comparing GFAAS data of citrate and PVP Ag-NPs in OECDss						
	Overtime ANOVA			ANOVA for STP		
	$C_{Total\ Ag}$ (µg*L^{-1})	%diss. Ag	%unr. Ag	$C_{Total\ Ag}$ (µg*L^{-1})	%diss. Ag	%unr. Ag
F	7.780	5.530	4.932	9.515	4.283	9.183
P-value	0.068	0.100	0.113	0.048	0.132	0.050
$F_{critical}$	10.128	10.128	10.128	9.277	9.277	9.277

A3-3.2 Two-way ANOVA test without replicate (α = 0.05) of the UV-Vis data (MA and the corresponded wavelength) of citrate and PVP Ag-NPs in OECDss and is components; samples collected at 0 hrs and 24 hrs (left at room temperature), 45 hrs (during aeration) and 48 hrs (during settling)

Table A3 - 19: Two way ANOVA without replicate (α = 0.05), comparing the UV-Vis data (MA and λmax) of citrate and PVP Ag-NPs in peptone, meat-extract, urea, K_2HPO_4, NaCl $CaCl_2$, $MgSO_4$ and OECDss media: before aeration (at 0 and 24 hrs), during aeration (at 45 hrs) and after settling (at 48 hrs).

ANOVA comparing UV-Vis data of citrate and PVP Ag-NPs in peptone				
	Overtime ANOVA		ANOVA for STP	
	Max. absorbance	λ_{max} (nm)	Max. absorbance	λ_{max} (nm)
F	13.890	5.400	5.897	3.4
P-value	0.034	0.103	0.089	0.171
$F_{critical}$	10.128	10.128	9.277	9.277
ANOVA comparing UV-Vis data of citrate and PVP Ag-NPs in meat-extract				
	Overtime ANOVA		ANOVA for STP	
	Max. absorbance	λ_{max} (nm)	Max. absorbance	λ_{max} (nm)
F	189.343	0.010	112.771	0.187
P-value	0.001	0.928	0.001	0.899
$F_{critical}$	10.128	10.128	9.277	9.277
ANOVA comparing UV-Vis data of citrate and PVP Ag-NPs in urea				
	Overtime ANOVA		ANOVA for STP	
	Max. absorbance	λ_{max} (nm)	Max. absorbance	λ_{max} (nm)
F	3.860	5.123	1.166	2.630
P-value	0.144	0.110	0.451	0.224
$F_{critical}$	10.128	10.128	9.277	9.277
ANOVA comparing UV-Vis data of citrate and PVP Ag-NPs in K_2HPO_4				
	Overtime ANOVA		ANOVA for STP	
	Max. absorbance	λ_{max} (nm)	Max. absorbance	λ_{max} (nm)
F	0.191	3.095	63.362	1.090
P-value	0.691	0.177	0.003	0.473
$F_{critical}$	10.128	10.128	9.277	9.277
ANOVA comparing UV-Vis data of citrate and PVP Ag-NPs in NaCl				
	Overtime ANOVA		ANOVA for STP	
	Max. absorbance	λ_{max} (nm)	Max. absorbance	λ_{max} (nm)
F	0.780	18.25	2.854	4.754
P-value	0.442	0.024	0.206	0.116
$F_{critical}$	10.128	10.128	9.277	9.277

ANOVA comparing UV-Vis data of citrate and PVP Ag-NPs in $CaCl_2$				
	Overtime ANOVA		**ANOVA for STP**	
	Max. absorbance	**λ_{max} (nm)**	**Max. absorbance**	**λ_{max} (nm)**
F	2.070	2.606	4.96	1.240
P-value	0.246	0.205	0.110	0.432
$F_{critical}$	10.128	10.128	9.277	9.277
ANOVA comparing UV-Vis data of citrate and PVP Ag-NPs in $MgSO_4$				
	Overtime ANOVA		**ANOVA for STP**	
	Max. absorbance	**λ_{max} (nm)**	**Max. absorbance**	**λ_{max} (nm)**
F	56.793	26.560	750.712	2.170
P-value	0.005	0.014	0.000	0.270
$F_{critical}$	10.128	10.128	9.277	9.277
ANOVA comparing UV-Vis data of citrate and PVP Ag-NPs in OECDss				
	Overtime ANOVA		**ANOVA for STP**	
	Max. absorbance	**λ_{max} (nm)**	**Max. absorbance**	**λ_{max} (nm)**
F	77.824	2.612	104.824	26.727
P-value	0.003	0.205	0.002	0.012
$F_{critical}$	10.128	10.128	9.277	9.277

A3-3.3 Two-way ANOVA test without replicate (α = 0.05) of the UV-Vis particles size using $model_1$ of citrate and PVP Ag-NPs in OECDss and is components; samples collected at 0 hrs and 24 hrs (left at room temperature), 45 hrs (during aeration) and 48 hrs (during settling)

Table A3 - 20: Two way ANOVA without replicate (α = 0.05), comparing the UV-Vis calculated size (from $model_1$) of citrate and PVP Ag-NPs in Peptone, meat-extract, urea, K_2HPO_4, NaCl $CaCl_2$, $MgSO_4$ media: before aeration (at 0 and 24 hrs), during aeration (at 45 hrs) and after settling (at 48 hrs).

ANOVA comparing UV-Vis size of citrate and PVP Ag-NPs								
	Overtime ANOVA				ANOVA for STP			
	Peptone	Meat-extract	Urea	K_2HPO_4	Peptone	Meat-extract	Urea	K_2HPO_4
F	5.417	0.111	5.121	3.103	3.412	0.106	2.628	1.090
P-value	0.102	0.795	0.109	0.176	0.170	0.799	0.224	0.473
$F_{critical}$	10.128	161.448	10.128	10.128	9.277	161.448	9.277	9.277
	Overtime ANOVA				ANOVA for STP			
	NaCl	$CaCl_2$	$MgSO_4$	OECDss	NaCl	$CaCl_2$	$MgSO_4$	OECDss
F	18.100	2.607	26.454	N/A	4.722	1.238	2.159	N/A
P-value	0.024	0.205	0.014	N/A	0.117	0.433	0.272	N/A
$F_{critical}$	10.128	10.128	10.128	N/A	9.277	9.277	9.277	N/A

A3-3.4 Two-way ANOVA test without replicate (α = 0.05) of the DLS data of citrate and PVP Ag-NPs in OECDss and is components; samples collected at 0 hrs and 24 hrs (left at room temperature), 45 hrs (during aeration) and 48 hrs (during settling)

Table A3 - 21: Two way ANOVA without replicate (α = 0.05), comparing the DLS data (Primary peak (nm), PDI, ZP (ZP, in mV)) of citrate and PVP Ag-NPs in peptone, meat-extract, urea, K_2HPO_4, NaCl $CaCl_2$, $MgSO_4$ and OECDss media: before aeration (at 0 and 24 hrs), during aeration (at 45 hrs) and after settling (at 48 hrs).

ANOVA comparing DLS data of citrate and PVP Ag-NPs in peptone						
	Overtime ANOVA			ANOVA for specific time point (STP)		
	Primary peak (nm)	PDI	ZP (mV)	Primary peak (nm)	PDI	ZP (mV)
F	0.009	13.79	0.561	2.073	7.874	4.467
P-value	0.931	0.034	0.508	0.282	0.062	0.125
$F_{critical}$	10.128	10.128	10.128	9.277	9.277	9.277
ANOVA comparing DLS data of citrate and PVP Ag-NPs in meat-extract						
	Overtime ANOVA			ANOVA for STP		
	Primary peak (nm)	PDI	ZP (mV)	Primary peak (nm)	PDI	ZP (mV)
F	0.538	0.774	2.215	14.173	0.542	3.836
P-value	0.516	0.444	0.233	0.028	0.686	0.149
$F_{critical}$	10.128	10.128	10.128	9.277	9.277	9.277
ANOVA comparing DLS data of citrate and PVP Ag-NPs in urea						
	Overtime ANOVA			ANOVA for STP		
	Primary peak (nm)	PDI	ZP (mV)	Primary peak (nm)	PDI	ZP (mV)
F	1.274	1.252	1.843	0.199	0.432	0.275
P-value	0.341	0.345	0.267	0.89	0.746	0.841
$F_{critical}$	10.128	10.128	10.128	9.277	9.277	9.277
ANOVA comparing DLS data of citrate and PVP Ag-NPs in K_2HPO_4						
	Overtime ANOVA			ANOVA for STP		
	Primary peak (nm)	PDI	ZP (mV)	Primary peak (nm)	PDI	ZP (mV)
F	3.250	0.564	4.064	0.700	0.260	2.173
P-value	0.170	0.507	0.137	0.611	0.851	0.270
$F_{critical}$	10.128	10.128	10.128	9.277	9.277	9.277
ANOVA comparing DLS data of citrate and PVP Ag-NPs in NaCl						
	Overtime ANOVA			ANOVA for STP		
	Primary peak (nm)	PDI	ZP (mV)	Primary peak (nm)	PDI	ZP (mV)
F	2.425	0.714	2.330	0.632	0.080	1.200
P-value	0.217	0.460	0.224	0.642	0.967	0.442
$F_{critical}$	10.128	10.128	10.128	9.277	9.277	9.277

ANOVA comparing DLS data of citrate and PVP Ag-NPs in $CaCl_2$						
	Overtime ANOVA			ANOVA for STP		
	Primary peak (nm)	PDI	ZP (mV)	Primary peak (nm)	PDI	ZP (mV)
F	5.990	0.600	0.738	0.880	2.100	1.300
P-value	0.092	0.495	0.453	0.541	0.279	0.417
$F_{critical}$	10.128	10.128	10.128	9.277	9.277	9.277
ANOVA comparing DLS data of citrate and PVP Ag-NPs in $MgSO_4$						
	Overtime ANOVA			ANOVA for STP		
	Primary peak (nm)	PDI	ZP (mV)	Primary peak (nm)	PDI	ZP (mV)
F	2.387	0.103	0.477	0.647	1.301	0.357
P-value	0.220	0.769	0.539	0.655	0.417	0.790
$F_{critical}$	10.128	10.128	10.128	9.277	9.277	9.277
ANOVA comparing DLS data of citrate and PVP Ag-NPs in OECDss						
	Overtime ANOVA			ANOVA for STP		
	Primary peak (nm)	PDI	ZP (mV)	Primary peak (nm)	PDI	ZP (mV)
F	1.259	0.211	0.693	5.560	2.465	1.274
P-value	0.344	0.677	0.466	0.100	0.239	0.423
$F_{critical}$	10.128	10.128	10.128	9.277	9.277	9.277

A3-3.5 Two-way ANOVA test without replicate (α = 0.05) of the TEM data (MA and the corresponded wavelength) of citrate and PVP Ag-NPs in OECDss and is components; samples collected at 0 hrs and 24 hrs (left at room temperature), 45 hrs (during aeration) and 48 hrs (during settling)

Table A3 - 22: Two way ANOVA without replicate (α = 0.05), comparing the TEM core size (nm) of citrate and PVP Ag-NPs in peptone and meat-extract media: before aeration (at 0 and 24 hrs), during aeration (at 45 hrs) and after settling (at 48 hrs).

ANOVA comparing TEM size of citrate and PVP Ag-NPs				
	in peptone		in meat-extract	
	Overtime ANOVA	ANOVA for STP	Overtime ANOVA	ANOVA for STP
F	16.85	4.950	9.183	0.712
P-value	0.026	0.111	0.056	0.607
$F_{critical}$	10.128	9.28	10.13	9.277
ANOVA comparing TEM size of citrate and PVP Ag-NPs				
	in urea		in K_2HPO_4	
	Overtime ANOVA	ANOVA for STP	Overtime ANOVA	ANOVA for STP
F	0.030	0.147	0.497	0.580
P-value	0.873	0.727	0.710	0.670
$F_{critical}$	10.128	9.28	10.13	9.277
ANOVA comparing TEM size of citrate and PVP Ag-NPs				
	in NaCl		in $CaCl_2$	
	Overtime ANOVA	ANOVA for STP	Overtime ANOVA	ANOVA for STP
F	0.005	2.875	1.248	0.552
P-value	0.950	0.204	0.345	0.681
$F_{critical}$	10.128	9.28	10.13	9.277
ANOVA comparing TEM size of citrate and PVP Ag-NPs				
	in $MgSO_4$		in OECDss	
	Overtime ANOVA	ANOVA for STP	Overtime ANOVA	ANOVA for STP
F	0.995	0.726	0.748	3.305
P-value	0.392	0.601	0.450	0.176
$F_{critical}$	10.128	9.28	10.13	9.277

A4 Appendix4: chapter 5 supplement

A4-1 UV-Vis particles size of citrate and PVP Ag-NPs in OECDss: treatment with and without aeration and absence of the activated sludge

A4-1.1 UV-Vis particles size of citrate and PVP Ag-NPs in OECDss: treatment with and without aeration and absence of the activated sludge; samples collected at 45 hrs (non-aeration phase and at 48 hrs (settling phase)

The average size (D) of the particles, calculated using the Drude and Mie model ($model_1$ (Equation A2 - 1)) showed that citrate and PVP-capped Ag-NPs present in an aerated WWTP increased in size over time and at each phase of the treatment - before aeration (at 0 and 24 hrs), during aeration (or at 45 hrs) and after aeration (at 48 hrs) (Figure A4 - 1, Table A4 - 1 and Table A4 - 2). With an estimated average size before exposure to the OECDss of 8.81 and 7.97 nm respectively, the citrate and PVP Ag-NPs size increased directly to 57.80 and 53.07% respectively after their dispersion (at 0 hrs) in the OECDss, reaching average sizes of 13.90 and 12.20 nm respectively. PVP Ag-NPs stayed constant in size after twenty-four hours of exposure, but citrate Ag-NPs average size was 70.26% larger (15.00 nm) than their initial.

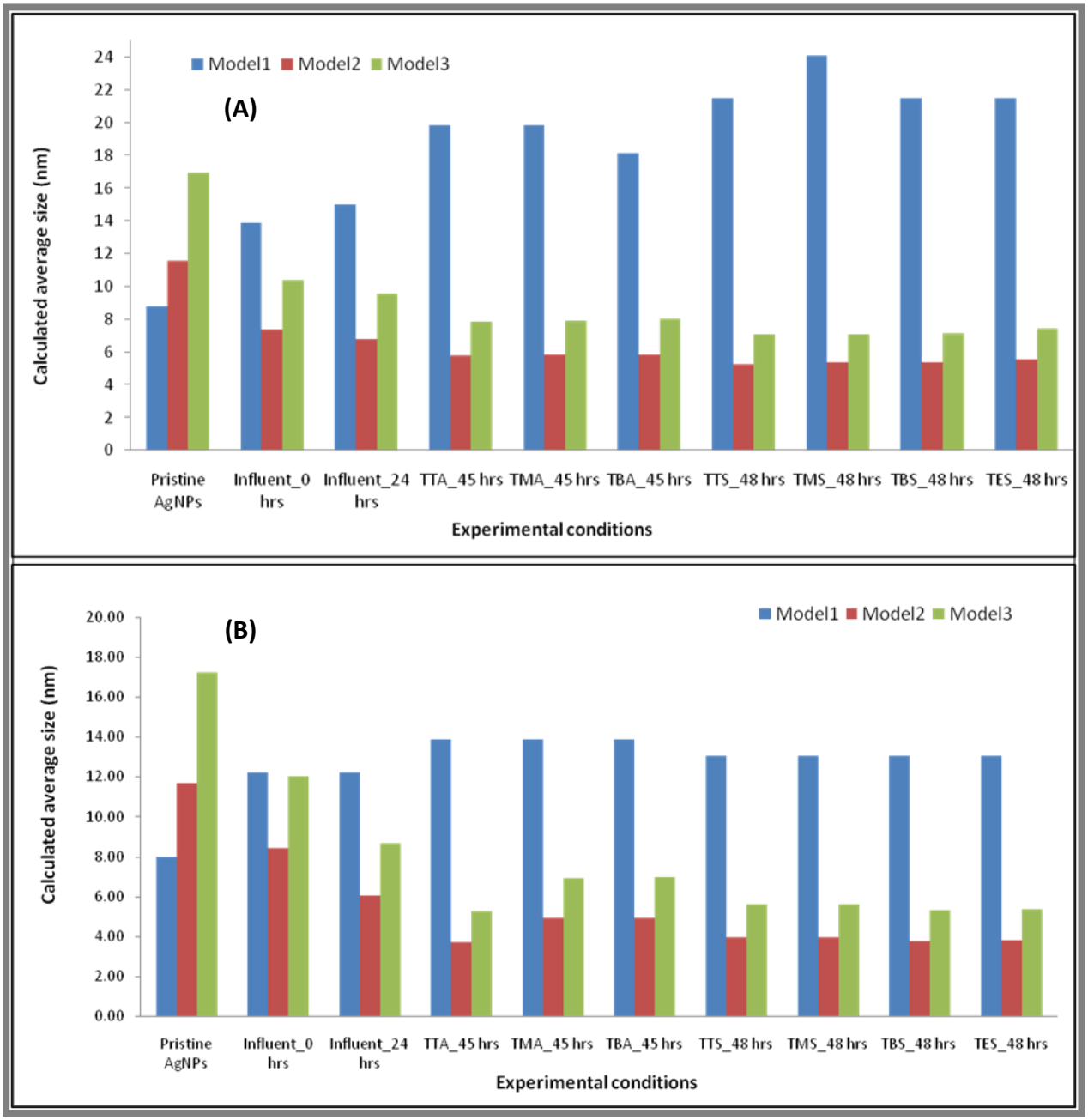

Figure A4 - 1: Citrate (A) and PVP (B) Ag-NPs in OECDss – Calculated average size of the particles from UV-Vis data using the Drude and Mie models before treatment (at 0 and 24 hrs) and during treatment with the samples collected from the top, middle and bottom of the SBR reactor at the aeration stage (TTA_45 hrs, TMA_45 hrs and TBA_45 hrs) and at the settling stage 48 hrs (TTS_48 hrs, TMS_48 hrs and TBS_48 hrs).

The treatment of the sewage in the SBR with aeration affected the average size of citrate Ag-NPs more than that of the PVP Ag-NPs. Indeed, during treatment, the citrate Ag-NPs agglomerated quite strongly. And as evidenced, their average size significantly increased to 125.10% (19.83 nm) at 45 hrs for samples collected at the top and in the middle of the SBR

reactor and 105.90% (18.14 nm) for the sample collected at the bottom of the reactor. This suggests the formation of (on average) dimers (2 particle clusters) of the citrate Ag-NPs. For the PVP Ag-NPs, the treatment of the OECDss had little to no effect on their size since the average value of the later had increased only to 74.40% (13.90 nm) at 45 hrs, and reduced to 13.05 nm (but still 63.74% compare to the pristine particles size) at 48 hrs. However, the size of the citrate Ag-NPs had increased to 144.40% (21.52 nm) at the top and bottom of the SBR reactor and to 173.21% (24.07 nm) in the middle, close in size to 3-particle agglomerates (on average).

When using $model_2$ (Equation A2 - 3) and $model_3$ (Equation A2 - 7) the changes in the average particle size was opposite to the trend revealed by $model_1$ which showed agglomeration of the particles (Figure A4 - 1, Table A4 - 1 and Table A4 - 2). In fact, the estimation of the particle size by $model_2$ and $model_3$ suggest that citrate and PVP Ag-NPs dispersed in OECDss dissolved within the first hour. The calculated values were in the same range for both models. Indeed, the average size of pristine citrate and PVP Ag-NPs were 11.58 and 11.69 nm respectively when using $model_2$ and 16.94 and 17.22 nm by applying $model_3$. At 0 hrs, after their dispersion in the media, both particles seemed to dissolve. However, $model_3$ showed higher degree dissolution of the particles with D being equal to 10.41 and 12.05 nm for citrate and PVP Ag-NPs respectively. Meaning there was a reduction of 56.48 and 30.02% respectively compared to their initial average size when using $model_3$. But, $model_2$ gave D equal to 7.37 and 8.43 respectively, i.e. there was a reduction in average size of 36.35% for the citrate Ag-NPs and 27.89% for the PVP Ag-NPs.

After 24 hrs, the citrate Ag-NPs size was mostly constant by both models with a value D of 6.81 nm ($model_2$) and 9.51 nm ($model_3$) with a reduction of 41.19% and 64.00% respectively, suggesting their dissolution was nearly nonexistent. But PVP Ag-NPs were found to have a high dissolution of the particles during this stage with an average size 48.25% ($model_2$) and 49.77% ($model_3$), corresponding to a D value of 6.05 nm and 8.65 nm respectively. These data are consistent with the UV-Vis data shown in Figures 5-4 and 5-5 above, where the PVP Ag-NPs showed greater loss of absorbance at 24 hrs compared to the citrate Ag-NPs. However, the GFAAS data in Figures 5-2 and 5-3 for the citrate and PVP Ag-NPs respectively, indicate a greater loss of Ag-NPs for citrate than for PVP coated.

The treatment of the sewage by aeration for twenty-one hours and then settling for three hours showed further dissolution of both citrate and PVP Ag-NPs since their average size was about 6 and 5 nm respectively according to $model_2$, and 8 and 7 nm respectively when $model_3$ was applied. Also, $model_2$ and $model_3$ showed that citrate and PVP Ag-NPs average size did not change during settling (at 48 hrs) as D was constant for both particle types.

The ANOVA test for $\alpha = 0.05$ (Table A4 - 24) was done by comparing the calculated average size (D) of the citrate Ag-NPs and PVP Ag-NPs in OECDss before aeration (at 0 and 24 hrs), during aeration (at 45 hrs) and settling (at 48 hrs). It was found that there was no significant difference in the average particle size before aeration using all three models since their corresponded F was lower than $F_{critical}$. Meaning, there was no significant difference between the mean sizes of both particle types before treatment. However, a significant difference in the particle size was found during and after aeration of the synthetic sewage since $F > F_{critical}$ in these cases.

Table A4 - 1: UV-Vis calculated size of citrate Ag-NPs in OECDss before and after treatment – Model$_1$ (function of FWHM and λ_{max}), model$_2$ (function of FWHM) and model$_3$ (function of FWHM) are deducted from Drude and Mie theory (Appendix 0).

	Model$_1$		Model$_2$		Model$_3$	
	NP size	%increase	NP size	%decrease	NP size	%decrease
Citrate Ag-NPs	8.81	0	11.58	0	16.95	0
Influent_0 hrs	13.90	57.80	7.37	36.35	10.41	56.48
Influent_24 hrs	15.00	70.26	6.81	41.19	9.54	64.00
TTA_45 hrs	19.83	125.10	5.80	49.91	7.86	78.50
TMA_45 hrs	19.83	125.10	5.83	49.65	7.9	78.15
TBA_45 hrs	18.14	105.90	5.85	49.48	8.02	77.11
TTS_48 hrs	21.52	144.27	5.28	54.40	7.07	85.32
TMS_48 hrs	24.07	173.21	5.40	53.37	7.11	84.97
TBS_48 hrs	21.52	144.27	5.35	53.80	7.16	84.54
TES_48 hrs	21.52	144.27	5.55	52.07	7.42	82.30

Table A4 - 2: UV-Vis calculated size of citrate Ag-NPs in OECDss before and after treatment – Model$_1$ (function of FWHM and λ_{max}), model$_2$ (function of FWHM) and model$_3$ (function of FWHM) are deducted from Drude and Mie theory (Appendix 0).

	Model$_1$		Model$_2$		Model$_3$	
	NP size	%increase	NP size	%decrease	NP size	%decrease
PVP Ag-NPs	7.97	0	11.69	0	17.22	0
Influent_0 hrs	12.20	53.07	8.43	27.89	12.05	30.02
Influent_24 hrs	12.20	53.07	6.05	48.25	8.65	49.77
TTA_45 hrs	13.90	74.40	3.72	68.18	5.26	69.45
TMA_45 hrs	13.90	74.40	4.91	58.00	6.93	59.76
TBA_45 hrs	13.90	74.40	4.93	57.83	6.96	59.58
TTS_48 hrs	13.05	63.74	3.96	66.12	5.62	67.36
TMS_48 hrs	13.05	63.74	3.96	66.12	5.62	67.36
TBS_48 hrs	13.05	63.74	3.75	67.92	5.33	69.05
TES_48 hrs	13.05	63.74	3.79	67.58	5.38	68.76

A4-1.2 UV-Vis particles size of citrate and PVP Ag-NPs in OECDss: treatment without aeration flow and absence of the activated sludge; samples collected at 45 hrs (non-aeration phase) and at 48 hrs (settling phase)

Table A4 - 2, shows the trend of the calculated average size (D) of citrate Ag-NPs in OECDss treated in the absence aeration. As we have seen above (Appendix A4-1.1), the D values determined using the Drude and Mie model show that the citrate Ag-NPs may have agglomerated ($model_1$: size increased) or dissolved ($model_2$ and $model_3$: size decreased). So, according to the D values given by all three models, the size of citrate Ag-NPs had increased from 8.81 nm to 13.05 nm ($model_1$), 11.58 nm ($model_2$) and 16.9 nm ($model_3$) within the first hour of their exposure to the synthetic sewage. But after 24 hrs, $model_2$ and $model_3$ showed a reduction of D to respectively 6.35 and 8.97 nm, whereas $model_1$ gave D constant.

During the non-aeration (stirring the media from 24 hrs to 45 hrs), according to $model_1$ the size of the particles was not affected, and after 3 hrs of settling (no stirring for 3 hrs), D had increased to 15.59 nm. Based on these results, we may conclude that even in the absence of aeration, citrate Ag-NPs present in WWTP undergo agglomeration. But these results contradict with the ones given by $model_2$ and $model_3$ which suggest further dissolution of citrate Ag-NPs for samples collected 45 hrs with D equal about 5 and 7 nm respectively. These sizes of the particles were maintained even after the settling phase at 48 hrs.

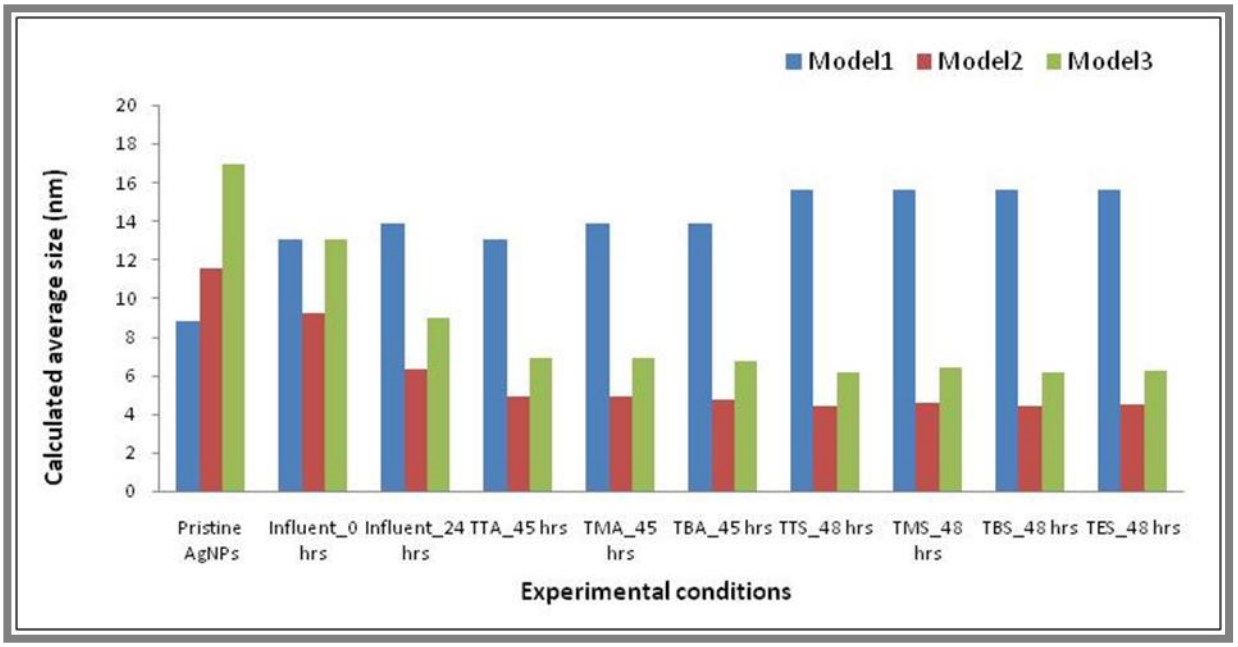

Figure A4 - 2: Citrate Ag-NPs in OECDss – Calculated average size of the particles by UV-Vis using the Drude and Mie models before and during treatment with no aeration.

The ANOVA test for $\alpha = 0.05$ (Table A4 - 26) was done by comparing the calculated average size (D) of the citrate Ag-NPs in OECDss under two conditions: treatment of the influent in the presence of an aeration flow (at 45 hrs) and absence of an aeration flow. It was found that there was a significant difference in the average particle size for all three models at 45 and 48 hrs. Meaning the aeration of the sewage would affect the Ag-NPs size, as it might accelerate their dissolution via oxidation and the dissolved particles could re-precipitate by forming larger particles as observed in section 5.3.1.4.

A4-2 DLS Average size of citrate and PVP Ag-NPs dispersed in OECDss: treatment in SBR plant with aeration and in absence of activated sludge.

Since the DLS signal of most the samples analysed had more than one peak, the Average Ag-NPs size given by the DLS was represented by the size of the scattering peak that contained a higher percentage volume and number of NPs.

❖ **Citrate Ag-NPs spiked in OECDss: treatment in SBR plant with aeration and in absence of activated sludge**

Table A4 - 3: DLS data of citrate capped Ag-NPs: average diameter (nm), percentage intensity, volume and number of each scattering peak.

Citrate pristine Ag-NPs: Z-average (nm) = 22.8 ± 0.1 and PDI = 0.30 ± 0.00				
	Average diameter (nm)	% Intensity	%Volume	% Number
Peak 1	34.9 ± 0.70	100.00 + 0.00	100.00 + 0.00	100.00 + 0.00
Peak 2	0.00 ± 0.00	0.00 ± 0.00	0.00 ± 0.00	0.00 ± 0.00
Peak 3	0.00 ± 0.00	0.00 ± 0.00	0.00 ± 0.00	0.00 ± 0.00

Table A4 - 4: DLS data of citrate Ag-NPs in OECDss before treatment in the SBR pilot plant at 0 hrs (Influent_0 hrs): average diameter (nm), percentage intensity, volume and number of each scattering peak.

Citrate Ag-NPs in OECDss before treatment in SBR pilot plant at 0 hrs: Influent_0 hrs Z-average (nm) = 33.6 ± 1.7 and PDI = 0.43 ± 0.01				
	Average diameter (nm)	% Intensity	%Volume	% Number
Peak 1	55.6 ± 5.7	96.8 + 3.9	97.9 + 1.8	100.0 + 0.0
Peak 2	2253.3 ± 1978.3	3.2 ± 3.9	2.1 ± 1.8	0.0 ± 0.0
Peak 3	0.0 ± 0.00	0.0 ± 0.0	0.0 ± 0.0	0.0 ± 0.0

Table A4 - 5: DLS data of citrate Ag-NPs in OECDss before treatment in the SBR pilot plant at 24 hrs (Influent_24 hrs): average diameter (nm), percentage intensity, volume and number of each scattering peak.

Citrate Ag-NPs in OECDss before treatment in SBR pilot plant at 24 hrs: Influent_24 hrs Z-average (nm) = 38.6 ± 4.0 and PDI = 0.38 ± 0.02				
	Average diameter (nm)	% Intensity	%Volume	% Number
Peak 1	53.3 ± 7.6	91.24 ± 5.9	92.40 ± 2.5	100.0 ± 0.0
Peak 2	2935.1 ± 1014.6	8.76 ± 5.9	7.6 ± 2.5	0.0 ± 0.0
Peak 3	0.0 ± 0.0	0.0 ± 0.0	0.0 ± 0.0	0.0 ± 0.0

Table A4 - 6: DLS data of citrate Ag-NPs in OECDss during treatment in the SBR pilot plant at 45 hrs, Test sample collected from the Top of the SBR tank during Aeration (TTA_45 hrs): average diameter (nm), percentage intensity, volume and number of each scattering percentage intensity, volume and number of each scattering peak.

Citrate Ag-NPs in OECDss during treatment in SBR pilot plant at 45 hrs: TTA_45 hrs Z-average (nm) = 45.2 ± 3.3 and PDI = 0.43 ± 0.01				
	Average diameter (nm)	% Intensity	%Volume	% Number
Peak 1	48.4 ± 5.2	75.5 ± 3.6	96.0 ± 0.6	100.0 ± 0.00
Peak 2	457.2 ± 49.4	24.5 ± 3.6	3.9 ± 0.6	0.0 ± 0.0
Peak 3	0.0 ± 0.0	0.0 ± 0.0	0.0 ± 0.0	0.0 ± 0.0

Table A4 - 7: DLS data of citrate Ag-NPs in OECDss during treatment in the SBR pilot plant at 45 hrs, Test sample collected from the Middle of the SBR tank during Aeration (TMA_45 hrs): average diameter (nm), percentage intensity, volume and number of each scattering peak.

Citrate Ag-NPs in OECDss during treatment in SBR pilot plant at 45 hrs: TMA_45 hrs Z-average (nm) = 34.7 ± 0.7 and PDI = 0.33 ± 0.04				
	Average diameter (nm)	**% Intensity**	**%Volume**	**% Number**
Peak 1	45.3 ± 2.6	94.3 ± 2.8	93.3 ± 2.2	100.0 ± 0.0
Peak 2	3241.5 ± 903.5	5.7 ± 2.8	6.7 ± 2.0	0.0 ± 0.0
Peak 3	0.0 ± 0.00	0.0 ± 0.0	0.0 ± 0.0	0.0 ± 0.0

Table A4 - 8: DLS data of citrate Ag-NPs in OECDss during treatment in the SBR pilot plant at 45 hrs, Test sample collected from the Bottom of the SBR tank during Aeration (TBA_45 hrs): average diameter (nm), percentage intensity, volume and number of each scattering peak.

Citrate Ag-NPs in OECDss during treatment in SBR pilot plant at 45 hrs: TBA_45 hrs Z-average (nm) = 38.6 ± 1.8 and PDI = 0.37 ± 0.02				
	Average diameter (nm)	**% Intensity**	**%Volume**	**% Number**
Peak 1	46.8 ± 3.1	87.7 ± 5.46	95.2 ± 1.9	100.0 ± 0.0
Peak 2	1329.8 ± 77.7	12.3 ± 5.46	4.8 ± 1.9	0.0 ± 0.0
Peak 3	0.0 ± 0.0	0.00 ± 0.0	0.0 ± 0.0	0.0 ± 0.0

Table A4 - 9: DLS data of citrate Ag-NPs in OECDss during treatment in the SBR pilot plant at 48 hrs, Test sample collected from the Top of the SBR tank during Settling (TTS_48 hrs): average diameter (nm), percentage intensity, volume and number of each scattering peak.

Citrate Ag-NPs in OECDss during treatment in SBR pilot plant at 48 hrs: TTS_48 hrs Z-average (nm) = 45.6 ± 3.6 and PDI = 0.44 ± 0.01				
	Average diameter (nm)	**% Intensity**	**%Volume**	**% Number**
Peak 1	44.6 ± 2.5	70.2 ± 5.7	96.1 ± 0.74	100.0 ± 0.0
Peak 2	364.2 ± 46.2	29.8 ± 5.7	3.9 ± 0.71	0.0 ± 0.0
Peak 3	0.0 ± 0.0	0.00 ± 0.0	0.00 ± 0.0	0.00 ± 0.0

Table A4 - 10: DLS data of citrate Ag-NPs in OECDss during treatment in the SBR pilot plant at 48 hrs, Test sample collected from the Middle of the SBR tank during Settling (TTS_48 hrs): average diameter (nm), percentage intensity, volume and number of each scattering peak.

Citrate Ag-NPs in OECDss during treatment in SBR pilot plant at 48 hrs: TMS_48 hrs **Z-average (nm) = 51.0 ± 1.1 and PDI = 0.42 ± 0.01**				
	Average diameter (nm)	**% Intensity**	**%Volume**	**% Number**
Peak 1	59.2 ± 2.6	78.3 ± 2.0	94.4 ± 0.6	100.0 ± 0.0
Peak 2	397.3 ± 3.0	21.7 ± 2.0	5.6 ± 0.6	0.0 ± 0.0
Peak 3	0.0 ± 0.0	0.0 ± 0.0	0.0 ± 0.	0.0 ± 0.0

Table A4 - 11: DLS data of citrate Ag-NPs in OECDss during treatment in the SBR pilot plant at 48 hrs, Test sample collected from the Bottom of the SBR tank during Settling (TTS_48 hrs): average diameter (nm), percentage intensity, volume and number of each scattering peak

Citrate Ag-NPs in OECDss during treatment in SBR pilot plant at 48 hrs: TBS_48 hrs Z-average (nm) = 65.5 ± 6.2 and PDI = 0.48 ± 0.03				
	Average diameter (nm)	% Intensity	%Volume	% Number
Peak 1	54.6 ± 3.5	57.4 ± 3.4	90.0 ± 2.1	100.0 ± 0.0
Peak 2	309.2 ± 28.2	42.6 ± 3.3	10.0 ± 2.1	0.0 ± 0.0
Peak 3	0.0 ± 0.0	0.0 ± 0.0	0.0 ± 0.0	0.0 ± 0.0

Table A4 - 12: DLS data of citrate Ag-NPs in OECDss during treatment in the SBR pilot plant at 48 hrs, Test sample collected from the Effluent of the SBR tank during Settling (TES_48 hrs): average diameter (nm), percentage intensity, volume and number of each scattering peak.

Citrate Ag-NPs in OECDss during treatment in SBR pilot plant at 48 hrs: TES_48 hrs Z-average (nm) = 49.7 ± 2.6 and PDI = 0.42 ± 0.02				
	Average diameter (nm)	% Intensity	%Volume	% Number
Peak 1	53.9 ± 5.9	74.9 ± 7.7	94.8 ± 1.0	100.0 ± 0.0
Peak 2	370.1 ± 77.2	25.1 ± 7.7	5.2 ± 1.0	0.0 ± 0.0
Peak 3	0.0 ± 0.0	0.0 ± 0.0	0.0 ± 0.0	0.0 ± 0.0

- **PVP Ag-NPs spiked in OECDss: treatment in SBR plant with aeration and in absence of activated sludge**

Table A4 - 13: DLS data of PVP capped Ag-NPs: average diameter (nm), percentage intensity, volume and number of each scattering peak.

PVP pristine Ag-NPs: Z-average (nm) = 36.8 ± 0.6 and PDI = 0.34± 0.06				
	Average diameter (nm)	% Intensity	%Volume	% Number
Peak 1	38.9 ± 1.6	75.7 ± 5.9	99.4 ± 0.1	100 ± 0.0
Peak 2	159.1 ± 15.7	24.3 ± 5.9	0.6 ± 0.1	0.0 ± 0.0
Peak 3	0.0 ± 0.0	0.0 ± 0.0	0.0 ± 0.0	0.0 ± 0.0

Table A4 - 14: DLS data of PVP Ag-NPs in OECDss before treatment in the SBR pilot plant at 0 hrs (Influent_0 hrs): average diameter (nm), percentage intensity, volume and number of each scattering peak.

PVP Ag-NPs in OECDss before treatment in SBR pilot plant at 0 hrs: Influent_0 hrs Z-average (nm) = 48.2 ± 8.7 and PDI = 0.47 ± 0.06				
	Average diameter (nm)	% Intensity	%Volume	% Number
Peak 1	38.7 ± 9.0	55.8 ± 9.4	89.5 ± 10.8	100.0 + 0.0
Peak 2	248.4 ± 160.9	34.6 ± 5.5	4.7 ± 2.9	0.0 ± 0.0
Peak 3	965.6 ± 1494.6	9.6 ± 7.9	5.8 ± 11.9	0.0 ± 0.0

Table A4 - 15: DLS data of PVP Ag-NPs in OECDss before treatment in the SBR pilot plant at 0 hrs (Influent_0 hrs): average diameter (nm), percentage intensity, volume and number of each scattering peak.

PVP Ag-NPs in OECDss before treatment in SBR pilot plant at 24 hrs: Influent_24 hrs Z-average (nm) = 56.1 ± 3.3 and PDI = 0.47 ± 0.07				
	Average diameter (nm)	% Intensity	%Volume	% Number
Peak 1	49.5 ± 6.7	66.4 ± 9.3	85.6 ± 8.2	100.0 ± 0.0
Peak 2	373.4 ± 204.3	31.6 ± 7.9	9.1 ± 6.1	0.0 ± 0.0
Peak 3	1073.3 ± 1969.6	2.0 ± 3.8	5.3 ± 8.3	0.0 ± 0.0

Table A4 - 16: DLS data of PVP Ag-NPs in OECDss during treatment in the SBR pilot plant at 45 hrs, Test sample collected from the Top of the SBR tank during Aeration (TTA_45 hrs): average diameter (nm), percentage intensity, volume and number of each scattering peak.

PVP Ag-NPs in OECDss during treatment in SBR pilot plant at 45 hrs: TTA_45 hrs Z-average (nm) = 50.8 ± 1.4 and PDI = 0.51 ± 0.02				
	Average diameter (nm)	% Intensity	%Volume	% Number
Peak 1	42.3 ± 2.4	60.4 ± 1.4	93.8 ± 1.0	100.0 ± 0.0
Peak 2	438.8 ± 27.9	39.6 ± 1.4	6.2 ± 1.0	0.0 ± 0.0
Peak 3	0.0 ± 0.0	0.0 ± 0.0	0.0 ± 0.0	0.0 ± 0.0

Table A4 - 17: DLS data of PVP Ag-NPs in OECDss during treatment in the SBR pilot plant at 45 hrs, Test sample collected from the Middle of the SBR tank during Aeration (TMA_45 hrs): average diameter (nm), percentage intensity, volume and number of each scattering peak

PVP Ag-NPs in OECDss during treatment in SBR pilot plant at 45 hrs: TMA_45 hrs Z-average (nm) = 39.6 ± 3.4 and PDI = 0.55 ± 0.09				
	Average diameter (nm)	% Intensity	%Volume	% Number
Peak 1	28.9 ± 6.2	55.20 ± 13.32	97.2 ± 1.86	100.0 ± 0.0
Peak 2	232.5 ± 60.4	37.55 ± 7.43	1.8 ± 0.77	0.0 ± 0.0
Peak 3	21.2 ± 42.3	6.9 ± 13.9	1.0 ± 0.45	0.0 ± 0.0

Table A4 - 18: DLS data of PVP Ag-NPs in OECDss during treatment in the SBR pilot plant at 45 hrs, Test sample collected from the Bottom of the SBR tank during Aeration (TBA_45 hrs): average diameter (nm), percentage intensity, volume and number of each scattering peak.

PVP Ag-NPs in OECDss during treatment in SBR pilot plant at 45 hrs: TBA_45 hrs Z-average (nm) = 55.9 ± 2.6 and PDI = 0.54 ± 0.02				
	Average diameter (nm)	% Intensity	%Volume	% Number
Peak 1	42.0 ± 14.7	38.6 ± 0.9	94.7 ± 1.4	100.0 ± 0.0
Peak 2	246.6 ± 91.4	49.7 ± 11.0	3.7 ± 1.5	0.0 ± 0.0
Peak 3	12.3 ± 10.8	11.7 ± 9.7	1.6 ± 2.7	0.0 ± 0.0

Table A4 - 19: DLS data of PVP Ag-NPs in OECDss during treatment in the SBR pilot plant at 48 hrs, Test sample collected from the Top of the SBR tank during Settling (TTS_48 hrs): average diameter (nm), percentage intensity, volume and number of each scattering peak.

PVP Ag-NPs in OECDss during treatment in SBR pilot plant at 48 hrs: TTS_48 hrs Z-average (nm) = 47.2 ± 6.3 and PDI = 0.600 ± 0.17				
	Average diameter (nm)	% Intensity	%Volume	% Number
Peak 1	28.3 ± 5.2	44.8 ± 3.8	87.0 ± 2.9	100.0 ± 0.0
Peak 2	190.5 ± 74.5	51.9 ± 4.5	3.9 ± 2.8	0.0 ± 0.0
Peak 3	4676.3 ± 613.7	3.4 ± 2.7	9.1 ± 1.7	0.0 ± 0.0

Table A4 - 20: DLS data of PVP Ag-NPs in OECDss during treatment in the SBR pilot plant at 48 hrs, Test sample collected from the Middle of the SBR tank during Settling (TMS_48 hrs): average diameter (nm), percentage intensity, volume and number of each scattering peak

PVP Ag-NPs in OECDss during treatment in SBR pilot plant at 48 hrs: TMS_48 hrs Z-average (nm) = 40.2 ± 1.5 and PDI = 0.50 ± 0.01				
	Average diameter (nm)	% Intensity	%Volume	% Number
Peak 1	34.5 ± 4.8	59.8 ± 6.9	97.6 ± 0.1	100.0 ± 0.0
Peak 2	206.0 ± 25.6	40.2 ± 6.9	2.4 ± 0.1	0.0 ± 0.0
Peak 3	0.0 ± 0.0	0.0 ± 0.0	0.0 ± 0.0	0.0 ± 0.0

Table A4 - 21: DLS data of PVP Ag-NPs in OECDss during treatment in the SBR pilot plant at 48 hrs, Test sample collected from the Bottom of the SBR tank during Settling (TBS_48 hrs): average diameter (nm), percentage intensity, volume and number of each scattering peak

PVP Ag-NPs in OECDss during treatment in SBR pilot plant at 48 hrs: TBS_48 hrs Z-average (nm) = 42.9 ± 3.2 and PDI = 0.53 ± 0.13				
	Average diameter (nm)	% Intensity	%Volume	% Number
Peak 1	26.0 ± 2.4	43.5 ± 4.6	90.9 ± 5.6	0.2 ± 0.4
Peak 2	142.7 ± 51.5	45.5 ± 3.7	5.6 ± 7.5	99.8 ± 0.4
Peak 3	2285.9 ± 1936.5	11.0 ± 7.9	3.4 ± 2.0	0.0 ± 0.0

Table A4 - 22: DLS data of PVP Ag-NPs in OECDss during treatment in the SBR pilot plant at 48 hrs, Test sample collected from the Effluent of the SBR tank during Settling (TES_48 hrs): average diameter (nm), percentage intensity, volume and number of each scattering peak.

PVP Ag-NPs in OECDss during treatment in SBR pilot plant at 48 hrs: TES_48 hrs Z-average (nm) = 60.6 ± 45.1 and PDI = 0.65 ± 0.13				
	Average diameter (nm)	% Intensity	%Volume	% Number
Peak 1	28.3 ± 3.2	34.4 ± 5.4	87.0 ± 7.8	100.0 ± 0.0
Peak 2	233.5 ± 73.8	51.6 ± 7.1	5.1 ± 3.0	0.0 ± 0.0
Peak 3	1684.1 ± 2085.2	14.0 ± 11.4	7.9 ± 7.6	0.00 ± 0.0

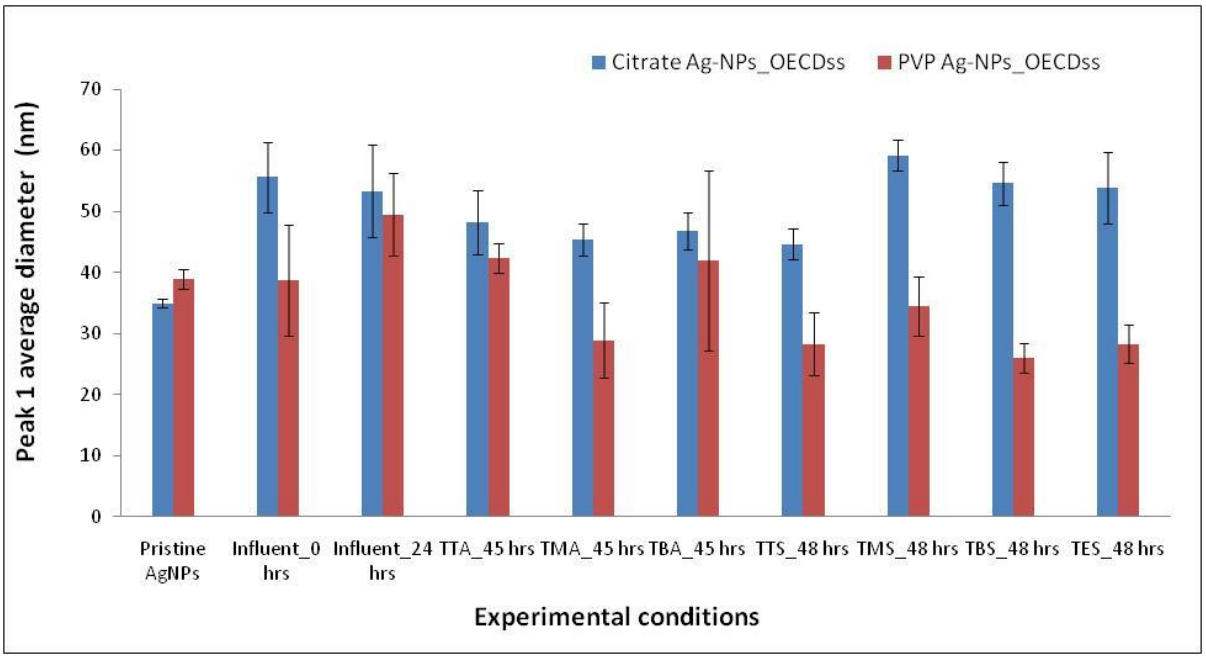

Figure A4 - 3: Variations of peak one size of citrate and PVP capped Ag-NPs in OECDss before (Pristine NPs, at 0 hrs and 24 hrs) and during treatment (at 45 hrs and 48 hrs) given by DLS: also known as average size distribution of the first peak (or peak representing a distribution off Ag-NPs with a maximum percentage of volume and number of particles.

A4-3 ANOVA test (α = 0.05) of GFAAS, UV-Vis of citrate and PVP Ag-NPs in OECDss: treatment with and without aeration; in presence and in absence on the activated sludge.

4.3.1.1. NOVA test (α = 0.05) of degree of dissolution of citrate and PVP Ag-NPs in the influent before treatment (at 0 and 24 hrs), during treatment by aeration and stirring (at 45 hrs) and after treatment or settling phase (at 48 hrs) in absence of activated sludge.

Table A4 - 23: ANOVA test (α = 0.05) of degree of dissolution of citrate and PVP Ag-NPs in the influent before treatment (at 0 and 24 hrs), during aeration (at 45 hrs), during settling (at 48 hrs) in absence of activated sludge.

Statistical test (ANOVA)									
	Before aeration (at 0 and 24 hrs)			During aeration (at 45 hrs)			During settling (at 48 hrs)		
Compared sample factor of citrate and PVP Ag-NPs	F	P-value	$F_{critical}$	F	P-value	$F_{critical}$	F	P-value	$F_{critical}$
Total Ag concentration ($C_{Total\ Ag}$)	0.017	0.908	18.513	29.923	0.005	7.709	10.376	0.018	5.987
Dissolved Ag concentration (C_{Ag+})	0.525	0.544	18.513	4.462	0.102	7.709	44.741	0.000	5.987
Estimated Ag-NPs concentration ($C_{Ag\text{-}NPs}$)	0.085	0.798	18.513	21.937	0.009	7.709	42.261	0.000	5.987

A4-1.3 ANOVA test (α = 0.05) of UV-Vis calculated average particle size of citrate and PVP Ag-NPs in OECDss before aeration (at 0 and 24 hrs), during aeration (at 45 hrs) and during settling (at 48 hrs) in absence of activated sludge.

Table A4 - 24: ANOVA test (α = 0.05) of average particle size of citrate and PVP Ag-NPs in OECDss before aeration (at 0 and 24 hrs), during aeration (at 45 hrs) and during settling (at 48 hrs) in absence of activated sludge. The average size of the Ag-NPs (D) was calculated using the Drude and Mie ($Model_1$)

Statistical test (ANOVA)									
	Before aeration			During aeration			During settling		
Compared sample factor of citrate and PVP Ag-NPs	F	P-value	$F_{critical}$	F	P-value	$F_{critical}$	F	P-value	$F_{critical}$
$Model_1$	16.736	0.055	18.513	90.756	0.000	7.709	204.100	0.000	5.987
$Model_2$	0.015	0.914	18.513	10.655	0.031	7.709	368.646	0.000	5.987
$Model_3$	0.045	0.852	18.513	7.494	0.052	7.709	238.110	0.000	5.987

A4-1.4 ANOVA test (α = 0.05) comparing the Ag concentration of citrate Ag-NPs OECDss when treated with aeration and without aeration in absence of activated sludge.

Table A4 - 25: ANOVA test (α = 0.05) of degree of dissolution of citrate Ag-NPs in OECDss used for treatment in the SBR with aeration and citrate Ag-NPs in OECDss used for treatment in the SBR without aeration. Samples collected from the influent before treatment (at0 and 24 hrs) and from the top, middle and bottom of the SBR tank during treatment at 48 hrs in absence of activated sludge.

Statistical test (ANOVA)									
	Before aeration (at 0 and 24 hrs)			During aeration (at 45 hrs)			During settling (at 48 hrs)		
Compared sample factor of citrate Ag-NPs with and without aeration	F	P-value	$F_{critical}$	F	P-value	$F_{critical}$	F	P-value	$F_{critical}$
Total Ag concentration ($C_{Total\ Ag}$)	2.206	0.276	18.513	5.170	0.085	7.709	7.989	0.030	5.987
Dissolved Ag concentration (C_{Ag+})	0.012	0.924	18.513	225.563	0.000	7.709	202.191	0.000	5.987
Estimated Ag-NPs concentration ($C_{Ag\text{-}NPs}$)	0.783	0.470	18.513	37.709	0.004	7.709	89.085	0.000	5.987

A4-1.5 ANOVA test (α = 0.05) of UV-Vis comparing calculated average particle size of citrate in OECDss only when treated with aeration and without aeration in absence of activated sludge.

Table A4 - 26: ANOVA test (α = 0.05) of average particle size of citrate and PVP Ag-NPs in OECDss before aeration (at 0 and 24 hrs), during treatment with and without aeration (at 45 hrs) and during settling (at 48 hrs) in absence of activated sludge. The average size of the Ag-NPs (D) was calculated using the Drude and Mie ($Model_1$)

Statistical test (ANOVA)									
	Before aeration (at 0 and 24 hrs)			During aeration (at 45 hrs)			During settling (at 48 hrs)		
Compared sample factor of citrate Ag-NPs with and without aeration	F	P-value	$F_{critical}$	F	P-value	$F_{critical}$	F	P-value	$F_{critical}$
$Model_1$	1.968	0.296	18.513	80.283	0.001	7.710	106.130	0.000	5.990
$Model_2$	0.221	0.685	18.513	708.500	0.000	7.710	185.022	0.000	5.990
$Model_3$	0.246	0.670	18.513	216.900	0.000	7.710	107.954	0.000	5.990

A4-1.6 ANOVA test (α = 0.05) comparing the Ag concentration of dispersed citrate and PVP Ag-NPs in OECDss when treated with aeration and in presence of activated sludge.

Table A4 - 27: ANOVA test (α = 0.05) of comparing Ag concentration of citrate and PVP Ag-NPs in OECDss used for treatment in the SBR with aeration. Samples collected from the influent (at 0 and 24 hrs), from the top, middle and bottom of the SBR reactor and during treatment at 45 and 48 hrs and from the effluent at 48 hrs in presence of activated sludge.

Statistical test (ANOVA)									
	Before aeration (at 0 and 24 hrs)			During aeration (at 45 hrs)			During settling (at 48 hrs)		
Compared sample factor of citrate and PVP Ag-NPs	F	P-value	$F_{critical}$	F	P-value	$F_{critical}$	F	P-value	$F_{critical}$
Total Ag concentration ($C_{Total\ Ag}$)	0.155	0.732	18.513	0.286	0.621	7.709	1.553	0.259	5.990
Dissolved Ag concentration (C_{Ag+})	0.250	0.670	18.513	0.036	0.860	7.709	0.076	0.792	5.990
Estimated Ag-NPs concentration ($C_{Ag\text{-}NPs}$)	0.194	0.703	18.513	0.424	0.550	7.709	2.034	0.204	5.990

A4-1 SEM image and EDS spectra of the OECDss only

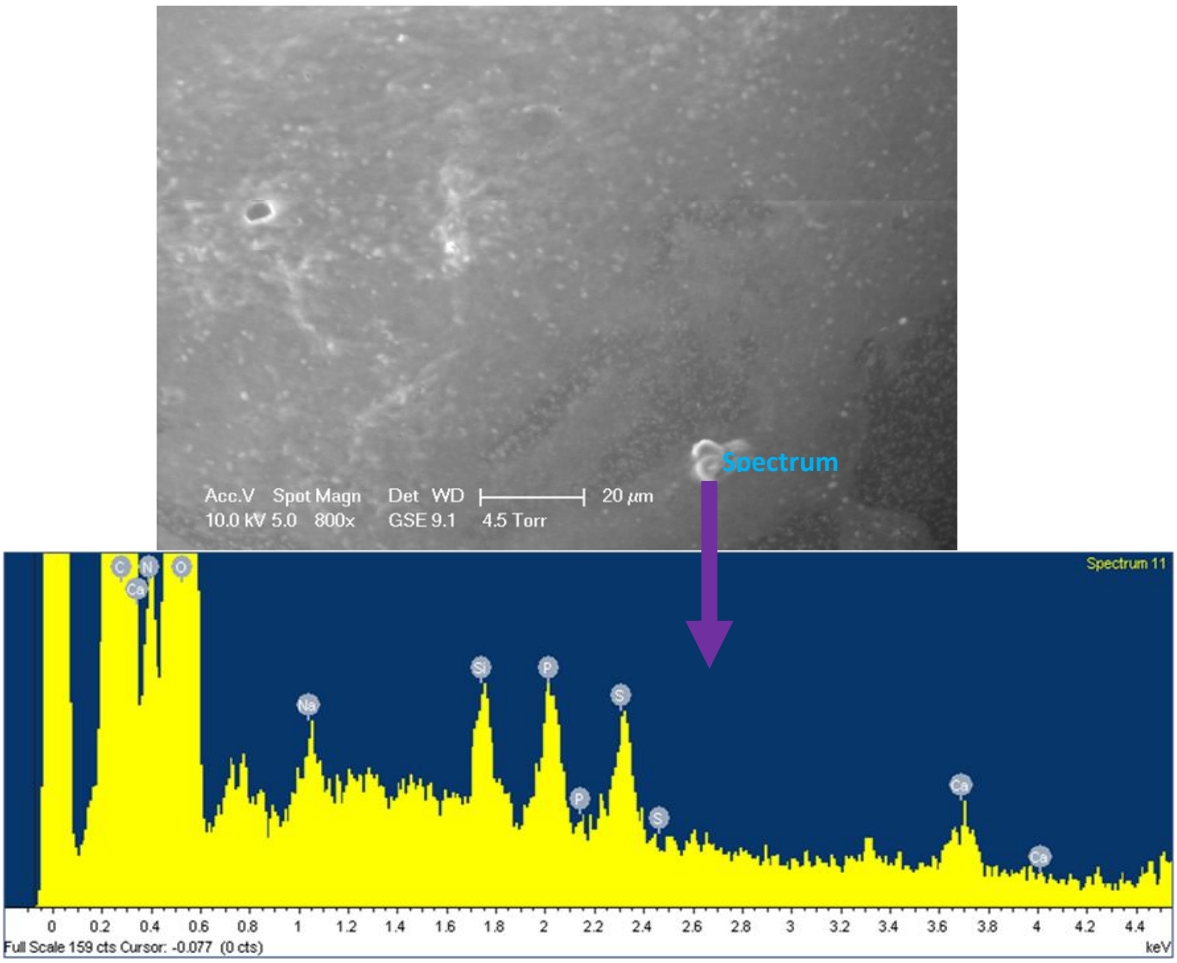

Figure A4 - 4: SEM image and EDS spectrum of the OECDss only.

A5 Appendix 5: Freundlich isotherm model summary for citrate and PVP Ag-NPs

Freundlich isotherm model Summary for PVP Ag-NPs

Model	R	R Square	Adjusted R Square	Std. Error of the Estimate	Change Statistics				
					R Square Change	F Change	df1	df2	Sig. F Change
1	.928[a]	.860	.843	.39918	.860	49.293	1	8	.000

a. Predictors: (Constant), LnCe

ANOVA[b]

Model		Sum of Squares	df	Mean Square	F	Sig.
1	Regression	7.855	1	7.855	49.293	.000[a]
	Residual	1.275	8	.159		
	Total	9.129	9			

a. Predictors: (Constant), LnCe

b. Dependent Variable: LnQe

Coefficients[a]

Model		Unstandardized Coefficients		Standardized Coefficients	t	Sig.	95.0% Confidence Interval for B	
		B	Std. Error	Beta			Lower Bound	Upper Bound
1	(Constant)	-3.951	.716		-5.517	.001	-5.602	-2.300
	LnCe	1.746	.249	.928	7.021	.000	1.172	2.319

a. Dependent Variable: LnQe

Freundlich isotherm model Summary for citrate Ag-NPs

Model	R	R Square	Adjusted R Square	Std. Error of the Estimate	Change Statistics				
					R Square Change	F Change	df1	df2	Sig. F Change
1	.958[a]	.918	.907	.29598	.918	89.150	1	8	.000

a. Predictors: (Constant), LnCe

ANOVA[b]

Model		Sum of Squares	Df	Mean Square	F	Sig.
1	Regression	7.810	1	7.810	89.150	.000[a]
	Residual	.701	8	.088		
	Total	8.511	9			

a. Predictors: (Constant), LnCe

b. Dependent Variable: LnQe

Coefficients[a]

Model		Unstandardized Coefficients		Standardized Coefficients	t	Sig.	95.0% Confidence Interval for B	
		B	Std. Error	Beta			Lower Bound	Upper Bound
1	(Constant)	-3.656	.458		-7.983	.000	-4.712	-2.600
	LnCe	1.598	.169	.958	9.442	.000	1.208	1.989

a. Dependent Variable: LnQe

References

(ISO), I. O. F. S. 2013. Agglomeration (definition). *ISO/TR 13097:2013(en).* ISO.

ABBT-BRAUN, G., LANKES, U. & FRIMMEL, F. H. 2004. Structural characterization of aquatic humic substances - The need for a multiple method approach. *Aquatic Sciences,* 66**,** 151-170.

ABOU EL-NOUR, K. M. M., EFTAIHA, A., AL-WARTHAN, A. & AMMAR, R. A. A. 2010. Synthesis and applications of silver nanoparticles. *Arabian Journal of Chemistry,* 3**,** 135-140.

AFSHINNIA, K., GIBSON, I., MERRIFIELD, R. & BAALOUSHA, M. 2016. The concentration-dependent aggregation of Ag NPs induced by cystine. *Science of the Total Environment,* 557**,** 395-403.

AGNIHOTRI, S., MUKHERJI, S. & MUKHERJI, S. 2014. Size-controlled silver nanoparticles synthesized over the range 5-100 nm using the same protocol and their antibacterial efficacy. *Rsc Advances,* 4**,** 3974-3983.

AIROUDJ, A., PLOUX, L. & ROUCOULES, V. 2015. Effect of Plasma Duty Cycle on Silver Nanoparticles Loading of Cotton Fabrics for Durable Antibacterial Properties. *Journal of Applied Polymer Science,* 132.

ALDRICH, S. *Meat-extract* [Online]. Available: http://www.sigmaaldrich.com/catalog/product/sial/70164?lang=en&region=GB.

AMUDA, O. S., GIWA, A. A. & BELLO, I. A. 2007. Removal of heavy metal from industrial wastewater using modified activated coconut shell carbon. *Biochemical Engineering Journal,* 36**,** 174-181.

ANOUAR, E., OSMAN, C., WEBER, J.-F. F. & ISMAIL, N. 2014. UV/Visible spectra of a series of natural and synthesised anthraquinones: experimental and quantum chemical approaches. *SpringerPlus,* 3**,** 233.

AQUANAL®-PROFESSIONAL. 2012a. *AQUANAL®-professional Cuvette test COD medium* [Online]. Available: http://www.sigmaaldrich.com/content/dam/sigma-aldrich/docs/Sigma-Aldrich/Instructions/1/37737_e.pdf.

AQUANAL®-PROFESSIONAL. 2012b. *AQUANAL®-professional Nitrogen Cuvette Test* [Online]. Available: http://www.sigmaaldrich.com/content/dam/sigma-aldrich/docs/Fluka/Instructions/1/70108_e.pdf.

AQUANAL®-PROFESSIONAL. 2012c. *AQUANAL®-professional Phosphate Cuvette Test, high* [Online]. Available: http://www.sigmaaldrich.com/content/dam/sigma-aldrich/docs/Fluka/Instructions/1/37744_e.pdf.

ARAUJO, R., CASTRO, A. C. M. & FIUZA, A. 2015. The use of nanoparticles in soil and water remediation processes. *Materials Today-Proceedings,* 2**,** 315-320.

ARVIDSSON, R., MOLANDER, S., SANDEN, B. A. & HASSELLOV, M. 2011. Challenges in Exposure Modeling of Nanoparticles in Aquatic Environments. *Human and Ecological Risk Assessment,* 17**,** 245-262.

ASHARANI, P., HANDE, M. P. & VALIYAVEETTIL, S. 2009. Anti-proliferative activity of silver nanoparticles. *BMC Cell Biology,* 10**,** 65.

ASHKARRAN, A. A. & BAYAT, A. 2013. Surface plasmon resonance of metal nanostructures as a complementary technique for microscopic size measurement. *International Nano Letters,* 3.

AXSON, J. L., STARK, D. I., BONDY, A. L., CAPRACOTTA, S. S., MAYNARD, A. D., PHILBERT, M. A., BERGIN, I. L. & AULT, A. P. 2015. Rapid Kinetics of Size and pH-Dependent Dissolution and Aggregation of Silver Nanoparticles in Simulated Gastric Fluid. *Journal of Physical Chemistry C,* 119**,** 20632-20641.

AZAM, A., AHMED, A. S., OVES, M., KHAN, M. S., HABIB, S. S. & MEMIC, A. 2012. Antimicrobial activity of metal oxide nanoparticles against Gram-positive and Gram-negative bacteria: a comparative study. *International Journal of Nanomedicine,* 7**,** 6003-6009.

AZIMI, Y., ALLEN, D. G., SETO, P. & FARNOOD, R. 2014. Effect of Activated Sludge Retention Time, Operating Temperature, and Influent Phosphorus Deficiency on Floc Physicochemical Characteristics and UV Disinfection. *Industrial & Engineering Chemistry Research,* 53**,** 12485-12493.

AZIZ, S. Q., AZIZ, H. A., YUSOFF, M. S. & BASHIR, M. J. K. 2011. Landfill leachate treatment using powdered activated carbon augmented sequencing batch reactor (SBR) process: Optimization by response surface methodology. *Journal of Hazardous Materials,* 189**,** 404-413.

AZONANO.COM. 2013. *Dynamic Light Scattering - Understanding the Basics* [Online]. Available: http://www.azonano.com/article.aspx?ArticleID=3662 [Accessed June 2013 2014].

BAALOUSHA, M., ARKILL, K. P., ROMER, I., PALMER, R. E. & LEAD, J. R. 2015. Transformations of citrate and Tween coated silver nanoparticles reacted with Na2S. *Science of the Total Environment,* 502**,** 344-353.

BAALOUSHA, M., MANCIULEA, A., CUMBERLAND, S., KENDALL, K. & LEAD, J. R. 2008. Aggregation and surface properties of iron oxide nanoparticles: Influence of pH and natural organic matter. *Environmental Toxicology and Chemistry,* 27**,** 1875-1882.

BAALOUSHA, M., NUR, Y., ROMER, I., TEJAMAYA, M. & LEAD, J. R. 2013. Effect of monovalent and divalent cations, anions and fulvic acid on aggregation of citrate-coated silver nanoparticles. *Science of the Total Environment,* 454**,** 119-131.

BAEK, Y. W. & AN, Y. J. 2011. Microbial toxicity of metal oxide nanoparticles (CuO, NiO, ZnO, and Sb2O3) to Escherichia coli, Bacillus subtilis, and Streptococcus aureus. *Sci Total Environ,* 409**,** 1603-8.

BAR-ILAN, O., ALBRECHT, R. M., FAKO, V. E. & FURGESON, D. Y. 2009. Toxicity Assessments of Multisized Gold and Silver Nanoparticles in Zebrafish Embryos. *Small,* 5**,** 1897-1910.

BASET, S., AKBARI, H., ZEYNALI, H. & SHAFIE, M. 2011. SIZE MEASUREMENT OF METAL AND SEMICONDUCTOR NANOPARTICLES VIA UV-Vis ABSORPTION SPECTRA. *Digest Journal of Nanomaterials and Biostructures,* 6**,** 709-716.

BASTUS, N. G., MERKOCI, F., PIELLA, J. & PUNTES, V. 2014. Synthesis of Highly Monodisperse Citrate-Stabilized Silver Nanoparticles of up to 200 nm: Kinetic Control and Catalytic Properties. *Chemistry of Materials,* 26**,** 2836-2846.

BELITZ, H. D., GROSCH, W. & SCHIEBERLE, P. 2009. *Food chemistry,* Berlin ; [London], Springer.

BENN, T. M. & WESTERHOFF, P. 2008a. Nanoparticle silver released into water from commercially available sock fabrics. *ENVIRONMENTAL SCIENCE & TECHNOLOGY,* 42**,** 4133-4139.

BENN, T. M. & WESTERHOFF, P. 2008b. Nanoparticle silver released into water from commercially available sock fabrics *ENVIRONMENTAL SCIENCE & TECHNOLOGY,* 42**,** 7025-7026.

BERKOWITZ, J., ANDERSON, M. A. & AMRHEIN, C. 2006. Influence of aging on phosphorus sorption to alum floc in lake water. *Water Research,* 40**,** 911-916.

BETTINA VOUTOU & STEFANAKI, E.-C. 2008. Electron Microscopy: The Basics. Thessalonik, Greece: Aristotle University of Thessaloniki.

BISWAS, A., WANG, T. & BIRIS, A. S. 2010. Single metal nanoparticle spectroscopy: optical characterization of individual nanosystems for biomedical applications. *Nanoscale,* 2**,** 1560-1572.

BISWAS, P. & WU, C.-Y. 2005. Nanoparticles and the Environment. *Journal of the Air & Waste Management Association,* 55**,** 708-746.

BLASER, S. A., SCHERINGER, M., MACLEOD, M. & HUNGERBUHLER, K. 2008. Estimation of cumulative aquatic exposure and risk due to silver: Contribution of nano-functionalized plastics and textiles. *Science of the Total Environment,* 390**,** 396-409.

BLINOVA, I., NISKANEN, J., KAJANKARI, P., KANARBIK, L., KAKINEN, A., TENHU, H., PENTTINEN, O. P. & KAHRU, A. 2013. Toxicity of two types of silver nanoparticles to aquatic crustaceans Daphnia magna and Thamnocephalus platyurus. *Environmental Science and Pollution Research,* 20**,** 3456-3463.

BOLEA, E., JIMENEZ-LAMANA, J., LABORDA, F., ABAD-ALVARO, I., BLADE, C., AROLA, L. & CASTILLO, J. R. 2014. Detection and characterization of silver nanoparticles and dissolved species of silver in culture medium and cells by AsFlFFF-UV-Vis-ICPMS: application to nanotoxicity tests. *Analyst,* 139**,** 914-922.

BOTHUN, G. D. 2008. Hydrophobic silver nanoparticles trapped in lipid bilayers: Size distribution, bilayer phase behavior, and optical properties. *J Nanobiotechnology,* 6**,** 13.

BOTIJA, M. O. 2006. *Characterisation and control of microthrix parvicella in a laboratory scale activated sludge plant.* Doctor of Philosophy Dissertation, University of Birmingham.

BRAR, S. K., VERMA, M., TYAGI, R. D. & SURAMPALLI, R. Y. 2010. Engineered nanoparticles in wastewater and wastewater sludge - Evidence and impacts. *Waste Management,* 30**,** 504-520.

BRITO, R. S., PINHEIRO, H. M., FERREIRA, F., MATOS, J. S. & LOURENCO, N. D. 2014. In situ UV-Vis spectroscopy to estimate COD and TSS in wastewater drainage systems. *Urban Water Journal,* 11**,** 261-273.

BUMBUDSANPHAROKE, N., CHOI, J. & KO, S. 2015. Applications of Nanomaterials in Food Packaging. *Journal of Nanoscience and Nanotechnology,* 15**,** 6357-6372.

BUZEA, C., PACHECO, I. I. & ROBBIE, K. 2007. Nanomaterials and nanoparticles: Sources and toxicity. *Biointerphases,* 2**,** Mr17-Mr71.

CAYUELA, A., SORIANO, M. L. & VALCÁRCEL, M. 2015. Reusable sensor based on functionalized carbon dots for the detection of silver nanoparticles in cosmetics via inner filter effect. *Analytica Chimica Acta*.

CHA, C. Y., SHIN, S. R., ANNABI, N., DOKMECI, M. R. & KHADEMHOSSEINI, A. 2013. Carbon-Based Nanomaterials: Multifunctional Materials for Biomedical Engineering. *Acs Nano,* 7**,** 2891-2897.

CHAI, H., YAO, J., SUN, J., ZHANG, C., LIU, W., ZHU, M. & CECCANTI, B. 2015. The effect of metal oxide nanoparticles on functional bacteria and metabolic profiles in agricultural soil. *Bull Environ Contam Toxicol,* 94**,** 490-5.

CHAKRABORTI, R. K. & KAUR, J. 2014. Noninvasive Measurement of Particle-Settling Velocity and Comparison with Stokes' Law. *Journal of Environmental Engineering,* 140.

CHEN, J. W., XIU, Z. M., LOWRY, G. V. & ALVAREZ, P. J. J. 2011. Effect of natural organic matter on toxicity and reactivity of nano-scale zero-valent iron. *Water Research,* 45**,** 1995-2001.

CHITTLEBOROUGH, D. J., TADJIKI, S., RANVILLE, J. F., SHANKS, F. & BECKETT, R. 2004. Soil colloid analysis by Flow Field-Flow Fractionation. *3rd Australian New Zealand Soils.* University of Sydney, Australia: The regional institute ltd.

CHOI, O., CLEUENGER, T. E., DENG, B. L., SURAMPALLI, R. Y., ROSS, L. & HU, Z. Q. 2009. Role of sulfide and ligand strength in controlling nanosilver toxicity. *Water Research,* 43**,** 1879-1886.

CHUN, M. S. & LEE, I. 2008. Rigorous estimation of effective protein charge from experimental electrophoretic mobilities for proteomics analysis using microchip electrophoresis. *Colloids and Surfaces a-Physicochemical and Engineering Aspects,* 318**,** 191-198.

COMFORT, K. K., MAURER, E. I., BRAYDICH-STOLLE, L. K. & HUSSAIN, S. M. 2011. Interference of silver, gold, and iron oxide nanoparticles on epidermal growth factor signal transduction in epithelial cells. *ACS Nano,* 5**,** 10000-8.

CONG, Y., BANTA, G. T., SELCK, H., BERHANU, D., VALSAMI-JONES, E. & FORBES, V. E. 2011. Toxic effects and bioaccumulation of nano-, micron- and ionic-Ag in the polychaete, Nereis diversicolor. *Aquat Toxicol,* 105**,** 403-11.

CUMBERLAND, S. A. & LEAD, J. R. 2009. Particle size distributions of silver nanoparticles at environmentally relevant conditions. *Journal of Chromatography A,* 1216**,** 9099-9105.

CURRI, M. L., COMPARELLI, R., COZZOLI, P. D., MASCOLO, G. & AGOSTIANO, A. 2003. Colloidal oxide nanoparticles for the photocatalytic degradation of organic dye. *Materials Science & Engineering C-Biomimetic and Supramolecular Systems,* 23**,** 285-289.

DABBOUSI, B. O., RODRIGUEZVIEJO, J., MIKULEC, F. V., HEINE, J. R., MATTOUSSI, H., OBER, R., JENSEN, K. F. & BAWENDI, M. G. 1997. (CdSe)ZnS core-shell quantum dots: Synthesis and characterization of a size series of highly luminescent nanocrystallites. *Journal of Physical Chemistry B,* 101**,** 9463-9475.

DALE, A. L., LOWRY, G. V. & CASMAN, E. A. 2013. Modeling Nanosilver Transformations in Freshwater Sediments. *ENVIRONMENTAL SCIENCE & TECHNOLOGY,* 47**,** 12920-12928.

DASARI, T. P. & HWANG, H. M. 2010. The effect of humic acids on the cytotoxicity of silver nanoparticles to a natural aquatic bacterial assemblage. *Science of the Total Environment,* 408**,** 5817-5823.

DEFRA 2012. Waste water treatment in the UK - 2012_Implementation of the European Union Urban waste water treatment directive - 91/271/EEC. *In:* DEPARTMENT FOR ENVIRONMENT, F. A. R. A. (ed.).

DELL'ORCO, D., LUNDQVIST, M., LINSE, S. & CEDERVALL, T. 2014. Mathematical modeling of the protein corona: implications for nanoparticulate delivery systems. *Nanomedicine,* 9**,** 851-858.

DESAI, R., MANKAD, V., GUPTA, S. K. & JHA, P. K. 2012. Size Distribution of Silver Nanoparticles: UV-Visible Spectroscopic Assessment. *Nanoscience and Nanotechnology Letters,* 4**,** 30-34.

DESTA, M. B. 2013. Batch Sorption Experiments: Langmuir and Freundlich Isotherm Studies for the Adsorption of Textile Metal Ions onto Teff Straw (Eragrostis tef) Agricultural Waste. *Journal of Thermodynamics,* 2013**,** 1-6.

DOMENECH, B., BASTOS-ARRIETA, J., ALONSO, A., MACANAS, J., MUNOZ, M. & N, D. 2012. Bifunctional Polymer-Metal Nanocomposite Ion Exchange Materials.

DOMINGOS, R. F., BAALOUSHA, M. A., JU-NAM, Y., REID, M. M., TUFENKJI, N., LEAD, J. R., LEPPARD, G. G. & WILKINSON, K. J. 2009. Characterizing Manufactured Nanoparticles in the Environment: Multimethod Determination of Particle Sizes. *ENVIRONMENTAL SCIENCE & TECHNOLOGY,* 43**,** 7277-7284.

DOOLETTE, C. L., MCLAUGHLIN, M. J., KIRBY, J. K., BATSTONE, D. J., HARRIS, H. H., GE, H. Q. & CORNELIS, G. 2013. Transformation of PVP coated silver nanoparticles in a simulated wastewater treatment process and the effect on microbial communities. *Chemistry Central Journal,* 7.

DUBBER, D. & GRAY, N. F. 2010. Replacement of chemical oxygen demand (COD) with total organic carbon (TOC) for monitoring wastewater treatment performance to minimize disposal of toxic analytical waste. *Journal of Environmental Science and Health Part a-Toxic/Hazardous Substances & Environmental Engineering,* 45**,** 1595-1600.

DUNESCIENCES. 2011. *Particle Size analysis of nanomaterials using ImageJ/Fiji* [Online]. Available: http://www.dunesciences.com/files/Particle_Size_Analysis_SOP.pdf [Accessed 09052014 2014].

DURAN, N., SILVEIRA, C. P., DURAN, M. & MARTINEZ, D. S. T. 2015. Silver nanoparticle protein corona and toxicity: a mini-review. *Journal of Nanobiotechnology,* 13.

EATON, A. D. & FRANSON, M. A. H. 2005. *Standard methods for the examination of water & wastewater,* Washington, DC, American Public Health Association.

EGC 2015. Wastewater Management European Green Capital.

EL BADAWY, A. M., LUXTON, T. P., SILVA, R. G., SCHECKEL, K. G., SUIDAN, M. T. & TOLAYMAT, T. M. 2010. Impact of Environmental Conditions (pH, Ionic Strength, and Electrolyte Type) on the Surface Charge and Aggregation of Silver Nanoparticles Suspensions. *ENVIRONMENTAL SCIENCE & TECHNOLOGY,* 44**,** 1260-1266.

ELLEGAARD-JENSEN, L., JENSEN, K. A. & JOHANSEN, A. 2012. Nano-silver induces dose-response effects on the nematode Caenorhabditis elegans. *Ecotoxicol Environ Saf,* 80**,** 216-23.

ELSASS, F. 2006. Transmission Electron Microscopy. *In:* F., B., G., T. B. K. & G., L. (eds.) *Handbook of Clay Science.* Elsevier.

ENGLEBIENNE, P., VAN HOONACKER, A. & VERHAS, M. 2003. Surface plasmon resonance: principles, methods and applications in biomedical sciences. *Spectroscopy-an International Journal,* 17**,** 255-273.

ESCUBED. 2011. *Zeta Potential – Electrophoresis* [Online]. Available: http://www.escubed.co.uk/sites/default/files/zeta_potential_(an011)_elecrophoresis.pdf.

FABREGA, J., FAWCETT, S. R., RENSHAW, J. C. & LEAD, J. R. 2009a. Silver Nanoparticle Impact on Bacterial Growth: Effect of pH, Concentration, and Organic Matter. *ENVIRONMENTAL SCIENCE & TECHNOLOGY,* 43**,** 7285-7290.

FABREGA, J., LUOMA, S. N., TYLER, C. R., GALLOWAY, T. S. & LEAD, J. R. 2011. Silver nanoparticles: Behaviour and effects in the aquatic environment. *Environment International,* 37**,** 517-531.

FABREGA, J., RENSHAW, J. C. & LEAD, J. R. 2009b. Interactions of Silver Nanoparticles with Pseudomonas putida Biofilms. *ENVIRONMENTAL SCIENCE & TECHNOLOGY,* 43**,** 9004-9009.

FANCHI, J. R. 2004. *Energy : technology and directions for the future,* Amsterdam ; London, Academic.

FARGASOVA, A., PRUCEK, R., RANC, V., PANACEK, A., KVITEK, L. & ZBORIL, R. 2015. Influence of various chloride ion concentrations on silver nanoparticle transformations and effectiveness in surface enhanced Raman scattering for different excitation wavelengths. *Rsc Advances,* 5**,** 9737-9744.

FARKAS, J., PETER, H., CHRISTIAN, P., GALLEGO URREA, J. A., HASSELLÖV, M., TUORINIEMI, J., GUSTAFSSON, S., OLSSON, E., HYLLAND, K. & THOMAS, K. V. 2011. Characterization of the effluent from a nanosilver producing washing machine. *Environment International,* 37**,** 1057-1062.

FARRE, M., SANCHIS, J. & BARCELO, D. 2011. Analysis and assessment of the occurrence, the fate and the behavior of nanomaterials in the environment. *Trac-Trends in Analytical Chemistry,* 30**,** 517-527.

FERNANDEZ-LOPEZ, C., MATEO-MATEO, C., ALVAREZ-PUEBLA, R. A., PEREZ-JUSTE, J., PASTORIZA-SANTOS, I. & LIZ-MARZAN, L. M. 2009. Highly Controlled Silica Coating of PEG-Capped Metal Nanoparticles and Preparation of SERS-Encoded Particles. *Langmuir,* 25**,** 13894-13899.

FISHERSCIENTIC. Available: https://www.fishersci.co.uk/shop/products/emd-millipore-sterifil-47mm-aseptic-vacuum-filter-system-holder/10320231#?keyword=Millipore+sterifil+filter+cell.

FOX, P. F., UNIACKE-LOWE, T., MCSWEENEY, P. L. H. & O'MAHONY, J. A. 2015. *Dairy Chemistry and Biochemistry*.

FRENCH, R. A., JACOBSON, A. R., KIM, B., ISLEY, S. L., PENN, R. L. & BAVEYE, P. C. 2009. Influence of Ionic Strength, pH, and Cation Valence on Aggregation Kinetics of Titanium Dioxide Nanoparticles. *Environmental Science & Technology,* 43**,** 1354-1359.

GAGNADRE, C., CARON, A., GUÉZÉNOC, H. & GROHENS, Y. 2009. Electron microscopy pictures, mathematical model and approximate solution of the surface potential. *Kybernetes,* 38**,** 780-788.

GALLARDO, O. A. D., MOIRAGHI, R., MACCHIONE, M. A., GODOY, J. A., PEREZ, M. A., CORONADO, E. A. & MACAGNO, V. A. 2012. Silver oxide particles/silver nanoparticles interconversion: susceptibility of forward/backward reactions to the chemical environment at room temperature. *Rsc Advances,* 2**,** 2923-2929.

GAO, J., POWERS, K., WANG, Y., ZHOU, H., ROBERTS, S. M., MOUDGIL, B. M., KOOPMAN, B. & BARBER, D. S. 2012. Influence of Suwannee River humic acid on particle properties and toxicity of silver nanoparticles. *Chemosphere,* 89**,** 96-101.

GAO, J., YOUN, S., HOVSEPYAN, A., LLANEZA, V. L., WANG, Y., BITTON, G. & BONZONGO, J. C. J. 2009. Dispersion and Toxicity of Selected Manufactured Nanomaterials in Natural River Water Samples: Effects of Water Chemical Composition. *ENVIRONMENTAL SCIENCE & TECHNOLOGY,* 43**,** 3322-3328.

GARRATT-REED, A. J. & BELL, D. C. 2003. *Energy-dispersive X-ray analysis in the electron microscope,* Oxford, BIOS.

GEERTSMA, R. E., WIJNHOVEN, S. W. P., PEIJNENBURG, W. J. G. M., HERBERTS, C. A., HAGENS, W. I., OOMEN, A. G., HEUGENS, E. H. W., ROSZEK, B., BISSCHOPS, J., GOSENS, I., VAN DE MEENT, D., DEKKERS, S., DE JONG, W. H., VAN ZIJVERDEN, M. & SIPS, A. J. A. M. 2009. Nano-silver - a review of available data and knowledge gaps in human and environmental risk assessment. *Nanotoxicology,* 3**,** 109-U78.

GLIGA, A. R., SKOGLUND, S., WALLINDER, I. O., FADEEL, B. & KARLSSON, H. L. 2014. Size-dependent cytotoxicity of silver nanoparticles in human lung cells: the role of cellular uptake, agglomeration and Ag release. *Particle and fibre toxicology,* 11**,** 1.

GLOVER, R. D., MILLER, J. M. & HUTCHISON, J. E. 2011. Generation of Metal Nanoparticles from Silver and Copper Objects: Nanoparticle Dynamics on Surfaces and Potential Sources of Nanoparticles in the Environment. *ACS Nano,* 5**,** 8950-8957.

GORUP, L. F., LONGO, E., LEITE, E. R. & CAMARGO, E. R. 2011. Moderating effect of ammonia on particle growth and stability of quasi-monodisperse silver nanoparticles synthesized by the Turkevich method. *Journal of Colloid and Interface Science,* 360**,** 355-358.

GOTTSCHALK, F. & NOWACK, B. 2011. The release of engineered nanomaterials to the environment. *Journal of Environmental Monitoring,* 13**,** 1145-1155.

GOTTSCHALK, F., SONDERER, T., SCHOLZ, R. W. & NOWACK, B. 2010. Possibilities and Limitations of Modeling Environmental Exposure to Engineered Nanomaterials by Probabilistic Material Flow Analysis. *Environmental Toxicology and Chemistry,* 29**,** 1036-1048.

GRAY, N. F. 2004. *Biology of wastewater treatment,* London, Imperial College Press.

GRILLO, R., ROSA, A. H. & FRACETO, L. F. 2015. Engineered nanoparticles and organic matter: A review of the state-of-the-art. *Chemosphere,* 119**,** 608-619.

GROKHALE, Y. P. 2010. *Synthesis and Modeling of Silver and Titanium Dioxide Naoparticles by Population Balance Equation.* Doctor of Enginieering Dissertation, Otto von Guericke University Madeburg.

GUO, X. S., LIANG, B., JIAN, J. M., ZHANG, Y. L. & YE, X. S. 2014. Glucose biosensor based on a platinum electrode modified with rhodium nanoparticles and with glucose oxidase immobilized on gold nanoparticles. *Microchimica Acta,* 181**,** 519-525.

GUTIERREZ, L., AUBRY, C., CORNEJO, M. & CROUE, J. P. 2015. Citrate-Coated Silver Nanoparticles Interactions with Effluent Organic Matter: Influence of Capping Agent and Solution Conditions. *Langmuir,* 31**,** 8865-8872.

HAFNER, B. 2011. *Introduction to the transmission electron microscopy primer* [Online]. Available: http://www.charfac.umn.edu/instruments/tem_primer.pdf.

HANDFORD, C. E., DEAN, M., HENCHION, M., SPENCE, M., ELLIOTT, C. T. & CAMPBELL, K. 2014. Implications of nanotechnology for the agri-food industry: Opportunities, benefits and risks. *Trends in Food Science & Technology,* 40**,** 226-241.

HARDESTY, J. H. & BASSAM, A. 2010. Spectrophotometry and the Beer-Lambert Law: An Important Analytical Technique in Chemistry.

HENGLEIN, A. & GIERSIG, M. 1999. Formation of colloidal silver nanoparticles: Capping action of citrate. *Journal of Physical Chemistry B,* 103**,** 9533-9539.

HOLDER, A. L., VEJERANO, E. P., ZHOU, X. & MARR, L. C. 2013. Nanomaterial disposal by incineration. *Environ Sci Process Impacts,* 15**,** 1652-64.

HOU, L. L., LI, K. Y., DING, Y. Z., LI, Y., CHEN, J., WU, X. L. & LI, X. Q. 2012. Removal of silver nanoparticles in simulated wastewater treatment processes and its impact on COD and NH4 reduction. *Chemosphere,* 87**,** 248-252.

HOUSECROFT, C. E. & CONSTABLE, E. C. 2010. *Chemistry : an introduction to organic, inorganic and physical chemistry,* Harlow, Prentice Hall.

HTTP://WWW.CHEMGUIDE.CO.UK/ANALYSIS/UVVISIBLE/SPECTROMETER.HTML. 03/0/2013].

HTTPS://WWW.MCILVAINECOMPANY.COM/GENERIC%20APPLICATIONS/WATER/MNCPL%20WASTEWATER.HTM. [Accessed 20/06/2013 2012].

HUSSAIN, M. A., SHAH, A., JANTAN, I., TAHIR, M. N., SHAH, M. R., AHMED, R. & BUKHARI, S. N. A. 2014. One pot light assisted green synthesis, storage and antimicrobial activity of dextran stabilized silver nanoparticles. *Journal of Nanobiotechnology,* 12.

HUYNH, K. A. & CHEN, K. L. 2011. Aggregation Kinetics of Citrate and Polyvinylpyrrolidone Coated Silver Nanoparticles in Monovalent and Divalent Electrolyte Solutions. *ENVIRONMENTAL SCIENCE & TECHNOLOGY***,** 110601141913062.

HVOLBAEK, B., JANSSENS, T. V. W., CLAUSEN, B. S., FALSIG, H., CHRISTENSEN, C. H. & NORSKOV, J. K. 2007. Catalytic activity of Au nanoparticles. *Nano Today,* 2**,** 14-18.

IRAVANI, S. 2011. Green synthesis of metal nanoparticles using plants. *Green Chemistry,* 13**,** 2638-2650.

IVASK, A., KURVET, I., KASEMETS, K., BLINOVA, I., ARUOJA, V., SUPPI, S., VIJA, H., KÄKINEN, A., TITMA, T. & HEINLAAN, M. 2014a. Size-dependent toxicity of silver nanoparticles to bacteria, yeast, algae, crustaceans and mammalian cells in vitro. *PloS one,* 9**,** e102108.

IVASK, A., KURVET, I., KASEMETS, K., BLINOVA, I., ARUOJA, V., SUPPI, S., VIJA, H., KAKINEN, A., TITMA, T., HEINLAAN, M., VISNAPUU, M., KOLLER, D., KISAND, V. & KAHRU, A. 2014b. Size-Dependent Toxicity of Silver Nanoparticles to Bacteria, Yeast, Algae, Crustaceans and Mammalian Cells In Vitro. *Plos One,* 9.

JACOBSON, A. R., MARTINEZ, C. E., SPAGNUOLO, M., MCBRIDE, M. B. & BAVEYE, P. 2005. Reduction of silver solubility by hurnic acid and thiol ligands during acanthite (beta-Ag2S) dissolution. *Environmental Pollution,* 135**,** 1-9.

JAMIESON, T., BAKHSHI, R., PETROVA, D., POCOCK, R., IMANI, M. & SEIFALIAN, A. M. 2007. Biological applications of quantum dots. *Biomaterials,* 28**,** 4717-32.

JIA, C. J. & SCHUTH, F. 2011. Colloidal metal nanoparticles as a component of designed catalyst. *Physical Chemistry Chemical Physics,* 13**,** 2457-2487.

JU-NAM, Y. & LEAD, J. R. 2008. Manufactured nanoparticles: An overview of their chemistry, interactions and potential environmental implications *S C I E N C E O F T H E T O T A L E N V I R O N M E N T,* 400**,** 3 9 6 – 4 1 4.

KAEGI, R., SINNET, B., ZULEEG, S., HAGENDORFER, H., MUELLER, E., VONBANK, R., BOLLER, M. & BURKHARDT, M. 2010. Release of silver nanoparticles from outdoor facades. *Environmental Pollution,* 158**,** 2900-2905.

KAEGI, R., VOEGELIN, A., ORT, C., SINNET, B., THALMANN, B., KRISMER, J., HAGENDORFER, H., ELUMELU, M. & MUELLER, E. 2012. Fate and transformation of silver nanoparticles in urban wastewater systems. *Water Research.*

KAEGI, R., VOEGELIN, A., ORT, C., SINNET, B., THALMANN, B., KRISMER, J., HAGENDORFER, H., ELUMELU, M. & MUELLER, E. 2013. Fate and transformation of silver nanoparticles in urban wastewater systems. *Water Research,* 47**,** 3866-3877.

KAEGI, R., VOEGELIN, A., SINNET, B., ZULEEG, S., HAGENDORFER, H., BURKHARDT, M. & SIEGRIST, H. 2011a. Behavior of Metallic Silver Nanoparticles in a Pilot Wastewater Treatment Plant. *ENVIRONMENTAL SCIENCE & TECHNOLOGY,* 45**,** 3902-3908.

KAEGI, R., VOEGELIN, A., SINNET, B., ZULEEG, S., HAGENDORFER, H., BURKHARDT, M. & SIEGRIST, H. 2011b. Behavior of Metallic Silver Nanoparticles in a Pilot Wastewater Treatment Plant. *ENVIRONMENTAL SCIENCE & TECHNOLOGY***,** 110405125242089.

KAEGI, R., VOEGELIN, A., SINNET, B., ZULEEG, S., HAGENDORFER, H., BURKHARDT, M. & SIEGRIST, H. 2011c. Behavior of silver nanoparticles in a pilot wastewater treatment plant: Supporting Information. *ENVIRONMENTAL SCIENCE & TECHNOLOGY,* 45**,** 3902–3908.

KANG, D., TANG, H., XIE, D. & KE, P. 2014. Adsorption abilities by heavy metals and inorganic particles and activated sludge in domestic wastewater treatment plant. *Chemical & Pharmaceutical Research,* 6**,** 2918-2926.

KANG, S., MAUTER, M. S. & ELIMELECH, M. 2009. Microbial Cytotoxicity of Carbon-Based Nanomaterials: Implications for River Water and Wastewater Effluent. *ENVIRONMENTAL SCIENCE & TECHNOLOGY,* 43**,** 2648-2653.

KAUR, I. P., KAKKAR, V., DEOL, P. K., YADAV, M., SINGH, M. & SHARMA, I. 2014. Issues and concerns in nanotech product development and its commercialization. *Journal of Controlled Release,* 193**,** 51-62.

KAZUMA, E. & TATSUMA, T. 2014. Localized surface plasmon resonance sensors based on wavelength-tunable spectral dips. *Nanoscale,* 6**,** 2397-2405.

KELLER, A. A., MCFERRAN, S., LAZAREVA, A. & SUH, S. 2013. Global life cycle releases of engineered nanomaterials. *Journal of Nanoparticle Research,* 15.

KELLER, A. A., VOSTI, W., WANG, H. T. & LAZAREVA, A. 2014. Release of engineered nanomaterials from personal care products throughout their life cycle. *Journal of Nanoparticle Research,* 16.

KELLER, A. A., WANG, H. T., ZHOU, D. X., LENIHAN, H. S., CHERR, G., CARDINALE, B. J., MILLER, R. & JI, Z. X. 2010. Stability and Aggregation of Metal Oxide Nanoparticles in Natural Aqueous Matrices. *ENVIRONMENTAL SCIENCE & TECHNOLOGY,* 44**,** 1962-1967.

KERNPHYSIK, I. F. 2003. *PIXE experimental set up in Cologne* [Online]. Available: https://www.ikp.uni-koeln.de/research/pixe/ 2014].

KHANDELWAL, N., KAUR, G., CHAUBEY, K. K., SINGH, P., SHARMA, S., TIWARI, A., SINGH, S. V. & KUMAR, N. 2014. Silver nanoparticles impair Peste des petits ruminants virus replication. *Virus Research,* 190**,** 1-7.

KHIN, M. M., NAIR, A. S., BABU, V. J., MURUGAN, R. & RAMAKRISHNA, S. 2012. A review on nanomaterials for environmental remediation. *Energy & Environmental Science,* 5**,** 8075-8109.

KIM, B., PARK, C. S., MURAYAMA, M. & HOCHELLA, M. F. 2010. Discovery and Characterization of Silver Sulfide Nanoparticles in Final Sewage Sludge Products. *ENVIRONMENTAL SCIENCE & TECHNOLOGY,* 44**,** 7509-7514.

KIM, H., JEONG, S. H., KAM, D. G., KIM, H. J., CHOI, S. M., LEE, M. B., BAE, S. W., LIM, J. H. & LEE, S. H. 2013. Developing a Site Index Model Considering Soil Characteristics for Pinus thunbergii Stands Grown on the West Coast of Korea. *Journal of the Korean Society for Applied Biological Chemistry,* 56**,** 173-180.

KIM, Y. H., LEE, D. K. & KANG, Y. S. 2005. Synthesis and characterization of Ag and Ag–SiO2 nanoparticles. *Colloids and Surfaces A: Physicochemical and Engineering Aspects,* 257–258**,** 273-276.

KING, S. M., JARVIE, H. P., BOWES, M. J., GOZZARD, E., LAWLOR, A. J. & LAWRENCE, M. J. 2015. Exploring controls on the fate of PVP-capped silver nanoparticles in primary wastewater treatment. *Environ. Sci.: Nano*.

KISER, M. A., WESTERHOFF, P., BENN, T., WANG, Y., PEREZ-RIVERA, J. & HRISTOVSKI, K. 2009. Titanium Nanomaterial Removal and Release from Wastewater Treatment Plants. *ENVIRONMENTAL SCIENCE & TECHNOLOGY,* 43**,** 6757-6763.

KLAINE, S. J., ALVAREZ, P. J. J., BATLEY, G. E., FERNANDES, T. F., HANDY, R. D., LYON, D. Y., MAHENDRA, S., MCLAUGHLIN, M. J. & LEAD, J. R. 2008. Nanomaterials in the environment: Behavior, fate, bioavailability, and effects. *Environmental Toxicology and Chemistry,* 27**,** 1825-1851.

KLAINE, S. J. & PEDRO J. J. ALVAREZ[2,] G. E. B., TERESA F. FERNANDES[4], RICHARD D. HANDY[5], DELINA Y. LYON[2], SHAILY MAHENDRA[2], MICHAEL J. MCLAUGHLIN[6], JAMIE R. LEAD[7] 2008. Nanomaterials in the environment: Behavior, fate, bioavailability, and effects[†]. *Environmental Toxicology and Chemistry,,* 27**,** 1825-1851.

KLECKA, G. M. & GONSIOR, S. J. 1984. Reductive Dechlorination of Chlorinated Methanes and Ethanes by Reduced Iron (Ii) Porphyrins. *Chemosphere,* 13**,** 391-402.

KOKURA, S., HANDA, O., TAKAGI, T., ISHIKAWA, T., NAITO, Y. & YOSHIKAWA, T. 2010. Silver nanoparticles as a safe preservative for use in cosmetics. *Nanomedicine-Nanotechnology Biology and Medicine,* 6**,** 570-574.

KREIBIG, U. 1974. Electronic Properties of Small Silver Particles - Optical-Constants and Their Temperature-Dependence. *Journal of Physics F-Metal Physics,* 4**,** 999-1014.

KREIBIG, U. & GENZEL, L. 1985. Optical-Absorption of Small Metallic Particles. *Surface Science,* 156**,** 678-700.

KRYSANOV, E. Y., PAVLOV, D. S., DEMIDOVA, T. B. & DGEBUADZE, Y. Y. 2010. Effect of nanoparticles on aquatic organisms. *Biology Bulletin,* 37**,** 406-412.

KUMAR, D., KUMARI, J., PAKRASHI, S., DALAI, S., RAICHUR, A. M., SASTRY, T. P., MANDAL, A. B., CHANDRASEKARAN, N. & MUKHERJEE, A. 2014. Qualitative toxicity assessment of silver

nanoparticles on the fresh water bacterial isolates and consortium at low level of exposure concentration. *Ecotoxicology and Environmental Safety,* 108**,** 152-160.

KUMAR, V. V. & ANTHONY, S. P. 2014. Highly selective silver nanoparticles based label free colorimetric sensor for nitrite anions. *Analytica Chimica Acta,* 842**,** 57-62.

LAJUNEN, T., VIITALA, L., KONTTURI, L. S., LAAKSONEN, T., LIANG, H., VUORIMAA-LAUKKANEN, E., VIITALA, T., LE GUEVEL, X., YLIPERTTULA, M., MURTOMAKI, L. & URTTI, A. 2015. Light induced cytosolic drug delivery from liposomes with gold nanoparticles. *Journal of Controlled Release,* 203**,** 85-98.

LAMBERTI, C. 2008. *Characterization of semiconductor heterostructures and nanostructures : biogeochemical interactions, health effects and remediation,* Amsterdam ; Oxford, Elsevier.

LE OUAY, B. & STELLACCI, F. 2015. Antibacterial activity of silver nanoparticles: A surface science insight. *Nano Today,* 10**,** 339-354.

LEAD, J. R. & SMITH, E. 2009. *Environmental and human health impacts of nanotechnology,* Chichester, Wiley-Blackwell.

LEVARD, C., REINSCH, B. C., MICHEL, F. M., OUMAHI, C., LOWRY, G. V. & BROWN, G. E. 2011. Sulfidation Processes of PVP-Coated Silver Nanoparticles in Aqueous Solution: Impact on Dissolution Rate. *ENVIRONMENTAL SCIENCE & TECHNOLOGY,* 45**,** 5260-5266.

LI, D., LYON, D. Y., LI, Q. & ALVAREZ, P. J. J. 2008. Effect of soil sorption and aquatic natural organic matter on the antibacterial activity of a fullerene water suspension. *Environmental Toxicology and Chemistry,* 27**,** 1888-1894.

LI, L. X. Y., HARTMANN, G., DOBLINGER, M. & SCHUSTER, M. 2013. Quantification of Nanoscale Silver Particles Removal and Release from Municipal Wastewater Treatment Plants in Germany. *ENVIRONMENTAL SCIENCE & TECHNOLOGY,* 47**,** 7317-7323.

LI, M. H., POKHREL, S., JIN, X., MADLER, L., DAMOISEAUX, R. & HOEK, E. M. V. 2011. Stability, Bioavailability, and Bacterial Toxicity of ZnO and Iron-Doped ZnO Nanoparticles in Aquatic Media. *ENVIRONMENTAL SCIENCE & TECHNOLOGY,* 45**,** 755-761.

LI, X., LENHART, J. J. & WALKER, H. W. 2012a. Aggregation Kinetics and Dissolution of Coated Silver Nanoparticles. *Langmuir,* 28**,** 1095-1104.

LI, X. A., LENHART, J. J. & WALKER, H. W. 2010a. Dissolution-Accompanied Aggregation Kinetics of Silver Nanoparticles. *Langmuir,* 26**,** 16690-16698.

LI, X. C., XIE, L. & ZHENG, X. J. 2012b. The comparison between the Mie theory and the Rayleigh approximation to calculate the EM scattering by partially charged sand. *Journal of Quantitative Spectroscopy & Radiative Transfer,* 113**,** 251-258.

LI, Z. Q., GREDEN, K., ALVAREZ, P. J. J., GREGORY, K. B. & LOWRY, G. V. 2010b. Adsorbed Polymer and NOM Limits Adhesion and Toxicity of Nano Scale Zerovalent Iron to E. coli. *ENVIRONMENTAL SCIENCE & TECHNOLOGY,* 44**,** 3462-3467.

LIESE, A. & HILTERHAUS, L. 2013. Evaluation of immobilized enzymes for industrial applications. *Chemical Society Reviews,* 42**,** 6236-6249.

LIM, J., YEAP, S. P., CHE, H. X. & LOW, S. C. 2013. Characterization of magnetic nanoparticle by dynamic light scattering. *Nanoscale Research Letters,* 8.

LIN, D. H., JI, J., LONG, Z. F., YANG, K. & WU, F. C. 2012. The influence of dissolved and surface-bound humic acid on the toxicity of TiO2 nanoparticles to Chlorella sp. *Water Research,* 46**,** 4477-4487.

LIN, X. B. & GU, N. 2014. Surface properties of encapsulating hydrophobic nanoparticles regulate the main phase transition temperature of lipid bilayers: A simulation study. *Nano Research,* 7**,** 1195-1204.

LIU, J. Y., PENNELL, K. G. & HURT, R. H. 2011. Kinetics and Mechanisms of Nanosilver Oxysulfidation. *ENVIRONMENTAL SCIENCE & TECHNOLOGY,* 45**,** 7345-7353.

LIU, X., JIN, X., CAO, B. & TANG, C. Y. 2014. Bactericidal activity of silver nanoparticles in environmentally relevant freshwater matrices: Influences of organic matter and chelating agent. *Journal of Environmental Chemical Engineering,* 2**,** 525-531.

LIVNEY, Y. D. 2010. Milk proteins as vehicles for bioactives. *Current Opinion in Colloid & Interface Science,* 15**,** 73-83.

LOMBI, E., DONNER, E., SCHECKEL, K. G., SEKINE, R., LORENZ, C., VON GOETZ, N. & NOWACK, B. 2014. Silver speciation and release in commercial antimicrobial textiles as influenced by washing. *Chemosphere,* 111**,** 352-358.

LOPEZ-SERRANO, A., OLIVAS, R. M., LANDALUZE, J. S. & CAMARA, C. 2014. Nanoparticles: a global vision. Characterization, separation, and quantification methods. Potential environmental and health impact. *Analytical Methods,* 6**,** 38-56.

LOWE, B. M., MAEKAWA, Y., SHIBUTA, Y., SAKATA, T., SKYLARIS, C. K. & GREEN, N. G. 2017. Dynamic behaviour of the silica-water-bio electrical double layer in the presence of a divalent electrolyte. *Phys Chem Chem Phys,* 19**,** 2687-2701.

LOWRY, G. V., ESPINASSE, B. P., BADIREDDY, A. R., RICHARDSON, C. J., REINSCH, B. C., BRYANT, L. D., BONE, A. J., DEONARINE, A., CHAE, S., THEREZIEN, M., COLMAN, B. P., HSU-KIM, H., BERNHARDT, E. S., MATSON, C. W. & WIESNER, M. R. 2012a. Long-Term Transformation and Fate of Manufactured Ag Nanoparticles in a Simulated Large Scale Freshwater Emergent Wetland. *ENVIRONMENTAL SCIENCE & TECHNOLOGY,* 46**,** 7027-7036.

LOWRY, G. V., ESPINASSE, B. P., BADIREDDY, A. R., RICHARDSON, C. J., REINSCH, B. C., BRYANT, L. D., BONE, A. J., DEONARINE, A., CHAE, S., THEREZIEN, M., COLMAN, B. P., HSU-KIM, H., BERNHARDT, E. S., MATSON, C. W. & WIESNER, M. R. 2012b. Long-Term Transformation and Fate of Manufactured Ag Nanoparticles in a Simulated Large Scale Freshwater Emergent Wetland. *ENVIRONMENTAL SCIENCE & TECHNOLOGY***,** 120430125425008.

LOWRY, G. V., GREGORY, K. B., APTE, S. C. & LEAD, J. R. 2012c. Transformations of Nanomaterials in the Environment. *ENVIRONMENTAL SCIENCE & TECHNOLOGY,* 46**,** 6893-6899.

LOZA, K., DIENDORF, J., SENGSTOCK, C., RUIZ-GONZALEZ, L., GONZALEZ-CALBET, J. M., VALLET-REGI, M., KOLLER, M. & EPPLE, M. 2014. The dissolution and biological effects of silver nanoparticles in biological media. *Journal of Materials Chemistry B,* 2**,** 1634-1643.

M. HOCHEDLINGER, H. PICHLER, HEISINGER, A. & HAAR, R. 2007. Online sewer monitoring by means of UV/VIS spectroscopy

MA, R., LEVARD, C., JUDY, J. D., UNRINE, J. M., DURENKAMP, M., MARTIN, B., JEFFERSON, B. & LOWRY, G. V. 2014. Fate of Zinc Oxide and Silver Nanoparticles in a Pilot Wastewater Treatment Plant and in Processed Biosolids. *ENVIRONMENTAL SCIENCE & TECHNOLOGY,* 48**,** 104-112.

MACE, S. & MATA-ALVAREZ, J. 2002. Utilization of SBR Technology for Wastewater Treatment: An Overview. *Industrial & Engineering Chemistry Research,* 41**,** 5539-5553.

MADOYAN, K. K., MELIKYAN, A. H. & MINASSIAN, H. R. 2012. Radiation Damping of Surface Plasmons in a Pair of Nanoparticles and in Nanoparticles near Interfaces. *Journal of Physical Chemistry C,* 116**,** 16800-16805.

MAHAPATRA, I., SUN, T. Y., CLARK, J. R. A., DOBSON, P. J., HUNGERBUEHLER, K., OWEN, R., NOWACK, B. & LEAD, J. 2015. Probabilistic modelling of prospective environmental concentrations of gold nanoparticles from medical applications as a basis for risk assessment. *Journal of Nanobiotechnology,* 13**,** 93.

MAKAROV, V. V., LOVE, A. J., SINITSYNA, O. V., MAKAROVA, S. S., YAMINSKY, I. V., TALIANSKY, M. E. & KALININA, N. O. 2014. "Green" Nanotechnologies: Synthesis of Metal Nanoparticles Using Plants. *Acta Naturae,* 6**,** 35-44.

MALEKI DIZAJ, S., MENNATI, A., JAFARI, S., KHEZRI, K. & ADIBKIA, K. 2015. Antimicrobial activity of carbon-based nanoparticles. *Adv Pharm Bull,* 5**,** 19-23.

MALVERN, I. L. 2013. Zetasizer Nano user manual. *In:* LTD., M. I. (ed.). Worcestershire: Malvern Instruments.

MANIKANDAN, D., MOHAN, S., MAGUDAPATHY, P. & NAIR, K. G. M. 2003. Blue shift of plasmon resonance in Cu and Ag ion-exchanged and annealed soda-lime glass: an optical absorption study. *Physica B-Condensed Matter,* 325**,** 86-91.

MANSFIELD, J. F. *An introduction to the Transmission Electron Microscopy-What it is and what it can do?* [Online]. Michigan. Available: http://www.emal.engin.umich.edu/courses/temchem2000/sld001.htm [Accessed 04/06/2013 2013].

MARTIN, M. N., ALLEN, A. J., MACCUSPIE, R. I. & HACKLEY, V. A. 2014. Dissolution, Agglomerate Morphology, and Stability Limits of Protein-Coated Silver Nanoparticles. *Langmuir,* 30**,** 11442-11452.

MATZKE, M., JURKSCHAT, K. & BACKHAUS, T. 2014. Toxicity of differently sized and coated silver nanoparticles to the bacterium Pseudomonas putida: risks for the aquatic environment? *Ecotoxicology,* 23**,** 818-829.

MAURER-JONES, M. A., GUNSOLUS, I. L., MURPHY, C. J. & HAYNES, C. L. 2013. Toxicity of Engineered Nanoparticles in the Environment. *Analytical Chemistry,* 85**,** 3036-3049.

MAVANI, K. & SHAH, M. 2013. Synthesis of Silver Nanoparticles by using Sodium Borohydride as a Reducing Agent. *International Journal of Engineering Research & Technology* 2.

MEESSEN, J. 2014. Urea synthesis. *Chemie Ingenieur Technik,* 86**,** 2180-2189.

MEESSEN, J. H. 2010. Urea. *ULLMANN'S Encyclopedia of Industrial Chemistry.* John Wiley and Sons.

MERRIFIELD, R. C. 2008. *Thesis.*

MICHELS, C., YANG, Y., SOARES, H. M. & ALVAREZ, P. J. J. 2015. Silver nanoparticles temporarily retard NO2- production without significantly affecting N2O release by Nitrosomonas europaea. *Environmental Toxicology and Chemistry,* 34**,** 2231-2235.

MILKFACTS.INFO. 2016. *Milk Protein* [Online]. Available: http://www.milkfacts.info/Milk%20Composition/Protein.htm.

MONTAZER, M., SHAMEI, A. & ALIMOHAMMADI, F. 2012. Synthesizing and stabilizing silver nanoparticles on polyamide fabric using silver-ammonia/PVP/UVC. *Progress in Organic Coatings,* 75**,** 379-385.

MORGENROTH, E., WILDERER, P. A., BARNARD, J., BOON, A., WILLIAMS, S., XIONG, F., WARE, A., PITMAN, T. & DE JONG, E. 1998. Sequencing batch reactor technology: Concepts, design and experiences (abridged) - Discussion. *Journal of the Chartered Institution of Water and Environmental Management,* 12**,** 314-321.

MORONES, J. R., ELECHIGUERRA, J. L., CAMACHO, A., HOLT, K., KOURI, J. B., RAMIREZ, J. T. & YACAMAN, M. J. 2005. The bactericidal effect of silver nanoparticles. *Nanotechnology,* 16**,** 2346-2353.

MUELLER, N. C. & NOWACK, B. 2008. Exposure modeling of engineered nanoparticles in the environment. *ENVIRONMENTAL SCIENCE & TECHNOLOGY,* 42**,** 4447-4453.

MULLER, B., SCHEYTT, T., ZIPPEL, M., HANNAPPEL, S., KLEIN-GOEDICKE, J. & DUSCHER, K. 2011. A New Approach to Calculate EMEA's Predicted Environmental Concentration for Human Pharmaceuticals in Groundwater at Bank Filtration Sites. *Water Air and Soil Pollution,* 217**,** 67-82.

MUMPER, C. K., OSTERMEYER, A. K., SEMPRINI, L. & RADNIECKI, T. S. 2013. Influence of ammonia on silver nanoparticle dissolution and toxicity to Nitrosomonas europaea. *Chemosphere,* 93**,** 2493-2498.

MYERS, M. N. 1997. Overview of field-flow fractionation. *Journal of Microcolumn Separations,* 9**,** 151-162.

MYERSON, A. S. 2002. *Handbook of industrial crystallization,* Boston ; Oxford, Butterworth-Heinemann.

NAKAMURA, T., HAYASHI, H. & EBINA, T. 2014. Preparation of copper nitride nanoparticles using urea as a nitrogen source in a long-chain alcohol. *Journal of Nanoparticle Research,* 16.

NANAYAKKARA, C. E., LARISH, W. A. & GRASSIAN, V. H. 2014. Titanium Dioxide Nanoparticle Surface Reactivity with Atmospheric Gases, CO2, SO2, and NO2: Roles of Surface Hydroxyl Groups and Adsorbed Water in the Formation and Stability of Adsorbed Products. *Journal of Physical Chemistry C,* 118**,** 23011-23021.

NANOCOMPOSIX. 2012. *Tech Note - Zeta and pH Curves for nanoComposix Citrate and PVP Capped Silver Nanoparticles* [Online]. nanoComposix. Available: http://www.nanocomposix.eu/sites/default/files/Tech%20Note%20-%20Zeta%20and%20pH%20Curves%20for%20nanoComposix%20Citrate%20and%20PVP%20Capped%20Silver%20Nanoparticles.pdf 2014].

NAVARRO, E., PICCAPIETRA, F., WAGNER, B., MARCONI, F., KAEGI, R., ODZAK, N., SIGG, L. & BEHRA, R. 2008. Toxicity of Silver Nanoparticles to Chlamydomonas reinhardtii. *ENVIRONMENTAL SCIENCE & TECHNOLOGY,* 42**,** 8959-8964.

NCI, A. F. N. I. C. 2005. *Microfluidics: The Flow of Innovation Continues* [Online]. Available: http://nano.cancer.gov/action/news/featurestories/monthly_feature_2005_aug.asp 2015].

NI, L. F., LI, Y., ZHANG, C., LI, L. Z., ZHANG, W. L. & WANG, D. W. 2016. Novel floating photocatalysts based on polyurethane composite foams modified with silver/titanium dioxide/graphene ternary nanoparticles for the visible-light-mediated remediation of diesel-polluted surface water. *Journal of Applied Polymer Science,* 133.

NINO-MARTINEZ, N., MARTINEZ-CASTANON, G. A., ARAGON-PINA, A., MARTINEZ-GUTIERREZ, F., MARTINEZ-MENDOZA, J. R. & RUIZ, F. 2008. Characterization of silver nanoparticles synthesized on titanium dioxide fine particles. *Nanotechnology,* 19**,** -.

NOGUEZ, C. 2007. Surface Plasmons on Metal Nanoparticles: The Influence of Shape and Physical Environment. *Journal of Physical Chemistry C,* 111**,** 3806-3819.

NOWACK, B. & BUCHELI, T. D. 2007. Occurrence, behavior and effects of nanoparticles in the environment. *Environmental Pollution,* 150**,** 5-22.

NOWACK, B., RANVILLE, J. F., DIAMOND, S., GALLEGO-URREA, J. A., METCALFE, C., ROSE, J., HORNE, N., KOELMANS, A. A. & KLAINE, S. J. 2012. Potential scenarios for nanomaterial release and subsequent alteration in the environment. *Environmental Toxicology and Chemistry,* 31**,** 50-59.

OECD 2001. OECD guideline for the testing of chemicals: Simulation Test - Aerobic Sewage Treatment 303 A: Activated Sludge Units.

PAL, A. K. & MOHAN, D. B. 2014. Fabrication of partially oxidized ultra-thin nanocrystalline silver films: effect of surface plasmon resonance on fluorescence quenching and surface enhanced Raman scattering. *Materials Research Express,* 1**,** 025014.

PAL, S., TAK, Y. K. & SONG, J. M. 2007. Does the antibacterial activity of silver nanoparticles depend on the shape of the nanoparticle? A study of the gram-negative bacterium Escherichia coli. *Applied and Environmental Microbiology,* 73**,** 1712-1720.

PARK, H. J., KIM, H. Y., CHA, S., AHN, C. H., ROH, J., PARK, S., KIM, S., CHOI, K., YI, J., KIM, Y. & YOON, J. 2013. Removal characteristics of engineered nanoparticles by activated sludge. *Chemosphere,* 92**,** 524-528.

PEARD, W. J. & PFLAUM, R. T. 1958. Interaction of Metal Ions with Heterocyclic Amines - Silver(I) Complexes. *Journal of the American Chemical Society,* 80**,** 1593-1596.

PEDERSEN, D. B. & DUNCAN, E. J. S. 2005. Surface Plasmon Resonance spectroscopy of gold nanoparticles coated substrates. Suffield - Canada: Defence Research and Development Canada.

PEIJNENBURG, W. J. G. M., BAALOUSHA, M., CHEN, J., CHAUDRY, Q., VON DER KAMMER, F., KUHLBUSCH, T. A. J., LEAD, J., NICKEL, C., QUIK, J. T. K., RENKER, M., WANG, Z. & KOELMANS, A. A. 2015. A review of the properties and processes determining the fate of engineered nanomaterials in the aquatic environment. *Critical Reviews in Environmental Science and Technology***,** 00-00.

PENG, S., MCMAHON, J. M., SCHATZ, G. C., GRAY, S. K. & SUN, Y. 2010. Reversing the size-dependence of surface plasmon resonances. *Proc Natl Acad Sci U S A,* 107**,** 14530-4.

PENN, M. R., PAUER, J. J. & MIHELCIC, J. R. Biochemical oxygen demand. *Encyclopedia of live support systems (EOLSS).*

PERKINELME. 2013. *Atomic Spectroscopy - A Guide to Selecting the Appropriate Technique and System* [Online]. Available: http://www.perkinelmer.co.uk/lab-solutions/resources/docs/BRO_WorldLeaderAAICPMSICPMS.pdf.

PHAM VAN DONG, CHU HAONG HA, LE TRAN BINH & KASBOHM, J. 2012. chemical synthesis and antibacterial activity of novel-shaped silver nanoparticles. *International Nano Letters,* 2**,** 9.

PICCINNO, F., GOTTSCHALK, F., SEEGER, S. & NOWACK, B. 2012a. Industrial production quantities and uses of ten engineered nanomaterials in Europe and the world. *Journal of Nanoparticle Research,* 14**,** 1-11.

PICCINNO, F., GOTTSCHALK, F., SEEGER, S. & NOWACK, B. 2012b. Industrial production quantities and uses of ten engineered nanomaterials in Europe and the world. *Journal of Nanoparticle Research,* 14.

PICCIOTTO, A., TORRISI, L., MARGARONE, D. & BELLUTTI, P. 2010. Particle size determination of silver nanoparticles generated by plasma laser ablation using a deconvolution method. *Radiation Effects and Defects in Solids,* 165**,** 706-712.

PINTO, V. V., FERREIRA, M. J., SILVA, R., SANTOS, H. A., SILVA, F. & PEREIRA, C. M. 2010. Long time effect on the stability of silver nanoparticles in aqueous medium: Effect of the synthesis and storage conditions. *Colloids and Surfaces a-Physicochemical and Engineering Aspects,* 364**,** 19-25.

PODILA, R., CHEN, R., KE, P. C., BROWN, J. M. & RAO, A. M. 2012. Effects of surface functional groups on the formation of nanoparticle-protein corona. *Applied Physics Letters,* 101.

POOLE, D. M. 2015. *Absorption of photons* [Online]. Available: http://www.kayelaby.npl.co.uk/atomic_and_nuclear_physics/4_2/4_2_1.html.

PRAETORIUS, A., SCHERINGER, M. & HUNGERBUHLER, K. 2012. Development of Environmental Fate Models for Engineered Nanoparticles-A Case Study of TiO2 Nanoparticles in the Rhine River. *ENVIRONMENTAL SCIENCE & TECHNOLOGY,* 46**,** 6705-6713.

PRATHNA, T. C., CHANDRASEKARAN, N. & MUKHERJEE, A. 2011. Studies on aggregation behaviour of silver nanoparticles in aqueous matrices: Effect of surface functionalization and matrix composition. *Colloids and Surfaces a-Physicochemical and Engineering Aspects,* 390**,** 216-224.

PYATENKO, A., SHIMOKAWA, K., YAMAGUCHI, M., NISHIMURA, O. & SUZUKI, M. 2004. Synthesis of silver nanoparticles by laser ablation in pure water. *Applied Physics A,* 79**,** 803-806.

QI, W. H. & WANG, M. P. 2005. Size and shape dependent lattice parameters of metallic nanoparticles. *Journal of Nanoparticle Research,* 7**,** 51-57.

QUIK, J. T., LYNCH, I., VAN HOECKE, K., MIERMANS, C. J., DE SCHAMPHELAERE, K. A., JANSSEN, C. R., DAWSON, K. A., STUART, M. A. & VAN DE MEENT, D. 2010. Effect of natural organic matter on cerium dioxide nanoparticles settling in model fresh water. *Chemosphere,* 81**,** 711-5.

R. GARCÍA & BÁEZ, A. P. Atomic Absorption Spectrometry (AAS). Mexico City, Mexico Universidad Nacional Autónoma de México,

Ciudad Universitaria.

RAI, M. E. O. C. & POSTEN, C. E. O. C. 2013. *Green biosynthesis of nanoparticles : mechanisms and applications*.

RASMUSSEN, S. 1992. *An introduction to statistics with data analysis,* Pacific Grove, Calif, Brooks/Cole ; Andover : International Thomson Pub. Services [distributor].

ROES, L., PATEL, M. K., WORRELL, E. & LUDWIG, C. 2012. Preliminary evaluation of risks related to waste incineration of polymer nanocomposites. *Science of the Total Environment,* 417**,** 76-86.

ROH, J., UMH, H. N., SIM, J., PARK, S., YI, J. & KIM, Y. 2013. Dispersion stability of citrate- and PVP-AgNPs in biological media for cytotoxicity test. *Korean Journal of Chemical Engineering,* 30**,** 671-674.

RÖMER, I. 2012. *The ecotoxicological and environmental behaviour and transformations of silver nanoparticles.* Doctor of Philosophy, The University of Birmingham.

RÖMER, I., WHITE, T. A., BAALOUSHA, M., CHIPMAN, K., VIANT, M. R. & LEAD, J. R. 2011. Aggregation and dispersion of silver nanoparticles in exposure media for aquatic toxicity tests. *Journal of Chromatography A*.

SAHA, K., CHATTOPADHYA, D., DASH, K., SAHA, U., TYAGI, P. K., GUPTA, M. M., PARAASHARI, A. & SHARMA, A. K. 1990. Sexually-Transmitted Diseases in Leprosy Patients in North and Northeastern India - a Futile Search for Human-Immunodeficiency-Virus Antibody. *International Journal of Leprosy and Other Mycobacterial Diseases,* 58**,** 660-665.

SALGIN, S., SALGIN, U. & BAHADIR, S. 2012. Zeta Potentials and Isoelectric Points of Biomolecules: The Effects of Ion Types and Ionic Strengths. *International Journal of Electrochemical Science,* 7**,** 12404-12414.

SALIERI, B., RIGHI, S., PASTERIS, A. & OLSEN, S. I. 2015. Freshwater ecotoxicity characterisation factor for metal oxide nanoparticles: A case study on titanium dioxide nanoparticle. *Science of the Total Environment,* 505**,** 494-502.

SCHIMPF, M. E. 1996. Tutorial: Field-Flow Fractionation. *the chemical educator,* 1.

SCHIMPF, M. E., CALDWELL, K. & GIDDINGS, J. C. 2000. *Field-flow fractionation handbook,* New York ; Chichester, Wiley-Interscience.

SCHNEID, A. C., PEREIRA, M. B., HOROWITZ, F., MAULER, R. S., MATTE, C. R., KLEIN, M. P., HERTZ, P. F., COSTA, T. M. H., DE MENEZES, E. W. & BENVENUTTI, E. V. 2015. Silver Nanoparticle Thin Films Deposited on Glass Surface Using an Ionic Silsesquioxane as Stabilizer and as Crosslinking Agent. *Journal of the Brazilian Chemical Society,* 26**,** 1004-1012.

SHANNAHAN, J. H., LAI, X. Y., KE, P. C., PODILA, R., BROWN, J. M. & WITZMANN, F. A. 2013. Silver Nanoparticle Protein Corona Composition in Cell Culture Media. *Plos One,* 8.

SHARMA, V. K. 2009. Aggregation and toxicity of titanium dioxide nanoparticles in aquatic environment--a review. *J Environ Sci Health A Tox Hazard Subst Environ Eng,* 44**,** 1485-95.

SHAW, R. 2014. Dynamic light scattering training achieving reliable nano particles sizing. Malvern, UK.

SHI, J. P., EVANS, D. E., KHAN, A. A. & HARRISON, R. M. 2001. Sources and concentration of nanoparticles (< 10 nm diameter) in the urban atmosphere. *Atmospheric Environment,* 35**,** 1193-1202.

SIGMAALDRICH. *Peptone from milk solids* [Online]. Available: http://www.sigmaaldrich.com/catalog/product/sigma/p6838?lang=en&region=GB.

SIGMAALDRICH. *Urea* [Online]. Available: http://www.sigmaaldrich.com/catalog/product/sigma/u0631?lang=en&region=GB.

SIMKA, W., PIOTROWSKI, J., ROBAK, A. & NAWRAT, G. 2009. Electrochemical treatment of aqueous solutions containing urea. *Journal of Applied Electrochemistry,* 39**,** 1137-1143.

SINGH, S., BHARTI, A. & MEENA, V. K. 2014. Structural, thermal, zeta potential and electrical properties of disaccharide reduced silver nanoparticles. *Journal of Materials Science-Materials in Electronics,* 25**,** 3747-3752.

SLATTER, D. H. 2003. *Textbook of small animal surgery,* Philadelphia, Pa. ; London, W. B. Saunders.

SOLOMON, T. 2001. The definition and unit of ionic strength. *Journal of Chemical Education,* 78**,** 1691-1692.

SPELLMAN, F. R. 2009. *Handbook of water and wastewater treatment plant operations,* Boca Raton, Fla., CRC ; London : Taylor & Francis [distributor].

STANLEY, S. 2014. Biological nanoparticles and their influence on organisms. *Current Opinion in Biotechnology,* 28**,** 69-74.

SUN, T. Y., GOTTSCHALK, F., HUNGERBUHLER, K. & NOWACK, B. 2014a. Comprehensive probabilistic modelling of environmental emissions of engineered nanomaterials. *Environ Pollut,* 185**,** 69-76.

SUN, T. Y., GOTTSCHALK, F., HUNGERBÜHLER, K. & NOWACK, B. 2014b. Comprehensive probabilistic modelling of environmental emissions of engineered nanomaterials. *Environmental Pollution,* 185**,** 69-76.

TADROS, T. 2013. Sedimentation of Particles in Suspensions *Encyclopedia of Colloid and Interface Science.* Springer Berlin Heidelberg.

TAI, J. T., LAI, C. S., HO, H. C., YEH, Y. S., WANG, H. F., HO, R. M. & TSAI, D. H. 2014. Protein Silver Nanoparticle Interactions to Colloidal Stability in Acidic Environments. *Langmuir,* 30**,** 12755-12764.

TAKEI, K., YU, Z., ZHENG, M., OTA, H., TAKAHASHI, T. & JAVEY, A. 2014. Highly sensitive electronic whiskers based on patterned carbon nanotube and silver nanoparticle composite films. *Proc Natl Acad Sci U S A,* 111**,** 1703-7.

TAO, N. J., BOUSSAAD, S., HUANG, W. L., ARECHABALETA, R. A. & D'AGNESE, J. 1999. High resolution surface plasmon resonance spectroscopy. *Review of Scientific Instruments,* 70**,** 4656-4660.

TEJAMAYA, M., RÖMER, I., MERRIFIELD, R. C. & LEAD, J. R. 2012. Stability of Citrate, PVP, and PEG Coated Silver Nanoparticles in Ecotoxicology Media. *ENVIRONMENTAL SCIENCE & TECHNOLOGY***,** 120321072752006.

TEJAMAYA, M., ROMER, I., STOLPE, B., BELINGA, M.-F. & LEAD, J. R. 2014. Characterisation and stability of polymer-capped AgNPs synthesised via ligand exchange method. 3.

TILAKI, R. M., ZAD, A. I. & MAHDAVI, S. M. 2006. Stability, size and optical properties of silver nanoparticles prepared by laser ablation in different carrier media. *Applied Physics a-Materials Science & Processing,* 84**,** 215-219.

TOMASZEWSKA, E., SOLIWODA, K., KADZIOLA, K., TKACZ-SZCZESNA, B., CELICHOWSKI, G., CICHOMSKI, M., SZMAJA, W. & GROBELNY, J. 2013. Detection Limits of DLS and UV-Vis Spectroscopy in Characterization of Polydisperse Nanoparticles Colloids. *Journal of Nanomaterials*.

TOOLBOXES.FLEXIBLELEARNING.NET.AU. *Study notes: Graphite Furnace Atomiser* [Online]. Available: http://toolboxes.flexiblelearning.net.au/demosites/series5/508/Laboratory/StudyNotes/snGrapFurnAtom.htm [Accessed 04/06/2013 2013].

TUCHIN, V. V. 2010. *Handbook of photonics for biomedical science,* Boca Raton, Fla., CRC.

TWC, T. T. W. C. Working Texas Style.

ULRICH, A., LOSERT, S., BENDIXEN, N., AL-KATTAN, A., HAGENDORFER, H., NOWACK, B., ADLHART, C., EBERT, J., LATTUADA, M. & HUNGERBUHLER, K. 2012. Critical aspects of sample handling for direct nanoparticle analysis and analytical challenges using asymmetric field flow fractionation in a multi-detector approach. *Journal of Analytical Atomic Spectrometry,* 27**,** 1120-1130.

UOB. 2014. *Microscopes and ancillary equipment* [Online]. Birmingham: University of Birmingham. Available: http://www.birmingham.ac.uk/facilities/electron-microscopy/microscopes/index.aspx.

VAN HOECKE, K., DE SCHAMPHELAERE, K. A., RAMIREZ-GARCIA, S., VAN DER MEEREN, P., SMAGGHE, G. & JANSSEN, C. R. 2011a. Influence of alumina coating on characteristics and effects of SiO2 nanoparticles in algal growth inhibition assays at various pH and organic matter contents. *Environ Int,* 37**,** 1118-25.

VAN HOECKE, K., DE SCHAMPHELAERE, K. A., VAN DER MEEREN, P., SMAGGHE, G. & JANSSEN, C. R. 2011b. Aggregation and ecotoxicity of CeO(2) nanoparticles in synthetic and natural waters with variable pH, organic matter concentration and ionic strength. *Environmental Pollution,* 159**,** 970-6.

VAN HOONACKER, A. & ENGLEBIENNE, P. 2006. Revisiting Silver Nanoparticle Chemical Synthesis and Stability by Optical Spectroscopy. *Current Nanoscience,* 2**,** 359-371.

VODNIK, V. V., BOZANIC, D. K., BIBIC, N., SAPONJIC, Z. V. & NEDELJKOVIC, J. M. 2008. Optical Properties of Shaped Silver Nanoparticles. *Journal of Nanoscience and Nanotechnology,* 8**,** 3511-3515.

WACKERLY, D. D., MENDENHALL, W. & SCHEAFFER, R. L. 2002. *Mathematical statistics with applications,* Pacific Grove, CA, Brooks/Cole Pub.

WAGNER, S., GONDIKAS, A., NEUBAUER, E., HOFMANN, T. & VON DER KAMMER, F. 2014. Spot the Difference: Engineered and Natural Nanoparticles in the Environment-Release, Behavior, and Fate. *Angewandte Chemie-International Edition,* 53**,** 12398-12419.

WANG, Y. F., WESTERHOFF, P. & HRISTOVSKI, K. D. 2012. Fate and biological effects of silver, titanium dioxide, and C-60 (fullerene) nanomaterials during simulated wastewater treatment processes. *Journal of Hazardous Materials,* 201**,** 16-22.

WANG, Y. L. & XIA, Y. N. 2004. Bottom-up and top-down approaches to the synthesis of monodispersed spherical colloids of low melting-point metals. *Nano Letters,* 4**,** 2047-2050.

WANG, Z. L. 2000. Transmission electron microscopy of shape-controlled nanocrystals and their assemblies. *Journal of Physical Chemistry B,* 104**,** 1153-1175.

WAYCHUNAS, G. A. 2009. Natural nanoparticle structure, properties and reactivity from X-ray studies. *Powder Diffraction,* 24**,** 89-93.

WEINBERG, H., GALYEAN, A. & LEOPOLD, M. 2011. Evaluating engineered nanoparticles in natural waters. *Trac-Trends in Analytical Chemistry,* 30**,** 72-83.

WESTERHOFF, P., SONG, G. X., HRISTOVSKI, K. & KISER, M. A. 2011. Occurrence and removal of titanium at full scale wastewater treatment plants: implications for TiO2 nanomaterials. *Journal of Environmental Monitoring,* 13**,** 1195-1203.

WHITELEY, C. M., VALLE, M. D., JONES, K. C. & SWEETMAN, A. J. 2013a. Challenges in assessing release, exposure and fate of silver nanoparticles within the UK environment. *Environmental Science-Processes & Impacts,* 15**,** 2050-2058.

WHITELEY, C. M., VALLE, M. D., JONES, K. C. & SWEETMAN, A. J. 2013b. Challenges in assessing release, exposure and fate of silver nanoparticles within the UK environment. *Environmental Science: Processes & Impacts,* 15**,** 2050-2058.

WIGGINTON, N. S., HAUS, K. L. & HOCHELLA, M. F. 2007. Aquatic environmental nanoparticles. *Journal of Environmental Monitoring,* 9**,** 1306-1316.

WILLIAMS, D. B. & CARTER, C. B. 1996. *Transmission electron microscopy : a textbook for materials science,* New York ; London, Plenum.

WU, Z. H., YANG, S. L. & WU, W. 2016. Shape control of inorganic nanoparticles from solution. *Nanoscale,* 8**,** 1237-1259.

XIU, Z. M., MA, J. & ALVAREZ, P. J. J. 2011. Differential Effect of Common Ligands and Molecular Oxygen on Antimicrobial Activity of Silver Nanoparticles versus Silver Ions. *Environmental Science & Technology,* 45**,** 9003-9008.

XIU, Z. M., ZHANG, Q. B., PUPPALA, H. L., COLVIN, V. L. & ALVAREZ, P. J. J. 2012. Negligible Particle-Specific Antibacterial Activity of Silver Nanoparticles. *Nano Letters,* 12**,** 4271-4275.

XU, W., JIN, W. P., LIN, L. F., ZHANG, C. L., LI, Z. S., LI, Y., SONG, R. & LI, B. 2014. Green synthesis of xanthan conformation-based silver nanoparticles: Antibacterial and catalytic application. *Carbohydrate Polymers,* 101**,** 961-967.

YANG, S. P., BAR-ILAN, O., PETERSON, R. E., HEIDEMAN, W., HAMERS, R. J. & PEDERSEN, J. A. 2013a. Influence of humic acid on titanium dioxide nanoparticle toxicity to developing zebrafish. *Environ Sci Technol,* 47**,** 4718-25.

YANG, Y., CHEN, Q., WALL, J. D. & HU, Z. Q. 2012. Potential nanosilver impact on anaerobic digestion at moderate silver concentrations. *Water Research,* 46**,** 1176-1184.

YANG, Y., GAJARAJ, S., WALL, J. D. & HU, Z. Q. 2013b. A comparison of nanosilver and silver ion effects on bioreactor landfill operations and methanogenic population dynamics. *Water Research,* 47**,** 3422-3430.

YANG, Y., ZHANG, C. Q. & HU, Z. Q. 2013c. Impact of metallic and metal oxide nanoparticles on wastewater treatment and anaerobic digestion. *Environmental Science-Processes & Impacts,* 15**,** 39-48.

YU, H. C., KANG, H. X., JIAO, Z. B., LU, G. X. & BI, Y. P. 2015. Tunable photocatalytic selectivity and stability of Ba-doped Ag3PO4 hollow nanosheets. *Chinese Journal of Catalysis,* 36**,** 1587-1595.

YU, Y., GU, L., WANG, C. L., DHANABALAN, A., VAN AKEN, P. A. & MAIER, J. 2009. Encapsulation of Sn@carbon Nanoparticles in Bamboo-like Hollow Carbon Nanofibers as an Anode Material in Lithium-Based Batteries. *Angewandte Chemie-International Edition,* 48**,** 6485-6489.

ZALUZEC, N. J. *X-Ray Energy Dispersive Spectroscopy In the Electron Microscope* [Online]. Available: http://tpm.amc.anl.gov/Lectures/Zaluzec-4-XEDS.ppt.pdf [Accessed 04/06/2013 2013].

ZHANG, F., WU, X. L., CHEN, Y. Y. & LIN, H. 2009. Application of Silver Nanoparticles to Cotton Fabric as an Antibacterial Textile Finish. *Fibers and Polymers,* 10**,** 496-501.

ZHANG, Y., CHEN, Y., WESTERHOFF, P., HRISTOVSKI, K. & CRITTENDEN, J. C. 2008. Stability of commercial metal oxide nanoparticles in water. *Water Research,* 42**,** 2204-2212.

ZHANG, Y., LEU, Y.-R., AITKEN, R. J. & RIEDIKER, M. 2015a. Inventory of Engineered Nanoparticle-Containing Consumer Products Available in the Singapore Retail Market and Likelihood of Release into the Aquatic Environment. *International Journal of Environmental Research and Public Health,* 12**,** 8717-8743.

ZHANG, Z., LIU, C., BAI, J., WU, C., XIAO, Y., LI, Y., ZHENG, J., YANG, R. & TAN, W. 2015b. Silver Nanoparticle Gated, Mesoporous Silica Coated Gold Nanorods (AuNR@MS@AgNPs): Low Premature Release and Multifunctional Cancer Theranostic Platform. *ACS Appl Mater Interfaces,* 7**,** 6211-9.

ZHAO, J., WANG, Z. Y., DAI, Y. H. & XING, B. S. 2013. Mitigation of CuO nanoparticle-induced bacterial membrane damage by dissolved organic matter. *Water Research,* 47**,** 4169-4178.

ZHAO, Q. Y., DUAN, R. Q., YUAN, J. L., QUAN, Y., YANG, H. & XI, M. R. 2014. A reusable localized surface plasmon resonance biosensor for quantitative detection of serum squamous cell carcinoma antigen in cervical cancer patients based on silver nanoparticles array. *International Journal of Nanomedicine,* 9**,** 1097-1104.

ZHOU, Z.-Y., TIAN, N., LI, J.-T., BROADWELL, I. & SUN, S.-G. 2011. Nanomaterials of high surface energy with exceptional properties in catalysis and energy storage. *Chemical Society Reviews,* 40**,** 4167-4185.

ZOOK, J. M., LONG, S. E., CLEVELAND, D., GERONIMO, C. L. A. & MACCUSPIE, R. I. 2011. Measuring silver nanoparticle dissolution in complex biological and environmental matrices using UV-visible absorbance. *Analytical and Bioanalytical Chemistry,* 401**,** 1993-2002.